Ollscoil na Gaillimhe
University of Galway

Provided by the author(s) and University of Galway in accordance with publisher policies. Please cite the published version when available.

Title	Elastin-like recombinamers-based hydrogel modulates the post-ischemic remodelling in a clinically-relevant model of myocardial infarction
Author(s)	Contessotto, Paolo
Publication Date	2019-04-17
Publisher	NUI Galway
Item record	http://hdl.handle.net/10379/15130

Downloaded 2024-04-17T00:53:01Z

Some rights reserved. For more information, please see the item record link above.

Elastin-like recombinamers-based hydrogel modulates the post-ischemic remodelling in a clinically-relevant model of myocardial infarction

A thesis submitted to the National University of Ireland for the degree of Doctor of Philosophy

Paolo Contessotto

February 2019

Centre for Research in Medical Devices, National University of Ireland, Galway

Research Supervisors: Prof. Abhay Pandit and Dr Michelle Kilcoyne

Table of Contents

Table of Contents ..... **i**
Table of Figures ..... **vii**
Table of Tables ..... **xx**
Acknowledgements ..... **xxii**
List of Abbreviations ..... **xxv**
Abstract ..... **xxxii**
Chapter One **1**
1.1 Introduction 2
1.2 Clinical aspects of MI 3
1.2.1 Classification of myocardial infarction 3
1.2.2 Cardiac functional behaviour 4
1.3 Biological substratum and roots for therapeutic approaches 8
1.3.1.1 Ischemic nature of myocardial infarction 8
1.3.1.2 Preventing the ischemic damage-associated cascade 8
1.3.2.1 Post-ischemic inflammatory phase 10
1.3.2.2 Macrophages and their secretome as key regulators 13
1.3.2.3 Evolution of cellular-based treatments 14
1.3.2.4 Acellular biomaterial-based therapeutic approaches 16
1.3.3.1 Fibrosis 24
1.3.3.2 Key molecules in the regulation of the fibrogenic program 26
1.3.4.1 Matrix metalloproteinases 27
1.3.4.2 Cardiac matrix-inspired therapeutic approaches 29
1.3.5.1 Angiogenesis 36
1.3.5.2 Angiogenesis-driven approaches 37
1.3.6.1 Cellular stress 53
1.3.6.2 Modulation of ischemic-derived cellular stress 54
1.3.7.1 Recruitment of growth factors 55
1.3.7.2 Growth factor-based tested treatments 56
1.3.8.1 Basis and relevance of glycobiology 57
1.3.8.2 Role of glycans as therapeutic modulators 58
1.4 Regenerative approaches 62
1.4.1 Cardiac stem cells 62
1.4.2 Strategies based on the re-entry of cardiomyocytes in the cell-cycle 63
1.5 Future directions 72

1.6 Conclusions 73
1.7 Project rationale: Elastin as an injectable biomaterial for the treatment of MI 76
1.8 Objectives and hypotheses 76
1.8.1 Chapter Two - Distinct differences in cellular membrane glycosylation reflect the regeneration potential of neonatal myocardial tissue 77
1.8.2 Chapter Three – An ovine model of non-transmural myocardial infarction 77
1.8.3 Chapter Four - Elastin-like recombinamers-based hydrogel modulates the post-ischemic remodelling in a clinically-relevant model of myocardial infarction 78
1.8.4 Chapter Five - Transcriptomic, proteomic and glycomic analyses to reveal the mechanism of modulation of post-ischemic remodelling by an elastin-based hydrogel 78
Chapter Two **122**
2.1 Introduction 123
2.2 Materials and methods 125
2.2.1 Tissue harvesting from adult and neonatal rats 125
2.2.2 Tissue processing and cryosectioning 125
2.2.3 Alcian blue staining to detected sulfated glycosaminoglycans 126
2.2.4 Glycosylation in myocardial tissue sections 126
2.2.5 Protein extraction and quantification 127
2.2.6 Protein labelling for lectin microarray analysis 127
2.2.7 Lectin microarray analysis on healthy myocardial tissue 128
2.2.8 Processing to extract *N*-glycans 129
2.2.9 Processing to extract *O*-glycans 130
2.2.10 *N*- and *O*-glycomic analysis 130
2.2.11 Peaks annotation and intensity calculation from LC-ESI-MS/MS analysis 131
2.2.12 Statistical analysis 131
2.3 Results 131
2.3.1 Glycosylation difference in sialic acid between cardiomyocytes cell surfaces and capillaries 132
2.3.2 Tissue glycosylation of adult left and right cardiac ventricles is similar across rat strains 133
2.3.3 Complex *N*-linked and sialylated glycan structures are more abundant in adult and distinctive structures were detected in neonatal myocardium 134
2.3.4 *O*-linked glycan analysis of neonatal and adult myocardium 135
2.3.5 Distinct tissue glycosylation between neonatal and adult myocardium 136
2.4 Discussion 156

2.5 Conclusions 159
2.6 References 160
Chapter Three **166**
3.1 Introduction 167
3.2 Materials and methods 169
3.2.1 Ovine model of non-full thickness myocardial infarction 169
3.2.2 Pain management and humane endpoints 170
3.2.3 Functional response by echocardiographic measurements 171
3.2.4 Harvesting and stereology 171
3.2.5 Tissue processing 172
3.2.6 Histological evaluation 172
3.2.7 Tissue processing for electron microscopy analyses 173
3.2.8 Analysis of ECM deposition by scanning electron microscopy 173
3.2.9 Subcellular evaluation by transmission electron microscopy analysis 174
3.2.10 Quantification of total sulfated GAGs 174
3.2.11 Quantification of heparan sulphate and chondroitin sulphate 175
3.2.12 Statistical analysis 175
3.3 Results 175
3.3.1 Ovine model of non-full thickness myocardial infarction 175
3.3.2 Degeneration of cardiomyocytes at the ultrastructure level 176
3.3.3 Post-ischemic myocardial remodelling 177
3.3.4 Quantification of glycosaminoglycans during the post-ischemic remodelling 177
3.4 Discussion 189
3.5 Conclusions 191
3.6 References 191
Chapter Four **199**
4.1 Introduction 200
4.2 Materials and methods 202
4.2.1 In vivo experimental plan 202
4.2.2 Preparation of ELRs for myocardial injection 202
4.2.3 Injection trials 203
4.2.4 Procedure for injection in vivo 203
4.2.5 Animal monitoring after injection procedures 204
4.2.6 Heart explants and tissue preservation 204
4.2.7 Isotropic uniform random sampling 204
4.2.8 Assessment of post-ischemic remodelling by histology 205

4.2.9 Immunofluorescence staining for capillaries, collagen type-I and cardiomyocytes 205
4.2.10 Quantification of fibrosis 206
4.2.11 Analysis of myocardial extracellular matrix 206
4.2.12 Quantification of matrix deposition 207
4.2.13 Evaluation of glycosylation in cellular membranes and ECM 207
4.2.14 Quantification of capillaries structures and angiogenesis 208
4.2.15 Functional response by echocardiographic measurements 208
4.2.16 Statistical analysis 208
4.3 Results 209
4.3.1 Multiple intra-myocardial injections of ELRs hydrogel 209
4.3.2 Fibrosis evaluation after ELRs hydrogel treatment 209
4.3.3 Application of Raman confocal microscopy for fibrosis detection 210
4.3.4 Glycobiology and angiogenesis assessment after ELRs hydrogel treatment 211
4.3.5 Total sulfated GAGs deposition and HS/CS ratio during remodelling 212
4.3.6 Evaluation of functional improvement 28 days after MI 213
4.4 Discussion 226
4.5 Conclusions 233
4.6 References 234
Chapter Five **243**
5.1 Introduction 244
5.2 Materials and methods 245
5.2.1 RNA extraction from sheep samples 245
5.2.2 Library preparation for RNA-sequencing analysis 246
5.2.3 RNA-sequencing and differential expression gene analysis 246
5.2.4 Protein extraction from sheep samples 246
5.2.5 Suspension trapping trypsin digestion before proteomic analysis 247
5.2.6 Proteomic label-free quantification 247
5.2.7 Ingenuity Pathway Analysis (IPA®) to analyse transcriptomic and proteomic data 249
5.2.8 Immunofluorescence to quantify $CD163^+$ cells and α-SMA^+ arterioles 249
5.2.9 Immunofluorescence and lectin histochemistry to validate GATA4 250
5.2.10 Release of *N*- and *O*-linked glycans from membrane proteins 251
5.2.11 *N*- and *O*-linked glycans detection by LC-ESI-MS/MS analyses 252
5.2.12 Quantification of mitochondrial parameters 253
5.2.13 Statistical analysis 253
5.3 Results 253

5.3.1 Significant remodelling-related pathways from RNA-sequencing 253
5.3.2 Inflammatory- and remodelling-related transcripts levels downregulation at day 28 post-MI 254
5.3.3 Alterations of angiogenic-related pathways and higher peri-vascular and arterioles density in the ischemic core after hydrogel treatment 255
5.3.4 *N*-glycome analysis validates the changes in terminal α-galactose associated with angiogenesis 256
5.3.5 *O*-glycome analysis of ischemic cardiac tissue 257
5.3.6 Higher retention of $GATA4^{+}$ cardiomyocytes and improved mitochondrial integrity in the border zone of the infarct after hydrogel treatment 258
5.4 Discussion 274
5.5 Conclusions 279
5.6 References 280
Chapter Six 287
6.1 Introduction 288
6.2 Summary 290
6.2.1 Chapter Two - Distinct differences in cellular membrane glycosylation reflect the regeneration potential of neonatal myocardial tissue 290
6.2.2 Chapter Three – An ovine model of non-transmural myocardial infarction 291
6.2.3 Chapter Four - Elastin-like recombinamers-based hydrogel modulates the post-ischemic remodelling in a clinically-relevant model of myocardial infarction 291
6.2.4 Chapter Five - Transcriptomic, proteomic and glycomic analyses to reveal the mechanism of modulation of post-ischemic remodelling by an elastin-based hydrogel 292
6.3 Limitations 296
6.3.1 Chapter Two - Distinct differences in cellular membrane glycosylation reflect the regeneration potential of neonatal myocardial tissue 296
6.3.2 Chapter Three – An ovine model of non-transmural myocardial infarction 296
6.3.3 Chapter Four - Elastin-like recombinamers-based hydrogel modulates the post-ischemic remodelling in a clinically-relevant model of myocardial infarction 297
6.3.4 Chapter Five - Transcriptomic, proteomic and glycomic analyses to reveal the mechanism of modulation of post-ischemic remodelling by an elastin-based hydrogel 298
6.4 Future directions 299
6.4.1 Analysis of glycosylation in iPSCs-derived cardiomyocytes 299
6.4.2 Endocardial delivery of a ELRs-based hydrogel for the treatment of myocardial infarction 300

6.4.3 Evaluation of the effect of ELRs-based hydrogel on macrophage polarisation 301
6.4.4 Glyco-functionalised ELRs-based hydrogel for the treatment of myocardial infarction 302
6.5 References 306
Appendices **316**
A.1 RNA extraction 317
A.2 Protein extraction in RIPA buffer 324
A.3 Membrane protein extraction 325
A.4 Preparation of 4% paraformaldehyde solution 325
A.5 Cryopreservation 326
A.6 Tissue processing for embedding in paraffin 328
A.7 Tissue sectioning using the microtome 329
A.8 Tissue sectioning using the cryostat 329
A.9 Periodate treatment of bovine serum albumin for lectin histochemistry 330
A.10 Lectin staining on cryosections 330
A.11 Lectin microarray on cardiac samples 331
A.12 Hematoxylin and eosin staining of tissue sections 333
A.13 Masson's Trichrome staining of tissue sections 333
A.14 Alcian blue staining of tissue sections 335
A.15 Verhoeff's Van-Gieson staining of tissue sections 335
A.16 Pentachrome staining of tissue sections 336
A.17 Sputter coating of samples for scanning electron microscopy analysis 336
A.18 Imaging by scanning electron microscopy 337
A.19 Processing of samples before transmission electron microscopy analysis 339
A.20 Automatic grid stainer before transmission electron microscopy analysis 340
A.21 Imaging by transmission electron microscopy 341
A.22 ELRs-based hydrogel fabrication 342
A.23 Confocal Raman microscopy 345
A.24 References 350
A.25 Patent submission, journal publications, conference proceedings and awards 351

Table of Figures

Chapter One

Figure 1.1 Illustration of type I myocardial infarction. The area located downstream the obstructed coronary blood vessel is quickly subjected to ischemia. The loss of millions of cardiomyocytes which were populating this area is the main reason for the further decrease in cardiac functional response……..7

Figure 1.2 Schematic of the main phases after MI. Millions of cardiomyocytes die within a few hours after the occurrence of the myocardial injury. The apoptotic wave can last until a few days after, together with the rise of the inflammatory infiltrates which were recruited in the ischemic site and last for the first three weeks after MI. After the activation of fibroblasts in myofibroblasts there is a progressive deposition of collagen which results in the formation of an irreversible scar……..11

Figure 1.3 Schematic of the infiltration of monocytes and macrophages in the ischemic myocardium. The secretion of tumour necrosis factor (TNF) by the monocytes and the reduction in laminin 10 and collagen IV is associated with the disruption of the basement membrane and the extravasation of immune cells in the ischemic area. Here, monocytes differentiate in macrophages to clear the apoptotic cellular debris……..12

Figure 1.4 Schematic of myocardial environment at the time of ischemia and at the end of the ischemic remodelling…….25

Figure 1.5 Schematic of the sprouting process leading to angiogenesis……..…….41

Figure 1.6 Schematic of different approaches to treat myocardial infarction. Acellular hydrogels, ECM-inspired treatments, growth-factor-based and cellular-based or a combination of these have been exploited in the recent decades. Abbreviations: PEG, polyethylene glycol; TIMP, tissue inhibitor of metalloproteinases; eNOS, endothelial nitric oxide synthase; FGF, fibroblast growth factor; HGF, hepatocyte growth factor; IGF, insulin growth factor; PDGF, platelet-derived growth factor; SDF, stromal cell-derived growth factor; VEGF, vascular endothelial growth factor; ADSCs, adipose-derived stem cells; BMSCs, bone-marrow-derived stem cells; CDCs, cardiac-derived stem cells; EPCs, endothelial progenitor cells; iPSCs, induced-pluripotent stem cells; MSCs, mesenchymal stem cells..……...60

Figure 1.7 Timeline of key findings related to myocardial ischemia over the last two decades. Landmark studies related to the cardiac remodelling and regenerative are highlighted in blue and the most promising therapeutic strategies are shown in yellow……..74

Figure 1.8 Modulation of post-ischemic remodelling. (A) Schematic of untreated ischemic core and border region characterised by poor stable angiogenesis, marked fibrosis and prolonged oxidative stress in the ischemic core, which leads to cardiomyocyte hypertrophy. (B) Schematic of modulated ischemic core after treatment with enhanced angiogenesis, lower fibrosis and pro-healing macrophage infiltration, that beneficially influence the physiological behaviour of cardiomyocytes in the border zone……....…75

Figure 1.9 3-D illustration showing the hypothesised modultation of the post-ischemic ECM microenvironment (MI-only) after the ELRs-based hydrogel treatment. Increased fibrosis and cardiomyocyte hypertrophy are more pronounced in the untreated pathological than in the hydrogel-treated condition…….80

Chapter Two

Figure 2.1 Alcian blue staining detects glycosaminoglycans (GAGs) present across the myocardial tissue. Alcian blue staining at pH 2.5 (A-B) allows the visualisation of GAGs present in the extracellular matrix, which become clearly evident in close proximity to vasculature structures (B). Alcian blue staining at pH 1 (C-D) shows just the highly sulfated GAGs, which are mostly concentrated just close to the artery walls (D). Erythrocytes are stained orange; all other cell nuclei are red. Images B and D are 40x magnification of areas selected from left ventricular tissue shown in images A and C. These tissues were harvested from adult healthy Lewis and Sprague Dawley rats. Scale bar in A,C = 100 μm, in B,D = 20 μm…….……..139

Figure 2.2 Lectin binding in left ventricle and relative quantification. The same patterns were detected in both Lewis (L) and Dark Agouti (DA) rats. WGA lectin binds to NeuAc and GlcNAc residues (A,B), DSA binds to GlcNAc glycans (D,E), MAA recognizes α-(2,3)-sialylated motifs (F,G), SNA-I binds to α-(2,6)-sialylated motifs (H,I) and ConA recognizes mannose and glucose (J,K). All lectin binding intensities were background-subtracted and quantified by Image J. Data are shown as

mean with standard deviation (C). Student's t-test, n=4-6 animals per group. Scale bar = 50 μm……...140

Figure 2.3 Hierarchical clustering of glycan moieties detected across the left and right ventricle in two different strains of healthy rat. Lectin microarrays showed the binding intensity to the glycans present in the membrane proteins extracted from the left (L) and right (R) ventricle from Fischer (A) and Lewis (B) strains of healthy rats. Hierarchical clustering showed an 80% similarity across all the samples tested with the exception of LA 1, which had a 70% similarity with the rest of the samples. Samples LA2 and RB3 showed a 92% similarity. Asialofetuin (ASF) was used as control glycoprotein and all lectin binding intensities were normalised. 90% laser scans were combined with 10% laser scans when intensity binding was saturated (above 60,000 RFU). The experiment was carried out in technical triplicate. N=3 animals per group……..141

Figure 2.4 Statistical analysis of lectin intensity binding of glycans detected across the left and right ventricle in two different strains of healthy rat. Lectin microarrays did not show any significant difference between either the left and right ventricle inside the same strain or across two different strains. 90% laser scans were combined with 10% laser scans when intensity binding was saturated (above 60,000 RFU). One-way ANOVA with Tukey's post hoc correction, n=3 animals per group……..…142

Figure 2.5 Extracted ion chromatography (EIC) of the most abundant *N*-linked glycans present in the membrane protein in neonatal and adult healthy myocardial tissue. (A) The six most abundant *N*-glycans structures at *m/z* 941 ($Man_9GlcNAc_2$), 1235 ($Man_5GlcNAc_2$), 1111 ($Neu5Ac_2Hex_5GlcNAc_4$), 1184 ($Neu5Ac_2Hex_5GlcNAc_4Fuc_1$) and 1658 ($Neu5Ac_4Hex_5GlcNAc_4Fuc_1$) were chosen to show the different relative percentage of Neu5Ac-α-(2,3)-Gal-, Neu5Ac-α-(2,6)-Gal-and Neu5Ac-α-(2,8)-Neu5Ac- in neonatal and adult left ventricular myocardial samples. (B) Adult-stage group showed a 5% increase in complex-type structures and a 6% decrease in the subgroup of high mannose structures compared to three-day-old neonatal. (C) Among total high mannose structures, $Man_6GlcNAc_2$ showed a 4% increase in relative percentage. The experiment was done using samples pooled from three different animals per group…….143

Figure 2.6 Extracted ion chromatography (EIC) of distinctive *N*- and *O*-linked glycans present in the membrane protein in neonatal and adult healthy myocardial tissue. (A) Three *N*-glycan structures were detected only in left ventricular myocardial neonatal sample at m/z 1022 ($[M-2H]^{2-}$ ions, high-mannose precursor), 881 ($[M-2H]^{2-}$ ions, hybrid-type), and 982 ($[M-2H]^{2-}$ ions, complex-type). (B) EIC of dominant core 1 and 2 *O*-glycans, one sulfated core 2 *O*-glycan ($[M-H]^{-}$ ions at m/z 1120) was detected exclusively in neonatal tissue (framed in red). The experiment was done using samples pooled from three different animals per group……145

Figure 2.7 Hierarchical clustering of healthy ventricular samples from neonatal and adult stages. Lectin microarrays showed the binding intensity to the glycans present in the membrane proteins extracted from the three-day-old neonatal (P), 14-day-old neonatal (PP) and adult (A) ventricular myocardial tissue from Sprague Dawley healthy rats. Hierarchical clustering showed an 80% similarity across all the samples tested with the exception of A 1, which had a 68% similarity with the rest of the samples. Three-day-old neonatal samples P1, P2 and P4 showed an 88% similarity and clustered together, showing the highest similarity inside the same group. Asialofetuin (ASF) was used as control glycoprotein and all lectin binding intensities were normalised. The experiment was carried out in technical triplicate. All 90% laser scan measurements recorded were below the saturation limit (60,000 RFU). N=4 animals per group……..…146

Figure 2.8 Higher complex *N*-glycans and lower core 1 *O*-glycans at early neonatal stage. (A) LC-ESI-MS/MS analysis showed trends of higher expression of complex *N*-glycans and lower core 1 *O*-glycans in adult left ventricular myocardial tissue from Sprague Dawley healthy rats. (B) One-way ANOVA with Tukey's post hoc correction confirmed a higher binding of lectins to complex *N*-glycans (TJA-I, DSA, NPA, and core 1 *O*-glycans lower. N=4 animals per group, *p<0.05, **p<0.01, ***p<0.001……...147

Figure 2.9 Higher fucosylation at early neonatal stage. (A) LC-ESI-MS/MS analysis showed a trend of higher expression of fucosylated *N*-glycans in three-day-old left ventricular myocardial tissue from Sprague Dawley healthy rats. (B) Lectin microarrays indicated an increased binding of three-day-old neonatal sample to AAL lectin……..148

Chapter Three

Figure 3.1 Quantification of decrease in ejection fraction (EF) at day 7 and 28 post-induction of MI. Echocardiographic data were used to calculate the ejection fraction (EF) values at each timepoint for all animals that survived to the induction of MI (A). Absolute changes in EF are shown 7 (7d MI) and 28 (28d MI) days after the surgical procedure. Data are reported as box-plots, Mann-Whitney *U* test, n=8 animals per group……...……..180

Figure 3.2 Gross explant images showing the scar formation 28 days after the ligation procedure. Healthy eight-month-old male sheep before (A,B) and 28 days after (C,D) the induction of myocardial infarction through the ligation of the side branches of the coronaries. A clear MI-area (framed in green) is visible in the cross section (D) by the whitish colouring of the region of the left ventricle effected. The infarct is non-transmural since it is not extended to the full thickness of the ventricular wall. Ruler = 1 mm……..…...181

Figure 3.3 Schematics of harvesting tissues from explanted hearts. After perfusion with PBS to remove the excess of blood, each heart was cross-sectioned in slices with a thickness of 1 cm from the atria to the apex. Clear MI areas were identified by the whitish colour and from there samples with a maximum size of 0.5 cm in every direction were taken from the core ischemic, the border and the remote regions. ……..182

Figure 3.4 Progressive cardiomyocyte vacuolisation at the ultrastructural level. Post-ischemic effects in the cardiomyocytes located in the infarct border zone were assessed at the ultrastructure level by TEM. Cytosolic disruption and progressive vacuolisation is clearly visible (red arrows) from healthy (A) to 7 days (B) and 28 days after MI (C). Moreover, clustering of the intercalated disks (circled in red) was seen at seven days after MI (D). Scale bar = 2 μm…….……..183

Figure 3.5 Accumulation of dense bodies in the mitochondria of cardiomyocytes. Mitochondria of cardiomyocytes located in the border zone of the infarct are effected by the accumulation of dense bodies (circled in red) seven days after the induction of myocardial infarction. Low (A) and high magnification (B,C,D) pictures show the extension and consistency of the pattern in a cardiomyocyte myofibril. Scale bar = 2 μm…….....184

Figure 3.6 Fibrotic deposition and inflammatory status at day 10 after MI. Post-ischemic myocardial remodelling was assessed in sheep myocardial left ventricle 10 days after the ligation procedure. Inflammatory infiltrate was seen by hematoxylin and eosin staining (A) and initial deposition of collagen was confirmed by Masson's Trichrome (B). Furthermore, glycosaminoglycans (GAGs) were present in the epicardium and also in the inner myocardial infarcted region (Alcian blue staining in (C)). Finally, pentachrome staining allowed the visualisation of muscle, collagen and GAGs components (D). Scale bar = 100 μm.……..185

Figure 3.7 Matrix deposition from activated myofibroblasts. Elongated-shaped myofibroblasts (red arrows) were detected across the ischemic zone 28 days after MI together with collagen deposition. Wavy-oriented typical collagen-like deposition was one of the signs of the formation of a clear scar as seen at the ultrastructural level. Scale bar = 2 μm……..…186

Figure 3.8 Structural differences seen 28 days post-injury. Comparison between healthy myocardial extracellular matrix (A) and fibrotic one 28 days after myocardial infarction (B). Collagen bundles are clearly innervating the matrix. Scale bar = 50 μm……..…187

Figure 3.9 Quantification of total sulfated glycosaminoglycans and heparan sulphate/chondroitin sulphate ratio from healthy to 7 and 28 days after MI. By dimethylmethylene blue assay (DMMB) total sulfated glycosaminoglycans were quantified (A) and then, after digestion with chondroitinase ABC, the ratio between heparan sulphate (HS) and chondroitin sulphate (CS) was calculated by a subtraction method (B). All the data were compared to healthy ventricular tissue. Data are reported as box-plots, one-way ANOVA with Tukey's post hoc correction, n=5 animals per group, ***p<0.001……....188

Chapter Four

Figure 4.1 *Ex vivo* injection trial in ovine heart. Representative images (A,B) of ELRs-hydrogel injection *ex vivo* in an ovine heart (1-mm ruler spacing) and correspondent H&E showing hydrogel penetration across the sarcomeres. Verhoeff's-Van Gieson staining is specific for elastin and illustrates intercalation of the hydrogel across the sarcomeres causing no damage to the integrity of

cardiomyocytes, vasculature structures and relative supporting collagen (D). Non-injected area is shown in C. Scale bar = 100 μm……..216
Figure 4.2 Schematics of the experimental groups. 14/43 sheep died because of the suture ligation procedure, corresponding to a 32.55% mortality. One out of seven PBS-injected and two out of nine ELRs-hydrogel-injected animals died after the injection procedure. One out of seven ELRs-hydrogel-injected sheep was excluded because of MI-related atrial fibrillation…….....217
Figure 4.3 Gross explant pictures showing the left ventricle at the macroscopic level. Representative pictures of gross explants from MI-only group (A) and ELRs-hydrogel group (B) 28 days after the induction of myocardial infarction. Clear MI-area (green rectangles) was visible by the whitish colouring of the region of the left ventricle effected in all animals at the time of harvesting. The infarcts were non-transmural since they were not extended to the full thickness of the left ventricular wall. Ruler = 1 mm……...218
Figure 4.4 Reduced fibrosis in the group treated with ELRs-hydrogel. Masson's Trichrome images (A) and relative quantification (C) of collagen deposition (stained in blue) across the ischemic areas in hydrogel-treated (star indicates an island of ELRs-hydrogel) compared against MI-only. TEM micrographs (B) illustrating the typical wavy structure of fibrotic collagen deposits (indicated by arrows) in the analyzed ischemic areas in both hydrogel-treated and MI-only, and their relative quantification (D). Scale bars = 100 μm in A, 2 μm in B. Data are reported as box-plots, Mann-Whitney *U* test, n=5 animals per group, *p<0.05……...……..219
Figure 4.5 Raman analysis of myocardial infarcted tissue. Averaged Raman spectra of 225 points scanned in 100 μm^2 ischemic areas in ELRs-treated, MI-only and healthy myocardial sections (A). The peak circled at 1246 cm^{-1} corresponds to reported collagen assignment. Heat maps (B,C,D) showing the localization of the integrated intensity of the 1246 cm^{-1} peak circled in (A), merged with confocal bright-field pictures of healthy (B), ELRs-treated (C) and MI-only myocardial sections (D). N=4 animals per group. Scale bars = 50 μm……...…220
Figure 4.6 Validation of a method of fibrosis detection by Raman spectroscopy. The characterisation and distribution of collagen fibres was validated by the comparison with gold standard Masson's Trichrome staining on consecutive sections from the same snap-frozen samples. Specifically, fibrotic deposition seen at 28 days after MI

(A) was confirmed by the high level expressed in the corresponding Raman heat map (B). Conversely, healthy myocardium (C) reflected in a considerably lower normalised integrated intensity in the Raman heat map (D)……....221

Figure 4.7 Relevant changes in *N*-acetyl-galactosamine and terminal α-galactose glycan expression after ELRs treatment. Heat map and hierarchical clustering of 49 lectin-microarray binding intensity to glycans present in membrane-proteins extracted from healthy (HLT), and either MI-only (M) or hydrogel-treated (H) animals in core ischemic (I), border (BZ) and remote (F) areas of MI. Asialofetuin (ASF) was used as glycoprotein control. Extracted quantification of GS-I-A4 and GS-I-B4 lectin binding intensity (B) across the different groups. GS-I lectin histochemistry counterstained with DAPI in ischemic regions 28 days after MI (C). Healthy adult myocardial rat tissue was used as positive control to stain endothelial cells. Pooled samples coming from four animals were analysed, error bars represent standard deviation of three replicates. One-way ANOVA followed by Dunnett's post hoc test, *p<0.05, ***p<0.001. Scale bar = 100 μm in C, 20 μm in D. ……..……222

Figure 4.8 Quantification of angiogenesis in ELRs-treated group. Co-localization of GS-I and CD31 staining in ischemic regions after hydrogel treatment (star indicates an island of ELRs-hydrogel) and in MI-only samples 28 days after MI (A). Higher magnification (B) and respective TEM micrograph (C) show the capillary components (E=endothelial cell, P=pericyte, R=red blood cell) in the ELRs-treated group. Quantification of number of capillaries (D) and radial diffusion (E) in the ischemic areas comparing MI-only with hydrogel-treated. Data are reported as box-plots, Student's t-test, n=5 animals per group, **p<0.01. Scale bars = 100 μm in A, 20 μm in B, 2 μm in C……..223

Figure 4.9 Quantification of total sulfated glycosaminoglycans and HS/CS ratio. Quantification of sulfated glycosaminoglycans by DMMB assay was performed on all the groups with the final endpoint of 28 days after MI. Statistical analysis by Dunnett's test confirmed a significant increase in pathologically-equivalent MI-only and PBS-treated groups but not in the ELRs-treated group (A). After enzymatic digestion, quantification of the ratio of heparan sulphate to chondroitin sulphate content showed a significant reduction in all the groups at 28 days, with a slight increase in the ELRs-treated group. Data are reported as box-plots, one-way

ANOVA followed by Dunnett's post hoc test, n=6 in hydrogel, n=5 in MI-only and healthy, n=4 in PBS, *p<0.05, **p<0.01……..224
Figure 4.10 Functional response 21 days after the ELRs-hydrogel injection. Echocardiographic data were used to calculate the ejection fraction (EF) values at each timepoint for all the groups of the study (A). Animals that did not show a decrease in EF at day seven post-MI were not considered for the functional analysis. Comparison of the absolute changes in EF before the surgical procedure and seven days after MI (B). Comparison of the absolute changes in EF before the injection procedure (performed at day seven post-MI) and 21 days after (28 days post-MI) (C). Data are reported as box-plots, Kruskal-Wallis ANOVA, n=4 animals in hydrogel, n=6 in PBS and MI-only, *p<0.05……225

Chapter Five

Figure 5.1 Volcano plots of DEG data from RNA-sequencing. Volcano plots showing the total genes significantly upregulated (log2(fold change) > 1.5) and downregulated (log2(fold change) < -1.5) across the core ischemic (IS), border (BZ) and remote regions (FAR) sampled from 7, 28 days MI-only (MI28D) and hydrogel-treated (HYD) groups. All differential expression gene (DEG) data were normalised to healthy baseline left ventricular samples. DEG data were analysed using the Wald's test and filtered by adjusted p-value<0.05, n=4 animals per group……....261
Figure 5.2 Significant pathways detected by IPA® analysis on RNA-seq data. DEG data from RNA-seq were analysed by IPA® analysis applying cut-offs of log2(Fold Change) > 1.5 and log2(Fold Change) < -1.5 and adjusted p-value<0.05. Dashed line shows a threshold of -Log(p-value) of 1.3, corresponding to p=0.05, that is the minimal level required to determine if a canonical pathway was significantly detected. Groups of MI-only at 7 and 28 days and hydrogel-treated are shown and grouped by relevant biological pathways. DEG data were analysed using the Wald's test and filtered by adjusted p-value<0.05, n=4 animals per group……..…..….262
Figure 5.3 Inflammatory and remodelling-related markers at day 28 post-MI. Differentially expressed genes (DEG) are expressed as log2(fold change) to the seven day post-MI levels. Inflammation, fibrosis and remodelling-related transcripts levels were measured in both the core ischemic (A,B) and border zones (C,D) of

infarcted hearts. DEG data were analysed using the Wald's test and filtered by adjusted p-value<0.05, n=4 animals per group, *p<0.05……..…263

Figure 5.4 Evaluation of angiogenic response 21 days after hydrogel injection. DEG data from RNA-seq were analysed by IPA® software to detect potential differences in the activation scores of pathways related to angiogenesis such as VEGF, HGF, ErbB and endothelin signalling (A). Ischemic core regions were stained for the presence of α-SMA$^+$ arterioles (B) and CD163$^+$ cells (D) in the hydrogel-treated and MI-only groups and quantified (C,E). Data are reported as box-plots, Mann-Whitney *U* test (n=4 in C and n=5 in E), *p<0.05. Scale bars = 100 μm in B, 20 μm in D……...264

Figure 5.5 Hierarchical clustering of *N*-glycomics data. Each subgroup of *N*-glycans (high mannose, hybrid and complex) was analysed by hierarchical clustering. A total number of 113 putative *N*-glycan structures were identified, divided in 18 high mannose (A), 17 hybrid (B) and 78 complex-type (C). Data are expressed as relative percentage of each putative *N*-glycan structure which was detected across the healthy and infarcted heart regions from untreated animals, 7 and 28 days after MI and hydrogel-injected. Regions of infarcted hearts are labelled as follows: is = core ischemic, bz = border zone, far = remote zone from the infarct. Each analysed sample was a pool of samples coming from three individuals……..…265

Figure 5.6 Proportional changes in main *N*-linked complex glycans compared to healthy baseline. *N*-linked glycans expressing α-(2,3)-sialylation (A), α-(2,6)-sialylation (B), NeuAc (C), NeuGc (D) and α-Gal (E) in the ischemic core and border regions of seven days post-MI, MI-only and hydrogel-treated were normalised to healthy levels. *N*-linked glycans were released from one pooled sample of three animals per group and region and analysed by LC-ESI-MS/MS. ……..…266

Figure 5.7 Proportional changes in main *O*-linked glycans compared to healthy. *O*-linked glycans expressing sialic acid (A), NeuAc (B), NeuGc (C) and α-gal (D) from the ischemic core and border regions were normalised to the healthy levels. *O*-linked glycans were released from one pooled sample of three animals per group and region and analysed by LC-ESI-MS/MS…….268

Figure 5.8 Hierarchical clustering of proteomic data. Hierarchical clustering on proteomic data showed two main clusters with a minimum similarity of 32%. Protein

entries were filtered by a unique peptide number of at least two. The ischemic core after treatment with the hydrogel clusters together with the border regions subgroup, in a distinctive way compared to the ischemic regions from PBS-injected and MI-only groups at both the day 7 and 28 post-MI. Moreover, the ischemic zone after treatment with the hydrogel showed a 72% minimum similarity with the cluster of the remote regions (samples A-D remote). Regions of infarcted hearts are labelled as follows: is = core ischemic, bz = border zone, far = remote zone from the infarct. Each analysed sample was a pool of samples coming from three individuals…….269

Figure 5.9 Significant pathways detected by IPA® analysis on proteomic data. Data from proteomic analysis (expressed as fold ratio to the healthy group), which had a unique peptide number of at least two, were analysed by IPA® analysis. Cut-offs of fold ratio > 1.5 and fold ratio < -1.5 were applied. Dashed line shows a threshold of -Log(p-value) of 1.3, corresponding to p=0.05, that is the minimal level required to determine if a canonical pathway was significantly detected. Groups of MI-only at 7 and 28 days and hydrogel-treated are shown and grouped by relevant biological pathways. Each analysed sample was a pool of samples coming from three individuals……...…..270

Figure 5.10 Fold change of relevant proteins involved in the remodelling in infarcted groups compared to healthy. Expression levels of myofibroblast-related markers vimentin and calponin 1 (A) together with ROS-scavengers cytochrome *c* and superoxide dismutase (B) as detected by nLC-ESI-MS/MS analysis. Regions are labelled as follows: is=core ischemic, bz=border, far=remote. Hyd=hydrogel-treated. Each analysed sample was a pool of samples from three individuals. Data are reported as average of two technical replicates……271

Figure 5.11 Detection and validation of GATA4 as a key upstream regulator. Delta of the activation z-score of upstream regulators between hydrogel-treated and MI-only group (A) highlighting GATA4 as top regulator (from IPA® analysis on RNA-seq data, n=4). Validation of $GATA4^+$ cardiomyocytes in the border zone in both treated and untreated groups (B) (star indicates an island of ELRs-hydrogel). Scale bars, 20 μm. Quantification of $GATA4^+$ cardiomyocytes indicates a higher count in the hydrogel-treated group (C). Data are reported as box-plots, Student's t-test, n=5 animals per group, **p<0.01……272

Figure 5.12 Mitochondrial swelling in the cardiomyocytes of the border zone. EM micrographs showing the mitochondria located between the myofibrils of the

cardiomyocytes from samples of the border zone (A). Mitochondrial volume (B), surface area of the outer membrane (C) and surface area of the inner membrane (D) were quantified across healthy, infarcted hearts at day 28 (MI-only) and hydrogel-treated hearts. Data are reported as box-plots, n=5 in MI-only, 6 in healthy and hydrogel. Kruskal-Wallis ANOVA, *p<0.05. Scale bars = 500 nm……273

Chapter Six

Figure 6.1 Graphical abstract of different glycosylation seen between neonatal and adult myocardial tissue (Chapter Two). The experimental flow included lectin histochemistry, PGC LC-ESI-MS/MS analyses (spectra) and lectin microarrays (heat-maps) to identify the glycan structures present in adult and neonatal myocardial tissues……294

Figure 6.2 Schematic representation of the improved remodelling observed in the ELRs-treated group (Chapter Four and Five). The ischemic core of the infarcted region is less fibrotic and more perfused by a capillary network 21 days after the multiple intra-myocardial injection of the ELRs-based hydrogel. This influences the preservation of a more physiological border zone, populated by a higher number of $GATA4^{+}$ cardiomyocytes……..…295

Figure 6.3 Endocardial delivery of the ELRs-based hydrogel in the infarcted left ventricular wall. ELRs-based hydrogel could be optimised for minimally invasive endocardial delivery to the left ventricular wall. A dual-barrel mixer prototype will need to be designed to ensure appropriate conditions to allow initial crosslinking of the ELRs. The ELRs-based hydrogel will need to be injected without being influenced by the transport through the catheter……..…304

Figure 6.4 Proposed study evaluating the effect of ELRs-based hydrogel matrix on macrophage polarisation. ELRs-based hydrogel porous matrix could be optimised to evaluate its spatial confinement effect on the expression of inflammatory markers in macrophages. This further study would also investigate if this matrix might favour a swift of macrophages towards a pro-healing state……305

Appendices

Figure A.1 Preliminary evaluation of RNA integrity after extraction……..…318

Figure A.2 Schematic of isotropic uniform random sampling. Infarcted hearts (a) were axially cut at 1 cm thickness (b). 0.5 cm-thick samples were taken from the ischemic, border and remote regions (c) and cut following the orientator method through ϕ (d) and cosine-weighted θ (e) clocks. Finally, after embedding sectioning and staining, isotropically-oriented sections were imaged and quantified by superimposing stereological squared grids (f)……..…327

Figure A.3 ϕ and θ clocks used to generate isotropic uniform random samples….328

Figure A.4 GS-I lectin histochemistry on ELRs-treated and MI-only animals 28 days post-MI and validation in neonatal healthy myocardial tissue. Scale bar = 20 μm…….331

Figure A.5 H&E images showing morphological integrity of ovine myocardial tissue following fixation and sucrose infiltration before embedding in OCT (A) and its partial disruption by immediate snap-freezing after harvesting (B). Scale bar = 100 μm…….334

Figure A.6 Transmission electron microscopy imaging showing the perfused capillaries (blue arrows) found in the proximity of cardiomyocytes (green arrow) and in the ischemic core regions across different animals in the ELRs-treated group. Wavy formed collagen (red arrow) was detected in the ischemic cores of both PBS-injected and ELRs-treated groups. Scale bar = 2 μm……...344

Figure A.7 Region of interest visualised by brightfield prior to Raman analysis…345

Figure A.8 Raman analysis of myocardial infarcted tissue. Averaged Raman spectra of 225 points scanned in 100 μm^2 areas in healthy (hlt) myocardial sections. N=3 animals……..…346

Figure A.9 Stereological grid super-imposed on Masson's Trichrome stained isotropic uniform random sample to quantify fibrosis. Area fraction of collagen was calculated from each low magnification image (10x). A grid made of 112 points was superimposed on each field of view and the points hitting collagen fibres were counted to get the area fraction values. A total ischemic area of 4.05 mm^2 was analysed per block. Scale bar = 100 μm……...…347

Figure A.10 Stereological grids to quantify capillaries, arterioles, $GATA4^+$ cardiomyocytes and $CD163^+$ cells. The number of $CD31^+$/GS-I^+ capillaries, α-SMA^+ arterioles, $GATA4^+$ cardiomyocytes and $CD163^+$ cells was calculated from each image. Confocal microscopy, 20x for vessel structures, scale bar = 100 μm. 40x for

GATA4 and CD163, scale bar = 20 μm. Four grids were superimposed on image and the objects of interest falling inside the grids were counted to get the numerical estimates……...348
Figure A.11 Acridine orange staining of cellular nuclei in the border zone of MI. Sections from healthy and border zones of the infarcted hearts were stained with acridine orange to visualize and quantify cellular nuclei following the nucleator method. Data were then used to normalise EM micrographs measurements and estimate relative mitochondrial swelling. n=5 in MI-only, 6 healthy and hydrogel-treated……349
Figure A.12 Schematics of HE5-cyclooctine and HRGD-azide elastin-like recombinamers (ELRs) sequences. The two ELRs crosslink by catalyst-free click-chemistry reaction to form a hydrogel. Elastin-derived VPGXG (X variable amino acid) pentapeptide is present on both ELRs, cell-adhesive sequence RGD is present on HRGD and matrix metalloproteinase (MMP)- and cathepsin K(Cat-K)-responsive sequences are present in the HE5 ELR…….349
Figure A.13 IPA® analysis highlighted an arrested inhibition of GATA4 in ELRs-treated group. Predicted inhibition (blue) of GATA4 as a key regulator in MI-only at 28 days post-MI is lost in the ELRs-treated group (light orange). In MI-only, this is linked with a marked expression of pro-fibrotic genes such as POSTN, COL1A1 and COL1A2 (framed in red). By contrast, in ELRs-treated condition the arrested inhibition of GATA4 is associated with EDN1 and FOS expression, which are markers of endothelial cell proliferation. Log2(fold change), P, and adjusted-P values from RNA-seq data are indicated below the gene names. ……..350

Table of Tables

Chapter One

Table 1.1 Clinical classification of type of myocardial infarction……...…6

Table 1.2 Acellular biomaterials for the treatment of MI……..18

Table 1.3 Extracellular matrix-inspired biomaterials for the treatment of MI……...31

Table 1.4 Combined approaches for the treatment of MI targeting angiogenesis….42

Table 1.5 Non-combined strategies for the treatment of MI…….....66

Chapter Two

Table 2.1 Lectins used for tissue histochemistry, their binding specificity, used concentration and inhibitory carbohydrate (150 mM)…….…138

Table 2.2 List of lectins printed on the lectin microarrays, with origin, abbreviation and carbohydrate specificity…….149

Table 2.3 *N*-linked glycan structures detected in adult and three-day-old neonatal healthy ventricular tissue. Each m/z value is provided with potential composition, putative structure retention time (RT), intensity and relative percentage (%)…..…151

Table 2.4 *O*-linked glycan structures detected in adult and three-day-old neonatal healthy ventricular tissue. Each m/z value is provided with potential composition, putative structure retention time (RT), intensity and relative percentage (%)……..155

Chapter Three

Table 3.1 MI models adopted in large animals……179

Chapter Four

Table 4.1 Optimised conditions for the injection of the ELRs hydrogel…….215

Appendices

Table A.1 Concentration (ng/μl), purity (A260/A280) and integrity (RIN) of RNA samples sent for RNA-sequencing……....319

Table A.2 List of components and reagents…….320

Table A.3 Routine program overnight for tissue processor…….....329

I certify that the thesis is all my own work and I have not obtained a degree in this University, or elsewhere, on the basis of this work

Acknowledgements

As easily predictable, I am writing this section after the whole thesis. The last five years have been a combination of diverse, and often contrasting, emotions. Several sources added drop by drop their contribution to influence and gradually transform my perspective of what it means to do a PhD. The primary source, my main academic supervisor Prof. Abhay Pandit, to whom I am eternally grateful for his support along this long path. The pursuit of precision and accuracy in performing and presenting the work of these years strengthened over time and it was inspired by the advice and behaviour of this supervisor. Since my project was firmly based on a multidisciplinary approach, I was co-supervised throughout by Dr Michelle Kilcoyne, and I will always recognise Michelle's brilliant guidance through the complex and not fully unveiled world of glycobiology. Another source of light on this route was Prof. Peter Dockery, whose lessons on stereology were a stimulating and unique opportunity to reinforce the results achieved over these years. Despite my troubled relationship with the clinicians so far, during this project I was always in contact with Dr Mark Da Costa. Our joined-up work resulted in the establishment of a clinically-relevant model of myocardial infarction. This required from us an infinite amount of work and travelling to Lithuania to perform all the procedures. My special thanks also to the members of the Graduate Research Committee, Dr Una Fitzgerald, Dr Dimitrios Zeugolis, Dr Manus Biggs and Dr Yuri Rochev for their comments and advices during these years.

Since my PhD started as part of the AngioMatTrain European project for the first three years, I would like to acknowledge all the other institutions involved for the exchange of knowledge. In particular, Prof. José Carlos Rodríguez-Cabello and Doriana Orbanić for their support and collaboration in providing the elastin-like recombinamers I needed to work on for the *in vivo* application. I would like to thank all the other members of the AngioMatTrain team who worked here in Galway: Dr Gesmi Milcovich, Dr Renza Spelat, Dr Christos Tapeinos and Grazia Marsico. Special thanks to Dr Sarah Gundy for organising such amazing events during that period.

Working in a lab populated by around 40 people sometimes it meant having to face multiple and unexpected issues, though, this was made easier by the continuous efforts of our hard-working lab manager Dr Oliver Carroll. Thanks also to Robert

Giblin and Vidoja Kovačević for their help with the ordering and delivery issues. I need to thank one of my most valued and unconventional collaborators, that is the person who probably contributed to the highest number of figures presented in this thesis, i.e. the graphic designer Maciek Doczyk. I will miss our discussions over how to make clear schematics of scientific concepts and observations. Infinite thanks to another companion along the way, Anthony Sloan, who was always helpful in checking the grammar of my documents. Probably because of his nice and polite manners for a long period I thought he was actually a British man. The "Ackowledgements" section is often peopled by names who will be sooner or later forgotten. For sure from this section I will never forget Keith Feerick, one of the most humble and hard-working professionals I ever met. Everyday I believe and hope he will be able to come back to this lab to give his precious contribution.

I would like to reserve a special mention for Juhi Samal and Ana Lúcia Rebelo, who I consider both amazing researchers and sincere friends. I wish all the best to the current generation of scientists in the lab, in particular to Dr Mihai Lomora, Dr Merari Chevalier and Dr Sergio Martin Saldana. Good luck to all the PhD students in the lab who are passionately working on their projects, I hope they will all achieve brilliant results and continue along their desired career path, either academic or industrial. Moreover, I would like to thank Prof. Lokesh Joshi, Dr Jared Gerlach, Dr Stephen Cunningham and Dr Marie Le Berre from the Glycobiology group for the fruitful discussions and meetings. Not to forget, the professionals from the Anatomy department, Dr Pierce Lalor, Dr Emma McDermott and Dr Mark Canney who were so helpful in getting practice with electron microscopy techniques and solving technical issues. Special dedication to Dr Peter Owens, after long hours of optimisation we were able together to revive the interest for using Raman spectroscopy here in Galway.

Lots of thanks to all the administrative professionals in CÚRAM I had the pleasure to work with: Tara Cosgrave, Mairéad Uí Fhátharta, Dr Stefania Spada, Carmel McGroarty-Mitchell and Dr Iain Shaw. It was a pleasure as well to be involved in education and public engagement activities by Claire Riordan and Andrea Fitzpatrick. I would also like to acknowledge Cristiana Pozzebon for solving some software-related bugs in the layout of this thesis.

During these five years I have had the opportunity to collaborate with several institutions in Europe. Dr Niclas Karlsson and Dr Jin Chunsheng from the Institute of Biomedicine in Gotheborg helped with the glycomic analysis, Prof Dulcé Papy-Garcia and Dr Sandrine Chantepie from CRRET laboratory in Paris contributed to the glycosaminoglycans analysis, and Prof. Fulvio Magni and Dr Clizia Chinello from Proteomics and Metabolomics Unit in Milan ran the proteomics. I would like to thank also the Lithuanian University of Health Sciences, in particular Prof. Dainius Pauza, Dr Kristina Rysevaite and Audrys Pauza for their support during the experiments in Kaunas. Thanks to all these scientists, it was possible to further investigate the mechanisms of our tested treatment for myocardial infarction.

At the present time of diverging views for the future of Europe, I can certainly attest to the combined strength and competence of all these institutions over this continent which is proof of our potential compactness. I acknowledge the European Union Seventh Framework Programme and the Science Foundation Ireland funding agencies for their support.

Finally, thank you to my parents Maria and Marco who always supported - sometimes with too much love - my work during my PhD and to whom I dedicate this thesis.

List of Abbreviations

AAL: *Aleuria aurantia* lectin

AAV: Adeno-Associated Viral vector

ABL: *Agaricus bisporus* lectin

ACC: American College of Cardiology

ACN: Acetonitrile

ADSC: Adipose-Derived Stem Cell

Ang II: Angiotensin II

ANG-1: Angiopoietin-1

ANOVA: Analysis Of Variance

APAF-1: Apoptotic Protease-Activating Factor 1

ASF: Asialofetuin

AUC: Area Under the Curve

BMMNC: Bone Marrow Mononuclear Cell

BPA: *Bauhinia purpurea* lectin

BSA: Bovine Serum Albumin

BZ: Border Zone

CAA: *Caragana arborescens* lectin

CABG: Coronary Artery Bypass Grafting

CAD: Coronary Artery Disease

Calsepa: *Calystegia sepium* lectin

CASP1: Caspase-1

Cat-K: Cathepsin-K

CD: Cluster of Differentiation

CDC: Cardiosphere-Derived Cell

CDG: Congenital Disorders of Glycosylation

cDNA: Complementary DNA

CHAM: Calcium Hydroxyapatite Microsphere

CK: Creatine Kinase

CM: Cardiomyocyte

CMC: Cardiac Mesenchymal stem Cell

Con A: Concanavalin A lectin

CPA: *Cicer arietinum* lectin

CRAMP: Cathelin-Related Anti-Microbial Peptide

CS: Chondroitin Sulphate

cTn: Cardiac Troponin

CXC: Cysteine-amino acid-Cysteine

DAPI: 4,6-diamidino-2-phenylindole

DBA: *Dolichos biflorus* lectin

DDR: DNA Damage Response

DEG: Differential Expressed Gene

DMMB: Dimethylmethylene Blue

DMOG: Dimethyloxalylglycine

DPX: Distyrene-Plasticizer-Xylene

DSA: *Datura stramonium* lectin

DTT: Dithiothreitol

ECG: Electrocardiogram

ECM: Extracellular Matrix

ED: End-Diastolic

EDTA: Ethylenediaminetetraacetic acid

EdU: 5-Ethynyl-29-deoxyuridine

EDV: End-Diastolic Volume

EF: Ejection Fraction

EIC: Extracted Ion Chromatography

ELR: Elastin-Like Recombinamer

EM: Electron Microscopy

EPC: Endothelial Progenitor Cell

EPO: Erythropoietin

ERBB: Epidermal growth factor family of receptor tyrosine kinases

ES: End-Systolic

ESC: European Society of Cardiology

ESI: Electrospray Ionisation

ESV: End-Systolic Volume

ET-1: Endothelin-1

EV: Extracellular Vesicle

FA: Formic Acid

FACS: Fluorescence-Activated Cell Sorting

FAR: Region remote from ischemic core

FDR: False Discovery Rate

FGF: Fibroblast Growth Factor

FITC: Fluorescein Isothiocyanate

FOV: Field Of View

FS: Fractional Shortening

FSTL1: Follistatin-Like 1

GAG: Glycosaminoglycan

Gal: Galactose

GalNAc: *N*-acetylgalactosamine

GD: Ganglioside

GHA: *Glechoma hederacea* lectin

GlcNAc: *N*-acetylglucosamine

GLP-1: Glucagon-like Peptide-1

GMP: Good Manufacturing Practice

GNA: *Galanthus nivalis* lectin

GS: *Griffonia simplicifolia* lectin

HA: Hyaluronic Acid

Hex: Hexose

HFpEF: Heart Failure with preserved Ejection Fraction

HGF: Hepatocyte Growth Factor

HGFR: Hepatocyte Growth Factor Receptor

HIF: Hypoxia-Inducible Factor

HLT: Healthy

HMDS: Hexamethyldisilazane

HPA: *Helix pomatia* lectin

HRE: Hypoxia-Response Element

HS: Heparan Sulphate

HYD: Hydrogel

IAA: Iodoacetamide

IGF: Insulin Growth Factor

IgG: Immunoglobulin G

IL: Interleukin

IPA: Ingenuity Pathway Analysis

iPSC: Induced Pluripotent Stem Cell

IS: Ischemic

LacdiNAc: *N*-Acetylgalactosaminyl

LAD: Left Anterior Descending artery

LAP: Latency Associated Peptide

LC-ESI-MS/MS: Liquid Chromatography-Electrospray Ionization-tandem Mass Spectrometry

Lch-B: *Lens culinaris* lectin

LPM: Linear Parameter Measurement

LTA: *Lotus tetragonolobus* lectin

LTQ: Linear Trap Quadrupole

LV: Left Ventricle

LVDA: Left Ventricle end Diastolic Area

LVDD: Left Ventricle end Diastolic Dimension

LVSA: Left Ventricle end Systolic Area

LVSD: Left Ventricle end Systolic Dimension

LXR/RXR: Liver X Receptors/Retinoid X Receptor

M-CSF: Macrophage Colony-Stimulating Factor

MAA: *Maackia amurensis* lectin

MeOH: Methanol

MI: Myocardial Infarction

miRNA: Micro RNA

MNC: Mononuclear Cell

MOA: *Marasmius oreades* lectin

MPA: *Maclura pomifera* lectin

mRNA: messenger RNA

MSC: Mesenchymal Stem Cell

NA: Not Available

NCAM: Neural Cell Adhesion Molecule

NeuAc: *N*-Acetylneuraminic acid

NeuGc: *N*-Glycolylneuraminic acid

NF: Nano-Fiber

NGF: Nerve Growth Factor

NIPAAm: *N*-isopropylacrylamide

nLC-ESI-MS/MS: nano-flow Liquid-Chromatography combined with tandem Mass Spectrometry

NO: Nitric Oxide

NPA: *Narcissus pseudonarcissus* lectin

NR4A1: Nuclear Receptor subfamily 4 group A member 1

NRP: Neuropilin

NS: Non-Significant

NSTEMI: Non-ST-segment Elevation Myocardial Infarction

OCT: Optimal Cutting Temperature compound

OM: Obtuse Marginal artery

PBS: Phosphate Buffer Saline

PCI: Percutaneous Coronary Intervention

PCR: Polymerase Chain Reaction

PDGF: Platelet-Derived Growth Factor

PECAM: Platelet Endothelial Cell Adhesion Molecule

PEG: Polyethylene Glycol

PFA: Paraformaldehyde

PHA-E: *Phaseolus vulgaris* isolectin E

PHD: Prolyl Hydroxylase

PHPLPP: PH domain Leucine-rich repeat Protein Phosphatase

PI3K: Phosphoinositide-3-Kinase

PIP2: Phosphatidylinositol Bisphosphate

PIP3: Phosphatidylinositol Triphosphate

PK: Proteinase K

PLGA: Poly(lactic-co-glycolic acid)

PNA: *Arachis hypogaea* lectin

PTEN: Protein/lipid phosphatase and Tensin homologue

PUFA: Polyunsaturated Fat

RA: Rapidly Adhering

RCA-I/120: *Ricinus communis* agglutinin

RFU: Relative Fluorescence Unit

RGD: Arginine-glycine-aspartic acid amino acids sequence

RIPA: Radioimmunoprecipitation Assay buffer

RNA-seq: RNA-sequencing

ROS: Reactive Oxygen Species

rpm: Revolutions Per Minute

RT: Room Temperature

SA: Slow-Adhering

SBA: *Glycine max* lectin

SDF: Stromal cell-Derived Factor

SDS: Sodium Dodecyl Sulfate

SEM: Scanning Electron Microscopy

sGAG: Sulfated Glycosaminoglycan

siRNA: Small Interfering RNA

SMA: Smooth Muscle Actin

SNA-I: *Sambucus nigra*-I lectin

ST6Gal-I: α-2,6-sialyltransferase

STA: *Solanum tuberosum* lectin

STEMI: ST-segment Elevation Myocardial Infarction

Sv: Surface density

TBS: Tris-Buffer Saline

TdT: Terminal deoxynucleotidyl Transferase

TEAB: Triethylammonium Bicarbonate

TEM: Transmission Electron Microscopy

TFA: Trifluoroacetic Acid

TGF: Transforming Growth Factor

Th: T-helper cell

TIC: Total Ion Current

TIMI: Thrombolysis In Myocardial Infarction

TIMP: Tissue Inhibitor of Metalloproteinase

TJA: *Trichosanthes japonica* lectin

TLR: Toll-Like Receptor

TNBS: Trinitrobenzene Sulfonic acid

TNF: Tumour Necrosis Factor

Treg: Regulatory T-cell

TSP-1: Thrombospondin-1

UHPLC: Ultra-High Performance Liquid Chomatography

URL: Upper Reference Limit

VEGF: Vascular Endothelial Growth Factor

VEGFR: Vascular Endothelial Growth Factor Receptor

VPGXG: Valine-proline-glycine-X-glycine amino acids sequence

VRA: *Vigna radiate* lectin

vWF: von Willebrand Factor

WGA: Wheat Germ Agglutinin

XIC: Extracted Ion Chromatogram

Abstract

Myocardial infarction (MI) belongs to the family of cardiovascular diseases and represents the primary cause of worldwide mortality. An increasing trend of morbidity and mortality has been recently reported by the World Health Organisation in the developing countries (2016). Despite the diversity of therapeutic approaches which included growth-factors and stem cells, no option can currently replace routinely performed surgical procedures such as percutaneous coronary intervention, coronary artery bypass grafting and, more rarely, heart transplantation.

This thesis starts with a literature review of the main phases and cellular components of the post-ischemic environment. The biological rationale of the therapeutic approaches adopted by other groups over recent decades is reported with no bias towards a specific therapeutic target, such as fibrosis, angiogenesis or cellular stress. This initial review portrays the current bottlenecks in the field and introduces the specific gaps that this thesis is addressing.

The mammalian heart possesses a regenerative capacity at its early neonatal stage, so the first study (Chapter Two) presented in this thesis investigated the distinctive features at that stage under a previously limited investigated perspective, i.e. glycosylation. Glycans are among the most relevant post-translational modifications, but because of their complexity and that advances in methods to study their expression are recent, little is known about their functional role, especially in the myocardial environment. In Chapter Two, a consistent glycosylation was seen across adult myocardial tissues in rats, which significantly differed from its early neonatal condition (three-day-old). Interestingly, the higher expression of glycan types like *N*-liked high mannose was comparable to the expression profile of studies which have characterised the glycosylation of undifferentiated cells.

Currently adopted animal models of MI do not reflect the increasing trend of non-transmural, focal infarcts seen in the hospitalised clinical cases. The most widely followed method of ligation of the the left anterior descending coronary induces full-thickness infarcts, which constitute a severe clinical condition from which the effected patient can hardly survive. To address this current limitation, an ovine

model of non-transmural myocardial infarction was developed and validated at functional, histological and protein level (Chapter Three).

Despite the promising results achieved in both small and large animal studies, recent meta-analyses highlighted the marginal effect of therapeutic strategies like bone-marrow derived stem cells once they are tested in the clinical trials. Increasing evidence has shown the crucial role that components of the extracellular matrix (ECM) can play to modulate the post-ischemic remodelling. Moreover, several types of acellular hydrogels have been demonstrated to promote a less fibrotic and more angiogenic microenvironment, however still none of these showed efficacy in the clinical trials. Elastin is a natural component of the cardiac ECM and can be mimicked by genetic engineering through the production of elastin-like recombinamers (ELRs). In this thesis, two ELRs named HE5 and HRGD which contain matrix metalloproteinase-responsive and cell-adhesive sequences, respectively, were used to fabricate acellular hydrogels. Following initial optimisation, the ELRs-based hydrogel was injected intra-myocardially in the infarcted ovine model seven days post-MI (Chapter Four). A functional recovery in ejection fraction, lower fibrosis and higher angiogenesis in the ischemic core region were observed 21 days after the multiple injection procedure. Therefore, high-throughput analyses at expression, protein and glycan level which are presented in Chapter Five validated the initial findings and further elucidated the mechanism of action of the ELRs-based hydrogel. GATA4 was detected by IPA® analysis as the most distinctive upstream regulator in the treated animals since its predicted inhibition seen in the untreated condition was reversed 21 days after the injection of the hydrogel. This finding was validated by immunofluorescence and further supported by a preserved integrity in the mitochondrial structures of the cardiomyocytes located in the border zone of the infarct. To summarise, the recovery in cardiac function after hydrogel injection, in combination with a clinically-inspired established model of non-full thickness MI and a realistic intervention time (seven days post-MI) provide this study with an additional advantage for its clinical translation.

To summarise, this thesis arises from the current biological and clinical gaps in the field and addresses them by the application of a multisciplinary approach. Through

the investigation of the relevance of glycobiology, the development of a clinically-relevant model of MI, the application of an ECM-inspired hydrogel and the understanding of its mechanism of action, a substantial contribution has been made in the field.

Chapter One

Introduction

Sections of this chapter will be submitted in the following manuscript:
Contessotto P. and Pandit A. “Biological rationale and actual impact of therapeutic strategies for myocardial infarction”.

1.1 Introduction

Myocardial infarction belongs to the family of cardiovascular diseases which accounts for approximately one third of worldwide mortality [Mozaffarian 2016, Roth]. A wide spectrum of risk factors contribute to the incidence of this pathology among the industrialized countries and in those subjected to a rising economic expansion, as confirmed by the most updated reports [Roth]. Nevertheless, in the last 25 years there was a clear trend of decreased incidence in regions with high socio-demographic index - which measures the income per individual - in contrast to a mild or unchanged incidence in most of the countries [Roth]. Among the most studied risk factors which are known to be associated with a higher incidence of cardiovascular diseases, diabetes, hypertension and cigarettes smoking, even in the use of the electronic cigarette were reported [Alzahrani]. In recent years, the belief in the correlation between the intake of saturated fat in the diet and the occurrence of cardiovascular diseases has been questioned by meta-analyses of previous trials. For instance, polyunsaturated fat (PUFA) consumption was shown to reduce coronary artery disease events in randomized controlled trials [Mozaffarian 2010], and the correlation between saturated fat consumption and higher cholesterol levels in serum did not translate to a higher incidence of coronary artery disease.

The definition of myocardial infarction was redefined in 2000 by a consensus statement of The Joint European Society of Cardiology (ESC) /American College of Cardiology Committee (ACC) [Consensus]. The rationale for the agreement of this document by both the ESC and the ACC stemmed from the need to include new indicators to the traditional three characteristics of chest discomfort: enzyme rise and a typical electrocardiogram (ECG) pattern [Consensus]. Briefly, the main difference was the introduction of the evaluation of biochemical markers which were demonstrated to indicate myocardial necrosis in the past decades to define a precise diagnosis [Lindahl, Ohman]. Specifically, to define an “acute, evolving or recent myocardial infarction”, a peak of either cardiac troponin (cTn) or creatine kinase (CK) the serum levels needed to be recorded together with at least one of the following: clinical symptoms of ischemia, pathologic Q waves in ECG, ST elevation or depression in ECG, or actual identification of a thrombus by coronary angioplasty intervention. Alternatively, pathologic findings of apoptotic cardiomyocytes were required [Saraste].

In the second consensus document - that was approved in 2007 [Thygesen 2007] - the criteria listed in the first consensus document were all confirmed but some of them were more precisely defined. First, cTn was defined as the preferential biomarker whose peak needed to fall in the range above the 99th percentile of the upper reference limit (URL). Second, percutaneous coronary interventions (PCI) which cause an increase of the biomarker above the 99th percentile of the URL in patients with initial normal values of troponin were considered as evidence of myocardial necrosis due to the procedure [Thygesen 2007]. If the same increase in cTn characterises a coronary artery bypass grafting (CABG), the definition of MI can be applied as well. On the other hand, the definition of "prior myocardial infarction" was applied in any of the following cases: evidence of pathologic Q waves in the ECG, pathological evidence of healed or healing MI or - a new indicator which was not present in the first consensus document - imaging showing a thinning of the viable myocardial segment effected by necrosis [Thygesen 2007].

Finally, in 2018 a Fourth Universal Definition of Myocardial Infarction Consensus Document was published and focused on the differentiation between myocardial injury and myocardial infarction. According to this last updated Consensus Document, the guidelines to define MI indicate still both the abovementioned variation in cTn levels "at least one value above the 99th percentile URL" [Thygesen 2018] and one of the previously defined criteria for ischemia (physical symptoms, ECG changes, pathological Q waves, imaging to detect loss of myocardium or abnormal regional wall motion and detection of a thrombus by angiography). Whether only a rise and/or fall in cTn is observed, the clinical case falls in the category of myocardial injury and no assignment of any of the five subgroups of MI can be made. CK serum levels continue to be regarded as much less sensitive and specific than cTn [Thygesen 2018].

1.2 Clinical aspects of MI

1.2.1 Classification of myocardial infarction

The latest agreement on the definition of myocardial infarction was published in 2018 [Thygesen 2018]. This document currently reports the most updated guidelines

regarding the clinical classification of myocardial infarction, which is based on five different types according to their specific aetiology, as summarized in Table 1.1.

Type 1 and type 2 are both defined as the clinical consequence of the pathological phenomenon of myocardial ischemia. Briefly, type 1 is the result of the blockage of a coronary artery by the detachment of an atherosclerotic plaque (Figure 1.1), whereas type 2 includes all the cases of myocardial ischemia which are not a direct consequence of a coronary artery disease. Specifically, type 2 embraces all the conditions which lead to an imbalance between the myocardial supply and the demand of oxygen, such as endothelial dysfunction, fixed atherosclerosis and coronary vasospasm [Thygesen 2012]. Type 3 MI is the most challenging in terms of its therapeutic targeting since it includes those patients subjected to quick cardiac death and so can be hardly diagnosed in a timely manner by the identification of the rise or fall of cTn or CK. In the last Consensus Document, distinction between sudden cardiac death and type 3 MI was stressed as one of the points to be clarified depending on the presence of ischemic ECG changes [Thygesen 2018]. Further autopsy examination can reassign the case to another MI type according to the outcome. Revascularization procedures are part of the everyday practice to induce reperfusion after the diagnosis of myocardial infarction in the clinical theatres. PCI and CABG are the most widely adopted techniques and can lead to procedural myocardial injuries which need to be confirmed by precise comparison of pre/post-procedure peaks of cTn. Whether imaging-based evidence of ischemia is also linked to either PIC or CABG-dependent myocardial injury, type 4 and type 5 MI occur. Specifically, type 4 has been recently divided in three subclasses: type 4a is associated with myocardial injury during PCI, type 4b with stent or scaffold-induced thrombosis, and type 4c is due to the recurrence of stenosis (restenosis) after angioplasty procedure [Thygesen 2018].

1.2.2 Cardiac functional behaviour

The cardiac remodelling process is a physiological response of the organ that is trying to compensate for the physical loss of millions of cardiomyocytes. Due to the loss of capacity of the mammalian cardiomyocytes to re-enter the cell cycle upon turning to the adult stage, the organ limits the loss of mechanical support needed to prevent its collapse through the deposition of collagen type I and III by the

myofibroblasts. On the other hand, the fibrotic process can be characterised by the chronic activation of myofibroblasts and uncontrolled scarring, and has been demonstrated to be an independent predictor of arrhytmias and sudden death in large cohorts of patients [Gulati, Leyva]. The dilatation of the ventricular chamber after the occurrence of MI reflects the pathological scenario of a progressive dysfunction in the contractile property of the whole organ. As a consequence of the Law of Laplace, the thickness of the left ventricular wall is inversely proportional to the physical stress exerted on the same wall by the blood pressure and therefore is one indicator of post-ischemic remodelling. The pathophysiological consequences of the wall thinning spread from the ischemic core to the border zone of the infarct [Wilson]. Here there is an increase in metabolic consumption of the residual segments of cardiomyocytes which survived the ischemic insult and that can be severely effected in their physiological contractile properties [Wang 2018c].

Table 1.1 Clinical classification of type of myocardial infarction.

MI Type	Aetiology	Characteristics	Reference
1	Rupture of the atherosclerotic plaque, blockage of the coronary artery following atherothrombotic coronary artery disease (CAD)	Patients affected have lower long-term mortality compared to that one of patients with type 2	Sandoval, Lambrecht, Falk
2	Myocardial ischemia due to imbalance between oxygen demand and supply, no acute thrombotic event	Elevated values of cTn, patients are less likely to receive therapy for CAD	Baron, Smilowitz, Cediel
3	Associated with new ischemic ECG changes or ventricular fibrillations without a precise aetiology	Changes in levels of cTn can be hardly detected. Low incidence: 3.6% among all MI cases. Physical exertion as a possible trigger	Dagres, Mittleman, Jangaard
4a	Myocardial injury due to percutaneous coronary intervention (PCI)	Associated to risk of TIMI (Thrombolysis In MI) major bleeding	Woudstra, Mehran
4b	Myocardial injury due to scaffold/stent intervention	Subtype defined only in the last Consensus Document (2018)	Garcia-Garcia
4c	Restenosis after angioplasty	Subtype defined only in the last Consensus Document (2018)	Thygesen 2018
5	Myocardial infarction due to coronary artery bypass grafting (CABG)	Elevated levels of cTn can be detected, possible renal dysfunction	Oikawa, Holzmann, Wang 2013a

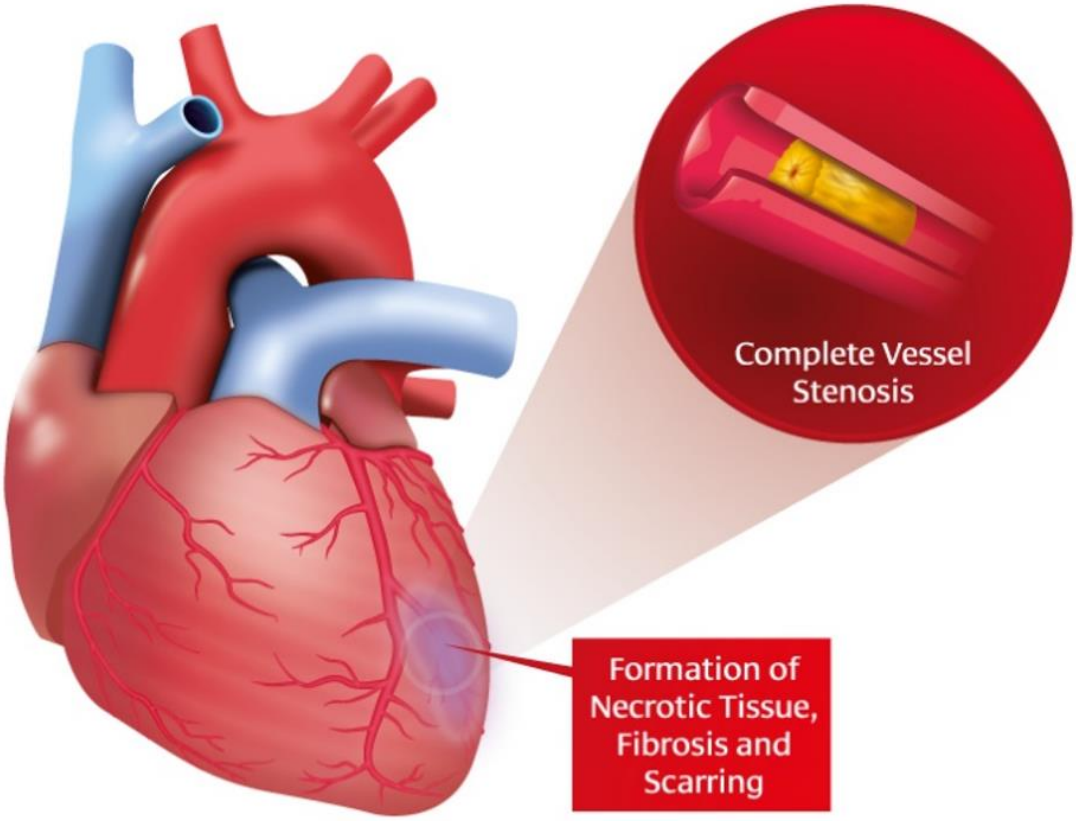

Figure 1.1 Illustration of type I myocardial infarction. The area located downstream the obstructed coronary blood vessel is quickly subjected to ischemia. The loss of millions of cardiomyocytes which were populating this area is the main reason for the further decrease in cardiac functional response.

1.3 Biological substratum and roots for therapeutic approaches

1.3.1.1 Ischemic nature of myocardial infarction

As summarized in the previous sections, the definition of myocardial infarction originates from the detection of the ischemic injury in the cardiomyocytes [Consensus]. Ischemic injury is one of the most studied types of insult that can severely affect the integrity of the cellular mechanisms, and the link between inflammation and ischemia is present across several clinical conditions [Eltzschig 2011 and 2014]. Examples of these pathologies include inflammatory bowel disease, ulcerative colitis, Crohn's disease, hind limb ischemia and myocardial infarction. Inflammatory hypoxia overlaps with aetiology of type 2 MI, where a severe imbalance between metabolic demand and supply leads to the myocardial injury. Hypoxia-inducible factors (HIFs) are crucial players in the molecular mechanisms behind hypoxia signalling [Semenza, Taylor]. The molecular mechanism of sensing and its relation with the biochemical pathway of HIF depends on the either normoxic or hypoxic conditions of the environment. In normoxia, HIF are polyubiquitylated and consequentially degraded due to the binding of E3 ubiquitin ligase to the α-subunit of HIF. This biological process is reversed in hypoxia, where the stabilization of the α-subunit induces its translocation in the nucleus. Here, following dimerization between the α- and the β- subunits, the complex binds to the hypoxia-response element (HRE) and promotes the activation of molecular pathways related to cell survival.

1.3.1.2 Preventing the ischemic damage-associated cascade

The induction of the normoxic state of HIF can be a target for the pharmacological manipulation of the prolyl hydroxylase (PHD) isoenzymes which are responsible for the hydroxylation of HIF which precedes the physiological polyubiquitinilation. This approach was applied to dimethyloxalylglycine (DMOG) and FG-4497 to target the catalytic domain of the inhibitor [Fraisl]. FG-4497 showed an improvement in clinical symptoms such as reduction in tumour necrosis factor (TNF)-α levels, colon length and weight loss in mice in which colitis was induced by trinitrobenzene sulfonic acid (TNBS) [Robinson]. A similar efficacy was demonstrated when

DMOG was tested in another murine model of colitis, which was induced by the injection of dextran sodium sulphate [Cummins].

In the case of the ischemia-reperfusion damage, a counterintuitive approach, defined as preconditioning, had been tested over recent decades. This consists in the preventive exposure to ischemia for short periods (minutes) before inducing severe and extended ischemic damage. The beneficial effect of such procedure on apoptosis and infarct size has been assessed [Piot]. Cycles of five minutes of ischemia and five minutes of reperfusion significantly reduced the infarct size from 58% to 11% when compared to non-preconditioned rats. Specifically, myocardial infarction was induced by the occlusion of the left anterior descending coronary vessel for 30 min followed by three hours of reperfusion [Piot]. In addition, in the preconditioned hearts the binding of terminal deoxynucleotidyl transferase (TdT) to fragmented DNA strands (TUNEL assay) was seen in fewer cells. This technique represents a well-established standard histochemical technique to localise apoptotic cells [Labat-Moleur, Christina].

The molecular pathways involved in the cardioprotective effect of preconditioning have been studied over the last two decades and include the phosphatidylinositol 3 kinase (PI3K)/Akt/mTOR signalling [Uchiyama, Tong, Hausenloy, Zhang, Dou]. Specifically, several recent studies investigated the molecular mechanisms of remifentanil, an opioid (μ-agonist) used for anaesthetic procedures [Irwin], which limited ischemic-reperfusion damage also in a pathological context different from that of the heart, such as small intestine and hepatic ischemic injuries [Shen 2016, Cui]. Exanatide, a peptide which binds to the glucagon-like peptide-1 (GLP-1) receptor, is a drug normally used for the treatment of diabetes mellitus type 2. Recent evidence has shown its efficacy in reducing the infarct size in patients that undergo PCI [Lønborg, Woo]. Currently, a phase III clinical trial named COMBAT-MI (NCT02404376) is recruiting 428 patients to evaluate the efficacy of the combination of remote ischemic conditioning with exanatide treatment.

1.3.2.1 Post-ischemic inflammatory phase

The lack of oxygenation following the obstruction of the coronary vessels causes the death of up to one billion cardiomyocytes in the effected portion of the left ventricle [Frangogiannis 2019]. As a consequence, alarmins are secreted by the injured myocardium to recruit the inflammatory cell populations responsible to mediate the sequential phases of the post-ischemic remodelling (Figure 1.2) [Frantz]. Inflammatory macrophages derive from the differentiation in the ischemic area of the monocytes which transvasated in the area due to the fenestrations in the basement membrane of the vasculature and execute the removal of the cellular debris (Figure 1.3). Macrophages also stimulate extracellular matrix (ECM) degradation to facilitate the accomplishment of this clearance function. Knockout studies have demonstrated that the recruitment of inflammatory macrophages and their secretome is essential for both our limited regenerative capacity at the neonatal stage [Aurora] and the physiological remodelling process which lead to the fibrotic remodelling [Hwang]. Several studies have considered the recruitment of monocytes and secretion of pro-inflammatory cytokines as one of the key means by which to avoid further complications in the stability of the injured myocardial microenvironment [Hwang, Weihrauch, Morimoto, Trial, Chung]. As an explicative example of a pro-inflammatory cytokine, continuous injection of macrophage colony-stimulating factor (M-CSF) for five days after the induction of MI in C57BL/6J mice reduced infarct size and promoted an angiogenic response without α-SMA$^+$ myofibroblasts accumulation [Morimoto]. The mechanism of action of such an improved cardiac remodelling was explained by the induction of bone marrow-derived CXCR4$^+$ cells in the infarct.

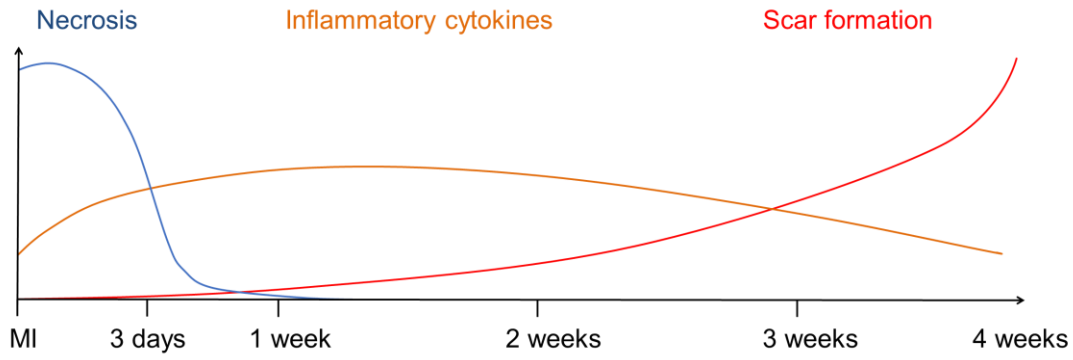

Figure 1.2 Schematic of the main phases after MI. Millions of cardiomyocytes die within a few hours after the occurrence of the myocardial injury. The apoptotic wave can last until a few days after, together with the rise of the inflammatory infiltrates which were recruited in the ischemic site and last for the first three weeks after MI. After the activation of fibroblasts in myofibroblasts there is a progressive deposition of collagen which results in the formation of an irreversible scar.

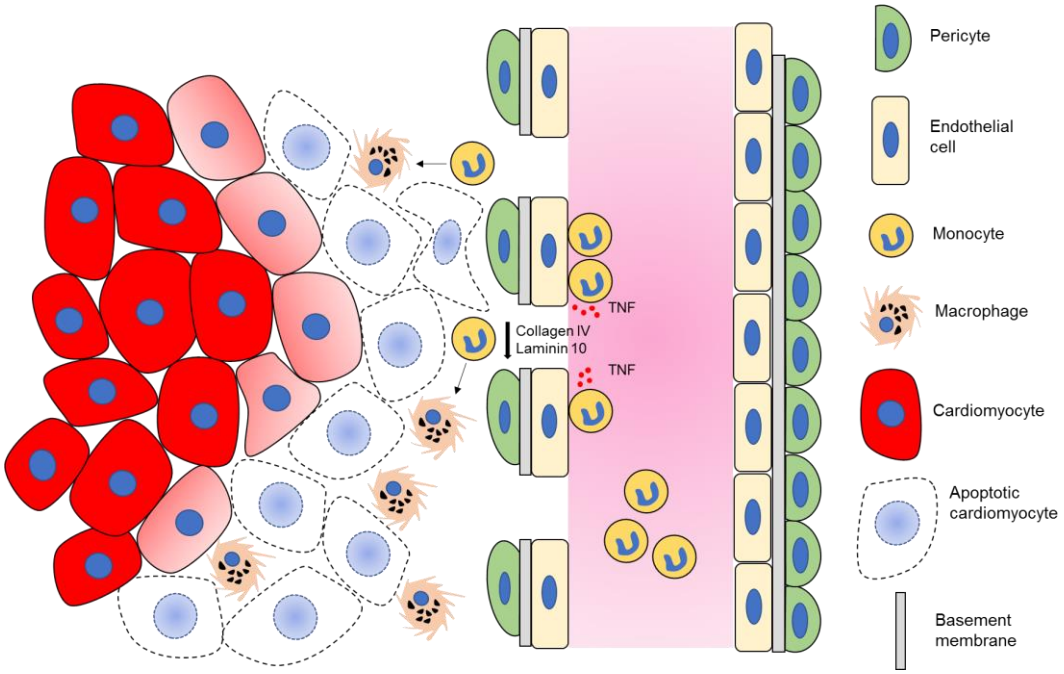

Figure 1.3 Schematic of the infiltration of monocytes and macrophages in the ischemic myocardium. The secretion of tumour necrosis factor (TNF) by the monocytes and the reduction in laminin 10 and collagen IV is associated with the disruption of the basement membrane and the extravasation of immune cells in the ischemic area. Here, monocytes differentiate in macrophages to clear the apoptotic cellular debris.

1.3.2.2 Macrophages and their secretome as key regulators

Macrophages are part of our innate immune response and their classification in pro-inflammatory (M1) and remodelling (M2) has always been questioned as a possible oversimplification of the actual complexity of macrophage populations *in vivo*. As a general concept, the pro-inflammatory macrophages were always associated with protection against infective insults, whereas the M2 were involved in the final wound healing response after a sterile insult. In the context of heart failure, the timely secretion of cytokines by macrophages is crucial in determining the resolution of the inflammatory phase towards the final healing of tissue. Indeed, they dictate the time of the different inflammatory cascades since the early phase after ischemia, when - by the release of TNF-α - they increase vascular permeability [Finsterbusch]. Specifically, the extravasation of the attracted neutrophils through the endothelial junctions is mediated by the cytokine-mediated communication between pericytes and neutrophils that determines gating and the formation of endothelial coatings to attract and engulf the inflammatory cells [Carman, Schenkel]. The transmigration of neutrophils through an orchestrated assembly of endothelial cells has been recently shown to be regulated by F-actin forces controlled by RhoA [Heemskerk]. Indeed, endothelial pores are both spatially and temporally confined during transmigration, thereby preventing tissue damage associated with vascular leakage [Heemskerk]. From the understanding of this step in the mechanism of action of leukocytes transendothelial migration, TNF-α-targeted therapies have been proven to limit inflammation, despite limitations such as variable patient response and increased risk of dysregulations in the immune regulation to prevent cancer outbreak [Udalova, Li 2017].

Once in the infarcted area, macrophages exert a role in most biological phenomena that characterise the outcome of myocardial ischemia such as fibrosis, angiogenesis and matrix remodelling. A relevant role in the activation of fibrotic programming by immune cells is linked to the toll-like receptor (TLR) 2 signalling since knockout studies confirmed significant reductions in cardiac hypertrophy and fibrosis [Wang 2017a, Higashikuni]. Generally, different pools of cytokines seem to be associated with the distinct phases of inflammation and fibrotic remodelling after ischemia. TNF-α, IL-1β and IL-6 are the most secreted cytokines during the inflammatory

phase whereas IL-10 and transforming growth factor (TGF)-β belong to the secretome of the alternatively activated macrophages [Frangogiannis 2019]. The switch from an inflammatory phase to a remodelling one is reflected by the activation of inhibitory mechanisms to block chronic inflammation and allow a fibrotic healing [Frangogiannis 2019]. Inside the family of cytokines which includes IL-19, IL-20, IL-22, IL-24, and IL-26, IL10 has a crucial role since it can both activate and be secreted by remodelling macrophages [Sziksz]. The secretion of growth factors and cytokines by the remodelling macrophages to distinguish themselves from the pro-inflammatory macrophages is the main source of activation of the myofibroblasts. Indeed, the secretion of IL10, TGF-β1, PDGF, and tissue inhibitors of metalloproteinases (TIMPs), is a hallmark for the transition from the inflammatory to the proliferative phase [Hulsmans]. However, macrophages are not the only components responsible for the activation of the myofibroblasts. HA and versican, a proteoglycan containing chondroitin sulphate, were also demonstrated to be contributing to the maintenance of the myofibroblast phenotype *in vitro* [Webber, Hattori]. Due to the lack of specific cell lineage studies, current knowledge does not allow the design of therapeutic options which do not exclude severe side effects or impairments of the remodelling response. Moreover, the significant reduction in fibrosis seen upon the blockage of pro-inflammatory cytokines *in vivo* simply represent the expected outcome of a drastic suppression of the healing response which is not necessarily converted in an improved remodelling and cardiac function [Kurrelmeyer, Sriramula, Mezzaroma].

1.3.2.3 Evolution of cellular-based treatments

The loss of relevant volumes of cardiomyocytes following ischemia cannot be physiologically replenished by the adult human heart, which is able to perform only a limited (1%) turnover of this type of cell [Bergmann]. Given their undifferentiated state, different types of stem cells have been tested over the last decades for the treatment of acute MI, and have shown consistent safety but controversial efficacy [Banerjee]. First-generation stem cells include bone marrow mononuclear (BMMNCs), adipose-derived (ADSCs), mesenchymal (MSCs) and hematopoietic stem cells ($CD34^+/CD133^+$). The main limitation of cellular-based approaches lies on the insufficient survival of the engrafted cells (around 2%) in the infarcted

myocardium [Hofmann, Hong 2014]. Despite this, significant long-term improvements are possible due to the paracrine action of the injected cells [Kinnaird 2004a,b]. Nevertheless, recent meta-analyses of trials using the first-generation stem cells for acute MI, that are BMMNCs, calculated mean improvements in EF and infarct size around 2-3%, with minimal clinical benefits [Fisher, Afzal]. Indeed, this slight overall improvement is due to the weight of the successful phase III trial REPAIR-AMI (NCT00279175, 204 patients enrolled), which presented a 5% absolute improvement in EF, together with a reduction in both the occurrence of MI and rehospitalisation [Schächinger 2006a,b]. These results followed the exciting positive trend that previously emerged from the outcome of smaller trials, namely TOPCARE-AMI and BOOST (NCT00224536), which enrolled 59 and 60 patients, respectively, even though a placebo group was not always included [Assmus, Schächinger 2004, Wollert 2004, Leistner]. Remarkably, in all these trials that showed positive results of BMMNCs infusion, the procedure was performed from three to five days after MI [Schächinger 2004 and 2006a, Wollert 2004]. Unfortunately, after REPAIR-AMI, following trials which globally recruited over 500 patients and tested the efficacy of BMMNCs for a follow-up comparable with the previous ones (from six to twelve months), did not show significant functional improvements or infarct size [Wollert 2017, Traverse, Perin, Sürder]. Therefore, there was the need for an additional phase III randomised, double-blinded and multicentre trials named BAMI (Effect of Intracoronary Reinfusion of Bone Marrow-Derived Mononuclear Cells; NCT01569178). This trial is recruiting 350 patients to test the efficacy of first-generation BMMNCs vs a placebo group [Mathur]. The estimated completion date is October 2019.

In addition, second-generation stem cells include induced pluripotent stem cells (iPSCs), embryonic stem cells, c-kit^{+} cardiac stem cells and cardiosphere-derived cells (CDCs). Clinical trials have started to assess the safety and efficacy of such therapeutic approaches, and delivered the first positive results in small cohorts of patients [Makkar, Malliaras 2014, Fernández-Avilés, Sanz-Ruiz]. Meanwhile, the main limitation of poor stem cell survival once in the inflamed and hypoxic microenvironment post-MI still can be addressed through a tailored delivery system. The inclusion of first-generation stem cells in bioengineered scaffolds can physically protect them from external insults and prolong their survival or, at minimum, extend

the effect of their paracrine signalling. Thereby, several studies in the last decade have focused on preclinical testing of scaffolds enriched with different types of stem cells [Chen 2013, 2014 and 2015, Christman, Liu, Gaffey].

1.3.2.4 Acellular biomaterial-based therapeutic approaches

Given the irreversible nature of the myocardial damage due to ischemia, the most direct approach of several preclinical studies was based on triggering the regenerative potential of the myocardial muscle, often by the employment of stem-cells-based strategies, such as cardiac progenitor cells [Makkar]. As shown in a recent meta-analysis in preclinical studies, the significant improvement in ejection fraction (EF), one of the main geometrical parameters by which to assess the functional recovery after MI, decreased from 11.7% to 5.2% once translated from small to large animal studies [Gyöngyösi]. Moreover, there are two main additional limitations of this approach. First, the high costs of the manufacturing processes associated with the production of stem cells and second, the intrinsic instability of undifferentiated cells which has a major impact on the shelf life of such an option. Thereby, the need for diversification in these approaches has encouraged preclinical testing of ECM-inspired therapies, which include acellular injectable biomaterials [O'Neill, Radisic]. Initially designed as engineering constructs able to target the mechanical dysfunction of the dilated heart wall, acellular biomaterials have been re-evaluated as agents able to provide pleiotropic benefits to the post-ischemic microenvironment [Landa, Ifkovits, Wassenaar]. In the recent years, several matrices such as alginate, chitosan, collagen, fibrin or hyaluronic acid (HA) have been tested *in vivo* for the treatment of MI [Mukherjee, Liu, Yu, Huang 2005, Gaffey]. The beneficial impact of hydrogels on the mechanical stability of the infarcted heart, which is based on the Law of Laplace, defined a common trend of functional improvements shared by the outcomes of different acellular biomaterials [Landa, Ifkovitz, Shu, Blackburn, Kadner, Yoon, Le, Leor 2009]. What remains to be harnessed is a minimum in the mechanical characteristics of the hydrogel to avoid the failure of certain types of acellular treatments, as seen in the case of certain HA-, alginate-based hydrogels and fibrin-alginate composite [Ifkovitz, Tous, Mukherjee, Purcell, Ruvinov].

Moreover, the identification of precise sites in the hydrogel which can behave as bioactive sites for either cellular recruitment or activation of growth factors provided a mechanistic explanation in addition to the benefits already carried with the mechanical stabilisation of the ventricular wall by the hydrogel [Huang 2005, Shu]. Accordingly, functionalisations without a precise biological rationale failed to provide an additional advantage to the biomaterial-based treatments [Tsur-Gang, Tous]. As an explicative example, poly(ethylene glycol) was first tested alone, resulting in either transient or totally absent benefit to the post-ischemic remodelling [Dobner, Rane]. In contrast, when PEG hydrogel was crosslinked with MMP1 and injected one week after the induction of MI, it induced a functional improvement together with an increase in the infarcted wall thickness [Kadner]. In addition, this study discussed the better outcome of a deferred delivery of the hydrogel than that with an immediate intervention. This approach is not feasibile in clinical practice. Conversely, a more recent study by Blackburn *et al*. involved three delivery times of a collagen type I-chondroitin sulphate-C hydrogel after MI (from three hours to two weeks post-surgery) and reported better results with the earliest timepoint [Blackburn]. In this study improvements included the whole spectrum of remodelling indices (functional response, fibrosis, angiogenesis and apoptosis), this therapeutic approach is strongly dependent on this composite nature. However, the benefit of this is lost when applied in a clinically-compatible therapeutic window [Blackburn]. Studies based on acellular biomaterial-based therapeutic approaches are listed in Table 1.2.

Table 1.2 Acellular biomaterials for the treatment of MI.

MI treatment tested	Species, sample size	Time of intervention	Functional response	Angiogenesis	Cell proliferation	Fibrosis	Mechanism	Ref.
Alginate hydrogel	Rats, N=13-15	1 w after MI or 2 months after MI	Significant improvement in EDV and ESV. NS change in FS	Myofibroblasts infiltration in the regions with degraded hydrogel	NA	NA	Early and chronic remodelling is improved by hydrogel physical support	Landa
Fibrin vs alginate	Rats, N=10	5 w after MI	Fibrin: deterioration of FS and LV systolic dimension. Alginate: significant increase in EF from 27.5% to 33.5%	Increase in arterioles density from 13 to 20-25/mm^2 with both alginate and fibrin	NA	Significant decrease from 16% to 12% in fibrin, NS decrease in alginate (14%)	Sustained physical support, fibrin has RGD which links $\alpha 5\beta 3$ integrin (VEGF activation)	Yu

Table 1.2 (Continued)

MI treatment tested	Species, sample size	Time of intervention	Functional response	Angiogenesis	Cell proliferation	Fibrosis	Mechanism	Ref.
Fibrin vs Matrigel® vs collagen	Rats, N=6	1 w after MI	NA	Significant increase in capillary density from 127 in PBS to 219 with Matrigel®, 232 with fibrin, 201/mm^2 with collagen (59 to 83% increase). NS change in arterioles	Significant increase in myofibroblasts invasion in ischemic area with collagen gel, but not with others	NS difference	RGD and fragment E from fibrin, HS proteoglycan in matrigel, binding sites to αvβ3 in collagen	Huang 2005
HA methacrylate hydrogel	Rats, N=6-7	2 d after MI	15% improvement in EF	NA	NA	NS difference	Interaction in TGFβ pathway	Le
Alginate	Pigs, N=4-7	4 days after MI	Significant improvement in systolic and diastolic areas, 40 to 50% with optimal concentration of alginate	Increased vessel count (qualitative)	NA	NA	Mechanical support by the injected material	Leor 2009

Table 1.2 (Continued)

MI treatment tested	Species, sample size	Time of intervention	Functional response	Angiogenesis	Cell proliferation	Fibrosis	Mechanism	Ref.
HA hydrogel	Rats, N=6	2w after MI	Significant improvement in EF from 18% in control to 43% in hydrogel group. Better haemodynamics	Significant increase in capillaries (from approx. 392 to 571 cap./mm^2). Significant increase in arterioles (from 12 to 19 art./ mm^2)	Significant reduction of apoptotic cells	Significant decrease in infarct size from 32% in control to 17% with hydrogel	Not clear mechanism of action, subacute model is not optimal to test efficacy	Yoon
Chitosan chloride (CSCl) hydrogel with RoY peptide	Rats, N=15	At the time of ligation	Significant increase in EF from 45% in PBS to 68% with RoY peptide, NS (55%), in hydrogel-only, significant improvement in FS with RoY peptide	Significant improvement in αSMA^+ vessels from 35/mm^2 in PBS to 43 in hydrogel-only and 68 with RoY peptide. Same trend for vWF^+ vessels	NA	Significant decrease in infarct size from 56% to 32% in CSCl-RoY and 40% in CSCl hydrogel	Activation of pAkt-pERK pathway	Shu

Table 1.2 (Continued)

MI treatment tested	Species, sample size	Time of intervention	Functional response	Angiogenesis	Cell prol.	Fibrosis	Mechanism	Ref.
HA hydrogel functionalised with hydroxyethyl methacrylate (HeMA)	Sheep, N=6-8	30 min after ligation	NS difference	Significant two-fold increase in α-SMA$^+$ vessels from approx. 7 in control to approx. 14 ves./mm^2 in HeMA groups in the middle of the infarct	NA	NS difference	Early timepoint injection affects material degradation and efficacy	Tous
Peptide-modified alginate hydrogels	Rats, N=6-9	1 w after MI	Significant improvement in LVSD, LVDD, LVDA, LVSA in alginate-only. Significant improvement in FS from 20% to 35% in alginate-only group	NS difference	NA	NS difference	Peptides do not enhance better remodelling	Tsur-Gang

Table 1.2 (Continued)

MI treatment tested	Species, sample size	Time of intervention	Functional response	Angiogenesis	Cell prol.	Fibrosis	Mechanism	Ref.
PEG hydrogel	Rats, N=11	At the time of ligation	Significant reduction in EDD 2 and 4 w after the injection. NS change in FS and all parameters at 13 w after injection	NA	Evidence of macrophage recruitment up to 13 w post-injection	Transient significant increase in wall thickness at 4 w, lost at 13 w	Temporary stabilization due to the bulking effect	Dobner
PEG hydrogel	Rats, N=7-8	9 d after MI	NS difference in EF, EDV, ESV	NS difference	NA	NA	Mechanical reinforce-ment is not sufficient to improve the remodelling	Rane
Fibrin-alginate composite	Pigs, N=8-9	1 w after MI	NS difference in EF, EDV and haemodynamics	Significant increase from 650 in saline to 850 cap./ mm^2 with composite	NA	NS difference	Alteration of collagen composition	Mukherjee

Table 1.2 (Continued)

MI treatment tested	Species, sample size	Time of intervention	Functional response	Angiogenesis	Cell prol.	Fibrosis	Mechanism	Ref.
PEG-based hydrogel polymerised MMP1	Rats, N=7-8	At the time of ligation (d0) / 1 w after MI	Significant improvement in FS and ESD in 1w group, NS in d0 group	NA	NA	NA	Tissue morphology 1 w post- MI might induce a bulking effect	Kadner
Collagen type I-chondroitin sulphate-C hydrogel injected at three different timepoints (3h, 1w and 2w)	Mice, N=5-20	3 h after MI / 1 w after MI / 2 w after MI	Significant increase in EF from 30% in control to 47% in hydrogel 3h and to 34% in hydrogel 1w. Better haemodynamics in hydrogel 3h group	Significant increase in capillaries from approx. 9 cap./FOV in control to 14 with hydrogel 3h, NS with hydrogel 1w. Significant increase in arterioles from approx. 5 in control to 8 art./FOV with hydrogel 3h or 1w	Significant increase in Ki67+/CD 31^+ cells 2d post-injection	Significant reduction in fibrosis from 27% to 15% in hydrogel 3h. Significant reduction in scar from 50% to 27% in hyd. 3h	Timely introduction of the matrix avoids the further worsening of heart remodelling	Blackburn

1.3.3.1 Fibrosis

The endpoint of the myocardial post-ischemic remodelling process involves the deposition of collagen type I and type III in the infarcted area, resulting in a fibrotic response (Figure 1.4). Although this is a way by which our organism tries to compensate for the loss of millions of cardiomyocytes due to ischemia, fibrosis is an independent predictor of morbidity and mortality also in the case of non-ischemic cardiomyopathies [Gulati, Leyva]. The major cells responsible for the deposition of collagen fibres are the myofibroblasts, which derive mostly from the transdifferentiation of the tissue-resident fibroblasts present in the myocardial tissue [Kanisicak]. The activation of myofibroblast and the progressive formation of a fibrotic scar in the ischemic tissue starts approximately from the seventh day post-MI, and the deposition of collagen remains minimal within the second week after ischemia [Lindsey 2012, Ma]. Generally, the infiltration of myofibroblasts in the ischemic core of the infarct is an indicator of a healing process that is resolving towards the formation of a stable scar, and for this reason it has been used as an indicator of beneficial remodelling in the evaluation of possible treatments for MI [Huang 2005, Lin]. Nevertheless, the consequent stiffness of the newly synthesized matrix is much higher than that of the original myocardial fibres and leads to systolic and diastolic dysfunctions [Frangogiannis 2017]. The disruption of the original architecture of myocardial layers leads to deformations in the ventricular chamber with altered contractile properties [Hales, Chen 2005]. Unfortunately, in several cases the persistent activation of myofibroblasts, which were demonstrated to populate the scar tissue even 17 years after MI [Willems], is not controlled by the microenvironment and the consequent arrhythmogenic responses can lead to the organ failure. For this reason, several studies have been conducted to identify the main molecules responsible for the transdifferentiation of fibroblasts in myofibroblasts, to further design a targeted therapy to stop the chronic activation of myofibroblasts. The factors identified include TGF-β1, endothelin-1, and angiotensin-II [Prunier, Rodriguez-Pascual, De Mello, Gourdie].

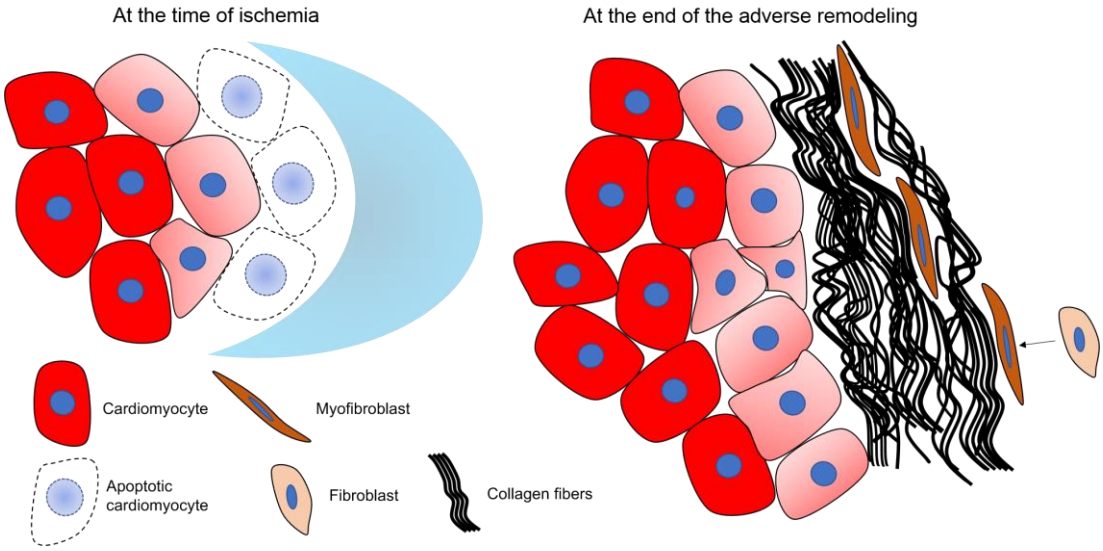

Figure 1.4 Schematic of myocardial environment at the time of ischemia and at the end of the ischemic remodelling.

1.3.3.2 Key molecules in the regulation of the fibrogenic program

TGF-β1 is one of the most studied growth factors because of its fundamental role throughout the inflammatory and remodelling processes. However, several studies have reported the expression of TGF-β1 at the developmental stage both in several cellular types such as chondrocytes, cardiomyocytes and in chronionic cells in the placenta and in the ECM of major organs (heart, pancreas, skin) [Thompson, Heine]. Specifically, the presence of transcripts of TGF-β1 and TGF-β2 isoforms were localised in the ovine trophectoderm at day 16 post-mating and in the placental endothelium up to day 30 [Doré]. One study focused on the effects of TGF-β1 deletion on mice embryos revealing extensive damage in multiple tissue components such as the aortic valve, atrioventricular septum and aorta, together with a higher apoptosis and delayed decrease of the endocardial cushion [Bartram]. All the three isoforms of TGF-β were detected in several studies investigating the expression of this growth factor in the acute phase after myocardial infarction [Deten, Hao, Wunsch]. In particular, the expression of TGF-β1 and TGF-β2 isoforms was localised in the infarct zone throughout the maturation phase after ischemia (two months post-MI) and TGF-β3 was detected even at a later timepoint (82 days post-MI) [Deten]. Moreover, the upregulation of TGF-β1 characterised not only the remodelling which follows MI induction by permanent ligation of the left anterior descending artery (LAD), but also in the case of reperfusion-induced damage. Indeed, in the latter TGF-β1 and IL-10 levels increase rapidly in the absence of mast cells and the less prominent increase of macrophage colony-stimulating factor (M-CSF) [Dewald].

One of the key findings was the correlation between the increased levels of TGF-β1 transcripts and the deposition of collagen type I in the infarct scar [Hao] which implicates the role of this molecule in the fibrogenic program that is dictated by the presence of myofibroblasts in the area. However, multiple studies have confirmed the expression of TGF-β1 in most of the main cellular types which are either effected or recruited by the onset of ischemia [Wünsch, van Amerongen, Weirather]. Specifically, TGF-β1 was expressed by cardiomyocytes [Wünsch], macrophages

since the moment of their recruitment to clear the cellular debris present in the damaged myocardium [van Amerongen], and by regulatory T-cells (Treg) [Weirather]. As confirmed by its secretion by the pro-healing Tregs, TGF-β1 is one of the key mediators to complete the healing process, thereby its potential as a target to modulate the uncontrolled activation of the fibrogenic program is a double-edged weapon. The crucial importance of this growth factor during the maturation phase needs a thorough knowledge of the cellular context together with the definition of the dose and timing of administration of the selected inhibitor to target its activation.

The canonical pathway of TGF-β activation starts with the dissociation of the latency associated peptide (LAP) which allows the release of the TGF-β dimer. Different molecules or conditions were demonstrated to play a role in the activation of TGF-β, such as the matricellular protein thrombospondin-1 (TSP-1), integrins, reactive oxygen species (ROS) and acidic pH [Annes]. TSP-1 is just one of the family of matricellular proteins that includes tenascin, ostepontin and periostin which were found to be associated with the conversion of fibroblasts into myofibroblasts. Knockout studies have shown how a higher myofibroblast density in the myocardial scar was seen in the absence of thrombospondin-1 [Frangogiannis 2005] whereas the deletion of osteopontin induced a reduction in interstitial fibrosis with no significant effect on the expression of TGF-β. As with the latter one, knockout of periostin lowered fibrosis and hypertrophy in a pressure-overload model and caused a persistent proliferative effect on myofibroblasts that was seen in the hypertrophic scar [Crawford, Oka 2007].

1.3.4.1 Matrix metalloproteinases

Unlike the factors responsible for the fibrotic response, there are proteins which are expressed from the early post-ischemic conditions up to the remodelling phase, such as matrix metalloproteinases (MMPs). MMPs are zinc-dependent endopeptidases that are crucial for the homeostasis of the ECM since - upon their expression - they determine the degradation of the matrix. MMPs expression can be counterbalanced by tissue inhibitors of metalloproteinases (TIMPs) to precisely regulate the proliferative and maturation phases after MI. Given the importance of the cardiac ECM in the activation or repression of signalling pathways which involve

fibroblasts, immune and vascular cells [Frangogiannis 2017], the origin, expression and function of this family of enzymes still represents a relevant point from which to understand and potentially target the post-ischemic remodelling process. Interestingly, MMPs have also been regarded as causative agents of the rupture of the atherosclerotic plaque, thus constituting *per se* an object of investigation in the aetiology of MI [Newby].

MMPs can be detected as early as ten minutes after the occurrence of MI following a coronary occlusion [Etoh], so their expression must be related to the earliest signalling in the ischemic context, and are thus likely linked to ROS generation and induced by necrotic cardiomyocytes. Evidence of expression of MMPs from cardiac cells and fibroblasts was assessed *in vitro* more than twenty years ago [Borg], but the real clinical importance of MMPs and balance with the TIMPs was studied only over the last decade, as temporal patterns in the MMP/TIMP ratio were evaluated in clinical cases [Webb]. Originally, MMPs action was associated with the ECM degradative process needed to open the way to the recruited macrophages which are designated to clear the necrotic cellular debris during the early inflammatory phase [Frangogiannis 2012]. Indeed, troponin I was identified as a target of MMP2 [Wang 2002], a gelatinase that can have intracellular targets like MMP1 [Limb]. In the case of MMP2, its inhibition prevented the degradation of the troponin I, which contributes to cardiac cell contractility, and improved the cardiac function [Wang 2002]. In contrast, MMP1 showed evidence of a protective intracellular effect by both preserving lamin A and hindering DNA degradation and caspase activation [Limb]. Specifically, MMP1 was found to be accumulated during the mitotic phase and localised in the nuclei and mitochondria.

The importance of an appropriate balance between MMPs and TIMPs can be understood in the drastic consequences of either an MMPs overexpression towards an excessively stiff matrix or a TIMPs prevalence that produces a mechanically weaker ECM. The first condition causes arrhytmias and irreversible electrical signalling dysregulation whereas the latter leads to cardiac rupture. Therefore, several studies focused on the close association between collagen degradation and expression of the respective MMPs collagenases both in knockout studies and clinical data [Foronjy, López, Matsumura, Lindsey 2018]. Remarkably, promising

results achieved in rodents after knockout of specific MMPs, such as the prevention of cardiac rupture following the deletion in MMP2 [Matsumura], provide us with only one side of the much more complex targeting of MMP/TIMP ratio in the clinical context. Nevertheless, such preliminary studies are essential to restrict the range of possible targeted therapeutic interventions based on ECM deposition. For instance, a recently published preclinical study tested the intracoronary injection of a recombinant TIMP3 at the time of reperfusion in pigs [Barlow]. In this study, a significant reduction in infarct size and left ventricular dilation was achieved using a clinically-compliant (percutaneous coronary intervention) delivery of the recombinant protein after ischemia-reperfusion damage. Indeed, previous data supported the rationale of this approach since knockout of TIMP3 demonstrated a worsening in systolic and diastolic function [Kandalam] and a more invasive sustained released of this protein from HA improved the cardiac remodelling in a large animal model [Eckhouse].

1.3.4.2 Cardiac matrix-inspired therapeutic approaches

Several cytokines and mediators of cell-ECM regulatory signalling can be either activated or inhibited according to their availability and recruitment in the post-ischemic cardiac ECM microenvironment, and this complex scenario cannot be accurately reproduced in an *in vitro* model yet. Indeed, most of the studies that demonstrated the efficacy of cardiac ECM-based approaches can reveal their mechanism of action only when focusing on a specific molecule rather than considering all the variables that can act in concert to determine the observed improved remodelling [Singleyn, Seif-Naraghi, Purcell, Chen 2016, Wassenaar, Eckhouse, Okada]. Remarkably, two impactful studies have demonstrated the efficacy of simple ECM proteins in both reducing the scarring and promoting cardiomyocytes regeneration when injected after ligation of LAD in rodents [Bassat, Kühn]. Interestingly, both these studies showed a similar functional improvement in EF of around 15% from baseline untreated animals, also supported by higher fractional shortening (FS) [Bassat, Kühn]. Secondly, whole ECM-based approaches have tested the efficacy of decellularised matrices which were derived from the small intestinal submucosa or from the heart itself [Singleyn, Seif-Naraghi, Wassenaar, Okada]. The studies performed by the Christman group involved delayed

administration of the decellularised ECM (one to two weeks after MI induction), avoiding an accelerated degradation by the harsh conditions of the early inflammatory phase (up to five days after MI induction), and thereby allowing consistent improvement in FS [Singleyn, Seif-Naraghi, Wassenaar]. In addition, recent work by Chen *et al*. demonstrated not only a functional recovery but also an additional proliferative effect on cardiomyocytes provided by decellularised zebrafish cardiac ECM [Chen 2016]. This finding suggests that ECM-dependent triggers are able to impact on the maladaptive remodelling that would be shared across different groups of vertebrates, independently of their innate cardiac regenerative capacity.

A targeted approach based on the modulation of the balance between MMPs and TIMPs adopted a sustained release of TIMP3 from hyaluronan hydrogels and was tested in large animal models [Eckhouse, Purcell]. By this continuous release of TIMP3 from the early inflammatory phase post-MI, the maladaptive remodelling was severely limited, as shown by consistent improvements in EF and haemodynamics [Eckhouse, Purcell]. However, contrasting results in terms of collagen deposition highlight how multiple effects which still need to be more precisely addressed can influence the alteration of the post-MI remodelling [Eckhouse, Purcell]. Indeed, the complexity of finding the right way to tune the ECM degradation towards a beneficial remodelling is the object of current complex systems including siRNA delivery against MMP2 from HA hydrogels [Wang 2018b]. Studies based on cardiac matrix-inspired therapeutic approaches are listed in Table 1.3.

Table 1.3 Extracellular matrix-inspired biomaterials for the treatment of MI.

MI treatment tested	Species, sample size	Time of intervention	Functional response	Angiogenesis	Cell proliferation	Fibrosis	Mechanism	Ref.
Periostin (ECM protein) with Gelfoam®	Rats, N=12-18	At the time of ligation	Significant increase in EF from 50% in control to 66% with periostin bound to Gelfoam®. Significant improvement in FS and EDD. Better haemodynamics with periostin	Significant four-fold increase in capillary density and 1.5-fold increase in arterioles with periostin	Periostin induces CM dedifferentia-tion, NS difference in c-kit+ cells	Significant reduction in scar size. Significant reduction in fibrosis from approx. 35% in control to 7% with periostin	Periostin induces the re-entry in cell-cycle of CM	Kühn
Agrin (ECM protein)	Mice, N=6-8	At the time of ligation	Significant improvement in EF from approx. 40% in control to 55% with agrin. Significant improvement in FS	NA	CM proliferative effect demonstrated *in vitro*	Significant reduction in fibrosis from 17% to 9%	Agrin provides a stimulus for CM regeneration	Bassat

Table 1.3 (Continued)

MI treatment tested	Species, sample size	Time of intervention	Functional response	Angiogenesis	Cell proliferation	Fibrosis	Mechanism	Ref.
Decellularised porcine ventricular ECM	Rats, N=6	2 w after MI	Significant increase from 55% to 62% in EF, significant improvement in ESV and EDD	NA	Increase in $Cnx43^+$ CM, three-fold increase in Ki67+ cells	NA	Matrix induces cellular proliferation and mechanical stability	Singelyn
Decellularised porcine ventricular ECM	Pigs, N=2-6	2 w after MI	Significant improvement by 20% in EF, improved EDV, ESV and global wall motion index	Foci of neovasculature detected	Residual endothelium in treatment	Significant decrease in fibrosis from 25% to 17%	Mechanical barrier against adverse remodelling	Seif-Naraghi
Decellularised normal (nzECM) and three-day-old zebrafish ECM (hzECM)	Mice, N=7	At the time of ligation	Significant improvement in EF from 40% to 60% in hzECM, and to 50% in nzECM. Significant improvements in ED and ES areas	NA	Significantly higher c-kit^+/$Ki67^+$ cells, $cTnT^+$/$Ki67^+$ CM and $ErbB2^+$/ $cTnT^+$ CM in nz/hzECM	NA	ErbB2 mediates the beneficial effects in mammalian ECM	Chen 2016

Table 1.3 (Continued)

MI treatment tested	Species, sample size	Time of intervention	Functional response	Angiogenesis	Cell prol.	Fibrosis	Mechanism	Ref.
Decellularised porcine ventricular ECM	Rats, N=7-8	1 w after MI	Significant increase in EF by 5% in treated group after 1 w. Significant improvement of ESV, NS in EDV. Better haemodynamics	NS increase in capillaries at 1 w and significant increase in arterioles from 35 to 55 art./ mm^2 at 1 w	Significant increase in GATA4, Nkx2.5, Tbx5, Tbx20 and c-kit	Significant decrease in interstitial fibrosis from 2.5% to 1.5%. Significant reduction in hypertrophy	Matrix provides the milieu necessary for the angiogenic and ECM-based effects	Wassenaar
Protease-degradable HA hydrogel with siRNA vs MMP2	Rats, N=6-7	At the time of ligation	Significant increase in EF from approx. 40% in control to 60% with combination. Better haemodynamics	NA	NA	NA	Addition of siRNA against MMP2 improves the remodelling	Wang 2018 b

Table 1.3 (Continued)

MI treatment tested	Species, sample size	Time of intervention	Functional response	Angioge-nesis	Cell proliferation	Fibrosis	Mechanism	Ref.
HA hydrogel containing recombinant TIMP-3 (rTIMP-3)	Pigs, N=7-8	At the time of ligation	Significant increase in EF from approx. 40% in control to approx. 50% in combined treatment. Significant improvement in EDV, better haemodynamics	NA	Increase α-SMA^{+} myofibroblast density	Significant reduction of MMP activity and increase in collagen content in treated groups	rTIMP-3 influences α-SMA+ cells-mediated remodelling	Eckhouse
MMP-responsive HA hydrogel releasing TIMP-3	Pigs, N=7	At the time of ligation	Significant increase in EF from 34% to 45% combined treatment, NS with HA-alone (from 34% to 37%). Better haemodynamics	NA	Significant decrease in fibrillar collagen from 44% to 35%, NS with HA only. Significant reduction in α-SMA+ cells	NA	Modulation of MMP/TIMP balance	Purcell

Table 1.3 (Continued)

MI treatment tested	Species, sample size	Time of intervention	Functional response	Angiogenesis	Cell proliferation	Fibrosis	Mechanism	Ref.
Porcine small intestinal submucosa-derived hydrogels (SIS form B and C)	Mice, N=6-9	At the time of ligation	Significant improvement in ESA and cardiac contractility with SIS-B, NS difference in other parameters with SIS-C	Significant increase in capillaries from 503 to 634 cap./mm^2 with SIS-B whereas trend of reduction with SIS-C	NA	Significant reduction in fibrosis from 63% in control to 47% in SIS-B	Content of FGF influences the efficacy of improved remodelling with SIS-B	Okada

1.3.5.1 Angiogenesis

The majority of tissues in our organism require constant oxygenation and supply of nutrients to fulfil their functions, and so the circulatory system is designed to reach even the regions most distant from the heart. In pathological contexts, such as ischemic diseases or cancer development, the enhancement or suppression of blood vessel formation from pre-existing vasculature - named angiogenesis - represents one of the most promising triggers to effectively remodel the effected microenvironment.
The requirement of endothelial cells as the primary source of angiogenesis was seen *in vitro* by Folkman and Haudenschild [Folkman], together with the concepts of "direct and indirect angiogenesis factors". HIF constitutes one of the well-known upstream signals which are able to induce an angiogenic response. After the translocation of the activated complex of HIF1α and HIF1β in the nucleus, the transcriptional effect includes the expression of vascular endothelial growth factor (VEGF) which is the most studied angiogenic molecule. Specifically, VEGFA and angiopoietin-1 (ANG-1) are needed from the early stages of the sprouting process since they stimulate the detachment of pericytes (Figure 1.5). These are mural cells coating the endothelium of blood vessels [Carmeliet]. Consequently, VEGF also stimulates the extravasation of proteins and immune cells which characterise the early inflamed ECM upon a sterile insult, such as $Ly6C^{hi}$CCR2 $CX3CR1^{low}$ monocytes in mice (equivalent to $CD14^{+}CD16^{-}$ in humans), neutrophils, MMP9 and MMP12 [Yabluchanskiy, Geissmann, Iyer]. Surprisingly, a recent study has evidenced the influence of gender in the liver X receptors/retinoid X receptor (LXR/RXR) signalling pathway after MI [DeLeon-Pennell]. Indeed, the dysruption of LXR/RXR pathway in female neutrophils, by acting on apolipoprotein F, resulted in an over 30% increase in survival and decreased cardiac rupture and ventricular dilation.

HIF1α also upregulates the CXC (two cysteines separated by one amino acid) chemokine stromal cell-derived factor 1α (SDF-1α), which in turn binds to its receptor CXCR4. SDF-1-CXCR4 axis stimulates the migration of hematopoietic and endothelial stem cells in the ischemic site, and lasts up to one week post-MI [Huang 2013, Zaruba, Askari]. The relevance of CXCR4 in revascularisation has been well

known for more than two decades when studies demonstrated its role in multiple organs [Tachibana, Zou].

Upon VEGF and ANG-1 stimulation, from the endothelium a leading cell named the tip cell and its neighbours, called stalk cells, constitute the sprouting unit which can elongate through the ECM following growth factor-dependent gradients. The main molecules involved in the guidance of the nascent vessel are VEGF receptor (VEGFR), neuropilins (NRPs), NOTCH, WNT and fibroblast growth factors (FGFs) [Carmeliet]. Moreover, ephrins and semaphorins (Semas) are proteins which regulate the filopodia elongations of the tip cell, and their relevance as key mediators of the angiogenic program has been shown both in ischemic and cancer-effected conditions [Yang 2016, Corà]. Indeed, the abovementioned Ly6C^{hi} cells are able to secrete Sema4a, which after its binding to the receptor PlexinD1, sustains angiogenesis by the enhancement of VEGFR2 [Meda]. Moreover, another member of the same family, Sema3a, has been identified together with neuropilin 1 (expressed by monocytes) as one regulator of vessel stabilisation after VEGF expression [Groppa 2015]. On the other hand, the regulatory role of EphrinB2/EphB4 through phospho-ERK1/2 has been demonstrated as an alternative mode of angiogenesis, that is achieved by vessel splitting and defined as intussusception [Groppa 2018]. The final stage of vessel formation is its coating by mural cells, such as pericytes and smooth muscle cells, to protect the nascent vasculatures from regression. The deposition of pericytes is driven by platelet derived growth factor (PDGF) B, ANG-1, TGF-β and NOTCH. Following the deposition of mural cells, the basement membrane also is put down to complete the vasculature maturation process.

1.3.5.2 Angiogenesis-driven approaches

Since a cardioprotective role on the border zone of the ischemic areas is well known to be elicited by the enhancement of angiogenesis, numerous therapeutic approaches based on direct angiogenic effect were tested in recent decades [Liu, Gaffey, Vera Janavel, Chen 2018, MacArthur, Lin, Kim]. An angiogenic response can result from molecular triggers with a completely diverse source such as direct growth factors signalling (VEGF, PDGF, FGF), cellular paracrine activity (BMMNCs, ADSCs, MSCs and endothelial progenitor cells) and biomaterial-derived degradation products

which can enhance an endogenous healing process (RGD sequence, integrin-binding sites, fragment E). Therefore, since an optimum treatment still needs to be widely recognized for its safe angiogenic effect and to be implemented in the clinical surgical procedures.

Anti-angiogenic therapies target VEGF in pathological scenarios such as tumours, macular degeneration and psoriasis [Kreuger, Mukkamala, Malecic], by contrast, in the infarcted heart, VEGF expression needs to be properly enhanced to achieve vascularisation. Intuitively, such an approach must avoid a tumorigenic long-term effect due to an uncontrolled VEGF expression [Goel]. Formation of angiomas was reported in the first pioneering studies which tested direct gene delivery of VEGF in rodents [Lee 2000, Schwarz]. Nevertheless, the possibility to transplant myoblasts transfected with the human $VEGF_{165}$ gene demonstrated a reduction in infarct size and a significantly improved haemodynamics in rodents without tumorigenesis [Suzuki]. Moreover, a positive effect on multiple remodelling indices was reported by the injection of plasmid-based $VEGF_{165}$ gene transfer in infarcted sheep [Vera Janavel]. Specifically, the beneficial effect was not limited to a marked angiogenic response, but was also characterised by lower myofibroblasts infiltration and fibrosis, and signs of cardiomyocytes mitosis [Vera Janavel]. Consistently, reduction in infarct size was seen by using non-viral vectors to deliver $VEGF_{165}$ four weeks after the ligation of the circumflex artery [Yockman].

More recently, improvements in cardioprotection and angiogenesis were obtained also by poly(disulfide amine) polymer-mediated transfection of $VEGF_{165}$ in skeletal myoblasts before injection in the rat infarcted myocardium [McGinn]. The potential of the synergistic effect of a temperature-sensitive, degradable hydrogel - made of polyethylene glycol (PEG) and δ-valerolactone (VL) - conjugated with $VEGF_{165}$ highlighted the benefit of biomaterial engineering-based approaches [Wu]. Advance towards a controlled release of $VEGF_{165}$ was achieved by Lin *et al.* by the combination of synthetic, non-immunogenic self-assembling peptide nanofibers with the growth factor, which was tested in the same study both in small (rats) and large animal models (mini-pigs) [Lin]. Here, the global view of the beneficial effects of a controlled release of VEGF, including EF, cellular proliferation and fibrosis, strongly emerged [Lin]. A similar engineering-based strategy using identical nanofibers by

the same author evaluated the cardioprotective effect of PDGF-BB delivery in infarcted rats [Hsieh 2006]. Activation of PI3K/Akt pathway in cardiomyocytes by PDGF-BB resulted in a reduction in apoptosis and infarct size, finally leading to a significant functional improvement [Hsieh 2006]. Consistent enhanced angiogenesis and reduced infarct size were achieved using nanofibers also with a combination of growth factors promoting both arteriogenesis and angiogenesis, PDGF-BB and FGF2, respectively [Kim].

Another scaffold-based system made of the copolymer poly(N-isopropylacrylamide-co-propylacrylic acid-co-butyl acrylate) (p[NIPAAm-co-PAA-co-BA]) showed to improve the therapeutic angiogenesis of basic fibroblast growth factor (bFGF) exploiting the acidic pH of the ischemic microenvironment [Garbern]. The sustained delivery of bFGF induced both angiogenesis and arteriogenesis together with functional improvements [Garbern]. However, another copolymer with a NIPAAm backbone designed to release bFGF and insulin growth factor (IGF) 1, was injected in the border zone of the infarct but did not lead to any significant angiogenesis [Nelson]. This unexpected outcome underlines the relevance of the timing of intervention in the post-ischemic context, where the difficulty to modulate the remodelling by a two weeks-delayed administration was seen in the case of cellular-based clinical trials [Traverse, Sürder].

The capacity of SDF-1α to mobilise $CD117^{+}$ bone marrow stem cells in the ischemic area was clearly demonstrated by Askari *et al*. [Askari], but still the timing of such action needs to be finely tuned for its full therapeutic aim [Ziff]. Recently, the intra-myocardial delivery of a SDF-1α synthetic analogue from a HA hydrogel induced an extended beneficial effect on remodelling, adding a marked reduction in fibrosis and an increase in EF to the expected enhancement of angiogenesis [MacArthur]. Moreover, a HA-SDF-1α hydrogel enriched with antimicrobial peptides-treated BMMNCs has recently been tested and a clear additional advantage to the angiogenic effect of HA-SDF-1α was not seen [Klyachkin].

Extended survival of first-generation stem cells for cardiovascular therapy was achieved by their delivery in hydrogel scaffolds, thereby their angiogenic paracrine signalling can also be prolonged in such constructs. Hsieh's group demonstrated the

additional advantage of HA hydrogel-BMMNCs combination compared to the individual groups both in small and large animal models [Chen 2013, 2014]. Angiogenesis and arteriogenesis were steadily achieved in these HA-BMMNCs systems and also supported by an approximate 50% relative decrease in scar size, and in such systems the highest improvements in functional recovery were also seen [Chen 2013, 2014]. Studies based on angiogenesis-driven approaches are listed in Table 1.4.

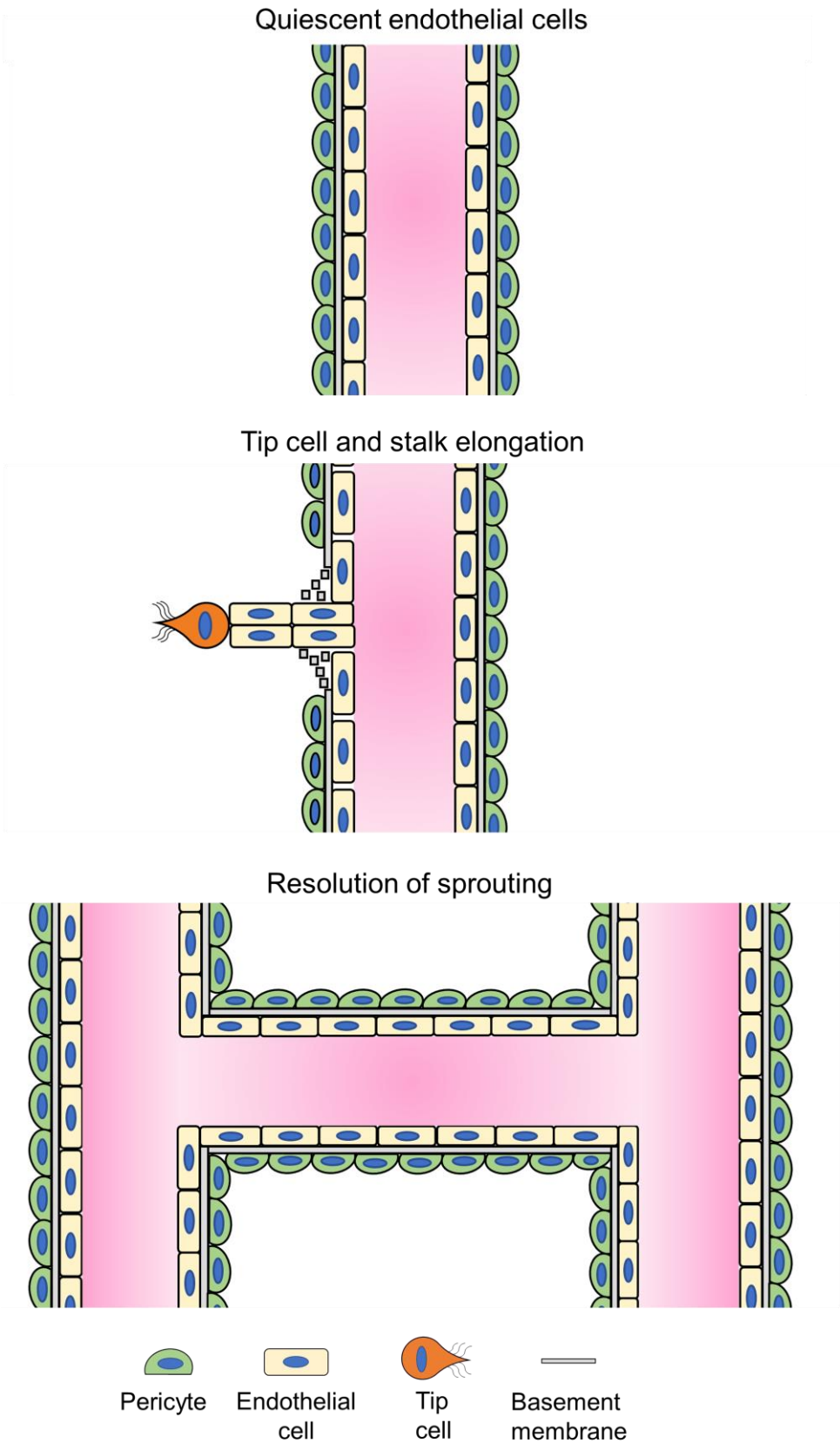

Figure 1.5 Schematic of the sprouting process leading to angiogenesis.

Table 1.4 Combined approaches for the treatment of MI targeting angiogenesis.

MI treatment tested	Species, sample size	Time of intervention	Functional response	Angiogenesis	Cell Prol.	Fibrosis	Mechanism	Ref.
VEGF-conjugated aliphatic polyester hydrogel	Rats, N=8-10	1 w after MI	Significant increase in EF by 10% in hydrogel-only and by 15% conjugated hydrogel. Significant reduction in EDV	Significant relative increase by 50% in blood vessel density in conjugated hydrogel	NA	Significant decrease in scar area by 10%	Extended effect by VEGF entrap-ment	Wu
Self-assembling peptide nano-fibers (NFs) with VEGF	Rats, N=8-10 Pigs, N=5-6	At the time of ligation	Rodent model: Significant improvement in FS with combined, NS with individual. Significant improvement of LVDS and LVDD with combined. Porcine model: Significant improvement in EF from 45% in control to 51% in combined, significant improvement in EDV and ESV with combined and individuals	In porcine model with combined: Two-fold significant increase in capillaries (from 250 to 600 cap./mm^2). Eight-fold increase in arterioles (from approx. 5 to 40 art./ mm^2). Significant increase in arterioles and capillaries in rodent model	Significant increased αSMA^+/ $Ki67^+$ cells only with combined	Significant reduction in collagen from. 17% in control to 3% in combined (remote region) Same trend with NFs-only	NFs provide the microenvi-ronmental cues to enhance arterio-genesis	Lin

Table 1.4 (Continued)

MI treatment tested	Species, sample size	Time of intervention	Functional response	Angiogenesis	Cell Prol.	Fibrosis	Mechanism	Ref.
Nanofibers with PDGF-BB	Rats, N=6-7	At the time of ligation	Significant improvement in FS, EDS and EDV with highest dose in combination	NS difference	Significant reduction in apoptotic cells with highest dose in combination. NS difference in $Ki67^+$ cells	Significant reduction in infarct size from 40% in control to 28% in combined	Induction of PI3K/Akt pathway by PDGF-BB improves survival of CM	Hsieh 2006
Self-assembling peptides with PDGF-BB and FGF2	Rats, N=6	At the time of ligation	Significant improvement in haemodynamics with combined	Five-fold increase in capillaries with combined, significant but lower increase with individual. Significant increase in arterioles density	Significant reduction in apoptotic CM	Significant reduction in infarct size from 36% in control to 9% in combined. Lower significant reductions with individual	Combination of PDGF-BB and FGF2 gives a functional and stable vessel network	Kim

Table 1.4 (Continued)

MI treatment tested	Species, sample size	Time of intervention	Functional response	Angiogenesis	Cell Prol.	Fibrosis	Mechanism	Ref.
poly(N-isopropylacrylamide-co-propylacrylic acid-co-butyl acrylate) (p[NIPAAm-co-PAA-co-BA]) with bFGF	Rats, N=8-16	At the time of ligation	Significant increase in FS from 25% in control to 35% in polymer with bFGF. Better haemodynamics	Significant increase (by 30%) in capillaries (from 200 to 275 cap./mm^2) and arterioles from 50 to 75 art./ mm^2	NA	NA	Angiogenic effect promoted by sustained bFGF delivery from pH responsive hydrogel	Garbern
NIPAAm hydrogel with bFGF and IGF1 (in PLGA microparticles)	Rats, N=9-10	2 w after MI	Significant improvements in fractional area change, EDA and ESA, independently of the addition of bFGF/IGF1	No significant differences in α-SMA$^+$ cells	Higher retention of injected GFs	NS difference	bFGF and IGF1 addition does not enhance the benefit	Nelson

Table 1.4 (Continued)

MI treatment tested	Species, sample size	Time of intervention	Functional response	Angiogenesis	Cell Prol.	Fibrosis	Mecha-nism	Ref.
HA hydrogel engineered with SDF-1 factor analogue (ESA)	Rats, N=8-15	At the time of ligation	Significant improvement in EF from 40% in control to 62% with combined, lower significance with HA-only	Significant four-fold increase in capillary density and three-fold increase with HA-only	Seven/eight-fold increase in $CXCR4^+$ progenitor cells	Significant decrease in fibrosis from 12% in control to 2% with combined and to 4% with HA-only	Preserva-tion of SDF1-CXCR4 axis	MacArthur
Cathelicidin peptides (CRAMPs)-treated BMMNCs and SDF-1 in HA-cyclodestrin hydrogels	Mice, N=7-15	At the time of ligation	Significant improvement in EF from 23% in control to 40% in combined. Significant improvement of ESV and EDV	Three-fold significant increase in capillaries (from 51 to 161 cap./mm^2) in combined	Significant more than two-fold increase in $BrdU^+$ CM in infarct and remote after combined	NS difference	CRAMPs augment the efficacy of BMSPCs	Klyachkin

Table 1.4 (Continued)

MI treatment tested	Species, sample size	Time of intervention	Functional response	Angiogenesis	Cell Prol.	Fibrosis	Mechanism	Ref.
Fibrin hydrogel with skeletal myoblasts	Rats, N=5-6	1 w after MI	NA	Significant increase in arterioles n. from 10 in control to 13 art./mm^2 in fibrin. Significant increase but lower comparing myoblast in fibrin with myoblast-alone	NA	Decrease in infarct size from 26 to 17%, no additional efficacy with myoblasts	Angiogenic effect of fibrin applied in ischemic MI scenario	Christman
Gelatin hydrogel with cardiomyocytes (CM)	Rats, N=5-10	At the time of ligation	Significant increase in EF from 55% to 67% in combined CM-hydrogel. Significant improvement in FS in combined	Significant three-fold increase in vWF$^+$ cells in combined treatment	GH enhanced retention of CM by approx. one third compared to PBS	NS difference	Enhance-ment paracrine effect of CM by retention in hydrogel	Nakajima

Table 1.4 (Continued)

MI treatment tested	Species, sample size	Time of intervention	Functional response	Angiogenesis	Cell Prol.	Fibrosis	Mechanism	Ref.
HA hydrogel with allogeneic bone marrow mononuclear cells (BMMNCs)	Rats, N=8	At the time of ligation	Significant improvement in EF from 35% in control to 45% in combined. Lower significance with individual treatments	Two/three-fold increase in both capillary and arteriole density only with combined group	NA	Significant reduction in scar size from approx. 45% in control to 20% with combined	Synergistic effect by combination of HA and BMMNCs individual benefits	Chen 2013
HA hydrogel with BMMNCs	Lanyu minipigs, N=7-8	At the time of ligation	Significant increase in systolic and diastolic thickness just in combined treatment. Maximum increase in EF is less than 5%	Significant increase in capillaries from 400 up to 600 cap./mm^2 with combined. Significant increase in arterioles from 80 to 250 art./mm^2 in combined	NA	Significant decrease in scar size from approx. 15% in control to approx. 7% with combined. Lower significance with individual	Combination of hydrogel and MNCs provide a synergistic effect	Chen 2014

Table 1.4 (Continued)

MI treatment tested	Species, sample size	Time of intervention	Functional response	Angiogenesis	Cell Prol.	Fibrosis	Mechanism	Ref.
Chitosan hydrogel with adipose-derived stem cells (ADSCs)	Rats, N=22	At the time of ligation	Significant increase in EF from 43% to 59%, significant increase in FS and improved haemodynamics with combined	Significant increase from 88 to 286 vessels/mm^2 in combined treatment (vWF). Increase to 220 vessels/mm^2 in chitosan-only	ADSC$^+$ for α-sarcomeric actinin, Cnx43, CD31, vWAg	Significant decrease in infarct size from 48% to 25% in combined and to 35% in hydrogel	ROS scavenging effect of chitosan combined to ADSCs regenerative potential	Liu
Autologous ADSCs embedded in platelet-rich fibrin scaffolds	Rats, N=8	At the time of ligation	Significant increase in EF from 43% in control to 55% in combined treatment. Sign. improv. in EDV and ESV	Significant increase in vessels from two ves./field in control to three in hydrogel-only and to seven in combined treatment	Significant increase in c-kit$^+$ and CXCR4$^+$ cells	Significant reduction in fibrosis by approx. 65% in combined treatment and by 30% in hydrogel-only	Extended effect of ADMSCs in the injected hydrogel system	Chen 2015

Table 1.4 (Continued)

MI treatment tested	Species, sample size	Time of intervention	Functional response	Angiogenesis	Cell Prol.	Fibrosis	Mechanism	Ref.
HA hydrogel with plasmid DNA-eNOS and ADSCs	Rats, N=25	At the time of ligation	Significant increase in EF from 35% to 70% using combined treatment, significant improvement also with all individual treatments. Significant improvements in FS, EDV and ESV	Qualitative increase in α-SMA, vWF	α-actinin staining increased in combined treatment	Significant decrease from approx. 65% in control to approx. 10% in combined treatment. Significant decrease also with individual treatments	Synergistic action of agents included in the hydrogel	Wang 2018a
HA shear-thinning hydrogel and endothelial progenitor cells	Rats, N=8-10	At the time of ligation	Significant increase in EF from 42% to 69% in combined, 57% with cell-only, 56% with hydrogel-only. Improved haemodynamics	Significant four-fold increase in vessels number, NS difference with either cell-only or gel-only	Significant increase in incorpora-ted EPCs	Significant reduction from 35% in control to 10% in combined	Enhance-ment of paracrine effects of progenitor cells in the hydrogel	Gaffey

Table 1.4 (Continued)

MI treatment tested	Species, sample size	Time of intervention	Functional response	Angiogenesis	Cell Prol.	Fibrosis	Mechanism	Ref.
HA-based hydrogel with extracellular vesicles (EV) or endothelial progenitor cells (EPC)	Rats, N=9-11	At the time of ligation	Significant increase in EF from approx. 30% in control to 50% with combination (either EV or EPC). Lower significance with HA- and EV-alone. Improved haemodynamics in all the treatment groups	Significant two-fold increase in capillaries and 50% increase in arterioles only with HA -EV. NS in other groups	NA	NA	Angiogenic response due to stable delivery of EVs from the hydrogel	Chen 2018
Porcine ECM hydrogel with HGF fragment	Rats, N=9-12	1 w after MI	NS difference	NS in capillary, significant increase in arterioles from 10 art./mm^2 in control to 50 in combined, NS with individual	NA	Significant reduction in interstitial fibrosis from 4% in control to 2% with combined	HGF fragment acts similarly to HGF and its efficacy is enhanced by prolonged release	Sonnenberg

Table 1.4 (Continued)

MI treatment tested	Species, sample size	Time of intervention	Functional response	Angiogenesis	Cell prol.	Fibrosis	Mechanism	Ref.
bFGF-gelatin hydrogel alone or with CDC or BMSC	Pigs, N=7-9	1 w after MI	Significant increase in EF from 32% to 37.1% in bFGF and to 38% in bFGF-CDC. Significant increase in wall motion from 46% to 58% in combined	Significant increase in arteriole number by 1.5-fold in bFGF group. NS difference between bFGF-CDC and b-FGF	Greater magnitude of myocyte conversion compared with the injection of hBMCs combined with bFGF	Significant decrease by 4% in infarct volume in bFGF-CDC, around 1-2% for individual	Synergistic action of bFGF with hCDCs to a stable vessel formation	Takehara
HA hydrogel with IGF-1/HGF	Rats, N=3-5	6 d after MI	NR	Two-fold increase in capillaries at 4 w, less evident increase at 1 w	Two-fold increase in $Ki67^{+}$ cells. $Gata4^{+}$ clusters in 80% of in combined, 40% in HGF/IGF-only, none in control	Significant lower fibrosis from 65% to 40% with combined	Sequential delivery IGF-HGF by HA hydrogel	Ruvinov

Table 1.4 (Continued)

MI treatment tested	Species, sample size	Time of intervention	Functional response	Angiogenesis	Cell prol.	Fibrosis	Mechanism	Ref.
PEG hydrogel with EPO	Rats, N=10-12	At the time of ligation	Significant improvement in EDD, ESV and FS with combined. Lower significant increase with all other individual groups. Better haemodynamics	Significantly higher vessel count with combined. Lower significant with EPO alone, NS with hydrogel	Significant reduction in apoptotic cells with combined, same trend with EPO-alone	Significant reduction in infarct size from 33% in control to 18% with combined	Enhancement of EPO effects by reservoir action of hydrogel	Wang 2009
pH-switchable PEG hydrogel with HGF and IGF-1	Pigs, N=3-4	4 w after MI (by catheter – transendo-cardial injection)	NR	NR	NR	Significant reduction in collagen content inside the scar from 25% in control to 13% with combined	Efficacy of IGF-1- and HGF-mediated reduction of fibrosis in a chronic model	Bastings

1.3.6.1 Cellular stress

The maintenance of homeostasis depends on molecular mechanisms and signals which regulate the cellular response to externals insults - generally defined as stress. Specifically, the source of insults can be either physico-chemical (DNA-damaging substances, radiations, toxins) or pathological (hypoxia, infective processes). Nevertheless, our organism can cope with these perturbations by the activation of specific mechanisms of self-defence, that involve the primary unit of the organism, i.e. the cell. The most immediate "cellular adaptation" upon an external insult is the DNA damage response (DDR). Damaged nucleotides in the chromosomes represent the highest risk of mutagenic transformation of our genome, with potential pathological consequences that are unpredictable including cancer-related and severe dysfunctional deficits [Satoh, Kikuchi 2003, Meister-Broekema, Hoeijmakers]. For this reason, at a cellular level in physiological conditions we possess cell-cycle checkpoints, tolerance and repair mechanisms which represent the first line of self-defence [Giglia-Mari]. However, in the cardiovascular field the main perturbation which is responsible for cardiac myocyte apoptosis is hypoxia [Frangogiannis 2012]. Specifically, lack of oxygenation can damage cardiac cells in an irreversible way within 20 min, and the apoptotic wave can last for hours after the occurrence of ischemia [Laflamme].

Myocardial necrosis is the triggering event for the consequent recruitment of inflammatory cells that produces a granulation tissue in the damaged area [Frangogiannis 2012]. The main difference between necrosis and apoptosis lies in the retention of an intact cellular membrane in the apoptotic cell, whereas the complete disruption and following release of cytosolic vacuoles and cytokines exacerbates the entity of inflammatory cells migration in the effected area [Konstantinidis]. Moreover, ROS-associated and calcium overload-dependent damage to cardiac mitochondria activate the intrinsic pathway of apoptosis. Indeed, due to the permeabilisation of the outer mitochondrial membrane, cytochrome *c* and apoptotic protease-activating factor 1 (Apaf-1) are released in the cytosol. This translocation induces the activation of the initiator caspase 9, which then completes the actual apoptotic program by activation of effector caspases 3, 6 and 7 [Xia].

Among the most widely studied pathways which have a role in the apoptotic program is the PI3K/Akt/mTOR signalling pathway. This pathway starts from the binding of growth factors, like IGF-1, to the respective tyrosine kinase receptors. Upon activation and conversion of phosphatidylinositol bisphosphate (PIP2) to triphosphate (PIP3), Akt, which is the fundamental mediator of the anti-apoptotic effect, is recruited. Studies have demonstrated the beneficial effects of Akt activation on cardiomyocytes survival and prevention of mitochondrial-mediated apoptosis [Uchiyama, Roberts, Bi, Su]. Interestingly, increased cytosolic localisation of phosphorylated Akt in females can be linked with the higher levels of estrogen in females [Camper-Kirby], which is known to have a protective action for the cardiovascular system [Knowlton]. Consistently, molecules which interfere with the downstream signalling of PI3K/Akt pathway, such as the dual protein/lipid phosphatase and tensin homologue (PTEN) and the PH domain leucine-rich repeat protein phosphatase (PHPLPP), cause an inhibitory effect on the pro-survival activation cascade [Chagpar, Miyamoto, Xing]. Nevertheless, such inhibitors have been recently associated with a protective role against pathological hypertrophy [Moc]. Thereby the identification of either the precise target or the suitable combination to achieve a beneficial modulation of such pathways will still require additional preliminary investigations.

1.3.6.2 Modulation of ischemic-derived cellular stress

Erythropoietin (EPO) is a glycoprotein cytokine which can stimulate the activation of the PI3K/Akt antiapoptotic pathway. Phase II and III trials that have tested the administration of EPO within a few hours of the reperfusion did not achieve functional improvements observed in small animal models [Najjar, Voors], so the delivery approach has been questioned. Inclusion of EPO inside either injectable hydrogel or patches has been tested [Klopsch, Wang 2009]. Although these studies were performed in small animal models, the reservoir action of the tested systems contributed to improved function and vascularisation, together with reduced fibrosis and cardiac cell apoptosis [Klopsch, Wang 2009].

Given the cause-effect relationship between the secretion of ROS and the activation of the DDR response, the scavenging of ROS in ischemia-reperfusion can potentially

reduce the cellular stress in such a pathological stage. ROS-responsive polymeric systems have been optimised and have reduced the infarction area, by the reduction of the pro-inflammatory and apoptotic effect of molecules such as hydrogen peroxide [Bae, Lee 2015, Park]. However, the complexity of hypoxia-induced molecular cascade was highlighted by the counterintuitive regenerative response observed upon induction of systemic hypoxaemia in mice for one week [Nakada]. Here, a conceptual switch from oxidative to glycolytic metabolism was applied systemically and enhanced the re-entry of cardiomyocytes in the cell cycle and their consequent proliferation [Nakada]. This work expands the conventional edges of ROS-associated damage towards the potential modulation of cardiomyocytes energetic efficiency. In fact, given the numerous factors which have a role in the storage and secretion of ROS, the observation of opposite outcomes related to their production suggest that the mechanism responsible for the activation of a fibrotic program rather than a regenerative one still needs to be made clear.

1.3.7.1 Recruitment of growth factors

Several cellular mechanisms such as growth, proliferation, differentiation, survival and inflammation are characterised by the orchestrated recruitment and activation/inhibition of polypeptides known as growth factors. These molecules are multifunctional, since they can both stimulate or inhibit the above-mentioned phenomena. The first pioneering work which highlighted the potential of growth factors as therapeutic tools was performed by Levi-Montalcini in 1952 [Levi-Montalcini]. This original work, which unravelled the potential of nerve growth factor (NGF), was expanded over the following decades, reaching the steps of *in vivo* testing of the biological activity of the delivered recombinant NGF [Colangelo] and reaching efficacy in Phase II clinical trials for the treatment of HIV-associated sensory neuropathy [McArthur]. In the cardiovascular field, hypertrophy has been widely studied and probably represents the most characterised adaptation of cardiac cells to ageing and pathological events, such as valvular dysfunctions or ischemia [Lyon, Oka 2014, Tham]. Intriguingly, cardiac hypertrophic response can share the same molecular pathway described in the previous section on cell survival, that is PI3K/Akt. A key study performed by Shiojima *et al*. demonstrated the importance of acute vs chronic activation of Akt in the context of cardiac hypertrophy [Shiojima].

By the establishment of a conditional transgenic activation of Akt in mice, it was shown that short periods (two weeks) of induction caused adaptive growth associated with a proportional angiogenic response. By contrast, long-term (six weeks) activation induced a maladaptive growth uncoupled with angiogenesis and prone to occurrence of heart failure [Shiojima]. The loss of the cardioprotective effect and increased cardiac injury was specifically associated with the overexpression of Akt3 in transgenic mice [Taniyama]. In addition to this, a different behaviour in response to a chronic condition of Akt activation depends on the type of growth factors expressed in maladaptive conditions. IGF-1 and endothelin 1 (ET-1) levels in human hypertrophic hearts were shown not to be correlated with ventricular dysfunction whereas angiotensin II (Ang II) was produced in hearts subjected to end-systolic wall stress [Serneri 1999]. By combining the evidence from following studies, the cardioprotective effect of IGF-1 contrasted with the hypertrophic response due to Ang II activation [Ainscough, Xu, Serneri 2001, González-Guerra].

1.3.7.2 Growth factor-based tested treatments

As already mentioned in the section related to angiogenesis, the balance between growth factors, as is the case with VEGF and PDGF, can determine the success of a potential therapeutic approach. Therefore, several approaches have finely tuned the release of angiogenic growth factor to achieve a stable and mature neovascularisation in the infarcted area. By the exploitation of the paracrine signalling triggered by a synthetic modified RNA which encoded for VEGF-A, Zangi *et al*. were able to show the efficacy of such growth factor to enliven the beneficial recruitment of epicardium-derived cells and their subsequent differentiation in endothelial and smooth muscle cells [Zangi]. Consequently, a marked reduction in fibrosis and enhancement of angiogenesis led to a significant 15% increase in EF as well as short- and long-term survival rates [Zangi]. Interestingly, recruitment of resident cardiac progenitor cells was reported upon combined injections of hepatocyte growth factor (HGF) and IGF-1 in a canine model, leading to the formation of new vessels and cardiac cells [Linke]. Here, the two growth factors were injected in the border zone of the infarct and induced remarkable improvements in the ventricular remodelling and EF, which were correlated with the degree of reported myocardial regeneration [Linke]. Nevertheless, the lack of technical quantification of fibrosis and

angiogenesis in the regenerated areas described a scenario which is hardly comparable with the other therapeutic approaches. The same growth factors (HGF/IGF-1) were sequentially delivered by a HA hydrogel in the infarcted rat myocardium, and in this study thorough analyses were performed to evaluate the overall tissue response [Ruvinov]. Indeed, two-fold increase in capillaries and absolute reduction in fibrosis by approximately 25% further supported the expected proliferative effect on $Ki67^+$ and $GATA^+$ cells [Ruvinov]. Nevertheless, the lack of functional data was a main limitation of this study. Interestingly, the beneficial reduction in fibrosis was observed also after treatment with a pH-switchable PEG hydrogel conjugated with HGF and IGF-1 in a chronic model of MI [Bastings]. Indeed, the decrease in collagen deposition was comparable with the HA-hydrogel incorporating the same growth factors [Ruvinov], using a porcine model [Bastings].

1.3.8.1 Basis and relevance of glycobiology

The flow of information to build and sustain the development of an organism and its functions goes from genes to proteins through the transcription and translation processes; this is the main point of the central dogma formulated by Crick [Crick]. Among the post-translational modifications, glycosylation is extensively present on cellular proteins and provides part of the complexity needed to regulate cell-cell and cell-ECM interactions [Varki]. The glycocalyx consists of the wide range of glycan modifications added to the protein backbone of cellular membrane proteins, the so called glycoproteins, that can be distinguished in either *N*- or *O*-glycans. *N*-glycans have their sugar chain bound to the terminal asparagine residue of the polypeptide and the first glycan of the chain is *N*-acetylglucosamine (GlcNAc) in eukaryotes. *O*-glycans are glycoproteins which display a chain of glycans starting with *N*-acetylgalactosamine (GalNAc) which attach via a covalent bond - similarly to *N*-glycans - to the terminal serine or threonine residue of the protein portion. The biosynthetic pathway which leads to the exposure of properly-folded *N*- and *O*-glycans on the cell membrane has multiple checkpoints in the two main compartments which regulate this process which are the endoplasmic reticulum and the Golgi apparatus [Bieberich, Cherepanova, Gerlach]. Disruptions in the enzymatic pathways that enable the formation of glycans can cause congenital disorders of glycosylation (CDG) which were noticed for the first time by Jaeken in 1980 [Jaeken

1980 and 2017, Brasil, Monticelli]. Defects in enzymes such as phosphomannomutase II or β1–4 galactosyltransferase can cause dramatic pathological conditions as mental retardation or myopathy with spontaneous haemorrhage and malformations, respectively [Keir, Freeze, Peters]. Despite the rising interest in the relevance of glycans since the period following the formulation of the central paradigm of molecular biology, limitations in the analytical techniques which are required to isolate and analyse these moieties have held back the potential for expansion in this field for several decades. Thanks to technological advances in the field of mass spectrometry analysis [Jensen, Frost, Yang 2018], specific methods for the processing and release of glycans from *N*- and *O*-glycoproteins can now be applied to evaluate the overall glycan complexity in the sample of interest, the approach defined as glycomics. Recent studies advanced the current knowledge in the remodelling processes of degenerative and cancer-related conditions [Paszek, Gonzalez, Mohd-Isa]. Nonetheless, the sensitivity of the glycome to the variability of the exogenous nutrients and the regulation of the salvage pathways severely limit the predictability of the expression levels of the glycans.

1.3.8.2 Role of glycans as therapeutic modulators

As a result of their biosynthesis, glycans are branched oligosaccharide structures and contain motifs which can bind to galectins or grow factor receptors. Therefore, alterations in the glycan structures can lead to dysregulation of the signalling responsible for cellular migration and ECM remodelling. For instance, the initial association seen between tumour progression and an increased β(1,6)-linked branching in *N*-glycans, was later characterised as part of a glyco-regulated EGFR/PI3K/Erk signalling pathway [Dennis, Lau]. In this case, the identification of the glycoenzyme which mediates this process, mannoside acetyl-glucosaminyltransferase 5, was confirmed by the reduction in tumour growth and metastases upon the knockout of the corresponding MGAT5 gene [Granovsky]. A key protein with a shared role both in the metastatic progression of tumour and in the induction of stable angiogenesis after ischemic, as mentioned above, is VEGFR2 [Stuttfeld]. A study described the signalling axis composed by galectin-1 and of VEGFR2 and its need for the enhancement of angiogenesis in refractory tumours which did not respond to anti-VEGF therapy [Croci]. In addition, a marked increase

in the expression of β(1,6)-linked branched *N*-glycans and a reduction in α(2,6)-NeuAc in endothelial cells included in the vascular network of the refractory tumours were observed [Croci]. Another observed mechanism of glyco-mediated, VEGF-independent enhanced migration of endothelial cells was based on the galectin-1 binding to the VEGFR co-receptor neuropilin-1 [Hsieh 2008]. In light of the role of galectin-1 in the fueling several types of tumour-associated angiogenesis, the pursued therapeutic approaches were focused on the synthesis of its inhibitors rather than towards a controlled enhancement for post-ischemic applications [Blanchard, Astorgues-Xerri]. In contrast, a different glycan-based approach is based on the regulation of the HGF receptor, as known as c-Met, by the sialic acid containing ganglioside (GD) 1α which results from the sialyltransferase ST6GALNAC5. In this case, evidence showed both the induction of a pro-tumorigenic c-Met-activated autocrine loop in canine kidney MDCK cells following the expression of ST6GALNAC5 gene and the correlation between mutations in the same gene and the occurrence of coronary artery diseases in a cohort of 160 patients [Chu, InanlooRahatloo]. Since most of the relevant studies were centred on understanding the role played by glycans in a dysregulated over-expression and activation of growth factors such as c-Met, VEGFR2, FGFR and ERBB [Markowska, Hsieh 2008, Croci, Merlin, Chu], extensive experiments will need to be designed to exploit such potential in the context of tissue repair.

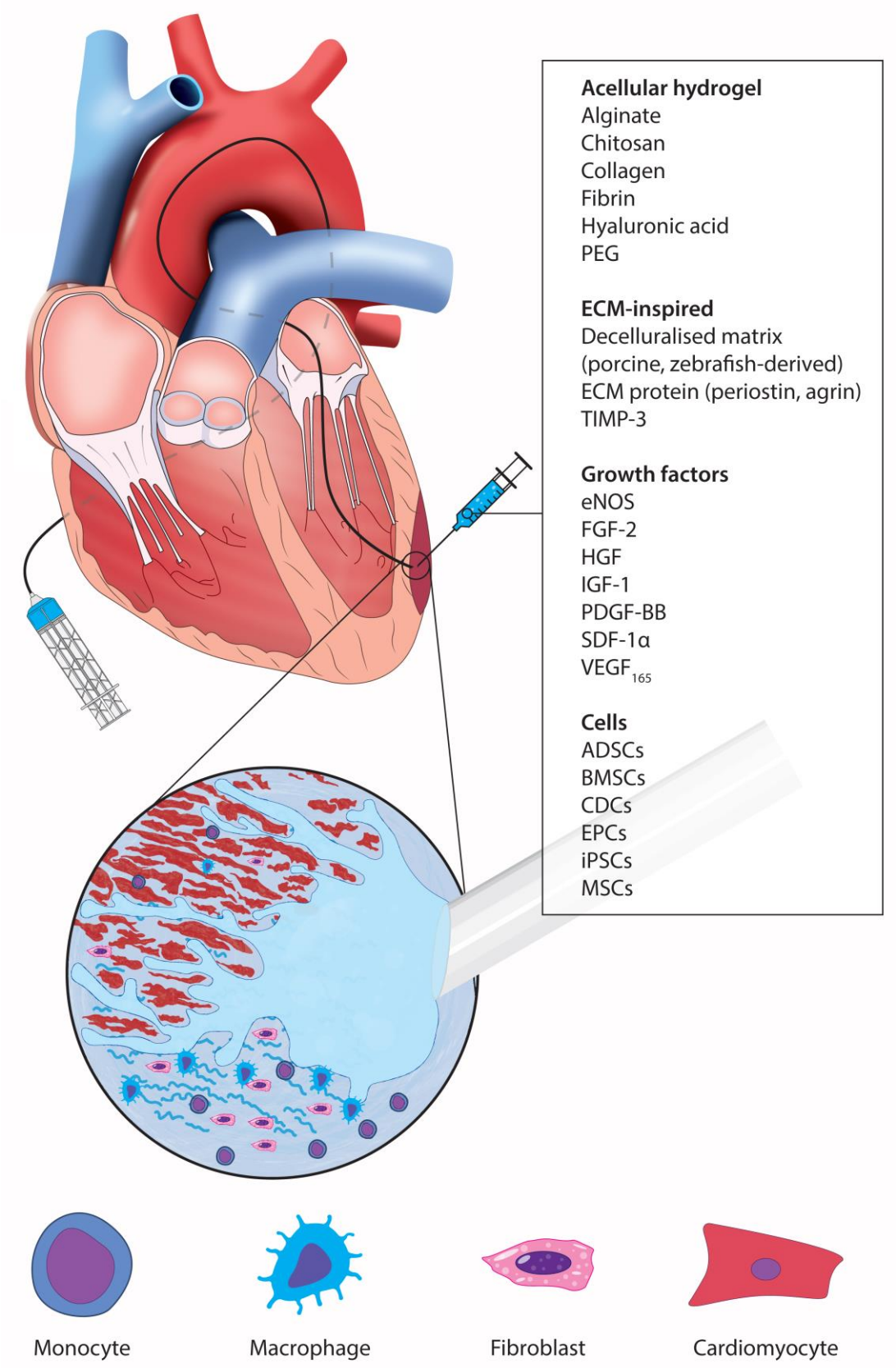

Figure 1.6 Schematic of different approaches to treat myocardial infarction. Acellular hydrogels, ECM-inspired treatments, growth-factor-based and cellular-based or a combination of these have been exploited in the recent decades.

Abbreviations: PEG, polyethylene glycol; TIMP, tissue inhibitor of metalloproteinases; eNOS, endothelial nitric oxide synthase; FGF, fibroblast growth factor; HGF, hepatocyte growth factor; IGF, insulin growth factor; PDGF, platelet-derived growth factor; SDF, stromal cell-derived growth factor; VEGF, vascular endothelial growth factor; ADSCs, adipose-derived stem cells; BMSCs, bone-marrow-derived stem cells; CDCs, cardiac-derived stem cells; EPCs, endothelial progenitor cells; iPSCs, induced-pluripotent stem cells; MSCs, mesenchymal stem cells.

1.4 Regenerative approaches

Cardiomyocytes are post-mitotic cells unable to re-enter the cell-cycle by definition at the adult stage and only in a time-limited way, around one-two days after birth [Porrello, Ye, Zhu]. Indeed, the exact rate of cardiomyocyte turnover has been estimated and corresponds to approximately 0.76% per year [Senyo]. Nevertheless, the concept of replacing the millions of cardiomyocytes which die following ischemia by inducing the repopulation of these cells - either by endogenous mechanisms or after external implantation - is one of the paths most widely investigated in cardiovascular research [Wysoczynski 2017, Bearzi, Bersell, Engel, Chimenti].

1.4.1 Cardiac stem cells

Among the most promising therapeutic approaches reported is the use of c-kit$^+$ cardiac stem cells (CSC), which were isolated from human hearts for the first time in 2007 [Bearzi]. Indeed, c-kit$^+$ CSC have shown their efficacy in improving the LV systolic function up to the phase I clinical trial SCIPIO (NCT00474461). However, the success of c-kit$^+$ stem cells has been disputed in terms of the cardiomyocyte regenerative capability in the mammalian heart which was claimed for the first time by Anversa's group in 2001 [Orlic]. Despite the claim by the same group of the existence of a lineage of c-kit$^+$ cardiac stem cells in the neonatal heart and their differentiation to myocytes by Notch1 [Urbanek], thorough studies redefined the actual differentiation potential of such stem cells towards the endothelial cell type [van Berlo, Sultana]. However, due to the poor survival of c-kit$^+$ cardiac stem cells injected in single dose in the infarcted myocardium [Hong 2013 and 2014], a straightforward change in the therapeutic approach towards administration of multiple doses of the same cells was tested in rats [Tokita, Guo]. Interestingly, the outcome of three administrations (35 days apart) of c-kit$^+$ cells resulted in a three-fold increase in EF, 50% relative reduction in scar and a greater myocyte density than in the single dose group [Tokita]. Nevertheless, expression of c-kit is not stable over culture and tends to be lost over a few passages, so a novel way to enrich for this type of cells was associated with their adhesion to plastic [Wysoczynski 2016]. Specifically, slow adhering (SA) and rapidly adhering (RA) stem cells expressed mesenchymal markers and, by comparison of the two types, SA stem cells resulted in

higher c-kit expression, angiogenic effect and functional improvement in mice [Wysoczynski 2016]. In a further study by the same group, the need for c-kit expression sorting for the therapeutic efficacy of such SA-cardiac mesenchymal stem cells (CMC) was negated [Wysoczynski 2018]. In this study, despite the lack of sorting for c-kit and negligible engraftment survival (below 1%), an improved remodelling was seen after SA-CMCs administration [Wysoczynski 2018]. Nevertheless, the details of the paracrine mechanism behind the reduced inflammation and fibrosis still need to be clarified in further studies.

1.4.2 Strategies based on the re-entry of cardiomyocytes in the cell-cycle

Another path to target myocardial regeneration started with the investigation of self-regenerating animal models like the zebrafish [Poss, Jopling, Kikuchi 2010]. Regenerated cardiomyocytes in zebrafish derive from the same type of cardiac cells which were not lost after the resection of the ventricle and that re-entered the cell cycle by dedifferentiation first, and then by proliferation [Jopling]. Cryoinjury has been also demonstrated to be a reliable method to induce cardiac regeneration in zebrafish [Chablais 2011 and 2012, Kikuchi 2010]. The mitotic checkpoint kinase *mps1* and the cell-cycle regulator *plk1* were shown to be required to accomplish the regenerative process [Poss, Jopling]. More recent studies were based on both the activation of these key regulators [Yin, Qin] and the detection of novel target genes to gain knowledge of the full mechanism of myocardial regeneration [Beauchemin, Zhang, Wang 2013b].

A key characteristic of mammalian cardiomyocytes is the presence of more than one nucleus inside the same cell (bi-/multi-nucleation) which was initially shown to be linked with its almost undetected ability to dedifferentiate [Bersell, Mahmoud, D'Uva]. Conversely, in a recent study both mononucleated and binucleated adult cardiomyocytes were demonstrated to have a comparable ability to re-enter the cell cycle when cocultured with neonatal ventricular myocytes [Wang 2017b]. To identify molecular regulators of cardiomyocyte re-entry in the cell cycle, the most interesting pool of candidates was made of ECM components inducing cardiomyocyte proliferation at the fetal stage such as periostin and neuregulin 1 (NRG1) [Pasumarthi]. Particularly with regard to the NRG1-ErbB2/4 receptor interaction, several studies assessed their need for a normal fetal cardiac

development since 1995 [Gassmann, Lee 1995, Meyer]. The key role of ErbB2 receptor in NRG1-induced embryonic development and early neonatal stage was then tested for its therapeutic potential after ischemic damage [D'Uva]. Remarkably, the sole reactivation of NRG1-ErbB2 signalling in adult mice using a generated a 'Tet-Off' transgenic mouse model (α*MHC–tTA;TetRE–caErbb2*) to express ErbB2 was sufficient to achieve cardiomyocyte dedifferentiation and proliferation [D'Uva]. In addition, the constitutive activation of ErbB2 induced cardiomegaly independently of the ageing stage of the mice (from early post-natal to adult), suggesting that this pathway is implicated also in the physiological hypertrophic growth of mammalian adult hearts. In this study the ideal conditions of a minimally scarred and volume-preserved post-ischemic myocardium were seen and supported by a complete functional recovery following both acute- (seven days post-MI) and chronic-MI (42 days post-MI) intervention [D'Uva]. However, the definition of the precise mechanism of action of ErbB2-dependent response has been shown to be more complex and associated with a concomitant angiogenesis [Yutzey, Reuter], as seen in zebrafish by applying experimental comparable settings [Gemberling].

Starting from the investigation of a zebrafish regenerative model, increasing evidence of the crucial role of the epicardium in cardiac repair and regeneration has been shown [Lepilina, Masters, Huang 2012, Wei]. After screening the proliferative capacity of epicardial-secreted factors, the cardiogenic potential of follistatin-like 1 (FSTL1) emerged and its delivery (recombinant hFSTL1) through a collagen epicardial patch was tested both in small and large animal models of MI, resulting in cardiomyocyte proliferation and functional improvement [Wei]. FSTL1-responsive cardiomyocytes are not adult cardiac cells, but a minor population of cells recruited in ischemic conditions which are able to re-enter the cell-cycle [Wei]. More recent studies have investigated the protective effect of FSTL1 on other cellular types involved in the posti-ischemic remodelling such as fibroblasts and mesenchymal stem cells [Shen 2019, Maruyama]. FSTL1 demonstrated to benefit also other pathological conditions such as hypertrophic cardiac pressure overload and heart failure with preserved ejection fraction (HFpEF) [Shimano, Tanaka, Wollert 2016]. Further studies will be needed to investigate the potential double-level role of FSTL1 as cardiac protecting agent and inducible enhancer of regeneration after ischemia.

Moreover, the glycosylation of FSTL1, as post-translational modification plays a crucial role in the proliferative effect induced by this factor [Wei, Magadum].

The application of a functional screening approach was chosen to test miRNAs capacity to induce cardiomyocyte proliferation, and the resulting best candidates were tested after inducing MI in mice [Eulalio]. Specifically, the delivery of miR199 and miR590 by adeno-associated viral vectors (AAV) limited the expansion of the infarcts and improved both EF and FS [Eulalio]. Since 5-ethynyl-29-deoxyuridine (EdU) was intraperitoneally administered every two days from the second day post-MI, EdU^+ nuclei counting highlighted a marked cellular proliferation only in the post-miR199/590 treatment groups up to 60 days [Eulalio]. Studies based on non-combined strategies are listed in Table 1.5. This approach based on the miRNA regulation of targets which inhibit the regenerative potential of the mammalian heart was followed and led to the discovery of additional regulators of cardiomyocyte proliferation, like miR34a [Yang 2015]. In this case, Bcl2, Cyclin D1, and Sirt1 were also identified as cell-cycle targets of miR34a-mediated modulation [Yang 2015].

Table 1.5 Non-combined strategies for the treatment of MI.

MI treatment tested	Species, sample size	Time of intervention	Functional response	Angiogenesis	Cell prol.	Fibrosis	Mechanism	Ref.
VEGF-A modRNA	Mice, N=5	At the time of ligation	Significant preservation of EF, compared to 15% decrease in control group	Significant enhancement of angiogenesis, checked for possible leaky structures	Prolifera-tion of $PECAM1^+$ cells	Significant decrease in fibrosis, from 35% to 15-20% with VEGF	KDR-dependent mechanism of epicardial progenitor cells differentiation to endothelial cells	Zangi
Plasmid encoding recombinant human (VEGF)165	Sheep, N=6-7	At the time of ligation	Wall motion scores similar 2 days post-AMI, tendency to improve 15 days later (NS)	Significant increase in arterioles at d10 from 18/mm^2 in control to 119/mm^2 in VEGF; at d15 from 26/mm^2 in control to 83/mm^2. Significant increase in n. cap. at d7 from 703/mm^2 to 1805/mm^2	Significant increase in CM mitotic in VEGF Two-fold higher density of cardiomyo-blasts	Significant decrease from 70% to 43% at day 10 and to 22% at day 15	Growth factors may display pleiotropic actions	Vera Janavel

Table 1.5 (Continued)

MI treatment tested	Species, sample size	Time of intervention	Functional response	Angiogenesis	Cell prol.	Fibrosis	Mechanism	Ref.
Ex-vivo activated human macrophages	Rats, N=8-9	At the time of ligation	Significant increase in FS from 20% in control to 30%	Significant increase in vessels from 10 in control to 25 ves./mm^2	Retention of activated macrophages in the infarct area, myofibroblasts accumulation	NR	Retention of activated macrophages in the infarct area	Leor 2006
T-reg cells (T-regs)	Mice, N=8	1, 4 or 12 w after MI	Significant increase in EF from 20% to 35%	NR	EdU$^+$ in proliferating CM after T-regs injections	Significant decrease in infarct size from 20% to 13%, 3 m after MI	T-regs act in a paracrine manner to promote CM proliferation after MI	Zacchigna
Neuregulin-1b glial growth factor 2	Pigs, N=5-8	1 w after MI, biweekly for 4 w	Significant improvement in EF (over 30%), diastolic volume and FS	NR	NR	Reduction in fibrosis by approx. 5% in the remote region	NRG-1b suppresses TGFb/ pSMAD3 pathway	Galindo

Table 1.5 (Continued)

MI treatment tested	Species, sample size	Time of intervention	Functional response	Angiogenesis	Cell prol.	Fibrosis	Mechanism	Ref.
IL-10 (50 μg/kg/day) infused subcuta-neously for 7 d	Mice, N=10-13	1 d after MI	Significant improvement in EF at 7d post-MI, 1.8-fold increase compared to control group (below 20% EF). Significant improvement in EDV and ESV	NR	Proliferation of fibroblasts and consequent activation promoted by macrophage type II	Significant reduction of collagen I secretion and ratio between collagen I and III	Swift of remodelling response towards a macrophage type II phenotype	Jung
Synthetic miRNAs	Mice, N=6-10	At the time of ligation	Significant increase in EF from 45% in control to 55% in miRNA group one month after	NR	Significant increase in EdU+ cells among proliferating CM after miRNA injections	Significant reduction in infarct size from 35% in control to 13%	Exogenous administra-tion of miRNAs stimulates CM proliferation	Eulalio

Table 1.5 (Continued)

MI treatment tested	Species, sample size	Time of intervention	Functional response	Angiogenesis	Cell prol.	Fibrosis	Mechanism	Ref.
HGF, IGF-1 injections	Dogs, N=6-8	At the time of ligation	Significant improvement in FS at 2 w and 3 w, reaching 50% control value at 4 w. Significant increased EF by 5% at 2w, and by 15% at 4 w	NR	11-, 16-, and 7-fold increase in progenitor cells per cm^3 of myocardium in the infarct, border zone, and remote area	NR	GFs induce translocation of resident progenitor cells to the infarct	Linke
Allogeneic and Syngeneic CDCs	Rats, N=5-8	At the time of ligation	Significant increase in EF from 37% in control to 55% in treatment. Significant increase in FS by 10% in treatment group	Significant increase in vessels from 25 ves./mm^2 in control to 30 ves./mm^2 (after 3 w)	Significant increase in c-kit^+, $BrdU^+$, $Ki67^+$ cells 3 w after injection	Decrease from 19% to 14% using syngeneic/ allogeneic	CDCs are clonogenic and exhibit multilineage potential	Malliaras 2012

Table 1.5 (Continued)

MI treatment tested	Species, sample size	Time of intervention	Functional response	Angiogenesis	Cell prol.	Fibrosis	Mechanism	Ref.
Infusion of cardiosphere-derived cells (CDCs)	Pigs, N=7	At the time of ligation	NS improvement in EF, significant improvement in haemodynamics	NR	NR	Significant decrease from 19.2% in control to 14.2%, 8 w after infusion	Increase in LV mass and possible regeneration associated with CDC	Johnston
Comparison CDC, BM-MSC, Ad-MSC, BM mononuclear cells	Mice, N=8-20	At the time of ligation	Significant increase in EF, from 20% in control to 37% in CDC group at three w. Improvement with other treatments is NS	NR	SA^{+}/engrafted cells in the surviving progeny of human CDCs, *in vivo* differentiation	NR	CDCs are clonogenic and exhibit multilineage potential	Li 2012

Table 1.5 (Continued)

MI treatment tested	Species, sample size	Time of intervention	Functional response	Angiogenesis	Cell prol.	Fibrosis	Mechanism	Ref.
Autologous endothelial progenitor cells (EPCs) or allogeneic mesenchymal stem cells (MSCs)	Pigs, N=10-12	1 w after MI	NS change in EF (around 45%) among all groups. Significant improvement in ESV (NS in EDV) in EPCs group	Two-fold significant increase in vessels (from 400 to 800 vessels/mm^2 in the border zone in EPCs group. NS in MSCs group	NR	Qualitative evaluation of scar. No difference in infarct size	Paracrine effect mediated by the infusion of EPCs in the infarct area	Dubois
Calcium hydroxyapatite microspheres (CHAM)	Sheep, N=5-13	At the time of ligation	Significant increase from 21% in control to 37% in high volume CHAM. NS increase with low volume CHAM. Same trend of significance in the improvement of EDV	NR	NR	Significant reduction in collagen content in CHAM group	Improved matrix stability thorugh TGFβ signalling	Dixon

1.5 Future directions

A comprehensive understanding of ischemia, inflammation, fibrosis, angiogenesis and cellular stress in the cardiac post-ischemic scenario is needed to formulate the most appropriate treatment for MI. The evaluation of the key cellular components involved in these processes (macrophages, growth factors, matrix metalloproteinases) combined with the exploration of benefits and limitations of the experimentally pursued therapeutic approaches is urgently needed in this field. Given the complexity of the post-ischemic microenvironment, the evaluation of the rationale behind initially promising treatments which did not reach success through the clinical phases can specifically identify the reasons for the limitation of such strategies. The current aims and strategies towards an optimum treatment for MI can be summarised as follows:

Aims

- Spatio-temporal orchestrated recruitment of pro-healing macrophage population.
- Reduction of maladaptive fibrotic remodelling and cardiac hypertrophy.
- Shift from a leaky and temporary vascular network to a perfused and physiologically-similar one.
- Induction of re-entry of cardiomyocytes in the cell-cycle and controlled proliferation.
- Identification of bottlenecks in current models of myocardial infarction.

Strategies

- Modulate the timing of inflammation by spatial confinement of inflammatory macrophages.
- ECM-dependent release of paracrine factors to prolong survival of introduced stem cells.
- Induce a time-limited shift in the cardiomyocytes metabolism from oxidative to anaerobic.
- Investigation of early-neonatal regenerative capacity.
- High-throughput analyses from the secretome of pro-healing macrophages and extracellular matrix to identify molecules able to enhance cardiomyocyte cell survival or proliferation.

- Establishment of clinically-relevant models of myocardial infarction.

1.6 Conclusions

The detection of a successful therapeutic strategy can require a comprehensive evaluation of the complexity which characterises the pathological scenario of interest. Myocardial ischemia is currently the first cause of worldwide mortality, with an increasing expansion in developing countries. Despite two decades of exciting experimental breakthroughs, none of the resulting strategies can now be preferred over surgical procedures such as coronary artery bypass graft or heart transplantation (Figure 1.7). In this chapter, ischemia, inflammation, fibrosis, angiogenesis, cellular stress as well as key cellular and molecular components were considered as therapeutic targets. By evaluating the benefits and limitations of the approaches which were founded on these phenomena, it is possible to weigh the rationale of each of these strategies. Given the multitide of variables which influence of the outcome of the experimented treatment, the pathological background was presented with an unbiased view towards any specific process or cellular component. Since the modulation of ischemic remodelling and the enhancement of myocardial regeneration are of equal importance, current studies in the field can also be focused towards a remodelling of the ischemic core and preservation of the functional integrity of the border zone (Figure 1.8).

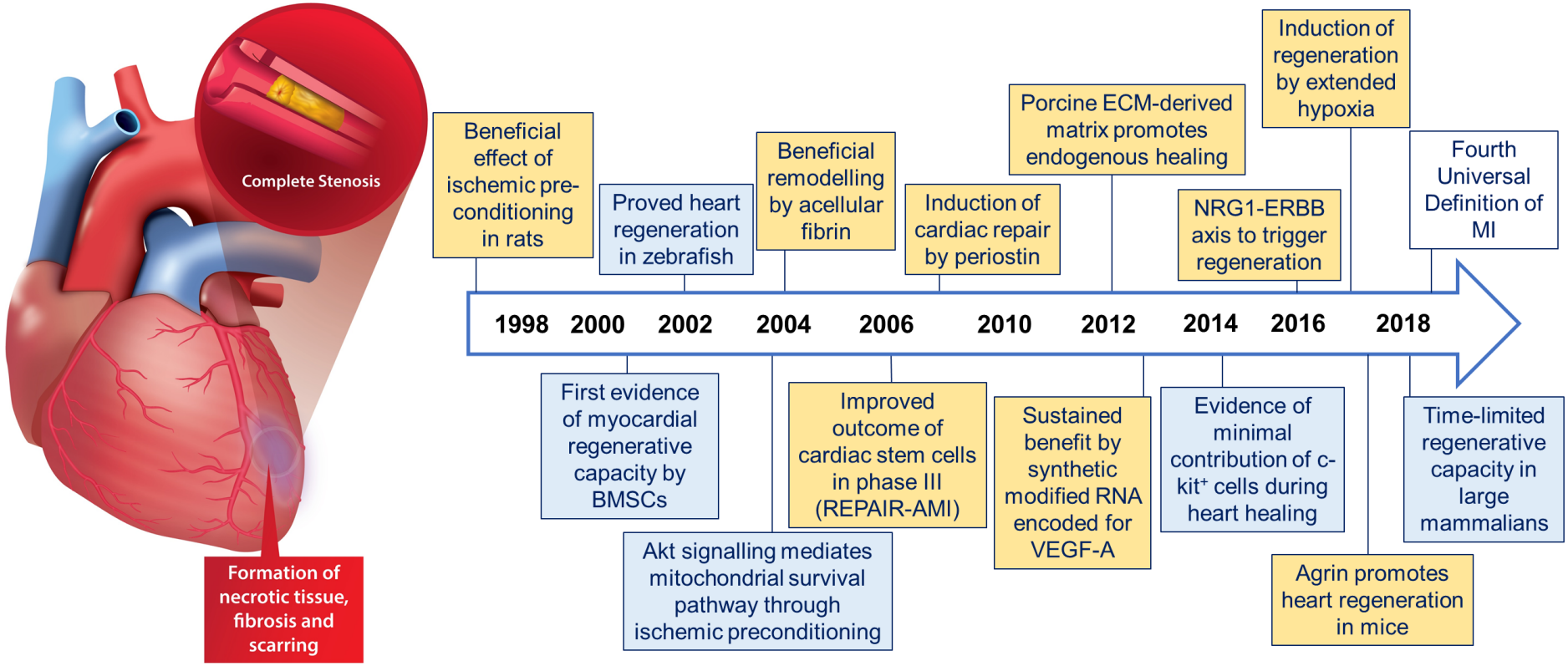

Figure 1.7 Timeline of key findings related to myocardial ischemia over the last two decades. Landmark studies related to the cardiac remodelling and regeneration are highlighted in blue and the most promising therapeutic strategies are shown in yellow.

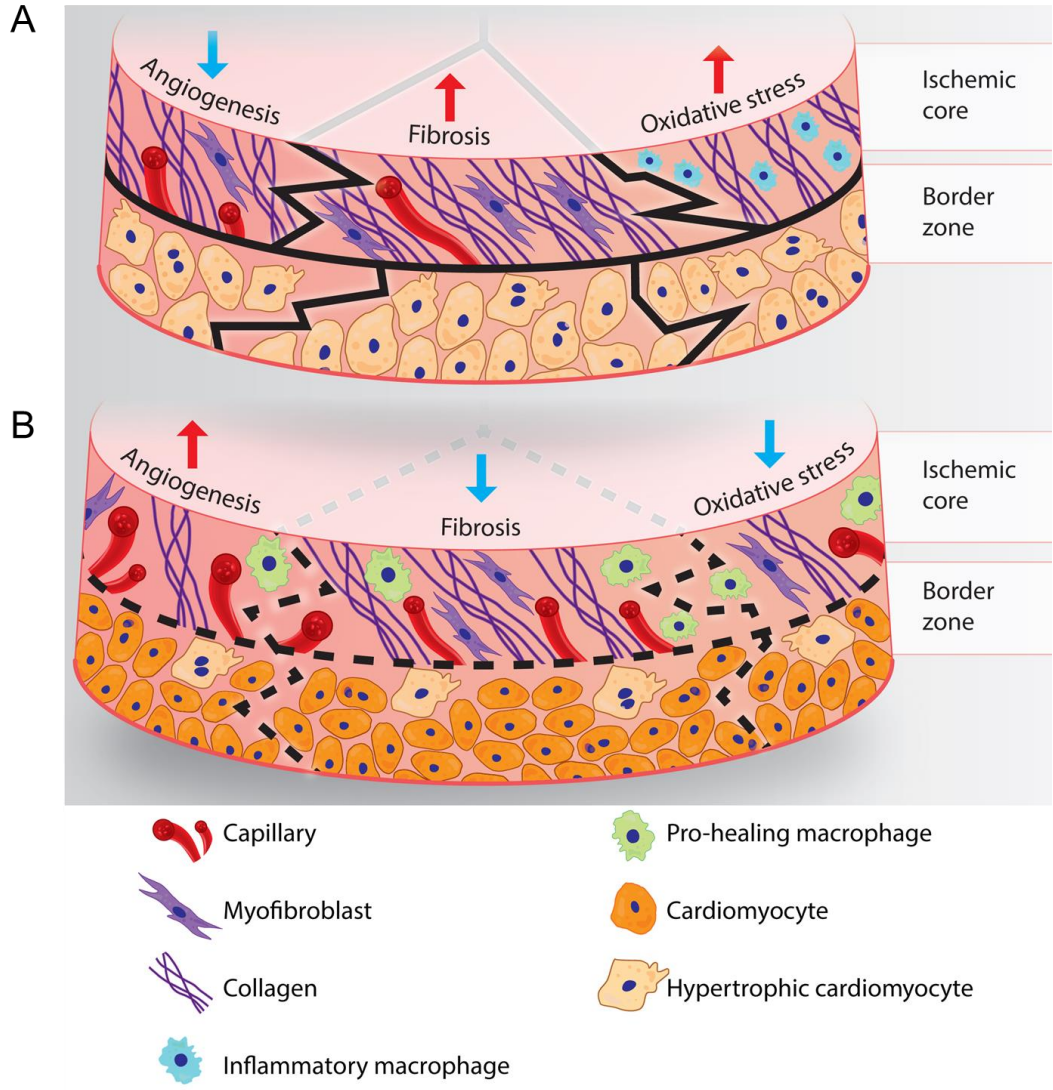

Figure 1.8 Modulation of post-ischemic remodelling. (A) Schematic of untreated ischemic core and border region characterised by poor stable angiogenesis, marked fibrosis and prolonged oxidative stress in the ischemic core, which leads to cardiomyocyte hypertrophy. (B) Schematic of modulated ischemic core after treatment with enhanced angiogenesis, lower fibrosis and pro-healing macrophage infiltration, that beneficially influence the physiological behaviour of cardiomyocytes in the border zone.

1.7 Project rationale: Elastin as an injectable biomaterial for the treatment of MI

The choice of the most suitable biomaterial therapeutic for the desired clinical need is a major challenge in current medical device development and preclinical testing. Elastin is one of the proteins which are abundantly present in the extracellular matrix of several tissue types such as myocardium, cartilage and skin [Mithieux]. Specifically, elastin fibres are derived from the coacervation and further crosslinking of the precursor tropoelastin molecules [Kozel]. The elastogenic activity resides in the main cellular components of the tissue network that can be endothelial cells, fibroblasts, chondrocytes, and keratinocytes.

Through the genetically-engineered fabrication of elastin-mimicking peptides called elastin-like recombinamers (ELRs), there is an opportunity to compensate for the poor availability of natural elastin and also to control the homogeneity of the biomaterial. Moreover, ELRs can be functionalised with specific motifs responsible for several biological functions including cell adhesiveness, degradability and interaction with the cellular microenvironment [Rodríguez-Cabello, Castellanos]. As a result, this functionalisation, together with the possibility to fabricate either hydrogel or microspherical constructs, has increased the range of applications of the ELRs. Several ELRs-based systems have already been studied for their efficacy and interaction with cellular components *in vitro* and *in vivo* over recent years [Staubli, González de Torre, Changi, Pescador]. Nevertheless, ELRs-based systems have never been tested in cardiac post-ischemic conditions either in small or large animal models of MI.

1.8 Objectives and hypotheses

The main aim of this thesis was to evaluate the effect of the intra-myocardial injection of an elastin-based hydrogel after the induction of MI in a clinically-relevant ovine model. Several phases were required to be completed before the *in vivo* testing, and comprehensive analyses were carried out to understand the mechanism of the hydrogel-mediated modulation of the post-ischemic remodelling (Figure 1.9). Moreover, a separate study on the glycosylation differences between early neonatal and adult myocardium in rat revealed glycans which are involved in the early regenerative potential of the mammalian cardiac tissue. The overall aim, hypothesis and objectives of each research chapter are outlined below.

1.8.1 Chapter Two - Distinct differences in cellular membrane glycosylation reflect the regeneration potential of neonatal myocardial tissue

Overall aim

To identify a glycan signature to distinguish the early neonatal from the adult myocardium.

Hypothesis

The glycosylation of myocardial cellular membrane proteins is consistent across ventricles at the adult stage but this changes at the early neonatal condition, reflecting a residual regenerative potential.

Objectives

- Evaluate myocardial glycan expression pattern between different adult rat strains.
- Compare the glycan pattern between the left and right ventricle.
- Perform a glycosylation analysis on the membrane proteins at various stages of cardiac maturity to identify distinctive features.

1.8.2 Chapter Three – An ovine model of non-transmural myocardial infarction

Overall aim

To establish an ovine model of non-transmural myocardial infarction.

Hypothesis

Focal infarcts can be consistently induced in sheep by multiple ligations lateral and parallel to the left anterior descending coronary artery from the first diagonal branch.

Objectives

- Optimise a procedure for the ligation of the side branches of the coronaries to induce non-transmural infarcts.
- Assess the significant decrease in cardiac function 28 days after the surgical procedure and the progressive fibrosis.
- Study the degeneration of cardiomyocytes at the ultrastructure level after ischemia.
- Evaluate and quantify the post-ischemic remodelling at the level of the extracellular matrix.

1.8.3 Chapter Four - Elastin-like recombinamers-based hydrogel modulates the post-ischemic remodelling in a clinically-relevant model of myocardial infarction

Overall aim

To evaluate the effect of the multiple intra-myocardial injection of an elastin-like recombinamers-based hydrogel on post-ischemic remodelling in an ovine model of non-transmural myocardial infarction.

Hypothesis

The multiple injection of an ELRs-based hydrogel seven days after MI can influence the endogenous remodelling towards a less fibrotic and more perfused ischemic core.

Objectives

- Optimise a procedure for the intra-myocardial injection of an ELRs-based hydrogel and evaluate the cardiac functional response 21 days after the hydrogel injection.
- Evaluate the effects of the hydrogel on fibrosis 21 days after the injection in the ischemic core of the infarct at histological and ultrastructural level.
- Investigate changes in total sulfated glycosaminoglycans (GAGs) and changes in GAGs ratio 21 days in the infarcted regions after the hydrogel injection by dimethylmethylene blue (DMMB) assay.
- Assess changes in the glycosylation of the membrane proteins in the ischemic core and border regions in response to the hydrogel 21 days after the injection by their binding to biologically relevant lectins.

1.8.4 Chapter Five - Transcriptomic, proteomic and glycomic analyses to reveal the mechanism of modulation of post-ischemic remodelling by an elastin-based hydrogel

Overall aim

To investigate the molecular mechanisms implicated in the improved remodelling after the treatment with an elastin-like recombinamers-based hydrogel.

Hypothesis

The multiple injection of an ELRs-based hydrogel seven days after MI causes an improved cardiac response which depends on the modulation of molecular mechanisms in the border zone of the infarct.

Objectives

- Identify the biological pathways that were altered after the hydrogel treatment by RNA-sequencing analysis.
- Evaluate the tissue response in membrane proteins glycosylation by LC-ESI-MS/MS glycomic analysis.
- Assess the modulation of tissue response after the hydrogel treatment by proteomic analysis.
- Validate the most prominent differences highlighted by RNA-sequencing and proteomic analyses to define a mechanism of action of the ELRs-hydrogel treatment.

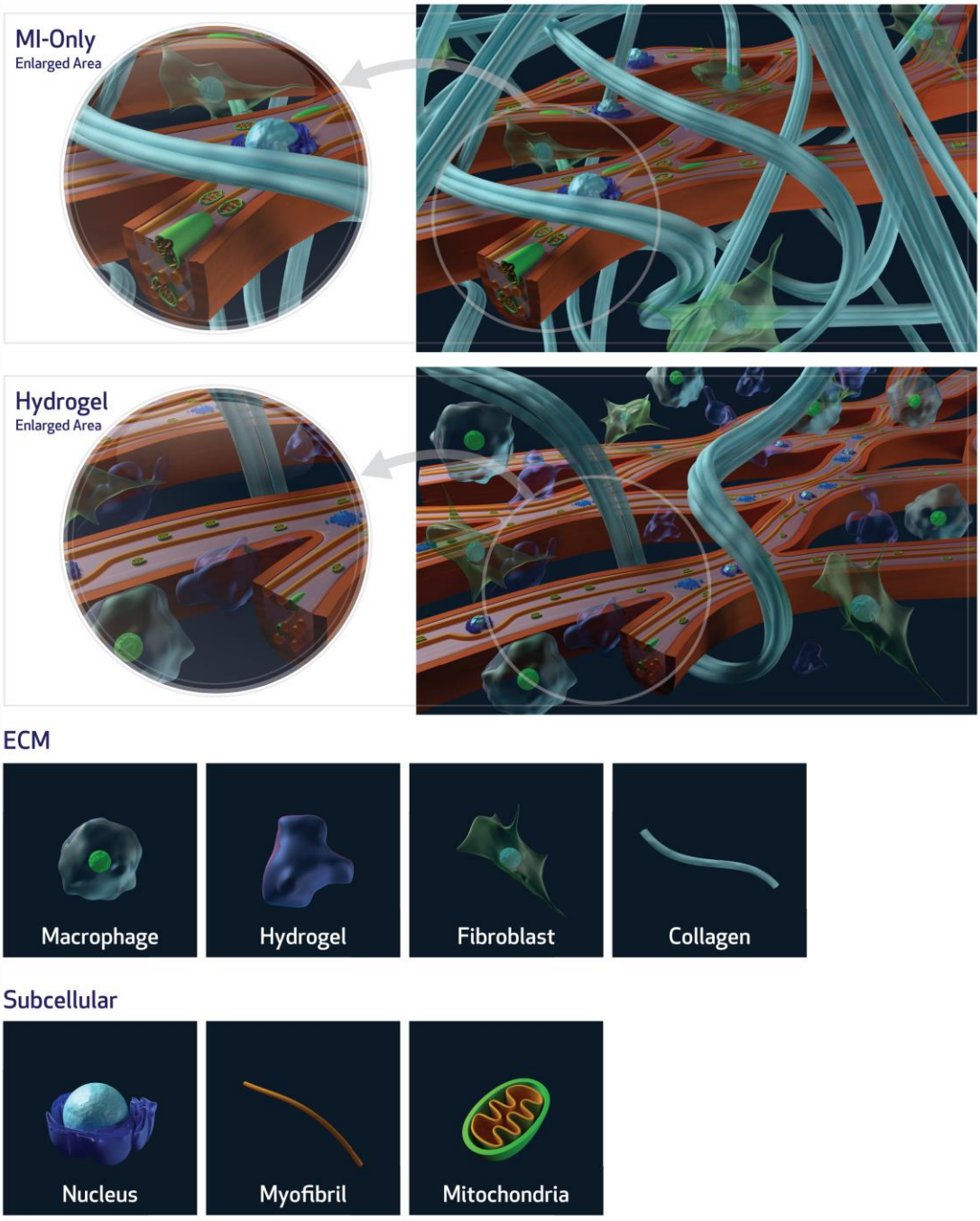

Figure 1.9 3-D illustration showing the hypothesised modulation of the post-ischemic ECM microenvironment (MI-only) after the ELRs-based hydrogel treatment. Increased fibrosis and cardiomyocyte hypertrophy are more pronounced in the untreated pathological than in the hydrogel-treated condition.

1.9 References

- Afzal MR, Samanta A, Shah ZI, Jeevanantham V, Abdel-Latif A, Zuba-Surma EK, Dawn B. Adult bone marrow cell therapy for ischemic heart disease: evidence and insights from randomized controlled trials. Circ Res. 2015 Aug 28;117(6):558-75
- Ainscough JF, Drinkhill MJ, Sedo A, Turner NA, Brooke DA, Balmforth AJ, Ball SG. Angiotensin II type-1 receptor activation in the adult heart causes blood pressure-independent hypertrophy and cardiac dysfunction. Cardiovasc Res. 2009 Feb 15;81(3):592-600
- Alzahrani T, Pena I, Temesgen N, Glantz SA. Association between electronic cigarette use and myocardial infarction. Am J Prev Med. 2018 Oct;55(4):455-461
- Annes JP, Munger JS, Rifkin DB. Making sense of latent TGFbeta activation. J Cell Sci. 2003 Jan 15;116(Pt 2):217-24
- Askari AT, Unzek S, Popovic ZB, Goldman CK, Forudi F, Kiedrowski M, Rovner A, Ellis SG, Thomas JD, DiCorleto PE, Topol EJ, Penn MS. Effect of stromal-cell-derived factor 1 on stem-cell homing and tissue regeneration in ischaemic cardiomyopathy. Lancet. 2003 Aug 30;362(9385):697-703
- Assmus B, Schächinger V, Teupe C, Britten M, Lehmann R, Döbert N, Grünwald F, Aicher A, Urbich C, Martin H, Hoelzer D, Dimmeler S, Zeiher AM. Transplantation of progenitor cells and regeneration enhancement in acute myocardial infarction (TOPCARE-AMI). Circulation. 2002 Dec 10;106(24):3009-17
- Astorgues-Xerri L, Riveiro ME, Tijeras-Raballand A, Serova M, Neuzillet C, Albert S, Raymond E, Faivre S. Unraveling galectin-1 as a novel therapeutic target for cancer. Cancer Treat Rev. 2014 Mar;40(2):307-19
- Aurora AB, Porrello ER, Tan W, Mahmoud AI, Hill JA, Bassel-Duby R, Sadek HA, Olson EN. Macrophages are required for neonatal heart regeneration. J Clin Invest. 2014 Mar;124(3):1382-92
- Bae S, Park M, Kang C, Dilmen S, Kang TH, Kang DG, Ke Q, Lee SU, Lee D, Kang PM. Hydrogen peroxide-responsive nanoparticle reduces myocardial ischemia/reperfusion injury. J Am Heart Assoc. 2016 Nov 14;5(11)

- Banerjee MN, Bolli R, Hare JM. Clinical studies of cell therapy in cardiovascular medicine: recent developments and future directions. Circ Res. 2018 Jul 6;123(2):266-287
- Barlow SC, Doviak H, Jacobs J, Freeburg LA, Perreault PE, Zellars KN, Moreau K, Villacreses CF, Smith S, Khakoo AY, Lee T, Spinale FG. Intracoronary delivery of recombinant TIMP-3 after myocardial infarction: effects on myocardial remodeling and function. Am J Physiol Heart Circ Physiol. 2017 Oct 1;313(4):H690-H699
- Baron T, Hambraeus K, Sundström J, Erlinge D, Jernberg T, Lindahl B; TOTAL-AMI study group. Type 2 myocardial infarction in clinical practice. Heart. 2015 Jan;101(2):101-6
- Bartram U, Molin DG, Wisse LJ, Mohamad A, Sanford LP, Doetschman T, Speer CP, Poelmann RE, Gittenberger-de Groot AC. Double-outlet right ventricle and overriding tricuspid valve reflect disturbances of looping, myocardialization, endocardial cushion differentiation, and apoptosis in TGF-beta(2)-knockout mice. Circulation. 2001 Jun 5;103(22):2745-52
- Bassat E, Mutlak YE, Genzelinakh A, Shadrin IY, Baruch Umansky K, Yifa O, Kain D, Rajchman D, Leach J, Riabov Bassat D, Udi Y, Sarig R, Sagi I, Martin JF, Bursac N, Cohen S, Tzahor E. The extracellular matrix protein agrin promotes heart regeneration in mice. Nature. 2017 Jul 13;547(7662):179-184
- Bastings MM, Koudstaal S, Kieltyka RE, Nakano Y, Pape AC, Feyen DA, van Slochteren FJ, Doevendans PA, Sluijter JP, Meijer EW, Chamuleau SA, Dankers PY. A fast pH-switchable and self-healing supramolecular hydrogel carrier for guided, local catheter injection in the infarcted myocardium. Adv Healthc Mater. 2014 Jan;3(1):70-8
- Bearzi C, Rota M, Hosoda T, Tillmanns J, Nascimbene A, De Angelis A, Yasuzawa-Amano S, Trofimova I, Siggins RW, Lecapitaine N, Cascapera S, Beltrami AP, D'Alessandro DA, Zias E, Quaini F, Urbanek K, Michler RE, Bolli R, Kajstura J, Leri A, Anversa P. Human cardiac stem cells. Proc Natl Acad Sci U S A. 2007 Aug 28;104(35):14068-73
- Beauchemin M, Smith A, Yin VP. Dynamic microRNA-101a and Fosab expression controls zebrafish heart regeneration. Development. 2015 Dec 1;142(23):4026-37

- Bergmann O, Zdunek S, Felker A, Salehpour M, Alkass K, Bernard S, Sjostrom SL, Szewczykowska M, Jackowska T, Dos Remedios C, Malm T, Andrä M, Jashari R, Nyengaard JR, Possnert G, Jovinge S, Druid H, Frisén J. Dynamics of cell generation and turnover in the human heart. Cell. 2015 Jun 18;161(7):1566-75
- Bersell K, Arab S, Haring B, Kühn B. Neuregulin1/ErbB4 signaling induces cardiomyocyte proliferation and repair of heart injury. Cell. 2009 Jul 23;138(2):257-70
- Beuscher HU, Günther C, Röllinghoff M. IL-1 beta is secreted by activated murine macrophages as biologically inactive precursor. J Immunol. 1990 Mar 15;144(6):2179-83
- Bi X, Zhang G, Wang X, Nguyen C, May HI, Li X, Al-Hashimi AA, Austin RC, Gillette TG, Fu G, Wang ZV, Hill JA. Endoplasmic reticulum chaperone GRP78 protects heart from ischemia/reperfusion injury through Akt activation. Circ Res. 2018 May 25;122(11):1545-1554
- Bieberich E. Synthesis, processing, and function of N-glycans in N-glycoproteins. Adv Neurobiol. 2014;9:47-70
- Blackburn NJ, Sofrenovic T, Kuraitis D, Ahmadi A, McNeill B, Deng C, Rayner KJ, Zhong Z, Ruel M, Suuronen EJ. Timing underpins the benefits associated with injectable collagen biomaterial therapy for the treatment of myocardial infarction. Biomaterials. 2015 Jan;39:182-92
- Blanchard H, Bum-Erdene K, Bohari MH, Yu X. Galectin-1 inhibitors and their potential therapeutic applications: a patent review. Expert Opin Ther Pat. 2016 May;26(5):537-54
- Borg KT, Burgess W, Terracio L, Borg TK. Expression of metalloproteases by cardiac myocytes and fibroblasts in vitro. Cardiovasc Pathol. 1997 Sep;6(5):261-9
- Brasil S, Pascoal C, Francisco R, Marques-da-Silva D, Andreotti G, Videira PA, Morava E, Jaeken J, Dos Reis Ferreira V. CDG Therapies: From bench to bedside. Int J Mol Sci. 2018 Apr 27;19(5)
- Camper-Kirby D, Welch S, Walker A, Shiraishi I, Setchell KD, Schaefer E, Kajstura J, Anversa P, Sussman MA. Myocardial Akt activation and gender:

increased nuclear activity in females versus males. Circ Res. 2001 May 25;88(10):1020-7

- Carman CV, Springer TA. A transmigratory cup in leukocyte diapedesis both through individual vascular endothelial cells and between them. J Cell Biol. 2004 Oct 25;167(2):377-88
- Carmeliet P, Jain RK. Molecular mechanisms and clinical applications of angiogenesis. Nature. 2011 May 19;473(7347):298-307
- Cediel G, Gonzalez-Del-Hoyo M, Carrasquer A, Sanchez R, Boqué C, Bardají A. Outcomes with type 2 myocardial infarction compared with non-ischaemic myocardial injury. Heart. 2017 Apr;103(8):616-622
- Chablais F, Jaźwińska A. Induction of myocardial infarction in adult zebrafish using cryoinjury. J Vis Exp. 2012 Apr 18;(62)
- Chablais F, Veit J, Rainer G, Jaźwińska A. The zebrafish heart regenerates after cryoinjury-induced myocardial infarction. BMC Dev Biol. 2011 Apr 7;11:21
- Chagpar RB, Links PH, Pastor MC, Furber LA, Hawrysh AD, Chamberlain MD, Anderson DH. Direct positive regulation of PTEN by the p85 subunit of phosphatidylinositol 3-kinase. Proc Natl Acad Sci U S A. 2010 Mar 23;107(12):5471-6
- Chen CH, Chang MY, Wang SS, Hsieh PC. Injection of autologous bone marrow cells in hyaluronan hydrogel improves cardiac performance after infarction in pigs. Am J Physiol Heart Circ Physiol. 2014 Apr 1;306(7):H1078-86
- Chen CH, Wang SS, Wei EI, Chu TY, Hsieh PC. Hyaluronan enhances bone marrow cell therapy for myocardial repair after infarction. Mol Ther. 2013 Mar;21(3):670-9
- Chen CW, Wang LL, Zaman S, Gordon J, Arisi MF, Venkataraman CM, Chung JJ, Hung G, Gaffey AC, Spruce LA, Fazelinia H, Gorman RC, Seeholzer SH, Burdick JA, Atluri P. Sustained release of endothelial progenitor cell-derived extracellular vesicles from shear-thinning hydrogels improves angiogenesis and promotes function after myocardial infarction. Cardiovasc Res. 2018 Jun 1;114(7):1029-1040
- Chen J, Liu W, Zhang H, Lacy L, Yang X, Song SK, Wickline SA, Yu X. Regional ventricular wall thickening reflects changes in cardiac fiber and sheet

structure during contraction: quantification with diffusion tensor MRI. Am J Physiol Heart Circ Physiol. 2005 Nov;289(5):H1898-907

- Chen WC, Wang Z, Missinato MA, Park DW, Long DW, Liu HJ, Zeng X, Yates NA, Kim K, Wang Y. Decellularized zebrafish cardiac extracellular matrix induces mammalian heart regeneration. Sci Adv. 2016 Nov 18;2(11):e1600844
- Chen YL, Sun CK, Tsai TH, Chang LT, Leu S, Zhen YY, Sheu JJ, Chua S, Yeh KH, Lu HI, Chang HW, Lee FY, Yip HK. Adipose-derived mesenchymal stem cells embedded in platelet-rich fibrin scaffolds promote angiogenesis, preserve heart function, and reduce left ventricular remodeling in rat acute myocardial infarction. Am J Transl Res. 2015 May 15;7(5):781-803
- Cherepanova N, Shrimal S, Gilmore R. N-linked glycosylation and homeostasis of the endoplasmic reticulum. Curr Opin Cell Biol. 2016 Aug;41:57-65
- Chimenti I, Smith RR, Li TS, Gerstenblith G, Messina E, Giacomello A, Marbán E. Relative roles of direct regeneration versus paracrine effects of human cardiosphere-derived cells transplanted into infarcted mice. Circ Res. 2010 Mar 19;106(5):971-80
- Christina M, Angelika HL, Bernd P, Martina P. Simultaneous detection of a cell surface antigen and apoptosis by microwave-sensitized TUNEL assay on paraffin sections. J Immunol Methods. 2006 Oct 20;316(1-2):163-6
- Christman KL, Vardanian AJ, Fang Q, Sievers RE, Fok HH, Lee RJ. Injectable fibrin scaffold improves cell transplant survival, reduces infarct expansion, and induces neovasculature formation in ischemic myocardium. J Am Coll Cardiol. 2004 Aug 4;44(3):654-60
- Chu C, Bottaro DP, Betenbaugh MJ, Shiloach J. Stable ectopic expression of ST6GALNAC5 induces autocrine MET activation and anchorage-independence in MDCK Cells. PLoS One. 2016 Feb 5;11(2):e0148075
- Chung AS, Kao WJ. Fibroblasts regulate monocyte response to ECM-derived matrix: the effects on monocyte adhesion and the production of inflammatory, matrix remodeling, and growth factor proteins. J Biomed Mater Res A. 2009 Jun 15;89(4):841-53
- Colangelo AM, Finotti N, Ceriani M, Alberghina L, Martegani E, Aloe L, Lenzi L, Levi-Montalcini R. Recombinant human nerve growth factor with a marked

activity in vitro and in vivo. Proc Natl Acad Sci U S A. 2005 Dec 20;102(51):18658-63

- Collins AR, Schnee J, Wang W, Kim S, Fishbein MC, Bruemmer D, Law RE, Nicholas S, Ross RS, Hsueh WA. Osteopontin modulates angiotensin II-induced fibrosis in the intact murine heart. J Am Coll Cardiol. 2004 May 5;43(9):1698-705
- Consensus statement: Myocardial infarction redefined--a consensus document of The Joint European Society of Cardiology/American College of Cardiology Committee for the redefinition of myocardial infarction. Eur Heart J. 2000 Sep;21(18):1502-13
- Corà D, Astanina E, Giraudo E, Bussolino F. Semaphorins in cardiovascular medicine. Trends Mol Med. 2014 Oct;20(10):589-98
- Crawford J, Nygard K, Gan BS, O'Gorman DB. Periostin induces fibroblast proliferation and myofibroblast persistence in hypertrophic scarring. Exp Dermatol. 2015 Feb;24(2):120-6
- Crick F. Central dogma of molecular biology. Nature. 1970 Aug 8;227(5258):561-3
- Croci DO, Cerliani JP, Dalotto-Moreno T, Méndez-Huergo SP, Mascanfroni ID, Dergan-Dylon S, Toscano MA, Caramelo JJ, García-Vallejo JJ, Ouyang J, Mesri EA, Junttila MR, Bais C, Shipp MA, Salatino M, Rabinovich GA. Glycosylation-dependent lectin-receptor interactions preserve angiogenesis in anti-VEGF refractory tumors. Cell. 2014 Feb 13;156(4):744-58
- Cui C, Yu F, Yin S, Yang Y, Jiao Y, Cheung C, Wang X, Qi B, Liu Y, Li P, Yu W, Xiao J, Yang L. Remifentanil preconditioning attenuates hepatic ischemia-reperfusion injury in rats via neuronal activation in dorsal vagal complex. Mediators Inflamm. 2018 May 10;2018:3260256
- Cummins EP, Seeballuck F, Keely SJ, Mangan NE, Callanan JJ, Fallon PG, Taylor CT. The hydroxylase inhibitor dimethyloxalylglycine is protective in a murine model of colitis. Gastroenterology. 2008 Jan;134(1):156-65
- D'Uva G, Aharonov A, Lauriola M, Kain D, Yahalom-Ronen Y, Carvalho S, Weisinger K, Bassat E, Rajchman D, Yifa O, Lysenko M, Konfino T, Hegesh J, Brenner O, Neeman M, Yarden Y, Leor J, Sarig R, Harvey RP, Tzahor E.

ERBB2 triggers mammalian heart regeneration by promoting cardiomyocyte dedifferentiation and proliferation. Nat Cell Biol. 2015 May;17(5):627-38

- Dagres N, Hindricks G. Risk stratification after myocardial infarction: is left ventricular ejection fraction enough to prevent sudden cardiac death? Eur Heart J. 2013 Jul;34(26):1964-71
- De Mello WC, Specht P. Chronic blockade of angiotensin II AT1-receptors increased cell-to-cell communication, reduced fibrosis and improved impulse propagation in the failing heart. J Renin Angiotensin Aldosterone Syst. 2006 Dec;7(4):201-5
- DeLeon-Pennell KY, Mouton AJ, Ero OK, Ma Y, Padmanabhan Iyer R, Flynn ER, Espinoza I, Musani SK, Vasan RS, Hall ME, Fox ER, Lindsey ML. LXR/RXR signaling and neutrophil phenotype following myocardial infarction classify sex differences in remodeling. Basic Res Cardiol. 2018 Aug 21;113(5):40
- Dennis JW, Laferté S, Waghorne C, Breitman ML, Kerbel RS. Beta 1-6 branching of Asn-linked oligosaccharides is directly associated with metastasis. Science. 1987 May 1;236(4801):582-5
- Deten A, Hölzl A, Leicht M, Barth W, Zimmer HG. Changes in extracellular matrix and in transforming growth factor beta isoforms after coronary artery ligation in rats. J Mol Cell Cardiol. 2001 Jun;33(6):1191-207
- Dewald O, Zymek P, Winkelmann K, Koerting A, Ren G, Abou-Khamis T, Michael LH, Rollins BJ, Entman ML, Frangogiannis NG. CCL2/Monocyte Chemoattractant Protein-1 regulates inflammatory responses critical to healing myocardial infarcts. Circ Res. 2005 Apr 29;96(8):881-9
- Dixon JA, Gorman RC, Stroud RE, Mukherjee R, Meyer EC, Baker NL, Morita M, Hamamoto H, Ryan LP, Gorman JH 3rd, Spinale FG. Targeted regional injection of biocomposite microspheres alters post-myocardial infarction remodeling and matrix proteolytic pathways. Circulation. 2011 Sep 13;124
- Dobner S, Bezuidenhout D, Govender P, Zilla P, Davies N. A synthetic non-degradable polyethylene glycol hydrogel retards adverse post-infarct left ventricular remodeling. J Card Fail. 2009 Sep;15(7):629-36

- Doré JJ Jr, Wilkinson JE, Godkin JD. Early gestational expression of transforming growth factor beta isoforms by the ovine placenta. Biol Reprod. 1995 Jul;53(1):143-52. Erratum in: Biol Reprod 1995 Aug;53(2):475-7
- Dou MY, Wu H, Zhu HJ, Jin SY, Zhang Y, He SF. Remifentanil preconditioning protects rat cardiomyocytes against hypoxia-reoxygenation injury via δ-opioid receptor mediated activation of PI3K/Akt and ERK pathways. Eur J Pharmacol. 2016 Oct 15;789:395-401
- Dubois C, Liu X, Claus P, Marsboom G, Pokreisz P, Vandenwijngaert S, Dépelteau H, Streb W, Chaothawee L, Maes F, Gheysens O, Debyser Z, Gillijns H, Pellens M, Vandendriessche T, Chuah M, Collen D, Verbeken E, Belmans A, Van de Werf F, Bogaert J, Janssens S. Differential effects of progenitor cell populations on left ventricular remodeling and myocardial neovascularization after myocardial infarction. J Am Coll Cardiol. 2010 May 18;55(20):2232-43
- Eckhouse SR, Purcell BP, McGarvey JR, Lobb D, Logdon CB, Doviak H, O'Neill JW, Shuman JA, Novack CP, Zellars KN, Pettaway S, Black RA, Khakoo A, Lee T, Mukherjee R, Gorman JH, Gorman RC, Burdick JA, Spinale FG. Local hydrogel release of recombinant TIMP-3 attenuates adverse left ventricular remodeling after experimental myocardial infarction. Sci Transl Med. 2014 Feb 12;6(223):223ra21
- Eltzschig HK, Bratton DL, Colgan SP. Targeting hypoxia signalling for the treatment of ischaemic and inflammatory diseases. Nat Rev Drug Discov. 2014 Nov;13(11):852-69
- Eltzschig HK, Eckle T. Ischemia and reperfusion--from mechanism to translation. Nat Med. 2011 Nov 7;17(11):1391-401
- Engel FB, Hsieh PC, Lee RT, Keating MT. FGF1/p38 MAP kinase inhibitor therapy induces cardiomyocyte mitosis, reduces scarring, and rescues function after myocardial infarction. Proc Natl Acad Sci U S A. 2006 Oct 17;103(42):15546-51
- Etoh T, Joffs C, Deschamps AM, Davis J, Dowdy K, Hendrick J, Baicu S, Mukherjee R, Manhaini M, Spinale FG. Myocardial and interstitial matrix metalloproteinase activity after acute myocardial infarction in pigs. Am J Physiol Heart Circ Physiol. 2001 Sep;281(3):H987-94

- Eulalio A, Mano M, Dal Ferro M, Zentilin L, Sinagra G, Zacchigna S, Giacca M. Functional screening identifies miRNAs inducing cardiac regeneration. Nature. 2012 Dec 20;492(7429):376-81
- Falk E, Nakano M, Bentzon JF, Finn AV, Virmani R. Update on acute coronary syndromes: the pathologists' view. Eur Heart J. 2013 Mar;34(10):719-28
- Fernández-Avilés F, Sanz-Ruiz R, Bogaert J, Casado Plasencia A, Gilaberte I, Belmans A, Fernández-Santos ME, Charron D, Mulet M, Yotti R, Palacios I, Luque M, Sádaba R, San Román JA, Larman M, Sánchez PL, Sanchís J, Jiménez MF, Claus P, Al-Daccak R, Lombardo E, Abad JL, DelaRosa O, Corcóstegui L, Bermejo J, Janssens S. Safety and efficacy of intracoronary infusion of allogeneic human cardiac stem cells in patients with ST-segment elevation myocardial infarction and left ventricular dysfunction. Circ Res. 2018 Aug 17;123(5):579-589
- Ferreira IG, Pucci M, Venturi G, Malagolini N, Chiricolo M, Dall'Olio F. Glycosylation as a main regulator of growth and death factor receptors signaling. Int J Mol Sci. 2018 Feb 15;19(2)
- Finsterbusch M, Voisin MB, Beyrau M, Williams TJ, Nourshargh S. Neutrophils recruited by chemoattractants in vivo induce microvascular plasma protein leakage through secretion of TNF. J Exp Med. 2014 Jun 30;211(7):1307-14
- Fisher SA, Zhang H, Doree C, Mathur A, Martin-Rendon E. Stem cell treatment for acute myocardial infarction. Cochrane Database Syst Rev. 2015 Sep 30;(9):CD006536
- Folkman J, Haudenschild C. Angiogenesis in vitro. Nature. 1980 Dec 11;288(5791):551-6
- Foronjy RF, Sun J, Lemaitre V, D'Armiento JM. Transgenic expression of matrix metalloproteinase-1 inhibits myocardial fibrosis and prevents the transition to heart failure in a pressure overload mouse model. Hypertens Res. 2008 Apr;31(4):725-35
- Fraisl P, Aragonés J, Carmeliet P. Inhibition of oxygen sensors as a therapeutic strategy for ischaemic and inflammatory disease. Nat Rev Drug Discov. 2009 Feb;8(2):139-52
- Frangogiannis NG, Ren G, Dewald O, Zymek P, Haudek S, Koerting A, Winkelmann K, Michael LH, Lawler J, Entman ML. Critical role of endogenous

thrombospondin-1 in preventing expansion of healing myocardial infarcts. Circulation. 2005 Jun 7;111(22):2935-42

- Frangogiannis NG. Regulation of the inflammatory response in cardiac repair. Circ Res. 2012 Jan 6;110(1):159-73
- Frangogiannis NG. The extracellular matrix in myocardial injury, repair, and remodeling. J Clin Invest. 2017 May 1;127(5):1600-1612
- Frangogiannis NG. Cardiac fibrosis: Cell biological mechanisms, molecular pathways and therapeutic opportunities. Mol Aspects Med. 2019 Feb;65:70-99
- Frantz S, Nahrendorf M. Cardiac macrophages and their role in ischaemic heart disease. Cardiovasc Res. 2014 May 1;102(2):240-8
- Freeze HH, Aebi M. Molecular basis of carbohydrate-deficient glycoprotein syndromes type I with normal phosphomannomutase activity. Biochim Biophys Acta. 1999 Oct 8;1455(2-3):167-78
- Frost DC, Li L. Recent advances in mass spectrometry-based glycoproteomics. Adv Protein Chem Struct Biol. 2014;95:71-123
- Gaffey AC, Chen MH, Venkataraman CM, Trubelja A, Rodell CB, Dinh PV, Hung G, MacArthur JW, Soopan RV, Burdick JA, Atluri P. Injectable shear-thinning hydrogels used to deliver endothelial progenitor cells, enhance cell engraftment, and improve ischemic myocardium. J Thorac Cardiovasc Surg. 2015 Nov;150(5):1268-76
- Galindo CL, Kasasbeh E, Murphy A, Ryzhov S, Lenihan S, Ahmad FA, Williams P, Nunnally A, Adcock J, Song Y, Harrell FE, Tran TL, Parry TJ, Iaci J, Ganguly A, Feoktistov I, Stephenson MK, Caggiano AO, Sawyer DB, Cleator JH. Anti-remodeling and anti-fibrotic effects of the neuregulin-1β glial growth factor 2 in a large animal model of heart failure. J Am Heart Assoc. 2014 Oct 23;3(5):e000773
- Garbern JC, Minami E, Stayton PS, Murry CE. Delivery of basic fibroblast growth factor with a pH-responsive, injectable hydrogel to improve angiogenesis in infarcted myocardium. Biomaterials. 2011 Mar;32(9):2407-16
- Garcia-Garcia HM, McFadden EP, Farb A, Mehran R, Stone GW, Spertus J, Onuma Y, Morel MA, van Es GA, Zuckerman B, Fearon WF, Taggart D, Kappetein AP, Krucoff MW, Vranckx P, Windecker S, Cutlip D, Serruys PW; Academic Research Consortium. Standardized end point definitions for coronary

intervention trials: The Academic Research Consortium-2 consensus document. Circulation. 2018 Jun 12;137(24):2635-2650

- Gassmann M, Casagranda F, Orioli D, Simon H, Lai C, Klein R, Lemke G. Aberrant neural and cardiac development in mice lacking the ErbB4 neuregulin receptor. Nature. 1995 Nov 23;378(6555):390-4
- Geissmann F, Jung S, Littman DR. Blood monocytes consist of two principal subsets with distinct migratory properties. Immunity. 2003 Jul;19(1):71-82
- Gemberling M, Karra R, Dickson AL, Poss KD. Nrg1 is an injury-induced cardiomyocyte mitogen for the endogenous heart regeneration program in zebrafish. Elife. 2015 Apr 1;4
- Gerhardt H, Golding M, Fruttiger M, Ruhrberg C, Lundkvist A, Abramsson A, Jeltsch M, Mitchell C, Alitalo K, Shima D, Betsholtz C. VEGF guides angiogenic sprouting utilizing endothelial tip cell filopodia. J Cell Biol. 2003 Jun 23;161(6):1163-77
- Gerlach JQ, Sharma S, Leister KJ, Joshi L. A tight-knit group: protein glycosylation, endoplasmic reticulum stress and the unfolded protein response. In: Agostinis P, Samali A, eds. Endoplasmic reticulum stress in health and disease. 1st Edition. Dordrecht: Springer, 2012. p. 23-39
- Giglia-Mari G, Zotter A, Vermeulen W. DNA damage response. Cold Spring Harb Perspect Biol. 2011 Jan 1;3(1):a000745
- Goel HL, Mercurio AM. VEGF targets the tumour cell. Nat Rev Cancer. 2013 Dec;13(12):871-82
- Gonzalez PS, O'Prey J, Cardaci S, Barthet VJA, Sakamaki JI, Beaumatin F, Roseweir A, Gay DM, Mackay G, Malviya G, Kania E, Ritchie S, Baudot AD, Zunino B, Mrowinska A, Nixon C, Ennis D, Hoyle A, Millan D, McNeish IA, Sansom OJ, Edwards J, Ryan KM. Mannose impairs tumour growth and enhances chemotherapy. Nature. 2018 Nov;563(7733):719-723
- González-Guerra JL, Castilla-Cortazar I, Aguirre GA, Muñoz Ú, Martín-Estal I, Ávila-Gallego E, Granado M, Puche JE, García-Villalón ÁL. Partial IGF-1 deficiency is sufficient to reduce heart contractibility, angiotensin II sensibility, and alter gene expression of structural and functional cardiac proteins. PLoS One. 2017 Aug 14;12(8):e0181760

- Gourdie RG, Dimmeler S, Kohl P. Novel therapeutic strategies targeting fibroblasts and fibrosis in heart disease. Nat Rev Drug Discov. 2016 Sep;15(9):620-38
- Granovsky M, Fata J, Pawling J, Muller WJ, Khokha R, Dennis JW. Suppression of tumor growth and metastasis in Mgat5-deficient mice. Nat Med. 2000 Mar;6(3):306-12
- Groppa E, Brkic S, Bovo E, Reginato S, Sacchi V, Di Maggio N, Muraro MG, Calabrese D, Heberer M, Gianni-Barrera R, Banfi A. VEGF dose regulates vascular stabilization through Semaphorin3A and the Neuropilin-1+ monocyte/TGF-β1 paracrine axis. EMBO Mol Med. 2015 Oct;7(10):1366-84
- Groppa E, Brkic S, Uccelli A, Wirth G, Korpisalo-Pirinen P, Filippova M, Dasen B, Sacchi V, Muraro MG, Trani M, Reginato S, Gianni-Barrera R, Ylä-Herttuala S, Banfi A. EphrinB2/EphB4 signaling regulates non-sprouting angiogenesis by VEGF. EMBO Rep. 2018 May;19(5)
- Gulati A, Jabbour A, Ismail TF, Guha K, Khwaja J, Raza S, Morarji K, Brown TD, Ismail NA, Dweck MR, Di Pietro E, Roughton M, Wage R, Daryani Y, O'Hanlon R, Sheppard MN, Alpendurada F, Lyon AR, Cook SA, Cowie MR, Assomull RG, Pennell DJ, Prasad SK. Association of fibrosis with mortality and sudden cardiac death in patients with nonischemic dilated cardiomyopathy. JAMA. 2013 Mar 6;309(9):896-908
- Guo Y, Wysoczynski M, Nong Y, Tomlin A, Zhu X, Gumpert AM, Nasr M, Muthusamy S, Li H, Book M, Khan A, Hong KU, Li Q, Bolli R. Repeated doses of cardiac mesenchymal cells are therapeutically superior to a single dose in mice with old myocardial infarction. Basic Res Cardiol. 2017 Mar;112(2):18
- Gyöngyösi M, Haller PM, Blake DJ, Martin Rendon E. Meta-analysis of cell therapy studies in heart failure and acute myocardial infarction. Circ Res. 2018 Jul 6;123(2):301-308
- Hales PW, Schneider JE, Burton RA, Wright BJ, Bollensdorff C, Kohl P. Histo-anatomical structure of the living isolated rat heart in two contraction states assessed by diffusion tensor MRI. Prog Biophys Mol Biol. 2012 Oct-Nov;110(2-3):319-30

- Hao J, Ju H, Zhao S, Junaid A, Scammell-La Fleur T, Dixon IM. Elevation of expression of Smads 2, 3, and 4, decorin and TGF-beta in the chronic phase of myocardial infarct scar healing. J Mol Cell Cardiol. 1999 Mar;31(3):667-78
- Hattori N, Carrino DA, Lauer ME, Vasanji A, Wylie JD, Nelson CM, Apte SS. Pericellular versican regulates the fibroblast-myofibroblast transition: a role for ADAMTS5 protease-mediated proteolysis. J Biol Chem. 2011 Sep 30;286(39):34298-310
- Hausenloy DJ, Tsang A, Mocanu MM, Yellon DM. Ischemic preconditioning protects by activating prosurvival kinases at reperfusion. Am J Physiol Heart Circ Physiol. 2005 Feb;288(2):H971-6
- Heemskerk N, Schimmel L, Oort C, van Rijssel J, Yin T, Ma B, van Unen J, Pitter B, Huveneers S, Goedhart J, Wu Y, Montanez E, Woodfin A, van Buul JD. F-actin-rich contractile endothelial pores prevent vascular leakage during leukocyte diapedesis through local RhoA signalling. Nat Commun. 2016 Jan 27;7:10493
- Heine U, Munoz EF, Flanders KC, Ellingsworth LR, Lam HY, Thompson NL, Roberts AB, Sporn MB. Role of transforming growth factor-beta in the development of the mouse embryo. J Cell Biol. 1987 Dec;105(6 Pt 2):2861-76
- Higashikuni Y, Tanaka K, Kato M, Nureki O, Hirata Y, Nagai R, Komuro I, Sata M. Toll-like receptor-2 mediates adaptive cardiac hypertrophy in response to pressure overload through interleukin-1β upregulation via nuclear factor κB activation. J Am Heart Assoc. 2013 Nov 18;2(6):e000267
- Hoeijmakers JH. DNA damage, aging, and cancer. N Engl J Med. 2009 Oct 8;361(15):1475-85
- Hofmann M, Wollert KC, Meyer GP, Menke A, Arseniev L, Hertenstein B, Ganser A, Knapp WH, Drexler H. Monitoring of bone marrow cell homing into the infarcted human myocardium. Circulation. 2005 May 3;111(17):2198-202
- Holzmann MJ, Sartipy U. Relation between preoperative renal dysfunction and cardiovascular events (stroke, myocardial infarction, or heart failure or death) within three months of isolated coronary artery bypass grafting. Am J Cardiol. 2013 Nov 1;112(9):1342-6
- Hong KU, Guo Y, Li QH, Cao P, Al-Maqtari T, Vajravelu BN, Du J, Book MJ, Zhu X, Nong Y, Bhatnagar A, Bolli R. c-kit+ Cardiac stem cells alleviate post-

myocardial infarction left ventricular dysfunction despite poor engraftment and negligible retention in the recipient heart. PLoS One. 2014 May 7;9(5):e96725

- Hong KU, Li QH, Guo Y, Patton NS, Moktar A, Bhatnagar A, Bolli R. A highly sensitive and accurate method to quantify absolute numbers of c-kit+ cardiac stem cells following transplantation in mice. Basic Res Cardiol. 2013 May;108(3):346
- Hsieh PC, Davis ME, Gannon J, MacGillivray C, Lee RT. Controlled delivery of PDGF-BB for myocardial protection using injectable self-assembling peptide nanofibers. J Clin Invest. 2006 Jan;116(1):237-48
- Hsieh SH, Ying NW, Wu MH, Chiang WF, Hsu CL, Wong TY, Jin YT, Hong TM, Chen YL. Galectin-1, a novel ligand of neuropilin-1, activates VEGFR-2 signaling and modulates the migration of vascular endothelial cells. Oncogene. 2008 Jun 12;27(26):3746-53
- Huang GN, Thatcher JE, McAnally J, Kong Y, Qi X, Tan W, DiMaio JM, Amatruda JF, Gerard RD, Hill JA, Bassel-Duby R, Olson EN. C/EBP transcription factors mediate epicardial activation during heart development and injury. Science. 2012 Dec 21;338(6114):1599-603
- Huang NF, Dewi RE, Okogbaa J, Lee JC, Jalilrufaihah A, Heilshorn SC, Cooke JP. Chemotaxis of human induced pluripotent stem cell-derived endothelial cells. Am J Transl Res. 2013 Aug 15;5(5):510-20
- Huang NF, Yu J, Sievers R, Li S, Lee RJ. Injectable biopolymers enhance angiogenesis after myocardial infarction. Tissue Eng. 2005 Nov-Dec;11(11-12):1860-6
- Hulsmans M, Sam F, Nahrendorf M. Monocyte and macrophage contributions to cardiac remodeling. J Mol Cell Cardiol. 2016 Apr;93:149-55
- Hwang MW, Matsumori A, Furukawa Y, Ono K, Okada M, Iwasaki A, Hara M, Miyamoto T, Touma M, Sasayama S. Neutralization of interleukin-1beta in the acute phase of myocardial infarction promotes the progression of left ventricular remodeling. J Am Coll Cardiol. 2001 Nov 1;38(5):1546-53
- Ifkovits JL, Tous E, Minakawa M, Morita M, Robb JD, Koomalsingh KJ, Gorman JH 3rd, Gorman RC, Burdick JA. Injectable hydrogel properties influence infarct expansion and extent of postinfarction left ventricular

remodeling in an ovine model. Proc Natl Acad Sci U S A. 2010 Jun 22;107(25):11507-12

- InanlooRahatloo K, Parsa AF, Huse K, Rasooli P, Davaran S, Platzer M, Kramer M, Fan JB, Turk C, Amini S, Steemers F, Gunderson K, Ronaghi M, Elahi E. Mutation in ST6GALNAC5 identified in family with coronary artery disease. Sci Rep. 2014 Jan 8;4:3595
- Irwin MG, Wong GT. Remifentanil and opioid-induced cardioprotection. J Cardiothorac Vasc Anesth. 2015 Jun;29 Suppl 1:S23-6
- Iyer RP, Patterson NL, Zouein FA, Ma Y, Dive V, de Castro Brás LE, Lindsey ML. Early matrix metalloproteinase-12 inhibition worsens post-myocardial infarction cardiac dysfunction by delaying inflammation resolution. Int J Cardiol. 2015 Apr 15;185:198-208
- Jaeken J, Péanne R. What is new in CDG? J Inherit Metab Dis. 2017 Jul;40(4):569-586
- Jaeken J, Vanderschueren-Lodeweyckx M, Casaer P, Snoeck L, Corbeel L, Eggermont E, Eeckels R. Familial psychomotor retardation with markedly fluctuating serum prolactin, FSH and GH levels, partial TBG-deficiency, increased serum arylsulphatase A and increased CSF protein: a new syndrome? Pediatr Res. 1980;14:179.
- Jaleel F, Ghanghro AB, Aqil S, Qureshi MS, Ashraf T. Imbalances of pro-inflammatory cytokines in myocardial infarction patients. Pak J Pharm Sci. 2018 Sep;31(5(Supplementary)):2103-2108
- Jangaard N, Sarkisian L, Saaby L, Mikkelsen S, Lassen AM, Marcussen N, Thomsen JL, Diederichsen ACP, Thygesen K, Mickley H. Incidence, frequency, and clinical characteristics of type 3 myocardial infarction in clinical practice. Am J Med. 2017 Jul;130(7):862.e9-862.e14
- Jeevanantham V, Butler M, Saad A, Abdel-Latif A, Zuba-Surma EK, Dawn B. Adult bone marrow cell therapy improves survival and induces long-term improvement in cardiac parameters: a systematic review and meta-analysis. Circulation. 2012 Jul 31;126(5):551-68
- Jensen PH, Karlsson NG, Kolarich D, Packer NH. Structural analysis of N- and O-glycans released from glycoproteins. Nat Protoc. 2012 Jun 7;7(7):1299-310

- Johnston PV, Sasano T, Mills K, Evers R, Lee ST, Smith RR, Lardo AC, Lai S, Steenbergen C, Gerstenblith G, Lange R, Marbán E. Engraftment, differentiation, and functional benefits of autologous cardiosphere-derived cells in porcine ischemic cardiomyopathy. Circulation. 2009 Sep 22;120(12):1075-83, 7 p following 1083
- Jopling C, Sleep E, Raya M, Martí M, Raya A, Izpisúa Belmonte JC. Zebrafish heart regeneration occurs by cardiomyocyte dedifferentiation and proliferation. Nature. 2010 Mar 25;464(7288):606-9
- Jung M, Ma Y, Iyer RP, DeLeon-Pennell KY, Yabluchanskiy A, Garrett MR, Lindsey ML. IL-10 improves cardiac remodeling after myocardial infarction by stimulating M2 macrophage polarization and fibroblast activation. Basic Res Cardiol. 2017 May;112(3):33
- Kadner K, Dobner S, Franz T, Bezuidenhout D, Sirry MS, Zilla P, Davies NH. The beneficial effects of deferred delivery on the efficiency of hydrogel therapy post myocardial infarction. Biomaterials. 2012 Mar;33(7):2060-6
- Kandalam V, Basu R, Abraham T, Wang X, Awad A, Wang W, Lopaschuk GD, Maeda N, Oudit GY, Kassiri Z. Early activation of matrix metalloproteinases underlies the exacerbated systolic and diastolic dysfunction in mice lacking TIMP3 following myocardial infarction. Am J Physiol Heart Circ Physiol. 2010 Oct;299(4):H1012-23
- Kanisicak O, Khalil H, Ivey MJ, Karch J, Maliken BD, Correll RN, Brody MJ, J Lin SC, Aronow BJ, Tallquist MD, Molkentin JD. Genetic lineage tracing defines myofibroblast origin and function in the injured heart. Nat Commun. 2016 Jul 22;7:12260
- Keir G, Winchester BG, Clayton P. Carbohydrate-deficient glycoprotein syndromes: inborn errors of protein glycosylation. Ann Clin Biochem. 1999 Jan;36 (Pt 1):20-36
- Kikuchi A. Tumor formation by genetic mutations in the components of the Wnt signaling pathway. Cancer Sci. 2003 Mar;94(3):225-9
- Kikuchi K, Holdway JE, Werdich AA, Anderson RM, Fang Y, Egnaczyk GF, Evans T, Macrae CA, Stainier DY, Poss KD. Primary contribution to zebrafish heart regeneration by gata4(+) cardiomyocytes. Nature. 2010 Mar 25;464(7288):601-5

- Kim JH, Jung Y, Kim SH, Sun K, Choi J, Kim HC, Park Y, Kim SH. The enhancement of mature vessel formation and cardiac function in infarcted hearts using dual growth factor delivery with self-assembling peptides. Biomaterials. 2011 Sep;32(26):6080-8
- Kinnaird T, Stabile E, Burnett MS, Lee CW, Barr S, Fuchs S, Epstein SE. Marrow-derived stromal cells express genes encoding a broad spectrum of arteriogenic cytokines and promote in vitro and in vivo arteriogenesis through paracrine mechanisms. Circ Res. 2004 Mar 19;94(5):678-85 (Kinnaird 2004a in the text)
- Kinnaird T, Stabile E, Burnett MS, Shou M, Lee CW, Barr S, Fuchs S, Epstein SE. Local delivery of marrow-derived stromal cells augments collateral perfusion through paracrine mechanisms. Circulation. 2004 Mar 30;109(12):1543-9 (Kinnaird 2004b in the text)
- Klopsch C, Skorska A, Ludwig M, Lemcke H, Maass G, Gaebel R, Beyer M, Lux C, Toelk A, Müller K, Maschmeier C, Rohde S, Mela P, Müller-Hilke B, Jockenhoevel S, Vollmar B, Jaster R, David R, Steinhoff G. Intramyocardial angiogenetic stem cells and epicardial erythropoietin save the acute ischemic heart. Dis Model Mech. 2018 Jun 22;11(6)
- Klyachkin YM, Idris A, Rodell CB, Tripathi H, Ye S, Nagareddy P, Asfour A, Gao E, Annabathula R, Ratajczak M, Burdick JA, Abdel-Latif A. Cathelicidin related antimicrobial peptide (CRAMP) enhances bone marrow cell retention and attenuates cardiac dysfunction in a mouse model of myocardial infarction. Stem Cell Rev. 2018 Oct;14(5):702-714
- Knowlton AA, Korzick DH. Estrogen and the female heart. Mol Cell Endocrinol. 2014 May 25;389(1-2):31-9
- Konstantinidis K, Whelan RS, Kitsis RN. Mechanisms of cell death in heart disease. Arterioscler Thromb Vasc Biol. 2012 Jul;32(7):1552-62
- Kreuger J, Phillipson M. Targeting vascular and leukocyte communication in angiogenesis, inflammation and fibrosis. Nat Rev Drug Discov. 2016 Feb;15(2):125-42
- Kühn B, del Monte F, Hajjar RJ, Chang YS, Lebeche D, Arab S, Keating MT. Periostin induces proliferation of differentiated cardiomyocytes and promotes cardiac repair. Nat Med. 2007 Aug;13(8):962-9

- Kurrelmeyer KM, Michael LH, Baumgarten G, Taffet GE, Peschon JJ, Sivasubramanian N, Entman ML, Mann DL. Endogenous tumor necrosis factor protects the adult cardiac myocyte against ischemic-induced apoptosis in a murine model of acute myocardial infarction. Proc Natl Acad Sci U S A. 2000 May 9;97(10):5456-61
- Labat-Moleur F, Guillermet C, Lorimier P, Robert C, Lantuejoul S, Brambilla E, Negoescu A. TUNEL apoptotic cell detection in tissue sections: critical evaluation and improvement. J Histochem Cytochem. 1998 Mar;46(3):327-34
- Lambrecht S, Sarkisian L, Saaby L, Poulsen TS, Gerke O, Hosbond S, Diederichsen ACP, Thygesen K, Mickley H. Different causes of death in patients with myocardial infarction type 1, type 2, and myocardial injury. Am J Med. 2018 May;131(5):548-554
- Landa N, Miller L, Feinberg MS, Holbova R, Shachar M, Freeman I, Cohen S, Leor J. Effect of injectable alginate implant on cardiac remodeling and function after recent and old infarcts in rat. Circulation. 2008 Mar 18;117(11):1388-96
- Lau KS, Partridge EA, Grigorian A, Silvescu CI, Reinhold VN, Demetriou M, Dennis JW. Complex N-glycan number and degree of branching cooperate to regulate cell proliferation and differentiation. Cell. 2007 Apr 6;129(1):123-34
- Le LV, Mohindra P, Fang Q, Sievers RE, Mkrtschjan MA, Solis C, Safranek CW, Russell B, Lee RJ, Desai TA. Injectable hyaluronic acid based microrods provide local micromechanical and biochemical cues to attenuate cardiac fibrosis after myocardial infarction. Biomaterials. 2018 Jul;169:11-21
- Lee D, Park S, Bae S, Jeong D, Park M, Kang C, Yoo W, Samad MA, Ke Q, Khang G, Kang PM. Hydrogen peroxide-activatable antioxidant prodrug as a targeted therapeutic agent for ischemia-reperfusion injury. Sci Rep. 2015 Nov 13;5:16592
- Lee KF, Simon H, Chen H, Bates B, Hung MC, Hauser C. Requirement for neuregulin receptor erbB2 in neural and cardiac development. Nature. 1995 Nov 23;378(6555):394-8
- Lee RJ, Springer ML, Blanco-Bose WE, Shaw R, Ursell PC, Blau HM. VEGF gene delivery to myocardium: deleterious effects of unregulated expression. Circulation. 2000 Aug 22;102(8):898-901

- Leistner DM, Fischer-Rasokat U, Honold J, Seeger FH, Schächinger V, Lehmann R, Martin H, Burck I, Urbich C, Dimmeler S, Zeiher AM, Assmus B. Transplantation of progenitor cells and regeneration enhancement in acute myocardial infarction (TOPCARE-AMI): final 5-year results suggest long-term safety and efficacy
- Leor J, Rozen L, Zuloff-Shani A, Feinberg MS, Amsalem Y, Barbash IM, Kachel E, Holbova R, Mardor Y, Daniels D, Ocherashvilli A, Orenstein A, Danon D. Ex vivo activated human macrophages improve healing, remodeling, and function of the infarcted heart. Circulation. 2006 Jul 4;114
- Leor J, Tuvia S, Guetta V, Manczur F, Castel D, Willenz U, Petneházy O, Landa N, Feinberg MS, Konen E, Goitein O, Tsur-Gang O, Shaul M, Klapper L, Cohen S. Intracoronary injection of in situ forming alginate hydrogel reverses left ventricular remodeling after myocardial infarction in Swine. J Am Coll Cardiol. 2009 Sep 8;54(11):1014-23
- Lepilina A, Coon AN, Kikuchi K, Holdway JE, Roberts RW, Burns CG, Poss KD. A dynamic epicardial injury response supports progenitor cell activity during zebrafish heart regeneration. Cell. 2006 Nov 3;127(3):607-19
- Levi-Montalcini R. Effects of mouse tumor transplantation on the nervous system. Ann N Y Acad Sci. 1952 Aug 8;55(2):330-44
- Leyva F, Taylor RJ, Foley PW, Umar F, Mulligan LJ, Patel K, Stegemann B, Haddad T, Smith RE, Prasad SK. Left ventricular midwall fibrosis as a predictor of mortality and morbidity after cardiac resynchronization therapy in patients with nonischemic cardiomyopathy. J Am Coll Cardiol. 2012 Oct 23;60(17):1659-67
- Li P, Zheng Y, Chen X. Drugs for Autoimmune Inflammatory Diseases: From Small Molecule Compounds to Anti-TNF Biologics. Front Pharmacol. 2017 Jul 12;8:460
- Li TS, Cheng K, Malliaras K, Smith RR, Zhang Y, Sun B, Matsushita N, Blusztajn A, Terrovitis J, Kusuoka H, Marbán L, Marbán E. Direct comparison of different stem cell types and subpopulations reveals superior paracrine potency and myocardial repair efficacy with cardiosphere-derived cells. J Am Coll Cardiol. 2012 Mar 6;59(10):942-53

- Limb GA, Matter K, Murphy G, Cambrey AD, Bishop PN, Morris GE, Khaw PT. Matrix metalloproteinase-1 associates with intracellular organelles and confers resistance to lamin A/C degradation during apoptosis. Am J Pathol. 2005 May;166(5):1555-63
- Lin YD, Luo CY, Hu YN, Yeh ML, Hsueh YC, Chang MY, Tsai DC, Wang JN, Tang MJ, Wei EI, Springer ML, Hsieh PC. Instructive nanofiber scaffolds with VEGF create a microenvironment for arteriogenesis and cardiac repair. Sci Transl Med. 2012 Aug 8;4(146):146ra109
- Lindahl B, Venge P, Wallentin L. Relation between troponin T and the risk of subsequent cardiac events in unstable coronary artery disease. The FRISC study group. Circulation. 1996 May 1;93(9):1651-7
- Lindsey ML, Zamilpa R. Temporal and spatial expression of matrix metalloproteinases and tissue inhibitors of metalloproteinases following myocardial infarction. Cardiovasc Ther. 2012 Feb;30(1):31-41
- Lindsey ML. Assigning matrix metalloproteinase roles in ischaemic cardiac remodelling. Nat Rev Cardiol. 2018 Aug;15(8):471-479
- Linke A, Müller P, Nurzynska D, Casarsa C, Torella D, Nascimbene A, Castaldo C, Cascapera S, Böhm M, Quaini F, Urbanek K, Leri A, Hintze TH, Kajstura J, Anversa P. Stem cells in the dog heart are self-renewing, clonogenic, and multipotent and regenerate infarcted myocardium, improving cardiac function. Proc Natl Acad Sci U S A. 2005 Jun 21;102(25):8966-71
- Liu Z, Wang H, Wang Y, Lin Q, Yao A, Cao F, Li D, Zhou J, Duan C, Du Z, Wang Y, Wang C. The influence of chitosan hydrogel on stem cell engraftment, survival and homing in the ischemic myocardial microenvironment. Biomaterials. 2012 Apr;33(11):3093-106
- Lønborg J, Vejlstrup N, Kelbæk H, Bøtker HE, Kim WY, Mathiasen AB, Jørgensen E, Helqvist S, Saunamäki K, Clemmensen P, Holmvang L, Thuesen L, Krusell LR, Jensen JS, Køber L, Treiman M, Holst JJ, Engstrøm T. Exenatide reduces reperfusion injury in patients with ST-segment elevation myocardial infarction. Eur Heart J. 2012 Jun;33(12):1491-9
- López B, González A, Querejeta R, Larman M, Díez J. Alterations in the pattern of collagen deposition may contribute to the deterioration of systolic function in

hypertensive patients with heart failure. J Am Coll Cardiol. 2006 Jul 4;48(1):89-96

- Lyon RC, Zanella F, Omens JH, Sheikh F. Mechanotransduction in cardiac hypertrophy and failure. Circ Res. 2015 Apr 10;116(8):1462-1476
- MacArthur JW Jr, Purcell BP, Shudo Y, Cohen JE, Fairman A, Trubelja A, Patel J, Hsiao P, Yang E, Lloyd K, Hiesinger W, Atluri P, Burdick JA, Woo YJ. Sustained release of engineered stromal cell-derived factor 1-α from injectable hydrogels effectively recruits endothelial progenitor cells and preserves ventricular function after myocardial infarction. Circulation. 2013 Sep 10;128(11 Suppl 1):S79-86
- Magadum A, Singh N, Kurian AA, Sharkar MTK, Chepurko E, Zangi L. Ablation of a single N-glycosylation site in human FSTL 1 induces cardiomyocyte proliferation and cardiac regeneration. Mol Ther Nucleic Acids. 2018 Dec 7;13:133-143
- Makkar RR, Smith RR, Cheng K, Malliaras K, Thomson LE, Berman D, Czer LS, Marbán L, Mendizabal A, Johnston PV, Russell SD, Schuleri KH, Lardo AC, Gerstenblith G, Marbán E. Intracoronary cardiosphere-derived cells for heart regeneration after myocardial infarction (CADUCEUS): a prospective, randomised phase 1 trial. Lancet. 2012 Mar 10;379(9819):895-904
- Malecic N, Young HS. Novel investigational vascular endothelial growth factor (VEGF) receptor antagonists for psoriasis. Expert Opin Investig Drugs. 2016;25(4):455-62
- Malliaras K, Li TS, Luthringer D, Terrovitis J, Cheng K, Chakravarty T, Galang G, Zhang Y, Schoenhoff F, Van Eyk J, Marbán L, Marbán E. Safety and efficacy of allogeneic cell therapy in infarcted rats transplanted with mismatched cardiosphere-derived cells. Circulation. 2012 Jan 3;125(1):100-12
- Malliaras K, Makkar RR, Smith RR, Cheng K, Wu E, Bonow RO, Marbán L, Mendizabal A, Cingolani E, Johnston PV, Gerstenblith G, Schuleri KH, Lardo AC, Marbán E. Intracoronary cardiosphere-derived cells after myocardial infarction: evidence of therapeutic regeneration in the final 1-year results of the CADUCEUS trial (CArdiosphere-Derived aUtologous stem CElls to reverse ventricUlar dySfunction). J Am Coll Cardiol. 2014 Jan 21;63(2):110-22

- Markowska AI, Liu FT, Panjwani N. Galectin-3 is an important mediator of VEGF- and bFGF-mediated angiogenic response. J Exp Med. 2010 Aug 30;207(9):1981-93
- Maruyama S, Nakamura K, Papanicolaou KN, Sano S, Shimizu I, Asaumi Y, van den Hoff MJ, Ouchi N, Recchia FA, Walsh K. Follistatin-like 1 promotes cardiac fibroblast activation and protects the heart from rupture. EMBO Mol Med. 2016 Aug 1;8(8):949-66
- Masters M, Riley PR. The epicardium signals the way towards heart regeneration. Stem Cell Res. 2014 Nov;13(3 Pt B):683-92
- Mathur A, Arnold R, Assmus B, Bartunek J, Belmans A, Bönig H, Crea F, Dimmeler S, Dowlut S, Fernández-Avilés F, Galiñanes M, Garcia-Dorado D, Hartikainen J, Hill J, Hogardt-Noll A, Homsy C, Janssens S, Kala P, Kastrup J, Martin J, Menasche P, Miklik R, Mozid A, San Román JA, Sanz-Ruiz R, Tendera M, Wojakowski W, Ylä-Herttuala S, Zeiher A. The effect of intracoronary infusion of bone marrow-derived mononuclear cells on all-cause mortality in acute myocardial infarction: rationale and design of the BAMI trial. Eur J Heart Fail. 2017 Nov;19(11):1545-1550
- Matsumura S, Iwanaga S, Mochizuki S, Okamoto H, Ogawa S, Okada Y. Targeted deletion or pharmacological inhibition of MMP-2 prevents cardiac rupture after myocardial infarction in mice. J Clin Invest. 2005 Mar;115(3):599-609
- McArthur JC, Yiannoutsos C, Simpson DM, Adornato BT, Singer EJ, Hollander H, Marra C, Rubin M, Cohen BA, Tucker T, Navia BA, Schifitto G, Katzenstein D, Rask C, Zaborski L, Smith ME, Shriver S, Millar L, Clifford DB, Karalnik IJ. A phase II trial of nerve growth factor for sensory neuropathy associated with HIV infection. AIDS Clinical Trials Group Team 291. Neurology. 2000 Mar 14;54(5):1080-8
- McGinn AN, Nam HY, Ou M, Hu N, Straub CM, Yockman JW, Bull DA, Kim SW. Bioreducible polymer-transfected skeletal myoblasts for VEGF delivery to acutely ischemic myocardium. Biomaterials. 2011 Jan;32(3):942-9
- Meda C, Molla F, De Pizzol M, Regano D, Maione F, Capano S, Locati M, Mantovani A, Latini R, Bussolino F, Giraudo E. Semaphorin 4A exerts a

proangiogenic effect by enhancing vascular endothelial growth factor-A expression in macrophages. J Immunol. 2012 Apr 15;188(8):4081-92

- Mehran R, Pocock S, Nikolsky E, Dangas GD, Clayton T, Claessen BE, Caixeta A, Feit F, Manoukian SV, White H, Bertrand M, Ohman EM, Parise H, Lansky AJ, Lincoff AM, Stone GW. Impact of bleeding on mortality after percutaneous coronary intervention results from a patient-level pooled analysis of the REPLACE-2 (randomized evaluation of PCI linking angiomax to reduced clinical events), ACUITY (acute catheterization and urgent intervention triage strategy), and HORIZONS-AMI (harmonizing outcomes with revascularization and stents in acute myocardial infarction) trials. JACC Cardiovasc Interv. 2011 Jun;4(6):654-64
- Meister-Broekema M, Freilich R, Jagadeesan C, Rauch JN, Bengoechea R, Motley WW, Kuiper EFE, Minoia M, Furtado GV, van Waarde MAWH, Bird SJ, Rebelo A, Zuchner S, Pytel P, Scherer SS, Morelli FF, Carra S, Weihl CC, Bergink S, Gestwicki JE, Kampinga HH. Myopathy associated BAG3 mutations lead to protein aggregation by stalling Hsp70 networks. Nat Commun. 2018 Dec 17;9(1):5342
- Merlin J, Stechly L, de Beaucé S, Monté D, Leteurtre E, van Seuningen I, Huet G, Pigny P. Galectin-3 regulates MUC1 and EGFR cellular distribution and EGFR downstream pathways in pancreatic cancer cells. Oncogene. 2011 Jun 2;30(22):2514-25
- Meyer D, Birchmeier C. Multiple essential functions of neuregulin in development. Nature. 1995 Nov 23;378(6555):386-90.
- Mezzaroma E, Mikkelsen RB, Toldo S, Mauro AG, Sharma K, Marchetti C, Alam A, Van Tassell BW, Gewirtz DA, Abbate A. Role of interleukin-1 in radiation-induced cardiomyopathy. Mol Med. 2015 Mar 26;21:210-8
- Mithieux SM, Wise SG, Weiss AS. Tropoelastin--a multifaceted naturally smart material. Adv Drug Deliv Rev. 2013 Apr;65(4):421-8
- Mittleman MA, Siscovick DS. Physical exertion as a trigger of myocardial infarction and sudden cardiac death. Cardiol Clin. 1996 May;14(2):263-70
- Miyamoto S, Purcell NH, Smith JM, Gao T, Whittaker R, Huang K, Castillo R, Glembotski CC, Sussman MA, Newton AC, Brown JH. PHLPP-1 negatively

regulates Akt activity and survival in the heart. Circ Res. 2010 Aug 20;107(4):476-84

- Moc C, Taylor AE, Chesini GP, Zambrano CM, Barlow MS, Zhang X, Gustafsson ÅB, Purcell NH. Physiological activation of Akt by PHLPP1 deletion protects against pathological hypertrophy. Cardiovasc Res. 2015 Feb 1;105(2):160-70
- Mohd Isa IL, Abbah SA, Kilcoyne M, Sakai D, Dockery P, Finn DP, Pandit A. Implantation of hyaluronic acid hydrogel prevents the pain phenotype in a rat model of intervertebral disc injury. Sci Adv. 2018 Apr 4;4(4):eaaq0597
- Monticelli M, Ferro T, Jaeken J, Dos Reis Ferreira V, Videira PA. Immunological aspects of congenital disorders of glycosylation (CDG): a review. J Inherit Metab Dis. 2016 Nov;39(6):765-780
- Morimoto H, Takahashi M, Shiba Y, Izawa A, Ise H, Hongo M, Hatake K, Motoyoshi K, Ikeda U. Bone marrow-derived CXCR4+ cells mobilized by macrophage colony-stimulating factor participate in the reduction of infarct area and improvement of cardiac remodeling after myocardial infarction in mice. Am J Pathol. 2007 Sep;171(3):755-66
- Mozaffarian D, Benjamin EJ, Go AS, Arnett DK, Blaha MJ, Cushman M, Das SR, de Ferranti S, Després JP, Fullerton HJ, Howard VJ, Huffman MD, Isasi CR, Jiménez MC, Judd SE, Kissela BM, Lichtman JH, Lisabeth LD, Liu S, Mackey RH, Magid DJ, McGuire DK, Mohler ER 3rd, Moy CS, Muntner P, Mussolino ME, Nasir K, Neumar RW, Nichol G, Palaniappan L, Pandey DK, Reeves MJ, Rodriguez CJ, Rosamond W, Sorlie PD, Stein J, Towfighi A, Turan TN, Virani SS, Woo D, Yeh RW, Turner MB; American Heart Association Statistics Committee; Stroke Statistics Subcommittee. Executive summary: Heart disease and stroke statistics--2016 update: A report from the American Heart Association. Circulation. 2016 Jan 26;133(4):447-54
- Mozaffarian D, Micha R, Wallace S. Effects on coronary heart disease of increasing polyunsaturated fat in place of saturated fat: a systematic review and meta-analysis of randomized controlled trials. PLoS Med. 2010 Mar 23;7(3):e1000252
- Mukherjee R, Zavadzkas JA, Saunders SM, McLean JE, Jeffords LB, Beck C, Stroud RE, Leone AM, Koval CN, Rivers WT, Basu S, Sheehy A, Michal G,

Spinale FG. Targeted myocardial microinjections of a biocomposite material reduces infarct expansion in pigs. Ann Thorac Surg. 2008 Oct;86(4):1268-76

- Mukkamala L, Bhagat N, Zarbin M. Practical lessons from protocol T for the management of diabetic macular edema. Dev Ophthalmol. 2017;60:109-124
- Murphy MP, Hartley RC. Mitochondria as a therapeutic target for common pathologies. Nat Rev Drug Discov. 2018 Nov 5
- Murry CE, Jennings RB, Reimer KA. Preconditioning with ischemia: a delay of lethal cell injury in ischemic myocardium. Circulation. 1986 Nov;74(5):1124-36
- Najjar SS, Rao SV, Melloni C, Raman SV, Povsic TJ, Melton L, Barsness GW, Prather K, Heitner JF, Kilaru R, Gruberg L, Hasselblad V, Greenbaum AB, Patel M, Kim RJ, Talan M, Ferrucci L, Longo DL, Lakatta EG, Harrington RA; REVEAL Investigators. Intravenous erythropoietin in patients with ST-segment elevation myocardial infarction: REVEAL: a randomized controlled trial. JAMA. 2011 May 11;305(18):1863-72
- Nakada Y, Canseco DC, Thet S, Abdisalaam S, Asaithamby A, Santos CX, Shah AM, Zhang H, Faber JE, Kinter MT, Szweda LI, Xing C, Hu Z, Deberardinis RJ, Schiattarella G, Hill JA, Oz O, Lu Z, Zhang CC, Kimura W, Sadek HA. Hypoxia induces heart regeneration in adult mice. Nature. 2017 Jan 12;541(7636):222-227
- Nakajima K, Fujita J, Matsui M, Tohyama S, Tamura N, Kanazawa H, Seki T, Kishino Y, Hirano A, Okada M, Tabei R, Sano M, Goto S, Tabata Y, Fukuda K. Gelatin hydrogel enhances the engraftment of transplanted cardiomyocytes and angiogenesis to ameliorate cardiac function after myocardial infarction. PLoS One. 2015 Jul 17;10(7):e0133308
- Nelson DM, Hashizume R, Yoshizumi T, Blakney AK, Ma Z, Wagner WR. Intramyocardial injection of a synthetic hydrogel with delivery of bFGF and IGF1 in a rat model of ischemic cardiomyopathy. Biomacromolecules. 2014 Jan 13;15(1):1-11
- Newby AC. Metalloproteinases promote plaque rupture and myocardial infarction: A persuasive concept waiting for clinical translation. Matrix Biol. 2015 May-Jul;44-46:157-66
- O'Neill HS, Gallagher LB, O'Sullivan J, Whyte W, Curley C, Dolan E, Hameed A, O'Dwyer J, Payne C, O'Reilly D, Ruiz-Hernandez E, Roche ET, O'Brien FJ, Cryan SA, Kelly H, Murphy B, Duffy GP. Biomaterial-enhanced cell and drug

delivery: Lessons learned in the cardiac field and future perspectives. Adv Mater. 2016 Jul;28(27):5648-61

- Ohman EM, Armstrong PW, Christenson RH, Granger CB, Katus HA, Hamm CW, O'Hanesian MA, Wagner GS, Kleiman NS, Harrell FE Jr, Califf RM, Topol EJ. Cardiac troponin T levels for risk stratification in acute myocardial ischemia. GUSTO IIA Investigators. N Engl J Med. 1996 Oct 31;335(18):1333-41
- Oikawa FTC, Hueb W, Nomura CH, Hueb AC, Villa AV, da Costa LMA, de Melo RMV, Rezende PC, Segre CAW, Garzillo CL, Lima EG, Ramires JAF, Filho RK. Abnormal elevation of myocardial necrosis biomarkers after coronary artery bypass grafting without established myocardial infarction assessed by cardiac magnetic resonance. J Cardiothorac Surg. 2017 Dec 29;12(1):122
- Oka T, Akazawa H, Naito AT, Komuro I. Angiogenesis and cardiac hypertrophy: maintenance of cardiac function and causative roles in heart failure. Circ Res. 2014 Jan 31;114(3):565-71
- Oka T, Xu J, Kaiser RA, Melendez J, Hambleton M, Sargent MA, Lorts A, Brunskill EW, Dorn GW 2nd, Conway SJ, Aronow BJ, Robbins J, Molkentin JD. Genetic manipulation of periostin expression reveals a role in cardiac hypertrophy and ventricular remodeling. Circ Res. 2007 Aug 3;101(3):313-21
- Okada M, Payne TR, Oshima H, Momoi N, Tobita K, Huard J. Differential efficacy of gels derived from small intestinal submucosa as an injectable biomaterial for myocardial infarct repair. Biomaterials. 2010 Oct;31(30):7678-83
- Orlic D, Kajstura J, Chimenti S, Jakoniuk I, Anderson SM, Li B, Pickel J, McKay R, Nadal-Ginard B, Bodine DM, Leri A, Anversa P. Bone marrow cells regenerate infarcted myocardium. Nature. 2001 Apr 5;410(6829):701-5
- Park S, Yoon J, Bae S, Park M, Kang C, Ke Q, Lee D, Kang PM. Therapeutic use of H2O2-responsive anti-oxidant polymer nanoparticles for doxorubicin-induced cardiomyopathy. Biomaterials. 2014 Jul;35(22):5944-53
- Pasumarthi KB, Field LJ. Cardiomyocyte cell cycle regulation. Circ Res. 2002 May 31;90(10):1044-54
- Paszek MJ, DuFort CC, Rossier O, Bainer R, Mouw JK, Godula K, Hudak JE, Lakins JN, Wijekoon AC, Cassereau L, Rubashkin MG, Magbanua MJ, Thorn KS, Davidson MW, Rugo HS, Park JW, Hammer DA, Giannone G, Bertozzi CR,

Weaver VM. The cancer glycocalyx mechanically primes integrin-mediated growth and survival. Nature. 2014 Jul 17;511(7509):319-25

- Perin EC, Willerson JT, Pepine CJ, Henry TD, Ellis SG, Zhao DX, Silva GV, Lai D, Thomas JD, Kronenberg MW, Martin AD, Anderson RD, Traverse JH, Penn MS, Anwaruddin S, Hatzopoulos AK, Gee AP, Taylor DA, Cogle CR, Smith D, Westbrook L, Chen J, Handberg E, Olson RE, Geither C, Bowman S, Francescon J, Baraniuk S, Piller LB, Simpson LM, Loghin C, Aguilar D, Richman S, Zierold C, Bettencourt J, Sayre SL, Vojvodic RW, Skarlatos SI, Gordon DJ, Ebert RF, Kwak M, Moyé LA, Simari RD; Cardiovascular Cell Therapy Research Network (CCTRN). Effect of transendocardial delivery of autologous bone marrow mononuclear cells on functional capacity, left ventricular function, and perfusion in chronic heart failure: the FOCUS-CCTRN trial. JAMA. 2012 Apr 25;307(16):1717-26
- Peters V, Penzien JM, Reiter G, Körner C, Hackler R, Assmann B, Fang J, Schaefer JR, Hoffmann GF, Heidemann PH. Congenital disorder of glycosylation IId (CDG-IId) -- a new entity: clinical presentation with Dandy-Walker malformation and myopathy. Neuropediatrics. 2002 Feb;33(1):27-32
- Pinho SS, Reis CA. Glycosylation in cancer: mechanisms and clinical implications. Nat Rev Cancer. 2015 Sep;15(9):540-55
- Piot CA, Padmanaban D, Ursell PC, Sievers RE, Wolfe CL. Ischemic preconditioning decreases apoptosis in rat hearts in vivo. Circulation. 1997 Sep 2;96(5):1598-604
- Porrello ER, Mahmoud AI, Simpson E, Hill JA, Richardson JA, Olson EN, Sadek HA. Transient regenerative potential of the neonatal mouse heart. Science. 2011 Feb 25;331(6020):1078-80
- Poss KD, Wilson LG, Keating MT. Heart regeneration in zebrafish. Science. 2002 Dec 13;298(5601):2188-90
- Prunier C, Pessah M, Ferrand N, Seo SR, Howe P, Atfi A. The oncoprotein Ski acts as an antagonist of transforming growth factor-beta signaling by suppressing Smad2 phosphorylation. J Biol Chem. 2003 Jul 11;278(28):26249-57
- Purcell BP, Barlow SC, Perreault PE, Freeburg L, Doviak H, Jacobs J, Hoenes A, Zellars KN, Khakoo AY, Lee T, Burdick JA, Spinale FG. Delivery of a matrix metalloproteinase-responsive hydrogel releasing TIMP-3 after myocardial

infarction: effects on left ventricular remodeling. Am J Physiol Heart Circ Physiol. 2018 Oct 1;315(4):H814-H825

- Qin Z, Barthel LK, Raymond PA. Genetic evidence for shared mechanisms of epimorphic regeneration in zebrafish. Proc Natl Acad Sci U S A. 2009 Jun 9;106(23):9310-5
- Radisic M, Christman KL. Materials science and tissue engineering: repairing the heart. Mayo Clin Proc. 2013 Aug;88(8):884-98
- Ramsden CE, Zamora D, Majchrzak-Hong S, Faurot KR, Broste SK, Frantz RP, Davis JM, Ringel A, Suchindran CM, Hibbeln JR. Re-evaluation of the traditional diet-heart hypothesis: analysis of recovered data from Minnesota Coronary Experiment (1968-73). BMJ. 2016 Apr 12;353:i1246
- Rane AA, Chuang JS, Shah A, Hu DP, Dalton ND, Gu Y, Peterson KL, Omens JH, Christman KL. Increased infarct wall thickness by a bio-inert material is insufficient to prevent negative left ventricular remodeling after myocardial infarction. PLoS One. 2011;6(6):e21571
- Reuter S, Soonpaa MH, Firulli AB, Chang AN, Field LJ. Recombinant neuregulin 1 does not activate cardiomyocyte DNA synthesis in normal or infarcted adult mice. PLoS One. 2014 Dec 29;9(12):e115871
- Roberts DJ, Tan-Sah VP, Smith JM, Miyamoto S. Akt phosphorylates HK-II at Thr-473 and increases mitochondrial HK-II association to protect cardiomyocytes. J Biol Chem. 2013 Aug 16;288(33):23798-806
- Robinson A, Keely S, Karhausen J, Gerich ME, Furuta GT, Colgan SP. Mucosal protection by hypoxia-inducible factor prolyl hydroxylase inhibition. Gastroenterology. 2008 Jan;134(1):145-55
- Rodríguez-Pascual F, Busnadiego O, González-Santamaría J. The profibrotic role of endothelin-1: is the door still open for the treatment of fibrotic diseases? Life Sci. 2014 Nov 24;118(2):156-64
- Roth GA, Johnson C, Abajobir A, Abd-Allah F, Abera SF, Abyu G, Ahmed M, Aksut B, Alam T, Alam K, Alla F, Alvis-Guzman N, Amrock S, Ansari H, Ärnlöv J, Asayesh H, Atey TM, Avila-Burgos L, Awasthi A, Banerjee A, Barac A, Bärnighausen T *et al.*, Global, regional, and national burden of cardiovascular diseases for 10 causes, 1990 to 2015. J Am Coll Cardiol. 2017 Jul 4;70(1):1-25

- Ruhrberg C, Gerhardt H, Golding M, Watson R, Ioannidou S, Fujisawa H, Betsholtz C, Shima DT. Spatially restricted patterning cues provided by heparin-binding VEGF-A control blood vessel branching morphogenesis. Genes Dev. 2002 Oct 15;16(20):2684-98
- Ruvinov E, Leor J, Cohen S. The promotion of myocardial repair by the sequential delivery of IGF-1 and HGF from an injectable alginate biomaterial in a model of acute myocardial infarction. Biomaterials. 2011 Jan;32(2):565-78
- Sandoval Y, Thordsen SE, Smith SW, Schulz KM, Murakami MM, Pearce LA, Apple FS. Cardiac troponin changes to distinguish type 1 and type 2 myocardial infarction and 180-day mortality risk. Eur Heart J Acute Cardiovasc Care. 2014 Dec;3(4):317-25
- Sanz-Ruiz R, Casado Plasencia A, Borlado LR, Fernández-Santos ME, Al-Daccak R, Claus P, Palacios I, Sádaba R, Charron D, Bogaert J, Mulet M, Yotti R, Gilaberte I, Bernad A, Bermejo J, Janssens S, Fernández-Avilés F. Rationale and design of a clinical trial to evaluate the safety and efficacy of intracoronary infusion of allogeneic human cardiac stem cells in patients with acute myocardial infarction and left ventricular dysfunction: The randomized multicenter double-blind controlled CAREMI trial (Cardiac Stem Cells in Patients With Acute Myocardial Infarction). Circ Res. 2017 Jun 23;121(1):71-80
- Saraste A, Pulkki K, Kallajoki M, Henriksen K, Parvinen M, Voipio-Pulkki LM. Apoptosis in human acute myocardial infarction. Circulation. 1997 Jan 21;95(2):320-3
- Satoh S, Daigo Y, Furukawa Y, Kato T, Miwa N, Nishiwaki T, Kawasoe T, Ishiguro H, Fujita M, Tokino T, Sasaki Y, Imaoka S, Murata M, Shimano T, Yamaoka Y, Nakamura Y. AXIN1 mutations in hepatocellular carcinomas, and growth suppression in cancer cells by virus-mediated transfer of AXIN1. Nat Genet. 2000 Mar;24(3):245-50
- Schächinger V, Assmus B, Britten MB, Honold J, Lehmann R, Teupe C, Abolmaali ND, Vogl TJ, Hofmann WK, Martin H, Dimmeler S, Zeiher AM. Transplantation of progenitor cells and regeneration enhancement in acute myocardial infarction: final one-year results of the TOPCARE-AMI Trial. J Am Coll Cardiol. 2004 Oct 19;44(8):1690-9

- Schächinger V, Erbs S, Elsässer A, Haberbosch W, Hambrecht R, Hölschermann H, Yu J, Corti R, Mathey DG, Hamm CW, Süselbeck T, Assmus B, Tonn T, Dimmeler S, Zeiher AM; REPAIR-AMI Investigators. Intracoronary bone marrow-derived progenitor cells in acute myocardial infarction. N Engl J Med. 2006 Sep 21;355(12):1210-21 (Schächinger 2006a in the text)
- Schächinger V, Erbs S, Elsässer A, Haberbosch W, Hambrecht R, Hölschermann H, Yu J, Corti R, Mathey DG, Hamm CW, Süselbeck T, Werner N, Haase J, Neuzner J, Germing A, Mark B, Assmus B, Tonn T, Dimmeler S, Zeiher AM; REPAIR-AMI Investigators. Improved clinical outcome after intracoronary administration of bone-marrow-derived progenitor cells in acute myocardial infarction: final 1-year results of the REPAIR-AMI trial. Eur Heart J. 2006 Dec;27(23):2775-83 (Schächinger 2006b in the text)
- Schenkel AR, Mamdouh Z, Muller WA. Locomotion of monocytes on endothelium is a critical step during extravasation. Nat Immunol. 2004 Apr;5(4):393-400
- Schimmel L, Heemskerk N, van Buul JD. Leukocyte transendothelial migration: A local affair. Small GTPases. 2017 Jan 2;8(1):1-15
- Schwarz ER, Speakman MT, Patterson M, Hale SS, Isner JM, Kedes LH, Kloner RA. Evaluation of the effects of intramyocardial injection of DNA expressing vascular endothelial growth factor (VEGF) in a myocardial infarction model in the rat--angiogenesis and angioma formation. J Am Coll Cardiol. 2000 Apr;35(5):1323-30
- Seif-Naraghi SB, Singelyn JM, Salvatore MA, Osborn KG, Wang JJ, Sampat U, Kwan OL, Strachan GM, Wong J, Schup-Magoffin PJ, Braden RL, Bartels K, DeQuach JA, Preul M, Kinsey AM, DeMaria AN, Dib N, Christman KL. Safety and efficacy of an injectable extracellular matrix hydrogel for treating myocardial infarction. Sci Transl Med. 2013 Feb 20;5(173):173ra25
- Semenza GL. Regulation of oxygen homeostasis by hypoxia-inducible factor 1. Physiology (Bethesda). 2009 Apr;24:97-106
- Senyo SE, Steinhauser ML, Pizzimenti CL, Yang VK, Cai L, Wang M, Wu TD, Guerquin-Kern JL, Lechene CP, Lee RT. Mammalian heart renewal by pre-existing cardiomyocytes. Nature. 2013 Jan 17;493(7432):433-6

- Serneri GG, Boddi M, Cecioni I, Vanni S, Coppo M, Papa ML, Bandinelli B, Bertolozzi I, Polidori G, Toscano T, Maccherini M, Modesti PA. Cardiac angiotensin II formation in the clinical course of heart failure and its relationship with left ventricular function. Circ Res. 2001 May 11;88(9):961-8
- Serneri GG, Modesti PA, Boddi M, Cecioni I, Paniccia R, Coppo M, Galanti G, Simonetti I, Vanni S, Papa L, Bandinelli B, Migliorini A, Modesti A, Maccherini M, Sani G, Toscano M. Cardiac growth factors in human hypertrophy. Relations with myocardial contractility and wall stress. Circ Res. 1999 Jul 9;85(1):57-67
- Shen H, Cui G, Li Y, Ye W, Sun Y, Zhang Z, Li J, Xu G, Zeng X, Zhang Y, Zhang W, Huang Z, Chen W, Shen Z. Follistatin-like 1 protects mesenchymal stem cells from hypoxic damage and enhances their therapeutic efficacy in a mouse myocardial infarction model. Stem Cell Res Ther. 2019 Jan 11;10(1):17
- Shen JT, Li YS, Xia ZQ, Wen SH, Yao X, Yang WJ, Li C, Liu KX. Remifentanil preconditioning protects the small intestine against ischemia/reperfusion injury via intestinal δ- and μ-opioid receptors. Surgery. 2016 Feb;159(2):548-59
- Shimano M, Ouchi N, Nakamura K, van Wijk B, Ohashi K, Asaumi Y, Higuchi A, Pimentel DR, Sam F, Murohara T, van den Hoff MJ, Walsh K. Cardiac myocyte follistatin-like 1 functions to attenuate hypertrophy following pressure overload. Proc Natl Acad Sci U S A. 2011 Oct 25;108(43):E899-906
- Shiojima I, Sato K, Izumiya Y, Schiekofer S, Ito M, Liao R, Colucci WS, Walsh K. Disruption of coordinated cardiac hypertrophy and angiogenesis contributes to the transition to heart failure. J Clin Invest. 2005 Aug;115(8):2108-18
- Shu Y, Hao T, Yao F, Qian Y, Wang Y, Yang B, Li J, Wang C. RoY peptide-modified chitosan-based hydrogel to improve angiogenesis and cardiac repair under hypoxia. ACS Appl Mater Interfaces. 2015 Apr 1;7(12):6505-17
- Singelyn JM, Sundaramurthy P, Johnson TD, Schup-Magoffin PJ, Hu DP, Faulk DM, Wang J, Mayle KM, Bartels K, Salvatore M, Kinsey AM, Demaria AN, Dib N, Christman KL. Catheter-deliverable hydrogel derived from decellularized ventricular extracellular matrix increases endogenous cardiomyocytes and preserves cardiac function post-myocardial infarction. J Am Coll Cardiol. 2012 Feb 21;59(8):751-63
- Smilowitz NR, Subramanyam P, Gianos E, Reynolds HR, Shah B, Sedlis SP. Treatment and outcomes of type 2 myocardial infarction and myocardial injury

compared with type 1 myocardial infarction. Coron Artery Dis. 2018 Jan;29(1):46-52

- Sonnenberg SB, Rane AA, Liu CJ, Rao N, Agmon G, Suarez S, Wang R, Munoz A, Bajaj V, Zhang S, Braden R, Schup-Magoffin PJ, Kwan OL, DeMaria AN, Cochran JR, Christman KL. Delivery of an engineered HGF fragment in an extracellular matrix-derived hydrogel prevents negative LV remodeling post-myocardial infarction. Biomaterials. 2015 Mar;45:56-63
- Sriramula S, Francis J. Tumor necrosis factor - alpha is essential for angiotensin II-induced ventricular remodeling: role for oxidative stress. PloS One. 2015 Sep 17;10(9):e0138372
- Stuttfeld E, Ballmer-Hofer K. Structure and function of VEGF receptors. IUBMB Life. 2009 Sep;61(9):915-22
- Su CC, Yang JY, Leu HB, Chen Y, Wang PH. Mitochondrial Akt-regulated mitochondrial apoptosis signaling in cardiac muscle cells. Am J Physiol Heart Circ Physiol. 2012 Feb 1;302(3):H716-23
- Sultana N, Zhang L, Yan J, Chen J, Cai W, Razzaque S, Jeong D, Sheng W, Bu L, Xu M, Huang GY, Hajjar RJ, Zhou B, Moon A, Cai CL. Resident c-kit(+) cells in the heart are not cardiac stem cells. Nat Commun. 2015 Oct 30;6:8701
- Sürder D, Manka R, Moccetti T, Lo Cicero V, Emmert MY, Klersy C, Soncin S, Turchetto L, Radrizzani M, Zuber M, Windecker S, Moschovitis A, Bühler I, Kozerke S, Erne P, Lüscher TF, Corti R. Effect of bone marrow-derived mononuclear cell treatment, early or late after acute myocardial infarction: twelve months CMR and long-term clinical results. Circ Res. 2016 Jul 22;119(3):481-90
- Suzuki K, Murtuza B, Smolenski RT, Sammut IA, Suzuki N, Kaneda Y, Yacoub MH. Cell transplantation for the treatment of acute myocardial infarction using vascular endothelial growth factor-expressing skeletal myoblasts. Circulation. 2001 Sep 18;104(12 Suppl 1):I207-12
- Tachibana K, Hirota S, Iizasa H, Yoshida H, Kawabata K, Kataoka Y, Kitamura Y, Matsushima K, Yoshida N, Nishikawa S, Kishimoto T, Nagasawa T. The chemokine receptor CXCR4 is essential for vascularization of the gastrointestinal tract. Nature. 1998 Jun 11;393(6685):591-4

- Takehara N, Tsutsumi Y, Tateishi K, Ogata T, Tanaka H, Ueyama T, Takahashi T, Takamatsu T, Fukushima M, Komeda M, Yamagishi M, Yaku H, Tabata Y, Matsubara H, Oh H. Controlled delivery of basic fibroblast growth factor promotes human cardiosphere-derived cell engraftment to enhance cardiac repair for chronic myocardial infarction. J Am Coll Cardiol. 2008 Dec 2;52(23):1858-1865
- Tanaka K, Valero-Muñoz M, Wilson RM, Essick EE, Fowler CT, Nakamura K, van den Hoff M, Ouchi N, Sam F. Follistatin like 1 regulates hypertrophy in heart failure with preserved ejection fraction. JACC Basic Transl Sci. 2016 Jun;1(4):207-221
- Taniyama Y, Ito M, Sato K, Kuester C, Veit K, Tremp G, Liao R, Colucci WS, Ivashchenko Y, Walsh K, Shiojima I. Akt3 overexpression in the heart results in progression from adaptive to maladaptive hypertrophy. J Mol Cell Cardiol. 2005 Feb;38(2):375-85
- Tham YK, Bernardo BC, Ooi JY, Weeks KL, McMullen JR. Pathophysiology of cardiac hypertrophy and heart failure: signaling pathways and novel therapeutic targets. Arch Toxicol. 2015 Sep;89(9):1401-38
- Thompson NL, Flanders KC, Smith JM, Ellingsworth LR, Roberts AB, Sporn MB. Expression of transforming growth factor-beta 1 in specific cells and tissues of adult and neonatal mice. J Cell Biol. 1989 Feb;108(2):661-9
- Thygesen K, Alpert JS, Jaffe AS, Chaitman BR, Bax JJ, Morrow DA, White HD; Executive Group on behalf of the Joint European Society of Cardiology (ESC)/American College of Cardiology (ACC)/American Heart Association (AHA)/World Heart Federation (WHF) Task Force for the Universal Definition of Myocardial Infarction. Fourth universal definition of myocardial infarction (2018). Circulation. 2018 Nov 13;138(20):e618-e651
- Thygesen K, Alpert JS, Jaffe AS, Simoons ML, Chaitman BR and White HD: the Writing Group on behalf of the Joint ESC/ACCF/AHA/WHF Task Force for the Universal Definition of Myocardial Infarction. Third universal definition of myocardial infarction. J Am Coll Cardiol. 2012 October 16, 2012:1581–98
- Thygesen K, Alpert JS, White HD, Joint ESC/ACCF/AHA/WHF Task Force for the Redefinition of Myocardial Infarction. Universal definition of myocardial

infarction. Eur Heart J 2007;28:2525–38; Circulation 2007;116:2634 –53; J Am Coll Cardiol 2007;50:2173–95

- Tokita Y, Tang XL, Li Q, Wysoczynski M, Hong KU, Nakamura S, Wu WJ, Xie W, Li D, Hunt G, Ou Q, Stowers H, Bolli R. Repeated administrations of cardiac progenitor cells are markedly more effective than a single administration: A new paradigm in cell therapy. Circ Res. 2016 Aug 19;119(5):635-51
- Tong H, Chen W, Steenbergen C, Murphy E. Ischemic preconditioning activates phosphatidylinositol-3-kinase upstream of protein kinase C. Circ Res. 2000 Aug 18;87(4):309-15
- Tous E, Ifkovits JL, Koomalsingh KJ, Shuto T, Soeda T, Kondo N, Gorman JH 3rd, Gorman RC, Burdick JA. Influence of injectable hyaluronic acid hydrogel degradation behavior on infarction-induced ventricular remodeling. Biomacromolecules. 2011 Nov 14;12(11):4127-35
- Traverse JH, Henry TD, Pepine CJ, Willerson JT, Zhao DX, Ellis SG, Forder JR, Anderson RD, Hatzopoulos AK, Penn MS, Perin EC, Chambers J, Baran KW, Raveendran G, Lambert C, Lerman A, Simon DI, Vaughan DE, Lai D, Gee AP, Taylor DA, Cogle CR, Thomas JD, Olson RE, Bowman S, Francescon J, Geither C, Handberg E, Kappenman C, Westbrook L, Piller LB, Simpson LM, Baraniuk S, Loghin C, Aguilar D, Richman S, Zierold C, Spoon DB, Bettencourt J, Sayre SL, Vojvodic RW, Skarlatos SI, Gordon DJ, Ebert RF, Kwak M, Moyé LA, Simari RD; Cardiovascular Cell Therapy Research Network (CCTRN). Effect of the use and timing of bone marrow mononuclear cell delivery on left ventricular function after acute myocardial infarction: the TIME randomized trial. JAMA. 2012 Dec 12;308(22):2380-9. Erratum in: JAMA. 2013 Jan 23;309(4):343. JAMA. 2015 Jul 7;314(1):86
- Trial J, Rossen RD, Rubio J, Knowlton AA. Inflammation and ischemia: macrophages activated by fibronectin fragments enhance the survival of injured cardiac myocytes. Exp Biol Med (Maywood). 2004 Jun;229(6):538-45
- Tsur-Gang O, Ruvinov E, Landa N, Holbova R, Feinberg MS, Leor J, Cohen S. The effects of peptide-based modification of alginate on left ventricular remodeling and function after myocardial infarction. Biomaterials. 2009 Jan;30(2):189-95

- Uchiyama T, Engelman RM, Maulik N, Das DK. Role of Akt signaling in mitochondrial survival pathway triggered by hypoxic preconditioning. Circulation. 2004 Jun 22;109(24):3042-9
- Udalova I, Monaco C, Nanchahal J, Feldmann M. Anti-TNF therapy. Microbiol Spectr. 2016 Aug;4(4)
- Urbanek K, Cabral-da-Silva MC, Ide-Iwata N, Maestroni S, Delucchi F, Zheng H, Ferreira-Martins J, Ogórek B, D'Amario D, Bauer M, Zerbini G, Rota M, Hosoda T, Liao R, Anversa P, Kajstura J, Leri A. Inhibition of notch1-dependent cardiomyogenesis leads to a dilated myopathy in the neonatal heart. Circ Res. 2010 Aug 6;107(3):429-41
- van Amerongen MJ, Harmsen MC, van Rooijen N, Petersen AH, van Luyn MJ. Macrophage depletion impairs wound healing and increases left ventricular remodeling after myocardial injury in mice. Am J Pathol. 2007 Mar;170(3):818-29
- van Berlo JH, Kanisicak O, Maillet M, Vagnozzi RJ, Karch J, Lin SC, Middleton RC, Marbán E, Molkentin JD. c-kit+ cells minimally contribute cardiomyocytes to the heart. Nature. 2014 May 15;509(7500):337-41
- Varki A. Biological roles of glycans. Glycobiology. 2017 Jan;27(1):3-49
- Vera Janavel G, Crottogini A, Cabeza Meckert P, Cuniberti L, Mele A, Papouchado M, Fernández N, Bercovich A, Criscuolo M, Melo C, Laguens R. Plasmid-mediated VEGF gene transfer induces cardiomyogenesis and reduces myocardial infarct size in sheep. Gene Ther. 2006 Aug;13(15):1133-42
- Vong LB, Bui TQ, Tomita T, Sakamoto H, Hiramatsu Y, Nagasaki Y. Novel angiogenesis therapeutics by redox injectable hydrogel - Regulation of local nitric oxide generation for effective cardiovascular therapy. Biomaterials. 2018 Jun;167:143-152
- Voors AA, Belonje AM, Zijlstra F, Hillege HL, Anker SD, Slart RH, Tio RA, van't Hof A, Jukema JW, Peels HO, Henriques JP, Ten Berg JM, Vos J, van Gilst WH, van Veldhuisen DJ; HEBE III Investigators. A single dose of erythropoietin in ST-elevation myocardial infarction. Eur Heart J. 2010 Nov;31(21):2593-600
- Wang W, Schulze CJ, Suarez-Pinzon WL, Dyck JR, Sawicki G, Schulz R. Intracellular action of matrix metalloproteinase-2 accounts for acute myocardial ischemia and reperfusion injury. Circulation. 2002 Sep 17;106(12):1543-9

- Wang T, Jiang XJ, Lin T, Ren S, Li XY, Zhang XZ, Tang QZ. The inhibition of postinfarct ventricle remodeling without polycythaemia following local sustained intramyocardial delivery of erythropoietin within a supramolecular hydrogel. Biomaterials. 2009 Sep;30(25):4161-7
- Wang TK, Stewart RA, Ramanathan T, Kang N, Gamble G, White HD. Diagnosis of MI after CABG with high-sensitivity troponin T and new ECG or echocardiogram changes: relationship with mortality and validation of the universal definition of MI. Eur Heart J Acute Cardiovasc Care. 2013 Dec;2(4):323-33 (Wang 2013a in the text)
- Wang J, Karra R, Dickson AL, Poss KD. Fibronectin is deposited by injury-activated epicardial cells and is necessary for zebrafish heart regeneration. Dev Biol. 2013 Oct 15;382(2):427-35 (Wang 2013b in the text)
- Wang JW, Fontes MSC, Wang X, Chong SY, Kessler EL, Zhang YN, de Haan JJ, Arslan F, de Jager SCA, Timmers L, van Veen TAB, Lam CSP, Kleijn DPV. Leukocytic Toll-Like Receptor 2 deficiency preserves cardiac function and reduces fibrosis in sustained pressure overload. Sci Rep. 2017 Aug 23;7(1):9193 (Wang 2017a in the text)
- Wang WE, Li L, Xia X, Fu W, Liao Q, Lan C, Yang D, Chen H, Yue R, Zeng C, Zhou L, Zhou B, Duan DD, Chen X, Houser SR, Zeng C. Dedifferentiation, proliferation, and redifferentiation of adult mammalian cardiomyocytes after ischemic injury. Circulation. 2017 Aug 29;136(9):834-848 (Wang 2017b in the text)
- Wang W, Tan B, Chen J, Bao R, Zhang X, Liang S, Shang Y, Liang W, Cui Y, Fan G, Jia H, Liu W. An injectable conductive hydrogel encapsulating plasmid DNA-eNOs and ADSCs for treating myocardial infarction. Biomaterials. 2018 Apr;160:69-81 (Wang 2018a in the text)
- Wang LL, Chung JJ, Li EC, Uman S, Atluri P, Burdick JA. Injectable and protease-degradable hydrogel for siRNA sequestration and triggered delivery to the heart. J Control Release. 2018 Sep 10;285:152-161 (Wang 2018b in the text)
- Wang H, Rodell CB, Zhang X, Dusaj NN, Gorman JH 3rd, Pilla JJ, Jackson BM, Burdick JA, Gorman RC, Wenk JF. Effects of hydrogel injection on borderzone

contractility post-myocardial infarction. Biomech Model Mechanobiol. 2018 Oct;17(5):1533-1542 (Wang 2018c in the text)

- Wassenaar JW, Gaetani R, Garcia JJ, Braden RL, Luo CG, Huang D, DeMaria AN, Omens JH, Christman KL. Evidence for mechanisms underlying the functional benefits of a myocardial matrix hydrogel for post-MI treatment. J Am Coll Cardiol. 2016 Mar 8;67(9):1074-86
- Webb CS, Bonnema DD, Ahmed SH, Leonardi AH, McClure CD, Clark LL, Stroud RE, Corn WC, Finklea L, Zile MR, Spinale FG. Specific temporal profile of matrix metalloproteinase release occurs in patients after myocardial infarction: relation to left ventricular remodeling. Circulation. 2006 Sep 5;114(10):1020-7
- Webber J, Meran S, Steadman R, Phillips A. Hyaluronan orchestrates transforming growth factor-beta1-dependent maintenance of myofibroblast phenotype. J Biol Chem. 2009 Apr 3;284(14):9083-92
- Wei K, Serpooshan V, Hurtado C, Diez-Cuñado M, Zhao M, Maruyama S, Zhu W, Fajardo G, Noseda M, Nakamura K, Tian X, Liu Q, Wang A, Matsuura Y, Bushway P, Cai W, Savchenko A, Mahmoudi M, Schneider MD, van den Hoff MJ, Butte MJ, Yang PC, Walsh K, Zhou B, Bernstein D, Mercola M, Ruiz-Lozano P. Epicardial FSTL1 reconstitution regenerates the adult mammalian heart. Nature. 2015 Sep 24;525(7570):479-85
- Weihrauch D, Arras M, Zimmermann R, Schaper J. Importance of monocytes/macrophages and fibroblasts for healing of micronecroses in porcine myocardium. Mol Cell Biochem. 1995 Jun 7-21;147(1-2):13-9
- Weirather J, Hofmann UD, Beyersdorf N, Ramos GC, Vogel B, Frey A, Ertl G, Kerkau T, Frantz S. Foxp3+ CD4+ T cells improve healing after myocardial infarction by modulating monocyte/macrophage differentiation. Circ Res. 2014 Jun 20;115(1):55-67
- Willems IE, Havenith MG, De Mey JG, Daemen MJ. The alpha-smooth muscle actin-positive cells in healing human myocardial scars. Am J Pathol. 1994 Oct;145(4):868-75
- Wilson EM, Moainie SL, Baskin JM, Lowry AS, Deschamps AM, Mukherjee R, Guy TS, St John-Sutton MG, Gorman JH 3rd, Edmunds LH Jr, Gorman RC, Spinale FG. Region- and type-specific induction of matrix metalloproteinases in

post-myocardial infarction remodeling. Circulation. 2003 Jun 10;107(22):2857-63

- Wollert KC, Meyer GP, Lotz J, Ringes-Lichtenberg S, Lippolt P, Breidenbach C, Fichtner S, Korte T, Hornig B, Messinger D, Arseniev L, Hertenstein B, Ganser A, Drexler H. Intracoronary autologous bone-marrow cell transfer after myocardial infarction: the BOOST randomised controlled clinical trial. Lancet. 2004 Jul 10-16;364(9429):141-8
- Wollert KC, Meyer GP, Müller-Ehmsen J, Tschöpe C, Bonarjee V, Larsen AI, May AE, Empen K, Chorianopoulos E, Tebbe U, Waltenberger J, Mahrholdt H, Ritter B, Pirr J, Fischer D, Korf-Klingebiel M, Arseniev L, Heuft HG, Brinchmann JE, Messinger D, Hertenstein B, Ganser A, Katus HA, Felix SB, Gawaz MP, Dickstein K, Schultheiss HP, Ladage D, Greulich S, Bauersachs J. Intracoronary autologous bone marrow cell transfer after myocardial infarction: the BOOST-2 randomised placebo-controlled clinical trial. Eur Heart J. 2017 Oct 14;38(39):2936-2943
- Wollert KC. Follistatin-like 1: Growing evidence for its beneficial role in heart failure. JACC Basic Transl Sci. 2016 Jun 27;1(4):222-223
- Woo JS, Kim W, Ha SJ, Kim JB, Kim SJ, Kim WS, Seon HJ, Kim KS. Cardioprotective effects of exenatide in patients with ST-segment-elevation myocardial infarction undergoing primary percutaneous coronary intervention: results of exenatide myocardial protection in revascularization study. Arterioscler Thromb Vasc Biol. 2013 Sep;33(9):2252-60
- Woudstra P, Grundeken MJ, van de Hoef TP, Wallentin L, Fox KA, de Winter RJ, Damman P. Prognostic relevance of PCI-related myocardial infarction. Nat Rev Cardiol. 2013 Apr;10(4):231-6
- Wu J, Zeng F, Huang XP, Chung JC, Konecny F, Weisel RD, Li RK. Infarct stabilization and cardiac repair with a VEGF-conjugated, injectable hydrogel. Biomaterials. 2011 Jan;32(2):579-86
- Wünsch M, Sharma HS, Markert T, Bernotat-Danielowski S, Schott RJ, Kremer P, Bleese N, Schaper W. In situ localization of transforming growth factor beta 1 in porcine heart: enhanced expression after chronic coronary artery constriction. J Mol Cell Cardiol. 1991 Sep;23(9):1051-62

- Wysoczynski M, Guo Y, Moore JB 4th, Muthusamy S, Li Q, Nasr M, Li H, Nong Y, Wu W, Tomlin AA, Zhu X, Hunt G, Gumpert AM, Book MJ, Khan A, Tang XL, Bolli R. Myocardial reparative properties of cardiac mesenchymal cells isolated on the basis of adherence. J Am Coll Cardiol. 2017 Apr 11;69(14):1824-1838
- Wysoczynski M, Khan A, Bolli R. New paradigms in cell therapy: Repeated dosing, intravenous delivery, immunomodulatory actions, and new cell types. Circ Res. 2018 Jul 6;123(2):138-158
- Xia P, Liu Y, Cheng Z. Signaling pathways in cardiac myocyte apoptosis. Biomed Res Int. 2016;2016:9583268
- Xing Y, Sun W, Wang Y, Gao F, Ma H. Mutual inhibition of insulin signaling and PHLPP-1 determines cardioprotective efficiency of Akt in aged heart. Aging (Albany NY). 2016 May;8(5):873-88
- Xu J, Carretero OA, Liao TD, Peng H, Shesely EG, Xu J, Liu TS, Yang JJ, Reudelhuber TL, Yang XP. Local angiotensin II aggravates cardiac remodeling in hypertension. Am J Physiol Heart Circ Physiol. 2010 Nov;299(5):H1328-38
- Yabluchanskiy A, Ma Y, Iyer RP, Hall ME, Lindsey ML. Matrix metalloproteinase-9: Many shades of function in cardiovascular disease. Physiology (Bethesda). 2013 Nov;28(6):391-403
- Yang Y, Cheng HW, Qiu Y, Dupee D, Noonan M, Lin YD, Fisch S, Unno K, Sereti KI, Liao R. MicroRNA-34a plays a key role in cardiac repair and regeneration following myocardial infarction. Circ Res. 2015 Aug 14;117(5):450-9
- Yang D, Jin C, Ma H, Huang M, Shi GP, Wang J, Xiang M. EphrinB2/EphB4 pathway in postnatal angiogenesis: a potential therapeutic target for ischemic cardiovascular disease. Angiogenesis. 2016 Jul;19(3):297-309
- Yang S, Chatterjee S, Cipollo J. The glycoproteomics-mass spectrometry for studying glycosylation in cardiac hypertrophy and heart failure. Proteomics Clin Appl. 2018 Feb 9
- Ye L, D'Agostino G, Loo SJ, Wang CX, Su LP, Tan SH, Tee GZ, Pua CJ, Pena EM, Cheng RB, Chen WC, Abdurrachim D, Lalic J, Tan RS, Lee TH, Zhang J, Cook SA. Early regenerative capacity in the porcine heart. Circulation. 2018 Dec 11;138(24):2798-2808

- Yin VP, Lepilina A, Smith A, Poss KD. Regulation of zebrafish heart regeneration by miR-133. Dev Biol. 2012 May 15;365(2):319-27
- Yockman JW, Choi D, Whitten MG, Chang CW, Kastenmeier A, Erickson H, Albanil A, Lee M, Kim SW, Bull DA. Polymeric gene delivery of ischemia-inducible VEGF significantly attenuates infarct size and apoptosis following myocardial infarct. Gene Ther. 2009 Jan;16(1):127-35
- Yoon SJ, Fang YH, Lim CH, Kim BS, Son HS, Park Y, Sun K. Regeneration of ischemic heart using hyaluronic acid-based injectable hydrogel. J Biomed Mater Res B Appl Biomater. 2009 Oct;91(1):163-71
- Yu J, Christman KL, Chin E, Sievers RE, Saeed M, Lee RJ. Restoration of left ventricular geometry and improvement of left ventricular function in a rodent model of chronic ischemic cardiomyopathy. J Thorac Cardiovasc Surg. 2009 Jan;137(1):180-7
- Yutzey KE. Regenerative biology: Neuregulin 1 makes heart muscle. Nature. 2015 Apr 23;520(7548):445-6
- Zacchigna S, Martinelli V, Moimas S, Colliva A, Anzini M, Nordio A, Costa A, Rehman M, Vodret S, Pierro C, Colussi G, Zentilin L, Gutierrez MI, Dirkx E, Long C, Sinagra G, Klatzmann D, Giacca M. Paracrine effect of regulatory T cells promotes cardiomyocyte proliferation during pregnancy and after myocardial infarction. Nat Commun. 2018 Jun 26;9(1):2432
- Zangi L, Lui KO, von Gise A, Ma Q, Ebina W, Ptaszek LM, Später D, Xu H, Tabebordbar M, Gorbatov R, Sena B, Nahrendorf M, Briscoe DM, Li RA, Wagers AJ, Rossi DJ, Pu WT, Chien KR. Modified mRNA directs the fate of heart progenitor cells and induces vascular regeneration after myocardial infarction. Nat Biotechnol. 2013 Oct;31(10):898-907
- Zaruba MM, Franz WM. Role of the SDF-1-CXCR4 axis in stem cell-based therapies for ischemic cardiomyopathy. Expert Opin Biol Ther. 2010 Mar;10(3):321-35
- Zhang R, Han P, Yang H, Ouyang K, Lee D, Lin YF, Ocorr K, Kang G, Chen J, Stainier DY, Yelon D, Chi NC. In vivo cardiac reprogramming contributes to zebrafish heart regeneration. Nature. 2013 Jun 27;498(7455):497-501
- Zhang R, Li L, Yuan L, Zhao M. Hypoxic preconditioning protects cardiomyocytes against hypoxia/reoxygenation-induced cell apoptosis via

sphingosine kinase 2 and FAK/AKT pathway. Exp Mol Pathol. 2016 Feb;100(1):51-8

- Zhu W, Zhang E, Zhao M, Chong Z, Fan C, Tang Y, Hunter JD, Borovjagin AV, Walcott GP, Chen JY, Qin G, Zhang J. Regenerative potential of neonatal porcine hearts. Circulation. 2018 Dec 11;138(24):2809-2816
- Ziff OJ, Bromage DI, Yellon DM, Davidson SM. Therapeutic strategies utilizing SDF-1α in ischaemic cardiomyopathy. Cardiovasc Res. 2018 Mar 1;114(3):358-367
- Zou YR, Kottmann AH, Kuroda M, Taniuchi I, Littman DR. Function of the chemokine receptor CXCR4 in haematopoiesis and in cerebellar development. Nature. 1998 Jun 11;393(6685):595-9
- Zymek P, Nah DY, Bujak M, Ren G, Koerting A, Leucker T, Huebener P, Taffet G, Entman M, Frangogiannis NG. Interleukin-10 is not a critical regulator of infarct healing and left ventricular remodeling. Cardiovasc Res. 2007 May 1;74(2):313-22

Chapter Two

Distinct differences in cellular membrane glycosylation reflect the regeneration potential of neonatal myocardial tissue

Sections of this chapter have been submitted in the following manuscript:
Contessotto P., Ellis B., Jin C., Karlsson N.G., Zorlotuna P., Kilcoyne M. and Pandit A. "Distinct glycosylation in membrane proteins reflects the regeneration potential of neonatal myocardial tissue" Under revision in *Matrix Biology*.

2.1 Introduction

Glycan moieties can regulate the cell-cell and cell-ECM interactions affecting several functions of an organism, including the development and ageing of its organs [Hu, Zalik, Huynh]. Due to the technical difficulties and relative novelty of techniques developed to assess the presence of different types of glycan moieties, so far a limited number of studies have evaluated at the specific structural level which glycans characterize fundamental tissues such as the cardiac muscle [Parker, InanlooRahatloo].

Pioneering studies started the investigation of glycan expression focusing mainly at the histological level, using both lectin histochemistry and electron microscopy to confirm and relatively quantify the presence of the different types of glycans across the myocardial and skeletal muscle tissues [Bardosi, Lawrenson, Frank, Gros]. Specifically, most of these studies differentiate for the heterogeneity of the binding signals coming from either the cytosolic or the membrane components of the tissue of interest, but they did not evaluate the glycan expression by quantitative methods. Therefore, no definitive conclusion could be drawn in relation to the localisation and importance of specific moieties across the cardiac tissue. In recent years, improvements in the extraction and analysis methods for glycoproteins and specifically for *N*-glycans have allowed the current analysis to be oriented towards the detection of precise subgroups and even single-structure glycans expressed in the cardiac muscle [Yang, Everest-Dass, Jensen].

Looking at the heart from a gross anatomical level, the distinction between the left and right ventricle is closely connected with the main functional role of the left ventricle in pumping oxygenated blood towards the circulatory system. In contrast, the right ventricle receives de-oxygenated blood and does not require the same complexity to regulate the infusion of blood through the entire body. Despite this major difference, the main cellular components of the two ventricles remain cardiomyocytes and fibroblasts, even though the thickness and length of the two walls vary. Only recent studies investigated whether cardiomyocytes belonging to either the left or right ventricular wall respond in different ways to ischemic injuries [Tracy, de Jonge]. The cellular membranes of cardiac cells and fibroblasts were already reported to be composed by glycan moieties, but no precise characterisation

was conducted to assess the relative abundance of these glycans using a method different from the classical lectin histochemistry (Bardosi, Lawrenson).

It is already a well-known and reported phenomenon that mammalian embryonic hearts have the capacity to regenerate [Drenckhahn]. Surprisingly, one-day-old neonatal mice is able to completely regenerate the heart portion resected (approximately 15% of the total organ volume) within three weeks [Porrello 2011]. The mammalian heart regenerative property is still retained through the initial stages after birth, whereas during the heart maturation from the post-neonatal to the adult stage the myocardial tissue loses the self-regenerative capacity [Haubner, Wang, Notari]. From a cellular perspective, myocardial infarction consists in a massive necrosis involving millions of cardiomyocytes located downstream in the tissue that is no longer perfused by the recently blocked coronaries. Consequently, there is now an urgent clinical need for an effective method to enhance cardiomyocytes proliferation in a post-ischemia scenario. Given the importance of glycans in the proliferation and differentiation mechanisms, they could be implicated in the early regenerative responses seen in the neonatal mammalian hearts. Specifically, the investigation of the consistency of the glycoprofile at the cellular membrane level could lead to precise modification between the neonatal condition and the adult fully differentiated one. Previous studies have established the co-localisation of sialic acid moieties at the level of cardiomyocytes membranes and endothelial cells, and thereby recognized them as key components of the interactions of these cells with the extracellular matrix. Moreover, the role of dysregulation of sialic acids in the ion channels activity which is fundamental for heart cells contractility, was defined [Monpetit].

For all these reasons, it is hypothesised that myocardial neonatal tissues distinguish their glycoprofile at the level of specific sialic acid and mannose-related structures from that of the fully differentiated and inter-ventricular conserved adult pattern.

Consequently, the objectives of this study are to:

- Evaluate the myocardial glycan expression pattern between different rat strains by lectin histochemistry.

- Compare the glycan pattern between left and right ventricles by lectin microarray analysis.

- Examine the glycosylation of the membrane proteins at various stages of cardiac maturity to identify distinctive features by LC-ESI-MS/MS and lectin microarray analyses.

2.2 Materials and methods

2.2.1 Tissue harvesting from adult and neonatal rats

All adult and neonatal rats were sacrificed at the endpoints planned in other studies, which did not affect the circulatory system; and carcasses were kindly made available for heart harvesting subject to the NUIG internal regulations. Specifically, adult Lewis and Dark Agouti rats were used to assess the glycoprofile between different species; secondly, adult Lewis and Fischer rats were used to check for differences between left and right ventricle of the heart; and finally, tissues from neonatal and their mother rat of the Sprague Dawley strain were used for the different stage intra-species comparison. Each animal was wiped with 70% ethanol at the level of the thorax where an incision was made to remove the skin layer and then the sternum was cut to gain access to the internal organs. The heart was clearly distinguishable because of its location in the upper part of the chest and its linkage to the lungs; it was then excised by cutting the great vessels. Upon extraction from the chest of the animal, each heart was immediately placed in PBS buffer and washed to remove the excess of blood. After this, the remaining great blood vessels and atria were removed using a fine blade and the heart was positioned in a cross-section orientation to clearly distinguish the left ventricle thick wall, the interventricular septum and the collapsed thin right ventricle.

2.2.2 Tissue processing and cryosectioning

Small samples from left and right ventricles of the adult hearts were immediately excised, washed briefly with PBS and snap-frozen using dry ice for further protein extraction. Similarly, ventricular samples from neonatal hearts were excised with fine scissors and snap-frozen. Samples from the left ventricle of the heart were fixed

on freshly prepared 4% paraformaldehyde solution (Appendix A.4) overnight at 4°C and washed with PBS to remove the excess fixative. Then, tissue samples were infiltrated in freshly prepared sterile-filtered 30% sucrose solution overnight at 4°C, embedded in OCT medium and stored at -80°C until cryosectioning (Appendix A.8). Sections having a thickness of 5 μm were obtained using the cryostat from the OCT blocks.

2.2.3 Alcian blue staining to detected sulfated glycosaminoglycans

Sections from healthy Lewis and Sprague-Dawley rats were assessed for the presence of glycosaminoglycans using Alcian blue solution in acetic acid (Appendix A.14). Briefly, after dehydration, sections were stained in Alcian Blue solution at either pH 2.5 or pH 1 for 30 min; the lower pH allowed the detection of highly sulfated GAGs. After rinsing in running tap water, sections were counterstained in Nuclear Fast Red for ten min. Finally, sections were quickly dehydrated through increasing ethanol dilutions, cleared in xylene and covered with the distyrene-plasticizer-xylene (DPX) mounting medium. A coverslip was put on the top of each slide and the mounting medium was left to solidify for a few hours before imaging under a light microscope (Leica, Germany).

2.2.4 Glycosylation in myocardial tissue sections

The cryosections were washed twice for three minutes each with TBS buffer (20 mM Tris-HCl, 100 mM NaCl, 1 mM, $CaCl_2$, 1 mM $MgCl_2$, pH 7.2) with 0.05% Tween-20 (TBS-T) and then once with just TBS buffer. After this, sections were blocked with 2% periodate-treated BSA (previously prepared as described in appendix A.9) in TBS for one hour at RT. Section were then quickly dipped in TBS before the incubation with the corresponding FITC-labelled lectin diluted in TBS for one hour at RT. Co-incubation with respective inhibitory control was performed to check the specificity of the glycan binding. Co-incubation was performed adding the haptenic sugar to the diluted lectin solution one hour before applying this combined solution to the sections. After the lectin incubation, sections were washed three times with TBS for three minutes each and then mounted using ProLong® Gold antifade with DAPI. The slides were kept at 4°C in the dark for one day before imaging (see the whole procedure in Appendix A.10). Imaging was performed using an IX81 inverted

epifluorescence microscope (Olympus, Japan). Eight to nine images per section of each tissue sample were taken using a 20x magnification after staining with DSA, MAA and SNA-I lectins and quantified using Image-J after background correction. Quantifications relative to WGA and ConA lectins were performed using images taken at 40x and 60x magnification, respectively.

2.2.5 Protein extraction and quantification

Cytosolic and membrane protein fractions were extracted from the snap-frozen tissue samples using the Mem-PER™ Plus Membrane Protein Extraction Kit. Each tissue sample weighing approximately 50 mg was washed in Cell Wash Solution and vortexed for 30 sec (Appendix A.3). After this, the tissue was cut finely into smaller pieces with scissors and put in a 2 ml tissue grinder. Permeabilization Buffer (with protease inhibitor cocktail) was added and tissue was homogenized manually until a uniform suspension was obtained. Then the suspension was incubated for ten min at 4°C. The homogenate was centrifuged at 16,000 g for 15 min and then the supernatant containing the cytosolic fraction was aliquoted and stored at -80°C. The pellet was resuspended with Solubilisation Buffer (with protease inhibitor cocktail) until a homogenous suspension was obtained. This was then incubated for 30 min at 4°C with shaking. This final homogenate was centrifuged at 16,000 g for 15 min and then the supernatant containing the membrane proteins was aliquoted and stored at 4°C. Protein quantification was assessed using a Micro BCA™ Protein Assay Kit, and the sample concentrations fell into the linear working range of the BSA standard curve.

2.2.6 Protein labelling for lectin microarray analysis

Membrane protein samples were thawed on ice and diluted in 1 M sodium bicarbonate (pH 8.2) to get a 100 mM solution. Each solution, containing approximately from 300 to 500 μg of protein, was transferred in an amber tube and incubated with 0.1 mg/ml solution of Alexa Fluor® 555-succinimidyl ester. The mixed solution was incubated for two hours at RT with gentle shaking and always protected from direct light. After the incubation, samples were transferred to a 3 kDa molecular weight cut-off Amicon® centrifugal filters and centrifuged at 4000 g for 25

min. Flow-through was discarded and filters filled with 4 ml of PBS buffer containing protease inhibitor cocktail. Filters were then centrifuged at 4000 g for 50 min and flow-through was discarded. Final samples of approximately 100 µl were aliquoted and stored at -80°C. From each sample, absorbances at 280 and 555 nm were measured by Nanodrop and protein concentration and labelling calculated.

2.2.7 Lectin microarray analysis on healthy myocardial tissue

Membrane protein samples previously labelled as described in section 2.2.5 were used for the lectin microarray analyses. All lectin microarrays were printed with 48 lectins (listed in Table 2.2 and Table A.2 in Appendices) according to an established protocol [Kilcoyne]. Each lectin microarray slide had a unique barcode indicating the printing batch. All the procedures described here prior to scanning needed to be performed in a dark room with red light. At the beginning, a titration experiment using a concentration of protein from 1 to 10 µg/ml was run to assess the optimum binding intensity of the sample to the printed lectins and to avoid saturation signals; therefore the chosen concentration for all the rat healthy samples was 2.5 µg/ml. Labelled membrane protein samples were thawed on ice and diluted in TBS-T (0.01% of Tween-20) to the optimal concentration in a final volume of 70 µl in a rubber eight-well gasket (Agilent Technologies, USA). Each slide was carefully assembled on the top of the loaded gaskets to avoid splashing of the samples and then incubated with gentle rotation (4 rpm) in a hybridization oven at 23°C for one hour (Appendix A.11). Following this, the slide was carefully disassembled after submerging it in TBS-T buffer and washed three times for three minutes each with gentle shaking in TBS-T. A final wash in TBS without Tween-20 was done before transferring the slides in empty falcon tubes and centrifuging them at 1500 g for five minutes. Finally, the slides were scanned immediately using G2505 microarray scanner (Agilent Technologies, USA) at 90% laser power. Image files showing the scanned lectin microarrays were processed using GenePix Pro v6.1.0.4 software (Molecular Devices, UK). Briefly, an adaptive diameter circular alignment based on 230 µm features was set in the options and grids were superimposed on the subarrays. Local background-corrected median feature intensity data were analysed and normalised to the median total intensity value of six replicate microarray slides. Clustering of the normalised data from the lectin microarrays was done using

Hierarchical Clustering Explorer v3.5 (HCE 3.5, University of Maryland). Data were imported and clustered by Euclidean distance with complete linkage.

2.2.8 Processing to extract *N*-glycans

Membrane protein samples from adult and neonatal healthy rats, which were extracted as described in section 2.2.4, were processed for *N*- and *O*-glycan analysis after optimising the starting concentration. At least 0.3 mg/ml of protein was needed from each sample before starting the procedure. Samples belonging to the same group but coming from three different animals were pooled together to get a final starting amount of membrane protein of at least 240 μg. Extract buffer was exchanged to 7 M urea via 30 kDa cut-off spin filter and incubated with 25 mM dithiothreitol at 56°C for 45 min. Then, reduced samples were alkylated with 62.5 mM iodoacetamide at RT for 50 min in the dark. After the alkylation, samples were trypsin-digested (5 μl) at 37°C overnight. The following day, acetone was added which was four-times the amount of the sample to precipitate the protein left at -20°C for 30 min. Samples were then washed twice with 500 μl of 60% methanol and pellets were air-dried using a SpeedVac concentrator (Thermo Fisher Scientific, USA). After adding 50 μl of 50 mM ammonium bicarbonate (pH 8.4) and 1 μl of PNGase F, samples were incubated at 37°C overnight. After the incubation with PNGase F, *N*-glycans that were present in the samples were separated from (*O*-glyco)peptides using a Sep-Pak® C18 cartridge (Waters Corporation, USA). Briefly, the cartridge was first conditioned with different dilutions (90% and 10%) of acetonitrile (ACN) in 0.5% trifluoroacetic acid (TFA), then with acetic acid (5% HAc). After applying the sample, both the eluent and washout with 5% HAc were combined. Samples containing *N*-glycans were subsequently dried with the SpeedVac at 30°C. Then *N*-glycans were reduced by incubation with 50 μl of a buffer made of 0.5 M sodium borohydride ($NaBH_4$) and 20 mM sodium hydroxide (NaOH) at 50°C overnight. The following day, *N*-glycans were desalted using a cation exchange resin AG® 50W-X8 (Bio-Rad, USA) packed onto a ZipTip® C18 tip (Merck, Germany). Samples were dried and then resuspended with 50 μl of methanol (MeOH) and dried with a SpeedVac at least three times to fully remove the traces of sodium borohydride. Finally, samples were stored at -20°C until the LC-MS/MS run.

2.2.9 Processing to extract *O*-glycans

The processing of *O*-glycans contained in the samples followed the same procedure for the *N*-glycans extraction until the elution with the use of the Sep-Pak® C18 cartridge (Waters Corporation, USA). During this step, *O*-glycopeptides were eluted by the addition of 65% ACN in 0.5% TFA. Samples were then dried with the SpeedVac at 30°C. Then, *O*-glycans were actually released by the reductive β-elimination reaction. Briefly, samples were incubated in a buffer containing 0.5 M sodium borohydride and 50 mM sodium hydroxide at 50°C overnight. The following day, samples were desalted using a cation exchange resin AG® 50W-X8 (Bio-Rad, USA) packed onto a ZipTip® C18 tip (Merck, Germany). Finally, samples containing *O*-glycans were resuspended with methanol (MeOH) and dried three times before storing at -20°C until LC-MS/MS analysis.

2.2.10 *N*- and *O*-glycomic analysis

Released glycans were resuspended in deionized water and analysed by liquid chromatograph-electrospray ionization tandem mass spectrometry (LC-ESI/MS) as previously reported [Mereiter]. The oligosaccharides were separated on a column (10 cm × 250 µm) packed in-house with 5 µm porous graphite particles (Hypercarb, Thermo-Hypersil, UK). The oligosaccharides were injected in the column and eluted with an ACN gradient (Buffer A, 10 mM ammonium bicarbonate; Buffer B, 10 mM ammonium bicarbonate in 80% ACN). The gradient (0-45% Buffer B) was eluted for 46 minutes, followed by a wash step with 100% Buffer B, and equilibrated with Buffer A in the following 24 min. A 40 cm × 50 µm i.d. fused silica capillary was used as transfer line to the ion source. The samples were analysed in negative ion mode on a LTQ linear ion trap mass spectrometer (Thermo Electron, USA), with an IonMax standard ESI source equipped with a stainless steel needle kept at –3.5 kV. Compressed air was used as nebuliser gas. The heated capillary was kept at 270°C, and the capillary voltage was –50 kV. A full scan (m/z 380-2000 two microscans, maximum 100 ms, target value of 30,000) was performed, followed by data-dependent MS^2 scans (two microscans, maximum 100 ms, target value of 10,000) with normalised collision energy of 35%, isolation window of 2.5 units, activation q=0.25 and activation time 30 ms. The threshold for MS^2 was set to 300 counts. Data

acquisition and processing were conducted with Xcalibur™ software (Version 2.0.7, Thermo Fisher Scientific, USA).

2.2.11 Peaks annotation and intensity calculation from LC-ESI-MS/MS analysis

Glycans were identified from their MS/MS spectra by manual annotation. For structural annotation, some assumptions were made in this study. The biosynthesis of *N*- and *O*-glycans was assumed to follow the classic pathways. Diagnostic fragmentation ions for *N*- and *O*-glycans were investigated as described [Everest-Dass]. Two terminal hexose (Hex2) units were presumed to be α-galactose (α-Gal) and two terminal *N*-Acetylglucosamine (HexNAc2) determinants were presumed to be *N*-Acetylglucosamine linked to a *N*-Acetylgalactosaminyl residue (LacdiNAc). Chain elongation was expected to be mediated by the addition of *N*-acetyllactosamine units. The annotated structures were submitted to the UniCarb-DR database (http://unicarb-dr.biomedicine.gu.se/references/351). For comparison of glycan abundances between samples, individual glycan structures were quantified relative to the total content by integration of the extracted ion chromatogram peak area. The area under the curve (AUC) of each structure was normalised to the total AUC and expressed as a percentage.

2.2.12 Statistical analysis

All statistical analysis was performed using Minitab™ Express software (Minitab, Inc. State College, USA). Data from lectin histochemistry were selected by significance as assessed by standard Student's t-test. Data from lectin microarray analysis were compared using one-way ANOVA with Tukey's post-hoc correction since they followed a normal distribution. Values were considered significant just with $p<0.05$.

2.3 Results

2.3.1 Glycosylation difference in sialic acid between cardiomyocytes cell surfaces and capillaries

With the aim to investigate the patterns of glycans expression across the myocardial left ventricle and their consistency, two strains of adult rat (Lewis and Fischer) were compared. Initially, the localisation of glycosaminoglycans in myocardial tissue was made visible by Alcian blue staining. Glycosaminoglycans such as heparan and chondroitin sulphate were clearly detected in the extracellular matrix surrounding the cardiomyocytes and in correspondence of the vasculature structures (Figure 2.1). Moreover, Alcian blue staining at pH 1 retained binding to highly sulfated mucopolysaccharides in the proximity of the *tunica externa* of the arteries (Figure 2.1). A panel of five lectins (Table 2.1) was selected for their binding to general mammalian type glycosylation, i.e. sialic acid, mannose (Man) and GlcNAc, to examine the local variation of the glycosylation within the myocardial left ventricles of both Lewis and Fisher strain adult rats. For both strains, *Maakia amurensis* agglutinin (MAA) binding was observed at the cardiomyocytes membranes which indicated the presence of terminal α-(2,3)-linked sialic acid residues on all cardiomyocyte cell surfaces (Figure 2.2 F,G). *Sambucus nigra* agglutinin isolectin-I (SNA-I) binding was localised with the capillaries between the cardiomyocytes but not on cardiomyocyte cell surfaces (Figure 2.2 H-I) which indicates that α-(2,6)-sialic acids are located discretely from α-(2,3)-linkages of sialic acids. No significant differences were seen in the binding intensity of MAA or SNA-I between the two strains. *Datura stramonium* agglutinin (DSA) was found to be more generic, binding both cardiomyocyte membranes and capillaries between cardiomyocytes (Figure 2.2 D,E) indicating an even distribution of terminal GlcNAc in the heart tissue. Wheat germ agglutinin (WGA) bound intensely to the same cellular surfaces which were bound by DSA, (Figure 2.2 A,B), consistent with its affinity for both GlcNAc but also with MAA and SNA-I binding due to WGA affinity for sialic acid regardless of linkage. Concanavalin A lectin (ConA) is usually employed in tissue histology studies to determine the presence and localisation of *N*-linked glycosylation as it binds preferentially to α-linked mannose (Man) residues in the core structures of all *N*-linked glycans [Naismith]. In both left ventricles, ConA binding was localised to both the cytosolic and the membrane portion of cardiomyocytes (Figure 2.2 J,K). This binding to organelles or structures is consistent with immature high mannose

glycans, *N*-linked glycans biosynthesised in the endoplasmic reticulum, and Golgi apparatus. ConA binding to the cellular surface of cardiomyocytes was also evident but this was not extended to capillary structures, which may indicate that complex *N*-linked glycans are in higher proportion in the capillaries indicated by the positive staining of the other lectins. The presence of *O*-linked glycans and/or glycolipids, which do not have Man residues, are also likely to contribute to the SNA-I MAA, DSA ad WGA binding.

2.3.2 Tissue glycosylation of adult left and right cardiac ventricles is similar across rat strains

Given the importance of glycans in the interaction with the ECM, any potential differences in the glycan composition of cardiomyocytes, which are present in two cardiac ventricles of the heart, could be an indicator of a different physiological function. Left and right ventricular tissue samples were harvested from four individuals from two different strains of healthy adult rats (Lewis and Fischer) and their membrane proteins extracted and processed specifically for the lectin microarray analysis (lectins are listed in Table 2.2). A heat map showing all the relative binding intensities to the lectins tested is shown in Figure 2.3. The lectin binding profiles of both the left and right membrane proteins showed a consistently high binding to WGA, SNA-I, both the isolectin I and II of *Trichosanthes japonica* (TJA), and *Ricinus communis* agglutinin (RCA-I/120). These data were consistent with the previous lectin histochemistry data that indicated the presence of complex-type glycans. High mannose-type glycan structures were detected by binding to *Lens culinaris* (Lch-B), *Calystegia sepium* (Calsepa), *Narcissus pseudonarcissus* (NPA) and *Galanthus nivalis* (GNA) lectins. Moreover, *Phaseolus vulgaris* isolectin E (PHA-E) indicated the presence of bi- and tri-antennary complex type glycans with terminal β-linked Gal residues. Finally, terminal α-linked galactose (α-Gal) was present across the cardiac ventricles in both the strains, as evidenced by the binding to *Maclura pomifera* (MPA), *Vigna radiate* (VRA) and *Marasmius oreades* (MOA) lectins. Binding to *Griffonia simplicifolia* (GS) isolectin B4 indicated that at least a proportion of the terminal α-Gal present was a component of the terminal Gal-α-(1,3)-Gal disaccharide.

Hierarchical clustering analysis of the lectin binding intensity data highlighted an 80% similarity across all the samples tested with the exception of one left ventricle from the Fischer strain, which had a similarity of 70% with the rest of the samples, and may have represented an outlier (Figure 2.3). None of the groups showed a clustering of all its individuals and so the individual variability did not allow the distinction of major differences due either to the ventricular or to the strain origin. Specifically, samples from both the left and right ventricles were clustered together with a total similarity percentage ranging from 80% (including all the samples apart from the outlier) to 92% related to two different samples harvested from different ventricles and strains (Figure 2.3). Furthermore, one-way ANOVA statistical analysis confirmed the outcome of the clustering since no significant difference was detected across the lectins that bound to high mannose- and complex-type glycans (Figure 2.4). Therefore, glycosylation of cardiac tissues was found to be consistent between left and right ventricles also between different rat strains.

2.3.3 Complex *N*-linked and sialylated glycan structures are more abundant in adult and distinctive structures were detected in neonatal myocardium

In order to assess any variation between neonatal and adult hart tissue glycosylation, structural characterisation of oligosaccharides from the tissue was performed. The *N*- and *O*-linked glycan structures of Sprague Dawley healthy three-day-old and adult myocardial left ventricles were analysed by liquid chromatography-mass spectrometry (LC-MS/MS) to identify any structural variations in detail (Figure 2.5 A). Seventy-three putative *N*-glycans were detected between the samples analysed (Table 2.3), showing an overall predominance of complex-type structures over high mannose and hybrid type, independently of the developmental stage (Figure 2.5 A). Specifically, the relative percentage of complex-type *N*-linked glycans increased from three-day-old to adult samples (56% and 61%, respectively) (Figure 2.5 B). Consequently, the amount of high mannose-type *N*-glycans decreased from 37% at early neonatal stage to 31% at the adult stage (Figure 2.5 B). The remaining hybrid-type structures were found to be 7% in neonatal and 8% in adult (Figure 2.5 B). However, the adult tended to have a shorter form of hybrid-type, whereas the neonatal tend to have a more sialylated (larger) form of hybrid-type. In the data analysed, the predominant high mannose structure was $Hex_9HexNAc_2$ (Man9) in

both neonatal and adult samples (Figure 2.5 C). Among all the high mannose structures quantified, the difference between the groups did not exceed 2%, apart from $Hex_6HexNAc_2$ (Man6) that decreased from 7% in neonatal to 2% in adult (Figure 2.5 C).

The adult tissue had higher expression of sialylated *N*-glycans (64%) but slightly lower core fucosylation (44%) than that of neonatal (57% and 47%, respectively), whereas the α-(2,6)-linked Neu5Ac level was similar (30%) in both samples. In addition, *N*-linked glycans with disialic acid terminus (Neu5Ac-α-(2,8)-Neu5Ac) in adult rat (10%) were higher than that in neonatal (1%). As shown in Figure 2.5 A, $Neu5Ac_4Hex_6HexNAc_5deHex_1$ (*m/z 1658*, di-sialylated) and $Neu5Ac_2Hex_5HexNAc_4$ (*m/z* 1111, without core fucosylation) were higher in adult stage (6% and 9%) compared to the neonatal one (1% and 2%), whereas $Neu5Ac_2Hex_5HexNAc_4deHex_1$ (*m/z* 1184, core fucosylated) showed a higher expression in neonatal (19%) than in the fully developed stage (13%). *N*-glycans containing terminal Gal-α-(1,3)-Gal disaccharides were similar between neonatal condition (9%) and adult stage (8%). As illustrated in Figure 2.6 A, one complex-type, containing terminal α-galactose (Gal-α-(1,3)-Gal-β-(1,4)-GlcNAc-β-(1,2)-Man-α-(1,3)-[Gal-α-(1-3)-Gal-β-(1,4)-GlcNAc-β-(1,2)-Man-α-(1,6)-]Man-β-(1,4)-GlcNAc-β-(1,4)-GlcNAcol, with [M-H] ion of *m/z* 1965 in Table 2.3), one high mannose-type (Glc-α-(1,3)-Man-α (1,2)-Man-α-(1,2)-Man-α-(1,3)[Man-α-(1,2)-Man-α-(1,3) - (Man-α-(1,2) - Man-α-(1,6)-Man-α-(1,6)]Man-β-(1,4)-GlcNAc-β-(1,4)-GlcNAcol, with [M-H] ion of *m/z* 2045 in Table 2.3) and one hybrid-type (GlcNAc-β-(1,2)-Man-α-(1,3)-[Man-α-(1,2)-Man-α-(1,3)(Man-α-(1,2)-Man-α-(1,6)-Man-α-(1-6)-]Man-β-(1,4)-GlcNAc-β-(1,4)-GlcNAcol, with [M-H] ion of *m/z* 1762-1 in Table 2.3) putative structures were detected only in the three-day-old group, all having relative percentages around 1%.

2.3.4 *O*-linked glycan analysis of neonatal and adult myocardium

O-glycome analysis revealed core 1 and 2 type *O*-glycans. A total of 15 *O*-glycans were identified across the samples analysed and most of these were sialylated (>90%) with either Neu5Ac or Neu5Gc (Table 2.4). Neither core 1 nor 2 *O*-glycans were found to be elongated with oligoLacNAc extension, probably due to high

sialylation (≥90%). In adult, the level of core 2 *O*-glycans was about 42%, while in neonatal the level was about 47%; on the other hand, core 1 *O*-glycans were similar between the two samples. Interestingly, a sulfated core 2 *O*-glycan ([M-H]-ion of *m/z* 1120, Table 2.4) was detected exclusively in neonatal tissue (7%), as shown in Figure 2.6 B. In addition, core 3 (GlcNAc-β-(1,3)-GalNAcol and sialyl-Tn (NeuAc-α-(2,6)-GalNAcol) structures had higher abundances in adult tissue than in neonatal (with [M-H]-ions of *m/z* 425 and 513, respectively, in Table 2.4). Neither ABO nor Lewis type antigens were detected in either of the samples.

2.3.5 Distinct tissue glycosylation between neonatal and adult myocardium

Early neonatal (three-day-old), later stage (14-day-old) and fully adult (eight-month-old) left ventricular tissues of Sprague-Dawley healthy rats were analysed by lectin microarray to confirm the variations in glycosylation elucidated by LC-MS/MS (Figure 2.7). Three profiles of the membrane glycans indicated binding to most of the same lectins that were described in the comparison between adult ventricles, although significantly different binding intensities suggested a different expression of certain glycan subgroups. The presence of high mannose glycans was suggested by binding to Lch-B, Calsepa, NPA, GNA and ConA lectins (Table 2.2). Glycans containing sialic acids binding to TJA isolectin I, MAA, SNA and WGA lectins were detected. Moreover in adult ventricles, high binding to RCA-I/120 lectin and PHA-E suggested that Gal-β-(1,4)-GlcNAc and bisecting GlcNAc, β-Gal/Gal-β-(1,4-GlcNAc were present among the complex type glycans. Similarly, terminal α-galactose was expressed also at the neonatal stages, as evidenced by the binding to MPA, MOA and GS-I-B4 (Figure 2.7). Hierarchical clustering of the lectin microarray binding intensity data showed an 80% similarity across all the samples profiled with the exception of one adult individual which had a similarity of 68% with the rest of the samples, and may have represented an outlier (Figure 2.7). Interestingly, three-day-old neonatal individuals showed an 88% similarity and clustered together, showing the highest similarity inside the same group. Groups of samples belonging to the 14-day-old stage and fully adult were clustered in a dispersed way; thus the individual variability inside each of those groups was higher than any distinct difference between the later stage neonatal and adult groups (Figure 2.7). One-way ANOVA analysis validated the trend in increased complex *N*-glycans

seen by LC-ESI-MS/MS (Figure 2.8 A). Specifically, a higher binding to TJA-I, *Solanum tuberosum* (STA), WGA, *Cicer arietinum* (CPA) and *Lotus tetragonolobus* (LTA) lectins (Table 2.2) indicated residues which can be present in complex *N*-glycans, such as α-(2,6)-linked sialic acid, GlcNAc, sialic acid, complex glycopeptides and α-(1,2/3)-linked fucose, respectively (Figure 2.8 B). Moreover, an increased binding to *Glycine max* (SBA), *Agaricus bisporus* (ABL) and *Arachis hypogaea* (PNA) lectins (Table 2.2) validated the increase of *O*-glycan core 1 residues (GalNAc and Gal-β-(1,3)-GalNAc) in adult, a rise which was barely seen from the *O*-glycome (Figure 2.8 B). In addition, a whole different ANOVA cluster showed a higher binding intensity in the adult group than that in the 14-day-old and it was composed by GalNAc-binding lectins RPbAI, SNA-II, *Dolichos biflorus* (DBA), *Glechoma hederacea* (GHA), *Bauhinia purpurea* (BPA), *Helix pomatia* (HPA) and GSL-I-A4 (Figure 2.8 B). Finally, the increase in fucosylation seen in neonatal *N*-glycans was reflected in an increased - although non-significant - binding to *Aleuria aurantia* (AAL) lectin (Figure 2.9). Interestingly, no relevant difference distinguished the three-day-old from the 14-day-old group, whereas the groups of lectins listed above confirm a different glycosylation between the three-day-old and the adult stage indicated by clustering analysis.

Table 2.1 Lectins used for tissue histochemistry, their binding specificity, used concentration and inhibitory carbohydrate (150 mM).

Lectin and abbreviation	Abbreviation	Binding specificity	Conc. (μg/ml)	Inhibitory carbohydrate
Sambucus nigra agglutinin isolectin-I	SNA-I	Neu5Ac/Gc-α(2,6)-Gal-β-(1,4)-GlcNAc-R	20	Lactose
Maackia amurensis agglutinin	MAA	Neu5Ac/Gc-α(2,3)-Gal-β-(1,4)-GlcNAc-R	15	Lactose
Concanavalin A lectin	Con A	α-linked Man, Glc, or GlcNAc	20	Man
Wheat germ agglutinin	WGA	GlcNAc, Neu5Ac/Gc	10	GlcNAc
Datura stramonium agglutinin	DSA	GlcNAc	15	GlcNAc

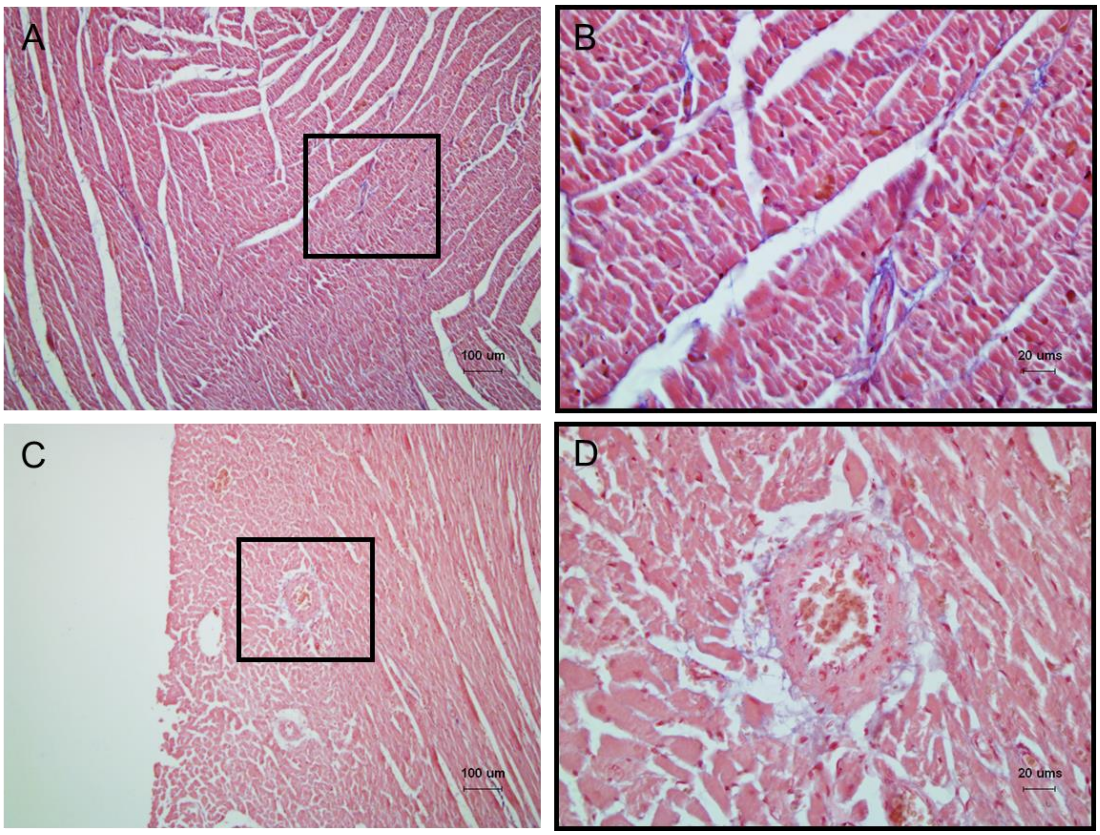

Figure 2.1 Alcian blue staining detects glycosaminoglycans (GAGs) present across the myocardial tissue. Alcian blue staining at pH 2.5 (A-B) allows the visualisation of GAGs present in the extracellular matrix, which become clearly evident in close proximity to vasculature structures (B). Alcian blue staining at pH 1 (C-D) shows just the highly sulfated GAGs, which are mostly concentrated just close to the artery walls (D). Erythrocytes are stained orange; all other cell nuclei are red. Images B and D are 40x magnification of areas selected from left ventricular tissue shown in images A and C. These tissues were harvested from adult healthy Lewis and Sprague Dawley rats. Scale bar in A,C = 100 μm, in B,D = 20 μm.

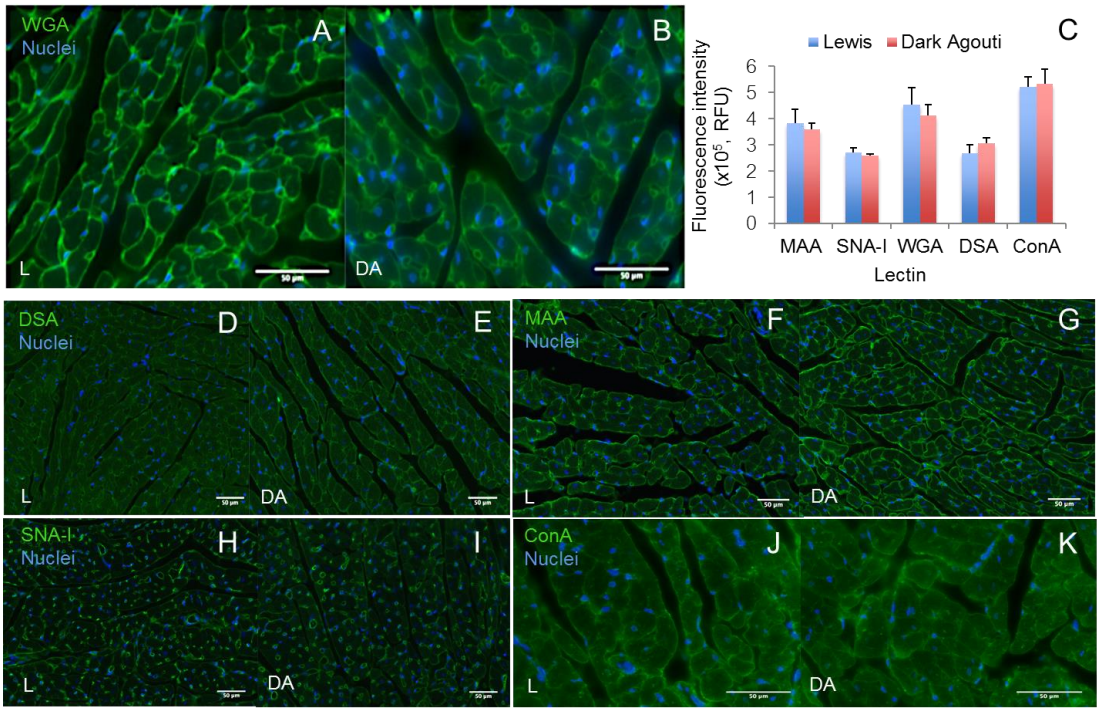

Figure 2.2 Lectin binding in left ventricle and relative quantification. The same patterns were detected in both Lewis (L) and Dark Agouti (DA) rats. WGA lectin binds to NeuAc and GlcNAc residues (A,B), DSA binds to GlcNAc glycans (D,E), MAA recognizes α-(2,3)-sialylated motifs (F,G), SNA-I binds to α-(2,6)-sialylated motifs (H,I) and ConA recognises mannose and glucose (J,K). All lectin binding intensities were background-subtracted and quantified by Image J. Data are shown as mean with standard deviation (C). Student's t-test, n=4-6 animals per group. Scale bar = 50 μm.

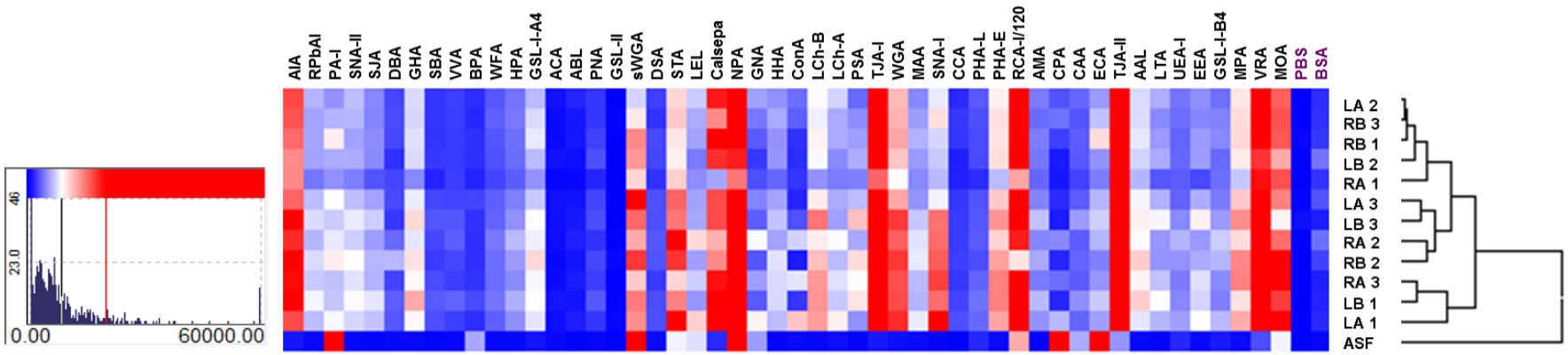

Figure 2.3 Hierarchical clustering of glycan moieties detected across the left and right ventricle in two different strains of healthy rat. Lectin microarrays showed the binding intensity to the glycans present in the membrane proteins extracted from the left (L) and right (R) ventricle from Fischer (A) and Lewis (B) strains of healthy rats. Hierarchical clustering showed an 80% similarity across all the samples tested with the exception of LA 1, which had a 70% similarity with the rest of the samples. Samples LA2 and RB3 showed a 92% similarity. Asialofetuin (ASF) was used as control glycoprotein and all lectin binding intensities were normalised. 90% laser scans were combined with 10% laser scans when intensity binding was saturated (above 60,000 RFU). The experiment was carried out in technical triplicate. N=3 animals per group.

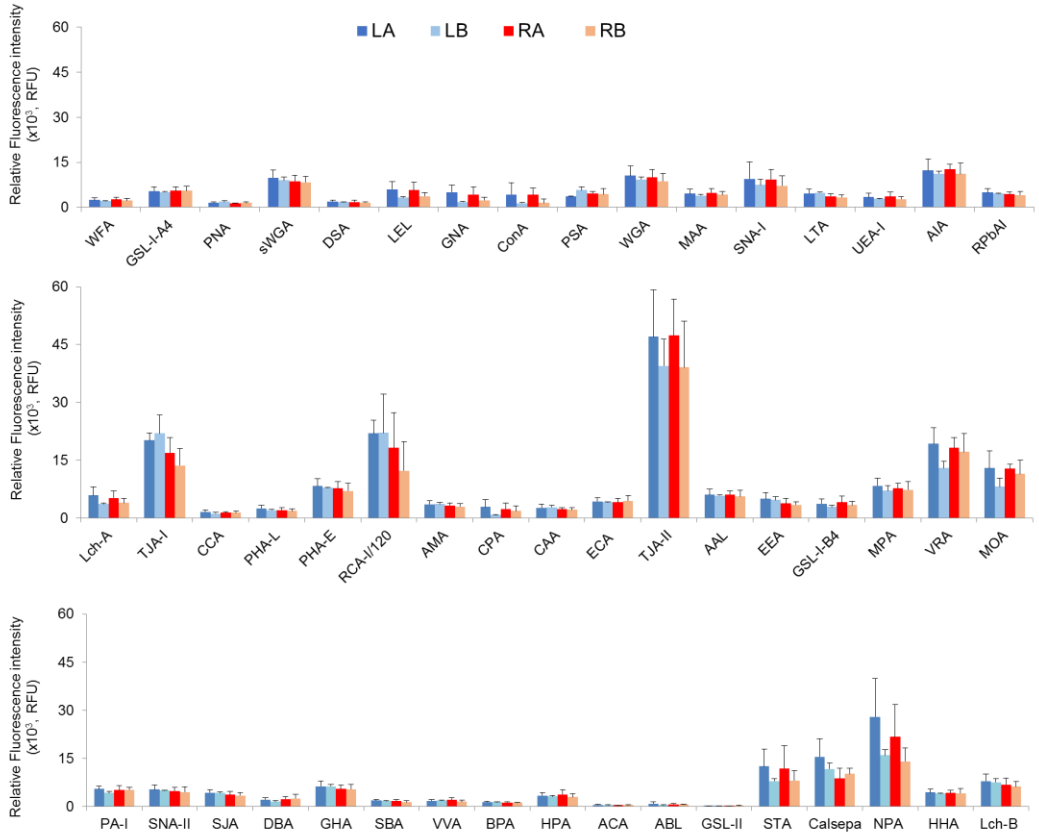

Figure 2.4 Statistical analysis of lectin intensity binding of glycans detected across the left and right ventricle in two different strains of healthy rat. Lectin microarrays did not show any significant difference between either the left and right ventricle inside the same strain or across two different strains. 90% laser scans were combined with 10% laser scans when intensity binding was saturated (above 60,000 RFU). One-way ANOVA with Tukey's post hoc correction, n=3 animals per group.

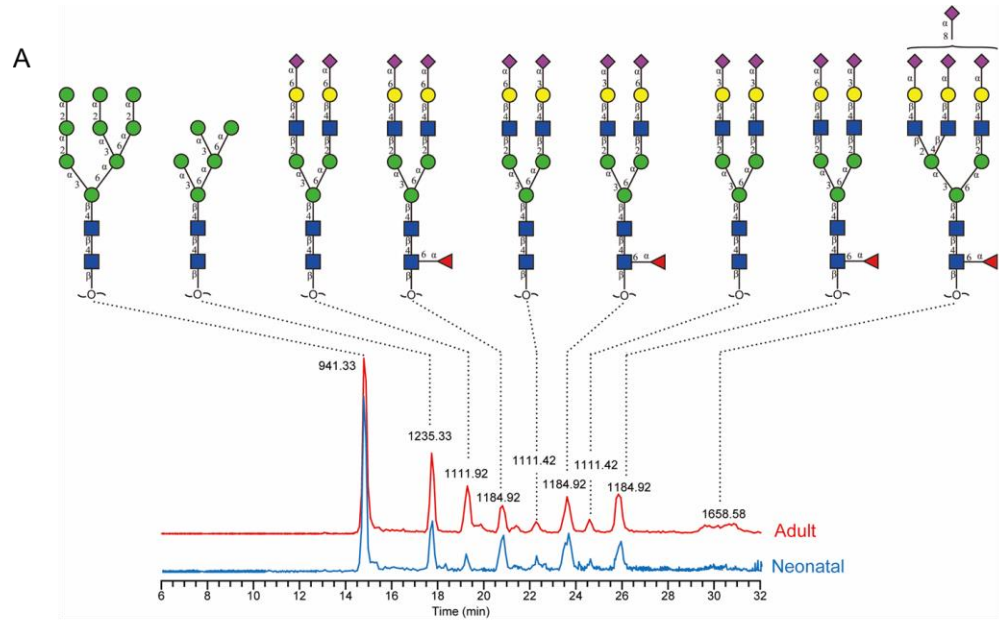

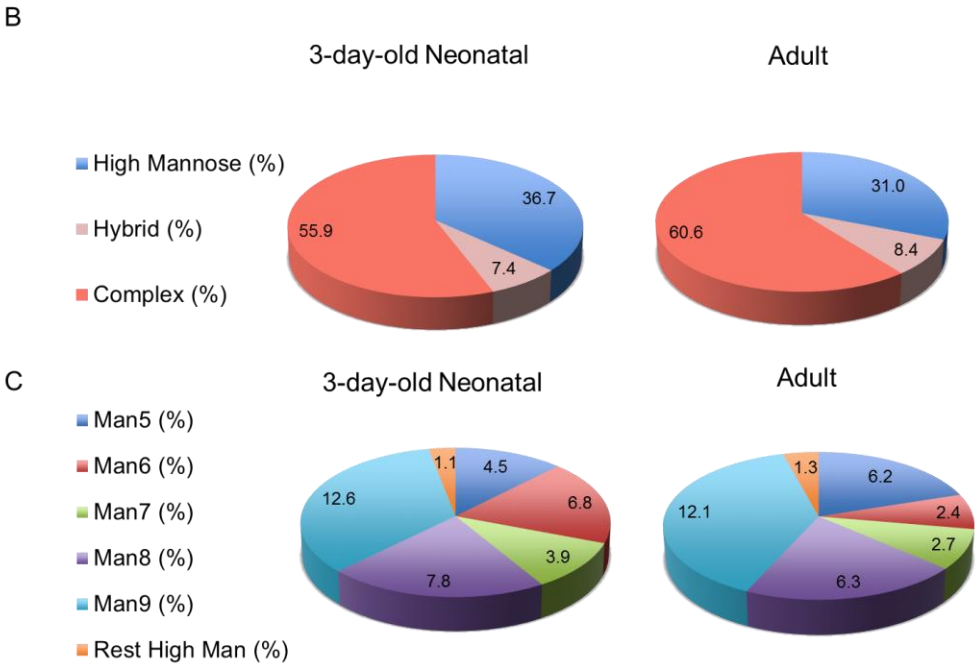

Figure 2.5 Extracted ion chromatography (EIC) of the most abundant *N*-linked glycans present in the membrane protein in neonatal and adult healthy myocardial tissue. (A) The six most abundant *N*-glycans structures at *m/z* 941 ($Man_9GlcNAc_2$), 1235 ($Man_5GlcNAc_2$), 1111 ($Neu5Ac_2Hex_5GlcNAc_4$), 1184 ($Neu5Ac_2Hex_5GlcNAc_4Fuc_1$) and 1658 ($Neu5Ac_4Hex_5GlcNAc_4Fuc_1$) were chosen to show the different relative percentage of Neu5Ac-α-(2,3)-Gal-, Neu5Ac-α-(2,6)-Gal-and Neu5Ac-α-(2,8)-Neu5Ac- in neonatal and adult left ventricular myocardial samples. (B) Adult-stage group showed a 5% increase in complex-type structures

and a 6% decrease in the subgroup of high mannose structures compared to three-day-old neonatal. (C) Among total high mannose structures, $Man_6GlcNAc_2$ showed a 4% increase in relative percentage. The experiment was done using samples pooled from three different animals per group.

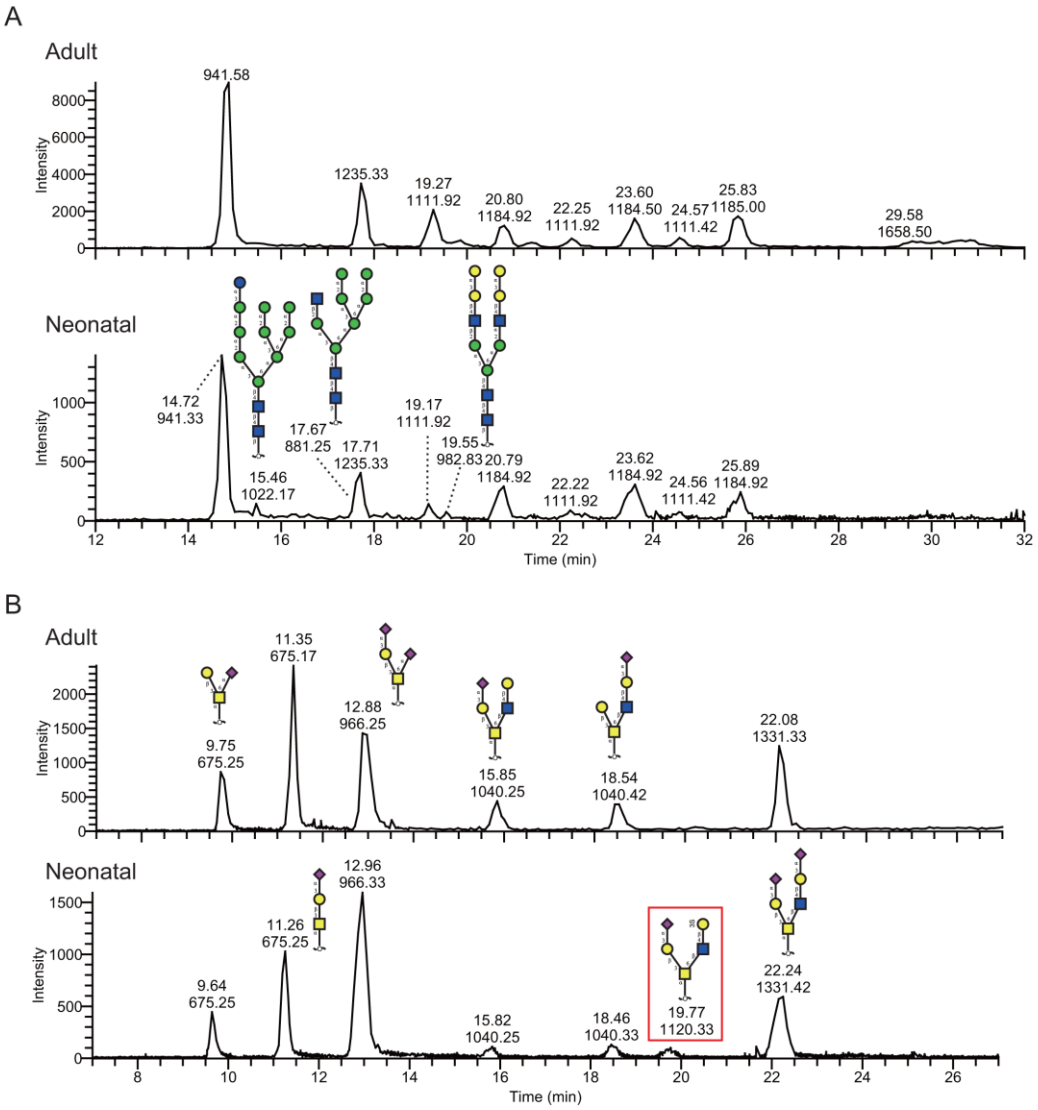

Figure 2.6 Extracted ion chromatography (EIC) of distinctive *N*- and *O*-linked glycans present in the membrane protein in neonatal and adult healthy myocardial tissue. (A) Three *N*-glycan structures were detected only in left ventricular myocardial neonatal sample at m/z 1022 ($[M-2H]^{2-}$ ions, high-mannose precursor), 881 ($[M-2H]^{2-}$ ions, hybrid-type), and 982 ($[M-2H]^{2-}$ ions, complex-type). (B) EIC of dominant core 1 and 2 *O*-glycans, one sulfated core 2 *O*-glycan ($[M-H]^{-}$ ions at m/z 1120) was detected exclusively in neonatal tissue (framed in red). The experiment was done using samples pooled from three different animals per group.

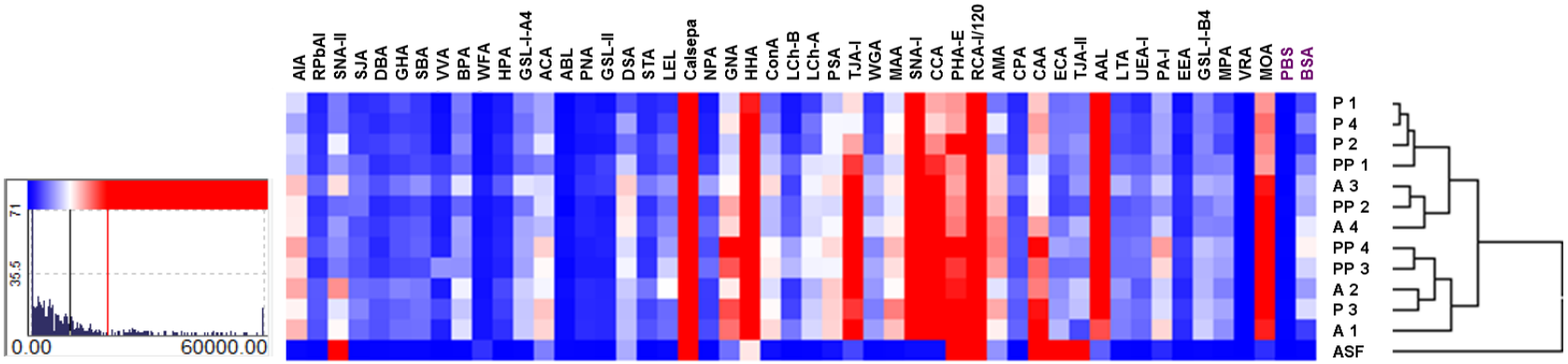

Figure 2.7 Hierarchical clustering of healthy ventricular samples from neonatal and adult stages. Lectin microarrays showed the binding intensity to the glycans present in the membrane proteins extracted from the three-day-old neonatal (P), 14-day-old neonatal (PP) and adult (A) ventricular myocardial tissue from Sprague Dawley healthy rats. Hierarchical clustering showed an 80% similarity across all the samples tested with the exception of A1, which had a 68% similarity with the rest of the samples. Three-day-old neonatal samples P1, P2 and P4 showed an 88% similarity and clustered together, showing the highest similarity inside the same group. Asialofetuin (ASF) was used as control glycoprotein and all lectin binding intensities were normalised. The experiment was carried out in technical triplicate. All 90% laser scan measurements recorded were below the saturation limit (60,000 RFU). N=4 animals per group.

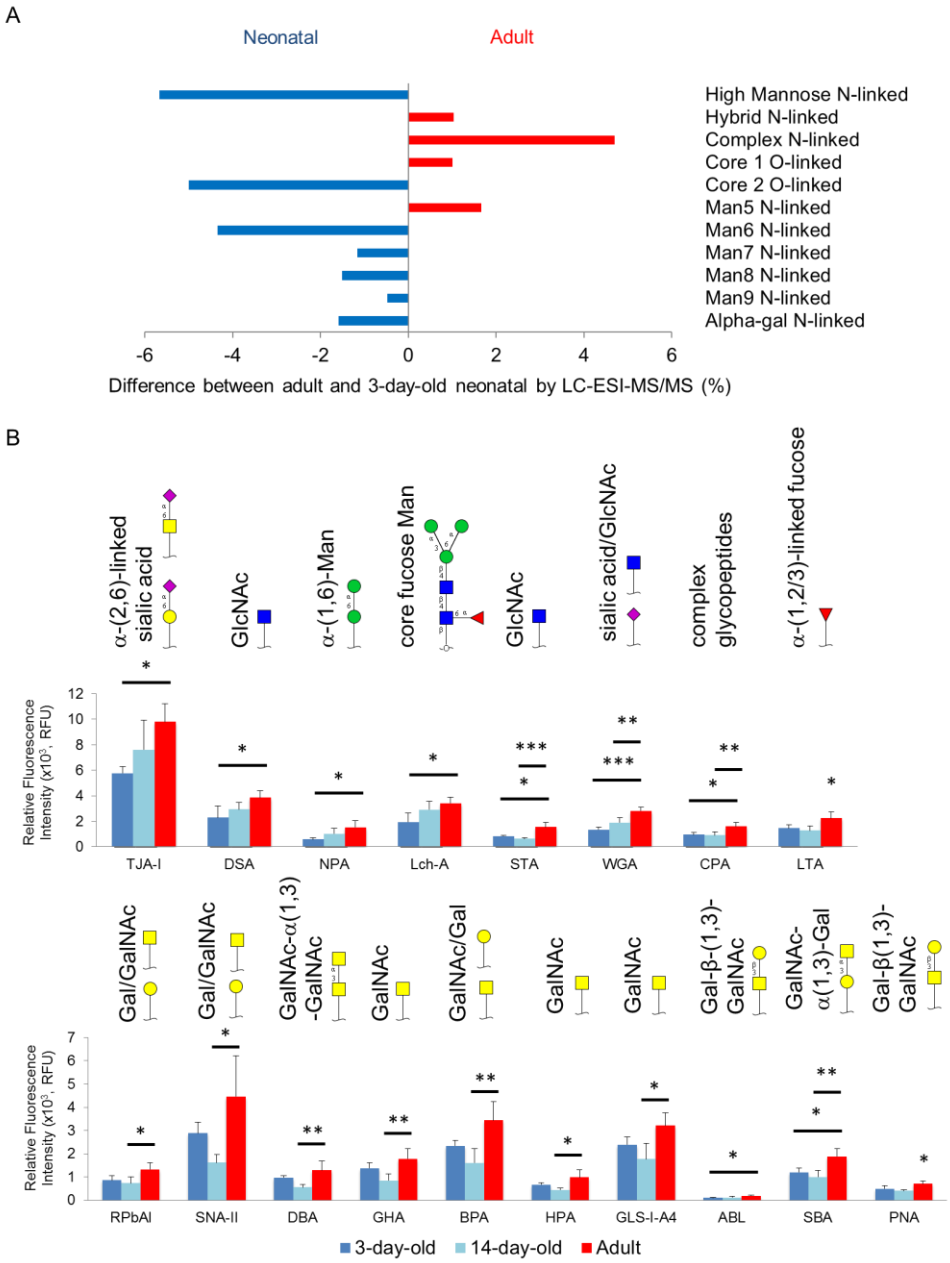

Figure 2.8 Higher complex *N*-glycans and lower core 1 *O*-glycans at early neonatal stage. (A) LC-ESI-MS/MS analysis showed trends of higher expression of complex *N*-glycans and lower core 1 *O*-glycans in adult left ventricular myocardial tissue from Sprague Dawley healthy rats. (B) One-way ANOVA with Tukey's post hoc correction confirmed a higher binding of lectins to complex *N*-glycans (TJA-I, DSA, NPA, upper panel), and core 1 *O*-glycans (lower panel). N=4 animals per group, *p<0.05, **p<0.01, ***p<0.001.

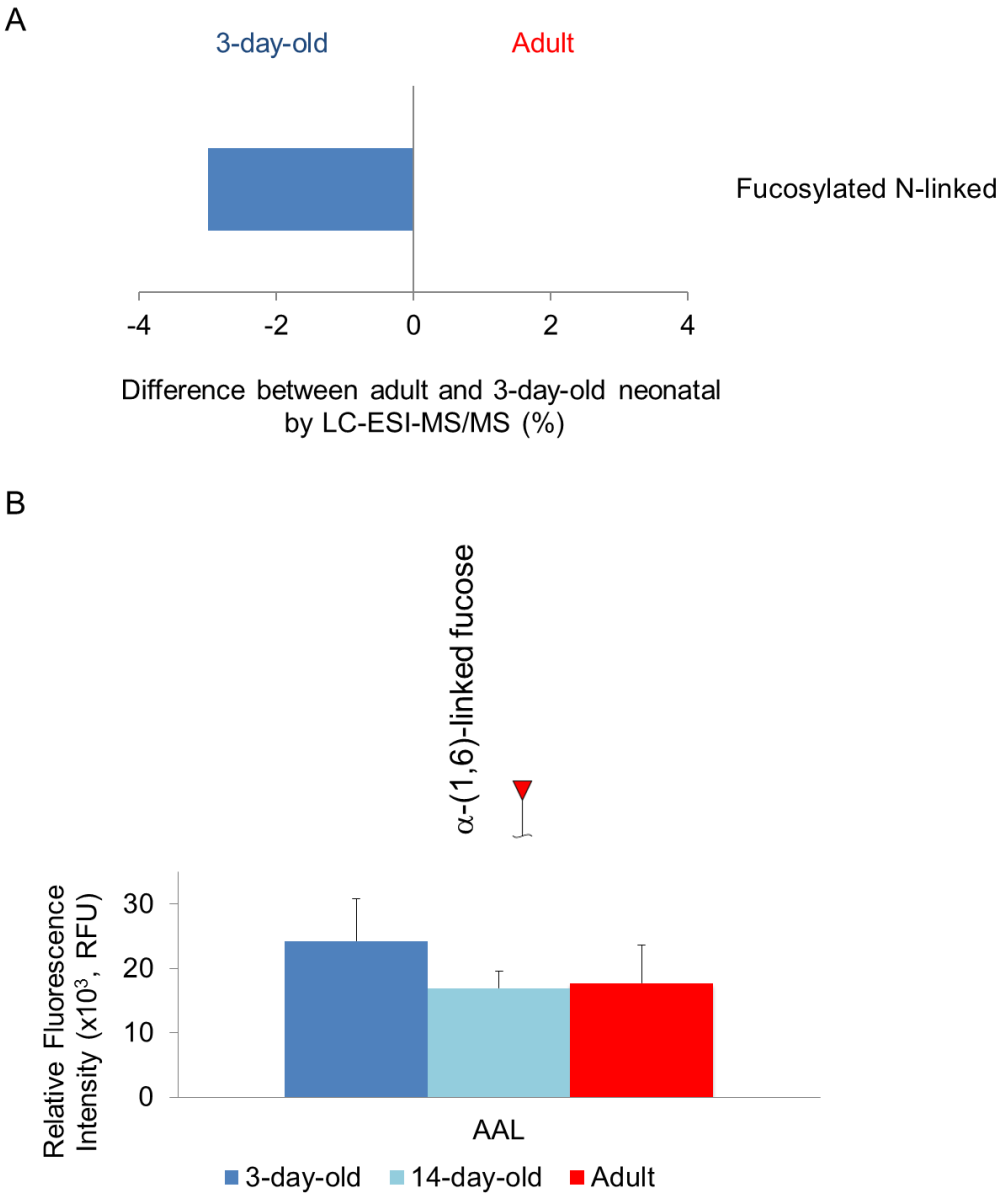

Figure 2.9 Higher fucosylation at early neonatal stage. (A) LC-ESI-MS/MS analysis showed a trend of higher expression of fucosylated *N*-glycans in three-day-old left ventricular myocardial tissue from Sprague Dawley healthy rats. (B) Lectin microarrays indicated an increased binding of three-day-old neonatal sample to AAL lectin.

Table 2.2 List of lectins printed on the lectin microarrays, with origin, abbreviation and carbohydrate specificity.

Lectin	Organism	Common name	Specificity
AIA, Jacalin	*Artocarpus integrifolia*	Jack fruit lectin	Gal (sialylation tolerant)
RPbAI	*Robinia pseudoacacia*	Black locust lectin	Gal, GalNAc
PA-I	*Pseudomonas aeruginosa*	Pseudomonas lectin	Gal, Gal derivatives
SNA-II	*Sambucus nigra*	Sambucus lectin-II	Gal/GalNAc
SJA	*Sophora japonica*	Pagoda tree lectin	β-GalNAc
DBA	*Dolichos biflorus*	Horse gram lectin	GalNAc-α-(1-3)-GalNAc
GHA	*Glechoma hederacea*	Ground ivy lectin	GalNAc
SBA	*Glycine max*	Soy bean lectin	GalNAc-α-(1-3)-Gal
VVA	*Vicia villosa*	Hairy vetch lectin	α-linked terminal GalNAc
BPA	*Bauhinia purpurea*	Camel's foot tree lectin	GalNAc/Gal
WFA	*Wisteria floribunda*	Japanese wisteria lectin	GalNAc/sulfated GalNAc
HPA	*Helix pomatia*	Garden snail lectin	α-linked terminal GalNAc
GSL-I-A4	*Griffonia simplicifolia*	Griffonia lectin-I A4	α-linked GalNAc
ACA	*Amaranthus caudatus*	Amaranthin	Sialylated/Gal-β-(1,3)-GalNAc
ABL	*Agaricus bisporus*	Edible mushroom lectin	Gal-β-(1,3)-GalNAc, GlcNAc
PNA	*Arachis hypogaea*	Peanut lectin	Gal-β-(1,3)-GalNAc
GSL-II	*Griffonia simplicifolia*	Griffonia/Bandeiraea lectin-II	GlcNAc
sWGA	*Triticum vulgaris*	Succinyl WGA	GlcNAc
DSA	*Datura stramonium*	Jimson weed lectin	GlcNAc
STA	*Solanum tuberosum*	Potato lectin	GlcNAc oligomers
LEL	*Lycopersicum eculentum*	Tomato lectin	GlcNAc-β-(1,4)-GlcNAc
Calsepa	*Calystegia sepium*	Bindweed lectin	Man/Maltose
NPA	*Narcissus pseudonarcissus*	Daffodil lectin	α-(1,6)-Man

Table 2.2 (Continued)

Lectin	Organism	Common name	Specificity
GNA	Galanthus nivalis	Snowdrop lectin	Man-α(1,3)-
HHA	Hippeastrum hybrid	Amaryllis agglutinin	Man-α(1,3)-Man-α(1,6)-
ConA	Canavalia ensiformis	Jack bean lectin	Man, Glc, GlcNAc
Lch-B	Lens culinaris	Lentil isolectin B	Man, fucose dependent
Lch-A	Lens culinaris	Lentil isolectin A	Man, fucose dependent
PSA	Pisum sativum	Pea lectin	Man, fucose dependent
TJA-I	Trichosanthes japonica	TJA One	Sialic acid-α-(2,6)-Gal(NAc)
WGA	Triticum vulgaris	Wheat germ agglutinin	NeuAc/GlcNAc
MAA	Maackia amurensis	Maackia agglutinin	Sialic acid-α-(2,3)-Gal(NAc)
SNA-I	Sambucus nigra	Sambucus lectin-I	Sialic acid-α-(2,6)-Gal(NAc)
CCA	Cancer antennarius	California crab	9-O-acetyl-sialic acid
PHA-L	Phaseolus vulgaris	Kidney bean leukoagglutinin	tri-/tetra-antennary β-Gal/Gal-β-(1,4)-GlcNAc
PHA-E	Phaseolus vulgaris	Kidney bean erythroagglutinin	biantennary, bisecting GlcNAc,β-Gal/Gal-β-(1,4-)GlcNAc
RCA-I/120	Ricinus communis	Castor bean lectin I	Gal-β-(1,4)-GlcNAc
AMA	Arum maculatum	Lords and Ladies agglutinin	Gal-β-(1,4)-GlcNAc
CPA	Cicer arietinum	Chickpea lectin	Complex glycopeptides
CAA	Caragana arborescens	Pea tree lectin	Gal-β-(1,4)-GlcNAc
ECA	Erythrina cristagalli	Cocks comb/coral tree lectin	Gal-β-(1,4)-GlcNAc oligomers
TJA-II	Trichosanthes japonica	TJA Two	Fuc-α(1,2)GalNAc-β(1-
AAL	Aleuria aurantia	Orange peel fungus lectin	α-(1,6)-linked Fuc
LTA	Lotus tetragonolobus	Lotus lectin	α-(1,3)-linked Fuc
UEA-I	Ulex europaeus	Gorse lectin-I	α-(1,2)-linked Fuc
EEA	Euonymous europaeus	Spindle tree lectin	α-Gal

Table 2.3 *N*-linked glycan structures detected in adult and three-day-old neonatal healthy ventricular tissue. Each m/z value is provided with potential composition, putative structure retention time (RT), intensity and relative percentage (%).

Mass	Composition	Putative structures	RT Adult	Intensity Adult	% Adult	RT Neo	Intensity Neonatal	% Neo
749	Hex2HexNAc2	Manα1-3Manβ1-4GlcNAcβ1-4GlcNAcol	14.3	659.6	0.5	nd	0.0	0.0
895	Hex2HexNAc2deHex1	Manα1-6Manβ1-4GlcNAcβ1-4(Fucα1-6)GlcNAcol	17.2	496.8	0.3	nd	0.0	0.0
911	Hex3HexNAc2	Manα1-3(Manα1-6)Manβ1-4GlcNAcβ1-4GlcNAcol	16.7	565.2	0.4	nd	0.0	0.0
1057	Hex3HexNAc2deHex1	Manα1-3(Manα1-6)Manβ1-4GlcNAcβ1-4(Fucα1-6)GlcNAcol	19.5	766.9	0.5	19.4	191.4	0.9
1073	Hex4HexNAc2	Manα1-3(Man-Manα1-6)Manβ1-4GlcNAcβ1-4GlcNAcol	16.0	719.8	0.5	nd	0.0	0.0
1235	Hex5HexNAc2	Manα1-3[Manα1-3(Manα1-6)Manα1-6]Manβ1-4GlcNAcβ1-4GlcNAcol	17.7	9028.7	6.2	17.7	1019.0	4.5
1397-1	Hex6HexNAc2	Manα1-2Manα1-3[Manα1-3(Manα1-6)Manα1-6]Manβ1-4GlcNAcβ1-4GlcNAcol	15.3	2814.7	1.9	15.2	1517.4	6.8
1397-2	Hex6HexNAc2	Manα1-3[Manα1-2Manα1-3(Manα1-6)Manα1-6]Manβ1-4GlcNAcβ1-4GlcNAcol	18.6	698.3	0.5	nd	0.0	0.0
1463	Hex3HexNAc4deHex1	GlcNAcβ1-2Manα1-3(GlcNAcβ1-2Manα1-6)Manβ1-4GlcNAcβ1-4(Fucα1-6)GlcNAcol	17.1	680.7	0.5	nd	0.0	0.0
1559-1	Hex7HexNAc2	Manα1-2Manα1-3[Manα1-3(Manα1-2Manα1-6)Manα1-6]Manβ1-4GlcNAcβ1-4GlcNAcol	14.6	1535.4	1.1	14.4	867.0	3.9
1559-2	Hex7HexNAc2	Manα1-2Manα1-2Manα1-3[Manα1-3(Manα1-6)Manα1-6]Manβ1-4GlcNAcβ1-4GlcNAcol	15.3	497.6	0.3	nd	0.0	0.0
1559-3	Hex7HexNAc2	Manα1-2Manα1-3[Manα1-2Manα1-3(Manα1-6)Manα1-6]Manβ1-4GlcNAcβ1-4GlcNAcol	15.5	1892.5	1.3	nd	0.0	0.0
1600-1	Hex6HexNAc3	Galβ1-4GlcNAcβ1-2Manα1-3[Manα1-3(Manα1-6)Man α1-6]Manβ1-4GlcNAcβ1-4GlcNAcol	16.1	983.7	0.7	nd	0.0	0.0
1600-2	Hex6HexNAc3	Galα1-3Galβ1-4GlcNAcβ1-2Manα1-3(Manα-Manα1-6)Manβ1-4GlcNAcβ1-4GlcNAcol	16.7	274.8	0.2	nd	0.0	0.0
1641	Hex5HexNAc4	Galβ1-4GlcNAcβ1-2Manα1-3(Galβ1-4GlcNAcβ1-2Manα1-6)Manβ1-4GlcNAcβ1-4GlcNAcol	16.6	338.9	0.2	nd	0.0	0.0
1666	Hex3HexNAc5deHex1	GlcNAcβ1-2Manα1-3(GlcNAcβ1-4)(GlcNAcβ1-2Manα1-6)Manβ1-4GlcNAcβ1-4(Fucα1-6)GlcNAcol	14.1	681.7	0.5	nd	0.0	0.0
1713-1	NeuAc1Hex4HexNAc3deHex1	NeuAcα2-3Galβ1-4GlcNAcβ1-2Manα1-3(Manα1-6)Manβ1-4GlcNAcβ1-4(Fucα1-6)GlcNAcol	18.9	161.6	0.1	nd	0.0	0.0
1713-2	NeuAc1Hex4HexNAc3deHex1	Manα1-3(NeuAcα2-3Galβ1-4GlcNAcβ1-2Manα1-6)Manβ1-4GlcNAcβ1-4(Fucα1-6)GlcNAcol	21.8	198.5	0.1	nd	0.0	0.0
1721	Hex8HexNAc2	Manα1-2Manα1-2Manα1-3[Manα1-3(Manα1-2Manα1-6)Manα1-6]Manβ1-4GlcNAcβ1-4GlcNAcol	14.6	6719.0	4.6	14.5	1757.0	7.8
1721	Hex8HexNAc2	Manα1-2Manα1-2Manα1-3[Manα1-2Manα1-3(Manα1-6)Manα1-6]Manβ1-4GlcNAcβ1-4GlcNAcol	15.5	2419.7	1.7	nd	0.0	0.0

Table 2.3 (Continued)

Mass	Composition	Putative structures	RT Adult	Intensity Adult	% Adult	RT Neo	Intensity Neonatal	% Neo
1729-1	NeuAc1Hex5HexNAc3	NeuAcα2-3Galβ1-4GlcNAcβ1-2Manα1-3(Manα1-6Manα1-6)Manβ1-4GlcNAcβ1-4GlcNAcol	16.3	506.3	0.3	nd	0.0	0.0
1729-2	NeuAc1Hex5HexNAc3	NeuAcα2-3Galβ1-4GlcNAcβ1-2Manα1-3(Manα1-3Manα1-6)Manβ1-4GlcNAcβ1-4GlcNAcol	20.0	1538.3	1.1	nd	0.0	0.0
1762-1	Hex7HexNAc3	GlcNAcβ1-2Manα1-3[Manα1-2Manα1-3(Manα1-2Manα1-6)Manα1-6]Manβ1-4GlcNAcβ1-4GlcNAcol	nd	0.0	0.0	17.6	232.3	1.0
1762-2	Hex7HexNAc3	Galα1-3Galβ1-4GlcNAcβ1-2Manα1-3[Manα1-3(Manα1-6)Manα1-6]Manβ1-4GlcNAcβ1-4GlcNAcol	18.2	492.2	0.3	nd	0.0	0.0
1787	Hex5HexNAc4deHex1	Galβ1-4GlcNAcβ1-2Manα1-3(Galβ1-4GlcNAcβ1-2Manα1-6)Manβ1-4GlcNAcβ1-4(Fucα1-6)GlcNAcol	18.5	343.0	0.2	18.5	337.6	1.5
1875-1	NeuAc1Hex5HexNAc3deHex1	NeuAcα2-3Galβ1-4GlcNAcβ1-2Manα1-3(Man-Manα1-6)Manβ1-4GlcNAcβ1-4(Fucα1-6)GlcNAcol	18.2	322.8	0.2	18.0	70.7	0.3
1875-2	NeuAc1Hex5HexNAc3deHex1	NeuAcα2-3Galβ1-4GlcNAcβ1-2Manα1-3(Man-Manα1-6)Manβ1-4GlcNAcβ1-4(Fucα1-6)GlcNAcol	21.3	2193.4	1.5	21.3	293.9	1.3
1883	Hex9HexNAc2	Manα1-2Manα1-2Manα1-3[Manα1-2Manα1-3(Manα1-2Manα1-6)Manα1-6]Manβ1-4GlcNAcβ1-4GlcNAcol	14.8	17655.7	12.1	14.7	2827.3	12.6
1891-1	NeuAc1Hex6HexNAc3	NeuAcα2-6Galβ1-4GlcNAcβ1-2Manα1-3[Manα1-3(Manα1-6)Manα1-6]Manβ1-4GlcNAcβ1-4GlcNAcol	17.5	967.3	0.7	17.5	315.0	1.4
1891-2	NeuAc1Hex6HexNAc3	NeuAcα2-3Galβ1-4GlcNAcβ1-2Manα1-3[Manα1-3(Manα1-6)Manα1-6]Manβ1-4GlcNAcβ1-4GlcNAcol	20.6	3112.6	2.1	20.6	500.0	2.2
1932-1	NeuAc1Hex5HexNAc4	Galβ1-4GlcNAcβ1-2Manα1-3(NeuAcα2-6Galβ1-4GlcNAcβ1-2Manα1-6)Manβ1-4GlcNAcβ1-4GlcNAcol	18.0	1414.8	1.0	17.9	167.3	0.7
1932-2	NeuAc1Hex5HexNAc4	Galβ1-4GlcNAcβ1-2Manα1-3(NeuAcα2-3Galβ1-4GlcNAcβ1-2Manα1-6)Manβ1-4GlcNAcβ1-4GlcNAcol	21.1	988.8	0.7	21.0	253.5	1.1
1949-1	Hex6HexNAc4deHex1	Galβ1-4GlcNAcβ1-2Manα1-3(Galα1-3Galβ1-4GlcNAcβ1-2Manα1-6)Manβ1-4GlcNAcβ1-4(Fucα1-6)GlcNAcol	19.8	816.3	0.6	19.8	134.9	0.6
1949-2	Hex6HexNAc4deHex1	Galα1-3Galβ1-4GlcNAcβ1-2Manα1-3(Galβ1-4GlcNAcβ1-2Manα1-6)Manβ1-4GlcNAcβ1-4(Fucα1-6)GlcNAcol	20.1	68.6	0.0	nd	0.0	0.0
1965	Hex7HexNAc4	Galα1-3Galβ1-4GlcNAcβ1-2Manα1-3(Galα1-3Galβ1-4GlcNAcβ1-2Manα1-6)Manβ1-4GlcNAcβ1-4GlcNAcol	nd	0.0	0.0	19.6	173.4	0.8
2037-1	NeuAc1Hex6HexNAc3deHex1	NeuAcα2-6Galβ1-4GlcNAcβ1-2Manα1-3[Manα1-3(Manα1-6)Manα1-6]Manβ1-4GlcNAcβ1-4(Fucα1-6)GlcNAcol	19.4	324.6	0.2	19.3	51.8	0.2
2037-2	NeuAc1Hex6HexNAc3deHex1	NeuAcα2-3Galβ1-4GlcNAcβ1-2Manα1-3[Manα1-3(Manα1-6)Manα1-6]Manβ1-4GlcNAcβ1-4(Fucα1-6)GlcNAcol	22.1	1236.7	0.8	22.0	200.5	0.9
2045	Hex10HexNAc2	Glcα1-3Manα1-2Manα1-2Manα1-3[Manα1-2Manα1-3(Manα1-2Manα1-6)Manα1-6]Manβ1-4GlcNAcβ1-4GlcNAcol	nd	0.0	0.0	15.5	250.0	1.1

Table 2.3 (Continued)

Mass	Composition	Putative structures	RT Adult	Intensity Adult	% Adult	RT Neo	Intensity Neonatal	% Neo
2078-1	NeuAc1Hex5HexNAc4deHex1	NeuAcα2-3Galβ1-4GlcNAcβ1-2Manα1-3(Galβ1-4GlcNAcβ1-2Manα1-6)Manβ1-4GlcNAcβ1-4(Fucα1-6)GlcNAcol	19.7	2892.1	2.0	19.6	935.1	4.2
2078-2	NeuAc1Hex5HexNAc4deHex1	Galβ1-4GlcNAcβ1-2Manα1-3(NeuAcα2-3Galβ1-4GlcNAcβ1-2Manα1-6)Manβ1-4GlcNAcβ1-4(Fucα1-6)GlcNAcol	22.6	3105.7	2.1	22.5	532.6	2.4
2094-1	NeuAc1Hex6HexNAc4	Galα1-3Galβ1-4GlcNAcβ1-2Manα1-3(NeuAcα2-3Galβ1-4GlcNAcβ1-2Manα1-6)Manβ1-4GlcNAcβ1-4GlcNAcol	19.3	707.1	0.5	19.2	105.0	0.5
2094-2	NeuAc1Hex6HexNAc4	NeuAcα2-3Galβ1-4GlcNAcβ1-2Manα1-3(Galα1-3Galβ1-4GlcNAcβ1-2Manα1-6)Manβ1-4GlcNAcβ1-4GlcNAcol	21.9	777.1	0.5	21.8	228.0	1.0
2111	Hex7HexNAc4deHex1	Galα1-3Galβ1-4GlcNAcβ1-2Manα1-3(Galα1-3Galβ1-4GlcNAcβ1-2Manα1-6)Manβ1-4GlcNAcβ1-4(Fucα1-6)GlcNAcol	21.1	1068.1	0.7	21.1	273.7	1.2
2223-1	NeuAc2Hex5HexNAc4	NeuAcα2-6Galβ1-4GlcNAcβ1-2Manα1-3(NeuAcα2-6Galβ1-4GlcNAcβ1-2Manα1-6)Manβ1-4GlcNAcβ1-4GlcNAcol	19.3	8802.4	6.0	19.2	177.7	0.8
2223-2	NeuAc2Hex5HexNAc4	NeuAcα2-6Galβ1-4GlcNAcβ1-2Manα1-3(NeuAcα2-3Galβ1-4GlcNAcβ1-2Manα1-6)Manβ1-4GlcNAcβ1-4GlcNAcol	21.4	1679.4	1.2	nd	0.0	0.0
2223-3	NeuAc2Hex5HexNAc4	NeuAcα2-6Galβ1-4GlcNAcβ1-2Manα1-3(NeuAcα2-3Galβ1-4GlcNAcβ1-2Manα1-6)Manβ1-4GlcNAcβ1-4GlcNAcol	22.4	2139.9	1.5	22.2	331.9	1.5
2223-4	NeuAc2Hex5HexNAc4	NeuAcα2-3Galβ1-4GlcNAcβ1-2Manα1-3(NeuAcα2-3Galβ1-4GlcNAcβ1-2Manα1-6)Manβ1-4GlcNAcβ1-4GlcNAcol	24.6	2518.0	1.7	24.6	336.0	1.5
2240-1	NeuAc1Hex6HexNAc4deHex1	Galα1-3Galβ1-4GlcNAcβ1-2Manα1-3(NeuAcα2-6Galβ1-4GlcNAcβ1-2Manα1-6)Manβ1-4GlcNAcβ1-4(Fucα1-6)GlcNAcol	20.8	4710.0	3.2	20.7	567.1	2.5
2240-2	NeuAc1Hex6HexNAc4deHex1	NeuAcα2-3Galβ1-4GlcNAcβ1-2Manα1-3(Galα1-3Galβ1-4GlcNAcβ1-2Manα1-6)Manβ1-4GlcNAcβ1-4(Fucα1-6)GlcNAcol	23.2	2630.0	1.8	23.2	653.3	2.9
2369-1	NeuAc2Hex5HexNAc4deHex1	NeuAcα2-6Galβ1-4GlcNAcβ1-2Manα1-3(NeuAcα2-3Galβ1-4GlcNAcβ1-2Manα1-6)Manβ1-4GlcNAcβ1-4(Fucα1-6)GlcNAcol	20.8	4873.2	3.3	20.7	1131.5	5.0
2369-2	NeuAc2Hex5HexNAc4deHex1	NeuAcα2-6Galβ1-4GlcNAcβ1-2Manα1-3(NeuAcα2-3Galβ1-4GlcNAcβ1-2Manα1-6)Manβ1-4GlcNAcβ1-4(Fucα1-6)GlcNAcol	23.6	6215.0	4.3	23.5	1420.5	6.3
2369-3	NeuAc2Hex5HexNAc4deHex1	NeuAcα2-3Galβ1-4GlcNAcβ1-2Manα1-3(NeuAcα2-3Galβ1-4GlcNAcβ1-2Manα1-6)Manβ1-4GlcNAcβ1-4(Fucα1-6)GlcNAcol	25.8	7379.5	5.1	25.9	1659.2	7.4
2514	NeuAc3Hex5HexNAc4	NeuAcα2-8NeuAcα2-3Galβ1-4GlcNAcβ1-2Manα1-3(NeuAcα2-3Galβ1-4GlcNAcβ1-2Manα1-6)Manβ1-4GlcNAcβ1-4GlcNAcol	22.7	2754.9	1.9	nd	0.0	0.0
2660-1	NeuAc3Hex5deHex4deHex1	NeuAcα2-8NeuAcα2-3Galβ1-4GlcNAcβ1-2Manα1-3(NeuAcα2-3Galβ1-4GlcNAcβ1-2Manα1-6)Manβ1-4GlcNAcβ1-4(Fucα1-6)GlcNAcol	24.0	693.7	0.5	nd	0.0	0.0
2660-2	NeuAc3Hex5deHex4deHex1	NeuAcα2-3Galβ1-4GlcNAcβ1-2Manα1-3(NeuAcα2-8NeuAcα2-3Galβ1-4GlcNAcβ1-2Manα1-6)Manβ1-4GlcNAcβ1-4(Fucα1-6)GlcNAcol	26.9	967.1	0.7	nd	0.0	0.0

Table 2.3 (Continued)

Mass	Composition	Putative structures	RT Adult	Intensity Adult	% Adult	RT Neo	Intensity Neonatal	% Neo
2734-1	NeuAc2Hex6HexNAc5deHex1	2NeuAc+Galβ1-4GlcNAcβ1-2(Galβ1-4GlcNAcβ1-4)Manα1-3(Galβ1-4GlcNAcβ1-2Manα1-6)Manβ1-4GlcNAcβ1-4(Fucα1-6)GlcNAcol	23.7	419.7	0.3	23.8	1754.5	7.8
2734-2	NeuAc2Hex6HexNAc5deHex1	2NeuAc+Galβ1-4GlcNAcβ1-2(Galβ1-4GlcNAcβ1-4)Manα1-3(Galβ1-4GlcNAcβ1-2Manα1-6)Manβ1-4GlcNAcβ1-4(Fucα1-6)GlcNAcol	25.2	869.0	0.6	25.0	71.5	0.3
2734-3	NeuAc2Hex6HexNAc5deHex1	2NeuAc+Galβ1-4GlcNAcβ1-2(Galβ1-4GlcNAcβ1-4)Manα1-3(Galβ1-4GlcNAcβ1-2Manα1-6)Manβ1-4GlcNAcβ1-4(Fucα1-6)GlcNAcol	26.1	1390.5	1.0	26.0	98.3	0.4
2734-4	NeuAc2Hex6HexNAc5deHex1	2NeuAc+Galβ1-4GlcNAcβ1-2(Galβ1-4GlcNAcβ1-4)Manα1-3(Galβ1-4GlcNAcβ1-2Manα1-6)Manβ1-4GlcNAcβ1-4(Fucα1-6)GlcNAcol	28.0	495.9	0.3	nd	0.0	0.0
2880-1	NeuAc3Hex6HexNAc5	3NeuAc+Galβ1-4GlcNAcβ1-2(Galβ1-4GlcNAcβ1-4)Manα1-3(Galβ1-4GlcNAcβ1-2Manα1-6)Manβ1-4GlcNAcβ1-4GlcNAcol	23.9	807.6	0.6	nd	0.0	0.0
2880-2	NeuAc3Hex6HexNAc5	3NeuAc+Galβ1-4GlcNAcβ1-2(Galβ1-4GlcNAcβ1-4)Manα1-3(Galβ1-4GlcNAcβ1-2Manα1-6)Manβ1-4GlcNAcβ1-4GlcNAcol	25.4	390.0	0.3	nd	0.0	0.0
2880-3	NeuAc3Hex6HexNAc5	3NeuAc+Galβ1-4GlcNAcβ1-2(Galβ1-4GlcNAcβ1-4)Manα1-3(Galβ1-4GlcNAcβ1-2Manα1-6)Manβ1-4GlcNAcβ1-4GlcNAcol	27.6	663.6	0.5	nd	0.0	0.0
3026-1	NeuAc3Hex6HexNAc5deHex1	3NeuAc+Galβ1-4GlcNAcβ1-2(Galβ1-4GlcNAcβ1-4)Manα1-3(Galβ1-4GlcNAcβ1-2Manα1-6)Manβ1-4GlcNAcβ1-4(Fucα1-6)GlcNAcol	24.9	1382.0	0.9	24.8	376.5	1.7
3026-2	NeuAc3Hex6HexNAc5deHex1	3NeuAc+Galβ1-4GlcNAcβ1-2(Galβ1-4GlcNAcβ1-4)Manα1-3(Galβ1-4GlcNAcβ1-2Manα1-6)Manβ1-4GlcNAcβ1-4(Fucα1-6)GlcNAcol	26.1	2655.1	1.8	nd	0.0	0.0
3026-3	NeuAc3Hex6HexNAc5deHex1	3NeuAc+Galβ1-4GlcNAcβ1-2(Galβ1-4GlcNAcβ1-4)Manα1-3(Galβ1-4GlcNAcβ1-2Manα1-6)Manβ1-4GlcNAcβ1-4(Fucα1-6)GlcNAcol	27.8	2658.1	1.8	27.3	157.9	0.7
3026-4	NeuAc3Hex6HexNAc5deHex1	3NeuAc+Galβ1-4GlcNAcβ1-2(Galβ1-4GlcNAcβ1-4)Manα1-3(Galβ1-4GlcNAcβ1-2Manα1-6)Manβ1-4GlcNAcβ1-4(Fucα1-6)GlcNAcol	30.2	3463.7	2.4	nd	0.0	0.0
3317-1	NeuAc4Hex6HexNAc5deHex1	4NeuAc+Galβ1-4GlcNAcβ1-2(Galβ1-4GlcNAcβ1-4)Manα1-3(Galβ1-4GlcNAcβ1-2Manα1-6)Manβ1-4GlcNAcβ1-4(Fucα1-6)GlcNAcol	27.1	141.1	0.1	nd	0.0	0.0
3317-2	NeuAc4Hex6HexNAc5deHex1	4NeuAc+Galβ1-4GlcNAcβ1-2(Galβ1-4GlcNAcβ1-4)Manα1-3(Galβ1-4GlcNAcβ1-2Manα1-6)Manβ1-4GlcNAcβ1-4(Fucα1-6)GlcNAcol	29.7	5113.0	3.5	30.0	164.0	0.7
3317-3	NeuAc4Hex6HexNAc5deHex1	4NeuAc+Galβ1-4GlcNAcβ1-2(Galβ1-4GlcNAcβ1-4)Manα1-3(Galβ1-4GlcNAcβ1-2Manα1-6)Manβ1-4GlcNAcβ1-4(Fucα1-6)GlcNAcol	30.6	3905.4	2.7	nd	0.0	0.0
3391	NeuAc3Hex7HexNAc6deHex1	3xNeuAc+Galβ1-4GlcNAcβ1-2(Galβ1-4GlcNAcβ1-4)Manα1-3[Galβ1-4GlcNAcβ1-2(Galβ1-4GlcNAcβ1-6)Manα1-6]Manβ1-4GlcNAcβ1-4(Fucα1-6)GlcNAcol	28.5	519.6	0.4	28.3	197.3	0.9
3682-1	NeuAc4Hex7HexNAc6deHex1	4xNeuAc+Galβ1-4GlcNAcβ1-2(Galβ1-4GlcNAcβ1-4)Manα1-3[Galβ1-4GlcNAcβ1-2(Galβ1-4GlcNAcβ1-6)Manα1-6]Manβ1-4GlcNAcβ1-4(Fucα1-6)GlcNAcol	30.2	1181.7	0.8	30.2	93.7	0.4
3682-2	NeuAc4Hex7HexNAc6deHex1	4xNeuAc+Galβ1-4GlcNAcβ1-2(Galβ1-4GlcNAcβ1-4)Manα1-3[Galβ1-4GlcNAcβ1-2(Galβ1-4GlcNAcβ1-6)Manα1-6]Manβ1-4GlcNAcβ1-4(Fucα1-6)GlcNAcol	33.2	303.6	0.2	nd	0.0	0.0
3973	NeuAc5Hex7HexNAc6deHex1	5xNeuAc+Galβ1-4GlcNAcβ1-2(Galβ1-4GlcNAcβ1-4)Manα1-3[Galβ1-4GlcNAcβ1-2(Galβ1-4GlcNAcβ1-6)Manα1-6]Manβ1-4GlcNAcβ1-4(Fucα1-6)GlcNAcol	35.9	1480.3	1.0	35.5	42.1	0.2

Table 2.4 *O*-linked glycan structures detected in adult and three-day-old neonatal healthy ventricular tissue. Each m/z value is provided with potential composition, putative structure retention time (RT), intensity and relative percentage (%).

Mass	Composition	Putative structures	RT Adult	Intensity Adult	% Adult	RT Neo	Intensity Neo	% Neo
384	Hex1HexNAc1	Galβ1-3GalNAcol	6.8	852.2	3.9	6.8	1037.0	4.3
425	HexNAc2	GlcNAcβ1-3GalNAcol	8.9	581.3	2.6	nd	0.0	0.0
513	NeuAc1HexNAc1	NeuAcα2-6GalNAcol	9.1	311.6	1.4	nd	0.0	0.0
587	Hex1HexNAc2	Galβ1-3(GlcNAcβ1-6)GalNAcol	9.2	96.2	0.4	nd	0.0	0.0
675-1	NeuAc1Hex1HexNAc1	Galβ1-3(NeuAcα2-6)GalNAcol	9.8	2274.0	10.3	9.6	1039.3	4.3
675-2	NeuAc1Hex1HexNAc1	NeuAcαα2-3Galβ1-3GalNAcol	11.4	3164.3	14.3	11.3	2896.0	12.1
691-1	NeuGc1Hex1HexNAc1	Galβ1-3(NeuGcα2-6)GalNAcol	9.7	66.3	0.3	15.2	1517.4	6.3
691-2	NeuGc1Hex1HexNAc1	NeuGcα2-3Galβ1-3GalNAcol	11.2	129.0	0.6	nd	0.0	0.0
749	Hex2HexNAc2	Galβ1-3(Galβ1-4GlcNAcβ1-6)GalNAcol	11.2	837.1	3.8	11.2	316.1	1.3
878	NeuAc1Hex1HexNAc2	NeuAcα2-3Galβ1-3(GlcNAcβ1-6)GalNAcol	13.5	151.6	0.7	nd	0.0	0.0
966	NeuAc2Hex1HexNAc1	NeuAcα2-3Galβ1-3(NeuAcα2-6)GalNAcol	13.0	5353.0	24.2	13.0	6140.1	25.6
1040-1	NeuAc1Hex2HexNAc2	NeuAcα2-3Galβ1-3(Galβ1-4GlcNAcβ1-6)GalNAcol	15.9	1157.5	5.2	15.8	1252.5	5.2
1040-2	NeuAc1Hex2HexNAc2	Galβ1-3(NeuAcα2-3Galβ1-4GlcNAcβ1-6)GalNAcol	18.5	1392.0	6.3	18.4	2536.0	10.6
1120	NeuAc1Hex2HexNAc2Sul1	NeuAcα2-3Galβ1-3[(3S)Galβ1-4GlcNAcβ1-6]GalNAcol	nd	0.0	0.0	19.8	1582.8	6.6
1331	NeuAc2Hex2HexNAc2	NeuAcα2-3Galβ1-3(NeuAcα2-3Galβ1-4GlcNAcβ1-6)GalNAcol	22.1	5708.3	25.9	22.2	5708.1	23.8

2.4 Discussion

Cardiac regenerative potential is present in mammals only at the early neonatal stage [Porrello 2011], and the rapid loss of this capability is a well-known limitation of this type of tissue after the occurrence of ischemic damage. Due to the importance of glycosylation in the regulation of the cellular microenvironment through interactions of the cell glycocalyx and the ECM, identifying glycosylation-related mechanisms associated with pathological degeneration could provide key targets for novel therapeutic strategies [Mohd Isa, Paszek]. Moreover, recently glycosylation differences of ECM and cells related to ageing were characterized [Collin], and in the cardiac field a precise correlation was found between the alterations in the structure and function of heparan sulphate and the physiological decline of growth factor recruitment in the ECM [Huynh].

Studies to characterize the glycosylation of the myocardial and skeletal muscle tissues have been mainly histologically based to date using lectins to indicate the presence of different types of glycosylation [Bardosi, Lawrenson, Frank, Gros]. Most of these studies differentiated for cytosolic or membrane localisation in the tissue of interest. Cardiomyocytes, fibroblasts and capillaries structures populate both ventricular walls of the heart and so far very few studies have focused on any possible regional-dependent different physiological responses to external insults [Tracy, de Jonge]. The work presented in this chapter not only localized the binding of a panel of biologically-relevant lectins to rat cardiomyocytes surfaces and capillaries, but assessed the consistency of the glycosylation expression across different strains of rat healthy left and right cardiac ventricles. Further, a differential localisation of terminal sialic acids with different linkages with α-(2,6)-sialylation located on capillaries and α-(2,3)-sialylation on the cardiomyocytes membranes was seen. SNA binding to capillaries but not to cardiomyocytes was likely to be as a result of the lack of α-(2,6)-sialic acids on the cell surface, consistently with what had been previously reported [Lawrenson]. From a ligand-receptor perspective, the consistent expression of α-(2,6)-sialic acids on surfaces of vessels could be a mechanism by which regulate the receptors implicated with angiogenesis, such as vascular endothelial growth factor receptor (VEGFR), hepatocyte growth factor receptor (HGFR) and epidermal growth factor-related ERBB receptor [Ferreira].

Recently, a high abundance of this linkage of sialic acid was assessed also in vessels characterizing anti-VEGF sensitive tumours [Croci] and the knockdown of α-2,6-sialyltransferase (ST6Gal-I) significantly reduced the motility of colon cancer cells [Qian].

The consistent expression of GlcNAc residues on the cardiomyocytes surfaces reflects previous findings [Bardosi, Emde] and indicates the relevance of this glycan in the composition of the glycocalyx which characterises the cellular membrane. Binding to DSA lectin was seen both by lectin histochemistry and microarrays, and indeed their binding residues GlcNAc-β-(1,4) and Gal-β-(1-4)-GlcNAc were detected also in the *N*-glycans structures by LC-MS/MS. Nevertheless, there were not relevant differences associated with the expression of these residues in the current ageing comparison.

The main limitation of the results hereby presented stems from the variability of the strains of rat and genders which were used for the initial determination of a healthy adult baseline, whereas the same strain was used for the final ageing comparison. Rat myocardial left ventricle tissues from two post-neonatal stages (three- and 14-day-old) had consistent glycosylation and both differed from adult glycosylation. After the recent advances in the development of LC-ESI-MS/MS to quantify *N*- and *O*-glycans [Jensen, Yang, Frost], it was possible to see for the first time in this study a higher expression of complex glycans on the cellular membrane and ECM in the adult stage than that in the early neonatal, including di-sialylated *N*-glycans (NeuAc-α(2-8)-NeuAc). The higher expression of complex-type structures correlates with the lectin microarray, in particular in the binding to WGA, CPA and LTA lectins. A higher binding to WGA reflected the increased sialylation in adult detected in *N*-glycans by LC-MS/MS. Previous studies have established the importance of both *N*- and *O*-linked glycans in the voltage gated ion channel activity which is fundamental for heart cells contractility [Monpetit, Schwetz]. Specifically, enzymatic desialylation experiments were performed to demonstrate the modulation of the functioning of voltage-gated potassium channels by *N*- and *O*-glycans [Schwetz 2010 and 2011], and the relevance of polysialic acid was highlighted on the conductive properties of cardiac cells. Deletion of the α-(2,8)-sialyltransferase 8B enzyme significantly affected the action potential of sodium channels in atrial

cardiomyocytes whereas this did not occur with ventricular cardiomyocytes [Montpetit]. In the current study, the higher expression of NeuAc-α(2-8)-NeuAc detected in the adult than in the neonatal ventricular whole membrane and ECM lysate could instead reflect the role of polysialic acid in the regulation of cell-ECM. This specific structure has been studied for the potential activation of fibroblast growth factor signalling by its expression on neural cell adhesion molecules (NCAM) [Kiselyov, Ferreira 2018].

N-linked glycan analysis showed a 5% increase in the portion of complex-type structures and a 6% decrease in the subgroup of high mannose structures in adult compared to three-day-old neonatal. Interestingly, the results of the LC-MS/MS analysis performed in this study identified a 4% increase in relative percentage of the $Man_6GlcNAc_2$-structure in neonatal cardiac tissue. The greater expression of this high mannose type structure in neonatal tissue may be an indication of stemness of the tissue, as high percentages of high mannose structures were detected in total protein lysates of pluripotent stem cells [Fujitani, Hasehira]. Therefore, the increase in surface expression of high mannose structures may be due to the temporary expansion of the endoplasmic reticulum which is needed for the translational processes more than being a sign of cellular stress [Cherepanova, Bieberich].
Moreover, in this study three *N*-glycan structures that were present only in the neonatal tissue were identified. Among these structures, a complex-type structure with terminal Gal-α-(1,3)-Gal disaccharide ([M-H] ion of *m/z* 1965) and a high mannose type structure, $Hex_{10}HexNAc_2$ (Glc_1Man_9) ([M-H]-ion of *m/z* 2045), were also previously not found in adult tissue [Parker]. The detection of $Hex_{10}HexNAc_2$ exclusively in neonatal tissue, together with increase in the abundance of $Man_6GlcNAc_2$, might indicate a different cellular-type composition at three days after birth, i.e. in the middle of the self-regenerating capability of the mammalian heart [Porrello 2011]. Finally, the observed decrease in high mannose-type *N*-glycans in myocardial total membrane samples upon ageing reflects the same trend seen in both differentiated cardiomyocytes and fibroblasts when compared to induced pluripotent stem cells (iPSCs) [Hasehira, Kawamura]. Nevertheless, the distinctive increase in the relative abundance of $Man_5GlcNAc_2$- in iPSCs [Hasehira] was not seen in the neonatal total membranes, whereas $Man_6GlcNAc_2$- and $Man_{10}GlcNAc_2$- accounted for the higher abundance in total high mannose retained at the early

neonatal stage (three days after birth). Consistent with these findings relative to high mannose-type *N*-glycans, the stemness of three-day-old neonatal tissue was highlighted also by two additional observations in this study. First, the reported decrease in sialylated *N*-glycans in neonatal was reported also when comparing differentiated cardiomyocytes to stem cells [Kawamura]. Second, the increase in core fucosylation seen both in *N*-linked glycans correlated with its already reported distinctive presence in undifferentiated (iPSCs) rather than in the somatic state (fibroblasts) [Hasehira].

Further, the current work is the first structural analysis of *O*-linked glycans in rat cardiac tissue, either neonatal or adult. Interestingly, in both neonatal and adult, unlike *O*-glycans containing both Neu5Ac and Neu5Gc, all detected sialylated *N*-glycans contained only Neu5Ac. This finding could be in contrast with the previously reported expression of Neu5Gc in the total lysate of cardiomyocytes and ventricular/atrial tissue [Hasehira, Montpetit], but the samples analysed in this study were membrane proteins. Therefore, the accumulation of *N*-linked glycans containing NeuGc in the intracellular portion as a result of a metabolic pathway might account for this difference [Bergfeld]. On the other hand, the retention of NeuGc on the epithelial cells whose glycocalyx contain *O*-linked glycans could justify why they were detected in both neonatal and adult. This limited localisation would also partially explain the detection of a sulfated core 2 *O*-glycan structure (NeuAc-α-(2-3)-Galβ1-3[(3S)Galβ1-4GlcNAcβ1-6]GalNAcol) which is a carbohydrate determinant present on the glycoproteins coating endothelial mucins such as CD34 [Arata-Kawai, Hernandez Mir].

2.5 Conclusions

In conclusion, these results show glycosylation in different stages of healthy myocardial tissue. Consistent glycosylation was shown across the left ventricular tissue and was demonstrated to be similar to that across the right ventricle. Moreover, rat maturation is associated with precise changes in *N*- and *O*-linked glycan structures which were screened by LC-ESI-MS/MS and validated by lectin microarray analysis. These findings represent a well-characterized basis of comparison for the investigation of glycosylation changes in the myocardial tissue in a pathological scenario such as ischemia or cardiac pressure overload. With the

identification of potential glycans targets in this work, the future glycan-targeted therapies might be designed to enhance an ECM-inspired restoration of the myocardial tissue following myocardial infarction.

2.6 References

- Arata-Kawai H, Singer MS, Bistrup A, Zante Av, Wang YQ, Ito Y, Bao X, Hemmerich S, Fukuda M, Rosen SD. Functional contributions of N- and O-glycans to L-selectin ligands in murine and human lymphoid organs. Am J Pathol. 2011 Jan;178(1):423-33
- Bardosi A, Bardosi L, Hendrys M, Wosgien B, Gabius HJ. Spatial differences of endogenous lectin expression within the cellular organization of the human heart: a glycohistochemical, immunohistochemical, and glycobiochemical study. Am J Anat. 1990 Aug;188(4):409-18
- Bergfeld AK, Pearce OM, Diaz SL, Pham T, Varki A. Metabolism of vertebrate amino sugars with N-glycolyl groups: elucidating the intracellular fate of the non-human sialic acid N-glycolylneuraminic acid. J Biol Chem. 2012 Aug 17;287(34):28865-81
- Bieberich E. Synthesis, Processing, and Function of N-glycans in N-glycoproteins. Adv Neurobiol. 2014;9:47-70
- Cherepanova N, Shrimal S, Gilmore R. N-linked glycosylation and homeostasis of the endoplasmic reticulum. Curr Opin Cell Biol. 2016 Aug;41:57-65
- Collin EC, Kilcoyne M, White SJ, Grad S, Alini M, Joshi L, Pandit AS. Unique glycosignature for intervertebral disc and articular cartilage cells and tissues in immaturity and maturity. Sci Rep. 2016 Mar 11;6:23062
- Croci DO, Cerliani JP, Dalotto-Moreno T, Méndez-Huergo SP, Mascanfroni ID, Dergan-Dylon S, Toscano MA, Caramelo JJ, García-Vallejo JJ, Ouyang J, Mesri EA, Junttila MR, Bais C, Shipp MA, Salatino M, Rabinovich GA. Glycosylation-dependent lectin-receptor interactions preserve angiogenesis in anti-VEGF refractory tumors. Cell. 2014 Feb 13;156(4):744-58
- de Jonge N, Lahpor JR, van Wichen DF, Kirkels H, Gmelig-Meyling FH, van den Tweel JG, Doevendans PA, de Weger RA. Similar left and right ventricular sarcomere structure after support with a left ventricular assist device suggests the

utility of right ventricular biopsies to monitor left ventricular reverse remodeling. Int J Cardiol. 2005 Feb 28;98(3):465-70

- Drenckhahn JD, Schwarz QP, Gray S, Laskowski A, Kiriazis H, Ming Z, Harvey RP, Du XJ, Thorburn DR, Cox TC. Compensatory growth of healthy cardiac cells in the presence of diseased cells restores tissue homeostasis during heart development. Dev Cell. 2008 Oct;15(4):521-33
- Emde B, Heinen A, Gödecke A, Bottermann K. Wheat germ agglutinin staining as a suitable method for detection and quantification of fibrosis in cardiac tissue after myocardial infarction. Eur J Histochem. 2014 Dec 17;58(4):2448
- Everest-Dass AV, Abrahams JL, Kolarich D, Packer NH, Campbell MP. Structural feature ions for distinguishing N- and O-linked glycan isomers by LC-ESI-IT MS/MS. J Am Soc Mass Spectrom. 2013 Jun;24(6):895-906
- Ferreira IG, Pucci M, Venturi G, Malagolini N, Chiricolo M, Dall'Olio F. Glycosylation as a main regulator of growth and death factor receptors signaling. Int J Mol Sci. 2018 Feb 15;19(2)
- Frank JS, Langer GA, Nudd LM, Seraydarian K. The myocardial cell surface, its histochemistry, and the effect of sialic acid and calcium removal on its structure and cellular ionic exchange. Circ Res. 1977 Nov;41(5):702-14
- Frost DC, Li L. Recent advances in mass spectrometry-based glycoproteomics. Adv Protein Chem Struct Biol. 2014;95:71-123
- Fujitani N, Furukawa J, Araki K, Fujioka T, Takegawa Y, Piao J, Nishioka T, Tamura T, Nikaido T, Ito M, Nakamura Y, Shinohara Y. Total cellular glycomics allows characterizing cells and streamlining the discovery process for cellular biomarkers. Proc Natl Acad Sci U S A. 2013 Feb 5;110(6):2105-10
- Gerlach JQ, Kilcoyne M, Eaton S, Bhavanandan V, Joshi L. Non-carbohydrate-mediated interaction of lectins with plant proteins. Adv Exp Med Biol. 2011;705:257-69
- Glass WF 2nd, Briggs RC, Hnilica LS. Use of lectins for detection of electrophoretically separated glycoproteins transferred onto nitrocellulose sheets. Anal Biochem. 1981 Jul 15;115(1):219-24
- Gros D, Bruce B, Challice CE, Schrevel J. Ultrastructural localization of concanavalin A and wheat germ agglutinin binding sites in adult and embryonic mouse myocardium. J Histochem Cytochem. 1982 Mar;30(3):193-200

- Hasehira K, Tateno H, Onuma Y, Ito Y, Asashima M, Hirabayashi J. Structural and quantitative evidence for dynamic glycome shift on production of induced pluripotent stem cells. Mol Cell Proteomics. 2012 Dec;11(12):1913-23
- Haubner BJ, Adamowicz-Brice M, Khadayate S, Tiefenthaler V, Metzler B, Aitman T, Penninger JM. Complete cardiac regeneration in a mouse model of myocardial infarction. Aging (Albany NY). 2012 Dec;4(12):966-77
- Hernandez Mir G, Helin J, Skarp KP, Cummings RD, Mäkitie A, Renkonen R, Leppänen A. Glycoforms of human endothelial CD34 that bind L-selectin carry sulfated sialyl Lewis x capped O- and N-glycans. Blood. 2009 Jul 16;114(3):733-41
- Hu H, Eggers K, Chen W, Garshasbi M, Motazacker MM, Wrogemann K, Kahrizi K, Tzschach A, Hosseini M, Bahman I, Hucho T, Mühlenhoff M, Gerardy-Schahn R, Najmabadi H, Ropers HH, Kuss AW. ST3GAL3 mutations impair the development of higher cognitive functions. Am J Hum Genet. 2011 Sep 9;89(3):407-14
- Huynh MB, Morin C, Carpentier G, Garcia-Filipe S, Talhas-Perret S, Barbier Chassefière V, van Kuppevelt TH, Martelly I, Albanese P, Papy-Garcia D. Age-related changes in rat myocardium involve altered capacities of glycosaminoglycans to potentiate growth factor functions and heparin sulfate-altered sulfation. J Biol Chem. 2012 Mar 30;287(14):11363-73
- InanlooRahatloo K, Parsa AF, Huse K, Rasooli P, Davaran S, Platzer M, Kramer M, Fan JB, Turk C, Amini S, Steemers F, Gunderson K, Ronaghi M, Elahi E. Mutation in ST6GALNAC5 identified in family with coronary artery disease. Sci Rep. 2014 Jan 8;4:3595
- Jensen PH, Karlsson NG, Kolarich D, Packer NH. Structural analysis of N- and O-glycans released from glycoproteins. Nat Protoc. 2012 Jun 7;7(7):1299-310
- Kawamura T, Miyagawa S, Fukushima S, Kashiyama N, Kawamura A, Ito E, Saito A, Maeda A, Eguchi H, Toda K, Miyagawa S, Okuyama H, Sawa Y. Structural changes in N-Glycans on induced pluripotent stem cells differentiating toward cardiomyocytes. Stem Cells Transl Med. 2015 Nov;4(11):1258-64
- Kilcoyne M, Twomey ME, Gerlach JQ, Kane M, Moran AP, Joshi L. Campylobacter jejuni strain discrimination and temperature-dependent glycome

expression profiling by lectin microarray. Carbohydr Res. 2014 May 7;389:123-33

- Kiselyov VV, Soroka V, Berezin V, Bock E. Structural biology of NCAM homophilic binding and activation of FGFR. J Neurochem. 2005 Sep;94(5):1169-79
- Lawrenson JG, Cassella JP, Hayes AJ, Firth JA, Allt G. Endothelial glycoconjugates: a comparative lectin study of the brain, retina and myocardium. J Anat. 2000 Jan;196 (Pt 1):55-60.
- Liu Y, McBride R, Stoll M, Palma AS, Silva L, Agravat S, Aoki-Kinoshita KF, Campbell MP, Costello CE, Dell A, Haslam SM, Karlsson NG, Khoo KH, Kolarich D, Novotny MV, Packer NH, Ranzinger R, Rapp E, Rudd PM, Struwe WB, Tiemeyer M, Wells L, York WS, Zaia J, Kettner C, Paulson JC, Feizi T, Smith DF. The minimum information required for a glycomics experiment (MIRAGE) project: improving the standards for reporting glycan microarray-based data. Glycobiology. 2016 Nov 22
- Mereiter S, Magalhães A, Adamczyk B, Jin C, Almeida A, Drici L, Ibáñez-Vea M, Gomes C, Ferreira JA, Afonso LP, Santos LL, Larsen MR, Kolarich D, Karlsson NG, Reis CA. Glycomic analysis of gastric carcinoma cells discloses glycans as modulators of RON receptor tyrosine kinase activation in cancer. Biochim Biophys Acta. 2016 Aug;1860(8):1795-808
- Mohd Isa IL, Abbah SA, Kilcoyne M, Sakai D, Dockery P, Finn DP, Pandit A. Implantation of hyaluronic acid hydrogel prevents the pain phenotype in a rat model of intervertebral disc injury. Sci Adv. 2018 Apr 4;4(4):eaaq0597
- Montpetit ML, Stocker PJ, Schwetz TA, Harper JM, Norring SA, Schaffer L, North SJ, Jang-Lee J, Gilmartin T, Head SR, Haslam SM, Dell A, Marth JD, Bennett ES. Regulated and aberrant glycosylation modulate cardiac electrical signaling. Proc Natl Acad Sci U S A. 2009 Sep 22;106(38):16517-22
- Nairn AV, Aoki K, dela Rosa M, Porterfield M, Lim JM, Kulik M, Pierce JM, Wells L, Dalton S, Tiemeyer M, Moremen KW. Regulation of glycan structures in murine embryonic stem cells: combined transcript profiling of glycan-related genes and glycan structural analysis. J Biol Chem. 2012 Nov 2;287(45):37835-56
- Naismith JH, Field RA. Structural basis of trimannoside recognition by concanavalin A. J Biol Chem. 1996 Jan 12;271(2):972-6

- Notari M, Ventura-Rubio A, Bedford-Guaus SJ, Jorba I, Mulero L, Navajas D, Martí M, Raya Á. The local microenvironment limits the regenerative potential of the mouse neonatal heart. Sci Adv. 2018 May 2;4(5):eaao5553
- Parker BL, Palmisano G, Edwards AV, White MY, Engholm-Keller K, Lee A, Scott NE, Kolarich D, Hambly BD, Packer NH, Larsen MR, Cordwell SJ. Quantitative N-linked glycoproteomics of myocardial ischemia and reperfusion injury reveals early remodeling in the extracellular environment. Mol Cell Proteomics. 2011 Aug;10(8):M110.006833
- Paszek MJ, DuFort CC, Rossier O, Bainer R, Mouw JK, Godula K, Hudak JE, Lakins JN, Wijekoon AC, Cassereau L, Rubashkin MG, Magbanua MJ, Thorn KS, Davidson MW, Rugo HS, Park JW, Hammer DA, Giannone G, Bertozzi CR, Weaver VM. The cancer glycocalyx mechanically primes integrin-mediated growth and survival. Nature. 2014 Jul 17;511(7509):319-25
- Péanne R, de Lonlay P, Foulquier F, Kornak U, Lefeber DJ, Morava E, Pérez B, Seta N, Thiel C, Van Schaftingen E, Matthijs G, Jaeken J. Congenital disorders of glycosylation (CDG): Quo vadis? Eur J Med Genet. 2017 Oct 25. pii: S1769-7212(17)30494-9
- Porrello ER, Mahmoud AI, Simpson E, Hill JA, Richardson JA, Olson EN, Sadek HA. Transient regenerative potential of the neonatal mouse heart. Science. 2011 Feb 25;331(6020):1078-80
- Qian J, Zhu CH, Tang S, Shen AJ, Ai J, Li J, Geng MY, Ding J. alpha2,6-hyposialylation of c-Met abolishes cell motility of ST6Gal-I-knockdown HCT116 cells. Acta Pharmacol Sin. 2009 Jul;30(7):1039-45
- Rao SV, Zeymer U, Douglas PS, Al-Khalidi H, White JA, Liu J, Levy H, Guetta V, Gibson CM, Tanguay JF, Vermeersch P, Roncalli J, Kasprzak JD, Henry TD, Frey N, Kracoff O, Traverse JH, Chew DP, Lopez-Sendon J, Heyrman R, Krucoff MW. Bioabsorbable intracoronary matrix for prevention of ventricular remodeling after myocardial infarction. J Am Coll Cardiol. 2016 Aug 16;68(7):715-23
- Saldova R, Kilcoyne M, Stöckmann H, Millán Martín S, Lewis AM, Tuite CM, Gerlach JQ, Le Berre M, Borys MC, Li ZJ, Abu-Absi NR, Leister K, Joshi L, Rudd PM. Advances in analytical methodologies to guide bioprocess engineering for bio-therapeutics. Methods. 2017 Mar 1;116:63-83

- Schulz BL, Packer NH, Karlsson NG. Small-scale analysis of O-linked oligosaccharides from glycoproteins and mucins separated by gel electrophoresis. Anal Chem. 2002 Dec 1;74(23):6088-97
- Schwetz TA, Norring SA, Bennett ES. N-glycans modulate K(v)1.5 gating but have no effect on K(v)1.4 gating. Biochim Biophys Acta. 2010 Mar;1798(3):367-75
- Tracy RE. Cardiac myocyte sizes in right compared with left ventricle during overweight and hypertension. J Am Soc Hypertens. 2014 Jul;8(7):457-63
- Varki A. Biological roles of glycans. Glycobiology. 2017 Jan;27(1):3-49
- Wang X, Ha T, Liu L, Hu Y, Kao R, Kalbfleisch J, Williams D, Li C. TLR3 mediates repair and regeneration of damaged neonatal heart through glycolysis dependent YAP1 regulated miR-152 expression. Cell Death Differ. 2018 Jan 22
- Yang S, Chatterjee S, Cipollo J. The glycoproteomics-mass spectrometry for studying glycosylation in cardiac hypertrophy and heart failure. Proteomics Clin Appl. 2018 Feb 9
- Zalik SE, Didier E, Didier P, Ledsham IM, Bayle D, Sanders EJ. Expression of the galactose-binding lectins during the formation of organ primordia in the chick embryo. Int J Dev Biol. 1994 Mar;38(1):55-68

Chapter Three

An ovine model of non-transmural myocardial infarction

Sections of this chapter have been submitted in the following manuscript: Contessotto P., Orbanić D., Da Costa M., Jin C., Owens P., Chantepie S., Papy-Garcia D., Chinello C., Magni F., Karlsson N.G., Kilcoyne M., Dockery P., Rodríguez-Cabello J.C. and Pandit A. "Elastin-like recombinamers-based hydrogel heals myocardial infarction in a clinically-relevant model". Under revision in *Nature Materials.*

3.1 Introduction

Myocardial infarction (MI) belongs to the family of cardiovascular diseases that accounts for approximately one third of worldwide mortality [Roger]. The occlusion of the coronaries by the detachment of an atherosclerotic plaque interrupts the constant oxygenation needed in the cardiac muscle and quickly induces the death of cardiomyocytes. The first necrotic phase leads to the migration of a massive inflammatory infiltrate which is made of macrophages and lymphocytes to the site of damage. Together with the inflammatory cells, the paracrine signalling coming from macrophages induces a massive recruitment of fibroblasts, which under the induction of specific growth factors and cytokines such as TGF-β1 and IL1β, transdifferentiate to the myofibroblast phenotype. Myofibroblasts are responsible for the deposition of collagen fibres which build the non-contractile scarring across the infarcted myocardium. At the clinical level, the scar formation in the left ventricle of the heart leads to a dyskinetic behaviour and a progressive dilation of the left ventricle chamber, and finally to heart failure with a high risk of mortality.

To reproduce this pathology at a preclinical level, different models have been studied and optimised to achieve a functional and molecular outcome similar to those seen in clinical cases. Preclinical studies from rodents to large animals such as porcine and ovine mainly induce myocardial infarction by the ligation of the coronaries, specifically with an established preference of the ligation of the left anterior descending coronary artery (LAD) [Chen, Holladay, Le, Song].

The first pioneering trials by Harris *et al*. in 1950 reported the induction of large gross infarcts in the canine left ventricle together with histamine release and delayed ectopic activity for four hours after the occlusion [Harris 1943 and 1950]. Specifically, the further the ligature was from the ostium of the left coronary artery, the lower was the mortality which reached a minimum value of 25% at the distance of 2.6 to 3 cm. At the same time, the percentage of animals effected by rapid ectopic systoles increased from 33 to 100% together with the increase in the distance of ligature. The main drawback of the LAD procedure which is currently being adopted in animal studies consists in the large extension of the infarcted area in the left ventricle which implicates a high associated mortality and poor resemblance of the actual clinical cases. Indeed, cardiomyopathies reported in the clinical theatres are partial and non-transmural infarcts, and often involve multiple small regions of the left ventricle. For this reason, methods to reproduce the clinical cases have already

begun to be optimised both to limit the extension of the infarct up to approximately 25% of the left ventricular mass of the infarct and to bring the overall mortality down to around 17% [Moainie, Schmitto].

At the molecular level, the deposition of collagen is the endpoint of the left ventricular remodelling process which compensates for the loss of cardiomyocytes. Indeed, the whole post-ischemia process can be seen as the path of an immunological response involving different populations of macrophages and inflammatory cells [Frangogiannis]. Specifically, the initial inflammation phase involves the migration of neutrophils into the ischemic area, and macrophages are responsible for the removal of dead cells and matrix debris resulting from the necrosis of cardiomyocytes. After this first inflammatory phase, macrophages are alternatively activated to promote a tissue reparative response which includes angiogenesis and formation of granulation tissue. Specifically, the macrophages that derive from the Ly-6C^{lo} monocytes and express vascular-endothelial growth factor drive a host healing response by the secretion of cytokines such as IL10 and TGF-β and lipid mediators [Frangogiannis]. The timely-orchestrated sequential expression of different types of macrophages determines the ventricular remodelling after ischemia, and a dysregulation in favour of a chronic pro-inflammatory state leads to higher hypertrophy, matrix degradation and worse cardiac function [Mann 2005]. It has also been shown that the depletion of neutrophils causes a dysregulation in the polarization of macrophages, an increase in fibrosis and finally leads to a hypokinetic behaviour of the left ventricular walls [Horckmans].

The final host response of cardiac tissue to an ischemic injury results in the fibrotic deposition of collagen type I and III. Due to the heterogeneity in this scarring process, the organ functionality can be severely effected by this process, with progressive dyskinetic behaviour of the left ventricle and possible heart failure. The main cellular players in this deposition are myofibroblasts whose role in the delay in the conduction of the electrical impulse and induction of arrythmogenicity has recently been the subject of studies [Vasquez, Rosker].

It is understood that post-ischemic myocardial remodelling affects the original composition of the cardiac extracellular matrix by the disruption of the initial balance of glycosaminoglycans, proteoglycans and other matrix components. This affects not only the structural and mechanical stability of the extracellular environment but also leads to serious consequences on the molecular pathways including the recruitment

of growth factors such as vascular endothelial growth factor (VEGF), platelet-derived growth factor (PDGF) and fibroblast growth factor (FGF). These growth factors have been extensively studied over recent decades for their therapeutic potential in the repair of the ischemic ventricular environment, investigating also the side effects of their unregulated expression [Yanagisawa-Miwa, Marsano, Lee, Detilleux, Hao].

In this study, it is hypothesised that a large animal model of non-full thickness myocardial infarction can be established and characterized at the gross anatomical, extracellular matrix and ultrastructure level.

Consequently, the objectives of this study are to:

- Optimise a procedure for the suture ligation from the first diagonal coronary to induce non-transmural infarcts.

- Assess the significant decrease in cardiac functionality 28 days after the surgical procedure and the progressive fibrosis.

- Study the degeneration of cardiomyocytes at the ultrastructure level after ischemia.

- Evaluate and quantify the post-ischemic remodelling at the level of the extracellular matrix.

3.2 Materials and methods

3.2.1 Ovine model of non-full thickness myocardial infarction

Romanov eight-month-old adult male sheep underwent an induction procedure of myocardial infarction through open thoracotomy. Animals were sedated with Telazol® 6 mg/kg (Zoetis, USA) and endotracheally intubated. Anesthesia was maintained with 1–2% isoflurane (Baxter, USA). The animals were monitored with electrocardiogram (ECG) and invasive arterial pressure measurements throughout the

procedure of anaesthesia. Animals received magnesium 2 mg intravenously (Pfizer, USA), and amiodarone 1.5 mg/kg intravenously (Pfizer, USA), before the infarction was induced and an intravenous infusion of amiodarone 0.01 mg/kg/min for 60 min afterwards, to prevent ventricular arrythmias. At induction and after surgeries, all sheep received intramuscular benzylpenicillin 600mg (Pfizer, USA) three times a day, and streptomycin 500mg twice daily (Pfizer, USA), for five days. For analgesia after surgeries, flunixin meglumine 2.2 mg/kg (Excella GmBH, Germany) was used for five days, and if lung oedema was detected, hydrocortisone 250 mg intravenous (Pfizer, USA) was administered three times a day.

Induction of myocardial infarction was performed by the ligation of multiple, strategic coronary artery ligations on the LV lateral to and parallel to the left anterior descending artery (LAD). Specifically, a left lateral thoracotomy was performed through the fourth intercostal space, followed by a pericardiotomy. Deep non-transmural ligations were performed with 2/0 PROLENE™ (Ethicon EMEA, Belgium) at 2 cm intervals lateral and parallel to the LAD from the first diagonal moving distally towards and up to 4 cm from the apex. The pericardium was closed with 4/0 PROLENE™ after obtaining absolute haemostasis, leaving a chest tube with its tip in the pericardial sac and the remnant holes in the left chest before the thoracotomy was closed in layers, and the animal recovered. Long blue sutures were used to ligate the coronaries and track the infarction site for the following treatment injection procedures.

3.2.2 Pain management and humane endpoints

Premedication and anesthetic drugs were evaluated by an anesthetist. After tracheal intubation, each animal was connected to a standard circle anesthetic circuit. Sevoflurane in oxygen was delivered by use of an out-of-circuit precision sevoflurane vaporizer. Premedication was performed for selected sheep, and carried out under sterile conditions performing intramuscular injection to administer medicines for the premedication: Xylazine (1 mg/kg, intramuscular) then butorphanol (0.2 mg/kg, intramuscular), without additional suffering. Butorphanol was repeated after 1 hour during operation for pain management. After surgery, animals were monitored for signs of pain and distress including reduced activity, failure to groom, reduced food or water intake, eye squinting or pale eyes, teeth

grinding, changes in posture, guarding, and aggressiveness. If these signs were observed, it was discussed with veterinary staff whether to provide appropriate interventions such as additional administration of analgesia (buprenorphine) and, in the event that the pain proved unmanageable, the animals were euthanized. At three weeks after surgery, animals were euthanized by pentobarbital sodium (5 mg/kg) injection under anaesthesia in line with the Veterinary Medical Association Guidelines. After five minutes, animals were checked for heart pulse. Animals which experienced undue pain or distress requiring humane intervention were euthanized in the same manner.

3.2.3 Functional response by echocardiographic measurements

Echocardiography measurements were recorded the day before each surgical procedure and before the study time points. The extension of the ischemic area was visible by the discoloration on the epicardial surface in the minutes following the suture ligation. No ST elevation was noted on ECG monitoring during this period, suggesting that although there were signs of ischaemic injury in the areas of suture ligation, this did not create a classic ST-elevation MI. All echocardiographic examinations were performed on unsedated standing animals. Images and windows for the echocardiographic protocol were derived from techniques described by Reef *et al*. for horses and more recently adapted for sheep by Hallowell *et al*. [Reef, Hallowell]. Examinations were performed by two cardiologists. Briefly, six two-dimensional (2-D) parasternal images were obtained from the right, and three 2-D parasternal images from the left [Reef, Hallowell]. A 5 MHz probe was employed and the console and software used was Mindray 7 (Mindray Bio-Medical Electronics Co. Ltd, China). Among the main surgical complications were arrhythmias which compromised the functionality of the whole organ and led to the death of the animal following heart failure.

3.2.4 Harvesting and stereology

Hearts were perfused with PBS to remove the excess of blood immediately after the explantation. Two washes with PBS were performed before starting with the cutting and harvesting. Each heart was cut axially using a brain knife, keeping a thickness of 1 cm for each slice from the ventricular region; then all the slices up until the apex

were laid on a white surface and pictures were taken before and after sampling. Rulers were placed next to the slices on the white surface to allow the quantification from the images taken with the photographic camera. A total of seven small samples (0.5 cm maximum in every direction) were harvested from the ischemic site, border and remote area per each heart for the different processings and analyses presented in this thesis. Specifically, samples for histological analysis were fixed on freshly prepared 4% paraformaldehyde overnight at 4°C. After this, samples were washed with PBS to remove the excess of fixative and then isotropic uniform random orientation was applied to avoid any bias in further stereological quantifications [Bergmann, Mühlfeld]. For this reason, samples were embedded in OCT following the orientator method (Figures A.2 and A.3 in Appendices). This ensures a complete independence from the anisotropic orientation of capillaries in the cardiac muscle [Mühlfeld]. Briefly, to follow the orientator method before OCT embedding, the sample was placed on a uniformly divided φ clock. After this, the cardiac sample was cut at an angle randomly picked between one and nine. Then the sample was put on a cosine-weighted θ clock and cut at an angle again randomly chosen between one and nine. At least three sections per heart were used for further histological and immunofluorescence experiments, as previously performed in large animals [Zhu].

3.2.5 Tissue processing

Sheep cardiac samples were processed for OCT embedding and cryosectioning until storage at -80°C as described in section 2.2.2. Additionally, samples from sheep sacrificed 10 days after the ligation surgical procedure were harvested and processed for paraffin embedding and sectioning (A.6, A.7 and Table A.3 in Appendices). Hand-made spherical moulds were used to ensure isotropic uniform random sampling, for those reasons indicated in section 3.2.4.

3.2.6 Histological evaluation

Samples processed as described in section 3.2.5 were sectioned at 5 μm (Appendix A.7) using a microtome (Leica, Germany) and the sections were stored at room temperature. Before any histological staining procedure, glasses were incubated at 60°C for ten minutes to melt the paraffin and then used for the desired histological staining. Masson's Trichrome, hematoxylin and eosin (H&E), Alcian blue and

pentachrome stainings (Appendices A.12, A.13, A.14 and A.16) were performed on samples harvested ten days after myocardial infarction.

3.2.7 Tissue processing for electron microscopy analyses

Samples from the ischemic, border and remote regions were harvested from healthy and infarcted hearts 7 and 28 days after the surgical procedure. All samples for transmission electron microscopy (TEM) analyses were processed as described in Appendices A.19 and A.20. Briefly, samples were first fixed in 2.5% gluteraldehyde for 24h at 4°C. After this, samples for TEM were washed in phosphate buffer and post-fixed in 1% osmium tetraoxide for 2 h at RT. Then, the samples were dehydrated in 30% (5 min), 50% (15 min), 70% (15 min), 95% (15 min) and pure ethanol (twice, 15 min each). After dehydration, samples were washed with pure ethanol twice for 15 min before the embedding process. This consisted of three steps of progressive infiltration of Araldite® epoxy resin with acetone in 2:1, 1:2 ratio and pure resin for 24 h each at RT. Finally, samples were transferred in new pure Araldite® epoxy resin and then thermally cross-linked at 60°C for 48 h until complete hardening of the samples. Samples were then ready to be further processed for TEM analysis as described in section 3.2.9. After fixation in 2.5% gluteraldehyde for 24 hours at 4°C, samples for scanning electron microscopy analysis (SEM) were left in 2% gluteraldehyde, 2% paraformaldehyde in 0.1 M sodium cacodylate buffer (pH 7.2) for a maximum of seven days at 4°C until further processing. Samples were washed with phosphate buffer three times, five minutes each, and then dehydrated through a series of graded alcohols i.e. 50%, 70%, 90% for 12 min each. Then, samples were completely dehydrated by submersion in pure ethanol twice for 12 min each and then in hexamethyldisilazane (HMDS) twice for 12 min each. Following this, tissues were dried overnight on a Petri dish before further processing prior to scanning electron microscopy (SEM) analysis as described in section 3.2.8.

3.2.8 Analysis of ECM deposition by scanning electron microscopy

Once the samples were processed and dried as described in section 3.2.7, two different contrast enhancing methods were tested before imaging by SEM. All SEM imaging was carried out on an S-2600N scanning electron microscope (Hitachi, Japan). Using the first method, samples were incubated in a chamber with iodine

vapour overnight at RT and then imaged using the backscatter mode at 15 kV. Using the second method, samples were gold coated (Appendix A.17) using a SC500 sputter coater (Bio-Rad, USA) and imaged using the secondary electron detector mode at 15 kV (Appendix A.18).

3.2.9 Subcellular evaluation by transmission electron microscopy analysis

After the polymerisation step described in section 3.2.7, resin embedded samples for transmission electron microscopy (TEM) analysis were trimmed, and semithin survey sections (500 nm thick) were cut using a glass knife. The sections were then stained with toluidine blue to verify the presence of the ischemic damage at the extracellular level. The resin blocks were further trimmed to the region of interest and, using a diamond knife, ultrathin sections (70-90 nm thick) were cut and picked up onto copper grids. To enhance contrast, the sections were post stained with 0.5% uranyl acetate for three min and 3% lead citrate for five min using an EM AC20 Auto Ultrastainer™ (Leica, Germany), as described in Appendix A.20. Imaging was performed using an H-7000™ transmission electron microscope (Hitachi, Japan) at 75kV and at magnifications of 3000x and 10000x. Five fields of view per sample were imaged.

3.2.10 Quantification of total sulfated GAGs

Approximately 200 mg of snap-frozen tissue from healthy and peri-infarct areas of MI-only at 7 and 28 days were processed to quantify the total sulfated glycosaminoglycans (GAGs) and heparan sulphate/chondroitin sulphate (HS/CS) ratio. Samples were then freeze-dried and powdered. The dried-powdered tissue was weighed and suspended in a buffer to final 25 mg of tissue/mL. Proteinase K (PK) was added to the tissue suspension to final 50 μg/mL and the sample was kept at 56°C overnight. PK was inactivated by 30 min at 90°C and samples were subjected to DNA by DNase (7.5 U/ml) and lipid elimination by chloroform extraction. Finally, extracted GAGs were dialysed, freeze-dried and subjected to GAGs quantification according to the 1,9-dimethylmethylene blue (DMMB) assay as previously described [Barbosa].

3.2.11 Quantification of heparan sulphate and chondroitin sulphate

For specific HS quantification, extracted GAGs were incubated with a cocktail of heparinases. Briefly, undigested GAGs, CS, were quantified according to the DMMB assay. In parallel, chondroitinase ABC (25 mU/sample, two hours at 37 °C) was used for specific CS elimination. Undigested GAGs, HS, were quantified according to the DMMB assay. Some samples were treated by both enzymes and used to confirm the absence of other GAGs in the tissue.

3.2.12 Statistical analysis

All statistical analysis was performed using Minitab Express™ software (Minitab, Inc. State College, USA). Data related to EF from echocardiographic measurements at day 7 and 28 post-MI were compared using Mann-Whitney *U* test. Data related to total sulfated GAGs and HS/CS ratio were analysed by one-way ANOVA with Tukey's post hoc correction. Values were considered significant only with $p<0.05$.

3.3 Results

3.3.1 Ovine model of non-full thickness myocardial infarction

Current preclinical models are the result of the conventional induction of myocardial infarction through the ligation of the left anterior descending coronary artery (LAD). A major limitation of this method is its poor resemblance to the real clinical cases where non-transmural rather than full thickness infarcts localize in the left ventricular wall. Moreover, the majority of the studies on myocardial infarction are performed in rodents which is an obvious limitation on their translation to the human cases. Therefore, a large animal model is required to resemble the clinical cases in the most accurate way to evaluate the effects both at the functional and histological level. Specifically, the ovine model has been extensively used to evaluate the recovery of heart functionality because of the similarity of the organ volume with that of the human one whereas results of the studies carried out in small rodents and rabbits lack this property [Ifkovits, Macarthur, Shimkunas, Bischoff]. As summarised in Table 3.1, previous MI studies performing the ligation of the LAD in large animals showed a decrease in EF of between 10 and 30%. In this study, multiple ligations were performed lateral and parallel to the LAD from the first

diagonal up to 4 cm from the apex to induce non-transmural infarcts in the left ventricle. An average reduction of 6.37±11.10% in EF was seen seven days after the injection procedure. EF further decreased, although not significantly, by 13.62±11.11% three weeks later (28 days post-MI) relative to the pre-MI levels (Figure 3.1). Consistency in the localisation of the infarct was achieved and the extension of the induced infarcts did not include the whole thickness of the left ventricular wall, as shown in Figure 3.2. All the hearts were sliced axially keeping a thickness of 1 cm per slice. Before cutting the whole heart, the localisation of the infarct was visualised by its proximity to the long blue suture that was used to ligate the coronaries and was left on the site for tracking purposes. After slicing, the infarcted region was seen by the discolouring of the left ventricular wall which is a sign of fibrotic remodelling that is totally absent in the healthy hearts (Figure 3.2). Therefore, sampling was carried out from the core ischemic progressively to the border and remote regions and specimens isotropically uniformly oriented to avoid any bias in the stereological quantification of cardiomyocytes and vasculature structures (Figure 3.3).

3.3.2 Degeneration of cardiomyocytes at the ultrastructure level

The first necrotic phase after ischemia consists in the loss of millions of cardiomyocytes in the effected area which will never be replaced due to the lack of a sufficient self-regenerating capability in adult mammals hearts. Nevertheless, the myocardial environment is programmed to compensate for this event by activating a sequential inflammatory and fibrotic remodelling of the effected region.

It is well known that the necrotic phase responsible for the loss of cardiomyocytes in the left ventricle does not last over the early hours after ischemia. Despite this, the influence of the highly pro-inflammatory environment on the border region is still a subject of debate. In this study, a progressive vacuolisation was detected in the same region inside the myofibrils from 7 to 28 days after MI (Figure 3.4 A-C). Interestingly, a consistent disruption of the intercalated disks was seen exclusively one week after MI (Figure 3.4 D). This is an additional sign of the structural disassembly of the cardiomyocytes myofibrils apparatus which is needed for their cellular contraction and thus the synchronous beating of the whole organ.

The integrity of the cardiomyocytes structure and its progressive degeneration was assessed in the border zone of the infarct. Moreover, in this study the cardiomyocytes located in the border zone showed an accumulation of dense bodies inside their mitochondria which is a sign of necrotic state (Figure 3.5). This is reported for the first time in a large mammal model of MI seven days after the surgical procedure.

3.3.3 Post-ischemic myocardial remodelling

In human and large mammals such as the sheep used in this study, the peak of the early acute inflammatory phase is expected to reduce around the fourth day after MI, together with a consistent activation of the pro-healing population of macrophages one week after ischemia. From the end of the first week after MI throughout the following four to six weeks, the myofibroblasts secrete collagen type I and III, and this was seen to be started by the use of Masson's Trichrome staining of the ischemic tissue harvested ten days after the surgical procedure (Figure 3.6 B). At the same time, consecutive sections were stained with H & E and Alcian blue to clearly visualize the remnants of the inflammatory infiltrate and the secretion of sulfated glycosaminoglycans in the same region (Figure 3.6 A,C).

At the endpoint of 28 days after MI, the complete deposition of a fibrotic scar was observed and the typical wavy-orientation of collagen fibres was assessed by electron microscopy. Collagen deposition was localized through the infarcted areas where myofibroblasts were recognized by their typical elongated shape (Figure 3.7). Additionally, the distribution of collagen fibres across the myocardial extracellular matrix was visible also by scanning electron microscopy, in contrast to the condition seen in the remote region, as shown in Figure 3.8.

3.3.4 Quantification of glycosaminoglycans during the post-ischemic remodelling

The reorganization of the extracellular matrix is one of the consequences of the post-ischemic remodelling in the left ventricular wall. The importance of GAGs in the regulation of inflammation and angiogenesis in the extracellular matrix has been investigated in several pathologies since these can be either directly or indirectly involved in the remodelling response. In this study, sulfated glycosaminoglycans

were extracted from snap-frozen samples of the peri-infarct zone harvested 7 and 28 days after the surgical procedure of the induction of MI.

By dimethylmethylene blue assay (DMMB), total sulfated glycosaminoglycans were quantified and then, after digestion with chondroitinase ABC, the ratio between heparan sulphate (HS) and chondroitin sulphate (CS) was calculated by a subtraction method. All the data were compared to healthy ventricular tissue. A progressive increase in the deposition of total sulfated GAGs was observed from 7 to 28 days after MI (Figure 3.9 A). Specifically, an increase from 0.33±0.13 μg/mg of healthy tissue to 0.89±0.30 μg/mg of ischemic tissue at day seven was seen. This trend was confirmed and became highly significant at day 28 ($p<0.001$), with a total quantity of sulfated GAGs of 3.09±0.90 μg/mg of tissue (Figure 3.9 A). It is worth noting that hyaluronic acid cannot be quantified by this method since it is a non-sulfated GAG.

After the total GAGs quantification, the ratio between HS and CS was calculated by a subtraction method after enzymatic digestion of the samples with chondroitinase ABC. This ratio changed with the progression of remodelling after ischemia, as shown in Figure 3.9 B. An increase in CS was seen at day seven post-MI, bringing the ratio HS/CS from 0.98±0.17 in healthy condition to 0.90±0.55 even though this was not significant ($p=0.93$). Nevertheless, this ratio continued to decrease reaching the value of 0.49±0.24 at day 28, showing a more pronounced ($p=0.12$) decrease than that of the healthy condition (Figure 3.9 B).

Table 3.1 MI models adopted in large animals.

Species, sample size	MI induction	Decrease in EF (%)	Reference
Adult Dorset sheep, N=9	Ligation of LAD and second diagonal coronary	10 (after 2 w)	Ifkovitz
Mature Yucatan minipigs, N=4	Percutaneous coil embolism infarct model	18 (after 2 w)	Seif-Naraghi
Mature Lanyu minipigs, N=7	Ligation of LAD	20 (after 1 d)	Chen
Pigs, N=7	Occlusion of LAD by balloon inflation, followed by reperfusion	From 35 to 45 (after 1 w)	Takehara
Mature Yorkshire pigs, N=9	Ligation of obtuse marginal 1 (OM1) and OM2	14 (after 1 w)	Mukherjee
Adult Mongrel dogs, N=6	Ligation of LAD	20 (after 2 w)	Linke
Pigs, N=7	Ligation of OM1 and OM2	16 (after 1 w)	Purcell
Yorkshire pigs, N=4	Ischemia-reperfusion	10 (after 1 w)	Ye
Adult sheep, N=13	Ligation of LAD and diagonal branches	31 (after 8 w)	Dixon
Adult sheep, N=10	Occlusion of LAD by balloon inflation, followed by reperfusion	20 (directly after MI)	Houtgraaf
Yorkshire pigs, N=5	Ligation of OM1 and OM2	15 (after 1 w)	Eckhouse
Adult Dorset sheep, N=7	Ligation of LAD and second diagonal coronary	From 10 to 15 (after 1 w)	Tous

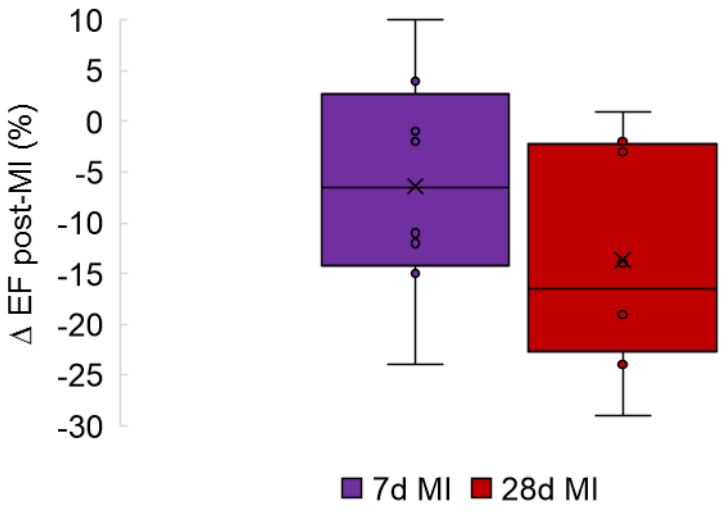

Figure 3.1 Quantification of decrease in ejection fraction (EF) at day 7 and 28 post-induction of MI. Echocardiographic data were used to calculate the ejection fraction (EF) values at each timepoint for all animals that survived to the induction of MI (A). Absolute changes in EF are shown 7 (7d MI) and 28 (28d MI) days after the surgical procedure. Data are reported as box-plots, Mann-Whitney *U* test, n=8 animals per group.

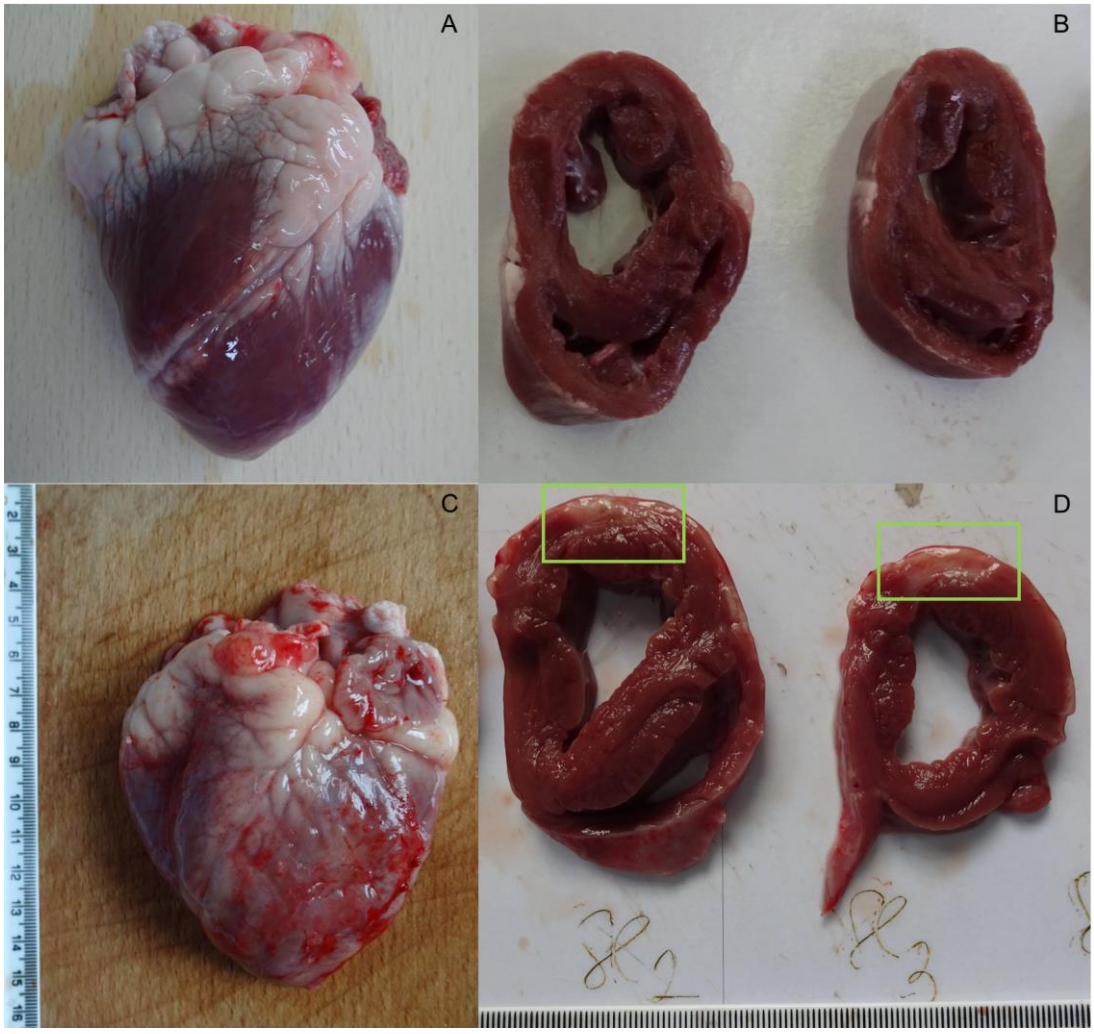

Figure 3.2 Gross explant images showing the scar formation 28 days after the ligation procedure. Healthy eight-month-old male sheep before (A,B) and 28 days after (C,D) the induction of myocardial infarction through the ligation of the side branches of the coronaries. A clear MI-area (framed in green) is visible in the cross section (D) by the whitish colouring of the region of the left ventricle effected. The infarct is non-transmural since it is not extended to the full thickness of the ventricular wall. Ruler = 1 mm.

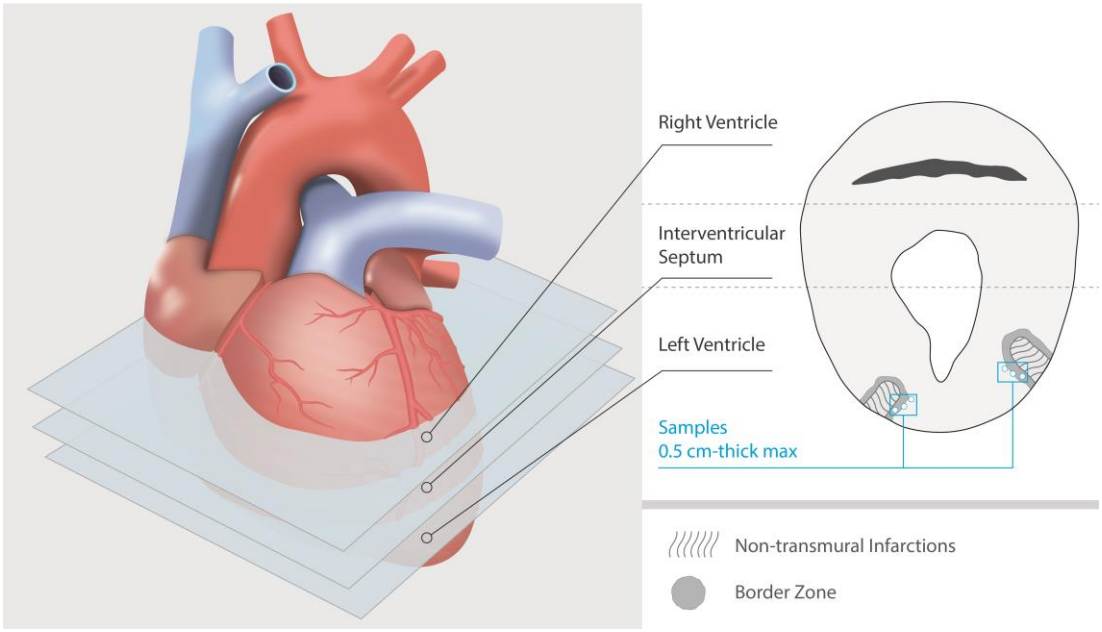

Figure 3.3 Schematics of harvesting tissues from explanted hearts. After perfusion with PBS to remove the excess of blood, each heart was cross-sectioned in slices with a thickness of 1 cm from the atria to the apex. Clear MI areas were identified by the whitish colour and from there samples with a maximum size of 0.5 cm in every direction were taken from the core ischemic, the border and the remote regions.

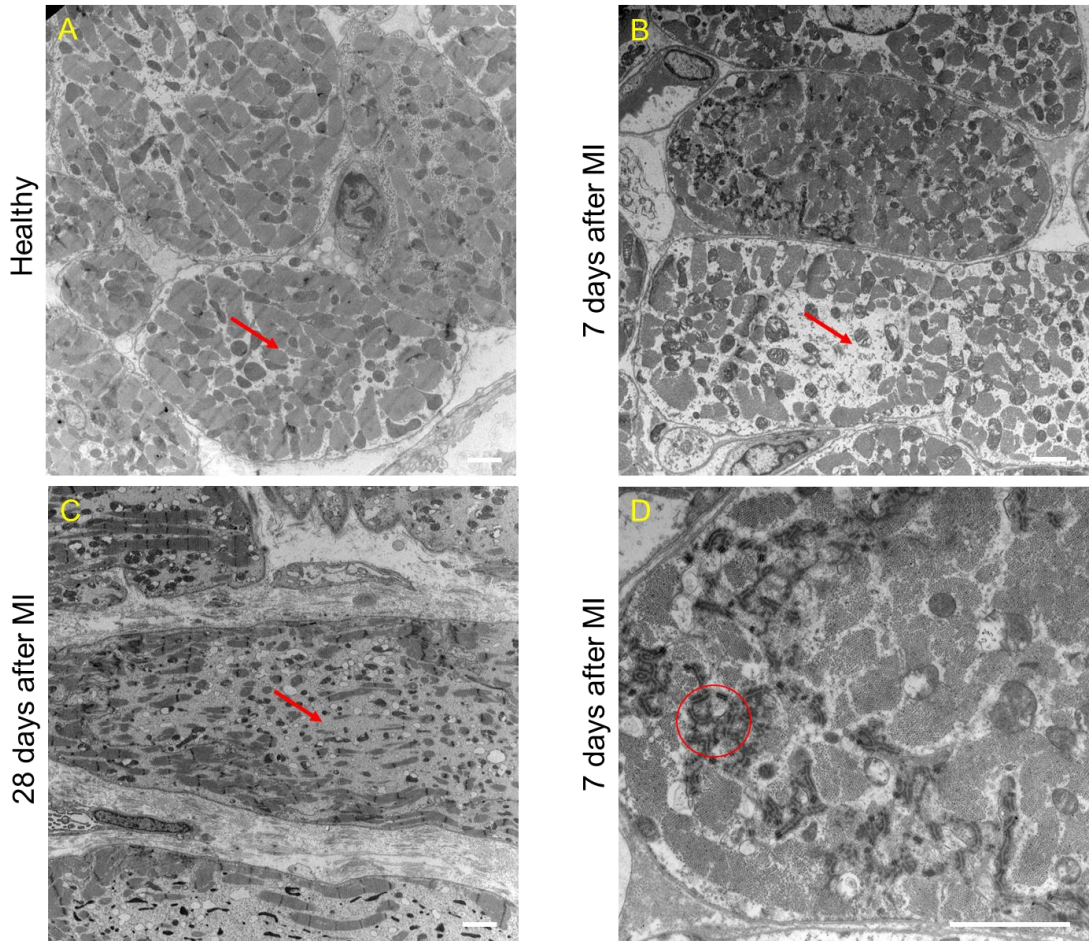

Figure 3.4 Progressive cardiomyocyte vacuolisation at the ultrastructural level. Post-ischemic effects in the cardiomyocytes located in the infarct border zone were assessed at the ultrastructure level by TEM. Cytosolic disruption and progressive vacuolisation is clearly visible (red arrows) from healthy (A) to 7 days (B) and 28 days after MI (C). Moreover, clustering of the intercalated disks (circled in red) was seen at seven days after MI (D). Scale bar = 2 μm.

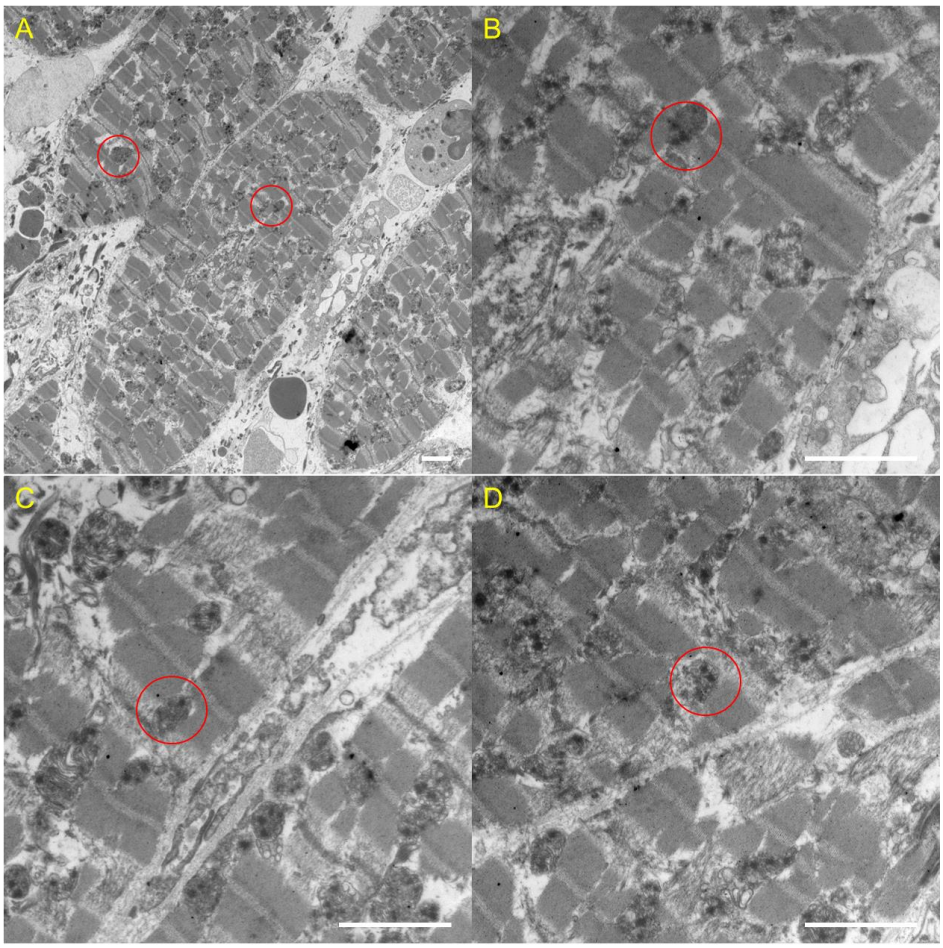

Figure 3.5 Accumulation of dense bodies in the mitochondria of cardiomyocytes. Mitochondria of cardiomyocytes located in the border zone of the infarct are effected by the accumulation of dense bodies (circled in red) seven days after the induction of myocardial infarction. Low (A) and high magnification (B,C,D) pictures show the extension and consistency of the pattern in a cardiomyocyte myofibril. Scale bar = 2 μm.

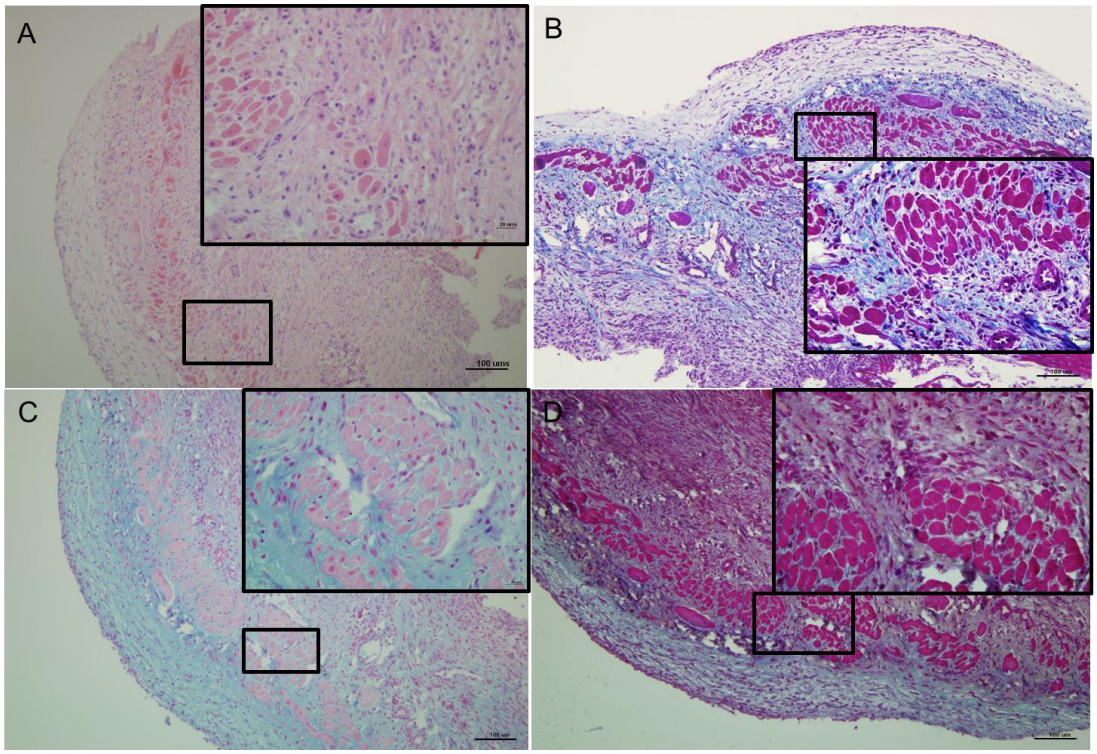

Figure 3.6 Fibrotic deposition and inflammatory status at day 10 after MI. Post-ischemic myocardial remodelling was assessed in sheep myocardial left ventricle 10 days after the ligation procedure. Inflammatory infiltrate was seen by hematoxylin and eosin staining (A) and initial deposition of collagen was confirmed by Masson's Trichrome (B). Furthermore, glycosaminoglycans (GAGs) were present in the epicardium and also in the inner myocardial infarcted region (Alcian blue staining in (C)). Finally, pentachrome staining allowed the visualisation of muscle, collagen and GAGs components (D). Scale bar = 100 μm.

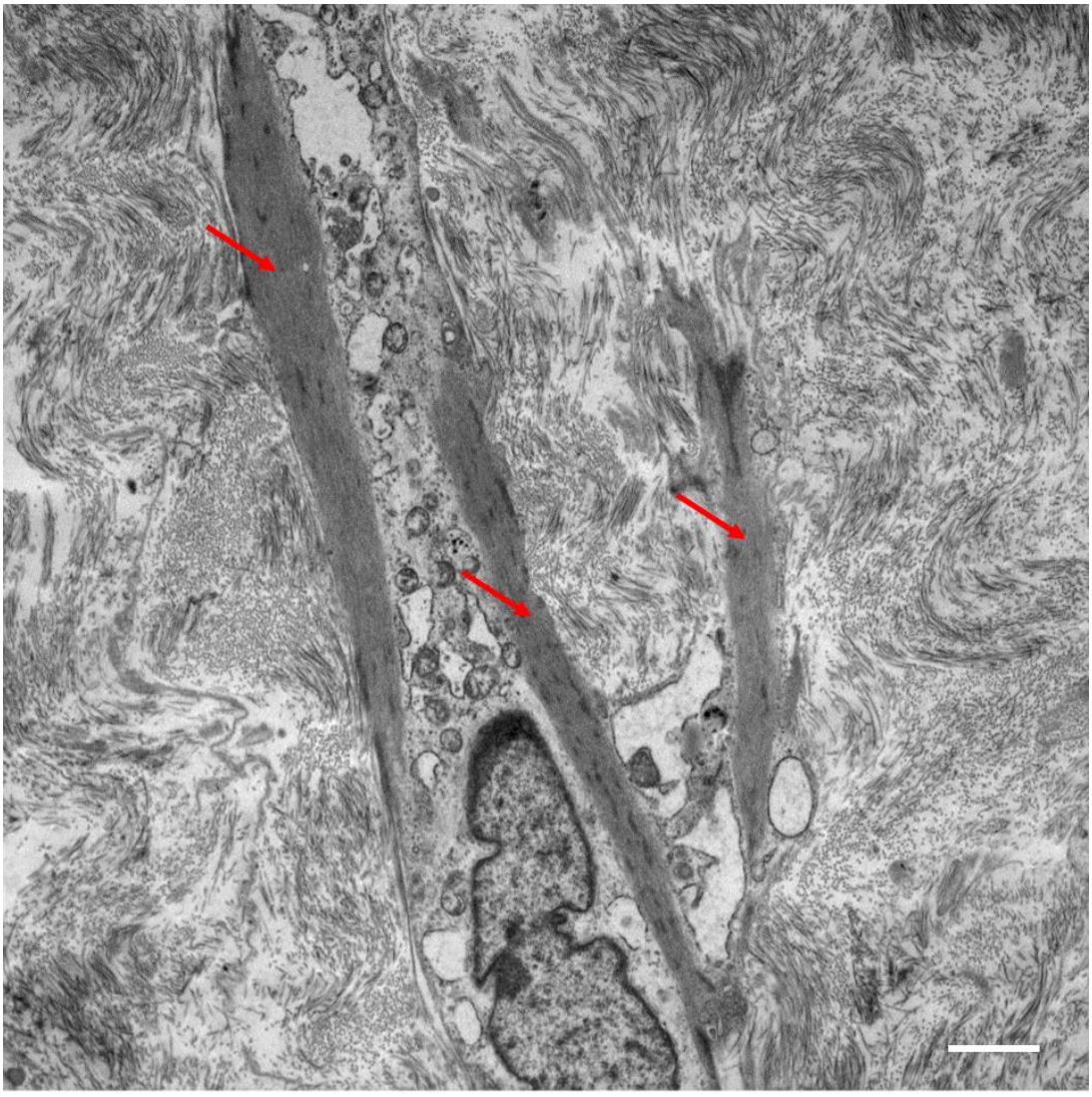

Figure 3.7 Matrix deposition from activated myofibroblasts. Elongated-shaped myofibroblasts (red arrows) were detected across the ischemic zone 28 days after MI together with collagen deposition. Wavy-oriented typical collagen-like deposition was one of the signs of the formation of a clear scar as seen at the ultrastructural level. Scale bar = 2 μm.

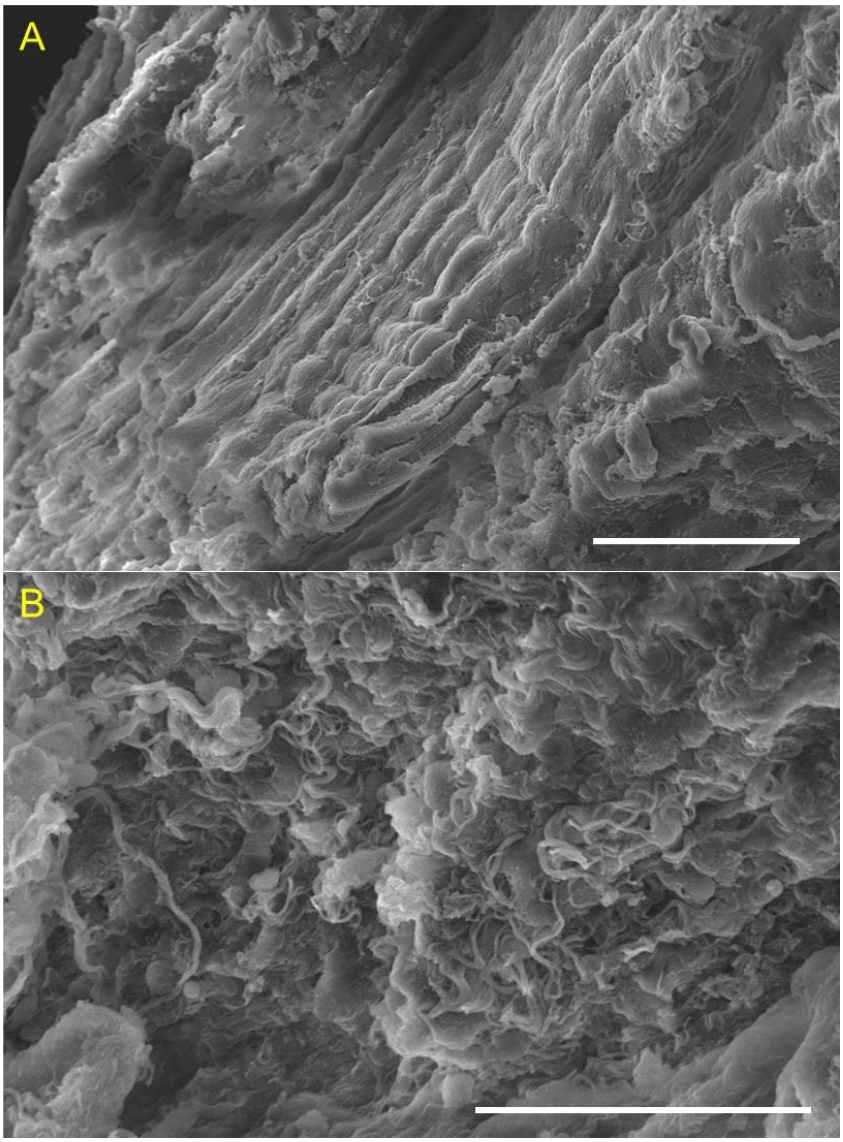

Figure 3.8 Structural differences seen 28 days post-injury. Comparison between healthy myocardial extracellular matrix (A) and fibrotic one 28 days after myocardial infarction (B). Collagen bundles are clearly innervating the matrix. Scale bar = 50 μm.

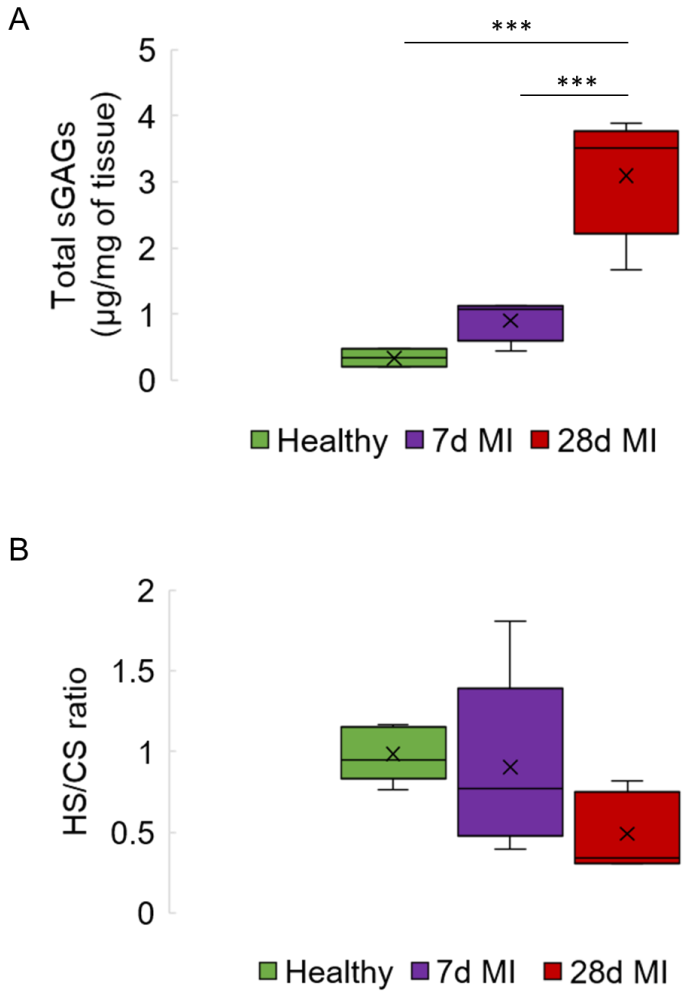

Figure 3.9 Quantification of total sulfated glycosaminoglycans and heparan sulphate/chondroitin sulphate ratio from healthy to 7 and 28 days after MI. By dimethylmethylene blue assay (DMMB) total sulfated glycosaminoglycans were quantified (A) and then, after digestion with chondroitinase ABC, the ratio between heparan sulphate (HS) and chondroitin sulphate (CS) was calculated by a subtraction method (B). All the data were compared to healthy ventricular tissue. Data are reported as box-plots, one-way ANOVA with Tukey's post hoc correction, n=5 animals per group, ***$p<0.001$.

3.4 Discussion

The minimal regenerative capacity of the heart represents a major limitation in the self-healing process of the cardiac tissue after ischemia. Indeed, during the first necrotic phase of MI, the loss of cardiomyocytes affects not only the core ischemic zone but also the border area, and heart failure is correlated with the extension of the damage in this area over the weeks that follow MI.

The method most widely used to reproduce MI in preclinical studies is based on the ligation of the left anterior descending coronary artery, at a variable distance from the apex of the heart [Chen, Holladay, Le, Song]. In contrast, in the model of MI outlined in this study multiple ligations were performed at the level of the first diagonal artery to reproduce patchy and non-transmural infarcts in the antero-lateral wall of the left ventricle. Adult male Romanov sheep were preferred over rodents to achieve a meaningful comparison in the functional outcome effect with that in the human cases. Moreover, preclinical studies were based on full thickness infarcts and immediate post-MI intervention which do not represent the majority of current clinical cases and thus might lead to clinically non-relevant outcomes [Roger, Rogers]. Notably, among patients surviving to hospital discharge, mortality is greater in NSTEMI than in STEMI patients [Fox]. In view of this, the current model is reflective of clinical presentation and practice to improve clinical outcomes in patients who develop significant injury and reduction in ejection fraction as a result of NSTEMI. Specifically, the average decrease in EF observed one (-6.3±11.10%) and four (-13±11.11%) weeks after the ligation procedure is lower than most of the reductions seen after the total occlusion of the LAD [Chen, Takehara, Linke, Dixon]. The variability seen in the decrease of this functional parameter reflects the range seen in clinical cases where multiple factors can influence the functional outcome [Miller]. Taking into account the pathological timeline of the post-ischemic remodelling, it was necessary to validate the progression of the pathology both at cellular and ECM-level. The progressive vacuolisation of the myofibrils of the cardiomyocytes located in the border zone confirmed the persistence of a necrotic effect in this specific region up to 28 days after the ligation procedure. Moreover, the accumulation of dense bodies inside the mitochondria seven days after MI further supported the extended effect of the early necrosis spreading from the core ischemic zone, as previously reported in a swine model intracoronary balloon occlusion [Galindo]. The electron-dense nature of these bodies is usually associated with

inorganic constituents such as Ca^{2+}, Mg^{2+} and $(CO_3)^{2-}$ which are the components of hydroxyapatite [Chinopoulos]. Therefore, the precipitation of these moieties can be a distinctive feature of a necrotic phenotype which was observed in other apoptotic contexts [Kiefmann, Mühling].

The transition from the early inflammatory phase to the proliferative phase was assessed by a histological evaluation at day 10 post-MI when both inflammatory infiltrate and the beginning of collagen deposition were observed. Indeed, the time-dependent cascade of different populations of inflammatory cells was extensively characterized over the last decade, and recent studies have been evaluating the relevance of the remodelling-related macrophages and regulatory T cells in the enhancement of a beneficial post-ischemic outcome [Horckmans, Zacchigna]. In the large animal model outlined in this study, the deposition of collagen fibres was validated at the ultrastructure level at day 28 post-MI in the proximity of the typically elongated-shape myofibroblasts. ECM remodelling was also clearly visible from the surface of the tested samples by SEM, although it was necessary to quantify the time-dependent deposition of ECM components.

GAGs are not only among the structurally fundamental moieties of the ECM; they also were seen to play a relevant role in both the TLR-related inflammatory response and in the enhancement of angiogenesis through the binding to growth factors [Olivares-Silva, Taylor, Prante]. Specifically, the release of HS chains by the activity of the matrix metalloproteinases is one of the triggers for the activation of the TLR4 receptor and consequent increase of IL1-β levels through the PI3K/Akt/NF-kB pathway. The continuous activation of this pathway leads to the TGF-β-dependent pro-fibrotic phenotype of cardiac fibroblasts. Therefore, in this study a quantification of total sulfated GAGs and HS/CS ratio was carried out to define their time-related deposition over the study timepoints. Interestingly, the significance of the deposition of the total sulfated GAGs was actually elevated only at day 28 post-MI, together with the observation of an increasing trend of deposition seven days after the ligation procedure. To further define how the balance between heparin sulphate and chondroitin sulphate varied during the post-ischemic remodelling, this study also included the quantification of the two different GAGs at the tested timepoints. In addition to the increase in the total sulfated GAGs, a marked drop in the HS levels

was reported only at the fully remodelled timepoint (28 days), even though the trend of decrease of HS and increase of CS was already visible at the end of the pro-inflammatory wave after MI (seven days).

3.5 Conclusions

A critical gap in the field of cardiovascular research is the definition of a large animal model that can resemble the clinical cases showing non-full thickness, localised infarcts rather than transmural infarcts in the left ventricular wall. This surgical procedure was therefore designed to induce non-transmural infarcts by multiple ligations that are parallel and lateral from the first diagonal of the LAD, and the evaluation of gross explants confirmed the non-transmural extension of the ischemic regions. Moreover, histological, ultrastructure and protein-related analyses were performed to assess whether the damaged areas followed the pathological timeline after MI. Extended effects of the necrosis in the border zone were seen at mitochondrial level and a quantification of the remodelling at ECM level was carried out focusing on those GAGs which are implicated in the inflammatory and remodelling phases after MI. A time-dependent deposition of chondroitin sulphate and reduction of heparin sulphate was seen over the four weeks of the post-ischemic remodelling. This model of non-full thickness MI resembles the non-transmural infarcts that are increasing among the hospitalised patients for which there are currently no therapeutic options.

3.6 References

- Barbosa I, Garcia S, Barbier-Chassefière V, Caruelle JP, Martelly I, Papy-García D. Improved and simple micro assay for sulfated glycosaminoglycans quantification in biological extracts and its use in skin and muscle tissue studies. Glycobiology. 2003 Sep;13(9):647-53
- Bergmann O, Zdunek S, Felker A, Salehpour M, Alkass K, Bernard S, Sjostrom SL, Szewczykowska M, Jackowska T, Dos Remedios C, Malm T, Andrä M, Jashari R, Nyengaard JR, Possnert G, Jovinge S, Druid H, Frisén J. Dynamics of cell generation and turnover in the human heart. Cell. 2015 Jun 18;161(7):1566-75

- Bischoff J, Casanovas G, Wylie-Sears J, Kim DH, Bartko PE, Guerrero JL, Dal-Bianco JP, Beaudoin J, Garcia ML, Sullivan SM, Seybolt MM, Morris BA, Keegan J, Irvin WS, Aikawa E, Levine RA. CD45 Expression in mitral valve endothelial cells after myocardial infarction. Circ Res. 2016 Nov 11;119(11):1215-1225
- Chen CH, Chang MY, Wang SS, Hsieh PC. Injection of autologous bone marrow cells in hyaluronan hydrogel improves cardiac performance after infarction in pigs. Am J Physiol Heart Circ Physiol. 2014 Apr 1;306(7):H1078-86
- Chinopoulos C, Adam-Vizi V. Mitochondrial Ca2+ sequestration and precipitation revisited. FEBS J. 2010 Sep;277(18):3637-51
- Detillieux KA, Sheikh F, Kardami E, Cattini PA. Biological activities of fibroblast growth factor-2 in the adult myocardium. Cardiovasc Res. 2003 Jan;57(1):8-19
- Dixon JA, Gorman RC, Stroud RE, Mukherjee R, Meyer EC, Baker NL, Morita M, Hamamoto H, Ryan LP, Gorman JH 3rd, Spinale FG. Targeted regional injection of biocomposite microspheres alters post-myocardial infarction remodeling and matrix proteolytic pathways. Circulation. 2011 Sep 13;124
- Eckhouse SR, Purcell BP, McGarvey JR, Lobb D, Logdon CB, Doviak H, O'Neill JW, Shuman JA, Novack CP, Zellars KN, Pettaway S, Black RA, Khakoo A, Lee T, Mukherjee R, Gorman JH, Gorman RC, Burdick JA, Spinale FG. Local hydrogel release of recombinant TIMP-3 attenuates adverse left ventricular remodeling after experimental myocardial infarction. Sci Transl Med. 2014 Feb 12;6(223):223ra21
- Fox KA, Dabbous OH, Goldberg RJ, Pieper KS, Eagle KA, Van de Werf F, Avezum A, Goodman SG, Flather MD, Anderson FA Jr, Granger CB. Prediction of risk of death and myocardial infarction in the six months after presentation with acute coronary syndrome: prospective multinational observational study (GRACE). BMJ. 2006 Nov 25;333(7578):1091
- Frangogiannis NG. Regulation of the inflammatory response in cardiac repair. Circ Res. 2012 Jan 6;110(1):159-73
- Galindo CL, Kasasbeh E, Murphy A, Ryzhov S, Lenihan S, Ahmad FA, Williams P, Nunnally A, Adcock J, Song Y, Harrell FE, Tran TL, Parry TJ, Iaci J, Ganguly A, Feoktistov I, Stephenson MK, Caggiano AO, Sawyer DB, Cleator

JH. Anti-remodeling and anti-fibrotic effects of the neuregulin-1β glial growth factor 2 in a large animal model of heart failure. J Am Heart Assoc. 2014 Oct 23;3(5):e000773

- Gardner RT, Habecker BA. Infarct-derived chondroitin sulfate proteoglycans prevent sympathetic reinnervation after cardiac ischemia-reperfusion injury. J Neurosci. 2013 Apr 24;33(17):7175-83
- Hallowell GD, Potter TJ, Bowen IM. Reliability of quantitative echocardiography in adult sheep and goats. BMC Vet Res. 2012 Sep 27;8:181
- Hao X, Silva EA, Månsson-Broberg A, Grinnemo KH, Siddiqui AJ, Dellgren G, Wärdell E, Brodin LA, Mooney DJ, Sylvén C. Angiogenic effects of sequential release of VEGF-A165 and PDGF-BB with alginate hydrogels after myocardial infarction. Cardiovasc Res. 2007 Jul 1;75(1):178-85
- Harris AS, Rojas AG. The initiation of ventricular fibrillation due to coronary occlusion. Exp Med Surg. 1943; 1:105
- Harris AS. Delayed development of ventricular ectopic rhythms following experimental coronary occlusion. Circulation. 1950; 1:1318
- Hashimoto H, Olson EN, Bassel-Duby R. Therapeutic approaches for cardiac regeneration and repair. Nat Rev Cardiol. 2018 Oct;15(10):585-600
- Holladay CA, Duffy AM, Chen X, Sefton MV, O'Brien TD, Pandit AS. Recovery of cardiac function mediated by MSC and interleukin-10 plasmid functionalised scaffold. Biomaterials. 2012 Feb;33(5):1303-14
- Horckmans M, Ring L, Duchene J, Santovito D, Schloss MJ, Drechsler M, Weber C, Soehnlein O, Steffens S. Neutrophils orchestrate post-myocardial infarction healing by polarizing macrophages towards a reparative phenotype. Eur Heart J. 2017 Jan 14;38(3):187-197
- Houtgraaf JH, de Jong R, Kazemi K, de Groot D, van der Spoel TI, Arslan F, Hoefer I, Pasterkamp G, Itescu S, Zijlstra F, Geleijnse ML, Serruys PW, Duckers HJ. Intracoronary infusion of allogeneic mesenchymal precursor cells directly after experimental acute myocardial infarction reduces infarct size, abrogates adverse remodeling, and improves cardiac function. Circ Res. 2013 Jul 5;113(2):153-66
- Ifkovits JL, Tous E, Minakawa M, Morita M, Robb JD, Koomalsingh KJ, Gorman JH 3rd, Gorman RC, Burdick JA. Injectable hydrogel properties

influence infarct expansion and extent of postinfarction left ventricular remodeling in an ovine model. Proc Natl Acad Sci U S A. 2010 Jun 22;107(25):11507-12

- Kiefmann M, Tank S, Keller P, Börnchen C, Rinnenthal JL, Tritt MO, Schulte-Uentrop L, Olotu C, Goetz AE, Kiefmann R. IDH3 mediates apoptosis of alveolar epithelial cells type 2 due to mitochondrial Ca(2+) uptake during hypocapnia. Cell Death Dis. 2017 Aug 24;8(8):e3005
- Le LV, Mohindra P, Fang Q, Sievers RE, Mkrtschjan MA, Solis C, Safranek CW, Russell B, Lee RJ, Desai TA. Injectable hyaluronic acid based microrods provide local micromechanical and biochemical cues to attenuate cardiac fibrosis after myocardial infarction. Biomaterials. 2018 Jul;169:11-21
- Lee RJ, Springer ML, Blanco-Bose WE, Shaw R, Ursell PC, Blau HM. VEGF gene delivery to myocardium: deleterious effects of unregulated expression. Circulation. 2000 Aug 22;102(8):898-901
- Linke A, Müller P, Nurzynska D, Casarsa C, Torella D, Nascimbene A, Castaldo C, Cascapera S, Böhm M, Quaini F, Urbanek K, Leri A, Hintze TH, Kajstura J, Anversa P. Stem cells in the dog heart are self-renewing, clonogenic, and multipotent and regenerate infarcted myocardium, improving cardiac function. Proc Natl Acad Sci U S A. 2005 Jun 21;102(25):8966-71
- Macarthur JW Jr, Cohen JE, McGarvey JR, Shudo Y, Patel JB, Trubelja A, Fairman AS, Edwards BB, Hung G, Hiesinger W, Goldstone AB, Atluri P, Wilensky RL, Pilla JJ, Gorman JH 3rd, Gorman RC, Woo YJ. Preclinical evaluation of the engineered stem cell chemokine stromal cell-derived factor 1 α analog in a translational ovine myocardial infarction model. Circ Res. 2014 Feb 14;114(4):650-9
- Mann DL, Bristow MR. Mechanisms and models in heart failure: the biomechanical model and beyond. Circulation. 2005 May 31;111(21):2837-49
- Marsano A, Maidhof R, Luo J, Fujikara K, Konofagou EE, Banfi A, Vunjak-Novakovic G. The effect of controlled expression of VEGF by transduced myoblasts in a cardiac patch on vascularization in a mouse model of myocardial infarction. Biomaterials. 2013 Jan;34(2):393-401
- Miller AL, Dib C, Li L, Chen AY, Amsterdam E, Funk M, Saucedo JF, Wang TY. Left ventricular ejection fraction assessment among patients with acute

myocardial infarction and its association with hospital quality of care and evidence-based therapy use. Circ Cardiovasc Qual Outcomes. 2012 Sep 1;5(5):662-71

- Moainie SL, Gorman JH 3rd, Guy TS, Bowen FW 3rd, Jackson BM, Plappert T, Narula N, St John-Sutton MG, Narula J, Edmunds LH Jr, Gorman RC. An ovine model of postinfarction dilated cardiomyopathy. Ann Thorac Surg. 2002 Sep;74(3):753-60
- Mühlfeld C, Nyengaard JR, Mayhew TM. A review of state-of-the-art stereology for better quantitative 3D morphology in cardiac research. Cardiovasc Pathol. 2010 Mar-Apr;19(2):65-82
- Mühling T, Duda J, Weishaupt JH, Ludolph AC, Liss B. Elevated mRNA-levels of distinct mitochondrial and plasma membrane Ca(2+) transporters in individual hypoglossal motor neurons of endstage SOD1 transgenic mice. Front Cell Neurosci. 2014 Nov 14;8:353
- Mukherjee R, Zavadzkas JA, Saunders SM, McLean JE, Jeffords LB, Beck C, Stroud RE, Leone AM, Koval CN, Rivers WT, Basu S, Sheehy A, Michal G, Spinale FG. Targeted myocardial microinjections of a biocomposite material reduces infarct expansion in pigs. Ann Thorac Surg. 2008 Oct;86(4):1268-76
- Olivares-Silva F, Landaeta R, Aránguiz P, Bolivar S, Humeres C, Anfossi R, Vivar R, Boza P, Muñoz C, Pardo-Jiménez V, Peiró C, Sánchez-Ferrer CF, Díaz-Araya G. Heparan sulfate potentiates leukocyte adhesion on cardiac fibroblast by enhancing Vcam-1 and Icam-1 expression. Biochim Biophys Acta. 2018 Mar;1864(3):831-842
- Prante C, Milting H, Kassner A, Farr M, Ambrosius M, Schön S, Seidler DG, Banayosy AE, Körfer R, Kuhn J, Kleesiek K, Götting C. Transforming growth factor beta1-regulated xylosyltransferase I activity in human cardiac fibroblasts and its impact for myocardial remodeling. J Biol Chem. 2007 Sep 7;282(36):26441-9
- Purcell BP, Barlow SC, Perreault PE, Freeburg L, Doviak H, Jacobs J, Hoenes A, Zellars KN, Khakoo AY, Lee T, Burdick JA, Spinale FG. Delivery of a matrix metalloproteinase-responsive hydrogel releasing TIMP-3 after myocardial infarction: effects on left ventricular remodeling. Am J Physiol Heart Circ Physiol. 2018 Oct 1;315(4):H814-H825

- Reef VB. Echocardiographic examination in the horse: the basics. Compend Contin Educ Pract Vet 1990; 12: 1312-1319
- Roger VL, Weston SA, Gerber Y, Killian JM, Dunlay SM, Jaffe AS, Bell MR, Kors J, Yawn BP, Jacobsen SJ. Trends in incidence, severity, and outcome of hospitalized myocardial infarction. Circulation. 2010 Feb 23;121(7):863-9
- Rogers WJ, Frederick PD, Stoehr E, Canto JG, Ornato JP, Gibson CM, Pollack CV Jr, Gore JM, Chandra-Strobos N, Peterson ED, French WJ. Trends in presenting characteristics and hospital mortality among patients with ST elevation and non-ST elevation myocardial infarction in the National Registry of Myocardial Infarction from 1990 to 2006. Am Heart J. 2008 Dec;156(6):1026-34
- Rosker C, Salvarani N, Schmutz S, Grand T, Rohr S. Abolishing myofibroblast arrhythmogeneicity by pharmacological ablation of α-smooth muscle actin containing stress fibers. Circ Res. 2011 Oct 28;109(10):1120-31
- Schmitto JD, Mokashi SA, Lee LS, Laurence R, Schotola H, Coelho-Filho O, Rajab TK, Kwong R, Bolman RM 3rd, Quintel M, Cohn LH, Chen FY. A novel, innovative ovine model of chronic ischemic cardiomyopathy induced by multiple coronary ligations. Artif Organs. 2010 Nov;34(11):918-22
- Seif-Naraghi SB, Singelyn JM, Salvatore MA, Osborn KG, Wang JJ, Sampat U, Kwan OL, Strachan GM, Wong J, Schup-Magoffin PJ, Braden RL, Bartels K, DeQuach JA, Preul M, Kinsey AM, DeMaria AN, Dib N, Christman KL. Safety and efficacy of an injectable extracellular matrix hydrogel for treating myocardial infarction. Sci Transl Med. 2013 Feb 20;5(173):173ra25
- Shimkunas R, Makwana O, Spaulding K, Bazargan M, Khazalpour M, Takaba K, Soleimani M, Myagmar BE, Lovett DH, Simpson PC, Ratcliffe MB, Baker AJ. Myofilament dysfunction contributes to impaired myocardial contraction in the infarct border zone. Am J Physiol Heart Circ Physiol. 2014 Oct 15;307(8):H1150-8
- Song M, Jang H, Lee J, Kim JH, Kim SH, Sun K, Park Y. Regeneration of chronic myocardial infarction by injectable hydrogels containing stem cell homing factor SDF-1 and angiogenic peptide Ac-SDKP. Biomaterials. 2014 Mar;35(8):2436-45
- Takehara N, Tsutsumi Y, Tateishi K, Ogata T, Tanaka H, Ueyama T, Takahashi T, Takamatsu T, Fukushima M, Komeda M, Yamagishi M, Yaku H, Tabata Y,

Matsubara H, Oh H. Controlled delivery of basic fibroblast growth factor promotes human cardiosphere-derived cell engraftment to enhance cardiac repair for chronic myocardial infarction. J Am Coll Cardiol. 2008 Dec 2;52(23):1858-1865

- Taylor KR, Gallo RL. Glycosaminoglycans and their proteoglycans: host-associated molecular patterns for initiation and modulation of inflammation. FASEB J. 2006 Jan;20(1):9-22
- Tous E, Ifkovits JL, Koomalsingh KJ, Shuto T, Soeda T, Kondo N, Gorman JH 3rd, Gorman RC, Burdick JA. Influence of injectable hyaluronic acid hydrogel degradation behavior on infarction-induced ventricular remodeling. Biomacromolecules. 2011 Nov 14;12(11):4127-35
- Troidl C, Möllmann H, Nef H, Masseli F, Voss S, Szardien S, Willmer M, Rolf A, Rixe J, Troidl K, Kostin S, Hamm C, Elsässer A. Classically and alternatively activated macrophages contribute to tissue remodelling after myocardial infarction. J Cell Mol Med. 2009 Sep;13(9B):3485-96
- Vasquez C, Morley GE. The origin and arrhythmogenic potential of fibroblasts in cardiac disease. J Cardiovasc Transl Res. 2012 Dec;5(6):760-7
- Yanagisawa-Miwa A, Uchida Y, Nakamura F, Tomaru T, Kido H, Kamijo T, Sugimoto T, Kaji K, Utsuyama M, Kurashima C, *et al*. Salvage of infarcted myocardium by angiogenic action of basic fibroblast growth factor. Science. 1992 Sep 4;257(5075):1401-3
- Ye L, Chang YH, Xiong Q, Zhang P, Zhang L, Somasundaram P, Lepley M, Swingen C, Su L, Wendel JS, Guo J, Jang A, Rosenbush D, Greder L, Dutton JR, Zhang J, Kamp TJ, Kaufman DS, Ge Y, Zhang J. Cardiac repair in a porcine model of acute myocardial infarction with human induced pluripotent stem cell-derived cardiovascular cells. Cell Stem Cell. 2014 Dec 4;15(6):750-61
- Zacchigna S, Martinelli V, Moimas S, Colliva A, Anzini M, Nordio A, Costa A, Rehman M, Vodret S, Pierro C, Colussi G, Zentilin L, Gutierrez MI, Dirkx E, Long C, Sinagra G, Klatzmann D, Giacca M. Paracrine effect of regulatory T cells promotes cardiomyocyte proliferation during pregnancy and after myocardial infarction. Nat Commun. 2018 Jun 26;9(1):2432

- Zhu W, Zhang E, Zhao M, Chong Z, Fan C, Tang Y, Hunter JD, Borovjagin AV, Walcott GP, Chen JY, Qin G, Zhang J. Regenerative potential of neonatal porcine hearts. Circulation. 2018 Dec 11;138(24):2809-2816

Chapter Four

Elastin-like recombinamers-based hydrogel modulates post-ischemic remodelling in a clinically-relevant model of myocardial infarction

Sections of this chapter have been submitted in the following manuscript: Contessotto P., Orbanić D., Da Costa M., Jin C., Owens P., Chantepie S., Papy-Garcia D., Chinello C., Magni F., Karlsson N.G., Kilcoyne M., Dockery P., Rodríguez-Cabello J.C. and Pandit A. "Elastin-like recombinamers-based hydrogel heals myocardial infarction in a clinically-relevant model". Under revision in *Nature Materials.*

4.1 Introduction

Myocardial infarction is one of the main causes of worldwide mortality. This is the clinical consequence of a limitation of cardiac tissue regeneration in mammals: unlike other tissues such as liver, skin and bone, the human myocardium is not able to regenerate once ischemic damage has occurred. Several approaches have been designed and tested to treat myocardial infarction over the past decades, but none of these has led to a final established clinical preference in the most advanced clinical trials [Chugh, Malliaras]. The employment of stem cells, growth factors or biomaterials has been tested either individually or in combination. However, an optimum system still needs to be designed and translated successfully in a clinical scenario.

In the field of tissue engineering, the increasing application of therapeutic biomaterials for a wide range of diseases has encouraged researchers to develop and test scaffold systems in a preclinical setting to deliver either stem cells or growth factors at the site of implantation. The choice of the most suitable therapeutic biomaterial for the desired clinical outcome is a major challenge in current medical device development. Elastin is one of the proteins which are abundantly present in the extracellular matrix of several tissue types such as myocardium, cartilage and skin [Mithieux]. Specifically, elastin fibres are derived from the coacervation and further crosslinking of the precursor tropoelastin molecules [Kozel]. The elastogenic activity resides in the main cellular components of the tissue network that can be endothelial cells, fibroblasts, chondrocytes, or keratinocytes.

Through the genetically-engineered fabrication of elastin-mimicking peptides called elastin-like recombinamers (ELRs), there is an opportunity to compensate for the limited availability of natural elastin and also to control the consistency of the biomaterial. Moreover, ELRs can be functionalised with specific motifs responsible for several interactions with the cellular microenvironment including cell adhesiveness and degradability [Rodríguez-Cabello, Castellanos]. As a result, this functionalisation, together with the possibility to fabricate various structural formats such as hydrogel or microspherical, has increased the possibility of applications.

Several ELRs-based systems have already been studied for their efficacy and interaction with cellular components *in vitro* and *in vivo* over recent years [Staubli, González de Torre, Changi, Pescador]. Variations in scaffold formulations are required depending on the delivery method in a specific pathological state and site of

implantation. In the myocardial microenvironment after ischemia, it is well known how the acute inflammatory, proliferation and remodelling phases dictate the host-response of the cardiac tissue to the ischemic insult [Frangogiannis]. Therefore, to design a potentially beneficial treatment for the post-ischemic remodelling requires a comprehensive understanding of the timing of the pathology. At the same time, there is a precise clinical need due to the organ's vulnerability to any invasive intervention after a heart attack. Ideally an intervention is possible through an epicardial or catheter-based procedure at one-week after the infarct. The key determinants of the success of a biomaterial-based therapy are the host foreign body response and the possible modulatory effect of the biomaterial on the inflammatory environment. Despite the detrimental effects of a chronic inflammatory situation in a healing environment [Liu, Li, Nahrendorf], there is evidence that the modulation of macrophage population is necessary for the achievement of an accelerated repair of the damaged environment [Jiang, Mantovani, Frantz, Saxena]. Therefore, a biomaterial system can be tailored to enhance the physiological angiogenesis and repair of the wounded tissue which is normally overcome by a fibrotic response and its unpredictable effects on the overall cardiac function.

In a study by Kadner *et al.*, the efficacy of a polyethylene glycol hydrogel was enhanced by its introduction after the acute phase of inflammation of myocardial infarction [Kadner]. Specifically, an uncontrolled fast degradation was avoided and a significant improvement at the functional level was observed. The investigation of the beneficial effects of an optimal timing in the delivery at the peak of inflammation from a synthetic scaffold has recently been assessed in muscle injury and regeneration [Cezar].

In light of these considerations, it is hypothesised that the intra-myocardial injection of an ELRs-based hydrogel seven days after MI can beneficially impact on the myocardial remodelling process after ischemia in an ovine model of non-transmural myocardial infarction.

Consequently, the objectives of this study are to:

- Optimise a procedure for the intra-myocardial injection of an ELRs-based hydrogel and evaluate the cardiac functional response 21 days after the hydrogel injection.

- Evaluate the effects of the hydrogel on fibrosis 21 days after the injection in the ischemic core of the infarct at histological and ultrastructural level.

- Investigate changes in total sulfated glycosaminoglycans (GAGs) and changes in GAGs ratio 21 days in the infarcted regions after the hydrogel injection by dimethylmethylene blue (DMMB) assay.

- Assess changes in the glycosylation of the membrane proteins in the ischemic core and border regions in response to the hydrogel 21 days after the injection by their binding to biologically relevant lectins.

4.2 Materials and methods

4.2.1 *In vivo* experimental plan

The procedure of myocardial infarction described in the section 3.2.1 was performed on 39 Romanov adult male sheep. Sheep were randomly assigned to ELRs, PBS, and MI-only groups; MI-only groups had a final endpoints of 7 and 28 days after the surgical procedure of coronaries ligation. A schematic representation of the experimental groups of this preclinical study is shown in Figure 4.2. Sheep were randomly assigned to ELRs, PBS, and MI-only groups; MI-only groups had as final endpoints 7 and 28 days after the surgical procedure of coronaries ligations. As regards the ELRs and PBS groups, animals were injected with either hydrogel or PBS seven days after the induction of MI, thereby following the same thoracotomy procedure with intra-myocardial injections in the left ventricular wall.

4.2.2 Preparation of ELRs for myocardial injection

Elastin-like recombinamers (ELRs) functionalised with azide (HRGD6) and cyclooctyne (HE5) groups for crosslinking were weighed in sterile conditions. ELRs

were resuspended in the appropriate quantities to keep the ratio HE5-cycloctyne:HRGD6-azide 1.79:1. ELRs were stored at 4°C until the day before they were required for injection, as detailed in Appendix A.22. Therefore, each ELR was dissolved in 750 µl of sterile water overnight at 4°C. Once the solutions were totally clear, 250 µl of HRGD6-azide was placed in a sterile eppendorf tube. To initiate hydrogel formation, 250 µl of HE5-cycloctyne was added to start the crosslinking of the recombinamers. Cold sterile tips were used to carry out this procedure and the eppendorf tube containing the mixed ELRs was kept on ice for exactly ten minutes before injection. Schematics showing the sequences of the two ELRs are illustrated in the Figure A.12 in Appendices.

4.2.3 Injection trials

The procedure for the optimisation of the intra-myocardial injection of the ELRs hydrogel was carried out using lamb hearts collected from a local abattoir. Different conditions were tested to assess the injectability of the crosslinked ELRs and their integration in the myocardial tissue, as detailed in Table 4.1. Briefly, the mixture of the two ELRs was left for crosslinking either at 4°C or at RT from an incubation time that varied from zero to 15 minutes. Every solution whose injectability was tested included 2 µl of Alcian blue solution as a dye to allow the immediate visualisation of the injected hydrogel in the left ventricular wall. Samples were excised from the injected and non-injected areas, processed for paraffin embedding, sectioned and stained by H&E and Verhoeff's-Van Gieson staining (Appendices A.12 and A.15).

4.2.4 Procedure for injection *in vivo*

A sterile syringe having a maximum capacity of 1 ml and a 25G needle was used to perform each intra-myocardial injection through the heart wall. Three injections were performed to the ischemic sites through the border zone. The border zone is the edge region between the site where ischemia was induced by coronary ligation and the healthy zone of the myocardial wall. Each injection carried a volume of 500 µl of hydrogel. The needle was carefully retracted after each injection to avoid backflow of the hydrogel solution. The surgeon performing the coronary ligation injury and injection procedures was blinded to the contents of the injectant.

4.2.5 Animal monitoring after injection procedures

After surgery, animals were monitored for signs of pain and distress including reduced activity, failure to groom, reduced food or water intake, eye squinting or pale eyes, teeth grinding, changes in posture, guarding, and aggressiveness. If these signs were observed, researchers engaged the veterinary staff whether to provide appropriate interventions such as additional administration of analgesia (buprenorphine); and in the event that the pain was unmanageable, the animals were euthanised. At three-weeks after surgery, animals were euthanised by pentobarbital sodium injection (5 mg/kg) under anaesthesia in line with the Veterinary Medical Association guidelines. After five minutes, animals were checked for pulse. Animals experiencing undue pain or distress requiring humane intervention were euthanised.

4.2.6 Heart explants and tissue preservation

Hearts were perfused with PBS to remove the excess of blood immediately after the explantation. Two washes with PBS were performed before initiating harvesting. Each heart was cut axially using a brain knife keeping a thickness of one cm for each slice from the ventricular region; then all the slices up until the apex were laid on a white surface and pictures were taken before and after sampling. Rulers were placed next to the slices on the white surface to allow the quantification from the images taken with a D90 photographic camera (Sony, Japan).

4.2.7 Isotropic uniform random sampling

Samples with a maximum thickness of 0.5 cm in every direction were harvested and embedded as described in the section 3.2.4 and shown in the Figure 3.3 in Chapter Three [Bergmann, Mühlfeld]. Isotropic uniform random sampling was required for further stereological quantification of volume fraction of fibrosis and angiogenesis-related parameters using appropriate stereological grids (Figures A.9 and A.10 in Appendices).

4.2.8 Assessment of post-ischemic remodelling by histology

Isotropic uniform random samples embedded in OCT were cut using a cryotome at a thickness of 5 μm (Appendix A.8). Each block was sectioned at three different levels, 200 μm-apart from the next. These serial sections were stained for Masson's Trichrome to visualize collagen fibres, collagen and nuclei (Appendix A.13). The imaging of all the serial sections was performed using a VS120 Virtual Slide Microscope (Olympus, Japan). Each section was first quickly scanned to optimise the focus until a 40x magnification was reached.

4.2.9 Immunofluorescence staining for capillaries, collagen type-I and cardiomyocytes

OCT-embedded sections with a thickness of 5 μm were used for all the immunofluorescence and lectin histochemistry experiments. Since the time of fixation in paraformaldehyde was optimised to get to the final overnight incubation at 4°C, this step did not affect the outcome of the immunofluorescence experiments and no antigen retrieval was necessary for any of the markers tested.

At the beginning of each experiment, sections stored at -80°C were left at RT for approximately 20 minutes before starting. Samples were first permeabilised with TBS-Tween (0.05%) twice for five minutes each, then washed with TBS for an additional five minutes. Blocking of the samples was carried out using 10% donkey serum for one hour at RT. Immunofluorescence experiments were performed using the following primary antibodies and dilutions: rabbit polyclonal to CD31 at 1:50, rabbit polyclonal to tropomyosin1α at 1:200, and rabbit polyclonal to collagen type I at 1:200. All primary antibodies were diluted in TBS-Tween (0.05%) and incubation was carried out at 4°C overnight. The following day, samples were washed with TBS-Tween three times for 15 minutes each and then incubated with anti-rabbit Alexa Fluor® 647-donkey secondary antibody at 1:500 dilution in TBS-Tween (0.05%) for one hour at RT. The undiluted secondary antibody was centrifuged for ten minutes at 10,000 rpm to precipitate aggregates before making the dilution. After the incubation, glasses were washed with TBS-Tween three times for 15 minutes each then mounted with Prolong® Gold with DAPI and coverslipped. Glasses were left to cure overnight at RT before sealing. Details of the antibodies used are listed in the Table A.2 in Appendices.

4.2.10 Quantification of fibrosis

Three fields of view were analysed per each serial section stained with Masson's Trichrome. A grid made of 112 points was superimposed on each field of view and the points hitting collagen fibres were counted to get the volume fraction values. By stereological measurements, a total ischemic area of 4.05 mm^2 was analysed per block (Figure A.9 in Appendices). Five animals were analysed from the MI-only group at 28 days after MI induction, and five animals from the hydrogel-treatment group which were sacrificed three weeks after the hydrogel injection (28 days after MI). To avoid bias, animals from at least two different batches of surgeries were analysed for each group.

4.2.11 Analysis of myocardial extracellular matrix

Samples were snap-frozen in liquid nitrogen/dry ice-cooled isopentane and embedded in OCT before storage at -80°C until processing. The day before the analysis, samples were cut using a cryostat at a thickness of 30 μm, left to adhere on quartz discs and stored at -80°C until analysis. Both samples from hydrogel-treated and MI-only control groups were histologically evaluated by Masson's Trichrome staining to assess the localisation inside the ischemic region before running the Raman analysis. Spectroscopy measurements were performed in reflection mode with a confocal Raman microscope (Witec Alpha 500) using 785 nm excitation. The detector grating used was 600 lines/mm, centred at 880 cm^{-1}. Spectra were collected using an Andor Ixus cooled charge coupled device (−60 °C). A 40x objective lens (NA 0.6) delivered the laser beam and collected the back-scattered light. Rayleigh scattering was blocked with the appropriate notch filter. The laser spot diameter was approximately 1 μm with a laser power of 0.05 mW (785 nm) used. The instrument calibration was verified using the maximum signal from a silicon standard at 520 cm^{-1} and spectral resolution was approximately 0.8 cm^{-1}. Typical measurements were performed with a 40 seconds integration time at each point taken at multiple positions (225) across the tissue sample in an area of 100 μm^2. Cosmic ray reduction, background corrections, spectrum averaging and Savitzky-Golay smoothing (4 point, 3rd order) were carried out using WITec Project FIVE® software (Witec, Germany). Normalisation to the peak at 1446 cm^{-1} and graphical analysis was performed using

Origin® version 9.1 (OriginLab, USA). All spectra described are plotted relative to the excitation wavelength. Additional details on the optimisation of the procedure using Raman confocal microscopy are described in section A.23 and Figures A.7 and A.8 in Appendices.

4.2.12 Quantification of matrix deposition

Samples for transmission electron microscopy (TEM) analysis were processed as previously described in section 3.2.7 and 3.2.9. Imaging was performed using an H-7000 transmission electron microscope (Hitachi, Japan) at 75kV and at magnifications of 3,000x and 10,000x. Five fields of view per sample were imaged. Quantification of collagen fibres was done by superimposing an 81-points grid on each picture and counting the intersections of the collagen fibres with the points of the grid. Only core ischemic areas were used for this quantification.

4.2.13 Evaluation of glycosylation in cellular membranes and ECM

Membrane proteins were extracted from snap-frozen samples as described in section 2.2.5 and labelled with Alexa Fluor® 555-succinimidyl ester following the procedure detailed in section 2.2.6. A titration experiment was performed to determine the optimal concentration of sheep membrane protein sample to be used for the lectin microarray experiment (5 μg/ml, diluted in TBS-Tween 0.05%). Samples from healthy, ELRs-hydrogel-treated and MI-only at 28 days groups were tested for their binding to a panel of 48 lectins. Asialofetuin was used as control at a concentration of 3 μg/ml. Equal amounts of labelled membrane proteins from three animals were pooled together so that a total of seven samples were analysed for their binding to lectins (in technical triplicate). Core ischemic, border and remote areas were analysed from the infarcted animals. Image files showing the scanned lectin microarrays were processed using GenePix Pro v6.1.0.4 software (Molecular Devices, UK). Briefly, an adaptive diameter circular alignment based on 230 μm features was set in the options and grids were superimposed on the subarrays. Local background-corrected median feature intensity data were analysed and normalised to the median total intensity value of three replicate microarray slides (Appendix A.11).

4.2.14 Quantification of capillaries structures and angiogenesis

Sections from the MI-only and ELRs-treated groups were double-stained with *Griffonia simplicifolia* (GS-I) lectin and anti-CD31 primary antibody after optimisation of the lectin histochemistry on ischemic tissues (Figure A.4 in Appendices). Briefly, samples were left to thaw at RT for 20 minutes and washed with TBS-Tween twice for three minutes each. Then samples were blocked with 3% periodated BSA for one hour at RT. After this, glasses were quickly dipped in TBS and incubated with the lectin at a concentration of 15 μg/ml for one hour at RT. The samples were then washed three times with TBS for three minutes each and then blocked with 3% periodated BSA for one hour at RT. Sections were then incubated with the primary antibody to CD31 listed in section 4.2.9 at 1:50 dilution overnight at 4°C. The following day, samples were washed with TBS-Tween twice for ten minutes each and then with TBS once for ten minutes. After the incubation for one hour at RT with anti-rabbit Alexa Fluor® 647-donkey secondary antibody, sections were washed with TBS-Tween twice for ten minutes each and then with TBS once for ten minutes. Finally, the glasses were mounted with Prolong® Gold with DAPI and coverslipped. Glasses were left to cure overnight at RT before sealing. All the procedures from incubation with the lectin to final mounting was performed avoiding direct light due to the sensitivity of FITC-labelled lectin. Imaging was done using a FluoView 1000 laser confocal microscope (Olympus, Japan) and five images were taken for each serial section at a magnification of 20x. Only capillaries structures (not bigger vasculature) were counted using an appropriate stereological grid which was superimposed on each image to quantify the total number per squared mm (Figure A.10 in Appendices).

4.2.15 Functional response by echocardiographic measurements

The same procedure described in section 3.2.3 was followed to record echocardiography measurements the day before each surgical procedure and before the study time points.

4.2.16 Statistical analysis

All statistical analyses were performed using Minitab™ Express software (Minitab, Inc. State College, USA). Data related to the quantification of the number of

capillaries and radial diffusion followed a normal distribution and were compared by Student's t-test. Data related to the area fraction of fibrosis did not follow a normal distribution, and so they were analysed by Mann-Whitney *U* test. Data from total sulfated GAGs quantification and lectin microarray analysis were analysed by one-way ANOVA with Dunnett's post-hoc correction using the baseline in healthy conditions as control group. Data from echocardiographic measurements were compared using Kruskal-Wallis ANOVA. Values were considered significant only with $p<0.05$.

4.3 Results

4.3.1 Multiple intra-myocardial injections of ELRs hydrogel

Elastin-like recombinamers (ELRs) functionalised with azide (HRGD6) and cyclooctyne (HE5) groups for crosslinking were used through the whole *in vivo* study. An *ex vivo* experiment was performed to assess the retention of the hydrogel – stained with Alcian blue dye - in the intra-myocardial injection site. Both visual inspection and Verhoeff's Van Gieson staining confirmed that the gelling of the hydrogel took place *in situ* (Figure 4.1). The incubation time and temperature of the two ELRs before injection were optimized, and the settings of ten minutes of incubation at 4°C were selected to proceed with the *in vivo* injections (Table 4.1).

Seven days after the surgical procedure of coronaries ligation previously described (Chapter Three, section 3.2.1), three injections of 500 ml of hydrogel each were delivered in the infarct zone. Sutures with 2/0 PROLENE™ (Ethicon, USA) clearly localised the MI site from the first diagonal moving distally towards and up to 4-5 cm from the apex. All the multiple-injection procedures in the ELRs-treated animals were successfully completed. Three weeks after the injection procedure, each sample was harvested following the method already described (Chapter Three, section 3.2.4) and gross explants were visually inspected before the sampling (Figure 4.3).

4.3.2 Fibrosis evaluation after ELRs hydrogel treatment

The formation of a fibrotic scar is the final result of the remodelling process programmed in the myocardial environment after ischemia. Even though this host response can help to stabilise the organ, it is not possible to predict whether this

scarring evolves towards a non-contractile area which impacts on the overall heart function. Moreover, fibrosis in an irreversible process which will not allow any further restoration of either vascularized or muscle-like tissue in the ischemic area.

For these reasons, therapeutic options for the enhancement of healthier post-ischemic myocardial remodelling should always evaluate the entity and composition of the scarring after the application of a treatment. In this study, a stereological approach based on the removal of the bias due to cardiac tissue orientation was applied at the sampling stage. This facilitated a quantitative evaluation of the fibrotic response in the sheep treated with ELRs-based hydrogel compared to an ischemic control group. The endpoint of all the groups of animals tested was 28 days after MI which is a well-established timepoint at which to estimate whether there is a relevant change in myocardial remodelling. The treatment with ELRs-hydrogel followed a multiple-injections procedure. Briefly, three injections of 500 μl of solution each were performed in the infarct area seven days after the surgical induction of MI. HE5-cyclooctine and HRGD-azide ELRs were mixed and left on ice for ten minutes before loading in a syringe with a 25G needle and administered to the ischemic left ventricular wall by intra-myocardial injection. At day 28 after MI, fibrosis quantification was performed from both conventional Masson's Trichrome-stained sections and from TEM micrographs (Figure 4.4 A,B). Interestingly, measurements from the two different methods showed a similar significant reduction in fibrosis; stereological grids were applied in both cases. Specifically, in the ischemic zones the area fraction of collagen stained by Masson's Trichrome decreased from 0.25±0.05 in the MI-only group to 0.14±0.04 in the hydrogel-treated group ($p=0.022$) (Figure 4.4), and from 0.35±0.10 in the MI-only to 0.17±0.04 in the ELRs-treated group ($p=0.036$) after quantification from EM micrographs (Figure 4.4 C,D). At the qualitative level, extensive scarring was seen in the MI-only group, and the typical wavy-oriented deposition of collagen fibres was clear from both histological and EM imaging (Figure A.6 in Appendices).

4.3.3 Application of Raman confocal microscopy for fibrosis detection

Histological and EM methods are extensively used as gold standards to characterise and quantify fibrosis after ischemia. Nevertheless, all standard histological, immunofluorescence and EM methods are time-consuming and produce significant

quantities of toxic and generally non-environmentally-friendly products. At the same time, several recent studies investigated the potential of spectroscopy techniques to analyse changes at the extracellular level in different conditions and systems [Votteler, Brauchle 2017].

In this study we optimised, validated and applied a method based on Raman confocal microscopy to visualize and estimate the presence of fibrosis in myocardial tissue. Raman spectroscopy has been extensively used for chemical fingerprinting, but not to the same extent as in the biological field. After a careful optimisation of the conditions required to achieve a consistent signal-to-noise ratio in the recording of Raman spectra across the same sample, myocardial sections from the different groups were tested for their molecular fingerprint. A significant difference between the ischemic tissues and the healthy ones was seen in the corresponding normalised peak integrated intensity at 1246 cm^{-1} ($p=0.025$) using four different animals (Figure 4.5). Since all the spectra were recorded using a confocal Raman machine, it was possible to localise the integrated intensity in the scanned tissue section and compare it with a standard from Masson's Trichrome stained section (Figure 4.6). Thus, this novel method was applied to establish whether it was possible to distinguish the reduction in fibrosis seen in the ELRs-treated group by conventional histology. The averaged spectra obtained from the 100 μm^2 areas scanned showed high intensities of the peaks at 934, 1447 and 1660 cm^{-1}, corresponding to troponin and cardiomyocytes, as previously detected in myocardial tissue [Brauchle 2016]. A distinct difference between the ELRs-treated and the infarcted areas was seen at 1246 cm^{-1}. Normalised peak integrated intensity-derived data showed significance between fibrotic regions and healthy myocardium ($p=0.019$, $n=4$) whereas hydrogel-treated samples did not show the same significant increased intensity ($p=0.79$, $n=4$). This data confirmed the results reported above.

4.3.4 Glycobiology and angiogenesis assessment after ELRs hydrogel treatment

The enhancement of angiogenesis is one of the main paths that had been extensively studied over the past decades to restore and improve the healing of myocardial tissue after ischemia. The expansion of vasculature structures from the existing ones is physiologically promoted during the proliferative phase of inflammation in response to VEGF signalling pathway. This response is not stable over the following weeks

due to the concurrent rising deposition of collagen fibres which prevents the migration of any other cellular component by occupying that space in the healing area. Moreover, an increasing number of studies are focusing on the involvement of glycan markers as key signals of inflammatory or degenerative paths [Grewal, Mohd Isa, Varki]. Therefore, in this study the approach was to conduct a lectin microarray screening on the membrane protein samples to detect initial relevant differences in the glycan markers.

A significant increase in sialylation and mannosylation was seen in the infarcted samples over that in the healthy condition independently of the regional difference of the sample i.e. core ischemic or remote (Figure 4.7 A). Most interestingly, focusing on the ELRs-treated and MI-only groups, relevant increases in the binding intensities to *Griffonia simplicifolia* isolectin A4 (GS-I-A4) ($p<0.05$) and GS-I-B4 ($p<0.001$), *Caragana arborescens* (CAA) and *Galanthus nivalis* (GNA) lectins were seen in the core ischemic regions three weeks after the injection of the hydrogel (Figure 4.7 A,B). Specifically, GS-I-B4 binds to terminal Gal-α-(1,3)-Gal, and this binding was already reported as a marker of endothelial cells and capillaries structures [Wälchli, He]. The localisation of the binding was assessed by lectin histochemistry and showed a migration of endothelial cells and as well as the probable formation of capillaries structures (Figure 4.7 C,D). To confirm that there was actually an enhancement of angiogenesis by the ELRs-hydrogel, binding to GS-I lectin was colocalised with the immunofluorescence staining against CD31 (Figure 4.8 A,B).

Using EM imaging, it was possible to distinguish the main components of the capillary structures i.e. endothelial cells, pericytes as well as the erythrocytes circulating in the lumen of these structures (Figure 4.8 C). Only GS-I+/CD31+ and up to 20 μm-size structures were counted as capillaries and stereologically quantified. The total number of capillaries significantly increased from 44±18 in MI-only conditions to 187±47 in ELRs-treated group ($p=0.012$, $n=5$). Consequently, the radial diffusion distance decreased from 63±13 in MI-only group to 29±3 in hydrogel-treated animals (Figure 4.8 D,E).

4.3.5 Total sulfated GAGs deposition and HS/CS ratio during remodelling

The relevance of glycosaminoglycans (GAGs) in the interaction between cells and the extracellular matrix had been exploited in the functionalisation of biomaterial-

based systems to enhance tissue healing [Rnjak-Kovacina]. In this large animal study, total sulfated GAGs and the ratio between heparan sulphate (HS) and chondroitin sulphate (CS) were quantified by DMMB assay in all the groups of the study to evaluate the remodelling at the extracellular matrix level.

The significant nine-fold increased deposition of sulfated GAGs already observed across the 7-day and 28-day timepoints (Chapter Three, section 3.3.4) was confirmed also in the two additional groups harvested 28 days after MI and analysed in this study, that included the PBS-treated and the ELRs hydrogel-treated animals. Statistical analysis by one-way ANOVA with Dunnett's test showed a significant seven-fold increase in the PBS group from the pre-infarct 0.33±0.13 μg/mg reaching the value of 2.45±1.69 μg/mg ($p=0.022$) which was comparable to the reported significant increase in the MI-only group at 28 days (3.09±0.89 μg/mg, $p=0.002$). The same trend was observed also in the hydrogel-treated group, but to a lesser extent and at a non-significant level, by the measurement of a total quantity of 1.73±1.07 μg/mg ($p=0.11$) (Figure 4.9 A).

To further investigate changes in the balance between heparan sulphate and chondroitin sulphate during the remodelling and to assess any variation following the ELRs-hydrogel injections, HS/CS ratio was quantified in the PBS-injected and ELRs-treated groups. From the baseline level in healthy conditions (0.97±0.02), a significant decrease by 47% and 53% in the HS/CS ratio was observed in the hydrogel-treated group (0.51±0.11, $p<0.01$) and in the PBS-injected animals, respectively (0.45±0.06, $p<0.01$) (Figure 4.9 B).

4.3.6 Evaluation of functional improvement 28 days after MI

Echocardiographic measurements were performed to track the main functional parameters of the hearts the day before every surgical procedure and at the endpoint of 28 days post-MI (Figure 4.10 A). Animals which showed an increase - although minimal - in ejection fraction (EF) seven days post-MI were not considered for the final functional analysis since the induction of the infarct may not have caused significant changes at this level. Nevertheless, the gross explants evaluation post-euthanasia did not exclude any animals from the histological and protein analyses presented in the previous sections. A consistent average decrease in EF by 10.8%,

8.3% and 9% was seen seven days post-MI in MI-only, PBS and hydrogel groups, with no significant difference across the groups (Figure 4.10 B). The decrease in EF due to the surgical procedure was completely reversed only in the ELRs-treated group, which showed a 16.2% improvement 21 days after the injection time (Figure 4.10 C). On the other hand, both the PBS-injected and MI-only groups continued to show a trend of decrease in EF at the same endpoint (-2.6% and -0.3%, respectively).

Table 4.1 Optimised conditions for the injection of the ELRs hydrogel.

Samples	Composition	Temp (°C)	V (µl)	Incubation time (min)	Remarks
1	HRGD6-azide + HE5-cyclooctine	4°C	100	0	Hydrogel is too fluid, has no gel characteristics. Injectability is easy. No high pressure required.
2	HRGD6-azide + HE5-cyclooctine	4°C	200	10	Hydrogel after ten minutes gives a gel characteristic. It is easy to inject and the gel diffusion is retained through the wall of the left ventricle.
3	HRGD6-azide + HE5-cyclooctine	4°C	100	15	Hydrogel after 15 minutes of incubation is highly gelled up and is very difficult to inject it into the heart muscle.
4	HRGD6-azide + HE5-cyclooctine	RT	100	5	Hydrogel is too fluid, has no gel characteristics. Injectability is easy. No high pressure required.
5	HRGD6-azide + HE5-cyclooctine	RT	200	10	Hydrogel after ten minutes gives a gel characteristic. It is easy to inject and the gel diffusion is retained through the wall of the left ventricle.

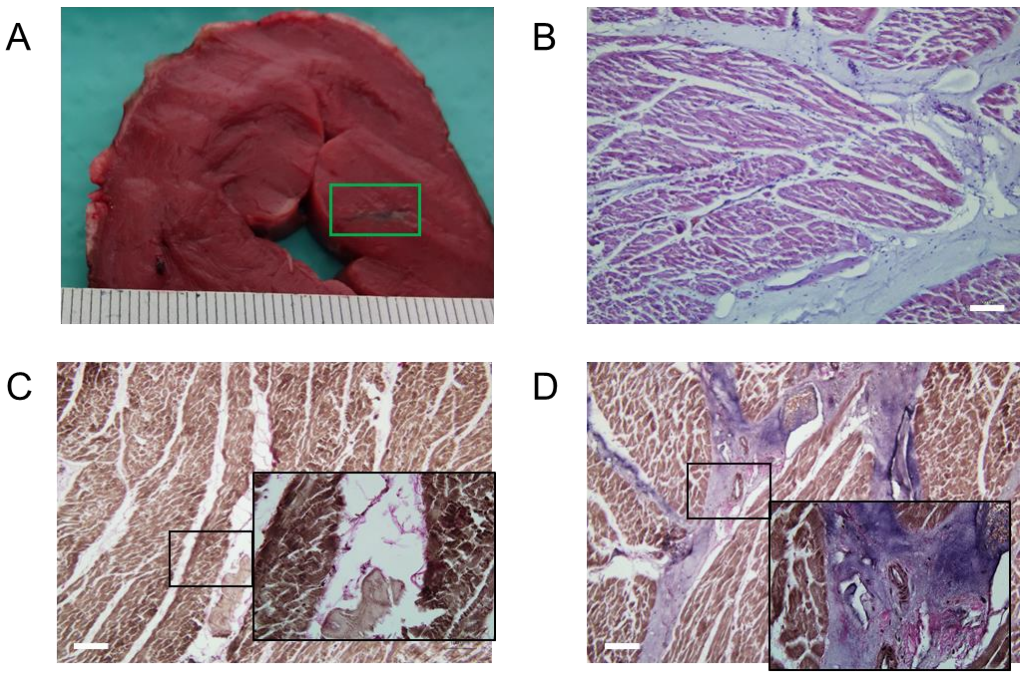

Figure 4.1 *Ex vivo* injection trial in ovine heart. Representative images (A,B) of ELRs-hydrogel injection *ex vivo* in an ovine heart (1-mm ruler spacing) and correspondent H&E showing hydrogel penetration across the sarcomeres. Verhoeff's-Van Gieson staining is specific for elastin and illustrates intercalation of the hydrogel across the sarcomeres causing no damage to the integrity of cardiomyocytes, vasculature structures and relative supporting collagen (D). Non-injected area is shown in C. Scale bar = 100 µm.

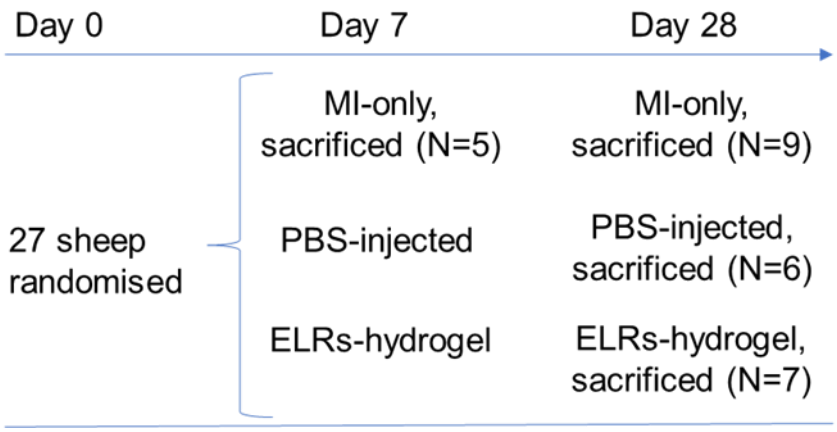

Figure 4.2 Schematic representation of experimental *in vivo* plan to test the efficacy of the ELRs-hydrogel. 9/39 sheep died because of the suture ligation procedure, corresponding to a 23.07% mortality. One out of seven PBS-injected and two out of nine ELRs-hydrogel-injected animals died after the injection procedure. One out of seven ELRs-hydrogel-injected sheep was excluded because of MI-related atrial fibrillation.

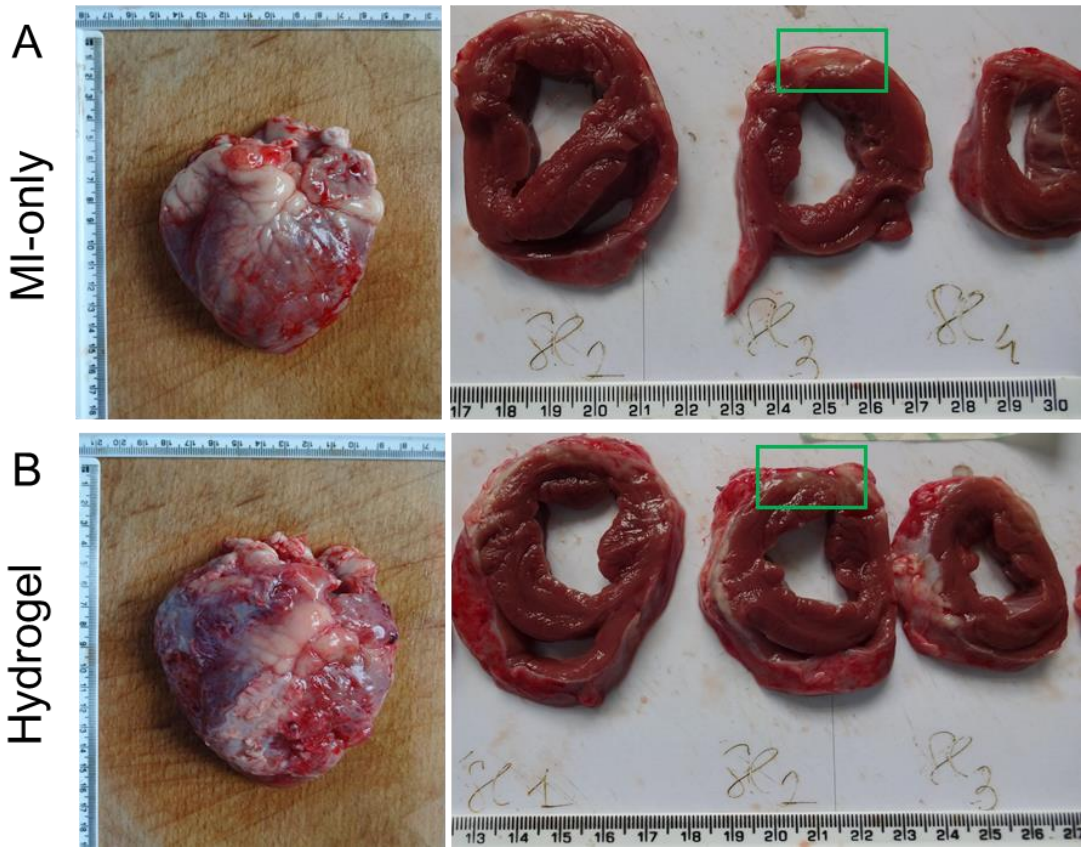

Figure 4.3 Gross explant pictures showing the left ventricle at the macroscopic level. Representative pictures of gross explants from MI-only group (A) and ELRs-hydrogel group (B) 28 days after the induction of myocardial infarction. Clear MI-area (green rectangles) was visible by the whitish colouring of the region of the left ventricle effected in all animals at the time of harvesting. The infarcts were non-transmural since they were not extended to the full thickness of the left ventricular wall. Ruler = 1 mm.

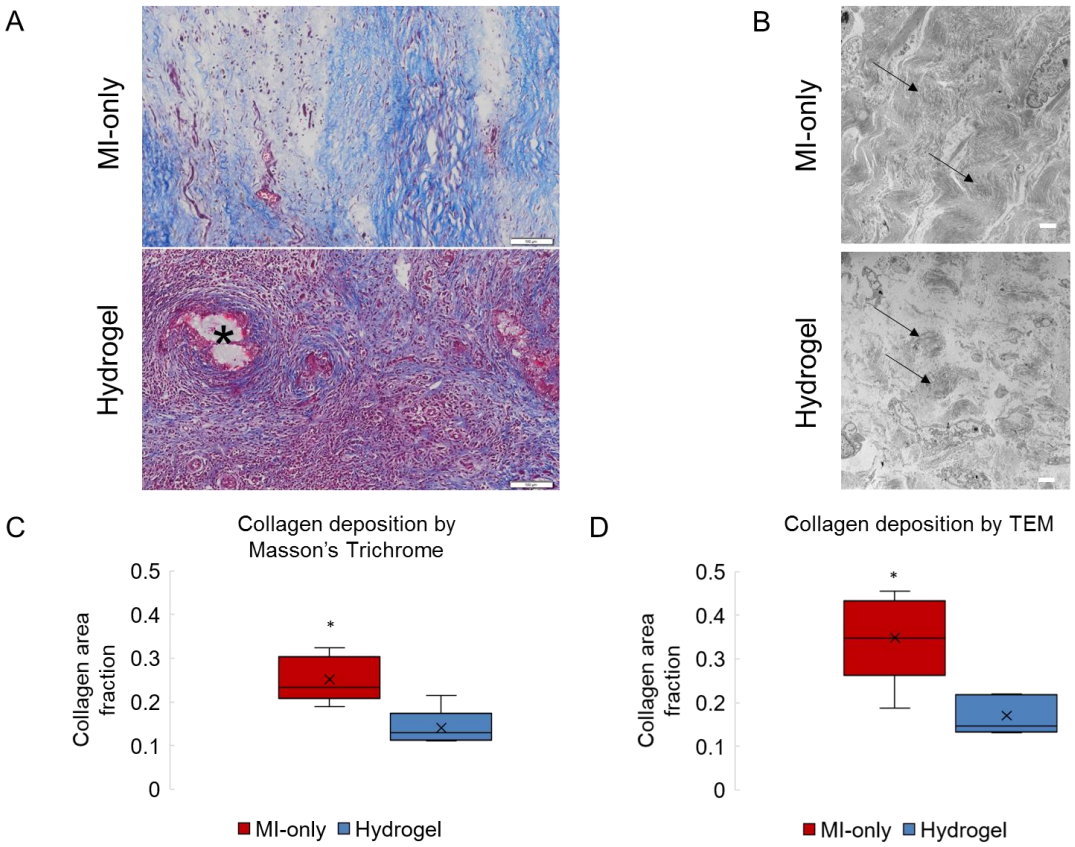

Figure 4.4 Reduced fibrosis in the group treated with ELRs-hydrogel. Masson's Trichrome images (A) and relative quantification (C) of collagen deposition (stained in blue) across the ischemic areas in hydrogel-treated (star indicates an island of ELRs-hydrogel) compared against MI-only. TEM micrographs (B) illustrating the typical wavy structure of fibrotic collagen deposits (indicated by arrows) in the analyzed ischemic areas in both hydrogel-treated and MI-only, and their relative quantification (D). Scale bars = 100 µm in A, 2 µm in B. Data are reported as box-plots, Mann-Whitney *U* test, n=5 animals per group, *p<0.05.

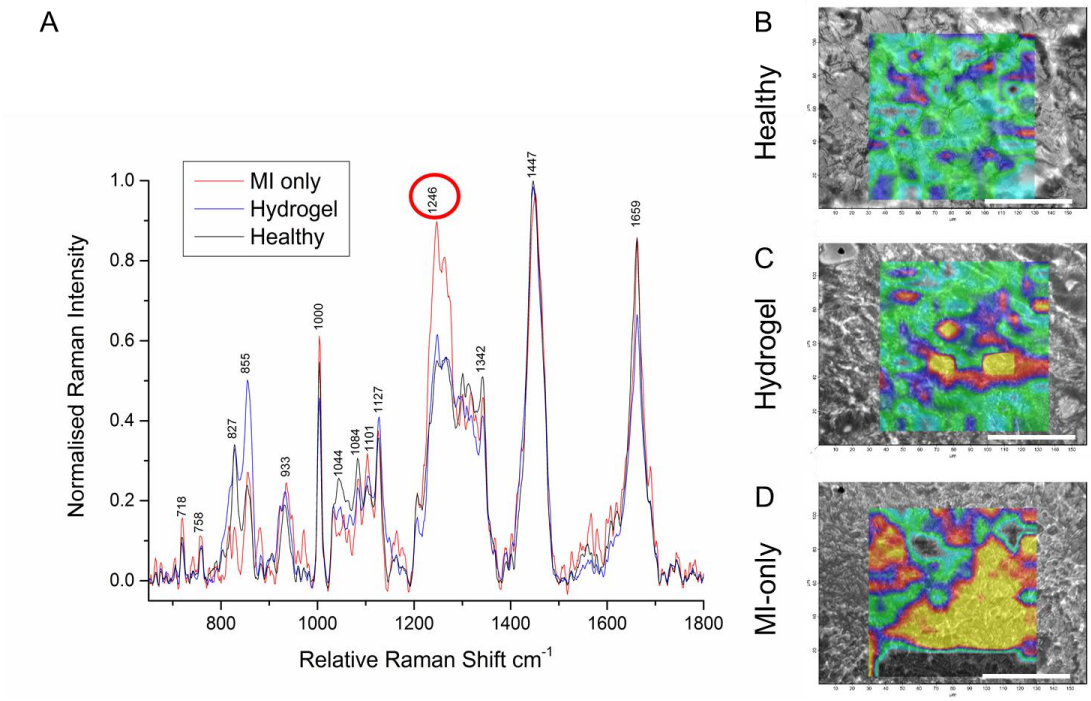

Figure 4.5 Raman analysis of myocardial infarcted tissue. Averaged Raman spectra of 225 points scanned in 100 µm^2 ischemic areas in ELRs-treated, MI-only and healthy myocardial sections (A). The peak circled at 1246 cm^{-1} corresponds to reported collagen assignment. Heat maps (B,C,D) showing the localization of the integrated intensity of the 1246 cm^{-1} peak circled in (A), merged with confocal bright-field pictures of healthy (B), ELRs-treated (C) and MI-only myocardial sections (D). N=4 animals per group. Scale bars = 50 µm.

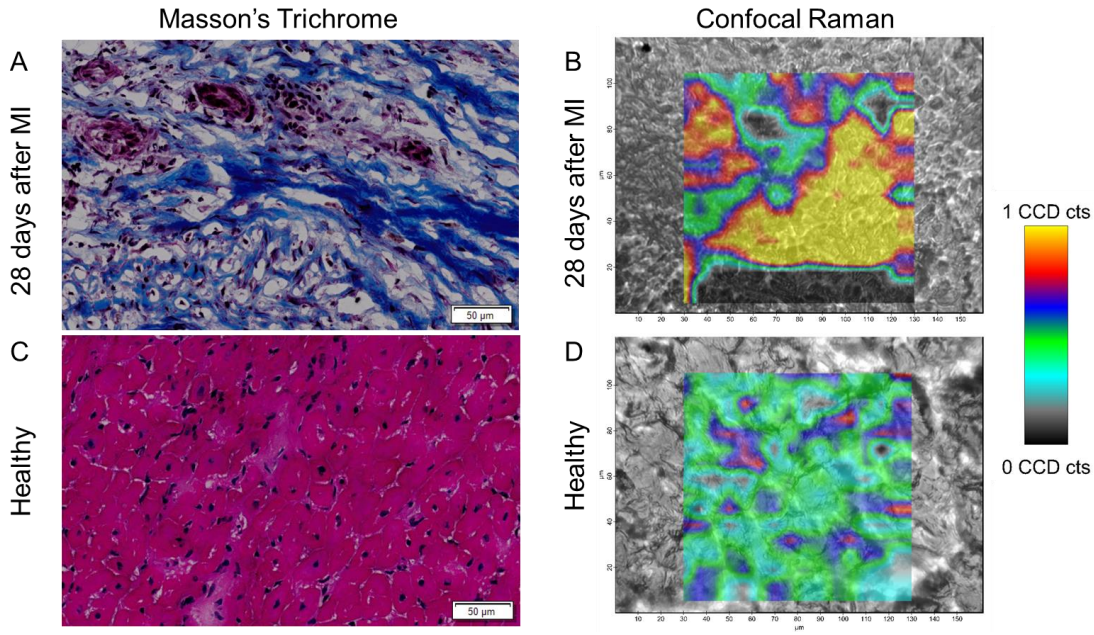

Figure 4.6 Validation of a method of fibrosis detection by Raman spectroscopy. The characterisation and distribution of collagen fibres was validated by the comparison with gold standard Masson's Trichrome staining on consecutive sections from the same snap-frozen samples. Specifically, fibrotic deposition seen at 28 days after MI (A) was confirmed by the high level expressed in the corresponding Raman heat map (B). Conversely, healthy myocardium (C) reflected in a considerably lower normalised integrated intensity in the Raman heat map (D).

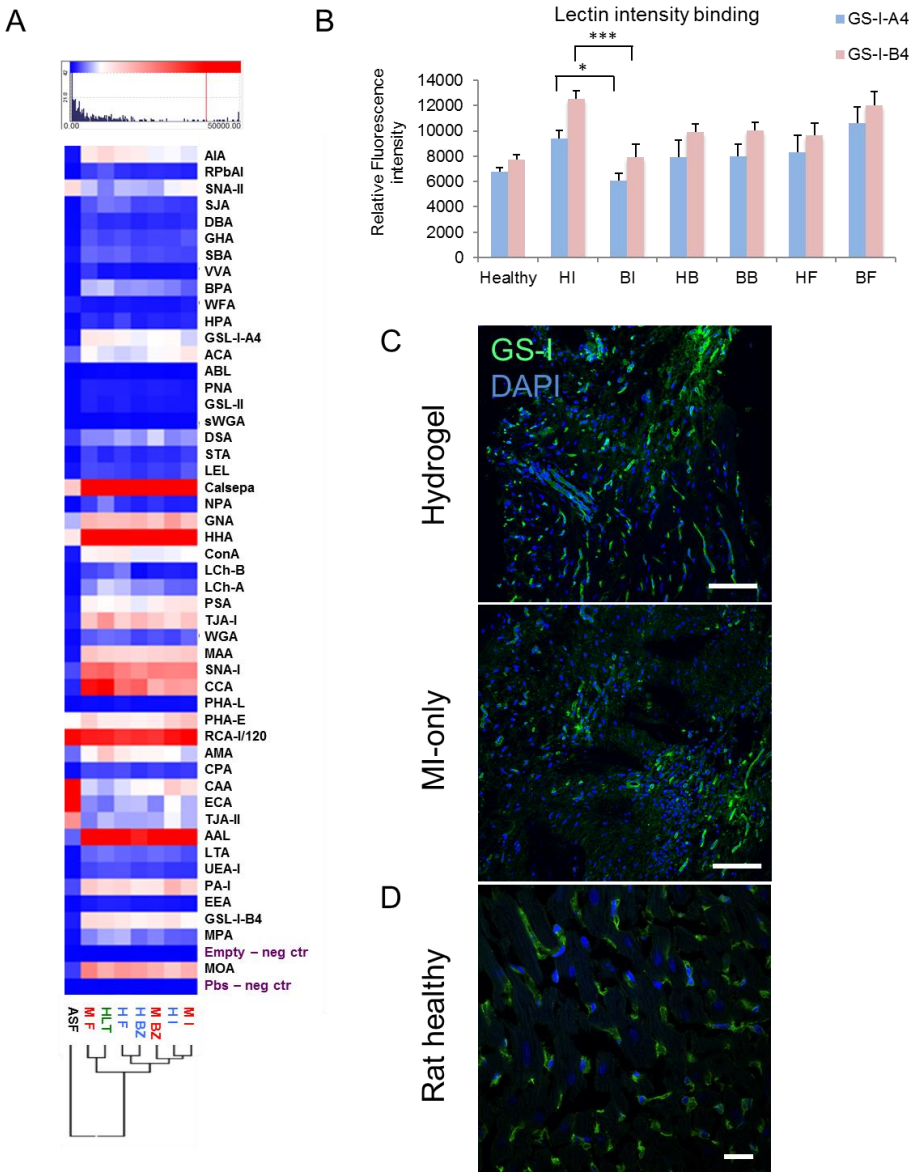

Figure 4.7 Relevant changes in *N*-acetyl-galactosamine and terminal α-galactose glycan expression after ELRs treatment. Heat map and hierarchical clustering of 49 lectin-microarray binding intensity to glycans present in membrane-proteins extracted from healthy (HLT) and either MI-only (M) or hydrogel-treated (H) animals in core ischemic (I), border (BZ) and remote (F) areas of MI. Asialofetuin (ASF) was used as glycoprotein control. Extracted quantification of GS-I-A4 and GS-I-B4 lectin binding intensity (B) across the different groups. GS-I lectin histochemistry counterstained with DAPI in ischemic regions 28 days after MI (C). Healthy adult myocardial rat tissue was used as positive control to stain endothelial cells. Pooled samples coming from four animals were analysed, error bars represent standard deviation of three replicates. One-way ANOVA followed by Dunnett's post hoc test, *$p<0.05$, ***$p<0.001$. Scale bar = 100 µm in C, 20 µm in D.

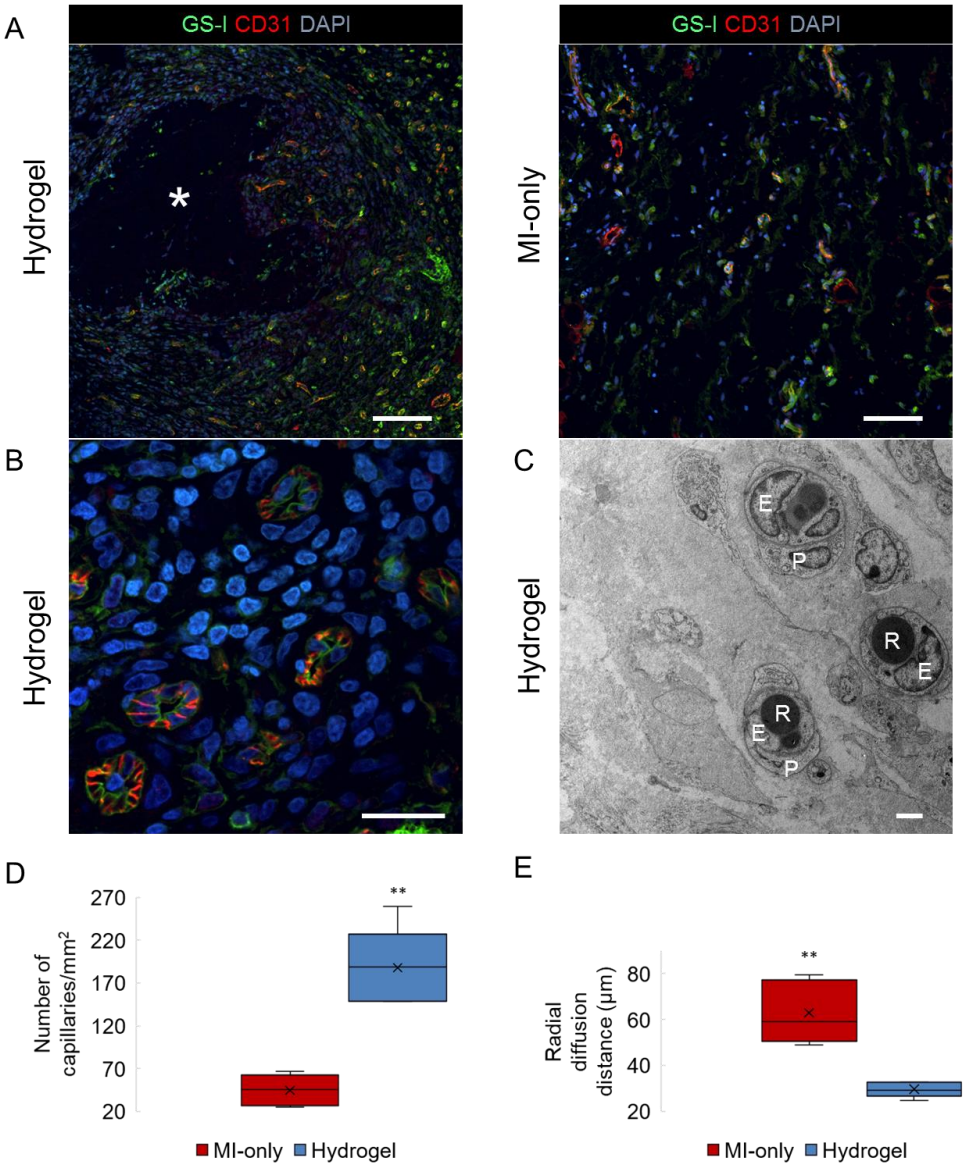

Figure 4.8 Quantification of angiogenesis in ELRs-treated group. Co-localization of GS-I and CD31 staining in ischemic regions after hydrogel treatment (star indicates an island of ELRs-hydrogel) and in MI-only samples 28 days after MI (A). Higher magnification (B) and respective TEM micrograph (C) show the capillary components (E=endothelial cell, P=pericyte, R=red blood cell) in the ELRs-treated group. Quantification of number of capillaries (D) and radial diffusion (E) in the ischemic areas comparing MI-only with hydrogel-treated. Data are reported as box-plots, Student's t-test, n=5 animals per group, **p<0.01. Scale bars = 100 µm in A, 20 µm in B, 2 µm in C.

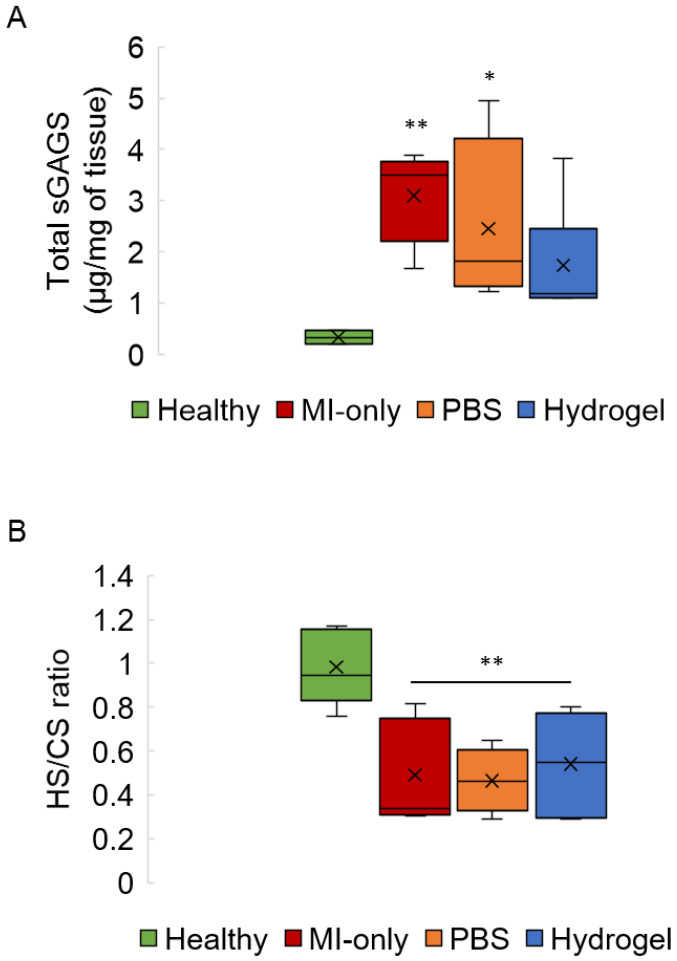

Figure 4.9 Quantification of total sulfated glycosaminoglycans and HS/CS ratio. Quantification of sulfated glycosaminoglycans by DMMB assay was performed on all the groups with the final endpoint of 28 days after MI. Statistical analysis by Dunnett's test confirmed a significant increase in pathologically-equivalent MI-only and PBS-treated groups but not in the ELRs-treated group (A). After enzymatic digestion, quantification of the ratio of heparan sulphate to chondroitin sulphate content showed a significant reduction in all the groups at 28 days, with a slight increase in the ELRs-treated group. Data are reported as box-plots, one-way ANOVA followed by Dunnett's post hoc test, n=6 in hydrogel, n=5 in MI-only and healthy, n=4 in PBS, *$p<0.05$, **$p<0.01$.

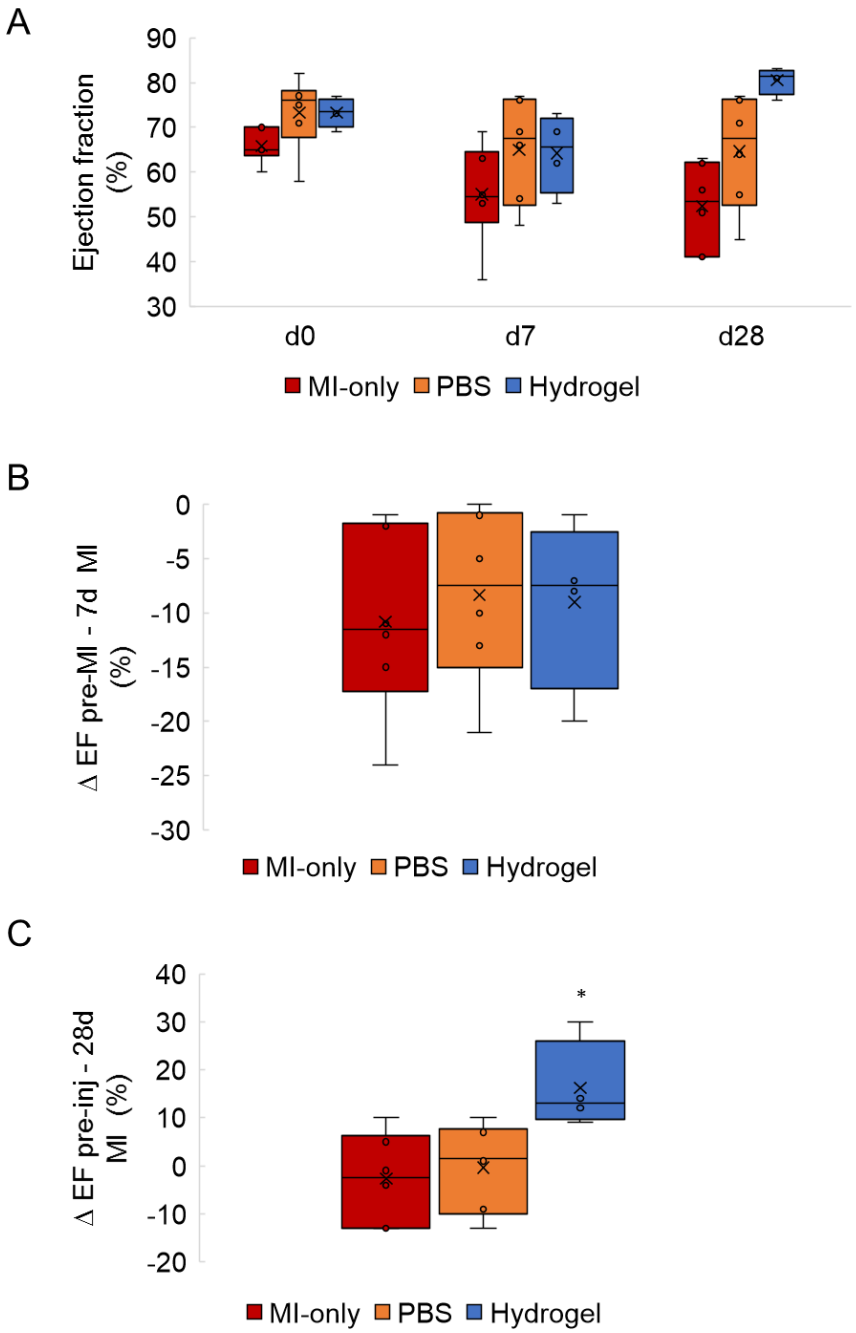

Figure 4.10 Functional response 21 days after the ELRs-hydrogel injection. Echocardiographic data were used to calculate the ejection fraction (EF) values at each timepoint for all the groups of the study (A). Animals that did not show a decrease in EF at day seven post-MI were not considered for the functional analysis. Comparison of the absolute changes in EF before the surgical procedure and seven days after MI (B). Comparison of the absolute changes in EF before the injection procedure (performed at day seven post-MI) and 21 days after (28 days post-MI) (C). Data are reported as box-plots, Kruskal-Wallis ANOVA, n=4 animals in hydrogel, n=6 in PBS and MI-only, *$p<0.05$.

4.4 Discussion

In this study, the efficacy of multiple intra-myocardial injections of an ELRs-based hydrogel in an ovine model of subendocardial MI was evaluated. Major efforts have been ongoing over recent decades in the design and *in vivo* testing of biomaterials which can modulate the post-ischemic remodelling towards a significant functional improvement that may ultimately reduce the occurrence of heart failure [O'Neill, Lee]. In the cardiovascular field, hydrogels are a preferential option due to their highly tuneable characteristics which include their injectability into the myocardial wall. In this work, a protocol of multiple intra-myocardial injections following the open thoracotomy was adopted. The injection procedure differed from protocols previously followed by other groups including Spinale *et al*., for the testing of hyaluronic acid- [Ifkovitz, Eckhouse] and fibrin-based hydrogels [Mukherjee]. Specifically, a decrease in the number of intra-myocardial injections from nine to three was adopted to avoid both incidental myocardial damage and atrial fibrillations following the invasive surgical procedure. Nevertheless, the total volume of hydrogel injected (1.5 ml per animal) lies in the range of testable efficacy for a large animal model, yet not excluding the possibility of increasing the dose to enhance or extend its effects over the 28 days time period tested in this preclinical study.

In recent years, matrices such as alginate, chitosan, collagen, fibrin or hyaluronic acid have been tested *in vivo* for the treatment of MI [Mukherjee, Liu, Yu, Huang, Gaffey]. While the main advantage shared by the intra-myocardial injection of most of these materials depends on the improvement of the wall stress in accordance with the law of Laplace [Lee]. Briefly, following the post-ischemic myocardial remodelling, the diameter of the left ventricle in both systolic and diastolic phases increases whereas the thickness of the wall, conversely, decreases. This profound and consistent geometrical change is irreversible and increases the stress exerted by the blood pressure on the left ventricular wall. Unfortunately, the absence of sufficient compensatory mechanisms and the progression of this wall stress leads to the occurrence of the organ failure. Consequently, increasing the thickness of the damaged ventricular wall by the injection of a matrix was demonstrated to significantly improve the functional outcome independently of the specific composition of the matrix used [Tous, Yu, Wang]. In this study, since improvements

in all the remodelling indices were seen (fibrosis, angiogenesis and functional response) evaluated one month after the multiple injection of the ELRs-hydrogel, the effect of the application of this matrix could derive from its bioactive properties. Due to its cell- (RGD sequences) and matrix metalloproteinases- (MMP)/cathepsin-responsive domains, this biomaterial has an intrinsic responsiveness to the post-ischemic. In this regard, the timing of the hydrogel delivery was likely to be crucial for its beneficial effects on fibrosis and angiogenesis. Indeed, it is well known that the ischemic remodelling begins with an acute inflammatory phase characterised by monocyte infiltration and secretion of IL-1β, TNF and IL6 pro-inflammatory cytokines by the population of the macrophages which early populate the ischemic region. The switch of macrophage population towards a remodelling phenotype begins from the fifth day post-MI [Troidl] and is one of the early events which characterise the end of the acute inflammatory phase and the peak of MMP upregulation. This is just one reason why the hydrogel was injected at the seventh day post-MI. An additional consideration which rationalised the timing of injection is the risk of ventricular ruptures during the first week after MI which, taken together with the normal clinical practice, makes this a more realistic intervention time. Recent work by Blackburn *et al*. compared the same timing of injection (seven days post-MI) with an immediate (three hours post-MI) and later one (two weeks post-MI) using a collagen type I-chondroitin sulphate-C hydrogel in mice [Blackburn]. Specifically, they have seen a 17% improvement in EF with the early injection of the hydrogel which was reduced to just 4% if injection was delayed to one week after MI. Significant reductions in fibrosis and apoptosis (caspase3^+ cells) together with an increase in angiogenesis only with the 3h post-MI injection led the authors to conclude that this was the optimal timing for injection [Blackburn]. Nevertheless, this contrasted with previous studies which used calcium-crosslinked alginate and PEG-based hydrogels both of which showed the beneficial effects of one-week post-MI injections [Landa, Kadner]. Also, the adopted timing of delivery has an intrinsic advantage over that of the three hours-post MI timing of injection tested by Blackburn *et al*. that it is not likely to be adopted in the clinical scenario, as mentioned also by the authors.

This study was performed using an ovine subendocardial model of myocardial infarction which markedly differs from the widely adopted model of ligation of LAD

and produces infarcts that are similar to the clinical cases of non-full thickness infarctions which require hospitalization, as explained in Chapter Three.

As a consequence, the average decrease in the EF seen across the three groups (hydrogel, PBS and MI-only) at one week post-surgery was in the range of 8-11% and animals not showing any type of decrease at seven days post-MI (two from the hydrogel group and two from the MI-only group) were excluded from functional analysis. This is the first-ever study which showed an average full-recovery in EF at 28 days post-MI compared to the pre-surgery situation in a large animal model. Comparing this data with a recently published preclinical study performed by the Christman group which tested the efficacy of an injectable ECM-derived hydrogel in pigs, the final results are comparable [Seif-Nairaghi]. Specifically, in that study, due to the direct ligation of the LAD, high decreases in EF - up to 25% - were induced [Seif-Nairaghi]. Nevertheless, that porcine-derived ECM matrix was able to promote a significant recovery reducing the deficit by up to 6% at two months post-injection. Interestingly, the data presented in this chapter followed the same pattern of EF improvement from the time of injection to the time of euthanasia (16% vs 20% improvement), although the endpoint of the study hereby presented was 28 days post-MI - so only three weeks after injection - whereas that comparable benefit was observed only three months after injection. Moreover, the limitation of the porcine ECM option towards its translational path stems from the potential residual presence of immunogenic antigen in the porcine ECM whereas the ELRs are produced in *E. coli* and do not possess xenogenic sequences. A study carried out by the Tzahor group evaluated the effect of the intra-myocardial injection of the ECM protein agrin following MI [Bassat]. Here the authors reported a recovery in EF at 28 days post-MI which grouped the treated animals together with the uninjured group; the study showed the capacity of agrin to induce cardiomyocytes regeneration as the driving force of this improvement. Since this preclinical evaluation was limited to mice, the functional improvements seen in a small animal still needs further confirmation in a more translationally-relevant model such as the one that is established in this thesis.

When an improvement in cardiac function is observed, previous research has studied remodelling parameters such as angiogenesis, fibrosis, apoptosis and cardiomyocytes proliferation. Histological and protein-based evaluation of the changes that occurred in the ECM from the time of injection to the endpoint of the study 21 days later are

reported in this chapter. A significant reduction in fibrosis in the ischemic core resulting from three independent techniques has been observed. Histological examination of collagen deposition was performed by both the traditional Masson's Trichrome staining and imaged at the lowest magnification and by TEM evaluation to confirm the typical wavy-orientation of fibrotic scar. The significance in the reduction was confirmed by both techniques and in similar terms. A reduction in fibrosis from 25% in control to 17% in the group treated with the decellularised porcine ECM has been reported [Seif-Naraghi], a result that is similar to the reduction in the collagen stained area seen in the current study (from 25% to 14%) three-weeks after the ELRs hydrogel injection. Moreover, the same trend of reduction in fibrosis was seen in another study where the efficacy of fibrin was tested in rats with and without the addition of myoblasts [Christman]. In this study the hydrogel was injected with the same timing, that is one week after the induction of MI. Moreover, to achieve a similar reduction in fibrosis (by approximately 50%) complex combinatorial systems needed to be formulated and tested. A combination of biomaterials with biomolecules has also been reported in the literature. Studies have included the use of chitosan hydrogels or patches with adipose-derived stem cells [Liu, Chen 2018] and hyaluronic acid hydrogel enriched with IGF-1/HGF growth factors [Ruvinov]. In addition, only those treatments based on firmly established mechanisms of action such as plasmid encoding recombinant human VEGF [Vera Janavel], ECM-inspired single proteins like agrin able to stimulate cardiomyocyte dedifferentiation [Bassat] or recently tested elastomeric polymers, like the poly(octamethylene maleate (anhydride) citrate (POMAC) [Montgomery], induced a comparable beneficial reduction in the scarring.

An additional technique adopted to validate the reduction in fibrosis was the confocal Raman spectroscopy analysis, a non-disruptive and non-contact method that has the potential to provide a full biochemical fingerprint of the analysed sample [Votteler, Pudlas]. Taking into consideration the rising interest in the application of this technique to the analysis of biological tissues [Monaghan, Brauchle 2017 and 2018] the application of the traditional spectroscopic Raman analysis with a confocal imaging of the core ischemic area of interest was optimised. It was sought to determine if any specific area of a Raman spectrum can be associated with the fibrotic remodelling and to compare healthy and ischemic tissues 28 days after MI

induction. Prior to staining of consecutive sections by Masson's Trichrome to confirm the collagen deposition, a consistent higher peak in correspondence of the 1246 cm^{-1} wavelength was detected. This peak was previously detected in the spectra recorded from Raman analysis of porcine aortic valves and murine myocardial ischemic tissues [Votteler, Monaghan] but was not associated with the fibrotic remodelling. This might be due to the limited (5-8%) fibrotic area seen in the ischemic sample from the murine infarcts previously analysed by Raman spectroscopy [Monaghan]. In addition, the combination of the laser scanning with confocal imaging allowed the visualization of the relative integrated intensity of the peak of interest in the scanned area. By comparing the resulting heat map of the intensity of the signal with a consecutive section stained with Masson's Trichrome, a clear visual matching was seen between the positivity of the stained collagen fibres and the intensity of the 1246 cm^{-1} wavelength peak across the ischemic tissue. This represents an interesting advance in the field in its potential impact as a novel diagnostic tool to detect the deposition of fibrotic collagen more quickly than using the standard histological evaluation. Specifically, several hours which are normally spent to achieve fixation of tissues and the follow-on steps required for a standard histological staining can be saved by this non-disruptive one hour-long scanning method on snap-frozen myocardial sections. Moreover, given the similar nature of collagen fibres scarring as the result of a pathological remodelling affecting multiple organs in the organism, the potential application of this method can be extended to other diseases such as lung fibrosis and diabetic ulcers.

Recently the expansion of the traditional boundaries which previously limited the glycobiological studies to infection-related immunobiology advanced the understanding of remodelling processes [Paszek, Gonzalez, Parker, Mohd Isa]. Therefore, to evaluate the changes in the glycosylation of cardiac ischemic tissue in response to the ELRs-hydrogel intervention, membrane-proteins extracted from infarcted samples were used to assess any sign of the biomaterial-mediated response with the most external components of the cellular environment. Initially the focus was on the validation of the results describing the reduction in fibrosis. Indeed, glycosaminoglycans (GAGs) are fundamental components of the myocardial ECM in physiological conditions, and a recent study illustrated the ageing-dependent variation in the expression of GAGs in terms of their decreased binding to growth

factors, like heparan sulphate (HS) [Huynh]. The changes in total sulfated GAGs were analysed first, and then any alteration in the ratio between HS and chondroitin sulphate (CS), another sulfated GAG abundantly present in the myocardial ECM [Nielsen], was assessed. The level of GAGs was already demonstrated to increase during the remodelling phase in both wound healing and in myocardial ischemia [Drobnik 2004, Drobnik 2013, Ghatak]. Moreover, this elevated expression was observed from three to six weeks after the induction of MI, a window that includes the endpoint of this study (four-weeks) [Drobnik 2004]. Results showed a time-dependent increase of total sulfated GAGs after MI which was significant compared to the uninjured animals at the endpoint and not only at one-week post-MI. In the ELRs-treated group, the accumulation of GAGs is reduced relative to the pathologically-equivalent groups, that are MI-only and PBS-injected. This finding reflects the reduced fibrotic scarring seen by Masson's Trichrome, TEM and Raman microscopy. Further analysis revealed the altered balance in the expression of HS and CS. In this analysis a significant change in the ratio at 28 days post-MI was seen, although the trend of increasing CS over HS was already detectable at seven days post-MI. The similar HS/CS ratios across all the study group at the endpoint led to the conclusion that this hydrogel intervention did not result in a differential rearrangement of the sulfated GAGs in the infarcted myocardium.

To assess the tissue response to the hydrogel injection, the expression of glycans present in the cellular membranes by lectin microarray analysis was screened. This technology allowed for the determination of the variation of glycan residues that could have been limited to specific subgroups of specificity such as mannose, sialic acid or fucose. Samples collected at 28 days post-MI were analysed, since any dysregulation detected at the earlier timepoint (seven days post-MI) was likely to be associated with the several lineages of inflammatory cells that remain present in the the healing microenvironment, with a consequent difficulty in distinguishing the multiple variables that determine those alterations. The glycan expression levels were markedly different when compared to pre-injury, but the significance was confined to a limited pool of residues. Specifically, in the subgroup of lectins binding to sialic acid, only α-(2,3)-linked sialic acid residues binding to *Maackia amurensis* (MAA) lectin were still significantly increased across all the groups compared to the uninjured. As shown in Chapter Two, this residue was localised in the cellular

membrane of cardiomyocytes and its stable increase at this timepoint is likely to be linked to the physiological hypertrophic response which is known to be one of the hallmarks of the post-ischemic cardiomyocytes response [Frangogiannis, Nielsen]. The most remarkable differences between the hydrogel-treated and MI-only groups were found in the expression of glycans localised in the core ischemic zones. In particular, higher expression of terminal Gal-α-(1,3)-Gal, Gal-β-(1,4)-GlcNAc disaccharides and Man-α-(1,3)- residue, which bound to *Griffonia simplicifolia* (GS) isolectin B4, *Caragana arborescens* (CAA) and *Galanthus nivalis* (GNA) lectins, respectively, was detected in the hydrogel group. Together with the validation of GS-I binding in ischemic tissues by lectin histochemistry, its expression that spread from the endothelial cells of healthy adult myocardial tissue was also confirmed. Thus the possibility to be focusing on a specificity dependent on a residual inflammatory cell population was excluded. Given the output of this glycobiology-based approach, it was hypothesised that migration of endothelial cells in the matrix occurred. This migration resulted in an angiogenic response that maturated together with the degradation of the hydrogel. The lectin used is an established reagent that can detect the formation of sprouting vasculature post-ischemia, as previously published in the cardiovascular field [Houtgraaf, Mukherjee, Rastogi 2008, Rastogi 2011]. To precisely quantify angiogenesis, the samples were stained with GS-I lectin and anti-CD31 antibody, a well-known marker of endothelial cells. Following stereological methods, a four-fold increase in the number of capillaries in the core of the infarct which is a distinct result in terms of angiogenic response, was observed. In this study the density of capillaries in the core ischemic zone was quantified. This zone is the most challenging microenvironment in which to induce sprouting of the vasculature network. Specifically, the data showed an average of 187 capillaries per squared mm in this region of the heart whereas studies testing the efficacy of angiogenic treatments in large animals reported much higher absolute numbers (ranging from 400 to 1000). These studies refer to the border zone of the infarct, where the original morphology and cellular composition of the tissue is more preserved [Houtgraaf, Lin, Dubois]. The current study, by contrast, demonstrated a significant increase in the same area of tissue which is normally irreversibly filled by the fibrotic scar and so, mostly acellular. This was confirmed by the minimal level of capillaries found in the MI-only group at 28 days (44 capillaries per squared mm).

In light of this consideration, if the four-fold increase seen after ELRs-hydrogel treatment is compared to a study testing collagen, fibrin and Matrigel® individually for their angiogenic potential in the infarct zone, the capillary density was limited to a two-fold increase [Huang]. In the reported study all the matrices showed a higher infiltration of myofibroblasts which contributed to a more beneficial remodelling process in the biomaterial-treated groups. In contrast, the current study demonstrated a lower deposition of collagen (which is typically secreted by myofibroblasts) in the ELRs-injected group and, in light of the angiogenic results at both protein and histological levels, the observed response is mediated by the migration of endothelial cells through the hydrogel matrix.

4.5 Conclusions

In this study the effects of the multiple injections of an ELRs-based hydrogel intra-myocardially seven days after the induction of focal infarcts in an ovine model were evaluated. Twenty-one days after the injection procedure, a beneficial remodelling in the ischemic core was observed. A significant improvement was seen in all the indices tested to compare the biomaterial-response to the pathophysiological situation in the MI-only group. Specifically, a significant reduction in fibrosis at 28 days post-MI was quantified. To validate the reliability of the adopted sampling method, additional independent analyses using EM and confocal Raman microscopy were carried out. Moreover, the decrease in total sulfated GAGs in the hydrogel group - assessed by DMMB assay - further confirmed the reduction in fibrosis. It is worth mentioning that these four techniques used four different methods of tissue processing - the same sample was never used for more than one independent method - and the results all remained consistent.

A glycobiology-based approach highlighted localised changes in the core ischemic zone between hydrogel-treated and non-treated animals which were then associated with an angiogenic response. Thus the hydrogel enhanced the recruitment of endothelial cells through the pores of its matrix. This distinguished the inner composition of the scarring tissue from that which was almost completely acellular seen without intervention 28 days post-MI. By the combination of both a reduction in fibrosis and an increase in angiogenesis in the ischemic core, cardiac function significantly improved and resulted in a full recovery in ejection fraction if compared to the pre-MI levels.

4.6 References

- Bassat E, Mutlak YE, Genzelinakh A, Shadrin IY, Baruch Umansky K, Yifa O, Kain D, Rajchman D, Leach J, Riabov Bassat D, Udi Y, Sarig R, Sagi I, Martin JF, Bursac N, Cohen S, Tzahor E. The extracellular matrix protein agrin promotes heart regeneration in mice. Nature. 2017 Jul 13;547(7662):179-184
- Bergmann O, Zdunek S, Felker A, Salehpour M, Alkass K, Bernard S, Sjostrom SL, Szewczykowska M, Jackowska T, Dos Remedios C, Malm T, Andrä M, Jashari R, Nyengaard JR, Possnert G, Jovinge S, Druid H, Frisén J. Dynamics of cell generation and turnover in the human heart. Cell. 2015 Jun 18;161(7):1566-75
- Blackburn NJ, Sofrenovic T, Kuraitis D, Ahmadi A, McNeill B, Deng C, Rayner KJ, Zhong Z, Ruel M, Suuronen EJ. Timing underpins the benefits associated with injectable collagen biomaterial therapy for the treatment of myocardial infarction. Biomaterials. 2015 Jan;39:182-92
- Brauchle E, Knopf A, Bauer H, Shen N, Linder S, Monaghan MG, Ellwanger K, Layland SL, Brucker SY, Nsair A, Schenke-Layland K. Non-invasive chamber-specific identification of cardiomyocytes in differentiating pluripotent stem cells. Stem Cell Reports. 2016 Feb 9;6(2):188-99
- Brauchle E, Bauer H, Fernes P, Zuk A, Schenke-Layland K, Sengle G. Raman microspectroscopy as a diagnostic tool for the non-invasive analysis of fibrillin-1 deficiency in the skin and in the in vitro skin models. Acta Biomater. 2017 Apr 1;52:41-48
- Brauchle E, Kasper J, Daum R, Schierbaum N, Falch C, Kirschniak A, Schäffer TE, Schenke-Layland K. Biomechanical and biomolecular characterization of extracellular matrix structures in human colon carcinomas. Matrix Biol. 2018 Aug;68-69:180-193
- Castellanos MI, Zenses AS, Grau A, Rodríguez-Cabello JC, Gil FJ, Manero JM, Pegueroles M. Biofunctionalization of REDV elastin-like recombinamers improves endothelialization on CoCr alloy surfaces for cardiovascular applications. Colloids Surf B Biointerfaces. (2015) 127:22-32.
- Cezar CA, Arany P, Vermillion SA, Seo BR, Vandenburgh HH, Mooney DJ. timed delivery of therapy enhances functional muscle regeneration. Adv Healthc Mater. 2017 Oct;6(19)

- Changi K, Bosnjak B, Gonzalez-Obeso C, Kluger R, Rodríguez-Cabello JC, Hoffmann O, Epstein MM. Biocompatibility and immunogenicity of elastin-like recombinamer biomaterials in mouse models. J Biomed Mater Res A. (2018) 106(4):924-934
- Chen J, Zhan Y, Wang Y, Han D, Tao B, Luo Z, Ma S, Wang Q, Li X, Fan L, Li C, Deng H, Cao F. Chitosan/silk fibroin modified nanofibrous patches with mesenchymal stem cells prevent heart remodeling post-myocardial infarction in rats. Acta Biomater. 2018 Oct 15;80:154-168
- Chiappini C, De Rosa E, Martinez JO, Liu X, Steele J, Stevens MM, Tasciotti E. Biodegradable silicon nanoneedles delivering nucleic acids intracellularly induce localized in vivo neovascularization. Nat Mater. 2015 May;14(5):532-9
- Christman KL, Vardanian AJ, Fang Q, Sievers RE, Fok HH, Lee RJ. Injectable fibrin scaffold improves cell transplant survival, reduces infarct expansion, and induces neovasculature formation in ischemic myocardium. J Am Coll Cardiol. 2004 Aug 4;44(3):654-60
- Chugh AR, Beache GM, Loughran JH, Mewton N, Elmore JB, Kajstura J, Pappas P, Tatooles A, Stoddard MF, Lima JA, Slaughter MS, Anversa P, Bolli R. Administration of cardiac stem cells in patients with ischemic cardiomyopathy: the SCIPIO trial: surgical aspects and interim analysis of myocardial function and viability by magnetic resonance. Circulation. 2012 Sep 11;126(11 Suppl1):S54-64
- Drobnik J, Szczepanowska A, Dabrowski R. Temporary augmentation of glycosaminoglycans content in the heart after left coronary artery ligation. Pathophysiology. 2004 Jul;11(1):35-39
- Drobnik J, Tosik D, Piera L, Szczepanowska A, Olczak S, Zielinska A, Liberski PP, Ciosek J. Melatonin-induced glycosaminoglycans augmentation in myocardium remote to infarction. J Physiol Pharmacol. 2013 Dec;64(6):737-44
- Dubois C, Liu X, Claus P, Marsboom G, Pokreisz P, Vandenwijngaert S, Dépelteau H, Streb W, Chaothawee L, Maes F, Gheysens O, Debyser Z, Gillijns H, Pellens M, Vandendriessche T, Chuah M, Collen D, Verbeken E, Belmans A, Van de Werf F, Bogaert J, Janssens S. Differential effects of progenitor cell populations on left ventricular remodeling and myocardial neovascularization after myocardial infarction. J Am Coll Cardiol. 2010 May 18;55(20):2232-43

- Eckhouse SR, Purcell BP, McGarvey JR, Lobb D, Logdon CB, Doviak H, O'Neill JW, Shuman JA, Novack CP, Zellars KN, Pettaway S, Black RA, Khakoo A, Lee T, Mukherjee R, Gorman JH, Gorman RC, Burdick JA, Spinale FG. Local hydrogel release of recombinant TIMP-3 attenuates adverse left ventricular epicardial after experimental myocardial infarction. Sci Transl Med. 2014 Feb 12;6(223):223ra21
- Frangogiannis NG. The inflammatory response in myocardial injury, repair, and remodelling. Nat Rev Cardiol. 2014 May;11(5):255-65
- Frantz S, Hofmann U, Fraccarollo D, Schäfer A, Kranepuhl S, Hagedorn I, Nieswandt B, Nahrendorf M, Wagner H, Bayer B, Pachel C, Schön MP, Kneitz S, Bobinger T, Weidemann F, Ertl G, Bauersachs J. Monocytes/macrophages prevent healing defects and left ventricular thrombus formation after myocardial infarction. FASEB J. 2013 Mar;27(3):871-81
- Gaffey AC, Chen MH, Venkataraman CM, Trubelja A, Rodell CB, Dinh PV, Hung G, MacArthur JW, Soopan RV, Burdick JA, Atluri P. Injectable shear-thinning hydrogels used to deliver endothelial progenitor cells, enhance cell engraftment, and improve ischemic myocardium. J Thorac Cardiovasc Surg. 2015 Nov;150(5):1268-76
- Ghatak S, Maytin EV, Mack JA, Hascall VC, Atanelishvili I, Moreno Rodriguez R, Markwald RR, Misra S. Roles of proteoglycans and glycosaminoglycans in wound healing and fibrosis. Int J Cell Biol. 2015;2015:834893
- González de Torre I, Ibáñez-Fonseca A, Quintanilla L, Alonso M, Rodríguez-Cabello JC. Random and oriented electrospun fibers based on a multicomponent, in situ clickable elastin-like recombinamer system for dermal tissue engineering. Acta Biomater. 2018 May;72:137-149
- Grewal PK, Holzfeind PJ, Bittner RE, Hewitt JE. Mutant glycosyltransferase and altered glycosylation of alpha-dystroglycan in the myodystrophy mouse. Nat Genet. 2001 Jun;28(2):151-4
- He C, Sun Y, Ren X, Lin Q, Hu X, Huang X, Su SB, Liu Y, Liu X. Angiogenesis mediated by toll-like receptor 4 in ischemic neural tissue. Arterioscler Thromb Vasc Biol. 2013 Feb;33(2):330-8
- Houtgraaf JH, de Jong R, Kazemi K, de Groot D, van der Spoel TI, Arslan F, Hoefer I, Pasterkamp G, Itescu S, Zijlstra F, Geleijnse ML, Serruys PW, Duckers

HJ. Intracoronary infusion of allogeneic mesenchymal precursor cells directly after experimental acute myocardial infarction reduces infarct size, abrogates adverse remodeling, and improves cardiac function. Circ Res. 2013 Jul 5;113(2):153-66

- Huang NF, Yu J, Sievers R, Li S, Lee RJ. Injectable biopolymers enhance angiogenesis after myocardial infarction. Tissue Eng. 2005 Nov-Dec;11(11-12):1860-6
- Huynh MB, Morin C, Carpentier G, Garcia-Filipe S, Talhas-Perret S, Barbier Chassefière V, van Kuppevelt TH, Martelly I, Albanese P, Papy-Garcia D. Age-related changes in rat myocardium involve altered capacities of glycosaminoglycans to potentiate growth factor functions and heparin sulfate-altered sulfation. J Biol Chem. 2012 Mar 30;287(14):11363-73
- Ibáñez-Fonseca A, Ramos TL, González de Torre I, Sánchez-Abarca LI, Muntión S, Arias FJ, Del Cañizo MC, Alonso M, Sánchez-Guijo F, Rodríguez-Cabello JC. Biocompatibility of two model elastin-like recombinamer-based hydrogels formed through physical or chemical cross-linking for various applications in tissue engineering and regenerative medicine. J Tissue Eng Regen Med. 2018 Mar;12(3):e1450-e1460
- Ifkovits JL, Tous E, Minakawa M, Morita M, Robb JD, Koomalsingh KJ, Gorman JH 3rd, Gorman RC, Burdick JA. Injectable hydrogel properties influence infarct expansion and extent of postinfarction left ventricular remodeling in an ovine model. Proc Natl Acad Sci U S A. 2010 Jun 22;107(25):11507-12
- Jiang B, Liao R. The paradoxical role of inflammation in cardiac repair and regeneration. J Cardiovasc Transl Res. 2010 Aug;3(4):410-6
- Kadner K, Dobner S, Franz T, Bezuidenhout D, Sirry MS, Zilla P, Davies NH. The beneficial effects of deferred delivery on the efficiency of hydrogel therapy post myocardial infarction. Biomaterials. 2012 Mar;33(7):2060-6
- Kozel BA, Rongish BJ, Czirok A, Zach J, Little CD, Davis EC, Knutsen RH, Wagenseil JE, Levy MA, Mecham RP. Elastic fiber formation: a dynamic view of extracellular matrix assembly using timer reporters. J Cell Physiol. 2006 Apr;207(1):87-96

- Landa N, Miller L, Feinberg MS, Holbova R, Shachar M, Freeman I, Cohen S, Leor J. Effect of injectable alginate implant on cardiac remodeling and function after recent and old infarcts in rat. Circulation. 2008 Mar 18;117(11):1388-96
- Lee RJ, Hinson A, Helgerson S, Bauernschmitt R, Sabbah HN. Polymer-based restoration of left ventricular mechanics. Cell Transplant. 2013;22(3):529-33
- Lin YD, Luo CY, Hu YN, Yeh ML, Hsueh YC, Chang MY, Tsai DC, Wang JN, Tang MJ, Wei EI, Springer ML, Hsieh PC. Instructive nanofiber scaffolds with VEGF create a microenvironment for arteriogenesis and cardiac repair. Sci Transl Med. 2012 Aug 8;4(146):146ra109
- Liu L, Wang Y, Cao ZY, Wang MM, Liu XM, Gao T, Hu QK, Yuan WJ, Lin L. Up-regulated TLR4 in cardiomyocytes exacerbates heart failure after long-term myocardial infarction. J Cell Mol Med. 2015 Dec;19(12):2728-40
- Liu Z, Wang H, Wang Y, Lin Q, Yao A, Cao F, Li D, Zhou J, Duan C, Du Z, Wang Y, Wang C. The influence of chitosan hydrogel on stem cell engraftment, survival and homing in the ischemic myocardial microenvironment. Biomaterials. 2012 Apr;33(11):3093-106
- Malliaras K, Makkar RR, Smith RR, Cheng K, Wu E, Bonow RO, Marbán L, Mendizabal A, Cingolani E, Johnston PV, Gerstenblith G, Schuleri KH, Lardo AC, Marbán E. Intracoronary cardiosphere-derived cells after myocardial infarction: evidence of therapeutic regeneration in the final 1-year results of the CADUCEUS trial (CArdiosphere-Derived aUtologous stem CElls to reverse ventricular dySfunction). J Am Coll Cardiol. 2014 Jan 21;63(2):110-22
- Mantovani A, Biswas SK, Galdiero MR, Sica A, Locati M. Macrophage plasticity and polarization in tissue repair and remodelling. J Pathol. 2013 Jan;229(2):176-85
- Mithieux SM, Wise SG, Weiss AS. Tropoelastin--a multifaceted naturally smart material. Adv Drug Deliv Rev. 2013 Apr;65(4):421-8
- Mohd Isa IL, Abbah SA, Kilcoyne M, Sakai D, Dockery P, Finn DP, Pandit A. Implantation of hyaluronic acid hydrogel prevents the pain phenotype in a rat model of intervertebral disc injury. Sci Adv. 2018 Apr 4;4(4):eaaq0597
- Monaghan MG, Holeiter M, Brauchle E, Layland SL, Lu Y, Deb A, Pandit A, Nsair A, Schenke-Layland K. Exogenous miR-29B delivery through a

hyaluronan-based injectable system yields functional maintenance of the infarcted myocardium. Tissue Eng Part A. 2018 Jan;24(1-2):57-67

- Montgomery M, Ahadian S, Davenport Huyer L, Lo Rito M, Civitarese RA, Vanderlaan RD, Wu J, Reis LA, Momen A, Akbari S, Pahnke A, Li RK, Caldarone CA, Radisic M. Flexible shape-memory scaffold for minimally invasive delivery of functional tissues. Nat Mater. 2017 Oct;16(10):1038-1046
- Mühlfeld C, Nyengaard JR, Mayhew TM. A review of state-of-the-art stereology for better quantitative 3D morphology in cardiac research. Cardiovasc Pathol. 2010 Mar-Apr;19(2):65-82
- Mukherjee R, Zavadzkas JA, Saunders SM, McLean JE, Jeffords LB, Beck C, Stroud RE, Leone AM, Koval CN, Rivers WT, Basu S, Sheehy A, Michal G, Spinale FG. Targeted myocardial microinjections of a biocomposite material reduces infarct expansion in pigs. Ann Thorac Surg. 2008 Oct;86(4):1268-76
- Nahrendorf M, Swirski FK, Aikawa E, Stangenberg L, Wurdinger T, Figueiredo JL, Libby P, Weissleder R, Pittet MJ. The healing myocardium sequentially mobilizes two monocyte subsets with divergent and complementary functions. J Exp Med. 2007 Nov 26;204(12):3037-47
- Nielsen SH, Mouton AJ, DeLeon-Pennell KY, Genovese F, Karsdal M, Lindsey ML. Understanding cardiac extracellular matrix remodeling to develop biomarkers of myocardial infarction outcomes. Matrix Biol. 2017 Dec 14
- O'Neill HS, Gallagher LB, O'Sullivan J, Whyte W, Curley C, Dolan E, Hameed A, O'Dwyer J, Payne C, O'Reilly D, Ruiz-Hernandez E, Roche ET, O'Brien FJ, Cryan SA, Kelly H, Murphy B, Duffy GP. Biomaterial-enhanced cell and drug delivery: Lessons learned in the cardiac field and future perspectives. Adv Mater. 2016 Jul;28(27):5648-61
- Parker BL, Palmisano G, Edwards AV, White MY, Engholm-Keller K, Lee A, Scott NE, Kolarich D, Hambly BD, Packer NH, Larsen MR, Cordwell SJ. Quantitative N-linked glycoproteomics of myocardial ischemia and reperfusion injury reveals early remodeling in the extracellular environment. Mol Cell Proteomics. 2011 Aug;10(8):M110.006833
- Paszek MJ, DuFort CC, Rossier O, Bainer R, Mouw JK, Godula K, Hudak JE, Lakins JN, Wijekoon AC, Cassereau L, Rubashkin MG, Magbanua MJ, Thorn KS, Davidson MW, Rugo HS, Park JW, Hammer DA, Giannone G, Bertozzi CR,

Weaver VM. The cancer glycocalyx mechanically primes integrin-mediated growth and survival. Nature. 2014 Jul 17;511(7509):319-25

- Pescador D, Ibáñez-Fonseca A, Sánchez-Guijo F, Briñón JG, Arias FJ, Muntión S, Hernández C, Girotti A, Alonso M, Del Cañizo MC, Rodríguez-Cabello JC, Blanco JF. Regeneration of hyaline cartilage promoted by xenogeneic mesenchymal stromal cells embedded within elastin-like recombinamer-based bioactive hydrogels. J Mater Sci Mater Med. 2017 Aug;28(8):115
- Pudlas M, Brauchle E, Klein TJ, Hutmacher DW, Schenke-Layland K. Non-invasive identification of proteoglycans and chondrocyte differentiation state by Raman microspectroscopy. J Biophotonics. 2013 Feb;6(2):205-11
- Rastogi S, Guerrero M, Wang M, Ilsar I, Sabbah MS, Gupta RC, Sabbah HN. Myocardial transfection with naked DNA plasmid encoding hepatocyte growth factor prevents the progression of heart failure in dogs. Am J Physiol Heart Circ Physiol. 2011 Apr;300(4):H1501-9
- Rastogi S, Imai M, Sharov VG, Mishra S, Sabbah HN. Darbepoetin-alpha prevents progressive left ventricular dysfunction and remodeling in nonanemic dogs with heart failure. Am J Physiol Heart Circ Physiol. 2008 Dec;295(6):H2475-82
- Rnjak-Kovacina J, Tang F, Whitelock JM, Lord MS. Glycosaminoglycan and proteoglycan-based biomaterials: Current trends and future perspectives. Adv Healthc Mater. 2018 Mar;7(6):e1701042
- Rodríguez-Cabello JC, González de Torre I, Ibañez-Fonseca A, Alonso M. Bioactive scaffolds based on elastin-like materials for wound healing. Adv Drug Deliv Rev. 2018 Apr;129:118-133
- Ruvinov E, Leor J, Cohen S. The promotion of myocardial repair by the sequential delivery of IGF-1 and HGF from an injectable alginate biomaterial in a model of acute myocardial infarction. Biomaterials. 2011 Jan;32(2):565-78
- Saxena A, Chen W, Su Y, Rai V, Uche OU, Li N, Frangogiannis NG. IL-1 induces proinflammatory leukocyte infiltration and regulates fibroblast phenotype in the infarcted myocardium. J Immunol. 2013 Nov 1;191(9):4838-48
- Seif-Naraghi SB, Singelyn JM, Salvatore MA, Osborn KG, Wang JJ, Sampat U, Kwan OL, Strachan GM, Wong J, Schup-Magoffin PJ, Braden RL, Bartels K, DeQuach JA, Preul M, Kinsey AM, DeMaria AN, Dib N, Christman KL. Safety

and efficacy of an injectable extracellular matrix hydrogel for treating myocardial infarction. Sci Transl Med. 2013 Feb 20;5(173):173ra25

- Staubli SM, Cerino G, Gonzalez De Torre I, Alonso M, Oertli D, Eckstein F, Glatz K, Rodríguez Cabello JC, Marsano A. Control of angiogenesis and host response by modulating the cell adhesion properties of an Elastin-Like Recombinamer-based hydrogel. Biomaterials. (2017) 135:30-41
- Tous E, Ifkovits JL, Koomalsingh KJ, Shuto T, Soeda T, Kondo N, Gorman JH 3rd, Gorman RC, Burdick JA. Influence of injectable hyaluronic acid hydrogel degradation behavior on infarction-induced ventricular remodeling. Biomacromolecules. 2011 Nov 14;12(11):4127-35
- Troidl C, Möllmann H, Nef H, Masseli F, Voss S, Szardien S, Willmer M, Rolf A, Rixe J, Troidl K, Kostin S, Hamm C, Elsässer A. Classically and alternatively activated macrophages contribute to tissue remodelling after myocardial infarction. J Cell Mol Med. 2009 Sep;13(9B):3485-96
- Varki A. Biological roles of glycans. Glycobiology. 2017 Jan;27(1):3-49
- Vera Janavel G, Crottogini A, Cabeza Meckert P, Cuniberti L, Mele A, Papouchado M, Fernández N, Bercovich A, Criscuolo M, Melo C, Laguens R. Plasmid-mediated VEGF gene transfer induces cardiomyogenesis and reduces myocardial infarct size in sheep. Gene Ther. 2006 Aug;13(15):1133-42
- Votteler M, Carvajal Berrio DA, Pudlas M, Walles H, Stock UA, Schenke-Layland K. Raman spectroscopy for the non-contact and non-destructive monitoring of collagen damage within tissues. J Biophotonics. 2012 Jan;5(1):47-56
- Wälchli T, Mateos JM, Weinman O, Babic D, Regli L, Hoerstrup SP, Gerhardt H, Schwab ME, Vogel J. Quantitative assessment of angiogenesis, perfused blood vessels and endothelial tip cells in the postnatal mouse brain. Nat Protoc. 2015 Jan;10(1):53-74
- Wang W, Tan B, Chen J, Bao R, Zhang X, Liang S, Shang Y, Liang W, Cui Y, Fan G, Jia H, Liu W. An injectable conductive hydrogel encapsulating plasmid DNA-eNOs and ADSCs for treating myocardial infarction. Biomaterials. 2018 Apr;160:69-81
- Yu J, Christman KL, Chin E, Sievers RE, Saeed M, Lee RJ. Restoration of left ventricular geometry and improvement of left ventricular function in a rodent

model of chronic ischemic cardiomyopathy. J Thorac Cardiovasc Surg. 2009 Jan;137(1):180-7

Chapter Five

Transcriptomic, proteomic and glycomic analyses to reveal the mechanism of modulation of post-ischemic remodelling by an elastin-like recombinamers-based hydrogel

Sections of this chapter have been submitted in the following manuscript: Contessotto P., Orbanić D., Da Costa M., Jin C., Owens P., Chantepie S., Papy-Garcia D., Chinello C., Magni F., Karlsson N.G., Kilcoyne M., Dockery P., Rodríguez-Cabello J.C. and Pandit A. "Elastin-like recombinamers-based hydrogel heals myocardial infarction in a clinically-relevant model". Under revision in *Nature Materials.*

5.1 Introduction

Since the first successful studies demonstrating the efficacy of acellular hydrogels for the improvement of post-ischemic cardiac remodelling [Christman 2004a,b], several studies with other acellular biomaterial systems have been reported. However, the biological mechanisms behind those cardiac improvements have been speculated [Landa, Leor, Singelyn].

Unfortunately, one of the most promising candidate in this field, that was calcium-crosslinked alginate, recently failed to show a significant improvement in cardiac function in a phase II trial [Rao]. Therefore, specific analyses centred on the biological mechanism rather than on the simple causative action of the biomaterial used would provide substantial advancements to the field.

To follow such an approach, biological mechanisms involving glycans will need to be included in the evaluation of tissue response to a biomaterial treatment. However, the complexity of glycobiology and the only recently established methods to precisely identify glycan structures [Jensen, Everest-Dass] make this assessment difficult. In the field of cardiac biology, recent studies have started to identify the classes of glycoproteins that are present and their involvement in pathological events such as hypertrophy by glycoproteomics analysis [Parker, Yang]. On the other hand, the role of glycan moieties as determinants of the specific binding between inflammatory cells and endothelial cells has been the objective of a variety of studies in the recent decades. Studies have been reported to elucidate the functional relevance of glycan ligands to the family of selectins which are crucially involved in all the main phases of leucocytes rolling and diapedesis during the inflammation process [Sackstein 2000 and 2008].

Moreover, to detect the molecular triggers behind the impact of a biomaterial treatment on ECM and cellular populations, standard high-throughput RNA sequencing (RNA-seq) and proteomic analyses can be used. A recent study by the Christman group focused on the detection and validation of the pathways which were altered after the injection of a decellularized myocardial matrix one week after the induction of MI in rats [Wassenaar]. Specifically, due to the wide range of alterations in inflammation, fibrosis, angiogenesis, apoptosis and progenitor cell recruitment that were demonstrated, the authors highlighted the multiple effect of the matrix in

all these biological phenomena instead of directing the attention to a specific or prevalent mechanism of action.

Consequently, the objectives of this study are to:

- Perform a RNA-sequencing analysis on total RNA samples from MI-only and ELRs-treated groups to identify which biological pathways were altered after the biomaterial treatment.

- Evaluate the tissue response in membrane protein and ECM glycosylation patterns by glycomic analysis.

- Run a proteomic analysis on total protein lysates to assess whether the tissue response was altered after the hydrogel treatment and comparable with previous histological evaluation.

- Validate the most prominent differences highlighted by RNA-sequencing and proteomic analyses and hypothesise a mechanism of action of the ELRs-hydrogel treatment.

5.2 Materials and methods

5.2.1 RNA extraction from sheep samples

Total RNA was extracted from the sheep samples harvested as described in section 3.2.4 and in Figure 3.2 and preserved in RNA*later*® at -80°C. Each sample, weighing approximately 50 mg, was finely minced and extracted in TRIzol™ by bead grinding using a Qiagen TissueLyser (Qiagen, USA) set at 50 oscillations per minute. Two cycles of ten minutes each were performed at 4°C and samples were visually inspected to ensure a complete homogenization. RNA extraction was then carried out by chloroform precipitation and purified using RNeasy® Mini Spin Columns, as detailed in the Appendix A.1. RNA was diluted in RNase-Free water and aliquoted before storing at -80°C. Samples were sent for RNA-seq analysis to Genewiz (USA)

prior to preliminary evaluation of RNA concentration, purity and integrity, as detailed in Figure A.1 and Table A.1 in Appendices.

5.2.2 Library preparation for RNA-sequencing analysis

RNA-seq library preparation used the NEBNext® Ultra™ RNA Library Prep Kit for Illumina by following the manufacturer's recommendations (New England Biolabs, Ipswich, USA). Briefly, mRNA were first enriched with Oligod(T) beads. Enriched mRNAs were fragmented for 15 minutes at 94 °C. The first strand and second strand cDNA were subsequently synthesized. cDNA fragments were end repaired and adenylated at 3'ends, and a universal adapter was ligated to cDNA fragments, followed by index addition and library enrichment with limited cycle PCR. The sequencing library was validated on the Agilent TapeStation (Agilent Technologies, USA), and quantified by using Qubit® 2.0 Fluorometer (Invitrogen, USA) as well as by quantitative PCR (Applied Biosystems, USA).

5.2.3 RNA-sequencing and differential expression gene analysis

RNA-seq was carried out using an Illumina MiSeq™ platform. Reads were demultiplexed to generate fastq files using a software Illumina BCL2FASTQ v2.19. R package DESeq2 was used to perform differential expression gene (DEG) analysis.

5.2.4 Protein extraction from sheep samples

Sheep tissue samples were harvested as described in section 3.2.4 and in Figure 3.2 and stored at -80°C. To extract proteins, tissues were minced in small pieces with a scalpel and homogenized in a tube containing RIPA lysis and extraction buffer with cOmplete™ EDTA-free protease inhibitor cocktail, as detailed in the Appendix A.2. The minced tissues were completely homogenized by the mechanical action of grinding beads using a Qiagen TissueLyser (Qiagen, USA) set at 50 oscillations per min. Two cycles of 15 minutes each were performed at 4°C and samples were visually inspected to ensure a complete homogenization. Samples were then left on ice for 15 minutes and centrifuged at 12,000 rpm for ten minutes at 4°C. The concentration of the homogenized samples was assessed using a Micro BCA™ Protein Assay Kit.

5.2.5 Suspension trapping trypsin digestion before proteomic analysis

Extracted proteins from sheep heart tissues were quantified by BCA assay and submitted to bottom-up proteomic sample preparation for LC-MS/MS analysis. A suspension trapping (S-Trap) method was adopted to concentrate samples and to remove detergent interference [Ludwig]. In particular, a digestion protocol based on S-trap™ Micro spin columns (ProtiFi, USA) was used following manufacturer's instructions. Tris-HCl was used in place of triethylammonium bicarbonate (TEAB) buffer both in sodium dodecyl sulfate (SDS) lysis buffer (1% SDS, 100 mM Tris-HCl, pH 7.55) and in binding buffer (90% aqueous methanol with a final concentration of 100 mM Tris-HCl, pH 7.1). Briefly, about 100 µg of estimated protein extracts was dried and resuspended in 25 µl of lysis buffer. Reduction of disulphide bonds was performed using 20 mM dithiothreitol (DTT) for ten minutes at 95ºC, and the alkylation by the addition of iodoacetamide (IAA) to a final concentration of 40 mM (incubated 30 minutes in the dark). Undissolved matter was removed by centrifugation for eight minutes at 13,000 g. Aqueous phosphoric acid at 1:10 was added (≈1.2% final concentration), subsequently, 165 µl of binding buffer was added. The acidified SDS lysate/methanol buffer mixture was loaded into the micro-column for protein trapping and trypsinization (1:25-enzyme:protein) according to manufacturer's protocol. After one hour of incubation at 37 ºC, peptides were eluted using centrifugation at 4,000 g with 40 µl each of 50 mM ammonium bicarbonate, then 0.2% formic acid (FA). Hydrophobic peptides were recovered with 35 µl of 50% ACN containing 0.2% FA. Pooled elution of each sample was dried and resuspended in 25 µl of loading solution (2% ACN, 0.1% trifluoroacetic acid). The peptide concentration was measured using a NanoDrop™ One/Onec Microvolume UV-Vis Spectrophotometer (Thermo Fisher Scientific, USA).

5.2.6 Proteomic label-free quantification

About 1.5 µg of peptide mixtures was injected into an Ultimate™ 3000 RSLCnano Ultra-High Performance Liquid Chomatography (UHPLC) system (Thermo Fisher Scientific, USA) coupled online with Impact HD™ UHR-QqToF (Bruker Daltonics, Germany). Each sample was analysed at least twice to minimize technical variability. Samples were loaded onto a pre-column (Dionex, Acclaim PepMap 100 C18,

cartridge, 300 µm) followed by a 50 cm nano-column (Dionex, ID 0.075 mm, Acclaim PepMap100, C18). The separation was performed at 40°C and at a flow rate of 300 nL/min using multistep four hours gradients of ACN as already reported [Chinello]. The column was on-line interfaced to a nanoBoosterCaptiveSpray™ electrospray ionisation (ESI) source (Bruker Daltonics). Data-dependent-acquisition mode was applied based on collision-induced dissociation (CID) fragmentation assisted by nitrogen as collision gas. Mass accuracy was improved using a specific lock mass (1221.9906 m/z) and a calibration segment (10 mM sodium formate cluster solution) before the beginning of the gradient for each single run. Acquisition parameters were set as already described [Liu 2015].

Data elaboration was performed through DataAnalysis™ v.4.1 Sp4 (Bruker Daltonics, Germany) and protein identities and relative abundancies were determined using PEAKS Studio 8.5 (Bioinformatics Solutions Inc., USA) [Zhang]. All duplicates for each sample were considered independently. An in-house constructed Uniprot's reference databases of *Ovis aries* (accessed Feb 2018, 556,825 sequences; 199,652,254 residues) were combined with a decoy database and implemented in the software. For protein identification, the following parameters were specified: enzymatic digestion performed by trypsin, allowing one missed cleavage; precursor mass tolerance was 20 ppm; fragment mass tolerance of 0.05 Da; carbamidomethylation (Cys) as fixed modification. To determine the false-positive identification rate, the estimated spectra was used against a decoy database. A false discovery rate (FDR) of ≤1%, with a peptide score of $-\text{Log}(p) \geq 20$ was considered adequate for confident protein identification. The de Novo ALC score was set ≥ 50%. Peptide feature based quantification was performed to calculate the relative protein and peptide abundance in the samples. Only confidently identified peptide features were matched and used for the estimation of the related signal intensity. Likewise, the area under the curve of the extracted ion chromatograms (XICs) was measured and used for the relative quantification between runs. Retention time shift tolerance was six minutes. Areas were normalised using TIC (Total Ion Current). To get the summed cumulative peak area of the protein, only unique peptides that are assigned to particular proteins were selected and only proteins that have more than two unique peptides were considered.

5.2.7 Ingenuity Pathway Analysis (IPA®) to analyse transcriptomic and proteomic data

Data from differentially expressed genes (DEG) analysis were converted from .csv to .xls files and gene column list was sorted to reference all the data relative to the different groups (7 days MI-only, 28 days MI-only and hydrogel-treated) to a summed up ID gene list. The created .xls file had columns reporting the log2(fold change) DEG data of each group compared to the healthy conditions and were loaded in Ingenuity Pathway Analysis (IPA®, Qiagen, USA) software according to the instructions. Cut-offs of log2(fold change) > 1.5 and log2(fold change) < -1.5 and adjusted p-value<0.05 were applied for core analysis. Moreover, comparative analysis was performed analysing the files relative to the core ischemic samples of seven days MI-only, 28 days MI-only and hydrogel-treated groups. Canonical pathway and upstream regulators data were compared by their activation z-score and associated p-value. Similarly, data from nano-flow liquid-chromatography combined with tandem mass spectrometry (nLC-ESI-MS/MS) label-free quantification were previously filtered for a unique peptide number above two and listed in a .xls file according to their fold change ratio to healthy conditions. The created .xls file had columns reporting the fold ratio of each group compared to the healthy conditions and was loaded in the IPA® software according to the instructions. Cut-offs of fold change > 1.5 and fold change < -1.5 were applied for core analysis. Moreover, comparative analysis was performed analysing the files relative to the core ischemic samples of seven days MI-only, 28 days MI-only, PBS-injected and hydrogel-treated groups.

5.2.8 Immunofluorescence to quantify $CD163^+$ cells and α-SMA^+ arterioles

OCT-embedded sections with a thickness of 5 μm were used for all the immunofluorescence and lectin histochemistry experiments. Since the time of fixation in paraformaldehyde was optimised to get to the final overnight incubation at 4°C, this step did not affect the outcome of immunofluorescence experiments and no antigen retrieval was necessary for any of the markers tested.

At the beginning of each experiment, sections stored at -80°C were left at RT for approximately 20 minutes before starting. Samples were first permeabilized with TBS-Tween (0.05%) twice for five minutes each, then washed with TBS for an

additional five minutes. Blocking of the samples was carried out using 10% donkey serum (Sigma) for one hour at RT. Immunofluorescence experiments were performed using the following primary antibodies and dilutions: rabbit polyclonal to α-smooth muscle actin (ab5694, Abcam, UK) at 1:200 and rabbit polyclonal to CD163 (ab87099, Abcam, UK) at 1:100. All primary antibodies were diluted in TBS-Tween (0.05%) and incubation was carried out at 4°C overnight. The following day, samples were washed with TBS-Tween three times for 15 minutes each and then incubated with anti-rabbit Alexa Fluor® 647-donkey secondary antibody respectively at 1:500 dilution in TBS-Tween (0.05%) for one hour at RT. The undiluted secondary antibody was centrifuged for ten minutes at 10000 rpm to precipitate aggregates before making the dilution. After the incubation, glasses were washed with TBS-Tween three times for 15 minutes each then mounted with Prolong® Gold with DAPI and coverslipped. Glasses were left to cure overnight at RT before sealing. Only $CD163^+$ cells or α-SMA^+ arterioles in the ischemic core (not in the border region) were counted using an appropriate stereological grid which was superimposed on each image to quantify the total number per squared mm. Details of the antibodies used are listed in the Table A.2 in Appendices.

5.2.9 Immunofluorescence and lectin histochemistry to validate GATA4

Sections from the MI-only and ELRs-treated groups were double stained with Wheat germ agglutinin (WGA) lectin and anti-GATA4 primary antibody after optimisation of this lectin-primary antibody protocol. Briefly, samples were left to thaw at RT for 20 minutes and washed with TBS-Tween twice for three minutes each. Then samples were blocked with 3% periodated BSA for one hour at RT. After this, glasses were quickly dipped in TBS and incubated with the lectin at a concentration of 20 μg/ml for one hour at RT. Following this, samples were washed three times with TBS for three minutes each and then blocked with 3% periodated BSA for one hour at RT. Sections were then incubated with the rabbit polyclonal primary antibody to GATA4 at 1:200 dilution overnight at 4°C. The following day, samples were washed with TBS-Tween twice for ten minutes each and then with TBS once for ten minutes. After the incubation for one hour at RT with anti-rabbit secondary antibody, sections were washed with TBS-Tween twice for ten minutes each and then with TBS once for ten minutes. Finally, the glasses were mounted with Prolong® Gold with DAPI

and coverslipped. Glasses were left to cure overnight at RT before sealing. All the procedures from incubation with the lectin to final mounting was performed avoiding direct light due to the sensitivity of FITC-labelled lectin. Imaging was done using a laser confocal microscope (Olympus FluoView 1000, Olympus America) and five images were taken for each serial section at a magnification of 40x. Only $GATA4^+$ cells in the border zone (not in the ischemic core region) were counted using an appropriate stereological grid which was superimposed on each image to quantify the total number of $GATA4^+$ cells per squared mm (Figure A.10 in Appendices).

5.2.10 Release of *N*- and *O*-linked glycans from membrane proteins

Membrane proteins were extracted from healthy, 7 days MI-only, 28 days MI-only, PBS-injected and hydrogel-treated groups were extracted. Membrane protein samples from sheep samples (240 µg) were pooled from three different animals. Extraction buffer was exchanged to 7 M urea via a 30 kDa MWCO centrifugal filter and incubated with 25 mM DTT at 56°C for 45 minutes. The reduced samples were then alkylated with 62.5 mM IAA at room temperature for 50 minutes in the dark. After alkylation, samples were treated with sequencing grade trypsin (1% w/w, Promega, Sweden) at 37°C overnight. Tryptic peptides were precipitated with 80% (v/v) acetone. The dried pellet was then washed twice with 500 µl of cold 60% methanol and pellets were air-dried. After adding 50 µl of 50 mM ammonium bicarbonate, pH 8.4, and 1 µl of PNGase F, samples were incubated at 37°C overnight. Released *N*-linked glycans were separated from (*O*-glyco)peptides using a Sep-Pak® C18 cartridge (Waters Corporation, USA). Briefly, the cartridge was first conditioned with different dilutions (90% and 10%) of acetonitrile (ACN) in 0.5% trifluoroacetic acid (TFA). After applying the sample, both the eluent and washout with 5% acetic acid were combined which contained released *N*-linked glycans. O-glycopeptides were eluted by the addition of 65% ACN in 0.5% TFA. Both samples were then dried at 30°C. Released *N*-linked glycans were reduced by 0.5 M sodium borohydride ($NaBH_4$) and 20 mM NaOH at 50°C overnight. *O*-linked glycans were released by the reductive β-elimination reaction. Briefly, samples were incubated in a buffer containing 0.5 M $NaBH_4$ and 50 mM NaOH at 50°C overnight. Reactions were quenched with glacial acetic acid, and samples were desalted and dried as previously described [Schulz].

5.2.11 *N*- and *O*-linked glycans detection by LC-ESI-MS/MS analyses

Released glycans were dissolved in deionized water and analysed by liquid chromatograph-electrospray ionization tandem mass spectrometry (LC-ESI/MS/MS) as previously reported [Mereiter]. The oligosaccharides were separated on a column (10 cm × 250 µm) packed in-house with 5 µm porous graphite particles (Hypercarb, Thermo-Hypersil, UK). The oligosaccharides were injected on to the column and eluted with an ACN gradient (Buffer A, 10 mM ammonium bicarbonate; Buffer B, 10 mM ammonium bicarbonate in 80% ACN). The gradient (0-45% Buffer B) was eluted for 46 minutes, followed by a wash step with 100% Buffer B, and equilibrated with Buffer A in the following 24 minutes. A 40 cm × 50 µm inner diameter fused silica capillary was used as transfer line to the ion source.

The samples were analysed in negative ion mode on a LTQ linear ion trap mass spectrometer (Thermo Electron, USA), with an IonMax standard ESI source equipped with a stainless steel needle kept at –3.5 kV. Compressed air was used as nebulizer gas. The heated capillary was kept at 270°C, and the capillary voltage was –50 kV. Full scan (m/z 380-2000 two microscans, maximum 100 ms, target value of 30,000) was performed, followed by data-dependent MS2 scans (two microscans, maximum 100 ms, target value of 10,000) with normalised collision energy of 35%, isolation window of 1.0 units, activation q=0.25 and activation time 30 ms). The threshold for MS2 was set to 300 counts. Data acquisition and processing were conducted with Xcalibur™ software (Version 2.0.7, Thermo Fisher Scientific, USA).

Glycan structures were identified from their MS/MS spectra by manual annotation. For structural annotation, some assumptions were made in this study. The structures of *N*- and *O*-linked glycans was assumed to follow the classic biosynthetic pathways. Diagnostic fragmentation ions for *N*- and *O*-glycans were investigated as previously described [Everest-Dass]. Terminal Hex2 units were presumed to be α-linked Gal. Chain elongation was expected to be mediated by the addition of N-acetyllactosamine (LacNAc) disaccharides. The annotated structures were submitted to the UniCarb-DR database (http://unicarb-dr.biomedicine.gu.se/references/352) according to MIRAGE guidelines [Liu 2016]. For comparison of glycan abundances between samples, individual structures were quantified relative to the total content by integration of the extracted ion chromatogram peak area. The area under the curve

(AUC) of each structure was normalised to the total AUC and expressed as a percentage. The peak area was processed by Progenesis QI (Nonlinear Dynamics, UK).

5.2.12 Quantification of mitochondrial parameters

Since the isector method [Tang] was applied for sampling, the volume density of mitochondria was calculated using the point counting method. Surface density (Sv) of both inner and outer mitochondrial membranes was estimated using a simple intersect counting technique [Weibel, Howard]. Specifically, the formula Sv= 2I/L where I = number of intersects with membranes and L is the total length of line applied to the sections was used. The relative estimates were combined with nuclear volumes derived from acridine orange staining (Figure A.11 in Appendices) to provide estimates of surface areas.

5.2.13 Statistical analysis

All statistical analyses were performed using Minitab™ Express software (Minitab, Inc. State College, USA). RNA-seq data were analysed using the Wald's test, which is a default statistical test for the DESeq2 package. Data from the quantification of α-SMA^+ arterioles and $CD163^+$ cells did not follow a normal distribution, and so they were analysed by Mann-Whitney *U* test. Mitochondrial data were analysed by Kruskal-Wallis ANOVA. Values were considered significant only with $p<0.05$.

5.3 Results

5.3.1 Significant remodelling-related pathways from RNA-sequencing

In Chapter Four the efficacy of intra-myocardial injections of ELRs-based hydrogel seven days after the induction of MI was evaluated and a significant improvement in the major remodelling indices was observed. Therefore, the potential involvement of biological pathways in this beneficial modulation of the myocardial microenvironment was investigated. Specifically, since the reduced fibrosis and enhanced angiogenesis reported in Chapter Four were related to the ischemic core,

RNA-seq, proteomic and glycomic analyses were performed on samples which were harvested from this zone.

Total RNA samples extracted from ischemic, border and remote regions from healthy, 7 days-old, 28 days-old MI and hydrogel-treated animals were extracted and sequenced after cDNA library preparation as described in the materials and methods section. A total of 40 bar-coded RNA samples gave 3,038,094,543 reads with a yield of 917,509 Mbases. The mean quality base score was 38.41, which means a possibility of incorrect base call of approximately 1 in 10,000.

After DEG analysis, a total of 18,222 genes were detected across the different groups. DEG data related to the ischemic core regions of infarcted each group were expressed as fold change to the baseline (healthy) levels and volcano plots highlighted a clear increase in the significantly different levels of transcripts in the infarcted zones rather than in the remote ones when compared to the healthy animals, as shown in Figure 5.1.

DEG data were then sorted by unique gene list for all the ischemic core groups and analysed by IPA® software. Taking into account a threshold of significance of $p<0.05$, several immunological and cardiovascular-related pathways were detected, as shown in Figure 5.2. Indeed, these pathways can be grouped by the traditional sequential timing of inflammatory, proliferative and maturation phases after MI. First, as regards the inflammatory phase: Inflammasome, TLR, leukocyte extravasation, IL6, HIF1α signalling, NO and ROS in macrophages, renin-angiotensin and atherosclerosis signalling pathways were significantly detected across all the infarcted groups. Moreover, several pathways associated with the proliferative and maturation phases were detected such as IL-12 in macrophages, IL-10, CD28 in T-helper cells, Th-1, Th-2, Rac, and fibrosis signalling were highlighted as potentially altered following the hydrogel treatment.

5.3.2 Inflammatory- and remodelling-related transcripts levels downregulation at day 28 post-MI

To determine whether any difference was present at gene level after the hydrogel treatment, DEG data of either inflammatory- or ECM remodelling-related markers were compared with those at the time of injection (seven days post-MI). Indeed, a significant trend of decreased expression of pro-inflammatory markers such as Tnf,

Il1a, Il1b both in the ischemic core and border zone of the infarct was seen independently of the treatment (Figure 5.3 A,C). In addition, at day 28 post-MI transcript levels of proliferative/maturation-related genes such as *IL10*, *MMP9*, *MMP12* were also markedly downregulated compared to three weeks before (Figure 5.3 A,C). However, no significant differences were detected between the two groups, thereby excluding both an enchanced either anti- or pro-inflammatory effect due to the biomaterial.

DEG data related to genes potentially associated with the fibrotic programming were also analysed, and a significant 3.5-fold increase in *NR4A1* levels after hydrogel treatment ($p=0.042$) in the ischemic core was found, which was followed by a 3.2-fold higher expression - although not significant ($p=0.12$) - in the border zone. By contrast, no significant differences were seen in the expression of *COL1A1*, *COL1A2*, *COL3A1*, *TGFB1*, *TGFB2*, *TGFB3*, *SMAD3*, *DCN*, *PDE1A* fibrotic markers. Interestingly, the fibrotic marker *POSTN* showed a downregulation by 1.9-fold in the hydrogel-treated ischemic core which was close to reaching significance ($p=0.06$).

5.3.3 Alterations of angiogenic-related pathways and higher peri-vascular and arterioles density in the ischemic core after hydrogel treatment

In section 4.3.4 (Chapter Four) a significant increase in the number of GS-I^+/$CD31^+$ capillaries in the ELRs-treated ischemic core compared to a poorly cellularised central region of ischemia in the MI-only group. So this finding adds strength to the hypothesis that there was a bioactive interaction between the ELRs-based scaffold and the recruited cellular populations during the proliferative phase.

To investigate further the molecular details of this effect, DEG data were analysed by IPA® software and focused on the angiogenic-related pathways, such as VEGF, HGF, ErbB and endothelin signalling. A trend of activation shared among all these pathways which had activation z-scores above 2.7 was observed, whereas in the control group - at the same timepoint - the activation z-scores of the same pathways all ranged between 1.1 and 2.1, as shown in Figure 5.4. A. However, the significance in the predicted activation of these pathways was reached only in the case of endothelin pathway ($p=0.03$) and was close to being achieved in the HGF pathway ($p=0.06$).

To hypothesise an angiogenic effect of the hydrogel, the expression of α-SMA (smooth muscle actin), a marker of mature vasculature, and CD163, which is usually expressed on myocardial peri-vascular macrophages were assessed by immunofluorescence. A five-fold increase in $CD163^+$ cells was seen in hydrogel-treated ischemic core ($p=0.02$) together with an approximated 50% increase ($p=0.03$) in the number of mature vessels ($\alpha\text{-}SMA^+$). Both the measurements followed a stereological approach and are comparable with all previously reported quantification of these structures per squared mm.

5.3.4 *N*-glycome analysis validates the changes in terminal α-galactose associated with angiogenesis

In section 4.3.4 (Chapter Four) a significant increased binding to terminal α-galactose (α-Gal) was reported in the ELRs-treated ischemic core by lectin microarray analysis and validated its co-localisation with $CD31^+$ vasculature structures. Here the expression of this specific glycan residue was validated by LC-ESI-MS/MS and its proportional change quantified in comparison to healthy conditions both in the ischemic and border zones.

During the sample processing prior to MS analysis, *N*-linked glycans were separated from the *O*-linked fraction and thereby analysed the two subgroups separately. Following annotation procedures, 113 putative *N*-glycan structures were identified, including 18 high mannose, 17 hybrid and 78 complex-type glycans (Figure 5.5). Hierarchical clustering analysis was performed for each *N*-linked glycan subgroup and a trend of distinction among the ischemic core, border and remote regions was seen across all the three subgroups. The reliability of the differences seen was supported by the consistent clustering of the healthy baseline group together with the remote regions - those ones less affected by the ischemic damage - in the infarcted groups.

Focusing on complex *N*-linked glycans, potential differences among different biologically-relevant residues that were shared by several putative *N*-glycan structures such as α-(2,6)- sialylation, α-(2,3)-sialylation and terminal α-Gal were evaluated. First, a clear increase in α-(2,3)-sialylation was observed, ranging from

20% to 33% in the central ischemic and border regions at the 28 day post-MI timepoint, independently of the treatment introduction. Interestingly, this increase was limited to approximately 10% in the correspondent regions at seven days post-MI (Figure 5.5 A), suggesting a linear increase over the remodelling. Moreover, focusing on the other type of sialic acid linkage, the proportional increase in α-(2,6)-sialylation was consistently above 10% in the ischemic core of all the infarcted groups. However, while the hydrogel-treated ischemic and border zones both showed a proportional increase close to 20%, in the MI-only correspondent regions the increment was limited to 16% and 7%, respectively (Figure 5.6 B). All the infarcted samples at day 28 showed a stronger expression of NeuAc, with a remarkable difference (18%) between the hydrogel-treated and non-treated in the ischemic core. Interestingly, a completely different pattern in the expression of the other sialylation type, that is NeuGc, opposed the hydrogel-treated (increase over 60%) to the MI-only (+6%) at the same timepoint in the ischemic core regions.

Finally, the most striking difference was seen in the trend of expression of terminal α-Gal. Here, the initial increase seen at day seven post-MI in the central and border regions (14% and 25%, respectively), was completely reversed 21 days later, when a marked drop down to - 20-25% was observed (Figure 5.5 C). However, the decrease did not occur in the ELRs-treated ischemic core, where the relative change was still similar to that at the injection timepoint (16% more than in healthy conditions), and the decrease was halved in the border zone compared to that of the control group (-9%).

5.3.5 *O*-glycome analysis of ischemic cardiac tissue

In this study the first-ever glycomic analysis of *O*-linked glycans from a large animal ischemic tissue was performed. Healthy and ischemic samples contained both core 1 and core 2 *O*-glycans, and the changes in the levels of α-Gal, sialylation and type of sialylation (NeuAc or NeuGc) were determined.

A constant increase in sialylated *O*-glycans was seen compared to the healthy baseline, starting from 5% in the ischemic core at day seven post-MI and reaching approximately 15-20% increase in the infarcted zones at 28d post-MI, independently of the treatment (Figure 5.7 A). Moreover, a clear higher expression of NeuAc was seen in the centre of the infarct both at the beginning and at the end of the

remodelling phase (+55% at day 28 post-MI), in contrast to a lower difference in the treated group (+28%), as shown in Figure 5.7 B. By contrast, a remarkable drop in the expression of NeuGc in the MI-only group was seen both in the border and core region (-20% and -78%, respectively). However, in the corresponding regions of the ELRs-treated group, the trend was severely limited and a difference of over 90% was observed compared to the non-treated levels (Figure 5.7 C). Finally, clear differences were also seen in the expression of α-Gal on *O*-glycans. As with the trend previously seen in *N*-glycans, α-Gal was still partially retained from the seven days post-MI timepoint (7%) in the ELRs-treated ischemic core (4%) but it was not detected in the corresponding region of the MI-only group (Figure 5.7 D). Interestingly, a consistent slight increase in the border zones of all the groups over that of to the healthy conditions was seen (2-4%).

5.3.6 Higher retention of GATA4$^+$ cardiomyocytes and improved mitochondrial integrity in the border zone of the infarct after hydrogel treatment

To understand whether a mechanism of action was responsible for the hydrogel-dependent functional improvement reported in section 4.3.6 (Chapter Four), the alterations in the molecular pathways were investigated by RNA-seq, as already mentioned in section 5.3.1, and proteomic analyses. Total proteins were extracted and processed for nLC-ESI-MS/MS label-free quantification and only peptides resulting from a false discovery rate (FDR) of ≤1%, peptide score of − Log (p-value) ≥ 20 were considered adequate for confident protein identification. Moreover, only unique peptides that are assigned to particular proteins were selected and only proteins that have more than two unique peptides were considered. After such processing, intensities were expressed as fold change to healthy conditions and analysed by hierarchical clustering. Interestingly, the ELRs-treated ischemic core did not cluster together with the central ischemic regions either from the seven days-old or from 28 days-old (PBS-injected or non-treated) infarcts. By contrast, the hydrogel-treated ischemic core clustered together with the border regions and even showed a 72% minimum similarity with that of the remote regions (Figure 5.8).

In addition, IPA® analysis confirmed the detection of significant pathways which are involved in the inflammatory response, such as acute phase response, LXR/RXR and FXR/RXR activation. Moreover, pathways related to the cell survival signalling were

detected, such as PI3K/AKT, IGF-1, actin cytoskeleton, integrin, protein kinase signalling and mitochondrial dysfunction (Figure 5.9). Then patterns consistent with those of an improved remodelling response were seen from the proteomic analysis. Specifically, myofibroblasts-related markers vimentin and calponin 1 were expressed at a much higher level in the ischemic core of both PBS and non-treated animals (about ten-fold in both) than that in the ELRs-treated group (around five-fold), and supported also by the contained increase in all the remote regions (Figure 5.10 A). Secondly, a pattern of increased expression of markers of ROS-scavenging, such as cytochrome *c* and superoxide dismutase, was observed in the hydrogel-treated border zone. In particular, the highest levels of the superoxide dismutase across all the infarcted samples analysed were seen in the border and remote regions of the hydrogel group. In addition, cytochrome *c* expression was consistently higher than the baseline only in the remote regions from the infarcts, except in the hydrogel group where it switched from the remote to the border zone (Figure 5.10 B).

To identify which potential molecular trigger was involved in the improved remodelling in the ELRs-treated group, the differences in the predicted activation scores were compared between the hydrogel-injected and non-treated groups at day 28 post-MI. Among the upstream regulators, the transcription factor GATA4 showed the highest difference between the two groups analysed. Specifically, during pathological remodelling, GATA4-associated z-score decreased from 7 to 28 days after MI. However, GATA4-associated z-score reversed the predicted inhibition (-1.87, p=0.001) in the MI-only after hydrogel injection (0.45, p=0.002), as shown in Figure 5.11 A and Figure A.13 in Appendices. Moreover, a similar trend, though to a lesser extent, was seen for TBX5, RHO, EPO and MYOCD molecules. On the other hand, CASP1 (caspase-1) was predicted to be activated at 7 days (z-score 2.41, p=0.001) and 28 days (z-score 1.84, p=0.014) in the MI-only group, but not in the hydrogel-treated group (z-score 0.29, p=0.033).

To validate this finding, $GATA4^+$ nuclei were stained by immunofluorescence and cardiomyocytes membranes bound by lectin histochemistry using WGA lectin in the border zone (Figure 5.11 B). $GATA4^+$ cardiomyocytes significantly increased (p=0.01) from 206±12 in MI-only to 305±30 in the ELRs-injected border zone of the infarct (Figure 5.11 C).

Furthermore, EM imaging validated the potential alterations highlighted by proteomic analysis in terms of mitochondrial dysfunction (Figure 5.9). Since mitochondria are the organelles that are most sensitive to pathological insults such as ischemia, a clear sign of cellular stress is represented by the swelling of these organelles inside the cardiomyocytes (Figure 5.12 A). Indeed, a significant two-fold increase in mitochondrial volumes ($p=0.03$), a over two-fold higher extension of inner ($p=0.04$) and a four-fold expansion of outer membrane area ($p=0.07$) over that of the healthy conditions were seen (Figure 5.12 B,C and D). Interestingly, the mitochondrial swelling was notably attenuated in all the parameters tested after the ELRs-treatment and never reached significance (Figure 5.12 B,C and D).

As a conclusion, IPA® analysis of GATA4-associated pathways showed the suppression of its inhibition after hydrogel-treatment, which is linked with Col1a1 Col1a2 and endothelin expression in the ECM, and Fos levels inside the nucleus (Figure A.13 in Appendices).

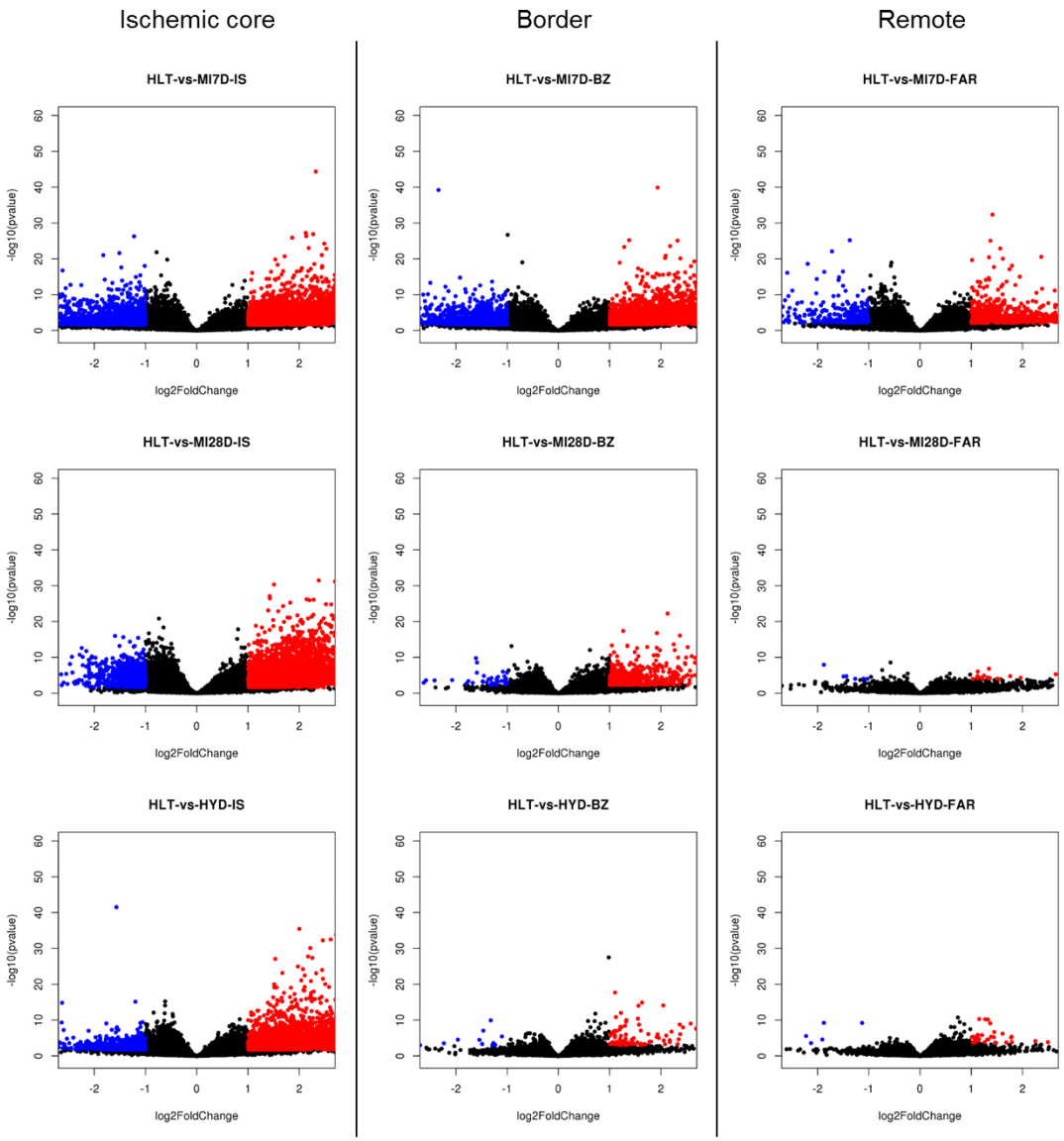

Figure 5.1 Volcano plots of DEG data from RNA-sequencing. Volcano plots showing the total genes significantly upregulated (log2(fold change) > 1.5) and downregulated (log2(fold change) < -1.5) across the core ischemic (IS), border (BZ) and remote regions (FAR) sampled from 7, 28 days MI-only (MI28D) and hydrogel-treated (HYD) groups. All differential expression gene (DEG) data were normalised to healthy baseline left ventricular samples. DEG data were analysed using the Wald's test and filtered by adjusted p-value<0.05, n=4 animals per group.

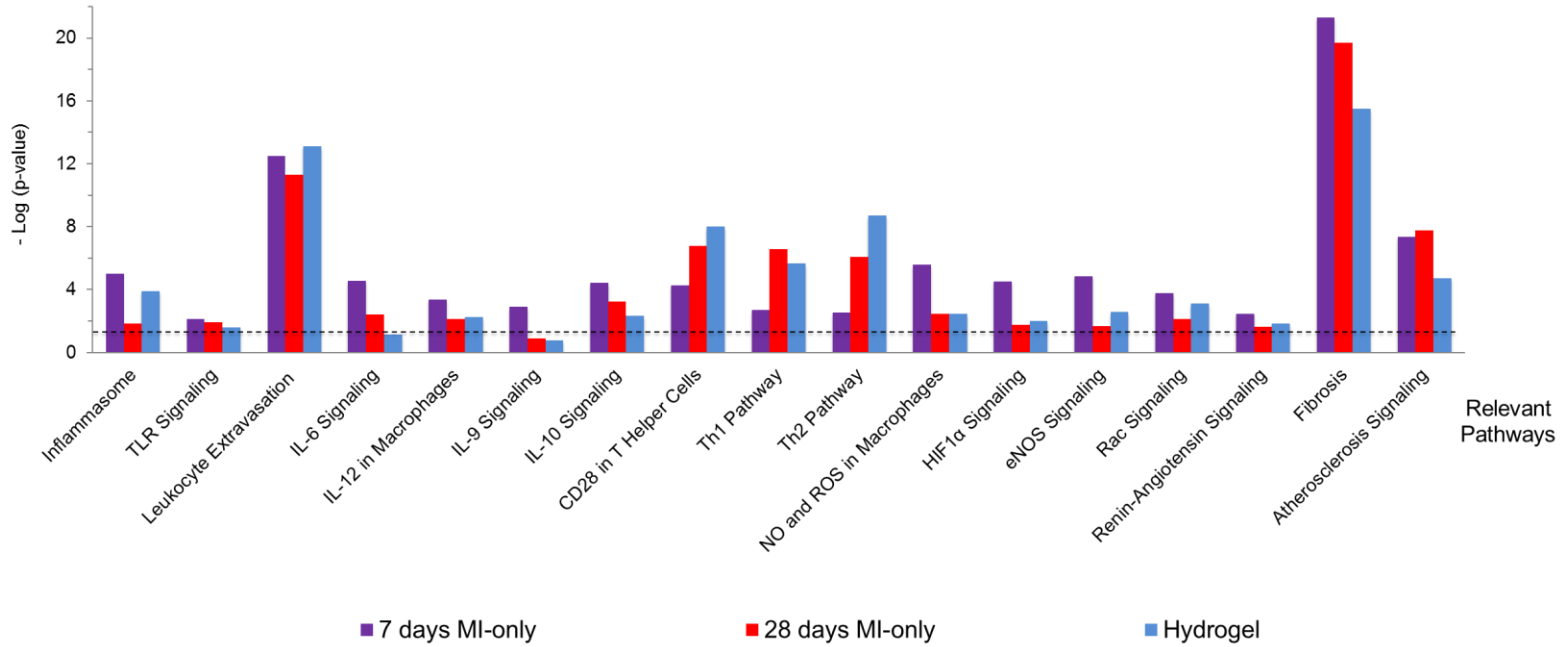

Figure 5.2 Significant pathways detected by IPA® analysis on RNA-seq data. DEG data from RNA-seq were analysed by IPA® analysis applying cut-offs of log2(Fold Change) > 1.5 and log2(Fold Change) < -1.5 and adjusted p-value<0.05. Dashed line shows a threshold of -Log(p-value) of 1.3, corresponding to p=0.05, that is the minimal level required to determine if a canonical pathway was significantly detected. Groups of MI-only at 7 and 28 days and hydrogel-treated are shown and grouped by relevant biological pathways. DEG data were analysed using the Wald's test and filtered by adjusted p-value<0.05, n=4 animals per group.

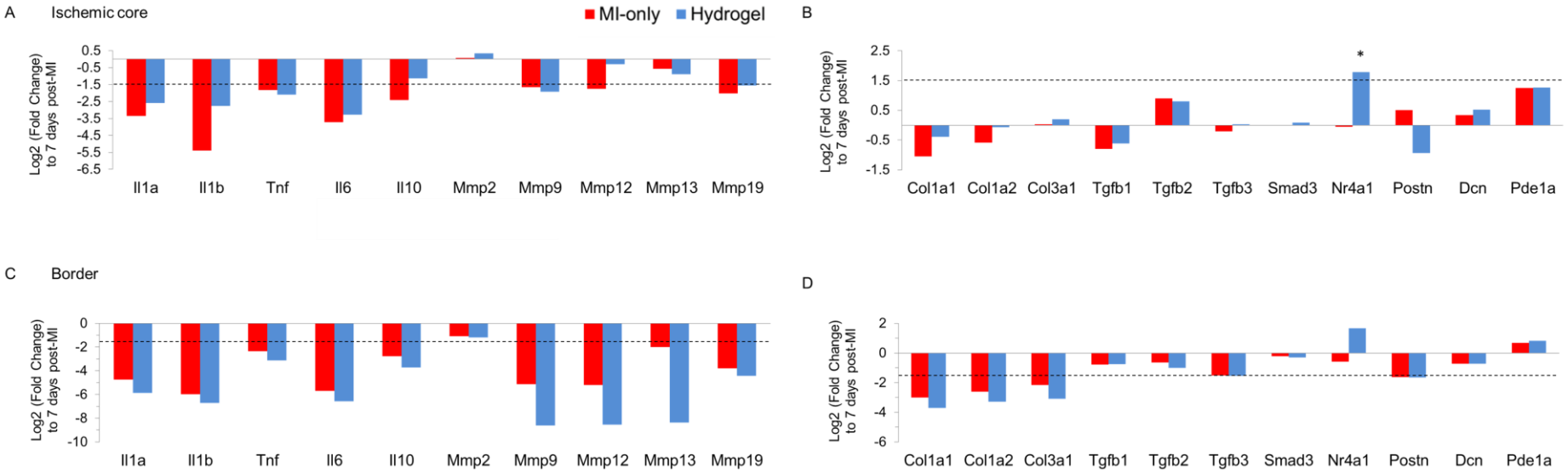

Figure 5.3 Inflammatory and remodelling-related markers at day 28 post-MI. Differentially expressed genes (DEG) are expressed as log2(fold change) to the seven day post-MI levels. Inflammation, fibrosis and remodelling-related transcripts levels were measured in both the core ischemic (A,B) and border zones (C,D) of infarcted hearts. DEG data were analysed using the Wald's test and filtered by adjusted p-value<0.05, n=4 animals per group, *p<0.05.

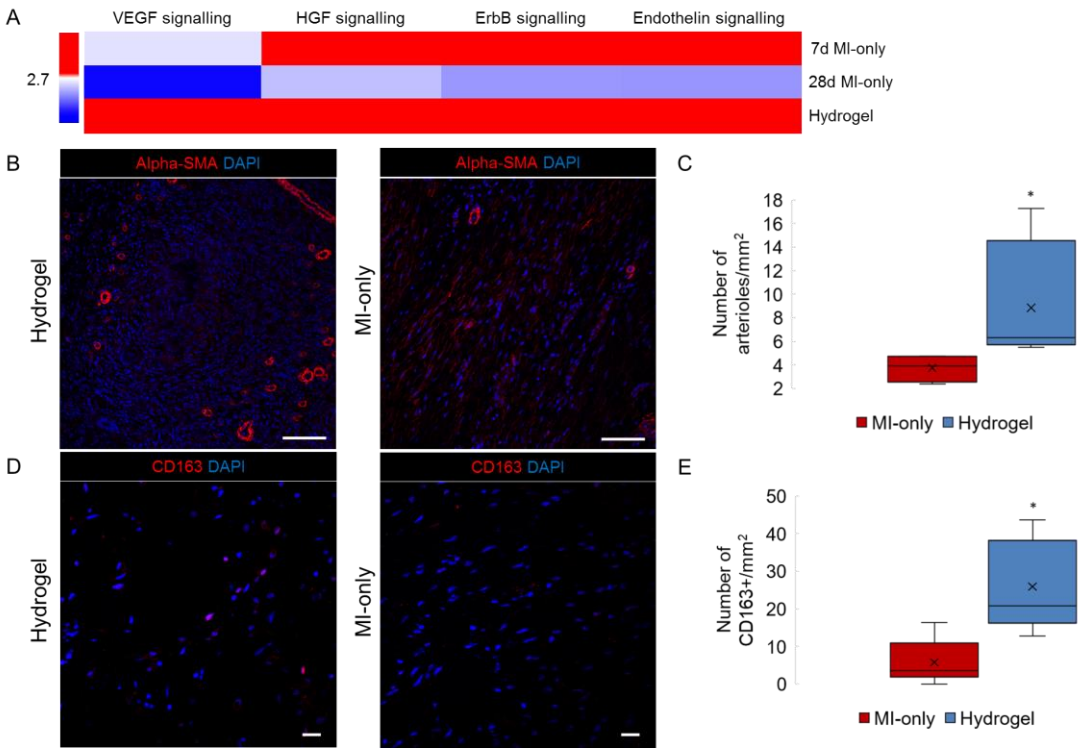

Figure 5.4 Evaluation of angiogenic response 21 days after hydrogel injection. DEG data from RNA-seq were analysed by IPA® software to detect potential differences in the activation scores of pathways related to angiogenesis such as VEGF, HGF, ErbB and endothelin signalling (A). Ischemic core regions were stained for the presence of α-SMA$^+$ arterioles (B) and CD163$^+$ cells (D) in the hydrogel-treated and MI-only groups and quantified (C,E). Data are reported as box-plots, Mann-Whitney *U* test (n=4 in C and n=5 in E), *p<0.05. Scale bars = 100 μm in B, 20 μm in D.

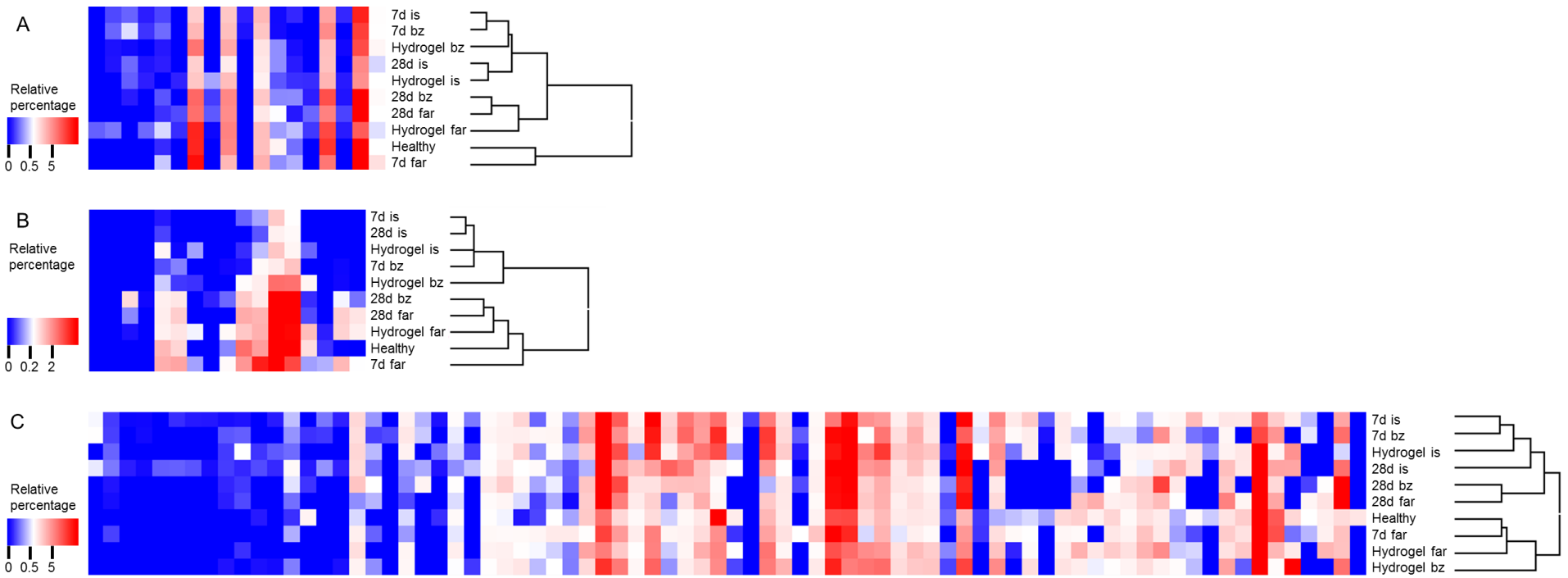

Figure 5.5 Hierarchical clustering of *N*-glycomics data. Each subgroup of *N*-glycans (high mannose, hybrid and complex) was analysed by hierarchical clustering. A total number of 113 putative *N*-glycan structures were identified, divided in 18 high mannose (A), 17 hybrid (B) and 78 complex-type (C). Data are expressed as relative percentage of each putative *N*-glycan structure which was detected across the healthy and infarcted heart regions from untreated animals, 7 and 28 days after MI and hydrogel-injected. Regions of infarcted hearts are labelled as follows: is = core ischemic, bz = border zone, far = remote zone from the infarct. Each analysed sample was a pool of samples coming from three individuals.

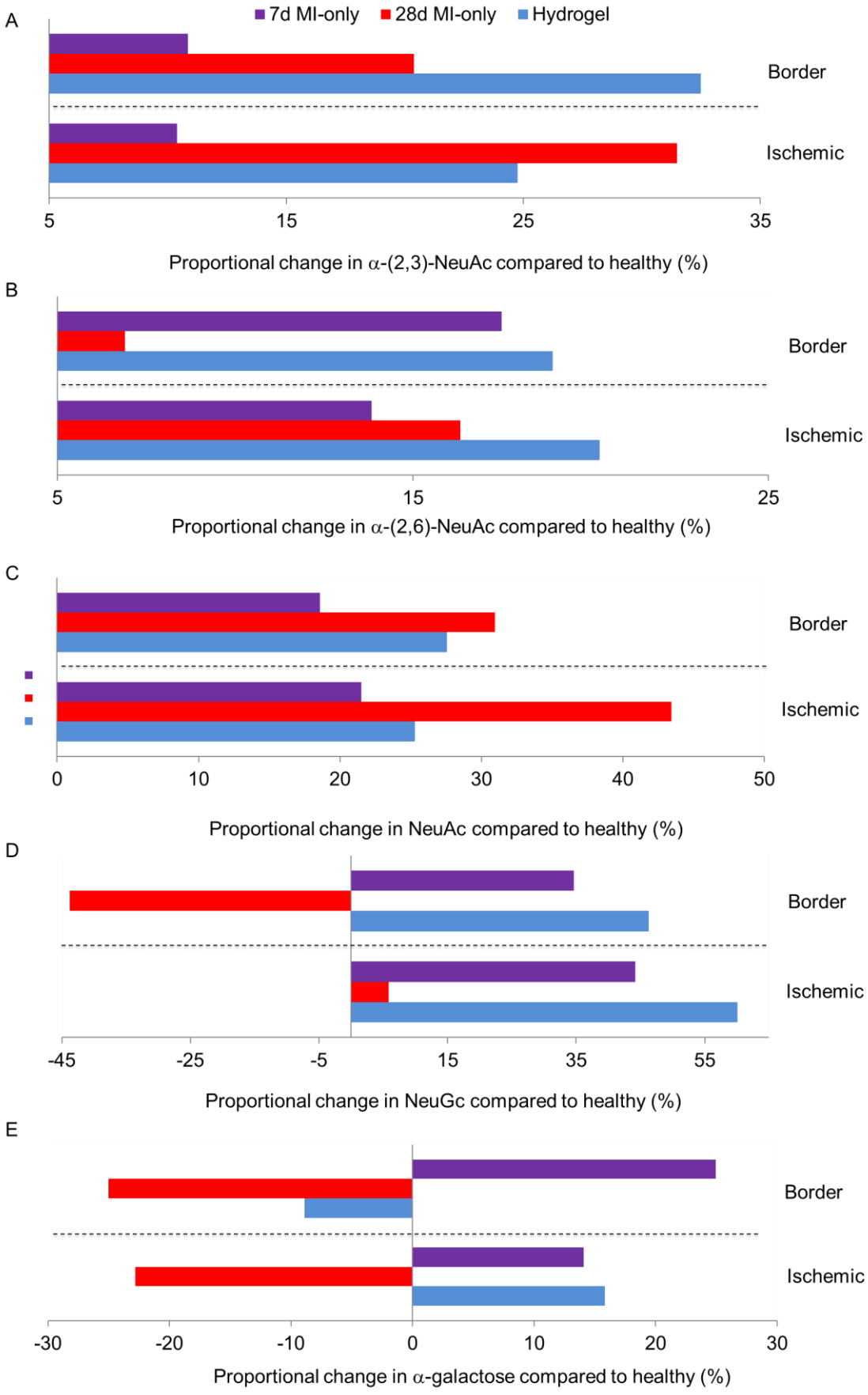
A
7d MI-only
28d MI-only
Hydrogel
Border
Ischemic
5
15
25
35
Proportional change in α-(2,3)-NeuAc compared to healthy (%)
B
Border
Ischemic
5
15
25
Proportional change in α-(2,6)-NeuAc compared to healthy (%)
C
Border
Ischemic
0
10
20
30
40
50
Proportional change in NeuAc compared to healthy (%)
D
Border
Ischemic
-45
-25
-5
15
35
55
Proportional change in NeuGc compared to healthy (%)
E
Border
Ischemic
-30
-20
-10
0
10
20
30
Proportional change in α-galactose compared to healthy (%)

Figure 5.6 Proportional changes in main *N*-linked complex glycans compared to healthy baseline. *N*-linked glycans expressing α-(2,3)-sialylation (A), α-(2,6)-sialylation (B), NeuAc (C), NeuGc (D) and α-Gal (E) in the ischemic core and border regions of seven days post-MI, MI-only and hydrogel-treated were normalised to healthy levels. *N*-linked glycans were released from one pooled sample of three animals per group and region and analysed by LC-ESI-MS/MS.

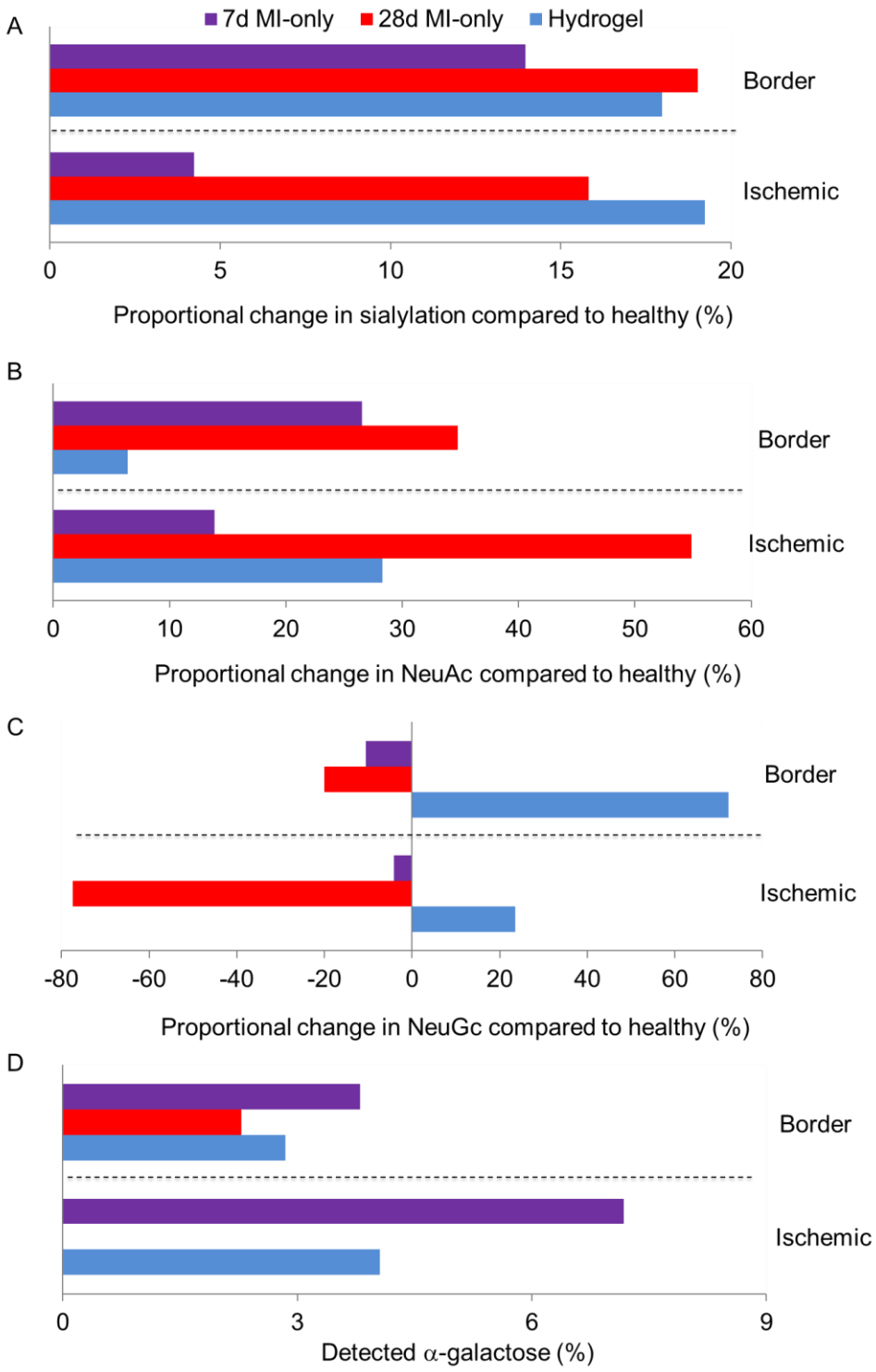

Figure 5.7 Proportional changes in main *O*-linked glycans compared to healthy. *O*-linked glycans expressing sialic acid (A), NeuAc (B), NeuGc (C) and α-Gal (D) from the ischemic core and border regions were normalised to the healthy levels. *O*-linked glycans were released from one pooled sample of three animals per group and region and analysed by LC-ESI-MS/MS.

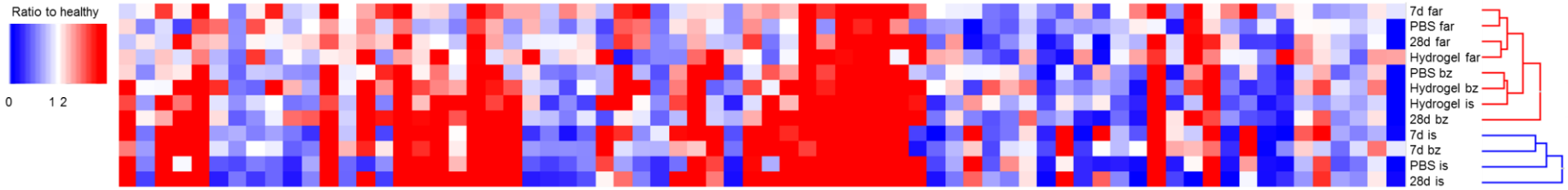

Figure 5.8 Hierarchical clustering of proteomic data. Hierarchical clustering on proteomic data showed two main clusters with a minimum similarity of 32%. Protein entries were filtered by a unique peptide number of at least two. The ischemic core after treatment with the hydrogel clusters together with the border regions subgroup, in a distinctive way compared to the ischemic regions from PBS-injected and MI-only groups at both the day 7 and 28 post-MI. Moreover, the ischemic zone after treatment with the hydrogel showed a 72% minimum similarity with the cluster of the remote regions (samples A-D remote). Regions of infarcted hearts are labelled as follows: is = core ischemic, bz = border zone, far = remote zone from the infarct. Each analysed sample was a pool of samples coming from three individuals.

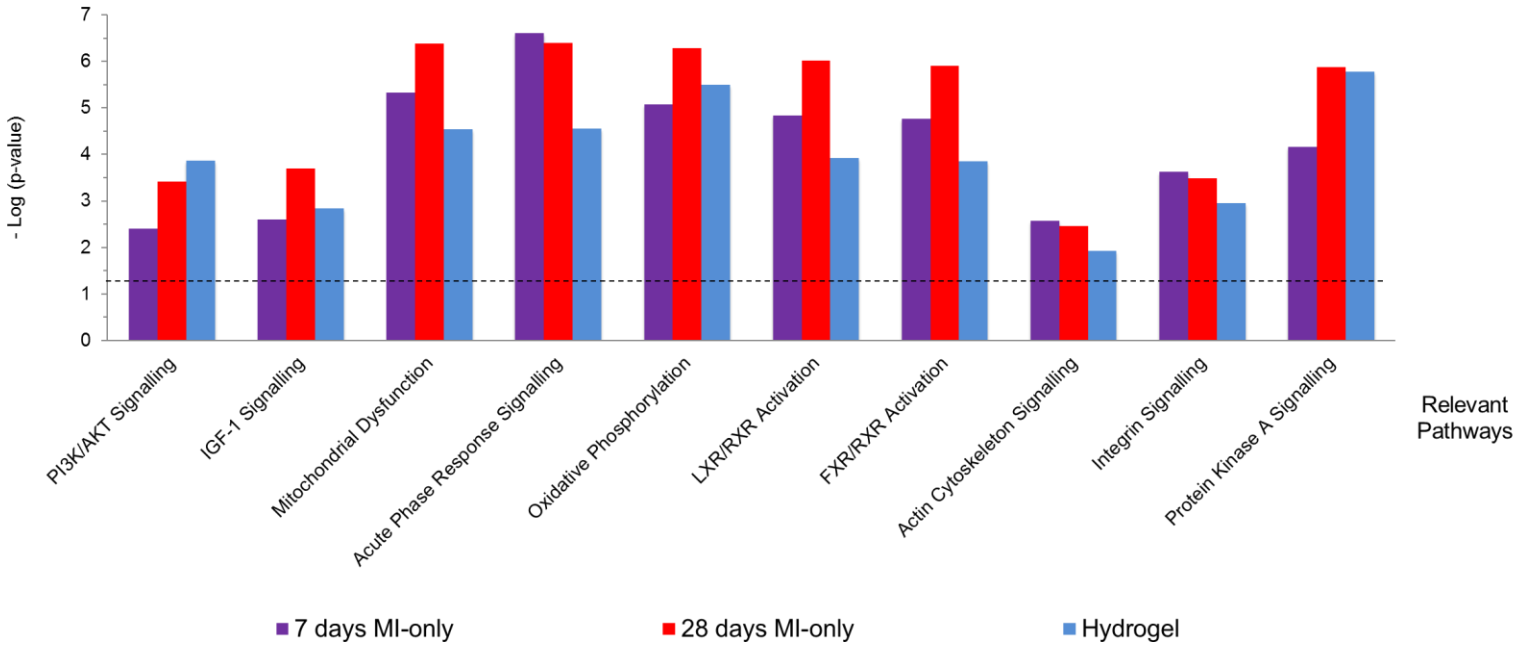

Figure 5.9 Significant pathways detected by IPA® analysis on proteomic data. Data from proteomic analysis (expressed as fold ratio to the healthy group), which had a unique peptide number of at least two, were analysed by IPA® analysis. Cut-offs of fold ratio > 1.5 and fold ratio < -1.5 were applied. Dashed line shows a threshold of -Log(p-value) of 1.3, corresponding to p=0.05, that is the minimal level required to determine if a canonical pathway was significantly detected. Groups of MI-only at 7 and 28 days and hydrogel-treated are shown and grouped by relevant biological pathways. Each analysed sample was a pool of samples coming from three individuals.

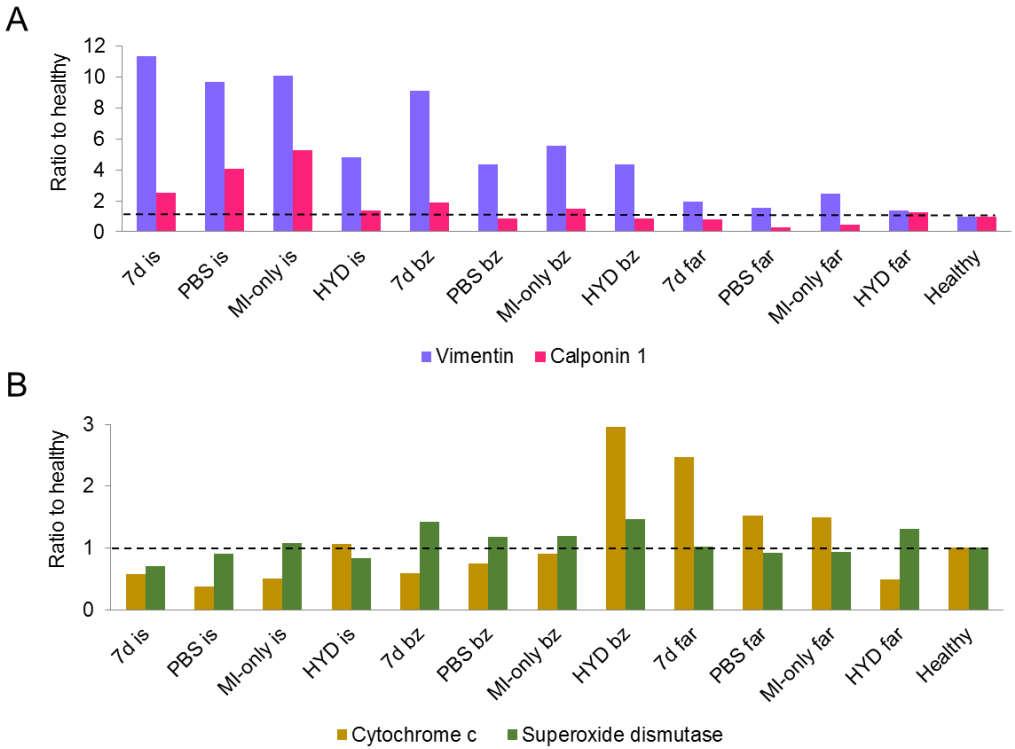

Figure 5.10 Fold change of relevant proteins involved in the remodelling in infarcted groups compared to healthy. Expression levels of myofibroblast-related markers vimentin and calponin 1 (A) together with ROS-scavengers cytochrome *c* and superoxide dismutase (B) as detected by nLC-ESI-MS/MS analysis. Regions are labelled as follows: is=core ischemic, bz=border, far=remote. Hyd=hydrogel-treated. Each analysed sample was a pool of samples from three individuals. Data are reported as average of two technical replicates.

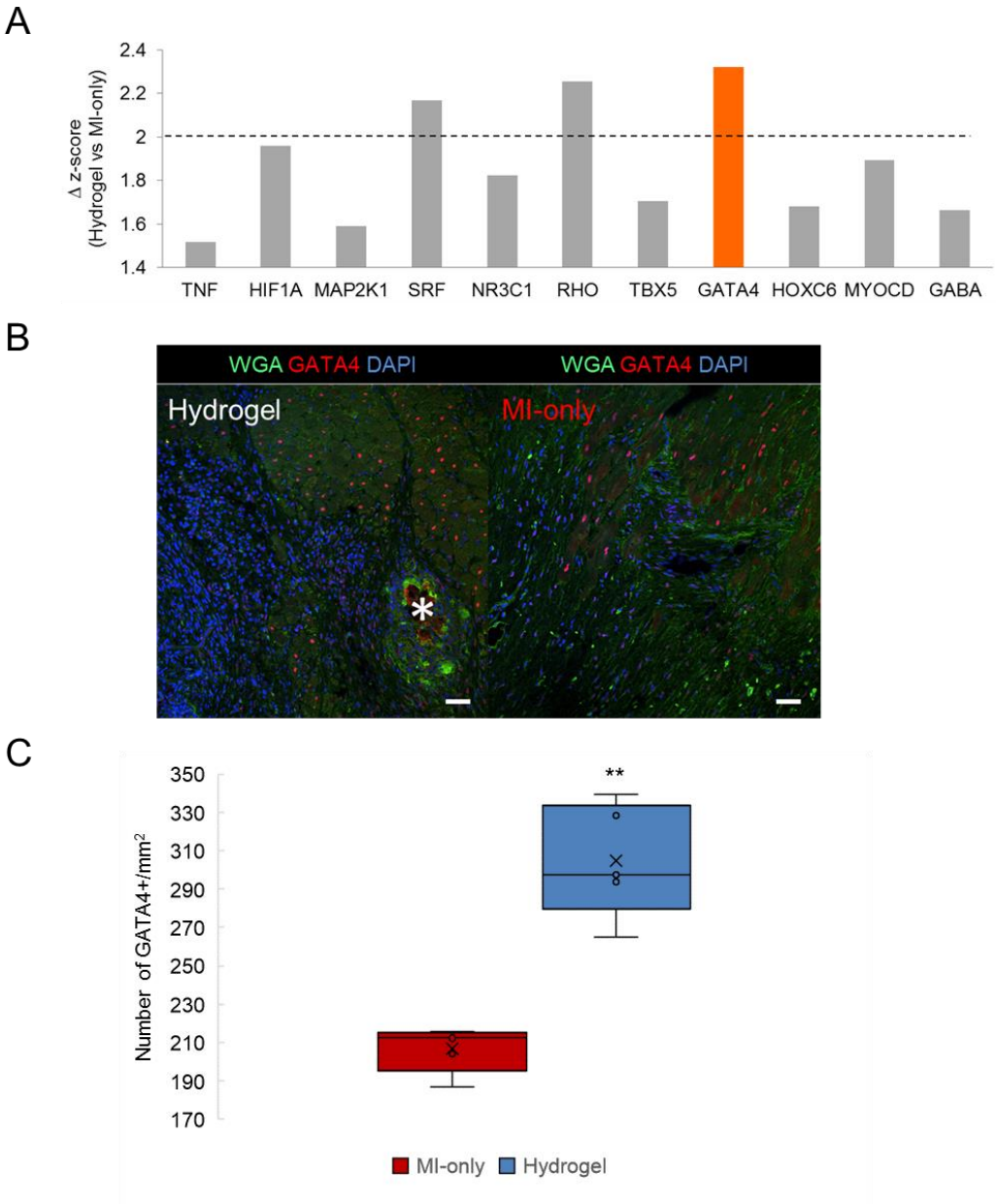

Figure 5.11 Detection and validation of GATA4 as a key upstream regulator. Delta of the activation z-score of upstream regulators between hydrogel-treated and MI-only group (A) highlighting GATA4 as top regulator (from IPA® analysis on RNA-seq data, n=4). Validation of $GATA4^+$ cardiomyocytes in the border zone in both treated and untreated groups (B) (star indicates an island of ELRs-hydrogel). Scale bars, 20 µm. Quantification of $GATA4^+$ cardiomyocytes indicates a higher count in the hydrogel-treated group (C). Data are reported as box-plots, Student's t-test, n=5 animals per group, **p<0.01.

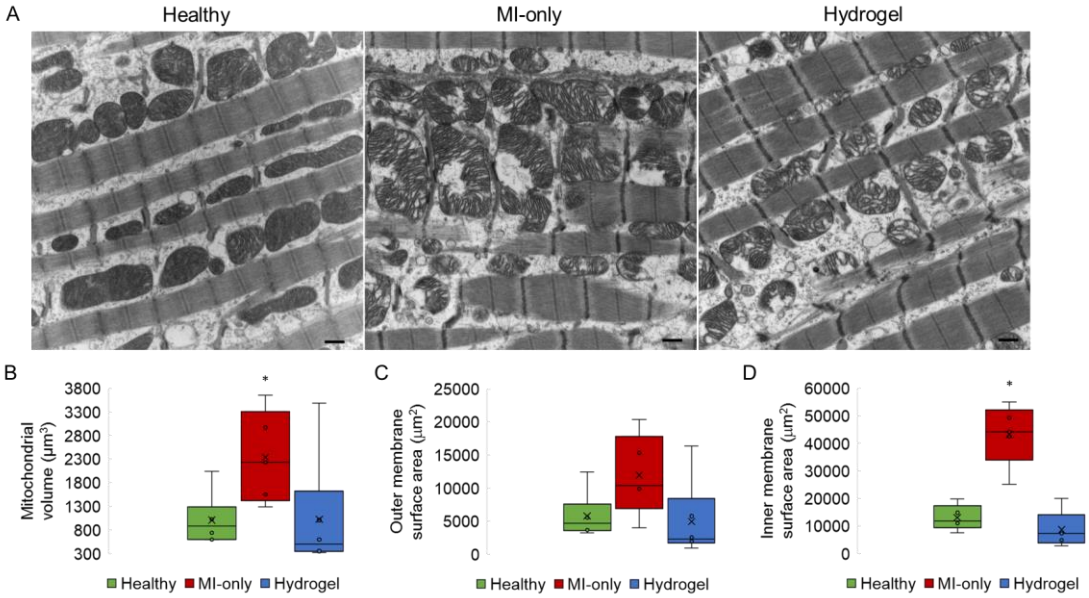

Figure 5.12 Mitochondrial swelling in the cardiomyocytes of the border zone. EM micrographs showing the mitochondria located between the myofibrils of the cardiomyocytes from samples of the border zone (A). Mitochondrial volume (B), surface area of the outer membrane (C) and surface area of the inner membrane (D) were quantified across healthy, infarcted hearts at day 28 (MI-only) and hydrogel-treated hearts. Data are reported as box-plots, n=5 in MI-only, 6 in healthy and hydrogel. Kruskal-Wallis ANOVA, *$p<0.05$. Scale bars = 500 nm.

5.4 Discussion

The overall aim of this chapter was to investigate the mechanisms responsible for the improvement seen in the main indices of post-ischemic remodelling 21 days after the injection of the ELRs-hydrogel. Indeed, only in the recent years have the molecular mechanisms behind the efficacy of a biomaterial treatment for a pathological condition been studied by high-throughput analyses [Wassenaar, Mohd Isa]. Therefore a comprehensive gene, protein and glycan-based approach was adopted to both support with additional data the hypothesis of a beneficial modulation of the remodelling by the hydrogel and to identify which pathways might be altered by this intervention.

This study represents a substantial advance in the field due to the wide spectrum of high-throughput techniques adopted, among which are RNA-seq, proteomic analysis by nLC-ESI-MS/MS and glycomic analysis by LC-ESI-MS/MS. By the combination of these methods we were able to expand all the findings observed at macroscopic and histological level. One of the crucial conclusions of the Chapter Four was a decreased fibrosis 21 days after the hydrogel injection (Section 4.3.2). According to the results achieved by RNA-seq, a minimal but consistent reduction in transcript levels of most genes associated with fibrotic programming from day 7 to day 28 post-MI was seen, but without any significant difference between hydrogel-treated and MI-only groups. The absence of a further reduction of Col1a1, Col1a2 and Col3a1 in an environment which was shown to be less fibrotic after hydrogel injection may be due to two main reasons. First, the high expression of these genes at day seven post-MI is an indication of their actual translation in collagen type I and III proteins, which start to be deposited by myofibroblasts during the second week after MI [van Amerongen], so at day 28 post-MI the requirement for a high expression of mRNA has been already physiologically discontinued. Second, several mechanisms are involved in the actual fibrotic deposition apart from the levels of transcripts of these genes. For instance, feedback mechanisms can regulate fibrosis and one of them has been recently identified to avoid a chronic activation of TGF-β signalling. This mechanism consisted in the negative feedback loop action of NR4A1 transcription factor and the knock-out model for this molecule demonstrated both a higher deposition of collagen and an increased number of myofibroblasts across several models of fibrosis [Palumbo-Zerr]. In this dataset Nr4a1 was significantly

lower in the ischemic core of non-treated animals during both the proliferative and maturation phases, whereas in ELRs-group it was not different from the healthy baseline, thereby resulting in a clear increase from the time of injection. A trend in increased expression was also seen - at a non-significant level - in the border zone of the infarct after hydrogel injection. Interestingly, the restoration of endogenously present Nr4a1 levels together with a lower fibrotic deposition was seen. A similar result was achieved by the pDNA polyplexes-mediated augmentation of this transcription factor in a rat model of fibrosis in the nucleus pulposus region of the intervertebral disc [Feng].

The diverse profile of ELRs-treated ischemic core was confirmed by hierarchical clustering analysis on proteomic data, where the similarity between PBS-injected and MI-only central regions of MI was not shared by the hydrogel-treated one. Specifically, the higher fibrosis assessed by histological evaluation in section 4.3.2 (Chapter Four) was here supported by a relevant increase in two myofibroblast markers - vimentin and calponin 1 - in both MI-only and PBS-injected groups. Interestingly, the higher increase seen here not only in vimentin but also in calponin which distinguishes this model of MI from results achieved in a reperfusion model, where myofibroblasts were vimentin^{+}/calponin^{-} [Frangogiannis 2000].

In the previous chapter (section 4.3.4) it was concluded that changes in the expression of specific glycan residues in cellular membrane proteins were associated with endothelial cell migration and a possible angiogenic response. Here, signs of this response were detectable at expression level by RNA-seq and the relative abundances of those glycan residues which actually distinguished the ELRs-mediated beneficial remodelling were quantified by LC-ESI-MS/MS.
IPA® analysis on DEG data highlighted a trend of retained activation of four angiogenic-related pathways (VEGF, HGF, ErbB and endothelin) three weeks post-ELRs injection, in contrast with a marked decrease seen in MI-only. In a recent work performed by Christman *et al.*, VEGF and FGF gene expression was mainly associated with a trend of increased arteriolar density seen one week after the matrix injection [Wassenaar]. Indeed, an appropriate balance in the expression of the growth factors implicated in the sprouting angiogenesis is crucial for the development of perfused and mature vasculature structures [Carmeliet, Greenberg]. Specifically,

VEGF was demonstrated to hinder the coating of vessels by pericytes, which is promoted by PDGF [Greenberg]. From IPA® analysis, the significance in predicted activation of the angiogenic pathways listed above was fully reached only for endothelin and almost for HGF (p=0.06), confirming that the ELRs-induced response was not driven by VEGF. Therefore, ischemic core regions were stained for α-SMA$^+$ arterioles and an increase of around 50% was seen. This result was comparable in terms of absolute number of arterioles per squared mm, as reported in studies testing the efficacy of angiogenic molecules, such as pleiotrophin and hyaluronan, in the ischemic myocardium [Christman 2005, Tous].

Over recent years several studies have focused on the development of systems which are able to drive the polarisation of macrophages towards a regulatory phenotype [Raimondo, Jain, Hoppstädter]. Indeed, the role of regulatory macrophages is one of the main triggers required for the pathophysiological switch from the inflammatory to proliferative and maturation phases post-ischemia [Frantz, Frangogiannis 2019]. The current RNA-seq dataset showed a trend of increased expression of markers associated with pro-remodelling macrophages, such as IL10, MRC1, MYC, EGR2 and PTGS1 [Jablonski]. The presence of CD163$^+$ cells was validated in the ischemic core regions, and a five-fold higher recruitment at day 28 post-MI was observed in ELRs-treated group. This finding, combined with the angiogenic data reported so far, represents an additional proof of an accelerated healing response in the central region of the infarct, one that was not exclusively affected by fibrotic scarring.

To support the overall hypothesis of a markedly different tissue profile in the ELRs-treated ischemic core, the current study was extended to glycomic analysis, this being the most sensitive technique to detect and quantify the relative abundance of glycan putative structures. Samples enriched in cellular membrane proteins were screened for the presence of both *N*- and *O*-linked glycans both in ischemic core and border regions of infarcted hearts. These results represent the first reported study to investigate changes in cardiac glycosylation profile following a biomaterial treatment.

Previous studies that determined alterations in glycosylation following myocardial infarction, were more centred on the validation of glycomic-based techniques for the identification of molecular changes in remodelling rather than in the definition of

precise glycosylation patterns and their alteration in response to a matrix-interacting treatment [Parker, Yang]. Indeed, technical advances in the methodologies to process and identify glycans by mass spectrometry have only recently developed, and these can now be used as tools to elucidate the biological role of glycans [Jensen, Everest-Dass, Cummings, Levery]. In this study the expression of α-Gal epitope that was detected by the high binding to GS-I-B4 in lectin microarrays, as shown in section 4.3.4 (Chapter Four), was validated. A clear pattern of increased abundance of both *N*- and *O*-glycans containing α-Gal was observed in ELRs-treated ischemic core, similar to that of the seven days post-MI timepoint. Indeed, the presence of terminal α-Gal was seen in a panel of putative *N*-glycans structures but its expression markedly dropped from day 7 to day 28 post-MI (over 35%), as a clear sign of a changed cellular membrane glycosylation. The retention of its expression 21 days after ELRs-hydrogel injections might depend on an extended recruitment of macrophages and endothelial cells in the central region of the infarct which had finally led to the formation of a more cellularised core than that affected by physiological scarring. The association of this endogenous increase of α-Gal with an improved post-ischemic remodelling recalls extensive studies carried out by Galili on the efficacy of α-Gal-coated liposomes and nanoparticles following wound healing [Wigglesworth, Galili 2010, Hurwitz]. In those experiments, they have demonstrated an accelerated curing and less fibrotic remodelling upon injection of α-Gal-coated systems, and that effect was modulated by the activation of the complement system. The main concern for the possible application of such a system would derive from the observation that anti-α-Gal antibodies are naturally produced in humans and actually represent a substantial fraction of overall circulating immunoglobulins (around 1%) [Galili 1984]. Despite this, the same authors have shown that the α-Gal-promoted recruitment of macrophages and consequent release of cytokines are completed within the following four weeks post-injection, with no further pro-inflammatory effect [Wigglesworth]. Interestingly, the application of α-Gal-coated nanoparticles led also to an angiogenic response in wounds of pigs where the enzyme responsible for α-Gal expression, that is α-(1,3)-galactosyltrasferase, was deleted, and thereby antibodies against this residue were circulating in the blood. Since the tested hydrogel in this study was not glyco-functionalised, the similarities between the α-Gal-characterized beneficial remodelling that was seen in myocardial tissue

and the already reported accelerated wound healing by Galili suggest that the efficacy of their functionalised system is due to the enhancement of an endogenously present mechanism of enhanced cellularised and less fibrotic remodelling. In support to this interpretation, α-Gal had already been found on porcine endothelial cell proteins, like von Willebrand factor, by its binding to human xenoreactive antibodies [Holzknecht]. Moreover, past studies reported the localisation of this glycan epitope across different types of vasculature (capillaries, arterioles, venules) and also on other components of the healing process, such as platelets and fibrinogen [Sandrin]. Indeed, the co-localisation of α-Gal-binding lectin GS-I^+/$CD31^+$ in capillaries - that was showed in section 4.3.4 (Chapter Four) - supports the hypothesis that α-Gal is more likely a marker of an endogenous angiogenic response - in this study driven by a glycan-free hydrogel - rather than a sufficient molecular trigger to promote a less fibrotic and accelerated healing, as shown by Galili.

Focusing on *O*-linked glycans, in addition to the detection of α-Gal in ELRs-treated ischemic core and not in MI-only, the expression of either NeuAc or NeuGc was evaluated in central and border infarcted regions . The distinction between these two types of sialylation revealed clear differences that were hidden behind a shared equivalently higher sialylation at 28 days post-MI. Indeed, hydrogel-treated animals showed an expression of the two types of sialylation that was more similar to the pre-MI condition, by limiting the extent of both the increase in NeuAc and the drop in NeuGc that characterized the MI-only ischemic core. The same trend was conserved also in the border region, with a further reduction in NeuAc and an increase in NeuGc, which reached an expression slightly higher than that of pre-MI, for the first time across all infarcted samples. Remarkably, higher expression of NeuGc was observed also in *N*-glycans extracted from ELRs-injected group, making this difference the most reflective of a different remodelling, together with α-Gal. Since the large majority of studies evaluating the relevance of NeuGc belong either to the field of cancer biology or to immunotherapy related to xenogeneic reactions [Mercado, He, Hernández, Krengel, Barone], very few works included data on the expression of NeuGc in myocardial tissue. The most relevant study was performed by the Bennett group, and a higher NeuGc/NeuAc ratio in adult than in neonatal myocardial tissue was observed [Montpetit]. However, this increase in NeuGc was

vaguely associated with cardiomyocytes development, and a precise quantification of the extent of this change was not provided.

In the present study it was demonstrated that upon ELRs-treatment, the ischemic core of the infarct was less fibrotic and more perfused than the untreated one, as also confirmed by stable differences in the glycosylation pattern of cellular membranes. A proposed mechanism of how this change in the core influenced the improved cardiac function was based the higher retention of $GATA4^+$ cardiomyocytes in the border zone of the infarct. GATA4 has been extensively studied as a marker of de-differentiation of cardiomyocytes and it is required for the mammalian heart regeneration at neonatal stage [Yu, Kikuchi]. Since to hypothesise a regenerative response after ischemia, precise growth factor-related differences would have been required and no evidence towards this direction was seen from RNA-seq and proteomic analyses, a different mechanism of action is proposed. Indeed, GATA4 was previously established as a marker of cardiac cell survival [Oka], and the retention of a higher number of $GATA4^+$ cardiomyocytes in the border region, together with a preserved mitochondrial integrity, represent the result of a protective action following the ELRs-hydrogel treatment. Specifically, the beneficial impact of the hydrogel injection in the central region of the infarct would have been crucial to avoid the formation of a highly compact fibrotic scarring and to promote, instead, an angiogenic response. Persistence of widely recognized markers of a beneficial remodelling at protein and glycan level, such as $CD163^+$ cells and α-Gal [Wigglesworth, Hurwitz, Raimondo, Montgomery, Hüttemann], up to 21 days after hydrogel injection supports the hypothesis of a matrix-dependent effect in the integrity and functionality of the cardiomyocytes which survived to ischemia at day seven.

5.5 Conclusions

In this chapter specific alterations at gene, protein and glycan level due to the injection of the ELRs-hydrogel were investigated. A differently remodelled ischemic core having a less fibrotic and more vascularised nature reflected its beneficial effects on the border zone of the infarct, where a higher retention of $GATA4^+$ cardiomyocytes was associated with a higher mitochondrial integrity. Thus, the synergistic effect of the remodelled ischemic core and the preserved border zone

strongly influenced the functional improvement and the infarct thickness 21 days after hydrogel injection. This is the first-ever preclinical study to both demonstrate the efficacy of an acellular biomaterial for the cardiac post-ischemic remodelling and to elucidate the molecular mechanisms behind its impact at gene, protein and glycan level. Substantial advances in the study of cell membrane glycosylation changes in the main specific glycan residues present in both *N*- and *O*-linked glycans after a biomaterial treatment have been reported for the first time. Furthermore, the combination of a clinically-inspired established model of non-transmural myocardial infarction with a realistic intervention time (seven days post-MI) provides this study with an additional advantage for clinical translation.

5.6 References

- Barone A, Benktander J, Teneberg S, Breimer ME. Characterization of acid and non-acid glycosphingolipids of porcine heart valve cusps as potential immune targets in biological heart valve grafts. Xenotransplantation. 2014 Nov-Dec;21(6):510-22
- Carmeliet P, Jain RK. Molecular mechanisms and clinical applications of angiogenesis. Nature. 2011 May 19;473(7347):298-307
- Chinello C, Stella M, Piga I, Smith AJ, Bovo G, Varallo M, Ivanova M, Denti V, Grasso M, Grasso A, Del Puppo M, Zaravinos A, Magni F. Proteomics of liquid biopsies: Depicting RCC infiltration into the renal vein by MS analysis of urine and plasma. J Proteomics. 2018 Apr 22
- Christman KL, Fang Q, Kim AJ, Sievers RE, Fok HH, Candia AF, Colley KJ, Herradon G, Ezquerra L, Deuel TF, Lee RJ. Pleiotrophin induces formation of functional neovasculature in vivo. Biochem Biophys Res Commun. 2005 Jul 15;332(4):1146-52
- Christman KL, Fok HH, Sievers RE, Fang Q, Lee RJ. Fibrin glue alone and skeletal myoblasts in a fibrin scaffold preserve cardiac function after myocardial infarction. Tissue Eng. 2004 Mar-Apr;10(3-4):403-9 (Christman 2004a in the text)
- Christman KL, Vardanian AJ, Fang Q, Sievers RE, Fok HH, Lee RJ. Injectable fibrin scaffold improves cell transplant survival, reduces infarct expansion, and

induces neovasculature formation in ischemic myocardium. J Am Coll Cardiol. 2004 Aug 4;44(3):654-60 (Christman 2004b in the text)

- Cummings RD, Pierce JM. The challenge and promise of glycomics. Chem Biol. 2014 Jan 16;21(1):1-15
- Everest-Dass AV, Abrahams JL, Kolarich D, Packer NH, Campbell MP. Structural feature ions for distinguishing N- and O-linked glycan isomers by LC-ESI-IT MS/MS. J Am Soc Mass Spectrom. 2013 Jun;24(6):895-906
- Feng G, Zhang Z, Dang M, Zhang X, Doleyres Y, Song Y, Chen D, Ma PX. Injectable nanofibrous spongy microspheres for NR4A1 plasmid DNA transfection to reverse fibrotic degeneration and support disc regeneration. Biomaterials. 2017 Jul;131:86-97
- Frangogiannis NG, Michael LH, Entman ML. Myofibroblasts in reperfused myocardial infarcts express the embryonic form of smooth muscle myosin heavy chain (SMemb). Cardiovasc Res. 2000 Oct;48(1):89-100
- Frangogiannis NG. Cardiac fibrosis: Cell biological mechanisms, molecular pathways and therapeutic opportunities. Mol Aspects Med. 2019 Feb;65:70-99
- Frantz S, Nahrendorf M. Cardiac macrophages and their role in ischaemic heart disease. Cardiovasc Res. 2014 May 1;102(2):240-8
- Galili U, Rachmilewitz EA, Peleg A, Flechner I. A unique natural human IgG antibody with anti-alpha-galactosyl specificity. J Exp Med. 1984 Nov 1;160(5):1519-31
- Galili U, Wigglesworth K, Abdel-Motal UM. Accelerated healing of skin burns by anti-Gal/alpha-gal liposomes interaction. Burns. 2010 Mar;36(2):239-51
- Greenberg JI, Shields DJ, Barillas SG, Acevedo LM, Murphy E, Huang J, Scheppke L, Stockmann C, Johnson RS, Angle N, Cheresh DA. A role for VEGF as a negative regulator of pericyte function and vessel maturation. Nature. 2008 Dec 11;456(7223):809-13
- He D, Fan X, Liu B, Tian Y, Zhang X, Kang L, Tai Y, Liu S, Wang Q, Li Q, Cai J. Generation and characterization of a IgG monoclonal antibody specific for GM3 (NeuGc) ganglioside by immunizing β3Gn-T5 knockout mice. Sci Rep. 2018 Feb 7;8(1):2561
- Hernández AM, Toledo D, Martínez D, Griñán T, Brito V, Macías A, Alfonso S, Rondón T, Suárez E, Vázquez AM, Pérez R. Characterization of the antibody

response against NeuGcGM3 ganglioside elicited in non-small cell lung cancer patients immunized with an anti-idiotype antibody. J Immunol. 2008 Nov 1;181(9):6625-34

- Holzknecht ZE, Platt JL. Identification of porcine endothelial cell membrane antigens recognized by human xenoreactive natural antibodies. J Immunol. 1995 May 1;154(9):4565-75
- Hoppstädter J, Seif M, Dembek A, Cavelius C, Huwer H, Kraegeloh A, Kiemer AK. M2 polarization enhances silica nanoparticle uptake by macrophages. Front Pharmacol. 2015 Mar 23;6:55
- Howard CV, Reed MG. Unbiased Stereology. 2nd Edition. Oxford: BIOS Scientific Publishers. 2005. p. 103-105
- Hurwitz ZM, Ignotz R, Lalikos JF, Galili U. Accelerated porcine wound healing after treatment with α-gal nanoparticles. Plast Reconstr Surg. 2012 Feb;129(2):242e-251e
- Hüttemann M, Pecina P, Rainbolt M, Sanderson TH, Kagan VE, Samavati L, Doan JW, Lee I. The multiple functions of cytochrome c and their regulation in life and death decisions of the mammalian cell: From respiration to apoptosis. Mitochondrion. 2011 May;11(3):369-81
- Jablonski KA, Amici SA, Webb LM, Ruiz-Rosado Jde D, Popovich PG, Partida-Sanchez S, Guerau-de-Arellano M. Novel markers to delineate murine M1 and M2 macrophages. PLoS One. 2015 Dec 23;10(12):e0145342
- Jain N, Vogel V. Spatial confinement downsizes the inflammatory response of macrophages. Nat Mater. 2018 Oct 22
- Jensen PH, Karlsson NG, Kolarich D, Packer NH. Structural analysis of N- and O-glycans released from glycoproteins. Nat Protoc. 2012 Jun 7;7(7):1299-310
- Kikuchi K, Holdway JE, Werdich AA, Anderson RM, Fang Y, Egnaczyk GF, Evans T, Macrae CA, Stainier DY, Poss KD. Primary contribution to zebrafish heart regeneration by gata4(+) cardiomyocytes. Nature. 2010 Mar 25;464(7288):601-5
- Krengel U, Bousquet PA. Molecular recognition of gangliosides and their potential for cancer immunotherapies. Front Immunol. 2014 Jul 21;5:325

- Landa N, Miller L, Feinberg MS, Holbova R, Shachar M, Freeman I, Cohen S, Leor J. Effect of injectable alginate implant on cardiac remodeling and function after recent and old infarcts in rat. Circulation. 2008 Mar 18;117(11):1388-96
- Leor J, Tuvia S, Guetta V, Manczur F, Castel D, Willenz U, Petneházy O, Landa N, Feinberg MS, Konen E, Goitein O, Tsur-Gang O, Shaul M, Klapper L, Cohen S. Intracoronary injection of in situ forming alginate hydrogel reverses left ventricular remodeling after myocardial infarction in Swine. J Am Coll Cardiol. 2009 Sep 8;54(11):1014-23
- Levery SB, Steentoft C, Halim A, Narimatsu Y, Clausen H, Vakhrushev SY. Advances in mass spectrometry driven O-glycoproteomics. Biochim Biophys Acta. 2015 Jan;1850(1):33-42
- Liu X, Chinello C, Musante L, Cazzaniga M, Tataruch D, Calzaferri G, James Smith A, De Sio G, Magni F, Zou H, Holthofer H. Intraluminal proteome and peptidome of human urinary extracellular vesicles. Proteomics Clin Appl. 2015 Jun;9(5-6):568-73
- Liu Y, McBride R, Stoll M, Palma AS, Silva L, Agravat S, Aoki-Kinoshita KF, Campbell MP, Costello CE, Dell A, Haslam SM, Karlsson NG, Khoo KH, Kolarich D, Novotny MV, Packer NH, Ranzinger R, Rapp E, Rudd PM, Struwe WB, Tiemeyer M, Wells L, York WS, Zaia J, Kettner C, Paulson JC, Feizi T, Smith DF. The minimum information required for a glycomics experiment (MIRAGE) project: improving the standards for reporting glycan microarray-based data. Glycobiology. 2016 Nov 22
- Ludwig KR, Schroll MM, Hummon AB. Comparison of in-solution, FASP, and s-trap based digestion methods for bottom-up proteomic studies. J Proteome Res. 2018 Jul 6;17(7):2480-2490
- Mercado CP, Quintero MV, Li Y, Singh P, Byrd AK, Talabnin K, Ishihara M, Azadi P, Rusch NJ, Kuberan B, Maroteaux L, Kilic F. A serotonin-induced N-glycan switch regulates platelet aggregation. Sci Rep. 2013 Sep 30;3:2795
- Mohd Isa IL, Abbah SA, Kilcoyne M, Sakai D, Dockery P, Finn DP, Pandit A. Implantation of hyaluronic acid hydrogel prevents the pain phenotype in a rat model of intervertebral disc injury. Sci Adv. 2018 Apr 4;4(4):eaaq0597
- Montgomery M, Ahadian S, Davenport Huyer L, Lo Rito M, Civitarese RA, Vanderlaan RD, Wu J, Reis LA, Momen A, Akbari S, Pahnke A, Li RK,

Caldarone CA, Radisic M. Flexible shape-memory scaffold for minimally invasive delivery of functional tissues. Nat Mater. 2017 Oct;16(10):1038-1046

- Montpetit ML, Stocker PJ, Schwetz TA, Harper JM, Norring SA, Schaffer L, North SJ, Jang-Lee J, Gilmartin T, Head SR, Haslam SM, Dell A, Marth JD, Bennett ES. Regulated and aberrant glycosylation modulate cardiac electrical signaling. Proc Natl Acad Sci U S A. 2009 Sep 22;106(38):16517-22
- Oka T, Maillet M, Watt AJ, Schwartz RJ, Aronow BJ, Duncan SA, Molkentin JD. Cardiac-specific deletion of Gata4 reveals its requirement for hypertrophy, compensation, and myocyte viability. Circ Res. 2006 Mar 31;98(6):837-45
- Palumbo-Zerr K, Zerr P, Distler A, Fliehr J, Mancuso R, Huang J, Mielenz D, Tomcik M, Fürnrohr BG, Scholtysek C, Dees C, Beyer C, Krönke G, Metzger D, Distler O, Schett G, Distler JH. Orphan nuclear receptor NR4A1 regulates transforming growth factor-β signaling and fibrosis. Nat Med. 2015 Feb;21(2):150-8
- Parker BL, Palmisano G, Edwards AV, White MY, Engholm-Keller K, Lee A, Scott NE, Kolarich D, Hambly BD, Packer NH, Larsen MR, Cordwell SJ. Quantitative N-linked glycoproteomics of myocardial ischemia and reperfusion injury reveals early remodeling in the extracellular environment. Mol Cell Proteomics. 2011 Aug;10(8):M110.006833
- Raimondo TM, Mooney DJ. Functional muscle recovery with nanoparticle-directed M2 macrophage polarization in mice. Proc Natl Acad Sci U S A. 2018 Oct 16;115(42):10648-10653
- Rao SV, Zeymer U, Douglas PS, Al-Khalidi H, White JA, Liu J, Levy H, Guetta V, Gibson CM, Tanguay JF, Vermeersch P, Roncalli J, Kasprzak JD, Henry TD, Frey N, Kracoff O, Traverse JH, Chew DP, Lopez-Sendon J, Heyrman R, Krucoff MW. Bioabsorbable intracoronary matrix for prevention of ventricular remodeling after myocardial infarction. J Am Coll Cardiol. 2016 Aug 16;68(7):715-23
- Sackstein R, Dimitroff CJ. A hematopoietic cell L-selectin ligand that is distinct from PSGL-1 and displays N-glycan-dependent binding activity. Blood. 2000 Oct 15;96(8):2765-74
- Sackstein R, Merzaban JS, Cain DW, Dagia NM, Spencer JA, Lin CP, Wohlgemuth R. Ex vivo glycan engineering of CD44 programs human

multipotent mesenchymal stromal cell trafficking to bone. Nat Med. 2008 Feb;14(2):181-7

- Sandrin MS, Osman N, McKenzie IF. Transgenic approaches for the reduction of Galalpha(1,3)Gal for xenotransplantation. Front Biosci. 1997 Apr 1;2:e1-11
- Schulz BL, Packer NH, Karlsson NG. Small-scale analysis of O-linked oligosaccharides from glycoproteins and mucins separated by gel electrophoresis. Anal Chem. 2002 Dec 1;74(23):6088-97
- Singelyn JM, Sundaramurthy P, Johnson TD, Schup-Magoffin PJ, Hu DP, Faulk DM, Wang J, Mayle KM, Bartels K, Salvatore M, Kinsey AM, Demaria AN, Dib N, Christman KL. Catheter-deliverable hydrogel derived from decellularized ventricular extracellular matrix increases endogenous cardiomyocytes and preserves cardiac function post-myocardial infarction. J Am Coll Cardiol. 2012 Feb 21;59(8):751-63
- Tang Y, Nyengaard JR. A stereological method for estimating the total length and size of myelin fibers in human brain white matter. J Neurosci Methods. 1997 May 16;73(2):193-200
- Tous E, Ifkovits JL, Koomalsingh KJ, Shuto T, Soeda T, Kondo N, Gorman JH 3rd, Gorman RC, Burdick JA. Influence of injectable hyaluronic acid hydrogel degradation behavior on infarction-induced ventricular remodeling. Biomacromolecules. 2011 Nov 14;12(11):4127-35
- van Amerongen MJ, Bou-Gharios G, Popa E, van Ark J, Petersen AH, van Dam GM, van Luyn MJ, Harmsen MC. Bone marrow-derived myofibroblasts contribute functionally to scar formation after myocardial infarction. J Pathol. 2008 Feb;214(3):377-86
- Wassenaar JW, Gaetani R, Garcia JJ, Braden RL, Luo CG, Huang D, DeMaria AN, Omens JH, Christman KL. Evidence for mechanisms underlying the functional benefits of a myocardial matrix hydrogel for post-MI treatment. J Am Coll Cardiol. 2016 Mar 8;67(9):1074-86
- Weibel, E.R. Stereological methods, Vol. 1: Practical methods for biological morphometry. London: Academic Press. 1979
- Wigglesworth KM, Racki WJ, Mishra R, Szomolanyi-Tsuda E, Greiner DL, Galili U. Rapid recruitment and activation of macrophages by anti-Gal/α-Gal

liposome interaction accelerates wound healing. J Immunol. 2011 Apr 1;186(7):4422-32

- Yang S, Chatterjee S, Cipollo J. The glycoproteomics-MS for studying glycosylation in cardiac hypertrophy and heart failure. Proteomics Clin Appl. 2018 Sep;12(5):e1700075
- Yu W, Huang X, Tian X, Zhang H, He L, Wang Y, Nie Y, Hu S, Lin Z, Zhou B, Pu W, Lui KO, Zhou B. GATA4 regulates Fgf16 to promote heart repair after injury. Development. 2016 Mar 15;143(6):936-49
- Zhang J, Xin L, Shan B, Chen W, Xie M, Yuen D, Zhang W, Zhang Z, Lajoie GA, Ma B. PEAKS DB: de novo sequencing assisted database search for sensitive and accurate peptide identification. Mol Cell Proteomics. 2012 Apr;11(4):M111.010587

Chapter Six

Summary and future directions

6.1 Introduction

Myocardial infarction (MI) represents the primary cause of worldwide mortality and its incidence is also spreading in the low- and middle-income countries [Global Health Estimates 2016]. The long-term survival after full thickness infarcts (STEMI) has now decreased significantly due to the success of primary percutaneous coronary intervention (PCI), with the only exception being that of the elderly (above 80 years) population [Pedersen, Velders, Waziri]. In most of the hospitalised patients with STEMIs, the occlusion of the proximal left anterior descending coronary (LAD) is not present, even though this usually results in the early death of the patient, hence the term "widow-maker's lesion". Furthermore, STEMI are increasingly treated with acute intervention, whereas patients without a ST-elevation myocardial infarction (NSTEMI) are not so treated, and there is an increased risk of reinfarction after an NSTEMI. Recurrent and silent NSTEMI can result in progressive deterioration of myocardial function and heart failure. Therefore, to address this clinical need a suitable model of MI needed to be established since the widely used model of LAD ligation causes full-thickness infarcts both in small and large animal models [Le, Leor, Chen, Montgomery, Bassat].

A wide range of therapeutic approaches for MI was tested experimentally over recent years, including cellular- and growth factor-based, or a combination of these [Zangi, Dubois, Johnston, Wang 2018, Takehara]. Given the limited, if not marginal positive results which emerged from the meta-analyses of cell-based trials for the treatment of MI [Gyöngyösi 2015, 2018], other promising strategies which showed significant results at the preclinical level have been considered [Bassat, Eulalio, Seif-Naraghi, Radisic 2013]. In particular, the intrinsic advantages of acellular hydrogels for their further translational path encouraged their development and experimental testing in both small and large animal models of MI [Leor, Christman, Ifkovits]. Nevertheless, the efficacy of an acellular hydrogel still needs to be demonstrated through the clinical trial phases [Frey, Rao]. Among the potential sources which can modulate the ischemic microenvironment there are the ECM components, and indeed some of the ECM-based treatments resulted in marked improvements both in the remodelling parameters and in the cardiac function [Bassat, Christman, Singelyn, Kühn]. Elastin is a naturally-present cardiac ECM protein which is produced by endothelial cells and fibroblasts [Mithieux]. Elastin fibres are derived from the

coacervation and further crosslinking of the precursor tropoelastin molecules [Kozel]. By genetically-engineering, it is possible to produce elastin-mimicking peptides called elastin-like recombinamers (ELRs) in *E.coli*. Moreover, the final sequence of such recombinamers can be adapted to include desired biologically-reactive functional groups such as RGD and MMP-responsive motifs [Rodríguez-Cabello, Castellanos].

To understand the myocardial environment and its pathological degeneration following ischemia, current studies are focusing on the recruitment, role and paracrine effects which were not initially unravelled due to the oversimplification of their role across the sequential inflammatory and proliferative phases after MI [Dewald, Frantz, Frangogiannis 2017 and 2019]. Glycans are among the less explored molecules in the myocardial microenvironment, despite their presence both in the ECM (proteoglycans and glycosaminoglycans) and on the cellular membranes (*N*- and *O*-glycans). The role of glycans in the modulation of growth factor-dependent intracellular signalling pathways highlighted key features of metastatic and inflammation-derived degenerative conditions in several organs of the body [Croci, Paszek, Mohd-Isa, Gonzalez]. Given the limited regenerative capacity of the mammalian myocardium at the neonatal stage [Porrello, Ye], expanding the analysis to the expression of partially-studied components like glycans can identify precise molecular patterns associated with that innate regenerative stage.

In light of these considerations, the main aims of this thesis are based on the investigation of the myocardial environment at different stages, during maturation and pathological (post-ischemia) conditions. Firstly, glycosylation profiles in early neonatal and adult stages were studied to identify eventual differences associated with a residual regenerative potential after birth. Secondly, a clinically-inspired ovine model of non-transmural MI was established and an ELRs-based hydrogel tested for its potential modulation of the post-ischemic remodelling. Finally, the mechanisms behind the remodelled regions after the injection of the ELRs-based treatment were studied at gene, protein and glycan level.

6.2 Summary

6.2.1 Chapter Two - Distinct differences in cellular membrane glycosylation reflect the regeneration potential of neonatal myocardial tissue

Mammalian adult cardiomyocytes are able to re-enter the cell-cycle only during the first one-two days after birth, thus avoiding the maladaptive remodelling which characterises post-ischemic phases in the adult [Porrello, Zhu]. The glycosylation profile in such early neonatal and adult conditions was studied in relation to the voltage gated ion channel activity from isolated cardiac myocytes [Montpetit, Schwetz]. In contrast, the current analysis included the identification of significant differences in the cellular membrane glycosylation from tissue samples harvested from neonatal and adult rats (Figure 6.1). A consistent expression of sialic acids, mannose and GlcNAc residues was assessed first in the adult myocardial tissue by their localisation in capillaries and cardiomyocytes membranes by lectin histochemistry. Moreover, a quantitatively-similar expression of these types of glycans on the cellular membranes of different strains of adult rat and across the left and right ventricle was validated by lectin microarray analysis. However, the scenario changed at the three-day-old neonatal stage, where an increase of high-mannose - and consequent decrease of complex - *N*-glycans were seen. $Man_6GlcNAc_2$ was identified as the main high mannose *N*-linked structure that was decreased in adult while a higher expression of sialylated *N*-linked glycans and lower core fucosylation for complex structures were associated with ageing. Three *N*-linked structures, one complex-, one hybrid- and one high mannose-type, were unique to the neonatal left ventricle. The occurrence of mucin core type 2 *O*-linked glycans were reduced in adult and one sulfated core type 2 *O*-linked structure was identified only in neonatal tissue. Interestingly, *O*-linked glycans from mature tissue contained both *N*-acetylneuraminic acid (Neu5Ac) and *N*-glycolylneuraminic acid (Neu5Gc), while all sialylated *N*-linked glycans detected contained only Neu5Ac. These differences in the glycosylation pattern resembled features described *in vitro* in undifferentiated cells [Fujitani, Hasehira], and distinctive putative structures at that stage were lost upon maturation.

6.2.2 Chapter Three – An ovine model of non-transmural myocardial infarction

Full-thickness infarcts were extensively reproduced in small and large animal studies which tested the efficacy of cellular- and biomaterial-based treatments [Dubois, Johnston, Wang 2018, Takehara]. However, such extended infarcts do not represent the most urgent clinical need related to MI, since the efficacy of PCI had already led to marked improvements in the long-term survival in those patients who survived to the occlusion of the LAD [Pedersen, Waziri]. Therefore, in the current study focal infarcts were induced in adult sheep by multiple ligations from the first diagonal up to 4-5 cm from the apex. Histological and protein analysis confirmed the progressive damage at the ultrastructure level in cardiomyocytes and the deposition of matrix and sulfated GAGs in the ECM. Since GAGs are required for the stabilisation of the fibrotic network which characterises the proliferative and remodelling phases after ischemia, their linear increase during the first four weeks after MI supports the histological analysis based on Masson's Trichrome, H&E, Alcian Blue, and electron microscopy. Interestingly, specific signs of deposition of dense bodies inside the mitochondria in the border zone of the infarct seven days after the induction of MI confirmed the long-term effect and reliability of the adopted surgical procedure. Finally, an average decrease in EF of 6.3% further confirmed the different extent of the damage induced by this surgical procedure which contrasts with the much higher reduction in EF seen after the conventional LAD ligation method [Leor, Montgomery, Bassat].

6.2.3 Chapter Four - Elastin-like recombinamers-based hydrogel modulates the post-ischemic remodelling in a clinically-relevant model of myocardial infarction

ECM-based approaches have recently shown promising results for the treatment of the infarcted heart both in small and large animal models [Bassat, Kühn, Singelyn]. Elastin is one of the cardiac ECM proteins and can be produced by genetic engineering to achieve recombinamers (named ELRs) which both preserve the distinctive pentapeptide VPGXG (present in the natural monomer tropoelastin) and can be further functionalised with motifs for specific biological interactions [Staubli, Castellanos]. However, the effect of an ELRs-based hydrogel system was not evaluated in any ischemic model thus far. In this study the procedure for the multiple

injection of the ELRs-based hydrogel was optimised and then its effects were evaluated in the ovine model of non-transmural MI described in Chapter Three. Significant reduced fibrotic remodelling and enhanced angiogenic responses were seen 21 days after the introduction of the hydrogel in the infarcted ventricular wall. The porous structure of the hydrogel and its functionalisation with RGD and MMPs/cathepsin K-responsive sequences allowed the recruitment of macrophages and endothelial cells, as already seen in other experimental conditions using different ELRs [Staubli]. The angiogenic response was first highlighted by strong changes in the glycosylation of the total cellular membrane proteins that showed a higher binding to *Griffonia simplicifolia* (GS)-I-B4 lectin in the ischemic core of the ELRs-treated infarcts. This higher binding corresponds to a higher expression of terminal α-galactose (α-Gal) that was co-localised with anti-CD31 staining to identify capillaries. Consequent stereological quantification indicated a four-fold increase in the number of capillaries in the hydrogel-treated ischemic cores. The migration of endothelial cells in the matrix of the hydrogel and the further formation of a vasculature network was possible also because of the limited fibrosis occurring in the same region. By the application of an isotropically uniform random sampling, consistent reductions in the quantity of the collagen-positive area were seen by Masson's Trichrome and EM. Moreover, parallel analyses focused on the whole molecular fingerprint of the tissue (Raman microscopy) and on the quantity of sulfated GAGs (DMMB assay) confirmed the less fibrotic environment in the treatment group.

6.2.4 Chapter Five - Transcriptomic, proteomic and glycomic analyses to reveal the mechanism of modulation of post-ischemic remodelling by an elastin-based hydrogel

Certain acellular systems have shown marked improvements in the myocardial post-ischemic remodelling but a precise mechanism of action still needs to be fully understood [Landa, Leor, Singelyn]. Only recently, high-throughput analyses started to elucidate the molecular pathways which determine the downstream effect triggered by the introduction of an ECM-inspired system to modulate a pathological condition [Wassenaar, Mohd-Isa]. In this chapter RNA-sequencing, nLC-ESI-MS/MS label-free quantification for proteomic and LC-ESI-MS/MS adapted for

glycomic analysis were performed on the infarcted samples. Ingenuity Pathway Analysis (IPA®) was run on both the transcriptomic and proteomic datasets, whereas the relative percentage of the annotated glycan structures was used as final output of the glycomic analysis. The enhanced angiogenic response described in Chapter Four was validated by the assessment of the variation in the activation z-scores of the main angiogenic-related pathways (VEGF, HGF, ErbB and endothelin signalling). In addition, immunofluorescence for α-SMA and its stereological quantification indicated a higher number of arterioles in the ELRs-treated ischemic cores. In such a microenvironment, increased recruitment of $CD163^+$ cells, usually defined as a marker of pro-healing macrophages, supported the other findings. Transcriptomic analysis at day 21 post-injection did not highlight either pro- nor anti-inflammatory effect of the ELRs-based treatment. The higher expression of α-Gal was detected by lectin microarray and histochemistry in the hydrogel-treated ischemic core (Chapter Four) and validated here by quantifying the relative percentage of terminal α-Gal after LS-ESI-MS/MS analysis on the *N*- and *O*-glycan fractions. The retention of this marker was region-specific since its presence decreased in the border zone of the same treated animals, even if to a lesser extent than in the untreated group. Finally, GATA4 emerged as the top upstream regulator in IPA® analysis on transcriptomic data and pathways linked to cellular survival were significantly detected among the canonical pathways also in the IPA®-analysed proteomic dataset. Indeed, $GATA4^+$ cardiomyocytes were found to be more preserved in the border zone of the infarct 21 days after the injection of the hydrogel. Key sensors of cellular integrity like mitochondria showed more physiological-like parameters at that timepoint. Thus, the proposed mechanism of action of hydrogel starts with the recruitment of macrophages and endothelial cells which surround and penetrate its matrix to form a vasculature network able to expand in a less fibrotic microenvironment. As a consequence, cardiomyocytes that survived to the early ischemic damage benefit the less fibrotic and more perfused nature of the contiguous ischemic core and show a better response both quantitatively (number of $GATA^+$ cells) and qualitatively (mitochondrial volume and membrane surface area). As a final result, the combination of a beneficially remodelled ischemic core and a more physiological border zone led to a recovery in cardiac function, indicated by the return of EF levels back to the pre-MI condition (Figure 6.2).

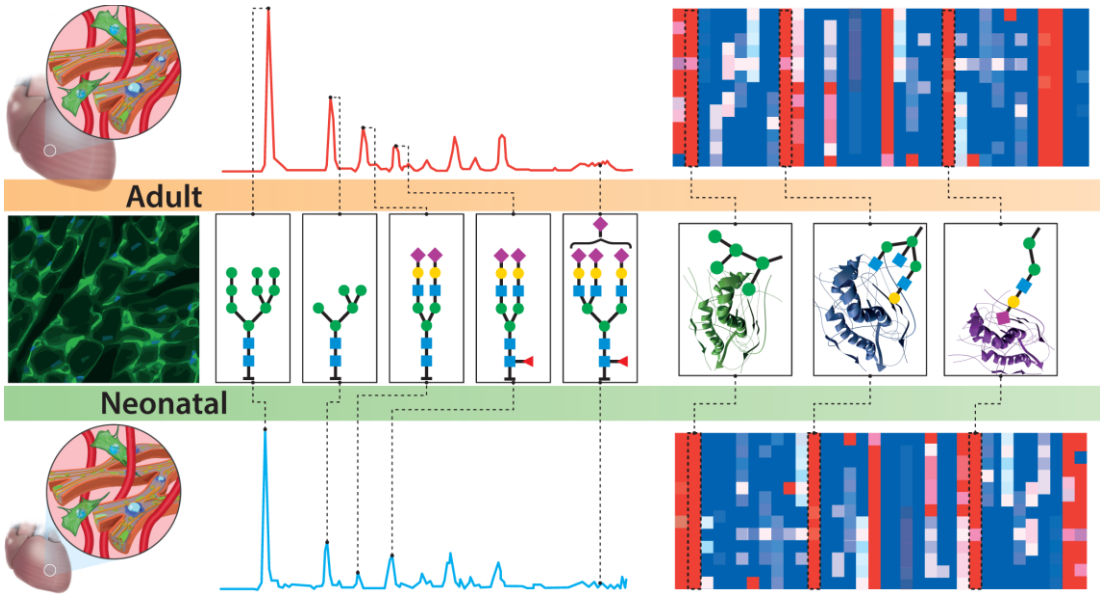

Figure 6.1 Graphical abstract of different glycosylation seen between neonatal and adult myocardial tissue (Chapter Two). The experimental flow included lectin histochemistry, PGC LC-ESI-MS/MS analyses (spectra) and lectin microarrays (heat-maps) to identify the glycan structures present in adult and neonatal myocardial tissues.

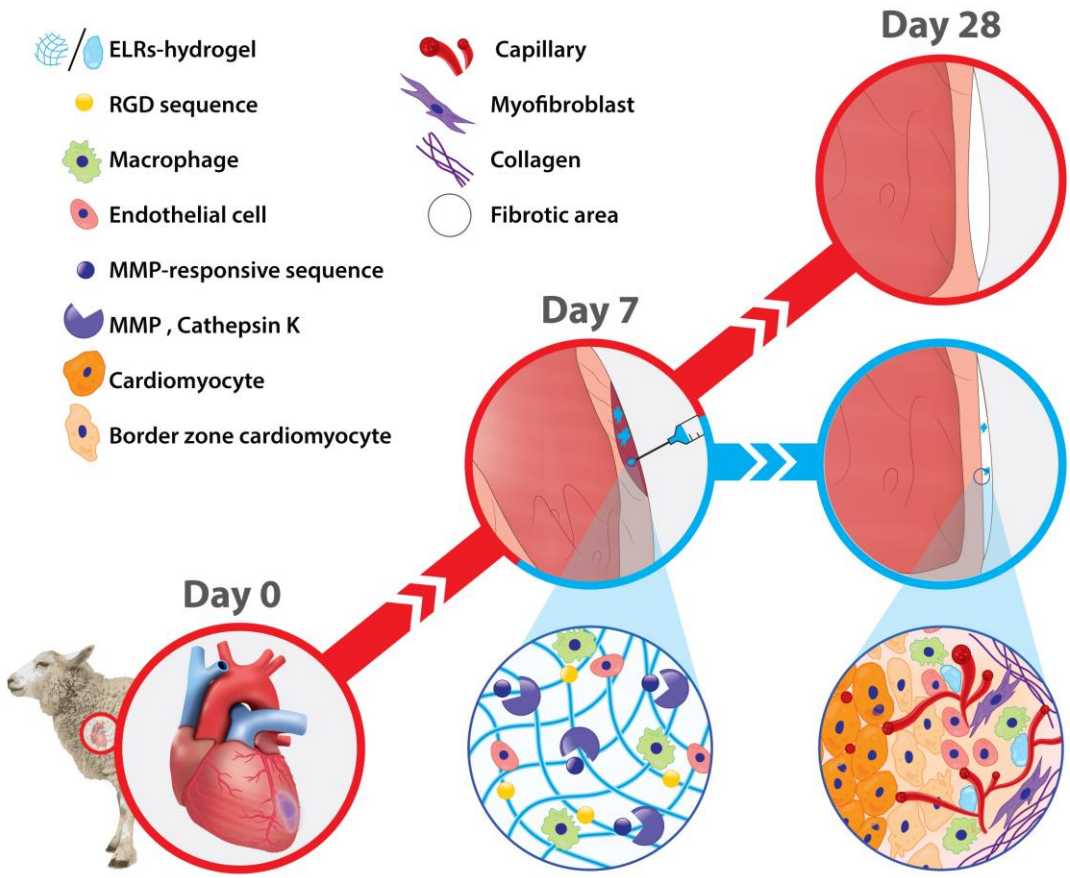

Figure 6.2 Schematic representation of the improved remodelling observed in the ELRs-treated group (Chapter Four and Five). The ischemic core of the infarcted region is less fibrotic and more perfused by a capillary network 21 days after the multiple intra-myocardial injection of the ELRs-based hydrogel. This influences the preservation of a more physiological border zone, populated by a higher number of $GATA4^{+}$ cardiomyocytes.

6.3 Limitations

6.3.1 Chapter Two - Distinct differences in cellular membrane glycosylation reflect the regeneration potential of neonatal myocardial tissue

The first part of this study showed a consistent glycosylation expressed on different species of rat and also across the left and right ventricles. Since the study was based on the tissue collection of hearts extracted from animals dedicated to studies designed from other research groups, and therefore pertaining to different experimental hypotheses, it was not possible to maintain the same gender in all the analysed samples in this first part of the study. However, these differences in the gender carried by the harvested animals did not result in overt changes of the glycosylation profile at the level of analysis performed. Nevertheless, consistency in the gender of the samples to be analysed will be a crucial requirement if studies were to focus on the glycan expression in serum samples [Ding, Ercan].

The glycomic LC-ESI-MS/MS analysis was performed using samples pooled from three individual animals. Protein concentration was similar across the samples within the same group, but the final protein concentration of the pooled sample was higher in the adult than in the neonatal sample. This generally does not have an effect on the number of *N*- and *O*-glycans detected as long as both the samples contain enough protein to release comparable *N*- and *O*-linked glycans during the processing steps. As seen in the final relative percentages, certain *N*- and *O*-glycans were detected only in the three-day-old sample, confirming that this did not affect the outcome of this study. However, if the relative abundance of a specific putative structure needs to be compared between two groups, the same concentration of protein is highly recommended before starting the processing to release *N*- and *O*-glycans.

6.3.2 Chapter Three – An ovine model of non-transmural myocardial infarction

In this chapter an ovine model of non-transmural MI was established by validations at functional, histological and protein level. Specifically, this model more closely resembles the majority of the critical clinical cases that are not STEMI with full-thickness infarcts. Consistently, seven days after the surgical induction of MI an average decrease in EF by 6.3% was seen, without the exclusion of any animal that was operated on and survived to the timepoint from this analysis. Nevertheless, in

the cardiovascular field imaging, techniques like MRI are adopted not only for clinical purposes but also in experimental studies since they can provide a precise measurement of the infarct size [Frey, Takehara, Johnston, Dubois]. Unfortunately, it was not possible to perform this imaging analysis in this study as all the experiments were carried out in a new pre-clinical facility. Despite this limitation, further analysis of the echocardiography measurements recorded will allow the quantification of additional parameters which are not presented in this thesis such as wall motion index, stroke volume, end-diastolic and end-systolic volume.

All the surgeries to induce MI were done after the opening of the chest cavity, a procedure named thoracotomy. This was required to perform both the ligations and to inject the hydrogel from the epicardium through the myocardial wall. However, this set-up is not an ideal clinical intervention. The administration of the ELRs-based hydrogel could be further optimised by a minimally-invasive procedure like a catheter endocardial delivery. As outlined in section 6.4.2, the physico-chemical characteristics of the hydrogel will need to be tested and probably re-optimised for this different delivery method. A crucial requirement will be the assessment of the consistency in the volume and dispersion path of hydrogel injected in the infarcted ventricular wall.

6.3.3 Chapter Four - Elastin-like recombinamers-based hydrogel modulates the post-ischemic remodelling in a clinically-relevant model of myocardial infarction

An ELRs-based hydrogel was tested for its efficacy in limiting the maladaptive remodelling which occurs in the post-ischemic cardiac microenvironment. A clinically-relevant ovine model of non-transmural MI was used for the assessment of the tissue and functional response 21 days after multiple intra-myocardial injections of the hydrogel. The significantly reduced fibrosis and enhanced angiogenesis seen at this endpoint can be compared with the outcome of preclinical studies using different either acellular or functionalised hydrogel systems, even though an additional evaluation at a further endpoint could have answered potential doubts regarding the long-term efficacy of the ELRs-hydrogel treatment. In particular, focusing on the angiogenic effect seen in the ischemic core, a later endpoint up to two months after the injection of the hydrogel would have been informative for evaluating the stage of

the "angiogenic switch" in such chronic condition. This study did not hypothesise the recruitment of progenitor cells in the injection region since RNA-sequencing and histological analyses highlighted a "conservative" response rather than a regenerative one. Despite the initial encouraging results related to cardiac stem cells and comparable cellular-based approaches, recent meta-analyses scaled down the actual functional effect of those treatments [Orlic, Gyöngyösi 2018, Wollert, Afzal, Fisher]. The alternative solution - now being pursued [Takita, Guo] - of increasing the number of cellular-based injections to prolong the paracrine effects of the marginal percentage (around 1-2%) of stem cells which survive in the ischemic microenvironment does not address the fundamental limitation of that approach. However, an impactful and durable benefit for the cardiac environment depends on the introduction of ECM components that can biomechanically interact with the endogenous cellular populations which are already recruited during the proliferative and remodelling phases. Therefore, further studies can reveal whether specific cellular populations, apart from the remodelling macrophages and the endothelial cells, are responsible for the improvements seen in the current work. Finally, the number of injections (three) and the total volume of hydrogel (1.5 ml) injected per animal aimed to minimise any injury due to the needle and to provide a proof-of-concept using a total volume which is relatively low for a large animal.

6.3.4 Chapter Five - Transcriptomic, proteomic and glycomic analyses to reveal the mechanism of modulation of post-ischemic remodelling by an elastin-based hydrogel

In this chapter the modulation of the ischemic remodelling by the ELRs-hydrogel (Chapter Four) was further investigated by high-throughput analyses. The identification of an upstream regulator associated with the hydrogel-dependent response (GATA4) was validated by immunofluorescence in the border region of the infarct. There, a higher retention of $GATA4^{+}$ cardiomyocytes and their preserved mitochondrial integrity have the potential to improve cardiac function. Late transcriptomic analysis on the samples harvested 21 days after the hydrogel injection indicated a trend of activation in the z-scores (VEGF, HGF, ErbB and endothelin signalling) which reached statistical significance only in the case of endothelin and was close to it in HGF signalling ($p=0.06$). This can be disputed as a sign of a non-

durable angiogenic response, but stereological quantification of α-SMA arterioles confirmed a higher perfusion in the ELRs-treated ischemic core. Nevertheless, in the proposed mechanism of action of the hydrogel, its potential mechanotransduction-dependent role was not included. In other words, the overall improvements in fibrosis and angiogenesis are striking and consistent, but the details of the cascade of molecular signalling which finally led to those outcomes were not fully elucidated. To address this question, additional earlier timepoints post-injection need to be included to assess the tissue response to this treatment. Moreover, the inclusion in the panel of analysis of fluorescence-activated cell sorting (FACS) after RNA isolation will contribute to the characterisation of the cellular populations involved and potentially interacting with the hydrogel.

6.4 Future directions

6.4.1 Analysis of glycosylation in iPSCs-derived cardiomyocytes

Glycans play a crucial role in cell-cell and cell-ECM communication and are widely expressed both in the ECM and on cellular membranes in the myocardial microenvironment [Parker, Montpetit, Huynh]. An extensive evaluation of glycosylation in relation to cancer metastasis led to the identification of precise mechanisms which enable the abnormal behaviour of growth factor receptor signalling pathways such as VEGFR2, c-MET, FGFR and ERBB [Markowska, Hsieh 2008, Croci, Merlin, Chu]. In contrast, the understanding of the role of glycans in wound healing, including ischemic damage still requires solid *in vitro* proof-of-principle studies. Among the second generation of stem cell-based treatments there are induced pluripotent stem cells (iPSCs) which became one of the most attractive therapeutic approaches since the possibility to reprogram pluripotency from adult human cells was demonstrated [Takahashi]. Therefore, iPSC-derived induced cardiomyocytes (iPSC-CMs) have been studied in cardiovascular tissue engineering [Zimmermann, Lian, Fonoudi]. The main limitation of this therapeutic strategy is the difficulty in mimicking the physiological electrical and mechanical properties of cardiomyocytes [Huang], and recently engineered platforms and imaging methods are addressing this issue [Nunes, Ribeiro]. Previous studies highlighted the importance of sialic acids in the regulation of Na^+ and K^+ voltage-gated ion channels

in the alterations of the cardiac electrical signalling coupled with arrhytmias [Montpetit, Ufret-Vincenty]. In light of these considerations, glycomic analyses of iPSC-CMs and adult healthy cardiomyocytes could identify which specific glycan structures are absent in the iPSC-CMs that have impaired electrical and mechanical properties. Moreover, after the regulation of the glyco-enzymes which are responsible for those alterations in the cellular membrane glycosylation, these engineered iPSC-CMs could be further improved in their subcellular organisation and electrophysiological behaviour in a recently established platform for their maturation, named *Biowire* [Nunes], before their final implantation *in vivo* through patch-based systems [Montgomery, Radisic 2016].

6.4.2 Endocardial delivery of a ELRs-based hydrogel for the treatment of myocardial infarction

The results reported in this thesis (Chapters Four and Five) have shown the efficacy of the intra-myocardial injection of elastin-like recombinamers (ELR)-based hydrogel in reducing fibrosis, enhancing angiogenesis and preserving the integrity of cardiomyocytes located in the border zone of the infarct. Briefly, the ELR-based hydrogel drives the combinatorial effect of being a soft barrier against fibrotic scarring and a molecular trigger for the recruitment and infiltration of endothelial cells and remodelling macrophages. A clinically relevant ovine model of focal infarcts was used to establish this efficacy. A continuation of this work will be focused on taking these initial results to the next phase to fulfil all the requirements for a clinical phase I trial. The hydrogel system will be adapted for a minimally invasive delivery, that is by an endocardial catheter procedure (Figure 6.3).

Firstly, the scale-up of the ELRs hydrogel will be carried out commercially by using a cost-effective bioreactor system. In addition, the design of an endocardial delivery of the current ELRs-hydrogel formulation needs to be made compatible with the gelling time of the hydrogel and its haemocompatibility tested. Secondly, the rheological and degradation properties need to be consistent after the scale up process. Since the final aim is to complete a clinical dossier for a phase I study, shelf-life studies will need to be conducted and all the production and application steps should be compliant with good manufacturing practice (GMP). Tissue and

functional response to the hydrogel endocardial delivery will include the assessment of fibrosis by Masson's Trichrome, electron microscopy and Raman analyses. The long-term angiogenic response will be evaluated both 21 days later and two months after the injection and quantified by stereological methods (immunostaining and lectin histochemistry). Finally, the functional response will need to be analysed by both echocardiographic and magnetic resonance imaging.

6.4.3 Evaluation of the effect of ELRs-based hydrogel on macrophage polarisation

Macrophages have a pivotal role during the inflammatory, proliferation and remodelling phases after MI [Frantz]. Most importantly, the sequential recruitment of pro-inflammatory and pro-healing populations of macrophages avoids the persistence of a chronic inflammatory state in the cardiac tissue. Therefore, the identification of markers and methods to precisely characterise these cellular populations is a useful step in evaluating their possible interaction with therapeutic strategies [Jablonski, Barros, Raimondo]. In light of the effect of an ELRs-based hydrogel injection seven-days after MI reported in this thesis, further work could be focused on the detailed molecular crosstalk at the interface between the hydrogel matrix and the ischemic tissue. The improved healing effect carried by the introduction of the hydrogel in this pathological scenario could be closely connected with a precise regulation of the transition between the pro-inflammatory to the pro-healing phenotype of macrophages.

The ELRs-based hydrogel evaluated for its efficacy in the current study possesses RGD motifs, which do not represent a specific binding sequence for either of the macrophage types. Nonetheless, the porous structure of the hydrogel, allows cellular invasion and becomes a spatial confinement for all the cellular types, including macrophages. Interestingly, a recent study by the Vogel's group elucidated the effect induced by different conditions of spatial confinement, including microporous structures, on the inhibition of the pro-inflammatory state of macrophages [Jain]. Appropriate *in vitro* studies can investigate the modulation of the ELRs-hydrogel porous matrix on the expression of canonical pro-inflammatory markers such as IL-6, CXCL9, IL-1β, and iNOS in lipopolysaccharide (LPS)-induced inflammatory conditions (Figure 6.4). Depending on the preliminary outcome, further optimisation

of the porous hydrogel matrix can determine the preferred matrix which would maximise the downregulation of the pro-inflammatory response. Upon *in vitro* evidence of this hypothesised mechanism, the ELRs-based hydrogel can be tested in a preclinical model during the first week after the induction of MI to evaluate any significant effect on the inflammatory phase and following remodelling. One of the crucial points will be to assess the impact of a potentially drastic reduction in fibrosis (even above the approximated 50% decrease reported in this thesis) with the long-term stability of the wall and risk of cardiac rupture, as evaluated when targeting macrophages post-MI [Takamura, Wang 2017].

6.4.4 Glyco-functionalised ELRs-based hydrogel for the treatment of myocardial infarction

One of the bottlenecks in cardiovascular tissue engineering is the enhancement of a stable and non-leaky vasculature network to perfuse the ischemic zones [Kreuger, Carmeliet]. Several studies focused on combinatorial approaches including VEGF, FGF and PDGF; however, an effective treatment did not reach success through the clinical phases [Kreuger]. Moreover, protein-based therapies have the intrinsic limitation of short half-lives and limited availability at the desired site. In contrast, the requirement of glycosaminoglycans (GAGs) for capillary branching and GAGs-growth factor interactions such as heparan sulphate (HS) and VEGF are well known [Ruhrberg, Gerhardt]. Nonetheless, the complexity in the synthesis of mimetics of extended and unbranched glycans such as HS and chondroitin sulphate (CS) hinders their potential as therapeutic options. In this thesis, an angiogenic response was seen 21 days after the ELRs-hydrogel injection and it was associated with the higher expression of one specific glycan epitope, α-galactose (α-Gal). The presence of this motif, validated also by LS-ESI-MS/MS, reflects the migration and sprouting of endothelial cells to form a capillary network, as the result of an endogenous response extended by the presence of the porous hydrogel matrix. Previous studies by Galili's group tested α-Gal-coated nanospheres and liposomes and observed accelerated wound healing [Wigglesworth, Galili 2010]. Importantly, the well-known immunogenic reaction to this glycan epitope in this pathological scenario is prevented due to the lack of its presentation on the cellular membranes. Specifically, in species (humans, apes and old world monkeys) and experimental conditions

(knock-out for α1,3 galactosyltransferase enzyme) where anti-α-Gal IgGs are present, they bind to α-Gal-coated nanoparticles, activate the complement system and recruit macrophages by the formation of complement cleavage chemotactic peptides [Galili 2015]. Finally, the interaction between the Fc portion of the anti-α-Gal IgG and the FcγR on macrophages activates the latter ones to secrete cytokines and growth factors to promote the endogenous healing [Galili 2015]. A further study based on this described mechanism and the expression of this epitope in an angiogenic response would include the functionalisation of the ELRs-based hydrogel with α-Gal to extend its pro-healing effect throughout the hydrogel degradation time in the ischemic environment.

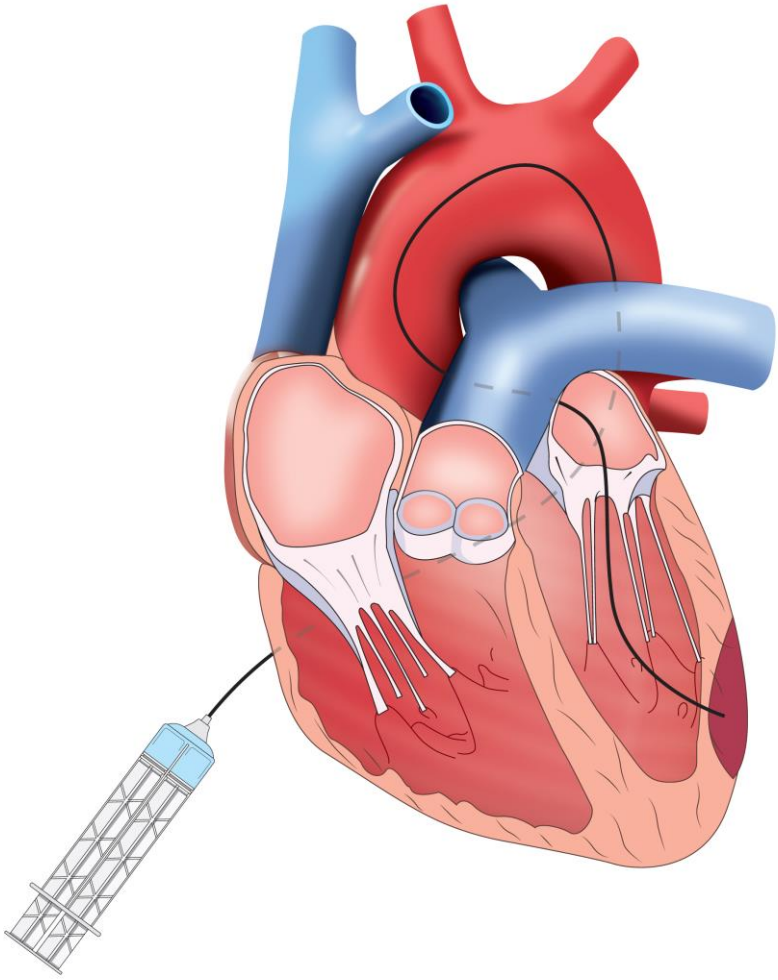

Figure 6.3 Endocardial delivery of the ELRs-based hydrogel in the infarcted left ventricular wall. ELRs-based hydrogel could be optimised for minimally invasive endocardial delivery to the left ventricular wall. A dual-barrel mixer prototype will need to be designed to ensure appropriate conditions to allow initial crosslinking of the ELRs. The ELRs-based hydrogel will need to be injected without being influenced by the transport through the catheter.

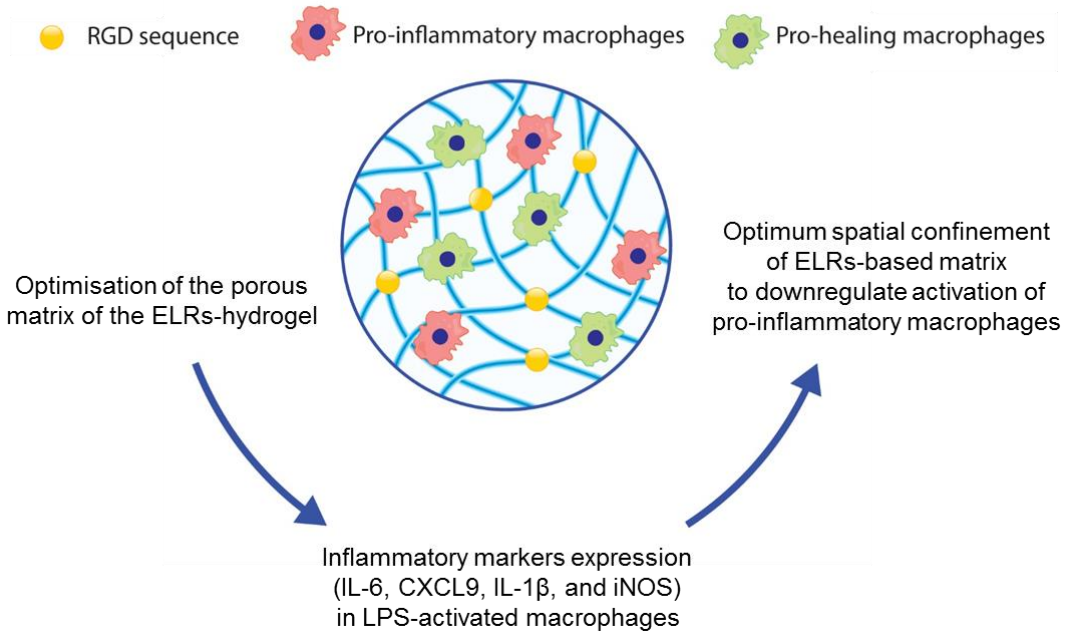

Figure 6.4 Proposed study evaluating the effect of ELRs-based hydrogel matrix on macrophage polarisation. ELRs-based hydrogel porous matrix could be optimised to evaluate its spatial confinement effect on the expression of inflammatory markers in macrophages. This further study would also investigate if this matrix might favour a swift of macrophages towards a pro-healing state.

6.5 References

- Afzal MR, Samanta A, Shah ZI, Jeevanantham V, Abdel-Latif A, Zuba-Surma EK, Dawn B. Adult bone marrow cell therapy for ischemic heart disease: evidence and insights from randomized controlled trials. Circ Res. 2015 Aug 28;117(6):558-75
- Barros MH, Hauck F, Dreyer JH, Kempkes B, Niedobitek G. Macrophage polarisation: an immunohistochemical approach for identifying M1 and M2 macrophages. PLoS One. 2013 Nov 15;8(11):e80908
- Bassat E, Mutlak YE, Genzelinakh A, Shadrin IY, Baruch Umansky K, Yifa O, Kain D, Rajchman D, Leach J, Riabov Bassat D, Udi Y, Sarig R, Sagi I, Martin JF, Bursac N, Cohen S, Tzahor E. The extracellular matrix protein agrin promotes heart regeneration in mice. Nature. 2017 Jul 13;547(7662):179-184
- Carmeliet P, Jain RK. Molecular mechanisms and clinical applications of angiogenesis. Nature. 2011 May 19;473(7347):298-307
- Castellanos MI, Zenses AS, Grau A, Rodríguez-Cabello JC, Gil FJ, Manero JM, Pegueroles M. Biofunctionalization of REDV elastin-like recombinamers improves endothelialization on CoCr alloy surfaces for cardiovascular applications. Colloids Surf B Biointerfaces. 2015 Mar 1;127:22-32
- Chen CH, Chang MY, Wang SS, Hsieh PC. Injection of autologous bone marrow cells in hyaluronan hydrogel improves cardiac performance after infarction in pigs. Am J Physiol Heart Circ Physiol. 2014 Apr 1;306(7):H1078-86
- Christman KL, Vardanian AJ, Fang Q, Sievers RE, Fok HH, Lee RJ. Injectable fibrin scaffold improves cell transplant survival, reduces infarct expansion, and induces neovasculature formation in ischemic myocardium. J Am Coll Cardiol. 2004 Aug 4;44(3):654-60
- Chu C, Bottaro DP, Betenbaugh MJ, Shiloach J. Stable ectopic expression of ST6GALNAC5 induces autocrine MET activation and anchorage-independence in MDCK Cells. PLoS One. 2016 Feb 5;11(2):e0148075
- Croci DO, Cerliani JP, Dalotto-Moreno T, Méndez-Huergo SP, Mascanfroni ID, Dergan-Dylon S, Toscano MA, Caramelo JJ, García-Vallejo JJ, Ouyang J, Mesri EA, Junttila MR, Bais C, Shipp MA, Salatino M, Rabinovich GA. Glycosylation-dependent lectin-receptor interactions preserve angiogenesis in anti-VEGF refractory tumors. Cell. 2014 Feb 13;156(4):744-58

- Dewald O, Zymek P, Winkelmann K, Koerting A, Ren G, Abou-Khamis T, Michael LH, Rollins BJ, Entman ML, Frangogiannis NG. CCL2/Monocyte Chemoattractant Protein-1 regulates inflammatory responses critical to healing myocardial infarcts. Circ Res. 2005 Apr 29;96(8):881-9
- Ding N, Nie H, Sun X, Sun W, Qu Y, Liu X, Yao Y, Liang X, Chen CC, Li Y. Human serum N-glycan profiles are age and sex dependent. Age Ageing. 2011 Sep;40(5):568-75
- Dubois C, Liu X, Claus P, Marsboom G, Pokreisz P, Vandenwijngaert S, Dépelteau H, Streb W, Chaothawee L, Maes F, Gheysens O, Debyser Z, Gillijns H, Pellens M, Vandendriessche T, Chuah M, Collen D, Verbeken E, Belmans A, Van de Werf F, Bogaert J, Janssens S. Differential effects of progenitor cell populations on left ventricular remodeling and myocardial neovascularization after myocardial infarction. J Am Coll Cardiol. 2010 May 18;55(20):2232-43
- Ercan A, Kohrt WM, Cui J, Deane KD, Pezer M, Yu EW, Hausmann JS, Campbell H, Kaiser UB, Rudd PM, Lauc G, Wilson JF, Finkelstein JS, Nigrovic PA. Estrogens regulate glycosylation of IgG in women and men. JCI Insight. 2017 Feb 23;2(4):e89703
- Fisher SA, Zhang H, Doree C, Mathur A, Martin-Rendon E. Stem cell treatment for acute myocardial infarction. Cochrane Database Syst Rev. 2015 Sep 30;(9):CD006536
- Fonoudi H, Ansari H, Abbasalizadeh S, Larijani MR, Kiani S, Hashemizadeh S, Zarchi AS, Bosman A, Blue GM, Pahlavan S, Perry M, Orr Y, Mayorchak Y, Vandenberg J, Talkhabi M, Winlaw DS, Harvey RP, Aghdami N, Baharvand H. A universal and robust integrated platform for the scalable production of human cardiomyocytes from pluripotent stem cells. Stem Cells Transl Med. 2015 Dec;4(12):1482-94
- Frangogiannis NG. The extracellular matrix in myocardial injury, repair, and remodeling. J Clin Invest. 2017 May 1;127(5):1600-1612
- Frangogiannis NG. Cardiac fibrosis: Cell biological mechanisms, molecular pathways and therapeutic opportunities. Mol Aspects Med. 2019 Feb;65:70-99
- Frantz S, Nahrendorf M. Cardiac macrophages and their role in ischaemic heart disease. Cardiovasc Res. 2014 May 1;102(2):240-8

- Frey N, Linke A, Süselbeck T, Müller-Ehmsen J, Vermeersch P, Schoors D, Rosenberg M, Bea F, Tuvia S, Leor J. Intracoronary delivery of injectable bioabsorbable scaffold (IK-5001) to treat left ventricular remodeling after ST-elevation myocardial infarction: a first-in-man study. Circ Cardiovasc Interv. 2014 Dec;7(6):806-12
- Fujitani N, Furukawa J, Araki K, Fujioka T, Takegawa Y, Piao J, Nishioka T, Tamura T, Nikaido T, Ito M, Nakamura Y, Shinohara Y. Total cellular glycomics allows characterizing cells and streamlining the discovery process for cellular biomarkers. Proc Natl Acad Sci U S A. 2013 Feb 5;110(6):2105-10
- Galili U, Wigglesworth K, Abdel-Motal UM. Accelerated healing of skin burns by anti-Gal/alpha-gal liposomes interaction. Burns. 2010 Mar;36(2):239-51
- Galili U. Acceleration of wound healing by α-gal nanoparticles interacting with the natural anti-Gal antibody. J Immunol Res. 2015;2015:589648
- Gerhardt H, Golding M, Fruttiger M, Ruhrberg C, Lundkvist A, Abramsson A, Jeltsch M, Mitchell C, Alitalo K, Shima D, Betsholtz C. VEGF guides angiogenic sprouting utilizing endothelial tip cell filopodia. J Cell Biol. 2003 Jun 23;161(6):1163-77
- Global Health Estimates 2016: Deaths by Cause, Age, Sex, by Country and by Region, 2000-2016. Geneva, World Health Organization; 2018
- Gonzalez PS, O'Prey J, Cardaci S, Barthet VJA, Sakamaki JI, Beaumatin F, Roseweir A, Gay DM, Mackay G, Malviya G, Kania E, Ritchie S, Baudot AD, Zunino B, Mrowinska A, Nixon C, Ennis D, Hoyle A, Millan D, McNeish IA, Sansom OJ, Edwards J, Ryan KM. Mannose impairs tumour growth and enhances chemotherapy. Nature. 2018 Nov;563(7733):719-723
- Guo Y, Wysoczynski M, Nong Y, Tomlin A, Zhu X, Gumpert AM, Nasr M, Muthusamy S, Li H, Book M, Khan A, Hong KU, Li Q, Bolli R. Repeated doses of cardiac mesenchymal cells are therapeutically superior to a single dose in mice with old myocardial infarction. Basic Res Cardiol. 2017 Mar;112(2):18
- Gyöngyösi M, Haller PM, Blake DJ, Martin Rendon E. Meta-analysis of cell therapy studies in heart failure and acute myocardial infarction. Circ Res. 2018 Jul 6;123(2):301-308
- Gyöngyösi M, Wojakowski W, Lemarchand P, Lunde K, Tendera M, Bartunek J, Marban E, Assmus B, Henry TD, Traverse JH, Moyé LA, Sürder D, Corti R,

Huikuri H, Miettinen J, Wöhrle J, Obradovic S, Roncalli J, Malliaras K, Pokushalov E, Romanov A, Kastrup J, Bergmann MW, Atsma DE, Diederichsen A, Edes I, Benedek I, Benedek T, Pejkov H, Nyolczas N, Pavo N, Bergler-Klein J, Pavo IJ, Sylven C, Berti S, Navarese EP, Maurer G; ACCRUE Investigators. Meta-Analysis of Cell-based CaRdiac stUdiEs (ACCRUE) in patients with acute myocardial infarction based on individual patient data. Circ Res. 2015 Apr 10;116(8):1346-60

- Hasehira K, Tateno H, Onuma Y, Ito Y, Asashima M, Hirabayashi J. Structural and quantitative evidence for dynamic glycome shift on production of induced pluripotent stem cells. Mol Cell Proteomics. 2012 Dec;11(12):1913-23
- Hsieh SH, Ying NW, Wu MH, Chiang WF, Hsu CL, Wong TY, Jin YT, Hong TM, Chen YL. Galectin-1, a novel ligand of neuropilin-1, activates VEGFR-2 signaling and modulates the migration of vascular endothelial cells. Oncogene. 2008 Jun 12;27(26):3746-53
- Huang NF, Serpooshan V, Morris VB, Sayed N, Pardon G, Abilez OJ, Nakayama KH, Pruitt BL, Wu SM, Yoon YS, Zhang J, Wu JC. Big bottlenecks in cardiovascular tissue engineering. Commun Biol. 2018 Nov 21;1:199
- Huynh MB, Morin C, Carpentier G, Garcia-Filipe S, Talhas-Perret S, Barbier Chassefière V, van Kuppevelt TH, Martelly I, Albanese P, Papy-Garcia D. Age-related changes in rat myocardium involve altered capacities of glycosaminoglycans to potentiate growth factor functions and heparin sulfate-altered sulfation. J Biol Chem. 2012 Mar 30;287(14):11363-73
- Ifkovits JL, Tous E, Minakawa M, Morita M, Robb JD, Koomalsingh KJ, Gorman JH 3rd, Gorman RC, Burdick JA. Injectable hydrogel properties influence infarct expansion and extent of postinfarction left ventricular remodeling in an ovine model. Proc Natl Acad Sci U S A. 2010 Jun 22;107(25):11507-12
- Jablonski KA, Amici SA, Webb LM, Ruiz-Rosado Jde D, Popovich PG, Partida-Sanchez S, Guerau-de-Arellano M. Novel markers to delineate murine M1 and M2 macrophages. PLoS One. 2015 Dec 23;10(12):e0145342
- Jain N, Vogel V. Spatial confinement downsizes the inflammatory response of macrophages. Nat Mater. 2018 Dec;17(12):1134-1144

- Johnston PV, Sasano T, Mills K, Evers R, Lee ST, Smith RR, Lardo AC, Lai S, Steenbergen C, Gerstenblith G, Lange R, Marbán E. Engraftment, differentiation, and functional benefits of autologous cardiosphere-derived cells in porcine ischemic cardiomyopathy. Circulation. 2009 Sep 22;120(12):1075-83, 7 p following 1083
- Kozel BA, Rongish BJ, Czirok A, Zach J, Little CD, Davis EC, Knutsen RH, Wagenseil JE, Levy MA, Mecham RP. Elastic fiber formation: a dynamic view of extracellular matrix assembly using timer reporters. J Cell Physiol. 2006 Apr;207(1):87-96
- Kreuger J, Phillipson M. Targeting vascular and leukocyte communication in angiogenesis, inflammation and fibrosis. Nat Rev Drug Discov. 2016 Feb;15(2):125-42
- Kühn B, del Monte F, Hajjar RJ, Chang YS, Lebeche D, Arab S, Keating MT. Periostin induces proliferation of differentiated cardiomyocytes and promotes cardiac repair. Nat Med. 2007 Aug;13(8):962-9
- Landa N, Miller L, Feinberg MS, Holbova R, Shachar M, Freeman I, Cohen S, Leor J. Effect of injectable alginate implant on cardiac remodeling and function after recent and old infarcts in rat. Circulation. 2008 Mar 18;117(11):1388-96
- Le LV, Mohindra P, Fang Q, Sievers RE, Mkrtschjan MA, Solis C, Safranek CW, Russell B, Lee RJ, Desai TA. Injectable hyaluronic acid based microrods provide local micromechanical and biochemical cues to attenuate cardiac fibrosis after myocardial infarction. Biomaterials. 2018 Jul;169:11-21
- Leor J, Tuvia S, Guetta V, Manczur F, Castel D, Willenz U, Petneházy O, Landa N, Feinberg MS, Konen E, Goitein O, Tsur-Gang O, Shaul M, Klapper L, Cohen S. Intracoronary injection of in situ forming alginate hydrogel reverses left ventricular remodeling after myocardial infarction in Swine. J Am Coll Cardiol. 2009 Sep 8;54(11):1014-23
- Lian X, Hsiao C, Wilson G, Zhu K, Hazeltine LB, Azarin SM, Raval KK, Zhang J, Kamp TJ, Palecek SP. Robust cardiomyocyte differentiation from human pluripotent stem cells via temporal modulation of canonical Wnt signaling. Proc Natl Acad Sci U S A. 2012 Jul 3;109(27):E1848-57

- Lindsey ML, Zamilpa R. Temporal and spatial expression of matrix metalloproteinases and tissue inhibitors of metalloproteinases following myocardial infarction. Cardiovasc Ther. 2012 Feb;30(1):31-41
- Markowska AI, Liu FT, Panjwani N. Galectin-3 is an important mediator of VEGF- and bFGF-mediated angiogenic response. J Exp Med. 2010 Aug 30;207(9):1981-93
- Merlin J, Stechly L, de Beaucé S, Monté D, Leteurtre E, van Seuningen I, Huet G, Pigny P. Galectin-3 regulates MUC1 and EGFR cellular distribution and EGFR downstream pathways in pancreatic cancer cells. Oncogene. 2011 Jun 2;30(22):2514-25
- Mithieux SM, Wise SG, Weiss AS. Tropoelastin--a multifaceted naturally smart material. Adv Drug Deliv Rev. 2013 Apr;65(4):421-8
- Mohd Isa IL, Abbah SA, Kilcoyne M, Sakai D, Dockery P, Finn DP, Pandit A. Implantation of hyaluronic acid hydrogel prevents the pain phenotype in a rat model of intervertebral disc injury. Sci Adv. 2018 Apr 4;4(4):eaaq0597
- Montgomery M, Ahadian S, Davenport Huyer L, Lo Rito M, Civitarese RA, Vanderlaan RD, Wu J, Reis LA, Momen A, Akbari S, Pahnke A, Li RK, Caldarone CA, Radisic M. Flexible shape-memory scaffold for minimally invasive delivery of functional tissues. Nat Mater. 2017 Oct;16(10):1038-1046
- Montpetit ML, Stocker PJ, Schwetz TA, Harper JM, Norring SA, Schaffer L, North SJ, Jang-Lee J, Gilmartin T, Head SR, Haslam SM, Dell A, Marth JD, Bennett ES. Regulated and aberrant glycosylation modulate cardiac electrical signaling. Proc Natl Acad Sci U S A. 2009 Sep 22;106(38):16517-22
- Nunes SS, Miklas JW, Liu J, Aschar-Sobbi R, Xiao Y, Zhang B, Jiang J, Massé S, Gagliardi M, Hsieh A, Thavandiran N, Laflamme MA, Nanthakumar K, Gross GJ, Backx PH, Keller G, Radisic M. Biowire: a platform for maturation of human pluripotent stem cell-derived cardiomyocytes. Nat Methods. 2013 Aug;10(8):781-7
- Orlic D, Kajstura J, Chimenti S, Jakoniuk I, Anderson SM, Li B, Pickel J, McKay R, Nadal-Ginard B, Bodine DM, Leri A, Anversa P. Bone marrow cells regenerate infarcted myocardium. Nature. 2001 Apr 5;410(6829):701-5
- Parker BL, Palmisano G, Edwards AV, White MY, Engholm-Keller K, Lee A, Scott NE, Kolarich D, Hambly BD, Packer NH, Larsen MR, Cordwell SJ.

Quantitative N-linked glycoproteomics of myocardial ischemia and reperfusion injury reveals early remodeling in the extracellular environment. Mol Cell Proteomics. 2011 Aug;10(8):M110.006833

- Paszek MJ, DuFort CC, Rossier O, Bainer R, Mouw JK, Godula K, Hudak JE, Lakins JN, Wijekoon AC, Cassereau L, Rubashkin MG, Magbanua MJ, Thorn KS, Davidson MW, Rugo HS, Park JW, Hammer DA, Giannone G, Bertozzi CR, Weaver VM. The cancer glycocalyx mechanically primes integrin-mediated growth and survival. Nature. 2014 Jul 17;511(7509):319-25
- Pedersen F, Butrymovich V, Kelbæk H, Wachtell K, Helqvist S, Kastrup J, Holmvang L, Clemmensen P, Engstrøm T, Grande P, Saunamäki K, Jørgensen E. Short- and long-term cause of death in patients treated with primary PCI for STEMI. J Am Coll Cardiol. 2014 Nov 18-25;64(20):2101-8
- Porrello ER, Mahmoud AI, Simpson E, Hill JA, Richardson JA, Olson EN, Sadek HA. Transient regenerative potential of the neonatal mouse heart. Science. 2011 Feb 25;331(6020):1078-80
- Radisic M, Christman KL. Materials science and tissue engineering: repairing the heart. Mayo Clin Proc. 2013 Aug;88(8):884-98
- Radisic M. Tissue engineering: Signals from within. Nat Mater. 2016 May 24;15(6):596-7
- Raimondo TM, Mooney DJ. Functional muscle recovery with nanoparticle-directed M2 macrophage polarization in mice. Proc Natl Acad Sci U S A. 2018 Oct 16;115(42):10648-10653
- Rao SV, Zeymer U, Douglas PS, Al-Khalidi H, White JA, Liu J, Levy H, Guetta V, Gibson CM, Tanguay JF, Vermeersch P, Roncalli J, Kasprzak JD, Henry TD, Frey N, Kracoff O, Traverse JH, Chew DP, Lopez-Sendon J, Heyrman R, Krucoff MW. Bioabsorbable intracoronary matrix for prevention of ventricular remodeling after myocardial infarction. J Am Coll Cardiol. 2016 Aug 16;68(7):715-23
- Ribeiro AJS, Schwab O, Mandegar MA, Ang YS, Conklin BR, Srivastava D, Pruitt BL. Multi-imaging method to assay the contractile mechanical output of micropatterned human iPSC-derived cardiac myocytes. Circ Res. 2017 May 12;120(10):1572-1583

- Rodríguez-Cabello JC, González de Torre I, Ibañez-Fonseca A, Alonso M. Bioactive scaffolds based on elastin-like materials for wound healing. Adv Drug Deliv Rev. 2018 Apr;129:118-133
- Ruhrberg C, Gerhardt H, Golding M, Watson R, Ioannidou S, Fujisawa H, Betsholtz C, Shima DT. Spatially restricted patterning cues provided by heparin-binding VEGF-A control blood vessel branching morphogenesis. Genes Dev. 2002 Oct 15;16(20):2684-98
- Sayed N, Liu C, Wu JC. Translation of human-induced pluripotent stem cells: From clinical trial in a dish to precision medicine. J Am Coll Cardiol. 2016 May 10;67(18):2161-2176
- Schwetz TA, Norring SA, Bennett ES. N-glycans modulate K(v)1.5 gating but have no effect on K(v)1.4 gating. Biochim Biophys Acta. 2010 Mar;1798(3):367-75
- Seif-Naraghi SB, Singelyn JM, Salvatore MA, Osborn KG, Wang JJ, Sampat U, Kwan OL, Strachan GM, Wong J, Schup-Magoffin PJ, Braden RL, Bartels K, DeQuach JA, Preul M, Kinsey AM, DeMaria AN, Dib N, Christman KL. Safety and efficacy of an injectable extracellular matrix hydrogel for treating myocardial infarction. Sci Transl Med. 2013 Feb 20;5(173):173ra25
- Singelyn JM, Sundaramurthy P, Johnson TD, Schup-Magoffin PJ, Hu DP, Faulk DM, Wang J, Mayle KM, Bartels K, Salvatore M, Kinsey AM, Demaria AN, Dib N, Christman KL. Catheter-deliverable hydrogel derived from decellularized ventricular extracellular matrix increases endogenous cardiomyocytes and preserves cardiac function post-myocardial infarction. J Am Coll Cardiol. 2012 Feb 21;59(8):751-63
- Staubli SM, Cerino G, Gonzalez De Torre I, Alonso M, Oertli D, Eckstein F, Glatz K, Rodríguez Cabello JC, Marsano A. Control of angiogenesis and host response by modulating the cell adhesion properties of an Elastin-Like Recombinamer-based hydrogel. Biomaterials. 2017 Aug;135:30-41
- Takahashi K, Tanabe K, Ohnuki M, Narita M, Ichisaka T, Tomoda K, Yamanaka S. Induction of pluripotent stem cells from adult human fibroblasts by defined factors. Cell. 2007 Nov 30;131(5):861-72
- Takamura M, Kurokawa K, Ootsuji H, Inoue O, Okada H, Nomura A, Kaneko S, Usui S. Long-term administration of eicosapentaenoic acid improves post-

myocardial infarction cardiac remodeling in mice by regulating macrophage polarization. J Am Heart Assoc. 2017 Feb 21;6(2)

- Takehara N, Tsutsumi Y, Tateishi K, Ogata T, Tanaka H, Ueyama T, Takahashi T, Takamatsu T, Fukushima M, Komeda M, Yamagishi M, Yaku H, Tabata Y, Matsubara H, Oh H. Controlled delivery of basic fibroblast growth factor promotes human cardiosphere-derived cell engraftment to enhance cardiac repair for chronic myocardial infarction. J Am Coll Cardiol. 2008 Dec 2;52(23):1858-1865
- Tokita Y, Tang XL, Li Q, Wysoczynski M, Hong KU, Nakamura S, Wu WJ, Xie W, Li D, Hunt G, Ou Q, Stowers H, Bolli R. Repeated administrations of cardiac progenitor cells are markedly more effective than a single administration: A new paradigm in cell therapy. Circ Res. 2016 Aug 19;119(5):635-51
- Ufret-Vincenty CA, Baro DJ, Santana LF. Differential contribution of sialic acid to the function of repolarizing K(+) currents in ventricular myocytes. Am J Physiol Cell Physiol. 2001 Aug;281(2):C464-74
- Velders MA, James SK, Libungan B, Sarno G, Fröbert O, Carlsson J, Schalij MJ, Albertsson P, Lagerqvist B. Prognosis of elderly patients with ST-elevation myocardial infarction treated with primary percutaneous coronary intervention in 2001 to 2011: A report from the Swedish Coronary Angiography and Angioplasty Registry (SCAAR) registry. Am Heart J. 2014 May;167(5):666-73
- Wang W, Tan B, Chen J, Bao R, Zhang X, Liang S, Shang Y, Liang W, Cui Y, Fan G, Jia H, Liu W. An injectable conductive hydrogel encapsulating plasmid DNA-eNOs and ADSCs for treating myocardial infarction. Biomaterials. 2018 Apr;160:69-81
- Wang Z, Huang S, Sheng Y, Peng X, Liu H, Jin N, Cai J, Shu Y, Li T, Li P, Fan C, Hu X, Zhang W, Long R, You Y, Huang C, Song Y, Xiang C, Wang J, Yang Y, Liu K. Topiramate modulates post-infarction inflammation primarily by targeting monocytes or macrophages. Cardiovasc Res. 2017 Apr 1;113(5):475-487
- Wassenaar JW, Gaetani R, Garcia JJ, Braden RL, Luo CG, Huang D, DeMaria AN, Omens JH, Christman KL. Evidence for mechanisms underlying the functional benefits of a myocardial matrix hydrogel for post-MI treatment. J Am Coll Cardiol. 2016 Mar 8;67(9):1074-86

- Waziri H, Jørgensen E, Kelbæk H, Stagmo M, Pedersen F, Lagerqvist B, James S, Køber L, Wachtell K. Short and long-term survival after primary percutaneous coronary intervention in young patients with ST-elevation myocardial infarction. Int J Cardiol. 2016 Jan 15;203:697-701
- Wigglesworth KM, Racki WJ, Mishra R, Szomolanyi-Tsuda E, Greiner DL, Galili U. Rapid recruitment and activation of macrophages by anti-Gal/α-Gal liposome interaction accelerates wound healing. J Immunol. 2011 Apr 1;186(7):4422-32
- Wollert KC, Meyer GP, Lotz J, Ringes-Lichtenberg S, Lippolt P, Breidenbach C, Fichtner S, Korte T, Hornig B, Messinger D, Arseniev L, Hertenstein B, Ganser A, Drexler H. Intracoronary autologous bone-marrow cell transfer after myocardial infarction: the BOOST randomised controlled clinical trial. Lancet. 2004 Jul 10-16;364(9429):141-8
- Ye L, D'Agostino G, Loo SJ, Wang CX, Su LP, Tan SH, Tee GZ, Pua CJ, Pena EM, Cheng RB, Chen WC, Abdurrachim D, Lalic J, Tan RS, Lee TH, Zhang J, Cook SA. Early regenerative capacity in the porcine heart. Circulation. 2018 Dec 11;138(24):2798-2808
- Zangi L, Lui KO, von Gise A, Ma Q, Ebina W, Ptaszek LM, Später D, Xu H, Tabebordbar M, Gorbatov R, Sena B, Nahrendorf M, Briscoe DM, Li RA, Wagers AJ, Rossi DJ, Pu WT, Chien KR. Modified mRNA directs the fate of heart progenitor cells and induces vascular regeneration after myocardial infarction. Nat Biotechnol. 2013 Oct;31(10):898-907
- Zhu W, Zhang E, Zhao M, Chong Z, Fan C, Tang Y, Hunter JD, Borovjagin AV, Walcott GP, Chen JY, Qin G, Zhang J. Regenerative potential of neonatal porcine hearts. Circulation. 2018 Dec 11;138(24):2809-2816
- Zimmermann WH, Melnychenko I, Wasmeier G, Didié M, Naito H, Nixdorff U, Hess A, Budinsky L, Brune K, Michaelis B, Dhein S, Schwoerer A, Ehmke H, Eschenhagen T. Engineered heart tissue grafts improve systolic and diastolic function in infarcted rat hearts. Nat Med. 2006 Apr;12(4):452-8

Appendices

A.1 RNA extraction

1. Thaw tissue samples stored at -80°C in RNA*later*™ stabilization solution.
2. Cut finely the samples with scissors wiped with RNase*Zap*™ Decontamination solution.
3. Add 1 ml TRIzol® per 50 mg of sample and one 5 mm-diameter stainless steel bead (Qiagen, Germany) in a round-bottom eppendorf tube.
4. Homogenise samples using the TissueLyser LT (Qiagen, Germany) tissue rupture set at 50 oscillations per min at 4°C. Make sure tissues are completely homogenised after 15 min. If necessary, repeat this step. Aspirate the homogenate.
5. Incubate the homogenate for 5 min at RT to dissociate nucleoprotein complexes.
6. Only the first sample was centrifuged for 1,200 rpm to check any eventual fat deposit. This was not observed so this step was skipped.
7. Add 200 µl of chloroform per 1 ml TRIzol®. Shake vigorously for 15 sec by inversion. Incubate for 5 min at RT.
8. Centrifuge at 13,300 rpm for 15 min at 4°C. After centrifugation, look at the three phases inside the eppendorf. The mRNA is located within the aqueous phase. Interphase and lower phenol-chloroform phase contain DNA and protein, respectively.
9. Carefully remove only the clear upper aqueous phase to a Rnase-free eppendorf. Do not touch the interface; if some is accidentally dispersed in the aqueous phase, centrifuge the sample again as detailed at point 8 and repeat this step.
10. Slowly add an equal volume of 70% ethanol in the transferred aqueous phase and mix by pipetting.
11. Tranfer up to 700 µl of sample from previous step to RNeasy® column to remove genomic DNA.
12. Centrifuge at 10,000 rpm for 15 sec at 4°C and discard the flow-through.
13. Add 700 µl RW1 buffer (RNeasy® kit) to the centre of the column, spin at 10,000 rpm for 15 sec and discard the flow-through.
14. Add 500 µl RPE buffer (RNeasy® kit) to the centre of the column, spin at 10,000 rpm for 15 sec and discard the flow-through.
15. Add 500 µl RPE buffer (RNeasy® kit) to the centre of the column, spin at 10,000 rpm for 2 min and discard the flow-through.

14. Transfer column to a new RNase-free 1.5 ml collection tube (RNeasy® kit). Add 30 µl RNase-free water onto the column, incubate at RT for one min and centrifuge for one min at 8,000 g.
15. Add washed 30 µl RNase-free water onto the column again and centrifuge at 10,000 rpm for one min.
16. Repeat step 15 by pipetting the flow-through again to the centre of the column and centrifuge at 10,000 rpm for one min.
17. Split the collected sample into 5 µl aliquots.
18. Determine the concentration of 1 µl RNA using the NanoDrop™ (Thermo Fisher Scientific, USA)
19. Calibrate the spectrometer with RNase-free water and measure the absorbance of the sample at 260 nm. The purity is determined from the ratio between the absorbance at 260 nm and the absorbance at 280 nm. This ratio should be between 1.8 and 2 to indicate pure RNA.

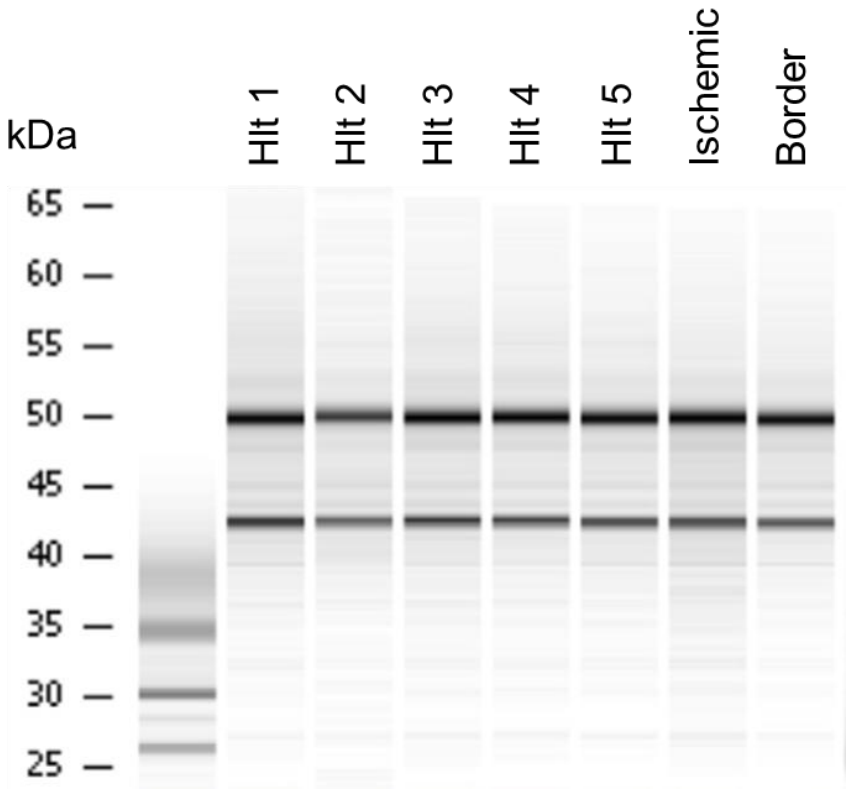

Figure A.1 Preliminary evaluation of RNA integrity after extraction.

Table A.1 Concentration (ng/µl), purity (A260/A280) and integrity (RIN) of RNA samples sent for RNA-sequencing.

Sample	Nanodrop 2000			Qubit	TapeStation
	Nucleic acid conc. (ng/µl)	A260/A280	A260/A230	Nucleic acid conc. (ng/µl)	RIN
HLT1-LV2	41.88	1.98	0.99	27.4	8.1
HLT1-LV2-2	39.9	1.99	0.98	29.6	8.2
HLT5-LV2	48.53	1.9	1.39	32.4	8.7
HLT5-LV2-2	50.34	2	1.39	37.6	8.5
HLT6	56.15	1.96	1.67	44.8	8.6
HLT6-2	44.35	2	1.68	35.4	8.5
HLT8	66.78	2.01	0.69	45.8	8.6
M28D1-IS	35.98	1.99	1.16	24.8	8.6
M28D1-IS	36.03	1.96	1.22	22	7.5
M28D1-BZ	83.9	1.97	1.48	62.8	8.2
M28D1-F	48.3	1.93	0.57	30	8.3
M28D1-F-2	45	2	0.54	29.2	8.4
M28D2-IS	127.6	2.02	0.79	87.4	8.3
M28D2-IS-2	96.56	2.07	0.64	72.2	8.1
M28D2-BZ	143.1	2.04	1.08	97.2	8.3
M28D2-F	49.7	2.01	1.97	34.4	8.3
M28D2-F-2	60.83	1.96	2.03	19.1	8.2
M28D3-IS	200.2	2.05	1.43	72.6	7.5
M28D3-BZ	102	1.95	1.45	32.2	8.4
M28D3-F	150.6	2.04	0.84	48.6	8.2
M28D4-IS	232.1	2.09	1.57	84.4	8.6
M28D4-BZ	231.4	2.1	0.95	75.2	8.4
M28D4-F	240.2	2.1	2.03	78.4	8.4
7D1-IS	255	2.11	1.68	87.6	8.1
7D1-BZ	233.9	2.1	1.64	80.2	8.2
7D1-F	236.8	2.06	1.98	84	8
7D2-IS	235.1	2.05	1.23	82.2	9.1
7D2-BZ	342.7	2.1	1.44	124	8.3
7D2-F	129.8	2.03	1.03	104	8.9
7D3-IS	505.6	2.03	1.78	93.4	9.4
7D3-BZ	227.1	2.08	2.01	73.6	9.3
7D3-F	96.48	2.07	0.81	65.4	9
7D4-IS	216.8	2.06	1.78	77	9.1
7D4-BZ	469.1	2.07	1.67	82.8	9.2

Table A.2 List of components and reagents.

Material	Supplier
Alexa Fluor® 555 succinimidyl ester	Thermo Fisher Scientific, USA
Cell wash solution	
Micro BCA™ protein assay kit	
Permeabilisation buffer	

ProLong™ gold antifade mountant with dapi	Sigma Aldrich, USA
RIPA lysis and extraction buffer	
RNA*later*™	
RNase*Zap*™	
RNase-free water	
Solubilisation buffer	
SuperFrost Plus™ slides	
TRIzol®	
Tween20®	
Acetic acid	
Acetonitrile (ACN)	
Acid fuchsin	
Acridine orange	
Alcian blue solution	
Alcoholic eosin y solution	
Anilin blue solution	
Biebrich scarlet-acid fuchsin solution	
Bovine serum albumin	
$CaCl_2$	
Chloroform	
Chondroitinase ABC	
Crocein scarlet	
Dimethylmethylene blue (DMMB) assay	
Dithiothreitol	
Donkey serum	
DPX mountant	
Fucose	
Galactose	
Gluteraldehyde	

Harris-modified hematoxylin solution	
HCl	
High grade BSA (A7638)	
Hexamethyldisilazane (HMDS)	
Iodoacetamide (IAA)	
Lead citrate	
Mannose	
$MgCl_2$	
NaCl	
N-acetylglucosamine	
Nuclear fast red solution	
Osmium tetroxide	
Paraformaldehyde (PFA)	
Phosphate buffer saline (PBS)	
Phosphotungstic acid	
Phosphomolybdic acid	
Sodium bicarbonate	
Sodium borohydride ($NaBH_4$)	
Sodium hydroxide (NaOH)	
Sodium thiosulfate	
Weigert's iron hematoxylin	
Trifluoroacetic acid	
Tris-buffered saline	
Trypsin	
Uranyl acetate	
Urea	
Amicon® centrifugal filters (3 kDa MW cut-off)	
Centrifugal filters (30 kDa MW cut-off)	Merck, Germany
Proteinase K	
Acetonitrile (ACN)	VWR International, USA

OCT compound	
Methanol	
PNGase F	Asparia Glycomics, Spain
Ethanol	Lennox, Ireland
Xylene	
Verhoeff's elastin stain kit	Clin-Tech, UK
cOmplete™, EDTA-free protease inhibitor cocktail	Roche, Switzerland
Bouin's solution	Medical Supply Co. Ltd, Ireland
Quartz discs (50.8mm diameter x 1.59 mm thick)	Alfa Aesar, USA
DNase	Qiagen, Germany
Disposable biopsy punch (0.4 mm-diameter)	Williams Medical Supply, UK
Araldite® epoxy resin	Electron Microscopy Sciences, USA
Sodium cacodylate buffer	
Rabbit polyclonal antibody to CD31 (ab28364)	Abcam, UK
Rabbit polyclonal antibody to CD163 (ab87099)	
Rabbit polyclonal antibody to collagen type I (ab34710)	
Rabbit polyclonal antibody to GATA4 (ab61170)	
Rabbit polyclonal antibody to tropomyosin1α (ab55915)	
Rabbit polyclonal antibody to α-smooth muscle actin (ab5694)	
Alexa Fluor® 647-Affinipure donkey anti-mouse IgG (H+L)	Jackson ImmunoResearch, USA
Alexa Fluor® 647-Affinipure donkey anti-rabbit IgG (H+L)	
Artocarpus integrifolia	

Robinia pseudoacacia	All these lectins were FITC-labelled and purchased from EY Laboratories Inc., USA
Pseudomonas aeruginosa	
Sambucus nigra	
Sophora japonica	
Dolichos biflorus	
Glechoma hederacea	
Glycine max	
Vicia villosa	
Bauhinia purpurea	
Wisteria floribunda	
Helix pomatia	
Griffonia simplicifolia	
Amaranthus caudatus	
Agaricus bisporus	
Arachis hypogaea	
Griffonia simplicifolia	
Triticum vulgaris	
Datura stramonium	
Solanum tuberosum	
Lycopersicum eculentum	
Calystegia sepium	
Narcissus pseudonarcissus	
Galanthus nivalis	
Hippeastrum hybrid	
Canavalia ensiformis	
Lens culinaris	
Lens culinaris	
Pisum sativum	
Trichosanthes japonica	
Triticum vulgaris	
Maackia amurensis	
Sambucus nigra	
Cancer antennarius	

Phaseolus vulgaris
Phaseolus vulgaris
Ricinus communis
Arum maculatum
Cicer arietinum
Caragana arborescens
Erythrina cristagalli
Trichosanthes japonica
Aleuria aurantia
Lotus tetragonolobus
Ulex europaeus
Euonymous europaeus
Griffonia simplicifolia
Maclura pomifera
Vigna radiata
Marasmius oreades

A.2 Protein extraction in RIPA buffer

1. Thaw tissue samples stored at -80°C in RIPA Lysis and Extraction Buffer with EDTA-free protease inhibitor cocktail and finely cut with scissors.
2. After cutting, submerge approximately 50 mg of sample in the same storage solution and top up with fresh RIPA buffer containing protease inhibitor cocktail up to 1.5 ml in a sterile round-bottom eppendorf.
3. Homogenise samples using the TissueLyser LT (Qiagen, Germany) tissue rupture set at 50 oscillations per min at 4°C. Make sure tissues are completely homogenised after 15 min. If necessary, repeat this step. Aspirate the homogenate.
4. Incubate on ice for 15 min.
5. Centrifuge at 12,000 rpm for 10 min at 4°C.
6. Aspirate the supernatant containing the total protein extract and make 200 µl aliquots.
7. Keep a small aliquot (50 µl) at 4°C to determine the protein concentration by the following day.

A.3 Membrane protein extraction

The procedure was performed using the Mem-PER™ Plus Membrane Protein Extraction Kit (Thermo Fisher Scientific, USA). Protein inhibitor cocktail was added to Permeabilisation and Solubilisation Buffer solution.

1. Thaw snap-frozen tissue samples stored at -80°C. Submerge approximately 40-50 mg of sample in 5 ml of Cell Wash Solution, vortex for 10 sec and discard wash.
2. Finely cut the samples with scissors and trasfer into a 2 ml tissue grinder. Add 1 ml of Permeabilisation Buffer and mechanically homogenise (at least 10 strokes).
3. Add 1 ml of Permeabilisation Buffer and tranfer the homogenate in a new tube for incubation on ice for 10 min.
4. Centrifuge at 16,000 g for 15 min at 4°C, remove the supernatant containing cytosolic proteins and store at -80°C.
5. Resuspend the pellet in 1 ml of Solubilisation Buffer until getting a homogeneous suspension.
6. Incubate for 30 min at 4°C with mixing.
7. Centrifuge at 16,000 g for 15 min at 4°C, remove the supernatant containing membrane proteins, aliquot and store at -80°C.
8. Keep a small aliquot (50 µl) at 4°C to determine the protein concentration by the following day.

A.4 Preparation of 4% paraformaldehyde solution

To make up a solution (1 L) of 4% paraformaldehyde (PFA) perform the following procedure in a fume hood.

1. Weigh out 40 g of paraformaldehyde powder wearing a nasal mask.
2. Dissolve powder in 800 ml dH_2O.
3. Heat the solution using a hotplate/stirrer to approximately 60°C. Once this temperature is reached, turn off the hotplate. Do not allow the solution to reach 65°C or greater.

4. Using a plastic pipette, slowly add 1M NaOH dropwise to the solution until it clears.
5. Make up the solution to a final volume of 1 L and allow to cool to RT.
6. Filter and store the solution at RT. Aliquot and store at -80°C if the solution is not used within the following two weeks.

A.5 Cryopreservation

1. Fix each sample with freshly prepared PFA 4% overnight at 4°C. (10 ml for each specimen).
2. Wash each sample with PBS three times for 10 min each.
3. Incubate each sample in 30% sterile-filtered sucrose solution (10 ml for each specimen).
4. Proceed when the specimen sinks to the bottom of the tube or leave overnight at 4°C.
5. Remove the excess of sucrose solution on filter paper and follow the orientator method to generate isotropic uniform random samples.
6. Position the sample on the center of the first ϕ clock and use a random number generator to decide which angle to cut at (Figure A.3).
7. Position the cut face of the sample down on the center of the second θ clock and use a random number generator to decide which angle to cut at (Figure A.3).
8. Position the cut face of the sample down on a plastic cryomold and fill it with OCT compound without exceeding the first ring of the mold.
9. Leave all the samples to equilibrate in OCT compound for 5-10 min.
10. Meanwhile, fill a polystyrene contained with liquid nitrogen until around 3 cm.
11. Position a small metal container filled with isopentane (2 cm) in the middle of the polystyrene box.
12. If possible, check the temperature inside the metal container using an ethanol thermometer to check that it is at least below -100°C. The solution should look turbid and whitish on the bottom and sides of the container once it reaches that temperature.
13. Firmly hold the cryomold vertically using a pair of tweezers and carefully submerge only the bottom and sides of the mold. Do not submerge completely the cryomold to avoid cracking inside the OCT-embedded sample.

14. Once the OCT turned its color to white, remove the specimen from the plastic mold and quickly transfer it on ice.
15. If processing more than five samples, be ready to eventually replace the liquid nitrogen to keep the isopentane bath at the right temperature over all the embedding procedure.
16. Do not leave the OCT embedded blocks for more than 5 min on ice and store them at -80°C.

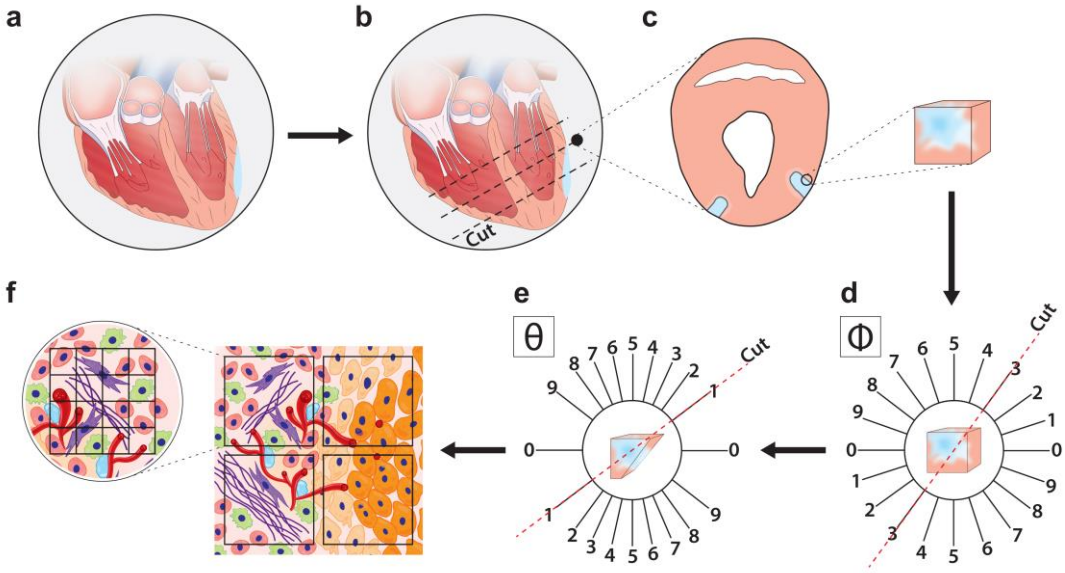

Figure A.2 Schematic of isotropic uniform random sampling. Infarcted hearts (a) were axially cut at 1 cm thickness (b). 0.5 cm-thick samples were taken from the ischemic, border and remote regions (c) and cut following the orientator method through ϕ (d) and cosine-weighted θ (e) clocks. Finally, after embedding sectioning and staining, isotropically-oriented sections were imaged and quantified by superimposing stereological squared grids (f).

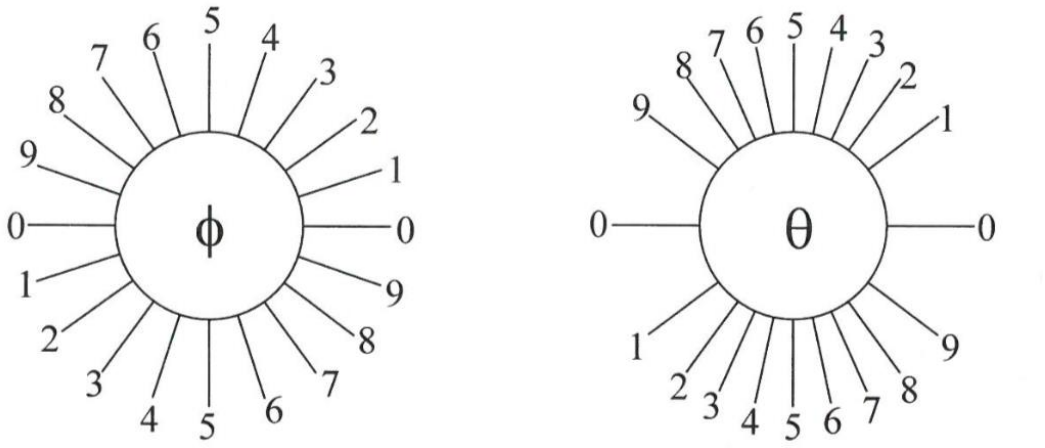

Figure A.3 ϕ and θ clocks used to generate isotropic uniform random samples.

A.6 Tissue processing for embedding in paraffin

1. Each tissue sample was fixed in 4% PFA overnight at 4°C.
2. Wash each sample with PBS three times for 10 min each.
3. Place each sample in a plastic cassette and label it with a pencil, keep the cassettes submerged in 70% ethanol solution.
4. Set the overnight processing using an Excelsior™ AS Tissue Processor (Thermo Fisher Scientific, USA), as detailed in Table A.3.
5. The following day, collect the samples from the paraffin wax bath (still at 62°C) and keep them in hot wax bath to avoid solidifying.
6. Quickly remove each sample from the cassette and place it in a plastic mold for embedding with fresh paraffin wax using an EG1150 Modular Tissue Embedding Center (Leica, Germany).
7. During the embedding procedure, make sure that the specimen has a thin layer of paraffin above the bottom of the plastic mold where it is embedded.
8. Leave the embedded samples to solidify for at least one hour on the refrigerated surface of the Tissue Embedding Center.

Table A.3 Routine program overnight for tissue processor.

Reagent	Duration (min)	Temperature (°C)
Ethanol 70%	Until start	RT
Ethanol 70%	45	RT
Ethanol 90%	45	RT
Ethanol 100% (1)	45	RT
Ethanol 100% (2)	60	RT
Ethanol 100% (3)	60	RT
Xylene (1)	45	RT
Xylene (2)	60	RT
Xylene (3)	75	RT
Paraffin wax (1)	60	62
Paraffin wax (2)	60	62
Paraffin wax (3)	60 - until collection	62

A.7 Tissue sectioning using the microtome

1. Leave the samples embedded in paraffin wax on the refrigerated surface of the Tissue Embedding Center for at least 1 h before starting to section. The face of the block which will be cut needs to lay on the refrigerated surface.
2. Fill the water bath with distilled water at an approximate hight of 5 cm and set the temperature to 50°C.
3. Position the paraffin block on the sample holder of a RM2235 microtome (Leica, Germany).
4. Set the cutting angle at 3° and cut specimens into 5 µm-thick sections.
5. Section a ribbon including three sections and transfer it onto the water bath using forceps. Collect the floating sections submerging SuperFrost Plus™ slides.
6. Leave the glasses to dry the excess of water and store at RT until use.
7. Before histological staining, make the section to adhere by incubating the glasses at 60°C for 10 min.

A.8 Tissue sectioning using the cryostat

1. Take the samples (OCT blocks) out of the -80°C freezer and place them at -20°C to equilibrate for at least 1 h.

2. Set the temperature inside the CM1850 cryostat (Leica, Germany) chamber at -25°C and move the required equipment for cutting inside the chamber (blades, brush, specimen stage).
3. Put a drop of OCT compound on the specimen stage and quickly position the samples embedded in OCT on the top of that. Leave the assembled specimen stage inside the chamber for one min.
4. Fix the specimen stage in the arm and use the motorised controls to adjust the distance between the blade and the OCT block.
5. Set the cutting angle at 3° and cut specimens into 5 μm-thick sections.
6. Avoid wrinkles and disruptions in the sections. After a prolonged use, move the blade laterally or change it.
7. Lift the cutting glass and quickly make the section adhere on the charged side of a SuperFrost Plus™ slide.
8. When applying serial sectioning, calculate at least 250 μm distance between the first section series and the following one. At the end of the sectioning, three sections taken at 250 μm-distance apart should be present on the same slide.
9. Label the slides and store at -80°C.

A.9 Periodate treatment of bovine serum albumin for lectin histochemistry

1. Use high grade BSA 10 mM periodic acid in 0.1 M sodium acetate, pH 4.5 made up fresh.
2. Dissolve BSA in the freshly made periodic acid solution (approx 5g/100 mL).
3. Incubate at RT for 6 h.
4. Dialyse against dH_2O (or PBS) with four changes over two days at 4 °C.

16. Lyophilise and store at 4 °C.

A.10 Lectin staining on cryosections

1. Leave the sections to warm at RT for 15-20 min.
2. Circle the sections using a hydrophobic marker (PAP pen).
3. Place the sections in a glass staining jar and wash with TBS-T three times (3 min each wash, gentle shaking).

4. Lay all the slides on a slide staining tray and incubate with 3% BSA (periodate-treated, high grade, made in TBS).
5. Wash with TBS twice (3 min each wash, gentle shaking).
6. From this point onwards, avoid exposure to direct light.
7. Incubate with the lectin solution (in TBS).
8. Wash with TBS three times (3 min each wash, gentle shaking).
9. If staining with antibody, should be done after lectin incubation.
10. Counterstain each section with one drop of with ProLong™ Gold Antifade Mountant with DAPI and coverslip.
11. Leave to cure in the dark for one day. Image within three days after curing.

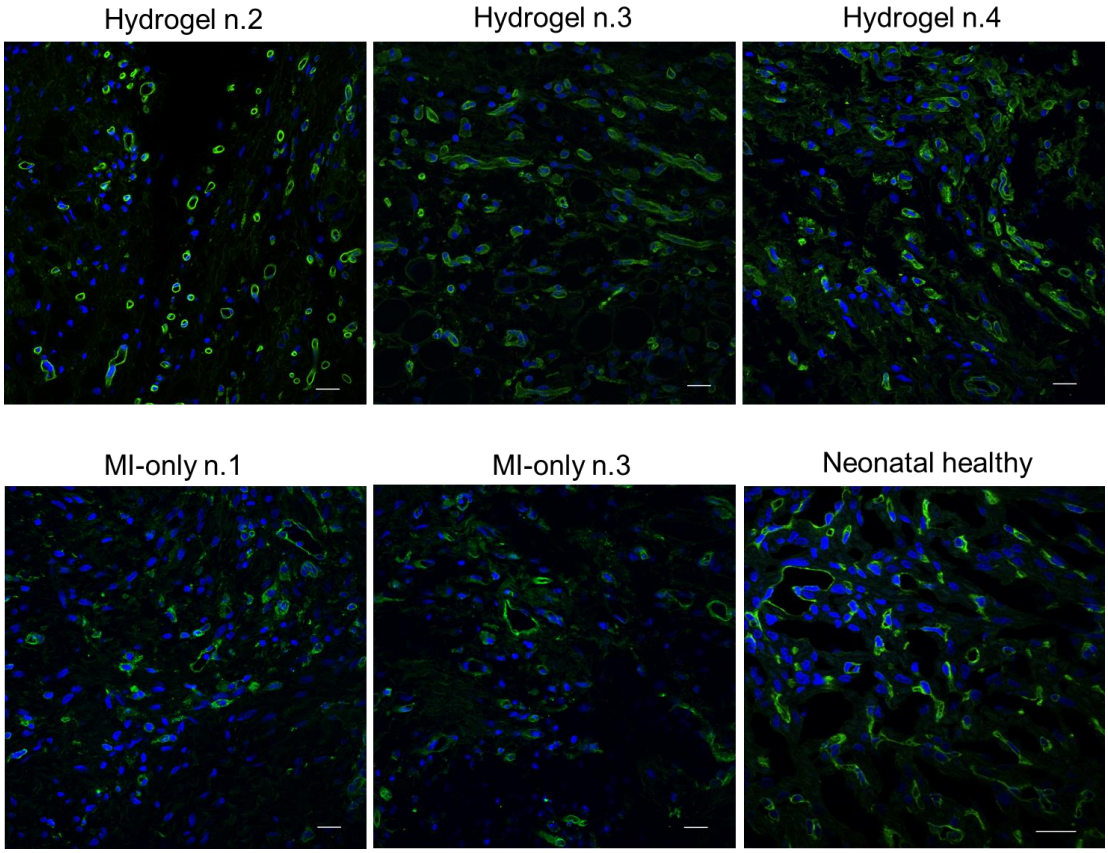

Figure A.4 GS-I lectin histochemistry on ELRs-treated and MI-only animals 28 days post-MI and validation in neonatal healthy myocardial tissue. Scale bar = 20 μm.

A.11 Lectin microarray on cardiac samples

All lectin microarrays were printed with 48 lectins (EY laboratories, USA) according to an established protocol [Kilcoyne]. Each lectin microarray slide had a unique

barcode indicating the printing batch. All the procedures described here prior to scanning needed to be performed in a dark room with red light. Membrane protein samples labelled with Alexa Fluor® 555 Succinimidyl Ester were thawed and a titration experiment using a concentration of protein from 1 to 10 μg/ml was run to assess the optimum binding intensity of the sample to the printed lectins and to avoid saturation signals; therefore the chosen concentration was 2.5 μg/ml and 5 μg/ml for all the rat and sheep samples, respectively. The procedure of the lectin microarray analysis is detailed below here.

1. Thaw labelled membrane protein samples on ice and dilute in TBS-T (0.01% of Tween-20) to the optimal concentration in a final volume of 70 μl in a rubber eight-well gasket (Agilent Technologies, USA).
2. Carefully assemble each slide (lectin-printed side) on the top of the loaded gaskets to avoid splashing of the samples.
3. Incubate with gentle rotation (4 rpm) in a hybridization oven at 23°C for 1 hour.
4. Carefully disassemble the slide and quickly submerge it in TBS-T buffer.
5. Place the slides in a glass staining jar filled with TBS-T with and wash three times (3 min each wash, gentle shaking).
6. Do a final wash in TBS without Tween-20 before transferring the slides in empty falcon tubes. Centrifuge at 1500 g for 5 min.
7. Scan the slides immediately using a G2505 microarray scanner (Agilent Technologies, USA) at 90% laser power.
8. Process image files showing the scanned lectin microarrays using GenePix Pro v6.1.0.4 software (Molecular Devices, UK). Superimpose grids having an adaptive diameter circular alignment based on 230 μm features in the options on the subarrays.
9. Extract background-corrected median feature intensity data for analysis.
10. Normalise data to the median total intensity value of six replicate microarray slides.
11. Run clustering of the normalised data using Hierarchical Clustering Explorer v3.5 (HCE 3.5, University of Maryland). Select Euclidean distance with complete linkage in the clustering options.

A.12 Hematoxylin and eosin staining of tissue sections

1. Leave the cryosections to warm at RT for 15-20 min. If using paraffin sections, incubate them at 60°C for 10 min to melt the paraffin.
2. If using paraffin sections, dewax in xylene (2 changes of 5 min each) and then rehydrate through graded alcohols (twice in 100%, 90%, 70%, 50%), 2 min each.
3. Wash in dH_2O for 2 min.
4. Stain in Harris-modified hematoxylin solution for 6 min.
5. Rinse in running tap water for 8 min.
6. Counterstain in alcoholic Eosin Y solution for 2 min.
7. Wash three times in dH_2O/running tap for 1 min.
8. Dehydrate through graded alcohols (70%, 90%, twice in 100%), 2 min each.
9. Clear in xylene, 2 changes of 5 min each.
10. Cover sections with DPX mountant and apply coverslip.
11. Leave slides in fume hood overnight.

A.13 Masson's Trichrome staining of tissue sections

1. Leave the cryosections to warm at RT for 15-20 min. If using paraffin sections, incubate them at 60°C for 10 min to melt the paraffin.
2. If using paraffin sections, dewax in xylene (two changes of 5 min each) and then rehydrate through graded alcohols (twice in 100%, 90%, 70%, 50%), 2 min each.
3. Wash in dH_2O for 2 min.
4. Mordant in Bouin's solution for 45 min at 65°C.
5. Wash in running tap water for 5 min to remove the picric acid.
6. Incubate in Weigert's iron hematoxylin working solution for 8 min.
7. Wash in running tap water for 5 min, rinse in distilled water.
8. Stain in Biebrich scarlet-acid fuchsin solution for 5 min.
9. Rinse in distilled water.
10. Incubate with phosphotungstic/phosphomolybdic acid in distilled water (1:1:2 ratio) for 10 min, discard solution.
11. Transfer directly into Aniline Blue solution for 5 min.
12. Rinse in distilled water.
13. Incubate in 1% acetic acid for 1 min, discard solution, rinse in distilled water.
14. Dehydrate through graded alcohols (70%, 90%, twice in 100%), 2 min each.
15. Clear in xylene, two changes of 5 min each.

16. Cover sections with DPX mountant and apply coverslip.
17. Leave slides in fume hood overnight.

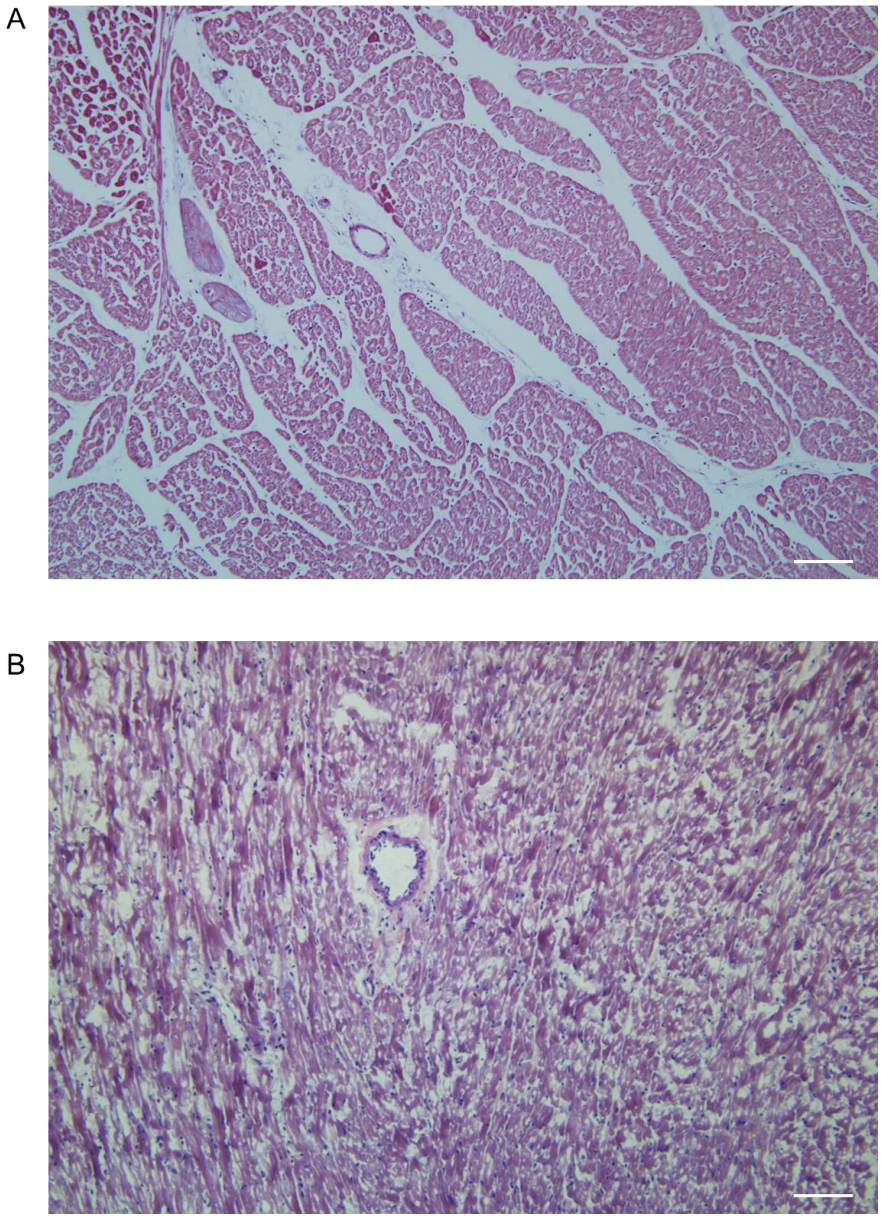

Figure A.5 H&E images showing morphological integrity of ovine myocardial tissue following fixation and sucrose infiltration before embedding in OCT (A) and its partial disruption by immediate snap-freezing after harvesting (B). Scale bar = 100 μm.

A.14 Alcian blue staining of tissue sections

Unless otherwise stated, the staining procedure Alcian Blue solution at pH 2.5 was used. To selectively identify sulfomucins and proteoglycans a low pH (pH 1) Alcian Blue solution was prepared.

1. Leave the cryosections to warm at RT for 15-20 min. If using paraffin sections, incubate them at 60°C for 10 min to melt the paraffin.
2. If using paraffin sections, dewax in xylene (2 changes of 5 min each) and then rehydrate through graded alcohols (twice in 100%, 90%, 70%, 50%), 2 min each.
3. Wash in dH_2O for 2 min.
4. Stain in Alcian Blue solution (1% in 3% acetic acid, pH 2.5) for 30 min.
5. Rinse in running tap water for 5 min.
6. Counterstain in Nuclear Fast Red solution for 10 min.
7. Wash in running tap water for 1 min.
8. Dehydrate through graded alcohols (70%, 90%, twice in 100%), 2 min each.
9. Clear in xylene, 2 changes of 10 min.
10. Cover sections with DPX mountant and apply coverslip.
11. Leave slides in fume hood overnight.

A.15 Verhoeff's Van-Gieson staining of tissue sections

1. Incubate paraffin sections at 60°C for 10 min to melt the paraffin.
2. Dewax in xylene (2 changes of 5 min each) and then rehydrate through graded alcohols (twice in 100%, 90%, 70%, 50%), 2 min each.
3. Wash in dH_2O for 2 min.
4. Stain in Verhoeff's hematoxylin solution for 1 h.
5. Rinse in running tap water for 5 min.
6. Incubate in 2% ferric chloride solution for 2 min.
7. Check staining under a light microscope.
8. Wash three times in dH_2O/running tap for 1 min.
9. Incubate in 5% sodium thiosulphate (freshly made) for 1 min.
10. Rinse in running tap water for 3 min.
11. Stain in Van-Gieson solution for 3 min.

12. Dehydrate through graded alcohols (70%, 90%, twice in 100%), 2 min each.
13. Clear in xylene, 2 changes of 5 min each.
14. Cover sections with DPX mountant and apply coverslip.
15. Leave slides in fume hood overnight.

A.16 Pentachrome staining of tissue sections

1. Incubate paraffin sections at 60°C for 10 min to melt the paraffin.
2. Dewax in xylene (2 changes of 5 min each) and then rehydrate through graded alcohols (twice in 100%, 90%, 70%, 50%), 2 min each.
3. Wash in dH_2O for 2 min.
4. Mordant in Bouin's solution for 45 min at 65°C.
5. Stain in Verhoeff's hematoxylin solution for 15 min.
6. Rinse in dH_2O and differentiate elastin fibres in 2% ferric cloride solution.
7. Wash in dH_2O for 2 min.
8. Check staining under a light microscope.
9. Incubate in 5% sodium thiosulphate (freshly made) for 1 min.
10. Rinse in running tap water for 3 min.
11. Incubate in 3% acetic acid for 3 min.
12. Stain with Alcian blue solution (pH 2.5) for 30 min.
13. Rinse in running tap water for 1 min and rinse in dH_2O.
14. Stain in Crocein scarlet-Acid fuchsin (4:1) for 2 min.
15. Wash three times in dH_2O and then dip for five times in 1% acetic acid.
16. Incubate in 5% phosphotungstic acid twice (2 min each).
17. Dip five times in 1% acetic acid.
18. Dehydrate through graded alcohols (70%, 90%, twice in 100%), 2 min each.
19. Clear in xylene, 2 changes of 5 min each.
20. Cover sections with DPX mountant and apply coverslip.
21. Leave slides in fume hood overnight.

A.17 Sputter coating of samples for scanning electron microscopy analysis

1. Lift the hinged lid up carefully and remove the glass chamber.
2. Place samples onto the specimen plate.

3. Ensure that the rubber seals of the glass chamber are cleaned of any dust or debris, replace onto the machine and carefully lower lid shut.
4. On the argon gas cylinder, open the mains valve. A pressure reading should appear on the main gauge. If not, the cylinder may be empty.
5. Open the brass ball valve enough to register a delivery reading of 5 Linear Parameter Measurement (LPM). The ball may fluctuate initially but will settle after a few sec.
6. Turn on the sputter coater by flicking the mains switch on the bottom left of the front panel.
7. Gently press down on the chamber lid and press the start button. Keep the lid pressed down for the first few sec of the run to make sure the chamber is properly sealed.
8. Observe the vacuum gauge on the bottom left hand side of the front panel. Check that the pointer needle begins to deflect from left to right indicating that the chamber is being evacuated.
9. Once the pressure gauge reaches between 0.1 and 0.05 Torr (usually 0.07 Torr), the coater will then cycle through the coating process automatically.
10. When coating is complete, the chamber will automatically depressurise and the red stop light will light. Check if the lid of the chamber is free, open the chamber, remove the samples and carefully close the lid. If the lid does not open freely, press the stop button to introduce more air into the chamber which will then allow the lid to be opened. Do not try and force the lid open.
11. Turn of the coater at the mains switch.
12. Turn of the brass ball valve and mains valve on the argon gas cylinder.
13. The samples are then ready to be viewed in the scanning electron microscope.

A.18 Imaging by scanning electron microscopy

To obtain an adequate signal, the scanning electron microscope must operate under high vacuum to minimise scattering of the low energy electron microscope by air molecules. Because of this, biological samples that contain any water will quickly become desiccated when placed in the vacuum which can induce morphological changes. To avoid this, samples need to be dried prior to imaging.

1. Before starting, look around the SEM workstation to check for spills, trip or electrical hazards.
2. To prepare sample on stub, screw the stub onto the appropriate sample holder. Check the height of the sample using the gate to ensure it is within the correct height limit.
3. On the SEM chamber door, ensure that the stage is at the specimen exchange position:
   - X = 20
   - Y = 20
   - Z = EX/EX boxes are aligned
   - Tilt = 0
4. Vent the sample chamber by pressing the green Air/Evac button on the front panel of the workstation. Wait for the door to open. A gap will appear between the chamber and door to indicate that the chamber has been fully vented. Do not force the chamber door open.
5. Carefully open the chamber door and place the sample in its holder in to the chamber.
6. Carefully and slowly, while keeping an eye on the camera screen, close the chamber door. Do not force the sample into the chamber.
7. Once the chamber door is closed, hold it firmly closed and evacuate the chamber by pressing the green Air/Evac button. Once the red bar begins to appear in the vacuum gauge display let go the door.
8. Set the desired imaging parameters. Ensure that the magnification is setting to its lowest value (x40).

   The recommended default settings for normal SE imaging are:
   - Accelerating voltage = 15 kV
   - Beam = 50
   - Working distance = 14 mm
   - Vacuum = High
   - In ‘Observation’ tab
9. Click on the ‘HV’ icon to turn on the beam. Click ‘ABC’ to automatically adjust brightness and contrast.

10. Select fast scan speed (‘Slow 1 or 2’) to locate region of interest and increase magnification.
11. Select ‘Reduce 1 or 2’. Adjust focus and click ‘ABC’. Brightness and contrast can also be adjusted manually using the brightness and contrast dials on the control panel.
12. Select slow scan speed (‘Slow 3’) and make sure focus, brightness and contrast are optimal. If not, go back to ‘Reduce’ scan and readjust.
13. This process (steps 3-5) may need to be repeated when gradually increasing the magnification.
14. To acquire image, click on the ‘M/H’ icon. The images will be temporarily saved in the software allow for batch saving.
15. Turn off the ‘HV’ by clicking on the icon.
16. On the SEM chamber door, ensure that the stage is at the specimen exchange position:
    - X = 20
    - Y = 20
    - Z = EX/EX boxes are aligned
    - Tilt = 0
17. Wait for the chamber to vent fully and carefully open the chamber door while keeping an eye on the camera screen to make sure the sample does not strike the detector.
18. Remove the sample from the chamber.
19. Close chamber door, hold closed and press green Air/Evac button to evacuate. The SEM must be kept under vacuum when not in use.

A.19 Processing of samples before transmission electron microscopy analysis

Small samples (around 0.3-thick in every direction) were harvested as described in section 3.2.4 and processed in the following way.

1. Fix each sample in 2.5% gluteraldehyde (fixative volume should be at least ten times the volume of the sample to be fixed), for 24h at 4°C.
2. Wash in PB (phosphate buffer) twice, 5 min each.
3. Post-fix in osmium tetroxide 1% for 2h at RT.

4. Dehydrate through graded alcohols (30%, 50%, 70%, 95%, 100% (twice)), 15 min each.
5. Wash in acetone twice, 15 min each.
6. Incubate in an acetone-araldite® resin mixture (ratio 2:1) for 24h.
7. Incubate in an acetone-araldite® resin mixture (ratio 1:2) for 24h.
8. Incubate in pure araldite® resin for 24h.
9. Transfer in new araldite® and leave in an oven at 60°C for 48h to allow resin polymerisation.

A.20 Automatic grid stainer before transmission electron microscopy analysis

After cutting the resin-embedded blocks using a diamond knife, a TEM automatic grid stainer EM AC20 (Leica, Germany) was used to process each sample. Before staining the grids, a wash programme must be run to ensure the chamber and tubes are clean.

1. Clean a grid carrier plate with 100% ethanol and rinse with dH_2O.
2. Open the chamber located on the left-hand side of the front panel of the machine and insert the empty grid carrier plate. Close and lock the chamber.
3. Turn the instrument on using the switch on the rear panel. Turn the two three-way valves to the 'W' position.
4. Select the W2 programme on the digital display and press start to begin wash run. The end of the wash is signalled by a beeping sound.
5. Clean the grid support plate with 100% ethanol.
6. For loading the grids, place the grid support plate into the plate holder frame and close the clamp using the thumb wheel.
7. Place grid support plate in frame over peg plate. Adjust grid plate on peg so that a grid slot is directly over the peg. Gently press the support plate down on the peg to open the slot.
8. Place the grid into the open slot and raise up the frame from the peg so that the edge of the grid is caught in the slot. Ensure that only the very edge of the grid is gripped in the slot.
9. Repeat until all grids are in place in the support plate and note the position of each grid if necessary.

10. Open the chamber door by turning the bayonet lock. Remove the grid support plate from the holder frame and insert into the holder on the chamber door with the grids facing in towards the chamber. Close and lock the chamber door.
11. Turn both of the 3-way valves to the 'S' position. Move to cursor to the desired contrast staining programme. Press start. Run the following staining sequence:
    - Wetting
    - Filling stain 1
    - Stain 1
    - Rinsing
    - Filling stain 2
    - Stain 2
    - Rinsing
    - Draining
12. The end of a contrasting run will signal with a sound. Open the chamber door and remove the grid support plate. Using filter paper, remove any excess water from the grids.
13. Place the grid support plate in the holder frame and allow to air dry. To remove grids, place 1 grid slot of the grid support plate in holder frame over the peg, press down gently and pick up grid.
14. Perform a post-staining wash step as described at points 2-4.

A.21 Imaging by transmission electron microscopy

1. First, remove grid holder (which will be in the 'Park' position) from TEM by flicking switch from Evac to Air. Wait 30 sec for system to switch to air.
2. From the park position, slowly and gently pull the grid holder straight out of the TEM until it comes to a stop. Hold tightly onto the grid holder when taking it out as any residual vacuum may cause the holder to be pulled back into the TEM.
3. Once the holder comes to a stop, gently turn the holder counter clockwise until it comes to a stop.
4. Gently pull the holder straight out of the TEM. Use one finger as an anchor so as to not cause the holder to strike the sides of the TEM as it is being pulled out.
5. Place holder onto platform. Release grid cover by pulling back spring clip. Rotate holder and cover will drop off.

6. Place grid into holder, replace cover and spring clip. Rotate holder a few times and tap gently to make sure grid and cover are secured.
7. Insert holder straight into TEM making sure that it is lined up correctly. Push holder gently in until it comes to a stop. Hold holder in position with heel of hand and flick switch from Air to Evac. Red light will come on.
8. Only when the red light switches off, turn the holder clockwise (long turn) until it comes to a stops and gently guide the holder into the TEM until it comes to a stop. There will be some resistance due to the vacuum, the vacuum will pull the holder into the TEM. Be sure to keep a grip on the handle when turning. This is the 'parked' position.
9. Turn the handle clockwise again (short turn) until it comes to a stop and guide the holder the rest of the way into the TEM.
10. Turn on HV by pressing the accelerating voltage button followed by the 75 button on the left panel. Remove cover from viewing window.
11. Once 75kV is achieved, turn up the filament all the way and observe beam on phosphor screen. Locate sample on the grid. Once found, lift up screen to begin using CCD camera. Place cover on viewing window.
12. Open AMT software on PC desktop.
13. Set image save path by performing the following:
    - File
    - Case Study
    - Create new case
    - Find your user folder and select
    - Input new file name
    - Click accept new case
    - Make sure filing cabinet box on left panel displays '001'
14. To view image on PC, click 'Click for live image'.

A.22 ELRs-based hydrogel fabrication

Hydrogel formation occurs at low temperature in a homogeneous manner. It can also take place at RT but the cross-linking/mesh formation will be slightly less homogeneous. The following procedure was always adopted before any either *ex vivo* or *in vivo* injection.

1. Calculate the amount of solvent for recombinamer dissolution at the desired concentration (the ratio in terms of equivalents among the recombinamers is HE5-cyclooctyne:HRGD6-azide=1.79:1 due to the difference in molecular weight and lysine residue modification rate).
2. Dissolve the polymer with cyclooctine on one side and the polymer with azide on the other at the desired concentration in cold (4°C) mQ H_2O or PBS solution.
3. Keep both solutions at 4°C till all the material is completely dissolved (at least overnight). Magnets should be avoided, if mixing is required, use a vortex.
4. Check that the polymer is completely dissolved by visual inspection. Solutions should be transparent.
5. Place the desired amount of HRGD-azide into a previously cooled eppendorf. Add the HE5-cyclooctine solution to the recipient by releasing the volume inside the previously one. Vortex the hydrogel solution and withdraw it with a cold tip.
6. Leave the mixed ELRs on ice and wait 10 min to allow initial crosslinking.
7. Aspirate the mix with a 1 ml volume syringe through a 25G needle and inject immediately.
8. Carefully retract the needle to avoid backflow of ELRs.

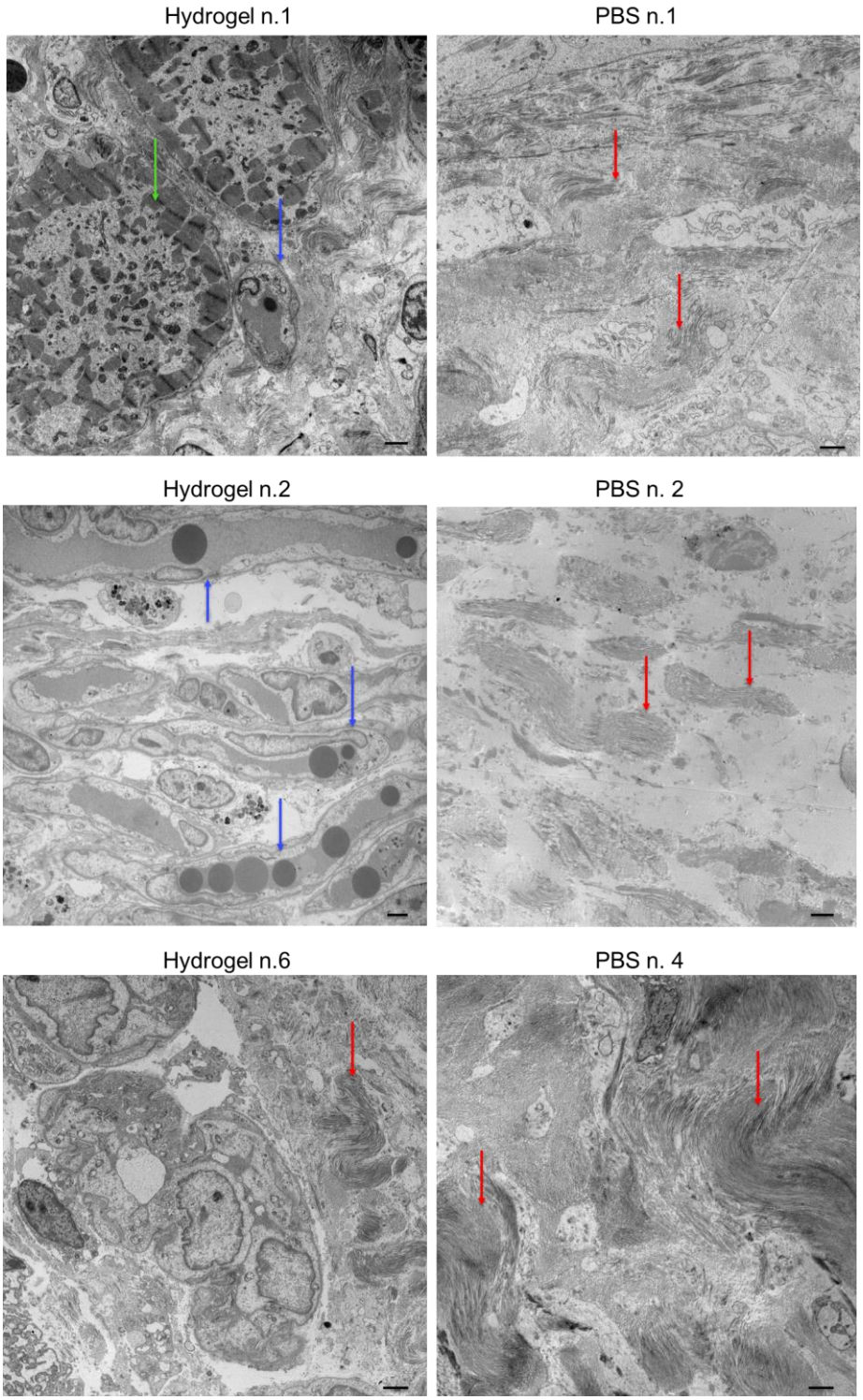

Figure A.6 Transmission electron microscopy imaging showing the perfused capillaries (blue arrows) found in the proximity of cardiomyocytes (green arrow) and in the ischemic core regions across different animals in the ELRs-treated group. Wavy formed collagen (red arrow) was detected in the ischemic cores of both PBS-injected and ELRs-treated groups. Scale bar = 2 μm.

A.23 Confocal Raman microscopy

Samples were harvested as described in section 3.2.4 and embedded in OCT using liquid nitrogen/dry ice-cooled isopentane before storage at -80°C until processing. Consistency in the spectral outcome was checked across three different healthy samples to set a baseline for comparison with pathological conditions, as shown in Figure A.8.

The following protocol was optimised for confocal Raman microscopy of myocardial tissue.

1. The day before analysis, section OCT blocks at 30 μm-thickness using a CM1850 cryostat (Leica, Germany) following the procedure described in A.8. Instead of using SuperFrost Plus™ slides, leave sections to adhere on quartz discs and store at -80°C until analysis.
2. Take serial sections as described in A.8 and perform Masson's Trichrome (A.13) to assess collagen deposition in each section which is consecutive to the sample which will be analysed by confocal Raman.
3. Set the alpha500 confocal Raman microscope (Witec, Germany) at 785 nm laser excitation (reflection mode, ~1 μm laser spot diameter, laser power 0.05 mW). Set detector grating at 600 lines/mm and centre of spectral detection at 880 cm^{-1}. Block Rayleigh scattering with the appropriate notch filter (785 nm).
4. Rotate objectives to select a 40x dry objective lens (NA 0.6).
5. Calibrate the instrument using a silicon standard (maximum signal at 520 cm^{-1}, spectral resolution of 0.8 cm^{-1}.
6. Place sample under the objective and locate region of interest in centre of field of view.
7. Direct the light path to the diffraction grating via fibre optic cable (which creates the confocal pinhole) and set the software to perform 225 spectral measurements across the sample in an area of 100 μm^2. An integration time of 40 sec was used for each measurement.

8. Apply cosmic ray reduction, background correction, spectrum averaging and Savitzky-Golay smoothing (4 point, 3rd order) using Project FIVE® software (Witec, Germany).
9. Normalise to the peak at 1446 cm^{-1} and graphical analysis was performed using Origin® version 9.1 (OriginLab, USA). All spectra described are plotted relative to the excitation wavelength.

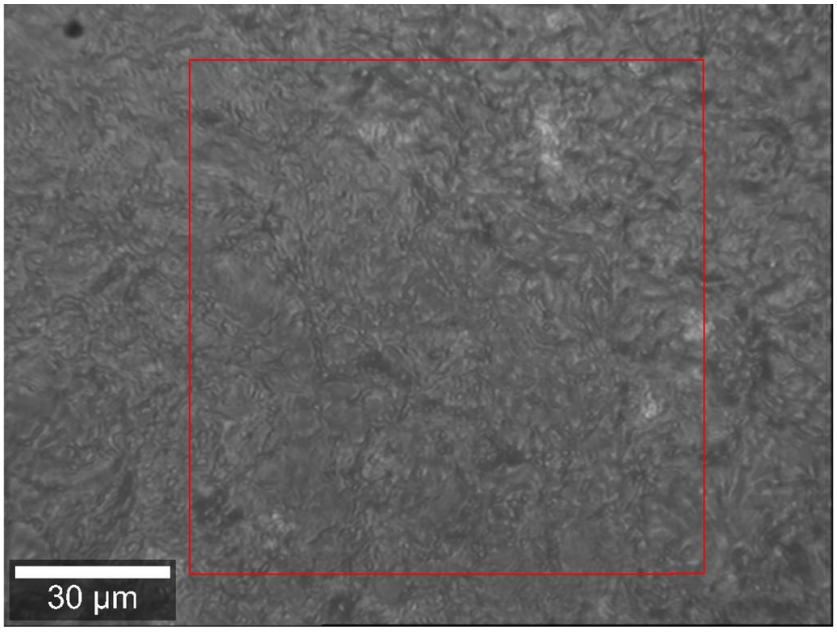

Figure A.7 Region of interest visualised by brightfield prior to Raman analysis.

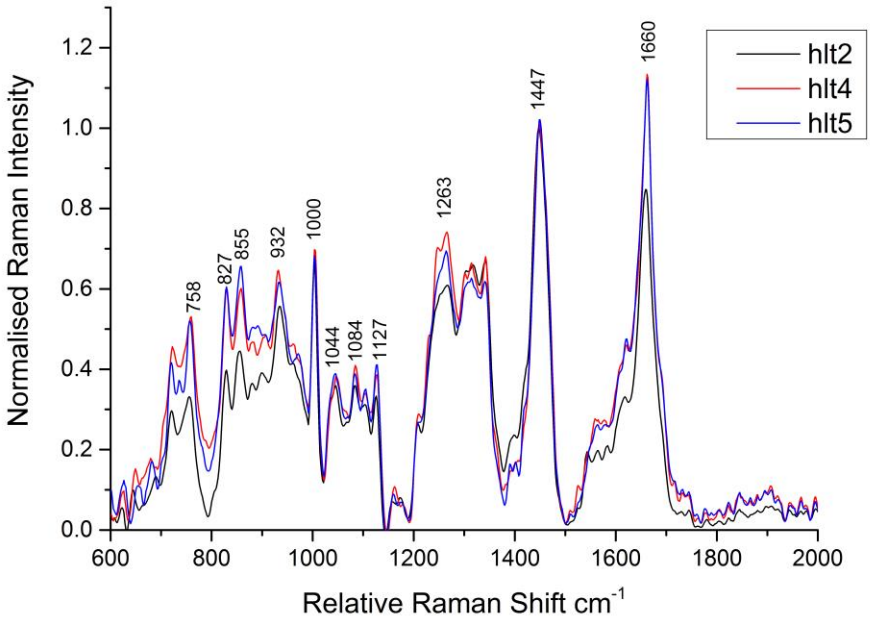

Figure A.8 Raman analysis of myocardial infarcted tissue. Averaged Raman spectra

of 225 points scanned in 100 μm^2 areas in healthy (hlt) myocardial sections. N=3 animals.

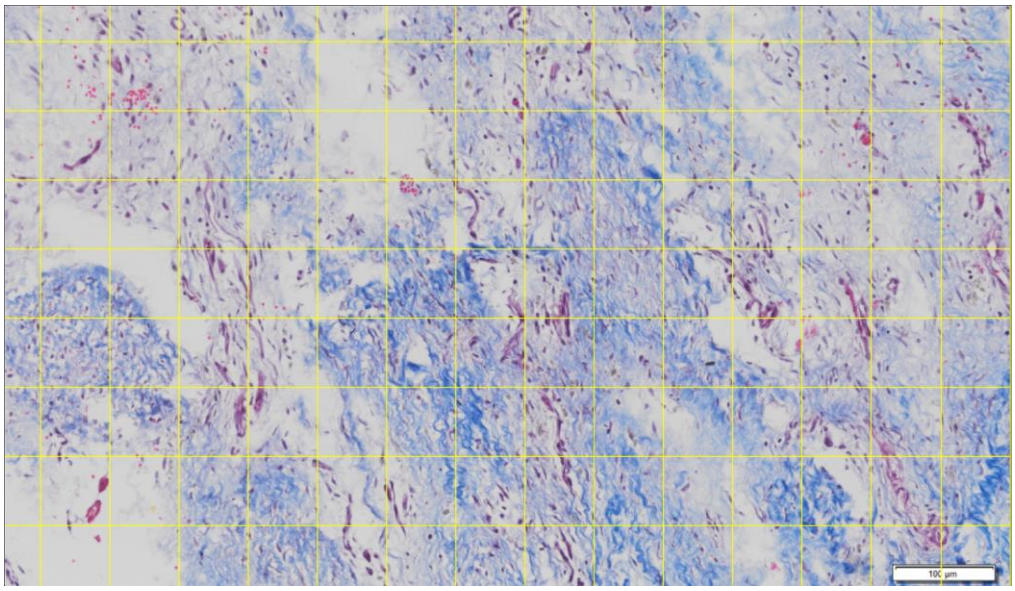

Figure A.9 Stereological grid super-imposed on Masson's Trichrome stained isotropic uniform random sample to quantify fibrosis. Area fraction of collagen was calculated from each low magnification image (10x). A grid made of 112 points was superimposed on each field of view and the points hitting collagen fibres were counted to get the area fraction values. A total ischemic area of 4.05 mm^2 was analysed per block. Scale bar = 100 μm.

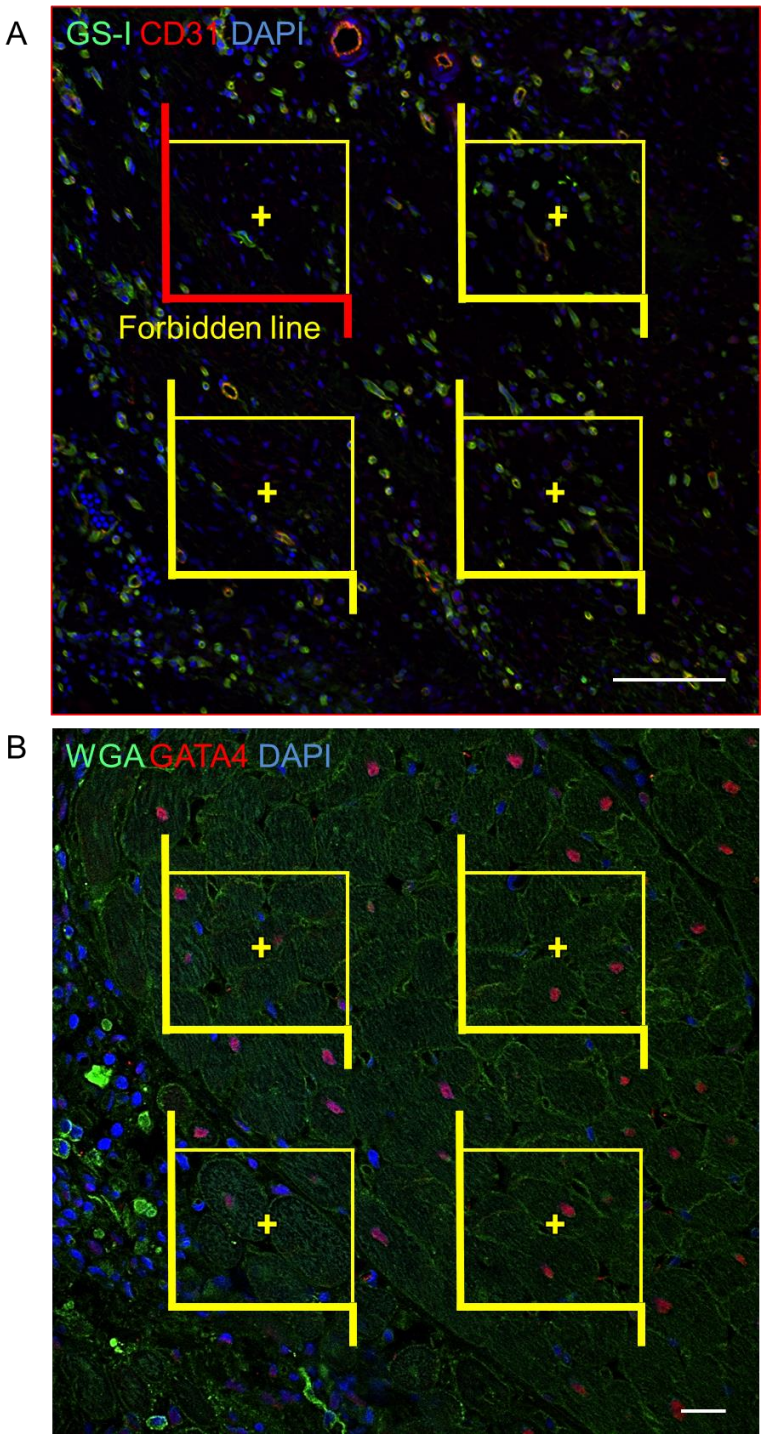

Figure A.10 Stereological grids to quantify capillaries, arterioles, GATA4$^+$ cardiomyocytes and CD163$^+$ cells. The number of CD31$^+$/GS-I$^+$ capillaries, α-SMA$^+$ arterioles, GATA4$^+$ cardiomyocytes and CD163$^+$ cells was calculated from each image. Confocal microscopy, 20x for vessel structures, scale bar = 100 μm. 40x for GATA4 and CD163, scale bar = 20 μm. Four grids were superimposed on image and the objects of interest falling inside the grids were counted to get the numerical estimates.

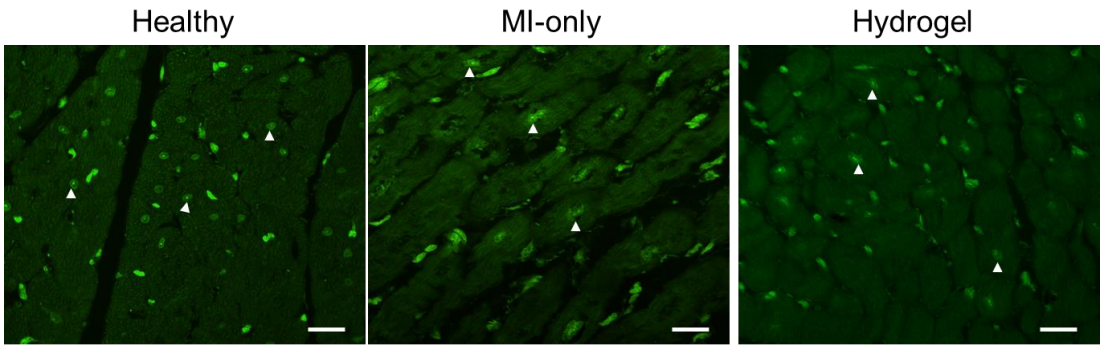

Figure A.11 Acridine orange staining of cellular nuclei in the border zone of MI. Sections from healthy and border zones of the infarcted hearts were stained with acridine orange to visualize and quantify cellular nuclei following the nucleator method. Data were then used to normalise EM micrographs measurements and estimate relative mitochondrial swelling. n=5 in MI-only, 6 healthy and hydrogel-treated.

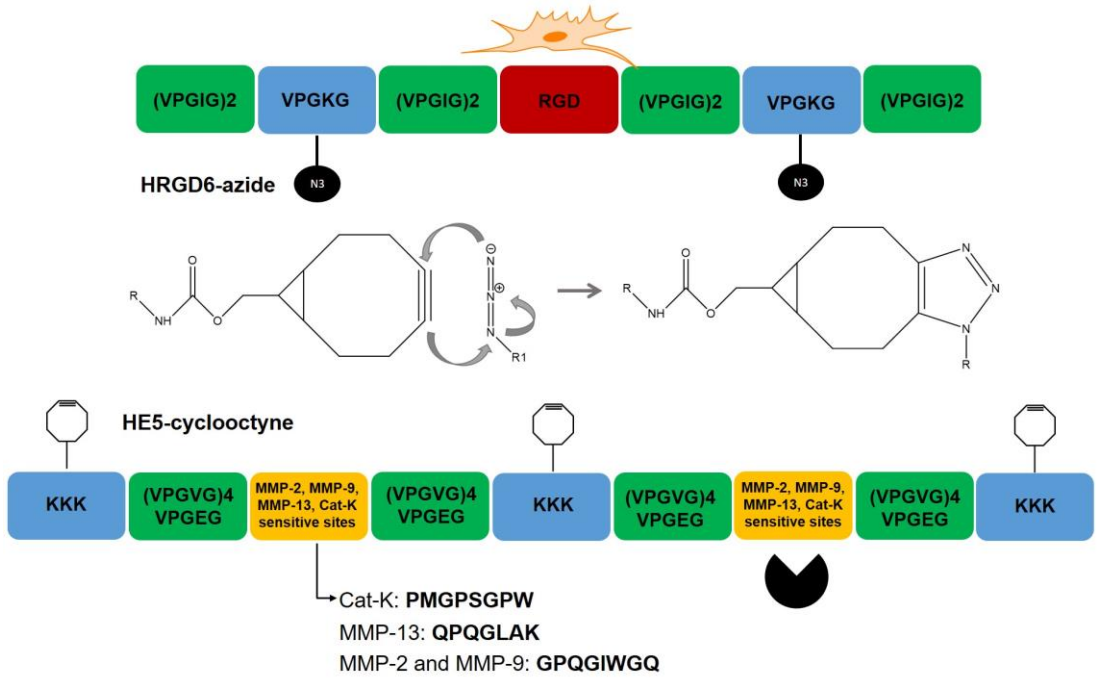

Figure A.12 Schematics of HE5-cyclooctine and HRGD-azide elastin-like recombinamers (ELRs) sequences. The two ELRs crosslink by catalyst-free click-chemistry reaction to form a hydrogel. Elastin-derived VPGXG (X variable amino acid) pentapeptide is present on both ELRs, cell-adhesive sequence RGD is present on HRGD and matrix metalloproteinase (MMP)- and cathepsin K(Cat-K)-responsive sequences are present in the HE5 ELR.

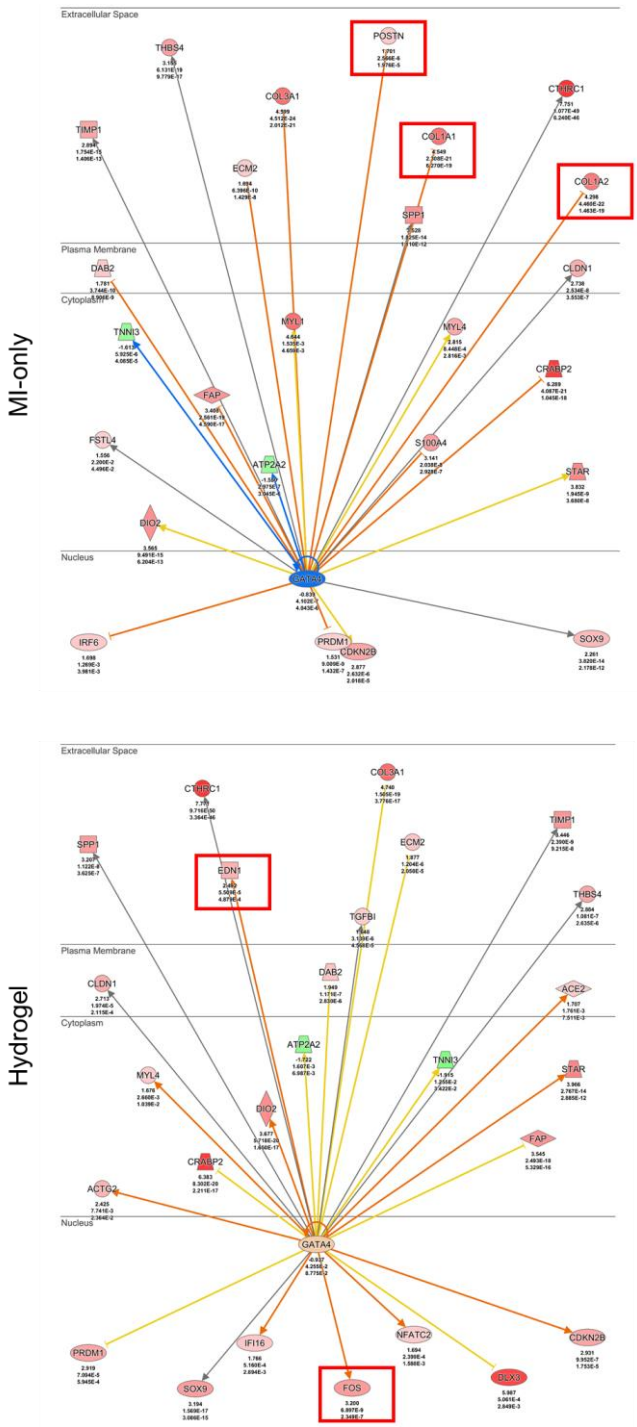

Figure A.13 IPA® analysis highlighted an arrested inhibition of GATA4 in ELRs-treated group. Predicted inhibition (blue) of GATA4 as a key regulator in MI-only at 28 days post-MI is lost in the ELRs-treated group (light orange). In MI-only, this is linked with a marked expression of pro-fibrotic genes such as POSTN, COL1A1 and COL1A2 (framed in red). By contrast, in ELRs-treated condition the arrested inhibition of GATA4 is associated with EDN1 and FOS expression, which are markers of endothelial cell proliferation. Log2(fold change), P, and adjusted-P values from RNA-seq data are indicated below the gene names.

A.24 References

- Mühlfeld C, Nyengaard JR, Mayhew TM. A review of state-of-the-art stereology for better quantitative 3D morphology in cardiac research. Cardiovasc Pathol. 2010 Mar-Apr;19(2):65-82
- Kilcoyne M, Twomey ME, Gerlach JQ, Kane M, Moran AP, Joshi L. Campylobacter jejuni strain discrimination and temperature-dependent glycome expression profiling by lectin microarray. Carbohydr Res. 2014 May 7;389:123-33

A.25 Patent submission, journal publications, conference proceedings and awards

Patent Submitted (1)

1. **Contessotto P.**, Da Costa M., Rodríguez-Cabello J.C. and Pandit A. "Treatment of myocardial infarction" patent filed at the European Patent Office on 26th September 2018.

Invention Disclosures Filed (2)

1. **Contessotto P.**, Owens P., Dockery P. and Pandit A. "Detection of myocardial fibrosis by Raman confocal microscopy" IDF filed in National University of Ireland Galway on 17th July 2018 (Tech-2018-023).
2. **Contessotto P.**, Da Costa M., Rodríguez-Cabello J.C. and Pandit A. "Elastin-like recombinamers hydrogel for the treatment of myocardial infarction" IDF filed in National University of Ireland Galway on 27th June 2017 (Tech-2017-043).

Published Manuscript (1)

1. Milcovich G., **Contessotto P.**, Marsico G., Ismail S. and Pandit A. "Synthetic/ECM-inspired hybrid platform for hollow microcarriers with ROS-triggered nanoporation hallmarks". *Scientific Reports*, 2017 Oct 13;7(1):13138.

Manuscripts Under Revision (2)

1. **Contessotto P.**, Ellis B., Jin C., Karlsson N.G., Zorlotuna P., Kilcoyne M. and Pandit A. "Distinct glycosylation in membrane proteins reflects the regeneration potential of neonatal myocardial tissue". In *Matrix Biology*.

2. **Contessotto P.**, Orbanić D., Da Costa M., Jin C., Owens P., Chantepie S., Papy-Garcia D., Chinello C., Magni F., Karlsson N.G., Kilcoyne M., Dockery P., Rodríguez-Cabello J.C. and Pandit A. "Elastin-like recombinamers-based hydrogel heals myocardial infarction in a clinically-relevant model". In *Nature Materials*.

Manuscripts Under Submission (1)

1. **Contessotto P.** and Pandit A. "Biological rationale and actual impact of therapeutic strategies for myocardial infarction".

Manuscripts to be Submitted (1)

1. Marsico G., Jin C., Sunny A.S., Brauchle E., Thomas D., **Contessotto P.**, Orbanić D., Rodríguez-Cabello J.C., Schenke-Layland K., Kilcoyne M., Karlsson N.G., McKullagh M. and Pandit A. "An elastin-based hydrogel induces muscle regeneration and angiogenesis in a hindlimb ischemia model modulating the glycosignature".

Published Book Chapter (1)

1. **Contessotto P.**, Browne S., Brody S. and Pandit A. "Cardiac valves: Biologic and Synthetic" In *Comprehensive Biomaterials II*, Elsevier, 2016.

Published Conference Abstracts (4)

1. **Contessotto P.**, Milcovich G., Spelat R., Marsico G., Chaturvedi A., Orbanić D., Flora T., Da Costa M., Rackauskas M., Amenitsch H., McCartin M., Rodríguez-Cabello J., Joshi L., Dockery P., Kilcoyne M. and Pandit A. (2016). "Towards an elastin-based hydrogel platform for the repair of myocardial infarction" *Front. Bioeng. Biotechnol.*, Conference Abstract: 10th World Biomaterials Congress. doi: 10.3389/conf.FBIOE.2016.01.02028.
2. Milcovich G., **Contessotto P.** and Pandit A. (2016). "Design of a protease and ROS responsive biomaterial approach to target drug delivery in inflamed tissue microenvironment" *Front. Bioeng. Biotechnol*., Conference Abstract: 10th World Biomaterials Congress, Montréal, Canada.
   doi: 10.3389/conf.FBIOE.2016.01.00936.

3. **Contessotto P.**, Spelat R., Marsico, G., Joshi L., Dockery P., Kilcoyne M. and Pandit A. (2016) "Comparing the myocardial glycoprofile across non-regenerative and regenerative models: an inner look at the extracellular environment" *eCells & Materials*, volume n.31, supplement 1, page 22, Conference Abstract: TERMIS-EU 2016 Conference, Uppsala, Sweden. doi: 10.22203/eCM.
4. Marsico G., Thomas D., **Contessotto P.**, Kilcoyne M., Joshi L., Quondamatteo F., McCullagh K. and Pandit A. (2016) "An insight into the glyco-environment of a murine model of hindlimb ischemia" *eCells & Materials*, volume n.31, supplement 1, page 190, Conference Abstract: TERMIS-EU 2016 Conference, Uppsala, Sweden. doi: 10.22203/eCM.

Conferences Proceedings (24, presenting author is underlined)

1. **Contessotto P.**, Orbanič D., Jin C., Owens P., Da Costa M., Karlsson N.G., Rodríguez-Cabello J.C., Dockery P., Kilcoyne M., Pandit A., "Post-ischemic myocardial remodeling and its modulation by an elastin-like recombinamers-based hydrogel". Podium presentation at Matrix Biology Ireland 2018 Meeting 21st November – 22nd November 2018, Galway, Ireland.
2. **Contessotto P.**, Orbanič D., Jin C., Owens P., Da Costa M., Cunningham S., Karlsson N.G., Rodríguez-Cabello J.C., Dockery P., Kilcoyne M., Pandit A., "Post-ischemic myocardial remodeling and its modulation by an elastin-like recombinamers-based hydrogel". Poster presentation at EMBO Workshop "The molecular and cellular basis of regeneration and tissue repair", 15th – 19th September 2018, Valletta, Malta.
3. Marsico G., Thomas D., Sunny A.A., Brauchle E., Orbanič D., **Contessotto P.**, Rodríguez-Cabello J.C., Schenke-Layland K., Kilcoyne M., McCullagh K., Pandit A., "Elastin-like hydrogel as a treatment for ischemic condition: an insight into the glycoenvironment". Poster presentation at EMBO Workshop "The molecular and cellular basis of regeneration and tissue repair", 15th – 19th September 2018, Valletta, Malta.
4. **Contessotto P.**, Orbanič D., Jin C., Owens P., Da Costa M., Cunningham S., Karlsson N.G., Rodríguez-Cabello J.C., Dockery P., Kilcoyne M., Pandit A., "Elastin-like recombinamers-based hydrogel modulates infarcted myocardium glycoprofile towards a regenerative state". Poster presentation at Benzon

Symposium "Glycotherapeutics: Emerging Roles of Glycans in Medicine", 27th – 30th August 2018, Copenhagen, Denmark.

5. **Contessotto P.**, Orbanič D., Jin C., Owens P., Da Costa M., Cunningham S., Karlsson N.G., Rodríguez-Cabello J.C., Dockery P., Kilcoyne M., Pandit A., "Elastin-like recombinamers-based hydrogel modulates infarcted myocardium glycoprofile towards a regenerative state". Research pitch at Biointerfaces International, 14th – 17th August 2018, Zurich, Switzerland.
6. **Contessotto P.**, Lalor P., Owens P., Orbanič D., Flora T., Da Costa M., Rodríguez-Cabello J.C., Joshi L., Dockery P., Kilcoyne M., Pandit A., "Elastin-like recombinamers-based hydrogel modulates infarcted myocardium glycoprofile towards a regenerative state". Podium presentation at Matrix Biology Ireland 2017 Meeting, 30th November – 1st December 2017, Dublin, Ireland.
7. Marsico G., Thomas D., Sunny A.S., Brauchle E., Orbanič D., **Contessotto P.**, Rodríguez-Cabello C., Schenke-Layland K., Kilkoyne M., McKullagh M., Pandit A., "Elastin-like hydrogel restored healthy ECM profile and GAGs contents in a mouse model of hindlimb ischemia", Podium presentation at Matrix Biology Ireland 2017 Meeting, 30th November – 1st December 2017, Dublin, Ireland.
8. Ellis B., **Contessotto P.**, Acun A., Can I., Pandit A., Zorlotuna P., "Myocardium-on-chip derived from characterized human iPSCs with capillary-like flow for personalized medicine". Podium presentation at Biomedical Engineering Society Annual Meeting, 11th - 14th October 2017, Phoenix, AZ, USA.
9. Marsico G., Thomas D., Sunny Akogwu A., **Contessotto P.**, Orbanič D., Rodríguez-Cabello J.C., McCullagh K. and Pandit A. "Angiogenesis in ischemic condition is induced by an elastin-like recombinamer (ELR) based hydrogel". Podium presentation at European Society of Biomaterials Conference, 4th – 8th September 2017, Athens, Greece.
10. **Contessotto P.**, Lalor P., Da Costa M., Owens P., Orbanič D., Flora T., Pauza A., Rodríguez-Cabello J.C., Joshi L., Dockery P., Kilcoyne M., Pandit A., "Elastin-like recombinamers-based hydrogel modulates infarcted myocardium glycoprofile towards a regenerative state". Podium presentation at Gordon Research Conference "Biomaterials and Tissue Engineering", 23rd – 28th July 2017, Holderness, NH, USA.

11. **Contessotto P.**, Lalor P., Orbanič D., Flora T., Pauza A.G., Da Costa M., Rodríguez-Cabello J.C., Joshi L., Dockery P., Kilcoyne M., Pandit A., "Elastin-like recombinamers-based hydrogel modulates infarcted myocardium glycoprofile towards a regenerative state". Podium presentation at TERMIS-EU Meeting, 26th – 30th June 2017, Davos, Switzerland.
12. **Contessotto P.***, Spelat R.*, Ellis B., Grealy M., Joshi L., Dockery P., Zorlutuna P., Kilcoyne M., Pandit A., "Glycosignatures from self-regenerating, neonatal and adult myocardial tissues are key targets for investigation of cardiac regeneration". Podium presentation at TERMIS-EU Meeting, 26th – 30th June 2017, Davos, Switzerland.
13. Marsico G., Thomas D., Sunny Akogwu A., **Contessotto P.**, Kilcoyne M., Joshi L., McCullagh K. and Pandit A., "Effect of ischemia on the glyco-environment: a study on a murine model". Podium presentation at TERMIS-EU Meeting, 26th – 30th June 2017, Davos, Switzerland.
14. Marsico G., Thomas D., **Contessotto P.**, Abbah S.A., Kaur J., Kilcoyne M., Joshi L., McCullagh K., Pandit A., "An insight into the glyco-environment of a murine model of hind limb ischemia", Podium presentation at Matrix Biology Ireland 2016 Meeting "Repairing the Matrix – Disease manifestation and therapeutic strategies", 16th - 18th November 2016, Galway, Ireland.
15. **Contessotto P.**, Spelat R., Marsico, G., Joshi L., Dockery P., Kilcoyne M., Pandit A., "Comparing the myocardial glycoprofile across non-regenerative and regenerative models: an inner look at the extracellular environment". Poster presentation at TERMIS-EU Meeting, 28th June – 1st July 2016, Uppsala, Sweden.
16. Marsico G., Thomas D., **Contessotto P.**, Kilcoyne M., Joshi L., Quondamatteo F., McCullagh K., Pandit A., "An insight into the glyco-environment of a murine model of hindlimb ischemia", Podium presentation at TERMIS-EU, 28th June – 1st July 2016, Uppsala, Sweden.
17. **Contessotto P.**, Milcovich G., Spelat R., Marsico G., Chaturvedi A., Orbanič D., Flora T., Da Costa M., Rackauskas M., Amenitsch H., McCartin M., Rodríguez-Cabello J., Joshi L., Dockery P., Kilcoyne M., Pandit A., "Towards an elastin-based hydrogel platform for the repair of myocardial infarction", Podium presentation at 10th World Biomaterials Congress, 17th – 22nd May 2016, Montréal, Canada.

18. Milcovich G., **Contessotto P.**, Pandit A. "Design of a protease and ROS responsive biomaterial approach to target drug delivery in inflamed tissue microenvironment", Poster presentation at 10th World Biomaterials Congress, 17th – 22nd May 2016, Montréal, Canada.
19. **Contessotto P.**, Browne S., Marsico G., Joshi L., Kilcoyne M., Pandit A., "Intra-species glycosylation differences in myocardial capillaries and cardiomyocytes", Poster presentation at Advanced Functional Polymers for Medicine, 23rd – 25th March 2015, Galway, Ireland.
20. Milcovich G., **Contessotto P.**, Pandit A., "Fabrication of ROS and protease responsive drug delivery systems", Poster presentation at Advanced Functional Polymers for Medicine, 23rd – 25th March 2015, Galway, Ireland.
21. Marsico G., Thomas D., **Contessotto P.**, Kilcoyne M., Joshi L., Quondamatteo F., Pandit A., "Glycoprofile expression in a murine model of critical limb ischemia", Poster presentation at Advanced Functional Polymers for Medicine, 23rd – 25th March 2015, Galway, Ireland.
22. **Contessotto P.**, Browne S., Marsico G., Joshi L., Kilcoyne M., Pandit A., "Glycoprofiling of rat myocardial tissue", Podium presentation at Matrix Biology Ireland 2014 Meeting, 19th - 21st November 2014, Galway, Ireland.
23. Marsico G., Thomas D., **Contessotto P.**, Kilcoyne M., Lokesh J., Quondamatteo F., Pandit A. Glycocalyx and ECM glycans modification in a murine model of critical limb ischemia", Podium presentation at Matrix Biology Ireland 2014 Meeting, 19th - 21st November 2014, Galway, Ireland.
24. Milcovich G., **Contessotto P.**, Marsico G., Orbanič D., Flora T., Rodríguez-Cabello J.C., Pandit A., "Fabrication of a multi-modal delivery system using a elastin-like recombinamer", Poster presentation at Advanced Functional Polymers for Medicine, 26th - 28th May 2014, Liege, Belgium.

Awards (2)

1. Travel award at EMBO Conference on "The Molecular & Cellular Basis of Regeneration and Tissue Repair", 15th – 19th September 2018, Malta.
2. Best poster presentation and travel award at Gordon Research Conference on "Biomaterials and Tissue Engineering", 23rd – 28th July 2017, Holderness, NH, USA.